THE UNIVERSITY OF TULSA
THE GRADUATE SCHOOL

ADVANCES IN WELL TESTING FOR SOLUTION-GAS-DRIVE RESERVOIRS

by
Dimitrios Georgios Hatzignatiou

A dissertation submitted in partial fulfillment of
the requirements for the degree of Doctor of Philosophy
in the Discipline of Petroleum Engineering
The Graduate School
The University of Tulsa
1990

THE UNIVERSITY OF TULSA
THE GRADUATE SCHOOL

ADVANCES IN WELL TESTING FOR SOLUTION-GAS-DRIVE RESERVOIRS

by

Dimitrios Georgios Hatzignatiou

A DISSERTATION
APPROVED FOR THE DISCIPLINE OF
PETROLEUM ENGINEERING

By Dissertation Committee

Albert C. Reynolds, Chairperson
Richard E. Thompson
Robin Thompson
[illegible]

ABSTRACT

Hatzignatiou, Dimitrios Georgios

(Doctor of Philosophy in Petroleum Engineering)

Advances in Well Testing for Solution-Gas-Drive Reservoirs

(454 pp. - Chapter VIII)

Directed by Professor Dr. Albert C. Reynolds, Jr.

(247 WORDS)

This work presents procedures for constructing relative permeability curves from well-test pressure data obtained at a well producing a solution-gas-drive reservoir. The effects of wellbore storage on the analysis of multiphase flow pressure data are also discussed.

It is shown that the relative permeability curves can be constructed from values of effective oil and gas permeabilities computed from well-test pressure data and application of nonlinear regression analysis techniques with Standing's correlation as the model function.

These computational procedures are also considered for heterogeneous solution gas drive systems and can be applied when the initial reservoir pressure is greater or equal to the initial bubble-point pressure.

The effect of wellbore storage on the analysis of pressure drawdown data obtained at a well producing a solution-gas-drive reservoir is also investigated. It is shown that effective oil permeability as a pointwise function of pressure can be computed directly from the measured values of the flowing wellbore pressure provided the sandface oil flow rate is measured and incorporated into the analysis. For cases where the sandface flow rate is measured, a new computational procedure for estimating oil saturation as a function of pressure is presented.

The effect of wellbore storage on the analysis of pressure buildup data obtained in a solution-gas-drive reservoir is also examined. Based on a superposition equation, new computational equations for obtaining rough estimates of effective oil and gas permeabilities as pointwise functions of pressure from the measured values of the shut-in wellbore pressure are presented.

ACKNOWLEDGEMENTS

I would first like to thank Dr. A. C. Reynolds, Jr., Professor of Petroleum Engineering and Mathematics, for the invaluable assistance he has provided and the continuous encouragement and patience he has shown throughout the course of this research, and for reading the countless revisions required in the development of this dissertation to its present form. I thank Drs. E. T. Guerrero, R. E. Thompson and L. G. Thompson for serving on my dissertation committee. I also extend my sincere thanks to Dr. Richard A. Redner, Associate Professor of Mathematics, for reviewing Chapter II and providing constructive remarks.

Throughout my PhD studies, I have received financial assistance in the form of teaching assistantships from the Petroleum Engineering Department of The University of Tulsa. Portions of this dissertation were financed by The University of Tulsa Petroleum Reservoir Exploitation Projects (TUPREP). I would like to thank both of these sources for financial support.

This work is dedicated to my wife, Kathy A. Hatzignatiou, my parents, Angeliki and Georgios Hatzignatiou, and my sister, Marlyn Hatzignatiou, for their love, patience, encouragement, support and trust.

ΑΦΙΕΡΩΣΗ

Αφιερωνετε στη μητερα μου Αγγελικη, στην αδελφη μου Μαρλυν, στο πατερα μου Γεωργιο, και στη συζυγο μου Καθη Χατζηγνατιου.

TABLE OF CONTENTS

TITLE PAGE i
APPROVAL PAGE ii
ABSTRACT iii
ACKNOWLEDGEMENTS v
TABLE OF CONTENTS vi
LIST OF TABLES xi
LIST OF FIGURES xiv

CHAPTER I INTRODUCTION 1
1.1 Literature Review 1
1.2 Outline 3

CHAPTER II NONLINEAR REGRESSION ANALYSIS TECHNIQUES 6
2.1 Introduction to Least Squares 6
2.2 Unconstrained Optimization Methods 7
2.2.1 Iterative Scheme 8
2.2.2 Acceptability and Convergence 9
2.2.3 Steepest Descent Method 10
2.2.4 Newton's Method 10
2.2.5 Directional Discrimination Method 11
2.2.6 The Gauss Method 11
2.2.7 Marquardt's Method 12
2.2.8 Cholesky's Decomposition 13
2.2.9 Modified Cholesky's Decomposition 15
2.2.10 Interpolation-Extrapolation 17
2.2.11 Termination Criteria 18
2.3 Constrained Optimization Methods 18

2.3.1 Penalty Functions 19
2.4 Estimation of Confidence Intervals 21
2.5 Review of Nonlinear Regression Analysis Methods . . 22

CHAPTER III DETERMINATION OF EFFECTIVE OR RELATIVE PERMEABILITY CURVES FROM WELL TESTS . . . 24
3.1 Introduction 24
3.2 Theoretical Background 27
3.2.1 Theory 1. Zero Critical Gas Saturation 30
3.2.2 Theory 2. Non-Zero Critical Gas Saturation . . 31
3.3 Mathematical Model 33
3.4 Simulator Data 34
3.5 Numerical Procedure 35
3.6 Results 38
3.6.1 Case 1: Zero Critical Gas Saturation, Zero Skin 38
3.6.1.1 Effects of the Duration of the Test 41
3.6.1.2 Effects of the Initial Value of kk_r^o 43
3.6.1.3 Effects of the Initial Guess 44
3.6.1.4 Effective (Relative) Permeability Curves . 45
3.6.1.5 Determination of Skin Factor 47
3.6.2 Case 2: Non-Zero Critical Gas Saturation, Zero Skin 54
3.6.3 Case 3: Zero Critical Gas Saturation, Non-Zero Skin 59

CHAPTER IV ESTIMATION OF EFFECTIVE PERMEABILITIES FOR RESERVOIRS INITIALLY ABOVE BUBBLE-POINT PRESSURE 66
4.1 Introduction 66
4.2 Mathematical Model and Simulator Data 67
4.3 Results 70
4.3.1 Zero Skin Cases 70

4.3.2 Non-Zero Skin Cases 85
4.4 Estimation of kk_{ro} and kk_{rg} Curves 93

CHAPTER V ESTIMATION OF EFFECTIVE PERMEABILITIES
FOR HETEROGENEOUS RESERVOIRS 99
5.1 Introduction 99
5.2 Mathematical Model 101
5.3 Simulator Data 101
5.4 Results 105
5.4.1 Zero Skin Cases 106
5.4.2 Non-Zero Skin Cases 137

CHAPTER VI EFFECT OF WELLBORE STORAGE
ON THE ANALYSIS OF
MULTIPHASE FLOW PRESSURE DATA 152
6.1 Introduction 152
6.2 Mathematical Model 154
6.3 General Notation and Definitions 155
6.4 Simulator Data 157
6.5 Theoretical Results 158
6.5.1 Effect of Wellbore Storage on
Pressure and Saturation 158
6.5.2 Rate-Normalization and Multirate
Pseudopressure Analysis 166
6.6 Computation of Oil Saturation 174
6.7 Computation of Effective Permeabilities 178
6.7.1 Effective Permeability as
a Function of Pressure 181
6.7.2 Influence of the Skin Factor 192
6.8 Pressure-Squared Method 202

6.8.1 Constant Rate Production 202
6.8.2 Pressure-Squared Analysis With
Logarithmic Convolution Time 207
6.8.3 Rate Normalization for
Pressure-Squared Method 208
6.9 Pressure-Squared Analysis Results 209
6.10 Pressure Method 223

CHAPTER VII EFFECT OF AFTERFLOW ON THE ANALYSIS
OF PRESSURE BUILDUP DATA FROM
SOLUTION-GAS-DRIVE RESERVOIRS 227
7.1 Introduction 227
7.2 Mathematical Model 229
7.3 General Notation and Definitions 230
7.4 Simulator Data 233
7.5 Theoretical Results 236
7.5.1 Rate-Normalization and Multirate
Pseudopressure Analysis 236
7.6 Computation of Oil Saturation 243
7.6.1 Influence of Skin Factor 247
7.6.2 Influence of Critical Gas Saturation 251
7.7 Computation of Effective Permeabilities 251
7.7.1 Effective Permeability as
a Function of Pressure 251
7.7.2 Influence of Skin Factor 262
7.7.3 Influence of Critical Gas Saturation 274
7.8 Pressure-Squared Method 279
7.8.1 Constant Rate Production 279
7.8.2 Pressure-Squared Analysis With
Logarithmic Convolution Time 287

7.8.3 Rate Normalization for
Pressure-Squared Method 288
7.9 Pressure-Squared Analysis Results 290
7.10 Pressure Method 310

CHAPTER VIII CONCLUSIONS 315

NOMENCLATURE 318
REFERENCES 323
APPENDIX A : ROCK AND FLUID PROPERTIES 329
APPENDIX B : SATURATION-PRESSURE RELATIONSHIP
DURING DRAWDOWN 334
APPENDIX C : SATURATION-PRESSURE RELATIONSHIP
IN TERMS OF THE RATIO k_{rg}/k_{ro}
DURING DRAWDOWN 336
APPENDIX D : DERIVATION OF EQUATION FOR COMPUTING
EFFECTIVE OIL PERMEABILITY
DURING DRAWDOWN 340
APPENDIX E : DERIVATION OF EQUATION FOR COMPUTING
EFFECTIVE OIL PERMEABILITY
DURING BUILDUP 341
APPENDIX F : TABLES 342

List of Tables

Table		Page
A-1	PVT Data - Set 1	329
A-2	Rock Properties - Set 1	330
A-3	PVT Data - Set 2	331
A-4	Rock Properties - Set 2	332
A-5	Rock Properties - Set 3	333
F-1	Simulated and Computed kk_{ro} Values Drawdown Test - Case 1	344
F-2	Simulated and Computed kk_{rg} Values Drawdown Test - Case 1	348
F-3	Parameter Values for the Computation of kk_{ro} and kk_{rg} Drawdown Test - Case 1	352
F-4	Simulated and Computed kk_{ro} Values Buildup Test - Case 1	356
F-5	Simulated and Computed kk_{rg} Values Buildup Test - Case 1	360
F-6	Parameter Values for the Computation of kk_{ro} and kk_{rg} Buildup Test - Case 1	364
F-7	Nonlinear Parameter Estimation Two Unknowns - Case 1	368
F-8	Nonlinear Parameter Estimation Three Unknowns - Case 1	369
F-9	Nonlinear Parameter Estimation Four Unknowns - Case 1	370
F-10	Effects of the Initial Guess on the Values of Estimated Parameters - Case 1	371

F-11 Approximate Confidence Intervals of Estimated Parameters with 95% Confidence - Case 1 372
F-12 Simulated and Computed kk_{ro} Values Drawdown Test - Case 3 374
F-13 Simulated and Computed kk_{rg} Values Drawdown Test - Case 3 375
F-14 Simulated and Computed kk_{ro} Values Drawdown Test - Case 1 377
F-15 Simulated and Computed kk_{ro} Values Buildup Test - Case 1 380
F-16 Simulated and Computed kk_{rg} Values Drawdown Test - Case 1 386
F-17 Simulated and Computed kk_{rg} Values Buildup Test - Case 1 389
F-18 Nonlinear Parameter Estimation Two Unknowns - Case 1 395
F-19 Nonlinear Parameter Estimation Three Unknowns - Case 1 396
F-20 Nonlinear Parameter Estimation Four Unknowns - Case 1 397
F-21 Simulated and Computed kk_{ro} Values Drawdown Test - Case 1 399
F-22 Simulated and Computed kk_{ro} Values Buildup Test - Case 1 402
F-23 Simulated and Computed kk_{rg} Values Drawdown Test - Case 1 405
F-24 Simulated and Computed kk_{rg} Values Buildup Test - Case 1 408
F-25 Simulated and Computed kk_{ro} Values Drawdown Test - Case 1a 412

F-26 Simulated and Computed kk_{ro} Values
Buildup Test - Case 1a 415
F-27 Simulated and Computed kk_{rg} Values
Drawdown Test - Case 1a 418
F-28 Simulated and Computed kk_{rg} Values
Buildup Test - Case 1a 421
F-29 Simulated and Computed kk_{ro} Values
Drawdown Test - Case 6 425
F-30 Simulated and Computed kk_{ro} Values
Buildup Test - Case 6 428
F-31 Simulated and Computed kk_{rg} Values
Drawdown Test - Case 6 431
F-32 Simulated and Computed kk_{rg} Values
Buildup Test - Case 6 434
F-33 Simulated and Computed S_o Versus p_{wf}
Relationship Drawdown Test - Case 2 438
F-34 Simulated and Computed kk_{ro} Values
Drawdown Test - Case 2 442
F-35 Simulated and Computed kk_{rg} Values
Drawdown Test - Case 2 445
F-36 Simulated and Computed kk_{ro} Values
Buildup Test - Case 2 449
F-37 Simulated and Computed kk_{rg} Values
Buildup Test - Case 2 452

List of Figures

Figure		Page
3.2.1	Effect of λ on the oil and gas relative permeability curves	29
3.2.2	Effect of S_{gc} on the oil and gas relative permeability curves	32
3.6.1	Effective oil permeability as a function of wellbore pressure; Case 1	39
3.6.2	Plot of effective oil and gas permeability curves; Case 1	46
3.6.3	Approximation of oil saturation/wellbore pressure relation; Case 1	49
3.6.4	Approximation of oil saturation/wellbore pressure relation; Case 1	50
3.6.5	Ratio of oil/gas effective permeability versus oil saturation; Case 1	51
3.6.6	Plot of dimensionless pseudopressure functions versus dimensionless time; Case 1	53
3.6.7	Effective oil permeability as a function of wellbore pressure; Case 2	55
3.6.8	Plot of effective oil and gas permeability curves; Case 2	57
3.6.9	Effective oil permeability as a function of wellbore pressure; Case 3	62
3.6.10	Plot of effective oil and gas permeability curves; Case 3	63
3.6.11	Plot of dimensionless pseudopressure functions versus dimensionless time; Case 3	65
4.2.1	Relative permeability curves; Set 1	69
4.3.1	Drawdown and buildup wellbore pressures; Case 1	71

4.3.2 Drawdown and buildup sandface oil saturation; Case 1 72
4.3.3 Effective oil permeability as a function of wellbore pressure; Case 1 73
4.3.4 Effective gas permeability as a function of wellbore pressure; Case 1 75
4.3.5 Drawdown and buildup wellbore pressures; Case 2 77
4.3.6 Drawdown and buildup sandface oil saturation; Case 2 78
4.3.7 Effective oil permeability as a function of wellbore pressure; Case 2 79
4.3.8 Effective gas permeability as a function of wellbore pressure; Case 2 81
4.3.9 Drawdown and buildup wellbore pressures; Case 3 82
4.3.10 Drawdown and buildup sandface oil saturation; Case 3 83
4.3.11 Effective oil permeability as a function of wellbore pressure; Case 3 84
4.3.12 Drawdown and buildup wellbore pressures; Case 4 86
4.3.13 Drawdown and buildup sandface oil saturation; Case 4 87
4.3.14 Effective oil permeability as a function of wellbore pressure; Case 4 88
4.3.15 Drawdown and buildup wellbore pressures; Case 5 90
4.3.16 Drawdown and buildup sandface oil saturation; Case 5 91
4.3.17 Effective oil permeability as a function of wellbore pressure; Case 5 92
4.4.1 Plot of effective oil and gas permeability curves; Case 1 96
4.4.2 Plot of effective oil and gas permeability curves; Case 1 98
5.3.1 Relative permeability curves; Set 3 103
5.4.1 Drawdown and buildup wellbore pressures; Case 1 107
5.4.2 Drawdown and buildup sandface oil saturation; Case 1 108
5.4.3 Effective oil permeability as a function of sandface oil saturation; Case 1 110

5.4.4 Effective gas permeability as a function of sandface oil saturation; Case 1 111
5.4.5 Drawdown and buildup wellbore pressures; Case 1a 115
5.4.6 Drawdown and buildup sandface oil saturation; Case 1a 116
5.4.7 Effective oil permeability as a function of sandface oil saturation; Case 1a 117
5.4.8 Effective gas permeability as a function of sandface oil saturation; Case 1a 118
5.4.9 Drawdown and buildup wellbore pressures; Case 2 120
5.4.10 Drawdown and buildup sandface oil saturation; Case 2 121
5.4.11 Effective oil permeability as a function of sandface oil saturation; Case 2 122
5.4.12 Effective gas permeability as a function of sandface oil saturation; Case 2 124
5.4.13 Drawdown and buildup wellbore pressures; Case 3 125
5.4.14 Drawdown and buildup sandface oil saturation; Case 3 126
5.4.15 Effective oil permeability as a function of sandface oil saturation; Case 3 127
5.4.16 Effective gas permeability as a function of sandface oil saturation; Case 3 129
5.4.17 Drawdown and buildup wellbore pressures; Case 4 131
5.4.18 Drawdown and buildup sandface oil saturation; Case 4 132
5.4.19 Effective oil permeability as a function of sandface oil saturation; Case 4 133
5.4.20 Drawdown and buildup wellbore pressures; Case 5 134
5.4.21 Drawdown and buildup sandface oil saturation; Case 5 135
5.4.22 Effective oil permeability as a function of sandface oil saturation; Case 5 136
5.4.23 Drawdown and buildup wellbore pressures; Case 6 139
5.4.24 Drawdown and buildup sandface oil saturation; Case 6 140

5.4.25 Effective oil permeability as a function of sandface oil saturation; Case 6 141
5.4.26 Drawdown and buildup wellbore pressures; Case 7 143
5.4.27 Drawdown and buildup sandface oil saturation; Case 7 144
5.4.28 Effective oil permeability as a function of sandface oil saturation; Case 7 145
5.4.29 Drawdown and buildup wellbore pressures; Case 8 147
5.4.30 Drawdown and buildup sandface oil saturation; Case 8 148
5.4.31 Effective oil permeability as a function of sandface oil saturation; Case 8 149
5.4.32 Effective gas permeability as a function of sandface oil saturation; Case 8 150
6.5.1 Effect of wellbore storage on the flowing wellbore pressure; Cases 1, 2 and 3 159
6.5.2 Effect of wellbore storage on the sandface oil saturation; Cases 1, 2 and 3 160
6.5.3 Sandface oil saturation as a function of flowing wellbore pressure; Cases 1, 2 and 3 162
6.5.4 Producing GOR versus flowing wellbore pressure for Cases 1, 2 and 3 163
6.5.5 Comparison of sandface flow rates for two wellbore storage models 164
6.5.6 Log-log plot of dimensionless pseudopressure versus dimensionless time; Cases 1, 2 and 3 165
6.5.7 Comparison of pseudopressure solution with liquid wellbore storage solution 167
6.5.8 Dimensionless Odeh-Jones plot in terms of pseudopressure; Cases 1, 2 and 3 170
6.5.9 Dimensionless Odeh-Jones plot in terms of pseudopressure; Cases 4, 5 and 6 171

6.5.10 Semilog plot of rate-normalized dimensionless pseudopressure versus dimensionless time; Cases 1-3 173
6.6.1 Plot of actual or computed sandface oil saturation versus flowing wellbore pressure; Case 2 177
6.6.2 Plot of actual or computed sandface oil saturation versus flowing wellbore pressure; Case 3 179
6.6.3 Plot of actual or computed sandface oil saturation versus flowing wellbore pressure; Case 4 180
6.7.1 Semilog plot of effective oil permeability versus dimensionless time; Case 2 183
6.7.2 Plot of effective oil permeability versus flowing wellbore pressure; Case 2 185
6.7.3 Plot of effective gas permeability versus flowing wellbore pressure; Case 2 186
6.7.4 Plot of effective oil permeability versus oil saturation; Case 2 188
6.7.5 Semilog plot of effective oil permeability versus dimensionless time; Case 3 189
6.7.6 Effective oil permeability versus flowing wellbore pressure; Case 3 190
6.7.7 Plot of simulated or computed oil saturation versus flowing wellbore pressure; Case 3 191
6.7.8 Effective oil permeability versus oil saturation; Case 3 193
6.7.9 Effective oil permeability versus dimensionless time; Case 4 . . . 194
6.7.10 Effective oil permeability versus flowing wellbore pressure; Case 4 196
6.7.11 Effective oil permeability versus dimensionless time; Case 4 . . . 197
6.7.12 Plot of effective gas permeability versus flowing wellbore pressure; Case 4 199
6.7.13 Effective oil permeability versus oil saturation; Case 4 200

6.7.14 Oil saturation versus flowing wellbore pressure; Case 4 201
6.7.15 Effective oil permeability versus oil saturation; Case 4 203
6.8.1 Oil mobility/FVF as a function of flowing wellbore pressure; Case 4 205
6.9.1 Log-log plot of change in pressure-squared versus time; Cases 1, 2 and 3 211
6.9.2 Semilog plot of change in pressure-squared versus time; Cases 1, 2 and 3 212
6.9.3 Rate-normalized change in pressure-squared versus logarithmic convolution time; Cases 1, 2 and 3 213
6.9.4 Semilog plot of rate-normalized change in pressure-squared versus time; Cases 1, 2 and 3 215
6.9.5 Log-log plot of change in pressure-squared versus time; Cases 4, 5 and 6 217
6.9.6 Semilog plot of change in pressure-squared versus time; Cases 4, 5 and 6 218
6.9.7 Rate-normalized change in pressure-squared versus logarithmic convolution time; Cases 4, 5 and 6 220
6.9.8 Semilog plot of rate-normalized change in pressure-squared versus time; Cases 4, 5 and 6 222
6.10.1 Semilog plot of rate-normalized pressure drop versus time; Cases 1, 2 and 3 224
6.10.2 Semilog plot of rate-normalized pressure drop versus time; Cases 4, 5 and 6 226
7.3.1 Comparison of dimensionless sandface flow rate change for two wellbore storage models 232
7.3.2 Comparison of pseudopressure solution with liquid wellbore storage solution 234
7.5.1 Dimensionless Odeh-Jones plot in terms of dimensionless pseudopressure; Cases 1-3 239

7.5.2 Semilog plot of rate-normalized dimensionless pseudopressure versus Horner time; Cases 1-3 242
7.5.3 Semilog plot of dimensionless pseudopressure versus Horner time; Cases 1-3 244
7.6.1 Variation of drawdown or buildup bubble-point pressure as a function of the wellbore pressure; Case 2 246
7.6.2 Approximation of sandface oil saturation/pressure relation; Case 2 248
7.6.3 Variation of drawdown or buildup bubble-point pressure as a function of the wellbore pressure; Case 5 249
7.6.4 Approximation of sandface oil saturation/pressure relation; Case 5 250
7.6.5 Variation of drawdown or buildup bubble-point pressure as a function of the wellbore pressure; Case 8 252
7.6.6 Approximation of sandface oil saturation/pressure relation; Case 8 253
7.7.1 Plot of effective oil permeability versus wellbore pressure; Cases 1-3 257
7.7.2 Effective oil permeability as a function of oil saturation; Cases 1-3 258
7.7.3 Effective gas permeability as a function of wellbore pressure; Cases 1-3 260
7.7.4 Effective gas permeability as a function of oil saturation; Cases 1-3 261
7.7.5 Effective oil permeability as a function of wellbore pressure; Cases 1-3 263
7.7.6 Effective oil permeability as a function of oil saturation; Cases 1-3 264
7.7.7 Effective gas permeability as a function of wellbore pressure; Cases 1-3 265

7.7.8 Effective gas permeability as a function of oil saturation; Cases 1-3 266
7.7.9 Effective oil permeability as a function of wellbore pressure from Eq. 7.7.3; Cases 1-3 267
7.7.10 Effective oil permeability as a function of wellbore pressure; Cases 4-6 268
7.7.11 Effective oil permeability as a function of oil saturation; Cases 4-6 270
7.7.12 Effective gas permeability as a function of wellbore pressure; Cases 4-6 271
7.7.13 Effective gas permeability as a function of oil saturation; Cases 4-6 272
7.7.14 Effective oil permeability as a function of wellbore pressure from Eq. 7.7.3; Cases 4-6 273
7.7.15 Effective oil permeability as a function of wellbore pressure; Cases 7-9 275
7.7.16 Effective oil permeability as a function of oil saturation; Cases 7-9 276
7.7.17 Effective gas permeability as a function of wellbore pressure; Cases 7-9 277
7.7.18 Effective gas permeability as a function of oil saturation; Cases 7-9 278
7.7.19 Effective oil permeability as a function of wellbore pressure from Eq. 7.7.3; Cases 7-9 280
7.8.1 Oil mobility/FVF as a function of wellbore pressure; Cases 1-3 282
7.8.2 Approximation of oil mobility/FVF for pressure-squared method 284
7.8.3 Effective oil permeability as a function of wellbore pressure; Case 4 286

7.9.1 Semilog plot of change in pressure-squared versus Horner time; Cases 1-3 291
7.9.2 Rate-normalized change in pressure-squared versus logarithmic convolution shut-in time; Cases 1-3 293
7.9.3 Semilog plot of rate-normalized change in pressure-squared versus Horner time; Cases 1-3 295
7.9.4 Dimensionless Odeh-Jones plot in terms of dimensionless pseudopressure; Cases 4-6 297
7.9.5 Semilog plot of rate-normalized dimensionless pseudopressure versus Horner time; Cases 4-6 298
7.9.6 Semilog plot of dimensionless pseudopressure versus Horner time; Cases 4-6 299
7.9.7 Semilog plot of change in pressure-squared versus Horner time; Cases 4-6 300
7.9.8 Rate-normalized change in pressure-squared versus logarithmic convolution shut-in time; Cases 4-6 302
7.9.9 Semilog plot of rate-normalized change in pressure-squared versus Horner time; Cases 4-6 304
7.9.10 Semilog plot of change in pressure-squared versus Horner time; Cases 7-9 305
7.9.11 Rate-normalized change in pressure-squared versus logarithmic convolution shut-in time; Cases 7-9 307
7.9.12 Semilog plot of rate-normalized change in pressure-squared versus Horner time; Cases 7-9 308
7.10.1 Semilog plot of rate-normalized change in pressure versus Horner time; Cases 1-3 311
7.10.2 Semilog plot of rate-normalized change in pressure versus Horner time; Cases 4-6 313

CHAPTER I
INTRODUCTION

1.1 LITERATURE REVIEW

Until recently analysis of multiphase flow well-test pressure data was conducted according to analysis techniques based on simple analogues of single-phase flow theory. Specifically, Perrine[1] and Martin[2] suggested that one can apply the single-phase flow analysis methods to multiphase flow pressure data to estimate the total mobility of the system. Perrine[1] stated that the partial differential pressure equation for multiphase flow can be derived from the single-phase one by replacing the single-phase mobility and compressibility by the total mobility and total compressibility of all phases present in the system. Martin[2] provided a theoretical explanation for Perrine's suggestion by combining the three partial differential equations for the oil, gas and water phases under the assumption that the pressure and saturation gradients are negligible.

Evinger and Muskat[3] studied the effect of multiphase flow on the productivity index of a well for steady state conditions and presented a procedure to compute the pressure, saturation and effective permeability profiles in a reservoir for the case that the producing GOR remains constant. Fetkovich[4] proposed analyzing multiphase flow data based on single-phase gas methods and derived expressions for transient, pseudosteady and steady state multiphase flow.

Motivated by the works of Evinger and Muskat[3] and Fetkovich[4], Raghavan[5] suggested semilog analysis techniques based on pseudopressure. These techniques assume radial flow to a completely-penetrating well producing a solution-gas-drive reservoir and assume that relative permeability curves as a function of oil saturation are known *a priori*.

Works presented recently by Bøe et al.[6] and Aanonsen[7] provided some theoretical basis for the use of pseudofunctions to approximately correlate multiphase flow solutions with the corresponding single-phase liquid solution and also provided computational equations for computing oil saturation as a function of pressure.

Motivated by the theoretical ideas of Refs. 6 and 7, Al-Khalifah et al.[8] and Serra et al.[9] achieved two major results on the analysis of well-testing pressure data obtained under multiphase flow conditions. The results were obtained independently and concurrently by the two sets of researchers. First, Al-Khalifah et al.[8] and Serra et al.[9] showed that one could compute effective permeability as a function of pressure directly from the measured flowing wellbore pressure. Refs. 8 and 9 also showed that one could estimate effective permeabilities as a function of saturation, or if absolute permeability is known[8], or can be estimated[9,10], one can construct approximate relative permeability curves directly from drawdown values of the wellbore pressure. Second, Al-Khalifah et al.[11] and Serra et al.[9,10,12] showed that one can analyze data by using a semilog plot of the wellbore pressure-squared versus time. The analysis can be used to obtain estimates of the initial value of effective oil permeability, the values of effective permeability at the last measured values of flowing wellbore pressure and the mechanical skin factor. The results of Refs. 8 and 9 consider only drawdown analysis. These results were extended to the analysis of buildup data in Refs. 10 and 12. Serra et al.[10,12] showed that a generalized form of superposition applies, provided the same pressure/saturation relationship is used in all pseudopressure functions. The authors extended their drawdown method for estimating oil and gas relative permeabilities to pressure buildup data and showed that the mechanical skin factor can be computed by using the pressure-squared method.

Regarding analysis based on a semilog plot of pressure-squared versus time, it should be noted that this analysis is applicable because the effective oil permeability can be approximated by a piecewise linear function of pressure. This result reflects the effect of saturation gradients caused by the development of a free gas phase as well as the variation in viscosity and FVF with pressure. In oil-water systems, there

exist cases where horizontal saturation gradients are negligible and, in such cases, data can be analyzed based on a semilog plot of pressure versus time; see Chu et al.[13]. Recently, Al-Khalifah et al.[14] presented an overview of the pressure-squared semilog analysis method vis-a-vis semilog analysis based on a plot of pressure versus time. Ref. 14 also showed that given a specified total flow rate, one could use a semilog plot of the change in pressure-squared divided by the oil flow rate to obtain a rough estimate of the initial oil permeability.

1.2 OUTLINE

Chapter II presents an overview of the nonlinear regression analysis methods used to obtain the unknown parameters needed to construct the effective or relative permeability curves based on Standing's[15] correlations.

Chapter III presents a procedure for estimating effective or relative permeability curves directly from well-test pressure data obtained under multiphase flow conditions. The basic procedure developed and discussed in this work combines computed effective permeability versus pressure values with nonlinear regression analysis techniques to determine the parameters involved in Standing's relative permeability correlations. The advantage of the proposed method is that it does not require direct knowledge or computation of oil saturation as a function of pressure. It is shown that, in many cases, the pressure data obtained from drawdown (single- or two-rate) and buildup tests is sufficient to determine accurate estimates of the parameters involved in Standing's relative permeability correlations. In particular, the computational procedures presented can be used to determine estimates of the pore size distribution index, connate water saturation, critical gas saturation and the effective (or relative) permeability of the non-wetting phase at irreducible wetting phase saturation. Once these parameters are determined, effective or relative permeability curves as a function of saturation can be generated without the direct knowledge or computation of sandface oil saturation.

In Chapter IV, we investigate the effects of initial reservoir pressure on the computation of effective permeabilities for reservoirs which are initially above the

bubble-point pressure. It is shown that the initial effective oil permeability may be estimated from drawdown and buildup pressure data. It is also shown that one can obtain accurate estimates of computed effective permeabilities as pointwise functions of wellbore pressure from drawdown data during the time period that the wellbore pressure is less than the initial bubble-point pressure. From the estimates of effective permeabilities obtained, it is shown that one can construct approximate effective or relative permeability curves either by nonlinear regression analysis techniques or by solving a nonlinear system of equations.

Chapter V investigates the effects of heterogeneities on the estimates of effective or relative permeabilities. The heterogeneous system considered in this work is that of a two-zone composite reservoir with different absolute permeability and/or relative permeability curves in the two regions. It is shown that the effective permeabilities estimated from pressure drawdown or buildup data reflect, at early times, the inner zone effective permeability data, and at later times reflect the outer zone effective permeability data for the oil phase. In general, the effective gas permeability of the outer zone cannot be obtained.

In Chapter VI, we investigate the effect of wellbore storage on the analysis of pressure drawdown data obtained at a well producing a solution-gas-drive reservoir. Wellbore storage effects are incorporated by specifying a sandface oil flow rate which increases exponentially from zero to the specified constant value of the oil flow rate at the surface. The equation used for the increasing sandface flow rate has been used previously in the petroleum engineering literature. Using new computational equations derived in this work, it is shown that effective oil permeability as a pointwise function of pressure can be computed directly from the measured values of the flowing wellbore pressure provided the sandface oil flow rate is measured and incorporated into the analysis. If the sandface flow rate is unknown, effective permeability can be computed only after wellbore storage effects become negligible, that is, using values of pressure which are unaffected by wellbore storage effects. In all cases, it is shown that a semilog plot of wellbore pressure-squared versus time represents a viable method for obtaining estimates of the effective oil permeabil-

ity at initial conditions, the effective oil permeability at the final value of flowing wellbore pressure and the mechanical skin factor. For cases where the sandface flow rate is measured, we present a new computational procedure for estimating oil saturation as a function of pressure. By combining the effective permeability versus pressure and oil saturation versus pressure results, one can approximately construct the effective oil permeability versus oil saturation curve. Unfortunately, the computational equation for computing oil saturation as a function of pressure is not highly accurate and is difficult to apply when the skin factor is positive.

Chapter VII examines the effect of wellbore storage on the analysis of pressure buildup data obtained in a solution-gas-drive reservoir. All results assume radial flow to a single well draining a solution-gas-drive reservoir with the initial reservoir pressure equal to the initial bubble-point pressure. Although connate water is present, water is immobile so that during production, only oil and gas flow within the reservoir. Wellbore storage effects are incorporated by specifying a sandface oil flow rate which, during shut-in, decreases exponentially from a stabilized constant value of the surface oil flow rate at the time of shut-in to zero. Based on a superposition equation, we present new computational equations for computing effective oil and gas permeabilities as pointwise functions of pressure from the measured values of the shut-in wellbore pressure. The computational equations require that the sandface oil flow rate is measured and incorporated into the analysis. By combining the computed effective permeability versus pressure relation with the oil saturation versus pressure results computed from the material balance equation, one can approximately construct the effective oil and gas permeability as functions of oil saturation. It is also shown that a semilog plot of shut-in pressure-squared versus Horner time represents a viable method for obtaining estimates of the effective oil permeability at the final value of shut-in wellbore pressure and the mechanical skin factor.

Finally, Chapter VIII summarizes the results and presents the conclusions obtained in this study.

CHAPTER II
NONLINEAR REGRESSION ANALYSIS TECHNIQUES

During the last few years, automated well-test methods have become a popular analysis tool in the petroleum industry. These methods estimate reservoir parameters by using nonlinear regression algorithms to match the observed response (pressure) with a model which is a function of the unknown parameters. Since the effectiveness of automated well-test methods depends on the robustness of the nonlinear regression algorithm used, we have performed extensive testing of nonlinear regression techniques presented previously in the petroleum literature.

2.1 Introduction to Least Squares Methods

The nonlinear parameter estimation problem consists of minimizing the following function[16]:

$$E = \sum_{i=1}^{m} \left[r_i(\vec{\theta}) \right]^2, \tag{2.1.1}$$

where E is the objective function and $r_i(\vec{\theta})$ are the residuals. The most frequently solved optimization problem is the data fitting problem where the residuals and the objective function are given by

$$r_i(\vec{\theta}) = y_i - F(\vec{\theta}, x_i), \tag{2.1.2)}$$

and

$$E = \sum_{i=1}^{m} \left[y_i - F(\vec{\theta}, x_i) \right]^2, \tag{2.1.3}$$

where $\{x_i, y_i\}$ is a set of values of the independent variable (x_i) and dependent variable (y_i) and $\vec{\theta}$ is the set of the n unknown parameters.

2.2 Unconstrained Optimization Methods

In many parameter estimation problems, we are required to find values $\vec{\theta}^*$ of the unknown parameters $\vec{\theta}$ such that the objective function E attains its maximum or minimum.

Using a Taylor series expansion, one may approximate the objective function E by truncating the series after the quadratic term to obtain

$$E^* = E|_{\vec{\theta}^o} + \sum_{k=1}^{n}(\theta_k - \theta_k{}^o)\frac{\partial E}{\partial \theta_k}|_{\vec{\theta}^o} + \frac{1}{2}\sum_{j=1}^{n}\sum_{k=1}^{n}(\theta_j - \theta_j{}^o)(\theta_k - \theta_k{}^o)\frac{\partial^2 E}{\partial \theta_j \partial \theta_k}|_{\vec{\theta}^o}. \quad (2.2.1)$$

The minimum of E^* can be obtained by differentiating Eq. 2.2.1 with respect to $\delta\theta_j = \theta_j - \theta_j{}^o$ and requiring

$$\frac{\partial E^*}{\partial \delta\theta_j} = 0. \quad (2.2.2)$$

This yields

$$\frac{\partial E^*}{\partial \delta\theta_j} = \frac{\partial E}{\partial \theta_j}|_{\vec{\theta}^o} + \sum_{k=1}^{n}\delta\theta_k \frac{\partial^2 E}{\partial \theta_j \partial \theta_k}|_{\vec{\theta}^o} = 0, \quad (2.2.3)$$

or

$$\sum_{k=1}^{n}\delta\theta_k \frac{\partial^2 E}{\partial \theta_j \partial \theta_k}|_{\vec{\theta}^o} = -\frac{\partial E}{\partial \theta_j}|_{\vec{\theta}^o}. \quad (2.2.4)$$

Writing Eq. 2.2.4 in vector form, one obtains

$$H\delta\vec{\theta} = -\vec{g}, \quad (2.2.5)$$

where $H = (h_{jk})$ is the Hessian matrix with elements given by

$$h_{jk} = \frac{\partial^2 E}{\partial \theta_j \partial \theta_k} = -2\sum_{i=1}^{m}\left[-\frac{\partial F}{\partial \theta_k}\frac{\partial F}{\partial \theta_j} + \left(y_i - F(\vec{\theta}^o, x_i)\right)\frac{\partial^2 F}{\partial \theta_k \partial \theta_j}\right]|_{\vec{\theta}^o}. \quad (2.2.6)$$

Throughout, $\vec{g}$ is the gradient vector with components given by

$$g_j = \frac{\partial E}{\partial \theta_j} = -2\sum_{i=1}^{m}\left[r_i(\vec{\theta}^o)\frac{\partial F(\vec{\theta}^o, x_i)}{\partial \theta_j}\right]|_{\vec{\theta}^o}. \quad (2.2.7)$$

Note that H is always a real symmetric matrix.

2.2.1 Iterative Scheme.

Every iterative scheme for a nonlinear unconstrained optimization problem requires an input initial guess $\vec{\theta}^1$ and proceeds to generate a sequence of estimates of the solutions $\vec{\theta}^2$, $\vec{\theta}^3$, ..., $\vec{\theta}^i$ which we hope will converge to $\vec{\theta}^*$ where the objective function $E(\vec{\theta}^*)$ attains its minimum value. The computation of the $\vec{\theta}^{i+1}$ is called the i^{th} iteration, $\vec{\theta}^i$ is the i^{th} iterate and the vector

$$\vec{\sigma}^i \equiv \vec{\theta}^{i+1} - \vec{\theta}^i, \tag{2.2.8}$$

is called the i^{th} step.

If for the i^{th} step the following inequality holds:

$$E(\vec{\theta}^{i+1}) < E(\vec{\theta}^i), \tag{2.2.9}$$

then the step and the iterative scheme are considered to be acceptable. Note, however, that this step may not guarantee convergence.

The general scheme of an acceptable method is as follows (see Ref. 16):

(i) Set $i = 1$ and provide an initial guess $\vec{\theta}^1$.

(ii) Determine a vector $\delta\vec{\theta}^i$ (step direction) in the direction of the i^{th} step.

(iii) Compute the step size ρ^i from the following equation:

$$\vec{\sigma}^i = \rho^i \delta\vec{\theta}^i, \tag{2.2.10}$$

so that the i^{th} step is acceptable. To do this, estimate the i^{th} iterate of the vector solution from

$$\vec{\theta}^{i+1} = \vec{\theta}^i + \rho^i \delta\vec{\theta}^i, \tag{2.2.11}$$

and require Eq. 2.2.9 to hold.

(iv) Use the termination criterion to check whether the solution vector $\vec{\theta}^{i+1}$ is the final solution. If the termination criterion is met, then denote the final solution by

$$\vec{\theta}^* = \vec{\theta}^{i+1}, \tag{2.2.12}$$

and stop the procedure. Otherwise, set i to $i + 1$ and proceed to the next iteration by returning to step (ii).

2.2.2 Acceptability and Convergence.

As described above, the solution vector at the i^{th} iteration computed from Eq. 2.2.11 is a function of the step size and it is given by

$$\vec{\theta}^{i+1}(\rho^i) = \vec{\theta}^i + \rho^i \delta\vec{\theta}^i, \tag{2.2.13}$$

and the objective function is

$$\Psi(\rho^i) \equiv E(\vec{\theta}^{i+1}(\rho^i)) = E(\vec{\theta}^i + \rho^i \delta\vec{\theta}^i). \tag{2.2.14}$$

Differentiating Eq. 2.2.14 with respect to ρ^i, one obtains

$$\frac{d\Psi}{d\rho^i} = \left(\frac{\partial\Psi}{\partial\vec{\theta}^{i+1}}\right)^T \left(\frac{\partial\vec{\theta}^{i+1}}{\partial\rho^i}\right) = \left(\frac{\partial\Psi}{\partial\vec{\theta}^{i+1}}\right)^T \delta\vec{\theta}^i, \tag{2.2.15}$$

where the superscript T denotes the transpose of a vector or a matrix.

Using Eq. 2.2.7, and evaluating Eq. 2.2.15 at $\rho^i = 0$, one obtains the directional derivative, Ψ', of E with respect to the vector $\delta\vec{\theta}^i$ at $\vec{\theta}^i$ to be

$$\Psi' = (\vec{g}^i)^T \delta\vec{\theta}^i. \tag{2.2.16}$$

Note that if $\Psi' < 0$ then Eq. 2.2.14 suggests that $E(\vec{\theta}^i)$ decreases when moving away from the $\vec{\theta}^i$ in the direction of $\delta\vec{\theta}^i$. In that case, Eq. 2.2.9 holds for some $\rho^i > 0$ and for this value of ρ^i, the proposed step is acceptable and the direction $\delta\vec{\theta}^i$ is an acceptable direction.

Bard[16] states and proves the following theorem;

Theorem : A direction $\delta\vec{\theta}^i$ is acceptable if and only if there exists a positive definite matrix Ω such that

$$\delta\vec{\theta}^i = -\Omega\vec{g}^i. \tag{2.2.17}$$

Note that this guarantees that $\Psi' < 0$, i.e., the objective function decreases in the direction of the step, but it is not sufficient to guarantee convergence of the algorithm.

Using Eq. 2.2.17, Eq. 2.2.11 can be rewritten as follows:

$$\vec{\theta}^{i+1} = \vec{\theta}^i - \rho^i \Omega\vec{g}^i, \tag{2.2.18}$$

which is the basic equation for obtaining the solution at the i^{th} iterate in a gradient method. The choice of the positive definite matrix, Ω, and the step size ρ^i differs for the various methods.

Suppose the proposed steps for all iterations are acceptable. Then the iteration scheme provides a sequence of acceptable points $E(\vec{\theta}^1), E(\vec{\theta}^2), E(\vec{\theta}^3), \ldots$ which are monotonically decreasing. If the sequence of the computed values of E has a lower limit, E_m, then this sequence will converge to E_m. If the sequence $\{\vec{\theta}^i\}$ also converges and if E is continuous then $E_m = E(\vec{\theta}^m)$. If at the i^{th} step $\vec{g}^i = \vec{0}$, then Eq. 2.2.18 implies that $\vec{\theta}^j = \vec{\theta}^i$ for $i \leq j$ which suggests that the point $\vec{\theta}^i$ is a stationary point. Thus, the gradient methods would not converge to the true minimum unless the objective function has no other stationary point. For practical purposes, convergence to a stationary point would be achieved if the matrix Ω is sufficiently positive definite and the step size is chosen so that the value of the objective function is decreased by a sufficiently large amount.

2.2.3 Steepest Descent Method.

In this method $\Omega = I$ and Eq. 2.2.17 yields

$$\delta\vec{\theta}^i = -\vec{g}^i. \tag{2.2.19}$$

The steepest descent is the simplest gradient method but it is not usually recommended because it is frequently very inefficient requiring a large number of steps to converge. For this reason we will not discuss this method further.

2.2.4 Newton's Method.

Suppose the Hessian matrix H is nonsingular. Then solving Eq. 2.2.5 for the i^{th} iterate, one obtains

$$\vec{\theta}^{i+1} = \vec{\theta}^i - H^{-1}\vec{g}^i, \tag{2.2.20}$$

where H^{-1} denotes the inverse of the Hessian matrix.

Eq. 2.2.20 defines the i^{th} iteration of Newton's method and, compared with the general gradient method formula given by Eq. 2.2.18, implies that in the Newton method $\rho = 1$ and $\Omega = H^{-1}$. Thus, Newton's method for nonlinear parameter

estimation problems consists of solving Eq. 2.2.5 for $\delta\vec{\theta} = -H^{-1}\vec{g}^{i}$ and updating the solution vector using

$$\vec{\theta}^{i+1} = \vec{\theta}^{i} + \delta\vec{\theta}, \tag{2.2.21}$$

until convergence is reached.

If the objective function is a quadratic function, then Newton's method converges in a single iteration and the solution vector $\vec{\theta}^{i+1}$ is a stationary point of E. Moreover, the solution $\vec{\theta}^{i+1}$ is a minimum if the inverse of the Hessian matrix, H^{-1}, is positive definite. In this case, the single step is also acceptable. If E is not quadratic, each step of Newton's method is acceptable as long as H^{-1} is positive definite matrix, but the method does not converge in a single iteration.

Newton's method, however, requires the evaluation of the second derivatives and has the following disadvantages:

(i) it may not converge if the Hessian matrix is not a positive definite matrix;

(ii) it might converge to a saddle point of the objective function instead of a minimum point; and,

(iii) it will always converge if the Hessian matrix is positive definite and the initial guess is close to a solution that minimizes the objective function E, but it will often diverge if the initial guess is not good.

2.2.5 Directional Discrimination Method.

To overcome the problem of indefiniteness in Newton's method, Greenstadt[17] proposed a method which factorizes the Hessian matrix using spectral decomposition and subsequently replaces all negative diagonal elements by their absolute values and all small diagonal elements by infinity, thus guaranteeing positive definiteness of the Hessian matrix H.

2.2.6 The Gauss Method.

An approximation of Newton's method can be derived by neglecting the second derivatives on the right hand side of Eq. 2.2.6 to obtain the Gauss method for nonlinear parameter estimation problems. Thus, in this case the elements of the

Hessian matrix are given by

$$h_{jk} = \frac{\partial^2 E}{\partial\theta_j \partial\theta_k} = 2\sum_{i=1}^{n} \frac{\partial F}{\partial\theta_k}\frac{\partial F}{\partial\theta_j}, \tag{2.2.22}$$

and the gradient vector $\vec{g}$ is still given by Eq. 2.2.7. The justification for the derivation of the Gauss method by neglecting the second derivatives in Eq. 2.2.6 can be seen as follows:

Using Eq. 2.1.2, Eq. 2.2.6 yields

$$h_{jk} = \frac{\partial^2 E}{\partial\theta_j \partial\theta_k} = -2\sum_{i=1}^{n}\left[-\frac{\partial F}{\partial\theta_k}\frac{\partial F}{\partial\theta_j} + r_i(\vec{\theta})\frac{\partial^2 F}{\partial\theta_k \partial\theta_j}\right]|_{\vec{\theta}^o}. \tag{2.2.23}$$

Since the residual $r_i(\vec{\theta}^o)$ is small, particularly close to the minimum of the objective function, Eq. 2.2.22 can be considered as a good approximation of Eq. 2.2.6.

The Gauss method is the most widely used method[16] for solving the nonlinear least squares problem since it does not require the evaluation of the second derivatives of the function F. Furthermore, setting the second derivatives in Eq. 2.2.6 equal to zero tends to make H positive definite. This guarantees that the method generates an acceptable direction at each step. Generally, Gauss' method with a good algorithm for choosing the step length should usually converge to a minimum, if one exists, but the method may be sensitive to computational instability if the system is ill-conditioned.

2.2.7 Marquardt's Method.

Marquardt[18] and Levenberg[19] presented a modification which can be applied to either the Newton or Gauss method to avoid problems associated with an ill-conditioned Hessian matrix, H. Their modification consists of adding a positive constant to the diagonal elements of the Hessian matrix which increases the magnitude of the eigenvalues of H. Therefore, using the basic equation for obtaining the solution at the i^{th} iterate, the matrix Ω becomes

$$\Omega \equiv (H + \xi B^2)^{-1}, \tag{2.2.24}$$

where B is a diagonal matrix with

$$B_{ii} = \begin{cases} |h_{ii}|, & \text{if } h_{ii} \neq 0; \\ 1, & \text{if } h_{ii} = 0; \end{cases}, \tag{2.2.25}$$

and ξ is a sufficiently large positive constant. Setting $B = I$ is also common.

The Newton-Marquardt method can be used to avoid negative eigenvalues of the original Hessian matrix and to ensure positive definiteness of the final Hessian matrix. The Gauss-Marquardt method can be used to ensure that all of the eigenvalues are sufficiently positive and thus, prevents a singular matrix.

We now give an outline of Marquardt's algorithm which is taken from Ref. 16.

Marquardt's Algorithm

(i) Set $i = 1$ and $\xi = 0.01$

(ii) At the beginning of each iteration compute the solution vector, $\vec{\theta}^{i+1}$, by using Eq. 2.2.17, and update the solution vector by using Eq. 2.2.21.

(iii) If the i^{th} iterate produces an acceptable step, accept the solution vector, $\vec{\theta}^{i+1}$, and replace the parameter ξ by

$$\xi = max(0.1\xi, \epsilon), \tag{2.2.26}$$

where $\epsilon \approx 10^{-7}$ is a small positive constant, and go back to step (ii).

(iv) Find a sufficiently small step size ρ^i such that Eq. 2.2.9 holds and compute the solution vector from Eq. 2.2.11. Finally, replace ξ by 10ξ and proceed to the next iteration.

2.2.8 Cholesky's Decomposition.

Let A be a real symmetric l x l matrix, D a diagonal l x l matrix and E a nonsingular l x l matrix which satisfy the following relationship:

$$A = EDE^T, \tag{2.2.27}$$

or in component form:

$$A_{ij} = \sum_{k=1}^{l} d_k E_{ik} E_{jk}, \tag{2.2.28}$$

where

$$d_k \equiv D_{kk}. \tag{2.2.29}$$

Then EDE^T is referred to as a spectral decomposition of A.

Assuming that A is a positive definite matrix, choosing $D = I$, where I is the l x l identity matrix, and specifying E to be a lower triagular matrix L, one can rewrite Eq. 2.2.27 as

$$A = LL^T, \tag{2.2.30}$$

or in component form:

$$A_{ij} = \sum_{k=1}^{l} L_{ik}L_{jk}, \tag{2.2.31}$$

or

$$A_{ij} = \sum_{k=1}^{j} L_{ik}L_{jk}; \qquad (j < i), \tag{2.2.32}$$

and

$$A_{ii} = \sum_{k=1}^{i} L_{ik}^2; \qquad (j = i), \tag{2.2.33}$$

Cholesky's method consists of solving Eqs. 2.2.32 and 2.2.33 recursively for the elements L_{ij} by the following algorithm.

Set $L_{11} = \sqrt{A_{11}}$, $L_{i1} = A_{i1}/L_{11}$ for $i = 1, 2, ..., l$. Then for each j, $j = 2, 3, ..., l$ apply the following two equations:

$$L_{jj} = \left(A_{jj} - \sum_{k=1}^{j-1} L_{jk}^2 \right)^{1/2}; \qquad (j = i), \tag{2.2.34}$$

and

$$L_{ij} = \left(A_{ij} - \sum_{k=1}^{j-1} L_{ik}L_{jk} \right) / L_{jj}; \qquad (i = j+1, j+2, ..., l). \tag{2.2.35}$$

Using the Cholesky decomposition of a matrix A, one can now solve a set of linear equations, such as

$$A\vec{x} = \vec{b}. \tag{2.2.36}$$

Using Eq. 2.2.30, the above matrix problem may be rewritten as

$$LL^T\vec{x} = \vec{b}, \tag{2.2.37}$$

or

$$L\vec{y} = \vec{b}, \tag{2.2.38}$$

where

$$\vec{y} = L^T\vec{x}. \tag{2.2.39}$$

Solving Eq. 2.2.38, one obtains the values of $\vec{y}$ to be

$$y_1 = \frac{b_1}{L_{11}}, \tag{2.2.40.1}$$

$$y_i = \left(b_i - \sum_{k=1}^{i-1} L_{ik}y_k\right)/L_{ii}; \qquad (i = 2,3,...,l). \tag{2.2.40.2}$$

Then one can solve Eq. 2.2.39 to obtain the unknown vector $\vec{x}$ as follows:

$$x_l = \frac{y_l}{L_{ll}}, \tag{2.2.41.1}$$

$$x_i = \left(y_i - \sum_{k=i+1}^{l} L_{ki}x_k\right)/L_{ii}; \qquad (i = l-1, l-2, ..., 1). \tag{2.2.41.2}$$

Cholesky's decomposition is the fastest direct method of solving Eq. 2.2.36 if the matrix A is symmetric positive definite.

2.2.9 Modified Cholesky's Decomposition.

Gill et al.[20] proposed a modification of Cholesky's factorization for the cases that the Hessian matrix, H, is symmetric indefinite matrix (i.e., H has both positive and negative eigenvalues). Their method is based on the assumptions that $H = LDL^T = LD^{1/2}D^{1/2}L^T$ where all elements of D are strictly positive and all elements of $LD^{1/2}$ satisfy a uniform bound, i.e., their absolute value is smaller than a positive number, β. The selection of β is based on the following criteria: (i) β is large enough such that positive definite matrices are not modified; (ii) the norm

of R (see Eq. 2.2.42) is minimized; and (iii) β is larger than the machine's precision. Their method consists of approximating the Hessian matrix, H, by a positive definite matrix, $\tilde{H}$, given by

$$\tilde{H} = LDL^T = H + R, \tag{2.2.42}$$

where R is a non-negative diagonal matrix.

An algorithm for the modified Cholesky factorization was proposed by Gill et al.[20] and is given here.

Modified Cholesky's Decomposition Algorithm

(i) Compute the quantities

$$\gamma = max\{|h_{ii}|, i = 1, 2, ..., n\}, \tag{2.2.43}$$

$$\xi = max\{|h_{ij}|, i < j, i, j = 1, 2, ..., n\}, \tag{2.2.44}$$

$$\nu = max\{1, \sqrt{n^2 - 1}\}, \tag{2.2.45}$$

and set

$$\beta^2 = max\{\gamma, \frac{\xi}{\nu}, \epsilon_M\}, \tag{2.2.46}$$

where ϵ_M denotes the machine's precision.

(ii) Initialize the column index $j = 1$ and define

$$c_{ii} = h_{ii}; \qquad i = 1, 2, ..., n. \tag{2.2.47}$$

(iii) Find the smallest index q such that

$$|c_{qq}| = max\{|c_{ii}|, i = j, ..., n\}, \tag{2.2.48}$$

and interchange the information corresponding to rows and columns q and j of H, i.e., row q is equal to column j and column j is equal to row q of the Hessian matrix, H.

(iv) Set

$$l_{js} = \frac{c_{js}}{d_s}; \qquad s = 1, 2, ..., j - 1, \tag{2.2.49}$$

compute

$$c_{ij} = h_{ij} - \sum_{s=1}^{j-1} l_{js} c_{is}; \qquad i = j+1, ..., n, \tag{2.2.50}$$

and set

$$\theta_j = max\{|c_{ij}|\}; \qquad j+1 \leq i \leq n. \tag{2.2.51}$$

In Eq. 2.2.50, the h_{ij}'s are the elements of the Hessian matrix.

(v) Define

$$d_j = max\{\delta, |c_{jj}|, \frac{\theta_j^2}{\beta^2}\}. \tag{2.2.52}$$

and compute the j^{th} diagonal elements of R from

$$r_j = d_j - c_{jj}, \tag{2.2.53}$$

where δ is a small positive quantity.

If $j = n$ exit.

(vi) Set

$$c_{ii} = c_{ii} - \frac{c_{ij}^2}{d_j}; \qquad i = j+1, ..., n. \tag{2.2.54}$$

Set $j = j + 1$ and go to (iii).

Note that l_{ij} ($i = 1, 2, ..., l$ and $j = 1, 2, ..., j$) denotes the ij^{th} element of the lower triangular matrix, L, d_j ($j = 1, 2, ..., l$) and $r_j (j = 1, 2, ..., l)$ denote the j^{th} elements of the positive diagonal matrix D and the non-negative diagonal matrix R, respectively.

2.2.10 Interpolation-Extrapolation.

Suppose the i^{th} iteration produces an acceptable direction. In this case, there always exists a number $\tilde{\eta}$ such that if $0 \leq \rho \leq \tilde{\eta}$, then $E(\vec{\theta}^{i+1}) < E(\vec{\theta}^{i})$. This is called interpolation method. On the other hand, if the iteration produced an acceptable direction for which the objective function decreased, we can try to find a different step size value which decreases the objective function even more. This is called extrapolation method.

Bard[16] provides an algorithm which can be used for the step size determination.

2.2.11 Termination Criteria.

An iterative computational procedure requires a criterion for stopping the search for the minimum objective function value. From a practical viewpoint, a stopping criterion recognizes convergence when the computed parameters do not change significantly, i.e.,

$$|\theta_j^{i+1} - \theta_j^i| \leq e_j; \qquad (j = 1,2,...,l), \tag{2.2.55}$$

where e_j $(j = 1,2,...,l)$ is a set of small numbers. These numbers may be input constant numbers or may be changed during the iterative procedure. In our nonlinear regression analysis method, we use Marquardt's[18] suggestion for updating the convergence criterion, i.e., we use the following equation:

$$e_j = 10^{-4}(\theta_j^i + 10^{-3}), \tag{2.2.56}$$

where the term 10^{-3} is added to avoid possible problems in the case that the solution vector $\vec{\theta}^i$ is close to $\vec{0}$.

The computational procedure can be also stopped if the number of iterations exceeds a maximum allowed number, since there is no point in allowing the procedure to continue if the method converges very slowly. One can derive another stopping criterion by substituting Eq. 2.2.11 into Eq. 2.2.55 to obtain

$$\rho^i|\delta\theta_j{}^i| \leq e_j; \qquad (j = 1,2,...,l), \tag{2.2.57}$$

which can be rearranged to yield the minimum admissible step size in the i^{th} iterate

$$\rho_{\min} \leq \min_j \frac{e_j}{|\delta\theta_j{}^i|}; \qquad (j = 1,2,...,l), \tag{2.2.58}$$

i.e., if the computational procedure yields a step size value such that $\rho < \rho_{\min}$, termination occurs.

2.3 Constrained Optimization Methods

The general objective of a nonlinear parameter algorithm is to find the values of the unknown parameters that minimize the objective function. If the unknown

parameters are allowed to assume any value, the estimation method is called unconstrained optimization. If, however, the unknown parameters are restricted to a certain region (subset of R^n), the estimation method is called constrained optimization. These restrictions may be due to prior information regarding the values that the unknown parameters can assume. For problems considered in this work the constraint functions are linear and of the following form:

$$c_l(\theta_l) = a_l\theta_l + b_l \geq 0; \qquad l = 1, 2, ..., nc, \tag{2.3.1}$$

where a_l and b_l are constants and n_c is the number of constraints.

Any of the inequality constraints of Eq. 2.3.1 can be changed to a constraint of the form

$$c_l(\theta_l) = 0. \tag{2.3.2}$$

We may also impose more than one constraint on each component of $\vec{\theta}$, i.e., $c_l(\theta_l) \geq 0$ and $d_l(\theta_l) \geq 0$.

2.3.1 Penalty Functions.

The above constraints can be implemented in the nonlinear parameter estimation algorithm by modifying the objective function in such a way that it remains almost unchanged in the interior of the permissible region, but increases rapidly as $\vec{\theta}$ approaches any boundary imposed by the inequality and/or equality constraints. This is accomplished by introducing a penalty function for each of the inequality constraints which is almost zero in the interior of the feasible region, but increases rapidly as the constraint function approaches zero from above. Thus, for the inequality of Eq. 2.3.1 we introduce the following penalty function:

$$\varsigma_l \equiv \frac{\alpha_l}{c_l(\vec{\theta})}, \tag{2.3.3}$$

where α_l are small positive constants.

Using this penalty function, one can modify the objective function to obtain

$$E^+(\vec{\theta}) = E(\vec{\theta}) + \sum_l \frac{\alpha_l}{c_l(\vec{\theta})}. \tag{2.3.4}$$

Fiacco and MacCormick[21] have shown that if $\vec{\theta}^+$ and $\vec{\theta}^*$ are the points, located in the permissible region, at which the objective functions $E^+(\vec{\theta}^+)$ and $E(\vec{\theta}^*)$ attain their minima, then

$$\lim_{\alpha_l \to 0} \vec{\theta}^+ = \vec{\theta}^*. \tag{2.3.5}$$

Expanding the objective function using Taylor's series and truncating this series after the quadratic term as in section 2.2, one can rewrite Eq. 2.3.4 as follows:

$$h_{jk}^+ = h_{jk} + \frac{\partial^2}{\partial\theta_j \partial\theta_k}\left(\sum_l \frac{\alpha_l}{c_l(\vec{\theta})}\right), \tag{2.3.6}$$

where h_{jk}^+ denotes the components of the modified Hessian matrix and h_{jk} is given by Eq. 2.2.6. Eq. 2.3.6 can be rewritten as

$$h_{jk}^+ = h_{jk} + \sum_l \frac{\partial^2 \varsigma_l(\vec{\theta})}{\partial\theta_j \partial\theta_k}. \tag{2.3.7}$$

Since the constraints c_l are paired independent for lower and upper bounds on the unknown parameters, $\vec{\theta}$, then

$$\frac{\partial^2 \varsigma_l(\vec{\theta})}{\partial\theta_j \partial\theta_k} = 0; \qquad j \neq k, \tag{2.3.8}$$

and thus, Eq. 2.3.7 yields

$$h_{jk}^+ = \begin{cases} h_{jk}, & \text{for } j \neq k; \\ h_{jk} + \sum_{l=1}^{nc} \frac{\partial^2}{\partial\theta_j^2}\left(\frac{\alpha_l}{c_l(\vec{\theta})}\right), & \text{for } j = k; \end{cases}, \tag{2.3.9}$$

where nc denotes the number of constraints.

Since

$$\frac{\partial^2}{\partial\theta_j^2}\left(\frac{\alpha_l}{c_l(\vec{\theta})}\right) = 2\frac{\alpha_l}{c_l^3(\vec{\theta})}\left(\frac{\partial c_l(\vec{\theta})}{\partial\theta_j}\right)^2, \tag{2.3.10}$$

Eq. 2.3.9 provides

$$h_{jk}^+ = \begin{cases} h_{jk}, & \text{for } j \neq k; \\ h_{jk} + 2\sum_{l=1}^{nc} \frac{\alpha_l}{c_l^3(\vec{\theta})}\left(\frac{\partial c_l(\vec{\theta})}{\partial\theta_j}\right)^2, & \text{for } j = k; \end{cases}. \tag{2.3.11}$$

Eq. 2.3.11 defines the Newton method components of the modified Hessian matrix H^+ obtained by including the penalty functions in the objective function.

For the Gauss method, the components h_{jk}^{+} can be derived from Eq. 2.3.11 by neglecting the second derivatives in the components, h_{jk}, of the original Hessian matrix.

For the constrained optimization methods, the gradient vector should also be modified by including the penalty functions to obtain

$$\vec{g}_j{}^{+} = \vec{g}_j + \sum_l \frac{\partial \zeta_l(\vec{\theta})}{\partial \theta_j}, \tag{2.3.12}$$

or

$$\vec{g}_j{}^{+} = -2\sum_{i=1}^{n} r_i(\vec{\theta})\frac{\partial F(\vec{\theta}, x_i)}{\partial \theta_j} - \sum_l \frac{\alpha_l}{c_l^2(\vec{\theta})}\frac{\partial c_l(\vec{\theta})}{\partial \theta_j}. \tag{2.3.13}$$

In order to obtain the values of the unknown parameters, one needs to solve the following modified problem:

$$H^{+}\delta\vec{\theta} = -\vec{g}^{+}, \tag{2.3.14}$$

which can be solved by any of the methods discussed earlier in this chapter.

2.4 Estimation of Confidence Intervals

After the computation of the best estimate $\vec{\theta}^{*}$, it is useful to provide estimates of the intervals that the components of the true solution of the problem lie in. If l, $0 \leq l \leq 1$, denotes the level of significance, then the true solution has a probability of $1-l$ to lie within the computed interval $[\omega_1, \omega_2]$, which is referred to as a $100(1-l)\%$ confidence interval.

In this work, we provide an approximate method of computing the confidence intervals for a nonlinear parameter problem (see Ref. 22). According to this method, if m is the number of data points and n the number of the unknown parameters, the mean square error is defined as

$$\eta = \frac{E(\vec{\theta})}{m-n}, \tag{2.4.1}$$

and the confidence interval for the j^{th} component of $\vec{\theta}$ will be

$$\left\{\theta_j^{*} - t_{l/2;m-n}[\Upsilon^{*}(\theta_j^{*})]^{1/2}; \theta_j^{*} + t_{l/2;m-n}[\Upsilon^{*}(\theta_j^{*})]^{1/2}\right\},$$

where $t_{l/2;m-n}$ denotes the value obtained from the t-distribution function for $m-n$ degrees of freedom, such that

$$P\left\{t \geq t_{l/2;m-n}\right\} = \frac{l}{2}, \tag{2.4.2}$$

$$\sqrt{\Upsilon^*(\theta_j^*)} = \sqrt{\eta e_{jj}}, \tag{2.4.3}$$

defines the standard error of the estimate of θ_j, and e_{jj} denotes the diagonal elements of the inverse of the Hessian matrix H^{-1}.

It is worth mentioning that the confidence interval is a function of the number of data points. More specifically, the greater the number of data points used, the narrower the confidence interval and the higher the confidence in the final answer.

2.5 Review of Nonlinear Regression Analysis Methods

In the petroleum literature, Rosa and Horne[23] have used the Gauss-Marquardt method in an automated well-test analysis procedure. Barua and Horne[24] found that the Gauss-Marquardt method often had difficulties in converging whenever the number of the estimated parameters was large or the effect of some of the parameters on the data was ill-defined.

To overcome these problems Barua et al.[25] modified the Newton-Greenstadt method to improve the robustness of the parameter estimation algorithm. Ref. 24 concluded that their method is unaffected by an increase of small eigenvalues which causes significant problems in the Gauss-Marquardt method.

Nanba and Horne[26] presented a new regression algorithm for automated well-test analysis which was based on Cholesky, and modified Cholesky factorization of symmetric positive definite matrices. As discussed earlier, the modified Cholesky factorization was proposed in 1983 by Gill et al.[20] and consists of approximating an indefinite Hessian matrix, H, by a positive definite Hessian matrix, $\tilde{H}$. A modification of this method was used by Nanba and Horne[27] to construct the oil and water relative permeability curves of water injection system. The authors used their regression algorithm in conjunction with the power-law model representation of oil

and water relative permeability and the multicomposite model solution of a water injection system to obtain the unknown parameters from an injection or a falloff test. Their method assumes that the reservoir profile for water saturation can be determined from the Buckley-Leverett frontal advance theory.

CHAPTER III
DETERMINATION OF EFFECTIVE OR RELATIVE PERMEABILITY CURVES FROM WELL TESTS

A procedure for estimating effective or relative permeability curves directly from well-test pressure data obtained under multiphase flow conditions is presented in this chapter. The procedure developed and discussed here combines computed effective permeability versus pressure values with nonlinear regression analysis techniques to determine the parameters involved in Standing's relative permeability correlations. The advantage of our method is that it does not require direct knowledge or computation of oil saturation as a function of pressure. The proposed technique is applied to several simulated drawdown pressure data, and some practical considerations involved in the proposed procedure are discussed.

For the nonlinear parameter estimation, we used the Gauss and Newton methods in forming the Hessian matrix H along with Cholesky and modified Cholesky factorization, respectively, in solving Eq. 2.2.5 and Bard's[16] line search method in updating the solution vector, $\vec{\theta}$.

3.1 INTRODUCTION

For solution-gas-drive reservoirs, Refs. 8-11 and 28 have provided methods for approximating the oil and gas effective permeabilities as a function of pressure directly from pressure drawdown and buildup data. Refs. 29 and 30 have presented modifications of the methods of Refs. 8-11 and 28 for cases where wellbore storage effects exist (see also Chapters 6 and 7). Here, we develop a new computational procedure that enables one to obtain the oil and gas effective permeability as a function of oil saturation by using Standing's[15] correlation in conjunction with the methods of Refs. 8-11 and 28-30. The results assume the two-phase radial flow of oil and gas to a well in an infinite-acting, solution-gas-drive reservoir.

The results of Refs. 8-11 and 28-30 show that, once wellbore storage effects become negligible, we can obtain good estimates of kk_{ro} and kk_{rg} from pressure drawdown data by applying the following equations:

$$(kk_{ro})_{p_{wf}} = \frac{-162.6q_o(\mu_o B_o)_{p_{wf}}}{hdp_{wf}/d\log t}, \tag{3.1.1}$$

and

$$(kk_{rg})_{p_{wf}} = \frac{-162.6q_g(t)(\mu_g B_g)_{p_{wf}}}{hdp_{wf}/d\log t}. \tag{3.1.2}$$

Eq. 3.1.1 assumes that q_o is constant and equal to the sandface flow rate. In Eq. 3.1.2, $q_g(t)$ denotes the sandface flow rate of free gas in scf/D, i.e.,

$$q_g(t) = q_{gt} - R_s q_o, \tag{3.1.3}$$

where q_{gt} is the total gas flow rate (free gas plus solution gas) at standard conditions. As shown in Refs. 9 and 28, during the infinite acting period, Eqs. 3.1.1 and 3.1.2 typically yield reasonably good estimates of effective permeabilities except at very early times.

The ratio of the effective permeabilities obtained from Eqs. 3.1.1 and 3.1.2 is exact even when Eqs. 3.1.1 and 3.1.2 yield inaccurate estimates of individual phase effective permeabilities. This can be seen as follows:

Dividing Eq. 3.1.2 by Eq. 3.1.1 and using Eq. 3.1.3, one obtains

$$\frac{kk_{rg}}{kk_{ro}} = \frac{(q_{gt} - R_s q_o)\mu_g B_g}{q_o \mu_o B_o}$$

$$= \frac{q_{gt}}{q_o}\frac{\mu_g B_g}{\mu_o B_o} - \frac{R_s \mu_g B_g}{\mu_o B_o} = R\frac{\mu_g B_g}{\mu_o B_o} - \frac{R_s \mu_g B_g}{\mu_o B_o}, \tag{3.1.4}$$

which is equivalent to

$$R = R_s + \frac{kk_{rg}/\mu_g B_g}{kk_{ro}/\mu_o B_o}. \tag{3.1.5}$$

Since Eq. 3.1.5 represents an exact physical relation, Eq. 3.1.4 is exact. It follows that if we compute kk_{ro} from Eq. 3.1.1 and kk_{rg} from Eq. 3.1.2 to obtain kk_{rg}/kk_{ro} as a function of pressure, we will obtain exact values provided we use the correct values of R_s, μ_o, μ_g, B_o and B_g in the computation. Of course, if we are

only interested in $(kk_{rg})/(kk_{ro})$, the value of this effective permeability ratio can be determined directly from Eq. 3.1.5 provided the producing GOR, phase viscosities and FVFs are known.

Eqs. 3.1.1 and 3.1.2 can be used to obtain estimates of kk_{ro} and kk_{rg} as a function of wellbore pressure. Combining these values with the sandface oil saturation versus wellbore pressure relation, one can determine the effective oil and gas permeabilities as a function of oil saturation; see Refs. 8-11 and 28-30. Refs. 8 through 10 and 29 have presented various forms of a differential equation, which can be solved to obtain S_o as a function of p_{wf}. However, when effective permeabilities as a function of pressure obtained from Eqs. 3.1.1 and 3.1.2 are used when solving the dS_o/dp_{wf} equation, we do not always obtain highly accurate estimates of S_o as a function of wellbore pressure. Therefore, combination of the two sets of computed data (kk_{rm}, $m = o, g$, versus p_{wf} and S_o as a function of p_{wf}) may give only very rough estimates of effective oil and gas permeabilities as functions of oil saturation.

Al-Khalifah et al.[11] have suggested that one can fit effective permeability data obtained from Eq. 3.1.1 to generate approximate effective oil permeability curves based on Standing's correlations. However, in Ref. 11 it was assumed that points on the effective oil permeability versus S_o curve could be obtained directly from pressure data obtained during a multirate test. This assumes that one can compute accurately S_o as a function of pressure directly from pressure and rate data. The results of Refs. 9, 10, 28 and 29 indicate that this assumption is not always valid.

The new procedure presented here applies nonlinear regression analysis to data obtained from Eqs. 3.1.1 and 3.1.2 to determine the parameters in Standing's relative permeability correlations. It is shown that our computational procedure eliminates the need to determine S_o values directly. In fact, once effective permeability curves have been estimated by our procedure, one can determine S_o for a given value of kk_{ro}.

3.2 THEORETICAL BACKGROUND

Standing[15] presented equations for two- and three-phase drainage relative permeability relationships. Here, we use his three-phase drainage relative permeability equations and assume throughout that the rock is strongly water wet with oil representing the intermediate wetting phase and gas representing the nonwetting phase. In the three-phase drainage relative permeability equations presented below, S_{iw} denotes irreducible water saturation. In this work, we assume that $S_{iw} = S_{wc}$ where S_{wc} denotes connate water saturation. Throughout, S_{gc} denotes the critical gas saturation.

The Standing[15] relative permeability correlations used in this work are as follows:

Mobile Water Phase

$$k_{rw} = (S_w^*)^{\frac{2+3\lambda}{\lambda}}, \tag{3.2.1}$$

Oil Phase

$$k_{ro} = k_r^o (S_o^*)^2 [(S_L^*)^{\frac{2+\lambda}{\lambda}} - (S_w^*)^{\frac{2+\lambda}{\lambda}}], \tag{3.2.2}$$

Gas Phase

$$k_{rg} = k_r^o \left(\frac{S_g - S_{gc}}{1 - S_{gc} - S_{iw}} \right)^2 \left[1 - (1 - (S_g^*))^{\frac{2+\lambda}{\lambda}} \right], \tag{3.2.3}$$

where

$$S_w^* = \frac{S_w - S_{iw}}{1 - S_{iw}}, \tag{3.2.4}$$

$$S_o^* = \frac{S_o}{1 - S_{iw}}, \tag{3.2.5}$$

$$S_g^* = \frac{S_g}{1 - S_{iw}}, \tag{3.2.6}$$

and

$$S_L^* = \frac{S_o + S_w - S_{iw}}{1 - S_{iw}} = S_o^* + S_w^*. \tag{3.2.7}$$

Note that:

$$S_o^* + S_g^* + S_w^* = 1. \tag{3.2.8}$$

In the preceding equations, λ is referred to as the pore size distribution index. According to Standing[15], the higher the value of λ is, the more uniform the pore size distribution; $\lambda = 0.5$ corresponds to a very wide range of pore sizes, $\lambda = 2$ corresponds to a wide range of pore sizes and $\lambda = 4$ corresponds to a medium range of pore sizes. Corey's[31] equations assume $\lambda = 2$, whereas Standing[15] suggests that a pore size index in the range of 0.6 to 1 is more common.

Fig. 3.2.1 shows the effect of λ on the oil and gas relative permeability curves computed from Eqs. 3.2.2 and 3.2.3. In generating these results, we used $S_{iw} = S_{wc} = 0.3$, $k_r^o = 0.7$ and $S_{gc} = 0.0$. Standing[15] states that k_r^o denotes the relative permeability of the nonwetting phase at irreducible wetting phase saturation and is incorporated into the oil and gas equations to adjust for the irreducible water saturation. Standing[15] suggested the following correlation for computing k_r^o:

$$k_r^o = 1.31 - 2.62S_{iw} + 1.1S_{iw}^2, \tag{3.2.9}$$

for $0.2 \leq S_{iw} \leq 0.5$. Ref. 15 also indicates that Eq. 3.2.9 should never be used for $S_{iw} > 0.5$ but can be used for $S_{iw} < 0.2$. However, k_r^o must satisfy $k_r^o \leq 1$. Thus, if Eq. 3.2.9 predicts $k_r^o > 1$, one should always use $k_r^o = 1$ in Eqs. 3.2.2 and 3.2.3. Note that Eq. 3.2.9 predicts $k_r^o > 1$ if $S_{iw} < 0.12487$. For a strongly water wet rock, however, one expects to have $S_{iw} \geq 0.2$. The relative permeability curves of Eqs. 3.2.2 and 3.2.3 represent effective permeabilities normalized by the true (single-phase) absolute permeability. In his computations, Standing[15] uses Eq. 3.2.9 to predict k_r^o for use in both Eqs. 3.2.2 and 3.2.3. By evaluating Eq. 3.2.2 at $S_g = 0$ and $S_w = S_{iw}$, we obtain

$$k_{ro}(S_o = 1 - S_{iw}, S_g = 0) = k_r^o. \tag{3.2.10}$$

Similarly, evaluation of Eq. 3.2.3 at $S_g = 1 - S_{iw}$ and $S_o = 0$ gives

$$k_{rg}(S_g = 1 - S_{iw}, S_o = 0) = k_r^o. \tag{3.2.11}$$

Thus Eq. 3.2.9 indicates that, for a strongly water wet rock, $k_{ro}(S_o = 1 - S_{iw}, S_g = 0) = k_{rg}(S_g = 1 - S_{iw}, S_o = 0)$.

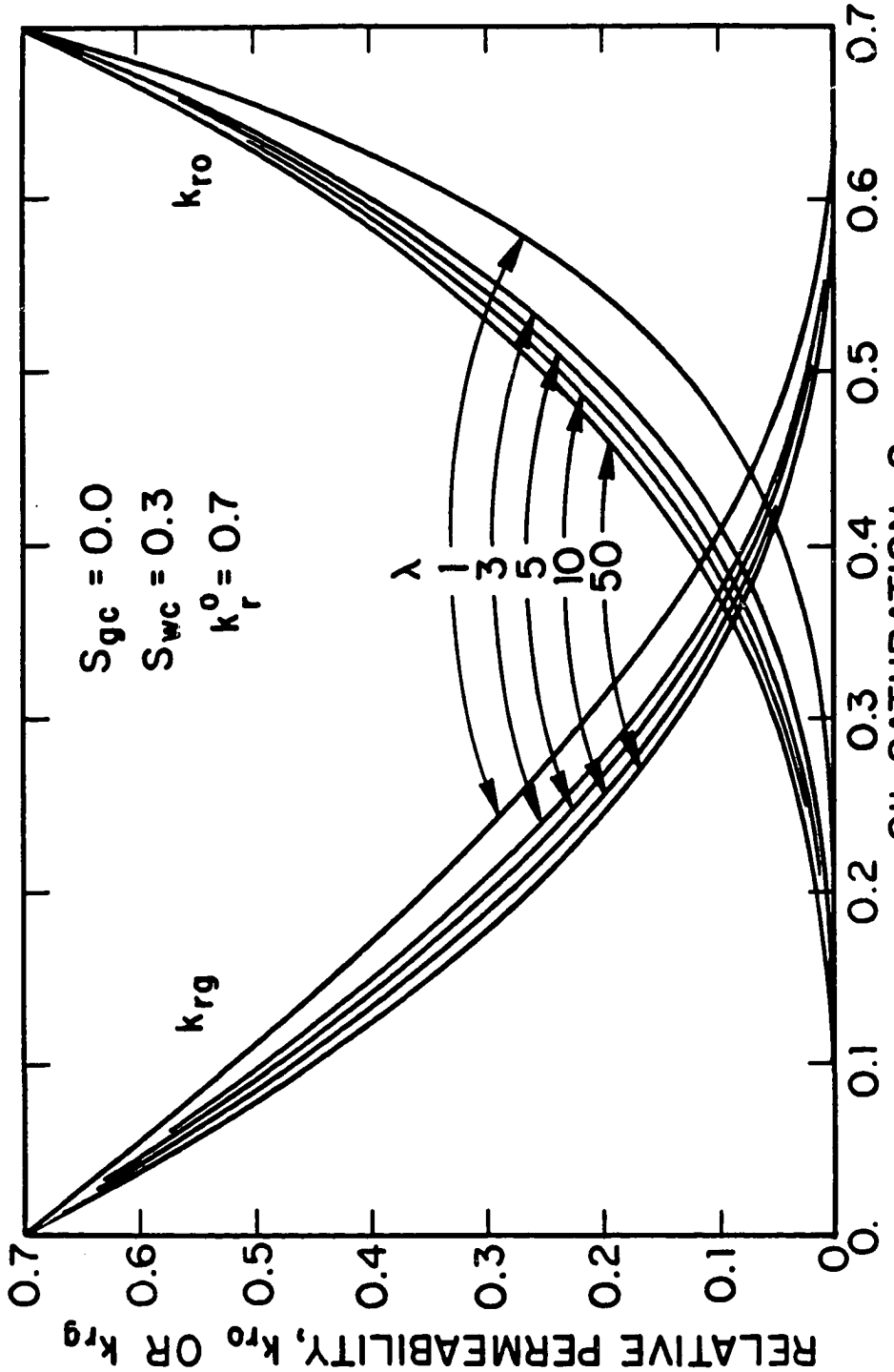

Fig. 3.2.1 - Effect of λ on the oil and gas relative permeability curves.

Throughout, it is assumed that water is immobile so that $S_w = S_{iw} = S_{wc}$. Under this assumption, Eqs. 3.2.4 and 3.2.7, respectively, imply that

$$S_w^* = 0, \tag{3.2.12}$$

and

$$S_L^* = S_o^*, \tag{3.2.13}$$

and Eq. 3.2.2 reduces to

$$k_{ro} = k_r^o(S_o^*)^2(S_o^*)^{\frac{2+\lambda}{\lambda}} = k_r^o(S_o^*)^{\frac{2+3\lambda}{\lambda}}. \tag{3.2.14}$$

Solving for S_o^* gives

$$S_o^* = \left(\frac{k_{ro}}{k_r^o}\right)^{\frac{\lambda}{2+3\lambda}} = \left(\frac{kk_{ro}}{kk_r^o}\right)^{\frac{\lambda}{2+3\lambda}}. \tag{3.2.15}$$

Eq. 3.2.15 holds regardless of whether $S_{gc} = 0$ or $S_{gc} > 0$. Also note that Eq. 3.2.14 implies that $k_{ro} = 0$ if and only if $S_o^* = 0$. Thus, Standing's correlation assumes that residual oil saturation is zero.

3.2.1 Theory 1. Zero Critical Gas Saturation.

Multiplying Eqs. 3.2.1 through 3.2.3, respectively, by k and using $S_{gc} = 0$ and $S_{wc} = S_{iw}$ so that Eqs. 3.2.12 and 3.2.13 hold, we obtain

$$kk_{rw} = 0, \tag{3.2.16}$$

$$kk_{ro} = kk_r^o(S_o^*)^{\frac{2+3\lambda}{\lambda}}, \tag{3.2.17}$$

$$kk_{rg} = kk_r^o(1 - S_o^*)^2(1 - (S_o^*)^{\frac{2+\lambda}{\lambda}}). \tag{3.2.18}$$

Solving Eq. 3.2.18 for S_o^*, one obtains

$$S_o^* = \left(\frac{k_{ro}}{k_r^o}\right)^{\frac{\lambda}{2+3\lambda}} = \left(\frac{kk_{ro}}{kk_r^o}\right)^{\frac{\lambda}{2+3\lambda}}. \tag{3.2.19}$$

Using Eq. 3.2.19, we can rearrange Eq. 3.2.18 to obtain

$$\frac{kk_{rg}}{kk_r^o} = \left(\frac{kk_{ro}}{kk_r^o}\right)\left(\frac{k_{rg}}{k_{ro}}\right) = \left[1 - \left(\frac{kk_{ro}}{kk_r^o}\right)^{\omega_1}\right]^2\left[1 - \left(\frac{kk_{ro}}{kk_r^o}\right)^{\omega_2}\right], \tag{3.2.20}$$

where

$$\omega_1 = \frac{\lambda}{2+3\lambda}, \tag{3.2.21}$$

and

$$\omega_2 = \frac{\lambda}{2+3\lambda}\frac{2+\lambda}{\lambda} = \omega_1\frac{2+\lambda}{\lambda} = \frac{2+\lambda}{2+3\lambda}. \tag{3.2.22}$$

Using Eq. 3.1.1, values of kk_{ro} can be computed accurately at the end of a drawdown test[8,28] and, as discussed previously, the values of k_{rg}/k_{ro} obtained from Eqs. 3.1.1 and 3.1.2 are exact at any time during the test. As discussed later, using values of kk_{ro} and $kk_{rg}/(kk_{ro})$ obtained from Eqs. 3.1.1 and 3.1.2 at two distinct values of p_{wf} in Eq. 3.2.20 yields a system of two equations which can be solved numerically to estimate the values of λ and $kk_r^o = kk_{ro}(S_o = 1 - S_{iw})$. More generally, one could use several computed values of kk_{ro} and $kk_{rg}/(kk_{ro})$ in Eq. 3.2.20 to obtain a system of nonlinear equations which can be solved by a nonlinear regression analysis technique to obtain estimates of λ, kk_r^o, S_{gc} and S_{iw}.

By computing the values of λ, kk_r^o, S_{gc} and S_{iw}, we determine the kk_{ro} and kk_{rg}versus S_o relationships of Eqs. 3.2.17 and 3.2.18. If k is known, then the values of k_{ro} and k_{rg} in terms of S_o also can be estimated. Alternatively, one can normalize the kk_{ro} and kk_{rg} curves by $kk_r^o = k_o(S_o = 1 - S_{iw})$ to obtain relative permeability curves.

3.2.2 Theory 2. Non-Zero Critical Gas Saturation.

In this case, $S_g - S_{gc} = 1 - S_o - S_{wc} - S_{gc} = 1 - S_o^*(1 - S_{wc}) - S_{wc} - S_{gc}$ and thus,

$$\frac{S_g - S_{gc}}{1 - S_{gc} - S_{iw}} = \frac{1}{1 - S_{gc} - S_{wc}}\Big[(1 - S_o^*)(1 - S_{wc}) - S_{gc}\Big]. \tag{3.2.23}$$

Substituting Eq. 3.2.23 into Eq. 3.2.3, multiplying the resulting equation by k and using $S_w^* = 0$ and $S_g^* = 1 - S_o^*$, one obtains

$$kk_{rg} = kk_r^o\left(\frac{1}{1 - S_{gc} - S_{wc}}\right)^2\Big[(1 - S_o^*)(1 - S_{wc}) - S_{gc}\Big]^2\Big[(1 - (S_o^*)^{\frac{2+\lambda}{\lambda}}\Big]. \tag{3.2.24}$$

The effect of S_{gc} on the oil and gas relative permeabilities versus oil saturation relationships is shown in Fig. 3.2.2 for $\lambda = 4$, $S_{wc} = 0.3$ and $k_r^o = 0.7$. Comparing

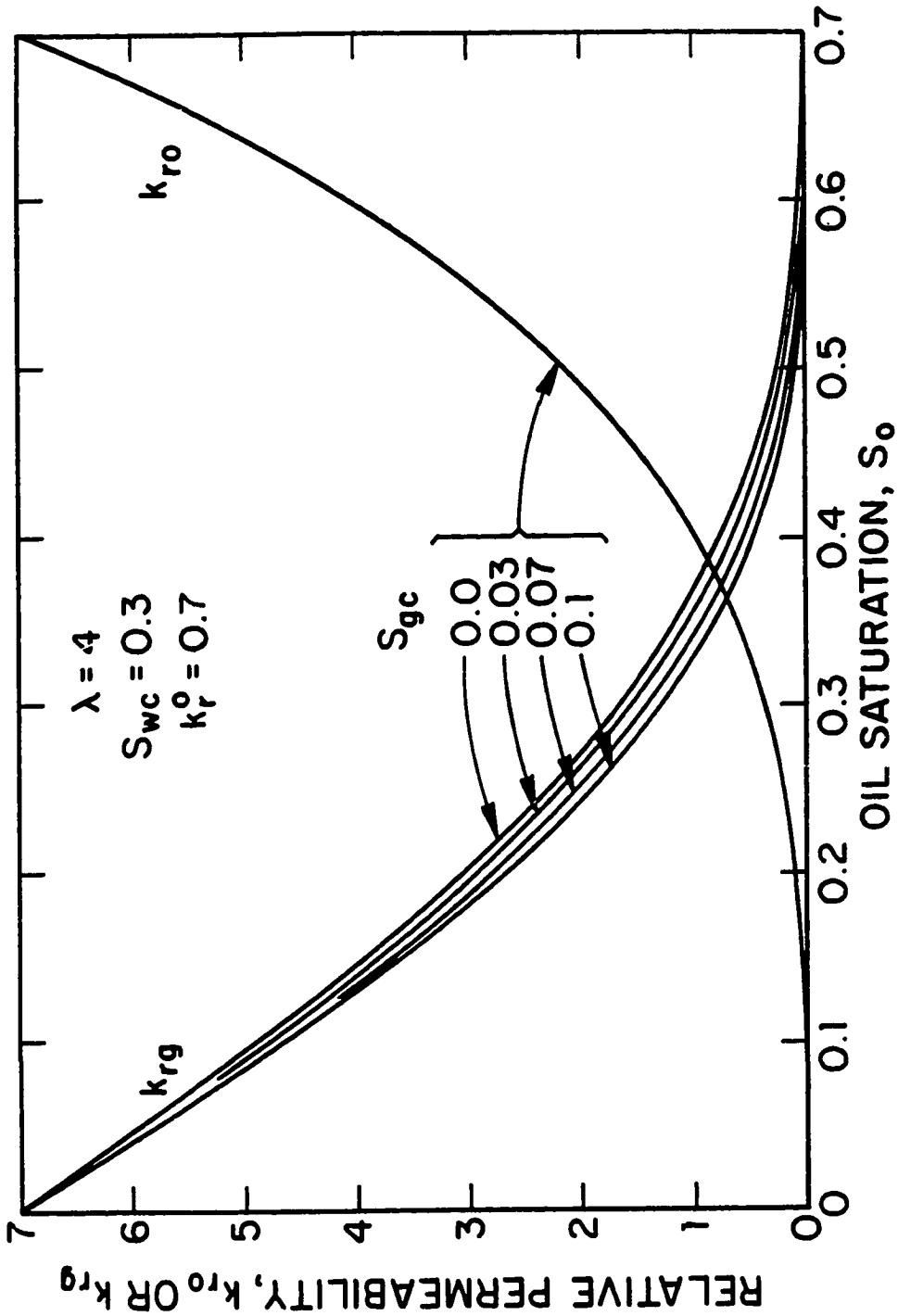

Fig. 3.2.2 - Effect of S_{gc} on the oil and gas relative permeability curves.

the results shown in Figs. 3.2.1 and 3.2.2, one can see that the critical gas saturation does not affect the k_{ro} and k_{rg} versus S_o results as much as λ does. Note k_{ro} does not depend on S_g and thus, is not affected by the value of S_{gc}; see Eqs. 3.2.2 and 3.2.3.

Use of the expression for S_o^* given by Eq. 3.2.15 in Eq. 3.2.24 with rearrangement gives

$$\frac{kk_{rg}}{kk_r^o} = \left(\frac{kk_{ro}}{kk_r^o}\right)\left(\frac{k_{rg}}{k_{ro}}\right) =$$

$$\left(\frac{1}{1-S_{gc}-S_{wc}}\right)^2\left[\left(1-\left(\frac{kk_{ro}}{kk_r^o}\right)^{\omega_1}\right)(1-S_{wc})-S_{gc}\right]^2\left[1-\left(\frac{kk_{ro}}{kk_r^o}\right)^{\omega_2}\right], \quad (3.2.25)$$

where the parameters ω_1 and ω_2 are given by Eqs. 3.2.21 and 3.2.22, respectively.

As discussed later, use of the values of kk_{ro} and $kk_{rg}/(kk_{ro})$ obtained from Eqs. 3.1.1 and 3.1.2 during the last part of a drawdown test, in Eq. 3.2.25 yields a system of nonlinear equations which can be solved numerically using nonlinear parameter estimation techniques to obtain estimates of λ, kk_r^o, S_{gc} and S_{iw}. In this chapter, Eqs. 3.1.1 and 3.1.2 were applied to simulated well-test pressure data generated from either the simulator of Ref. 28 or the simulator of Ref. 33.

3.3 Mathematical Model

As in Refs. 8-11 and 28-30, we consider radial flow to a completely penetrating well at the center of a cylindrical solution-gas-drive reservoir. The top, bottom and outer reservoir boundaries are assumed to be sealed, i.e., no flow boundaries. All the results presented, however, are for the infinite-acting period and thus, are not affected by the outer reservoir boundary. Gravity and capillary effects are neglected. Although Refs. 29 and 30 considered wellbore storage effects, all results presented in this Chapter assume wellbore storage effects are negligible. For all cases considered, water is immobile and water saturation remains fixed at S_{wc} = 0.3. All results presented pertain to the infinite-acting period, that is, the closed outer boundary has no influence on the results obtained.

Finally, absolute permeability is assumed to be constant in the reservoir, but the model allows a different value of absolute permeability in the skin zone. The

skin zone is modeled as a concentric region with absolute permeability k_s which is different from the absolute permeability of the reservoir. Whenever the skin factor is nonzero, the permeability of the skin zone is computed using Hawkins'[32] formula:

$$s = \left(\frac{k}{k_s} - 1\right) \ln\left(\frac{r_s}{r_w}\right), \tag{3.3.1}$$

where r_s denotes the radius of the skin zone.

3.4 SIMULATOR DATA

Tables A-1 and A-2, respectively, give "Set 1" PVT data and relative permeability data and Tables A-3 and A-4, respectively, give "Set 2" PVT data and relative permeability data. Throughout, the wellbore radius, external reservoir radius, reservoir thickness, porosity, and absolute permeability are specified as $r_w = 0.328$ ft, $r_e = 6600$ ft, $h = 15.547$ ft, $\phi = 0.3$ and $k = 10$ md, respectively, but the values of these parameters have no influence on the validity of the procedures and conclusions presented in this chapter. All results presented pertain to the infinite-acting period, that is, the closed outer boundary has no influence on the results obtained.

In this Chapter, results are presented for the following three cases:

Case 1

$q_o = 150$ STB/D ; s = 0 ; $S_{gc} = 0.0$; No wellbore storage ; Data Set 1;

Case 2

$q_o = 150$ STB/D ; s = 0 ; $S_{gc} = 0.07$; No wellbore storage ; Data Set 2;

Case 3

$q_{o1} = 50$ STB/D for $t_1 = 0.5$ days ; $q_{o2} = 100$ STB/D for $t_2 = 1.0$ days ; s = 5 ; $S_{gc} = 0.0$; No wellbore storage ; Set 2 PVT data and Set 1 relative permeability data.

For Case 1, the critical gas saturation is $S_{gc} = 0.0$, the initial reservoir pressure and bubble-point pressure values are equal and given by $p_i = p_{bi} = 3460$ psi. The initial values of total compressibility, oil viscosity and oil FVF are specified as $c_{ti} = 0.23564 \times 10^{-4}$ psi^{-1}, $\mu_{oi} = 0.43059$ cp and $B_{oi} = 1.5882$ RB/STB, respectively. The PVT and relative permeability data, Set 2, for Case 2 are shown

in Tables A-3 and A-4 and are the data used in Ref. 30. For this set of data, the critical gas saturation is $S_{gc} = 0.07$, the initial reservoir pressure and bubble-point pressure values are equal and given by $p_i = p_{bi} = 4000$ psi. The initial values of total compressibility, oil viscosity and oil FVF, respectively, are specified as $c_{ti} = 0.27604 \times 10^{-4}$ psi $^{-1}$, $\mu_{oi} = 0.41313$ cp and $B_{oi} = 1.48301$ RB/STB. The PVT data for Case 3 are given in Table A-3 (Set 2) and relative permeability data for Case 3 are given in Table A-2 (Set 1). For Case 3, the critical gas saturation is $S_{gc} = 0.0$, the initial reservoir pressure and bubble-point pressure values are equal and given by $p_i = p_{bi} = 4201.6$ psi. The initial values of total compressibility, oil viscosity and oil FVF are specified as $c_{ti} = 0.25616 \times 10^{-4}$ psi $^{-1}$, $\mu_{oi} = 0.391$ cp and $B_{oi} = 1.516$ RB/STB, respectively. For all three sets of data, the values of connate water saturation and residual oil saturation are held fixed with $S_{wc} = S_{iw} = 0.3$ and $S_{or} = 0.0$, respectively.

The reservoir simulator used to generate the numerical results for Cases 1 and 2 is a version of the variable bubble-point, black-oil simulator which has been described in Ref. 28. For the last case, Case 3, the results were obtained from the commercial black-oil simulator ECLIPSE[33]. For all cases considered, the external reservoir radius is $r_e = 6600$ ft which is sufficiently large so that the pressure and saturation changes in the near wellbore region are not affected by outer boundary effects.

Case 1 considers a problem where both skin effects and critical gas saturation are negligible. Case 2 allows us to examine the effects of a non-zero critical gas saturation on the proposed computational procedures neglecting the presence of a skin zone. Finally, Case 3 considers the effects of a skin zone with absolute permeability less than the reservoir one, but assumes the critical gas saturation is zero.

3.5 Numerical Procedure

We have shown earlier in this chapter that Standing's[15] relative permeability

correlations yield the following general equation:

$$\left(\frac{kk_{ro}}{kk_r^o}\right)\left(\frac{k_{rg}}{k_{ro}}\right) =$$

$$\left(\frac{1}{1-S_{gc}-S_{wc}}\right)^2\left[\left(1-\left(\frac{kk_{ro}}{kk_r^o}\right)^{\omega_1}\right)(1-S_{wc})-S_{gc}\right]^2\left[1-\left(\frac{kk_{ro}}{kk_r^o}\right)^{\omega_2}\right], \quad (3.5.1)$$

where k_r^o denotes the relative permeability of the nonwetting phase at irreducible wetting phase saturation. For the cases we consider the parameters ω_1 and ω_2 are given by Eqs. 3.2.21 and 3.2.22, respectively.

For the notation described earlier the residual function of the nonlinear parameter estimation is given by

$$r_j(\vec{\theta}) = -(kk_{ro})_j\left(\frac{k_{rg}}{k_{ro}}\right)_j + kk_r^o\left(\frac{1}{1-S_{gc}-S_{wc}}\right)^2$$

$$\left[\left(1-\left(\frac{(kk_{ro})_j}{kk_r^o}\right)^{\omega_1}\right)(1-S_{wc})-S_{gc}\right]^2\left[1-\left(\frac{(kk_{ro})_j}{kk_r^o}\right)^{\omega_2}\right], \quad (3.5.2)$$

for $j = 1, 2, ..., m$. Here $(kk_{ro})_j$ and $(k_{rg}/k_{ro})_j = (kk_{rg}/kk_{ro})_j$, respectively, denote values of effective permeabilities computed from Eqs. 3.1.1 and 3.1.2 using pressure drawdown data.

The objective function to be minimized is

$$E = \sum_{j=1}^{m}\left[r_j(\vec{\theta})\right]^2, \quad (3.5.3)$$

where

$$\vec{\theta} = (\theta_1, \theta_2, \theta_3, \theta_4) = (\lambda, kk_r^o, S_{gc}, S_{wc}). \quad (3.5.4)$$

Since the values of the unknown parameters are bounded, we used the penalty function method (see Refs. 16 and 20) to restrict the region in which the solution vector, $\vec{\theta}$, should be located. The following restrictions were used in the present problem:

$$0.5 \leq \lambda \leq 10, \quad (3.5.5)$$

$$k_b < kk_r^o, \quad (3.5.6)$$

$$0 \leq S_{gc} \leq 1, \tag{3.5.7}$$

and

$$0 \leq S_{wc} \leq 1, \tag{3.5.8}$$

where k_b represents the last value of kk_{ro} computed from a buildup test by the method of Ref. 10. The restrictions given by Eqs. 3.5.7 and 3.5.8 are obvious and the restriction of Eq. 3.5.5 has been justified earlier in this Chapter; however, the restriction of Eq. 3.5.6 needs further discussion. The reason for using this restriction is that the last value of kk_{ro} obtained from buildup data by the method of Ref. 10 always lies below the initial value of kk_{ro} which is equal to kk_r^o.

The numerical estimation of the unknown parameters λ, kk_r^o, S_{gc} and S_{wc} is based on an iterative scheme which has been discussed in Chapter 2, i.e., solve Eq. 2.2.5 for $\delta\vec{\theta}$ and update the solution vector using Eq. 2.2.11 until convergence is reached. At the first step, one needs to provide initial guesses of those parameters. For λ, we have restricted our initial guess to any value such as $0.5 \leq \lambda \leq 7$. For an infinite-acting system, an excellent approximation for the initial estimate of $kk_r^o = kk_{ro}(S_o = 1 - S_{wc}, S_g = 0)$ is the last value of kk_{ro} computed from pressure buildup data; see Ref. 10. The reason for choosing the last computed kk_{ro} value from a buildup test as an initial guess is that this value is always the closest one to the value of the effective oil permeability at $S_o = 1 - S_{wc}$. One can instead extrapolate computed values of kk_{ro} to $p = p_{bi}$ where p_{bi} denotes the initial bubble-point pressure to obtain an initial estimate of kk_r^o. This can be done by fitting a line through the final few values of kk_{ro} computed from buildup data and extrapolating this line to p_{bi} to estimate kk_r^o. Alternately, we can fit a line through both the final computed drawdown kk_{ro} value obtained from Eq. 3.1.1 and the final buildup value of kk_{ro} computed from the computational procedure given in Refs. 10, 28, and 30 and extrapolate this line to $p = p_{bi}$. In general, this will tend to yield a slight underestimate of kk_r^o. If buildup data are not available, then k_r^o can be estimated from Standing's correlations (see Eq. 3.2.9). If no such data is available one can set $k_r^o = 1$. Note, however, that if one sets $k_r^o = 1$ or determines k_r^o from Eq.

3.2.9, then one needs the value of absolute permeability, k, in order to obtain the initial estimate of kk_r^o. Results obtained in this research study have indicated that one could use any value of kk_{ro} computed from a drawdown test as both the lower bound in Eq. 3.5.6 and the initial estimate of kk_r^o without significantly affecting the values of the estimated parameters. We always restrict the initial values for the two unknown parameters, S_{gc} and S_{wc}, to the interval $0.0 < S_{gc} \leq 0.4$ and $0.0 < S_{wc} \leq 0.4$, respectively. The reason we did not use $S_{gc} = 0.0$ or $S_{wc} = 0.0$ as the initial guesses in the nonlinear regression analysis methods is because we perform divisions by S_{gc} and S_{wc} in the formulation of the penalty functions.

At each iteration, the values of the unknown parameters λ, kk_r^o, S_{gc} and S_{wc} are updated using a line search proposed by Ref. 16. This method helps to speed up the convergence of the nonlinear parameter estimation algorithm and sometimes prevent it from diverging. The procedure is repeated until the maximum absolute value of the difference between two successive iterations is less or equal to a specified tolerance.

From the values of λ, kk_r^o, S_{gc} and S_{wc} obtained, the effective oil permeability can be computed from Eq. 3.2.17, whereas the effective gas permeability is obtained from

$$kk_{rg} = kk_r^o \left(\frac{S_g - S_{gc}}{1 - S_{gc} - S_{wc}} \right)^2 \left[1 - (1 - (S_g^*))^{\frac{2+\lambda}{\lambda}} \right]. \tag{3.5.9}$$

For gas saturation values in the interval $0 < S_g < S_{gc}$, i.e., for $S_g - S_{gc} < 0$, the term $(S_g - S_{gc})/(1 - S_{gc} - S_{wc})$ of Eq. 3.5.9 is negative. In this case, one should set the entire term equal to zero which gives $kk_{rg} = 0$ (see Eqs. 3.5.9 and 3.2.24).

3.6 Results

In this section, we present results which demonstrate the applicability of the proposed computational method for determining effective permeability curves.

3.6.1 Case 1: Zero Critical Gas Saturation, Zero Skin.

Fig. 3.6.1 presents a plot of the kk_{ro} values versus the wellbore pressure for Case 1. The relative permeability curves for Case 1 (Table A-2) were generated by

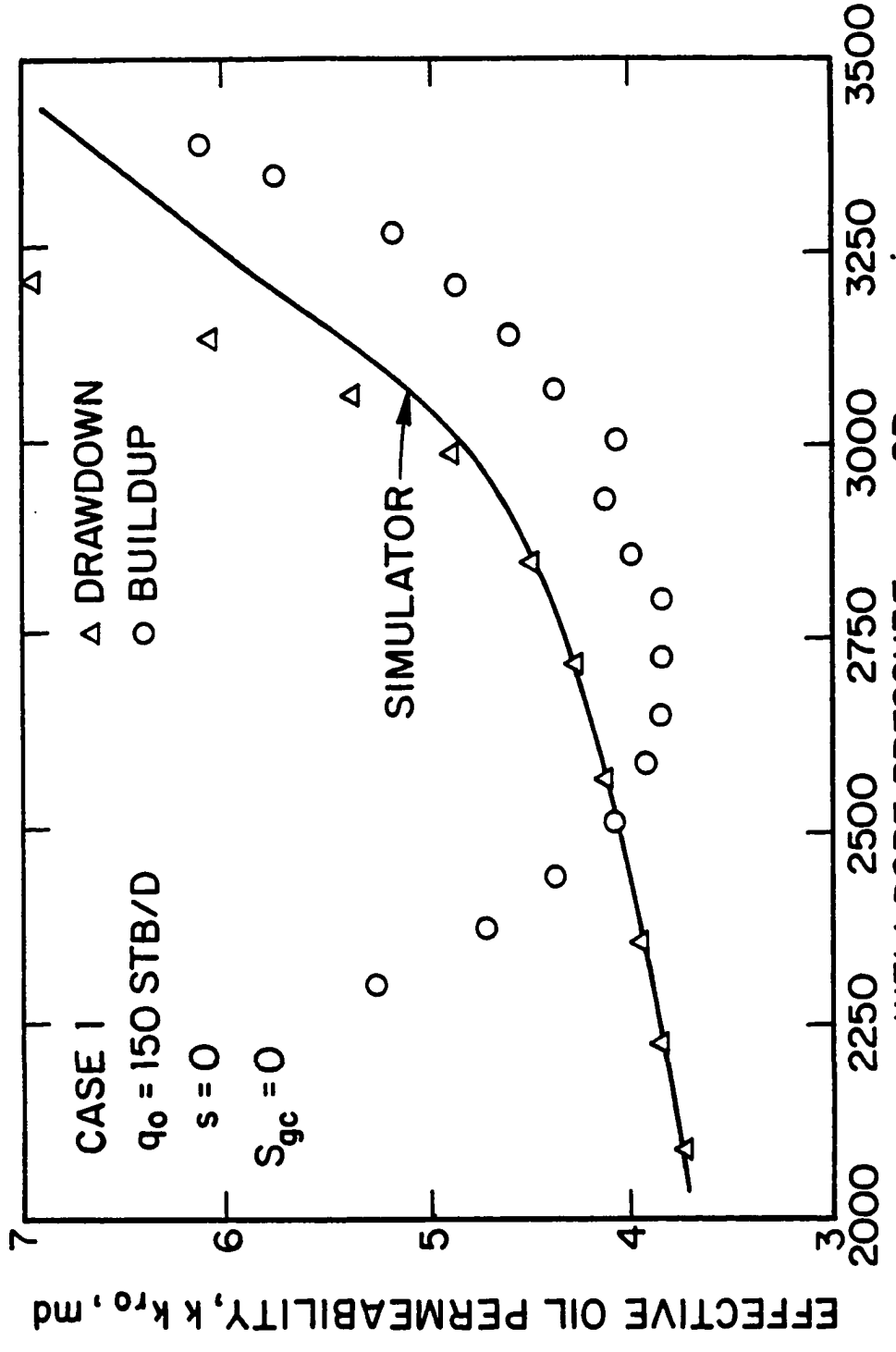

Fig. 3.6.1 - Effective oil permeability as a function of wellbore pressure; Case 1.

Standing's correlations (Eqs. 3.2.17 and 3.2.18) with $\lambda = 2$, $kk_r^o = 0.7$, $S_{gc} = 0.0$, and $S_{iw} = S_{wc} = 0.3$. Recall that for this case the skin factor, critical gas saturation and wellbore storage coefficient are all zero and the oil flow rate is constant and equal to $q_o = 150$ STB/D. Finally, the duration of both the drawdown and buildup tests is $t_p = 5$ days ($t_D \approx 6.76 \times 10^5$). The simulated and computed kk_{ro} and kk_{rg} versus the wellbore pressure p_{wf} are shown in Tables F-1 and F-2. In Table F-1, columns 1 and 2 show the time and wellbore pressure data, columns 3 and 4 show the sandface oil saturation and the effective oil permeability data obtained from the simulator and column 5 shows the kk_{ro} values computed from Eq. 3.1.1. In Table F-2, column 1 shows the wellbore pressure data, column 2 shows the effective gas permeability data obtained from the simulator and column 3 shows the kk_{rg} values computed from Eq. 3.1.2. Finally, Table F-3 shows the values of the parameters needed to compute kk_{ro} and kk_{rg} from Eqs. 3.1.1 and 3.1.2. Tables F-4 through F-6 show the simulated and computed data for the buildup test and their description is similar to the one for Tables F-1 through F-3, respectively. The solid line in Fig. 3.6.1 corresponds to simulator values, the triangular data points represent the kk_{ro} values computed from a drawdown pressure versus time data by using Eq. 3.1.1 and the circular data points represent the kk_{ro} values computed from buildup pressure versus shut-in time data by using the computational procedure of Ref. 10, i.e., by application of the following equation:

$$kk_{ro} = \frac{162.6 q_o (\mu_o B_o)_{p_{ws}}}{h dp_{ws}/d\log\left(\frac{t\Delta t}{t+\Delta t}\right)} = -\frac{162.6 q_o (\mu_o B_o)_{p_{ws}}}{h dp_{ws}/d\log R_{H1}}, \qquad (3.6.1)$$

where R_{H1} denotes the primary Horner time ratio, i.e., $R_{H1} = (t + \Delta t)/\Delta t$. The results of this figure show that the computed kk_{ro} values at the end of the drawdown test are in good agreement with the simulator kk_{ro} values. Using all the computed drawdown values of kk_{ro} and k_{rg}/k_{ro} corresponding to $kk_{ro} \leq 4.592$ in our nonlinear regression analysis program, we were able to obtain estimates of the unknown parameters λ, kk_r^o, S_{gc} and S_{wc} by using the Gauss method. More specifically, we used penalty function in forming the Hessian matrix, H, Cholesky factorization in solving Eq. 2.2.5, and Bard's[16] line search method in updating the solution vector

in Eq. 2.2.11.

Assuming that the values of S_{gc} and S_{wc} are known *a priori* and using $kk_r^o = k_b = 6.2958$ md and $\lambda = 1$ as initial guesses, the values of the estimated parameters obtained are $kk_r^o = 6.999$ md and $\lambda = 2.007$. These values are essentially identical to the correct values of $kk_r^o = 7.0$ md and $\lambda = 2.0$. Table F-7 shows the variation of the estimated parameters with respect to the iteration number. The approximate confidence intervals of the estimated parameters with 95% confidence[22] are: 6.95 md $\leq kk_r^o \leq$ 7.057 md and $1.949 \leq \lambda \leq 2.065$.

Assuming that only the value of S_{wc} is known and using $kk_r^o = k_b = 6.2958$ md, $\lambda = 1$ and $S_{gc} = 1.0 \times 10^{-10}$ as initial guesses, the values of the estimated parameters obtained are $kk_r^o = 6.999$ md, $\lambda = 2.007$ and $S_{gc} = 1.91 \times 10^{-10}$. These values are in excellent agreement with the correct values of $kk_r^o = 7.0$ md, $\lambda = 2.0$ and $S_{gc} = 0.0$. Table F-8 shows the values of the unknown parameters for each iteration. The approximate confidence intervals of the estimated parameters with 95% confidence[22] are: 6.932 md $\leq kk_r^o \leq$ 7.049 md, $2.007 \leq \lambda \leq 2.124$ and $0.0 \leq S_{gc} \leq 5.837 \times 10^{-2}$.

Assuming none of the four parameters is known *a priori* and using $kk_r^o = k_b = 6.2958$ md, $\lambda = 1$, $S_{gc} = 1.0 \times 10^{-10}$ and $S_{wc} = 0.1$ as initial guesses, the values of the estimated parameters obtained are $kk_r^o = 6.990$ md, $\lambda = 2.181$, $S_{gc} = 6.92 \times 10^{-10}$ and $S_{wc} = 0.2749$. These values are in good agreement with the correct values of $kk_r^o = 7.0$ md, $\lambda = 2.0$, $S_{gc} = 0.0$ and $S_{wc} = 0.3$. The variation of the estimated parameters as a function of iteration number is shown in Table F-9. The approximate confidence intervals of the estimated parameters with 95% confidence[22] are: 6.93 md $\leq kk_r^o \leq$ 7.051 md, $2.120 \leq \lambda \leq 2.242$, $0.0 \leq S_{gc} \leq 6.10 \times 10^{-2}$ and $0.214 \leq S_{wc} \leq 0.336$.

3.6.1.1 Effects of the Duration of the Test.

A very important point is that the duration of the test can be reduced from $t_p = 5$ days without the values of the estimated parameters changing significantly. To illustrate this point, we considered a three-day drawdown test followed by a

three-day buildup. Using the computed values of kk_{ro} and k_{rg}/k_{ro} from a three-day pressure drawdown test with $kk_r^o = k_b = 6.2958$ md and $\lambda = 1$ as initial guesses, the values of the estimated parameters obtained are $kk_r^o = 7.007$ md and $\lambda = 1.946$. Note that these values are about the same as the ones obtained from a five-day drawdown test followed by a five-day buildup test. The approximate confidence intervals of the estimated parameters with 95% confidence[22] are: 6.949 md $\leq kk_r^o \leq$ 7.066 md and $1.889 \leq \lambda \leq 2.005$. Assuming that only the value of S_{wc} is known and using the computed values of kk_{ro} and k_{rg}/k_{ro} from a three-day pressure drawdown test with $kk_r^o = k_b = 6.2958$ md, $\lambda = 1$ and $S_{gc} = 1.0 \times 10^{-10}$ as initial guesses, the values of the estimated parameters obtained are $kk_r^o = 7.007$ md, $\lambda = 1.946$ and $S_{gc} = 1.94 \times 10^{-10}$. The approximate confidence intervals of the estimated parameters with 95% confidence[22] are: 6.949 md $\leq kk_r^o \leq$ 7.066 md, $1.888 \leq \lambda \leq$ 2.005 and $0.0 \leq S_{gc} \leq 5.86 \times 10^{-2}$. Assuming none of the four parameters is known *a priori* and using $kk_r^o = k_b = 6.2958$ md, $\lambda = 1$, $S_{gc} = 1.0 \times 10^{-10}$ and $S_{wc} = 0.1$ as initial guesses, the values of the estimated parameters obtained are $kk_r^o = 6.996$ md, $\lambda = 2.132$, $S_{gc} = 5.78 \times 10^{-10}$ and $S_{wc} = 0.2613$. The approximate confidence intervals of the estimated parameters with 95% confidence[22] are: 6.935 md $\leq kk_r^o \leq$ 7.057 md, $2.072 \leq \lambda \leq 2.195$, $0.0 \leq S_{gc} \leq 6.12 \times 10^{-2}$ and $0.200 \leq S_{wc} \leq 0.322$.

For the one-day drawdown test followed by a one-day buildup test using $kk_r^o = k_b = 6.2958$ md and $\lambda = 1$ as initial guesses, the values of the estimated parameters obtained are $kk_r^o = 7.020$ md and $\lambda = 1.852$ which do not differ significantly from the ones estimated from a five-day or a three-day drawdown pressure test. The approximate confidence intervals of the estimated parameters with 95% confidence[22] are: 6.961 md $\leq kk_r^o \leq$ 7.078 md and $1.793 \leq \lambda \leq 1.910$. Assuming that only the value of S_{wc} is known and using the computed values of kk_{ro} and k_{rg}/k_{ro} from an one-day pressure drawdown test with $kk_r^o = k_b = 6.2958$ md, $\lambda = 1$ and $S_{gc} = 1.0 \times 10^{-10}$ as initial guesses, the values of the estimated parameters obtained are $kk_r^o = 7.020$ md, $\lambda = 1.852$ and $S_{gc} = 1.36 \times 10^{-9}$. The approximate confidence intervals of the estimated parameters with 95% confidence[22] are: 6.961 md $\leq kk_r^o \leq$ 7.079 md, $1.793 \leq \lambda \leq 1.911$ and $0.0 \leq S_{gc} \leq 5.89 \times 10^{-2}$. Assuming none of the

four parameters is known *a priori* and using $kk_r^o = k_b = 6.2958$ md, $\lambda = 1$, $S_{gc} = 1.0 \times 10^{-10}$ and $S_{wc} = 0.1$ as initial guesses, the values of the estimated parameters obtained are $kk_r^o = 7.012$ md, $\lambda = 1.924$, $S_{gc} = 5.49 \times 10^{-9}$ and $S_{wc} = 0.2669$. These values agree well with the ones estimated from a five-day or a three-day pressure drawdown test. The approximate confidence intervals of the estimated parameters with 95% confidence[22] are: 6.953 md $\leq kk_r^o \leq$ 7.016 md, $1.865 \leq \lambda \leq 1.984$, $0.0 \leq S_{gc} \leq 5.94 \times 10^{-2}$ and $0.207 \leq S_{wc} \leq 0.326$.

3.6.1.2 Effects of the Initial Value of kk_r^o.

Here, we show that instead of using the last kk_{ro} value from pressure buildup data as our initial estimate of kk_r^o, one could use a value of computed kk_{ro} from pressure drawdown data as an initial guess. For the case where the values of S_{gc} and S_{wc} are known and using the values of kk_{ro} and k_{rg}/k_{ro} computed from Eqs. 3.1.1 and 3.1.2 from a three-day pressure drawdown test with $kk_r^o = 4.592$ md and $\lambda = 1$ as initial guesses, the values of the estimated parameters obtained are $kk_r^o = 6.9981$ md and $\lambda = 1.9973$. Note that these values are almost identical to the values that we estimated using the last kk_{ro} value computed from pressure buildup data as the initial guess for kk_r^o. This implies that we do not need a highly accurate initial estimate of kk_r^o in order to apply nonlinear regression analysis techniques. The approximate confidence intervals of the estimated parameters with 95% confidence[22] are: 6.94 md $\leq kk_r^o \leq$ 7.057 md and $1.939 \leq \lambda \leq 2.056$. Assuming that only the value of S_{wc} is known *a priori* and using the computed values of kk_{ro} and k_{rg}/k_{ro} from a three-day pressure drawdown test with $kk_r^o = k_b = 4.592$ md, $\lambda = 1$ and $S_{gc} = 1.0 \times 10^{-10}$ as initial guesses, the values of the estimated parameters obtained are $kk_r^o = 6.998$ md, $\lambda = 1.997$ and $S_{gc} = 3.80 \times 10^{-10}$. The approximate confidence intervals of the estimated parameters with 95% confidence[22] are: 6.94 md $\leq kk_r^o \leq$ 7.057 md, $1.94 \leq \lambda \leq 2.056$ and $-5.86 \times 10^{-2} \leq S_{gc} \leq 5.86 \times 10^{-2}$. Assuming that none of the four parameters is known *a priori* and using $kk_r^o = k_b = 4.592$ md, $\lambda = 1$, $S_{gc} = 1.0 \times 10^{-10}$ and $S_{wc} = 0.1$ as initial guesses, the values of the estimated parameters obtained are $kk_r^o = 6.999$ md, $\lambda = 2.050$, $S_{gc} = 6.33 \times 10^{-10}$ and

$S_{wc} = 0.2543$. These values agree well with the ones estimated using the last kk_{ro} value computed from pressure buildup data as the initial guess for kk_r^o. Finally, the approximate confidence intervals of the estimated parameters with 95% confidence[22] are: 6.94 md $\leq kk_r^o \leq$ 7.059 md, $1.991 \leq \lambda \leq 2.109$, $0.0 \leq S_{gc} \leq 5.95 \times 10^{-2}$ and $0.195 \leq S_{wc} \leq 0.314$.

3.6.1.3 Effects of the Initial Guess.

A synopsis of the effects of the initial guess on the values of estimated parameters and the corresponding confidence intervals is presented in Tables F-10 and F-11, respectively, for the case where the well was produced for five days at $q_o = 150$ STB/D and then shut-in for 5 days. The last column of Table F-10 gives the number of iterations used to obtain convergence of the nonlinear regression analysis algorithm to obtain the estimates ("results") of the parameters given in Table F-10. The correct or actual values of the parameters are given in the last row of Table F-10.

For the initial guesses 1 through 6, it was assumed that the values of S_{gc} and S_{wc} are known *a priori* and thus, only the values of kk_r^o and λ were estimated from the nonlinear regression analysis technique. The initial guess for λ ranged from 0.5 to 7.0 and the initial guess for kk_r^o was either the last kk_{ro} value computed from pressure buildup data or a kk_{ro} value computed from pressure drawdown data. As can be seen from Table F-10, for initial guesses #1 through #5, the estimated kk_r^o and λ values are quite accurate compared to the true solution. The length of the confidence interval for the same cases, shown in Table F-11, is small which indicates high confidence in the estimated parameter values. For the I.G. #6 case, the initial estimates of both kk_r^o and λ are reasonably poor. In this case, the nonlinear regression algorithm yields $\lambda = 3.187$ as compared to the correct value of $\lambda = 2$.

For the initial guesses #7 and #8, it was assumed that only the value of S_{wc} is known *a priori* and thus, nonlinear regression analysis was applied to yield estimates of kk_r^o, λ and S_{gc}. Generally, we found that the presence of S_{gc} as an additional

unknown parameter has little effect on the accuracy of the estimated values of λ and kk_r^o. The length of the confidence interval for the three unknown parameters estimation problem is small for both kk_r^o and λ, but quite large for S_{gc}. The large confidence interval length for the critical gas saturation is attributed to the fact that the correct value of critical gas saturation ($S_{gc} = 0$) is on the boundary of the permissible region introduced by the penalty function method used.

For initial guesses #9 through #13, it was assumed that none of the four parameters is known *a priori* and thus, the nonlinear regression analysis algorithm was applied to obtain estimates of kk_r^o, λ, S_{gc} and S_{wc}. Tables F-10 and F-11 show that as the number of estimated parameters increases, the estimated values obtained from the nonlinear regression techniques depend heavily on the initial guess. If the initial guess is far from the true solution, the nonlinear regression techniques may either converge to the wrong solution or even diverge. As shown in Table F-10, extremely poor estimates of S_{wc} are obtained for I.G. #12 and I.G. #13, however, even in these cases, we obtained reasonable estimates of k_r^o and λ.

3.6.1.4 Effective (Relative) Permeability Curves.

Using the parameter values estimated by nonlinear regression analysis in Eqs. 3.2.17 and 3.5.9, one can compute the oil and gas effective permeability curves given by Standing's correlations. Fig. 3.6.2 shows a graph of effective oil and gas permeabilities versus oil saturation. The solid curves represent the correct (simulator) oil and gas effective permeability curves, whereas the data points correspond to the oil and gas effective permeabilities computed using the values of the parameters estimated from the nonlinear regression analysis for the five-day drawdown case. The circular data points correspond to the case where only λ and kk_r^o were estimated by regression analysis and S_{wc} and S_{gc} were assumed known. The square data points correspond to the case where the three parameters, λ, kk_r^o and S_{wc}, were obtained from regression analysis. The triangular data points correspond to the case where all four parameters were estimated by regression analysis. In all cases, we obtain good estimates of the actual effective permeability curves. For the case where four

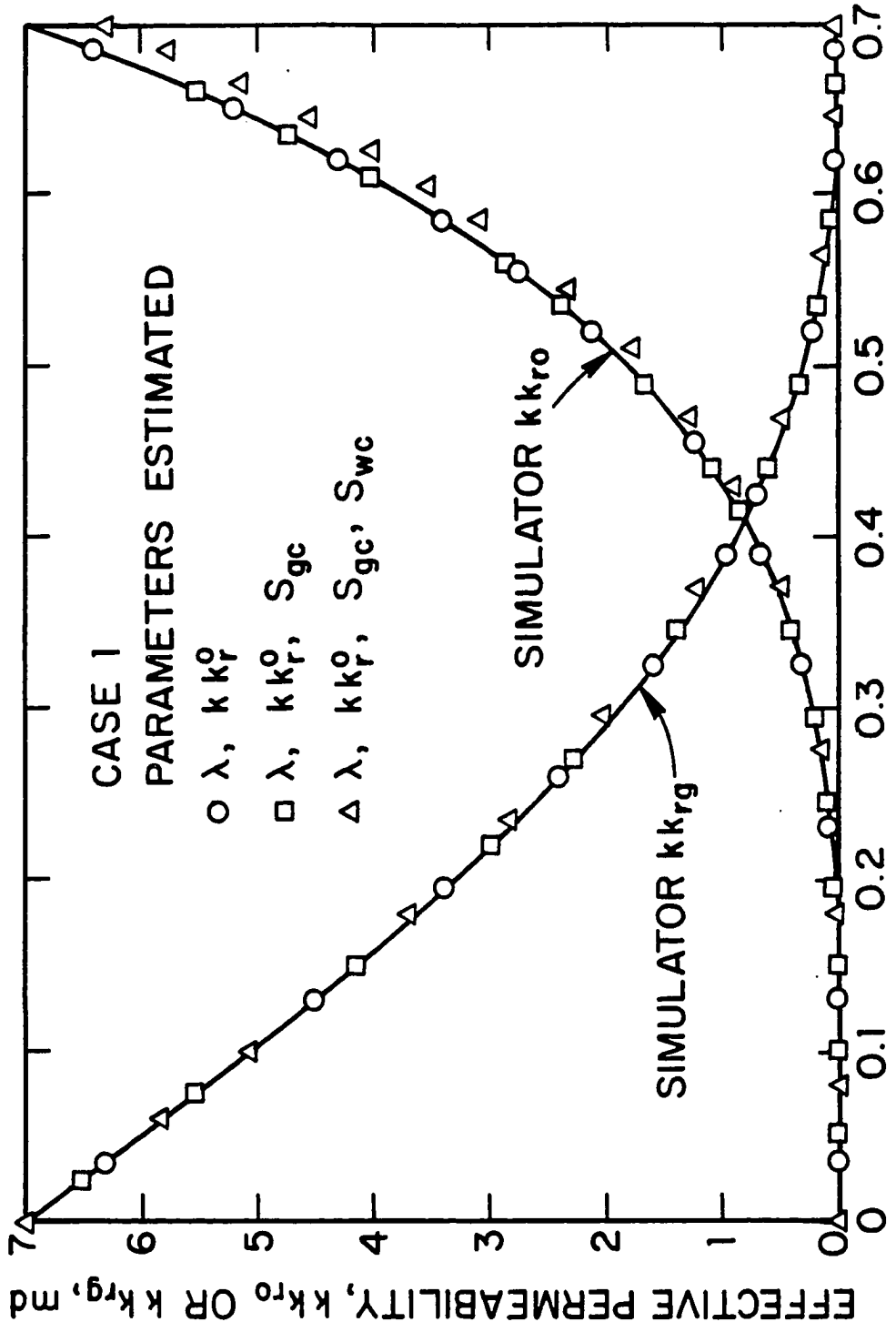

Fig. 3.6.2 - Plot of effective oil and gas permeability curves; Case 1.

parameters were estimated by regression analysis, the resulting kk_{ro} versus S_o curve is less accurate due to the fact that regression analysis gave $S_{wc} = 0.2749$ as compared to the correct value of $S_{wc} = 0.300$.

3.6.1.5 Determination of Skin Factor.

Having estimated the effective permeability curves, one could use the Bøe et al.[6] or the Evinger-Muskat[3] method as in Ref. 5 to determine the sandface oil saturation/wellbore pressure relationship. In the first case, one needs to solve a first order ordinary differential equation, whereas in the second case one needs to make use of Eq. 3.1.5. If the correct S_o versus p_{wf} relation can be obtained, this result can be combined with the kk_{ro} versus S_o curve generated by regression analysis (see Fig. 3.6.2) to obtain an accurate estimate of kk_{ro} as a function of pressure and then to generate the dimensionless wellbore pseudopressure function,

$$p_{pwD} = \frac{h\int_{p_{wf}}^{p_i} \frac{kk_{ro}}{\mu_o B_o} dp}{141.2 q_o}, \tag{3.6.2}$$

as a function of dimensionless time, t_D, defined by

$$t_D = \frac{6.328 \times 10^{-3} kk_{roi} t}{\phi c_{ti} \mu_{oi} r_w^2}, \tag{3.6.3}$$

where i denotes the initial value, i.e., the value at p_i and thus, kk_{roi} can be approximated by the value of kk_r^o obtained from regression analysis. If accurate estimates of kk_{ro} versus S_o and kk_r^o are obtained from regression analysis and the correct S_o versus p_{wf} can be determined accurately, then our measured pressure data can be converted to accurate p_{pwD} versus t_D data with Eqs. 3.6.2 and 3.6.3. Since

$$p_{pwD} = 1.151 \log\left(\frac{4t_D}{e^\gamma}\right) + s, \tag{3.6.4}$$

is approximately correct during the infinite-acting period, see Refs. 5-7, 9 and 28, the skin factor can then be estimated from the obvious rearrangement of Eq. 3.6.4.

In Fig. 3.6.3, we have plotted the sandface oil saturation versus the wellbore pressure for the cases where only two and three unknown parameters were estimated from nonlinear regression analysis, i.e., we used the effective permeability

data shown by circular or square data points in Fig. 3.6.2. The solid curve corresponds to the simulator values, whereas the circular data points represent the oil saturation/pressure relationship computed from the Bøe et al.[6] method and the square data points represent the oil saturation/pressure relationship obtained from the Evinger-Muskat[3] method. Note that both methods yield very accurate estimates of the oil saturation/pressure relationship.

Fig. 3.6.4 shows results similar to those of Fig. 3.6.3. The results of Fig. 3.6.4 are for the case where all four parameters (λ, kk_r^o, S_{gc} and S_{wc}) were estimated from regression analysis; i.e., we have used the effective permeability data shown by triangular data points in Fig. 3.6.2. The solid curve corresponds to simulator values, whereas the circular data points represent the oil saturation/pressure relationship computed from the Bøe et al.[6] method and the square data points represent the oil saturation/pressure relationship obtained from the Evinger-Muskat[3] method.

The results of Fig. 3.6.4 reveal that, at early times, the Bøe et al.[6] method yields highly accurate estimates of the sandface oil saturation as a function of the wellbore pressure. At later times ($p_{wf} < 3100$ psi), the S_o versus p_{wf} relation obtained from both the Bøe et al.[6] and the Evinger-Muskat[3] methods overestimates the simulator value of $S_o(p_{wf})$. The values computed from the Evinger-Muskat[3] method follow the same trend as the simulator values but lie above them throughout the duration of the test. This can be explained by examining Fig. 3.6.5 where the values of k_{rg}/k_{ro} are plotted versus oil saturation. As can be seen in Fig. 3.6.5, the k_{rg}/k_{ro} values computed when all four parameters were estimated by regression analysis (triangular data points) fall above the correct (simulator) values (solid curve), whereas the k_{rg}/k_{ro} results obtained using two (circular data points) or three (square data points) estimated parameters are very accurate compared with the simulator values.

The procedure we follow to compute the k_{rg}/k_{ro} values by the Evinger-Muskat[3] method is as follows: (i) use the estimated effective or relative permeability values obtained using Standing's correlations to determine the k_{rg}/k_{ro} versus oil saturation relationship; (ii) compute the k_{rg}/k_{ro} versus pressure relationship by using Eq.

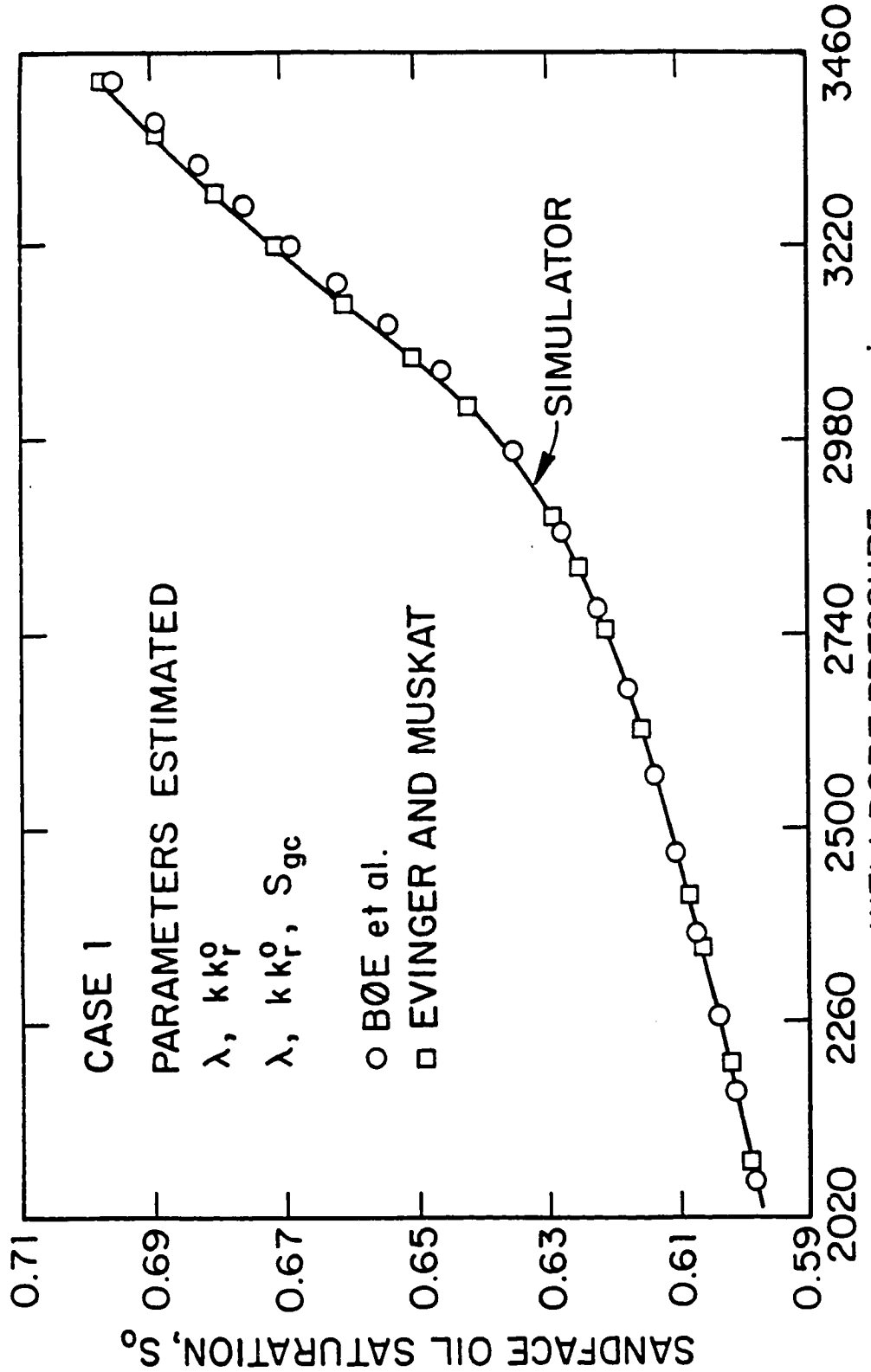

Fig. 3.6.3 - Approximation of oil saturation/wellbore pressure relation; Case 1.

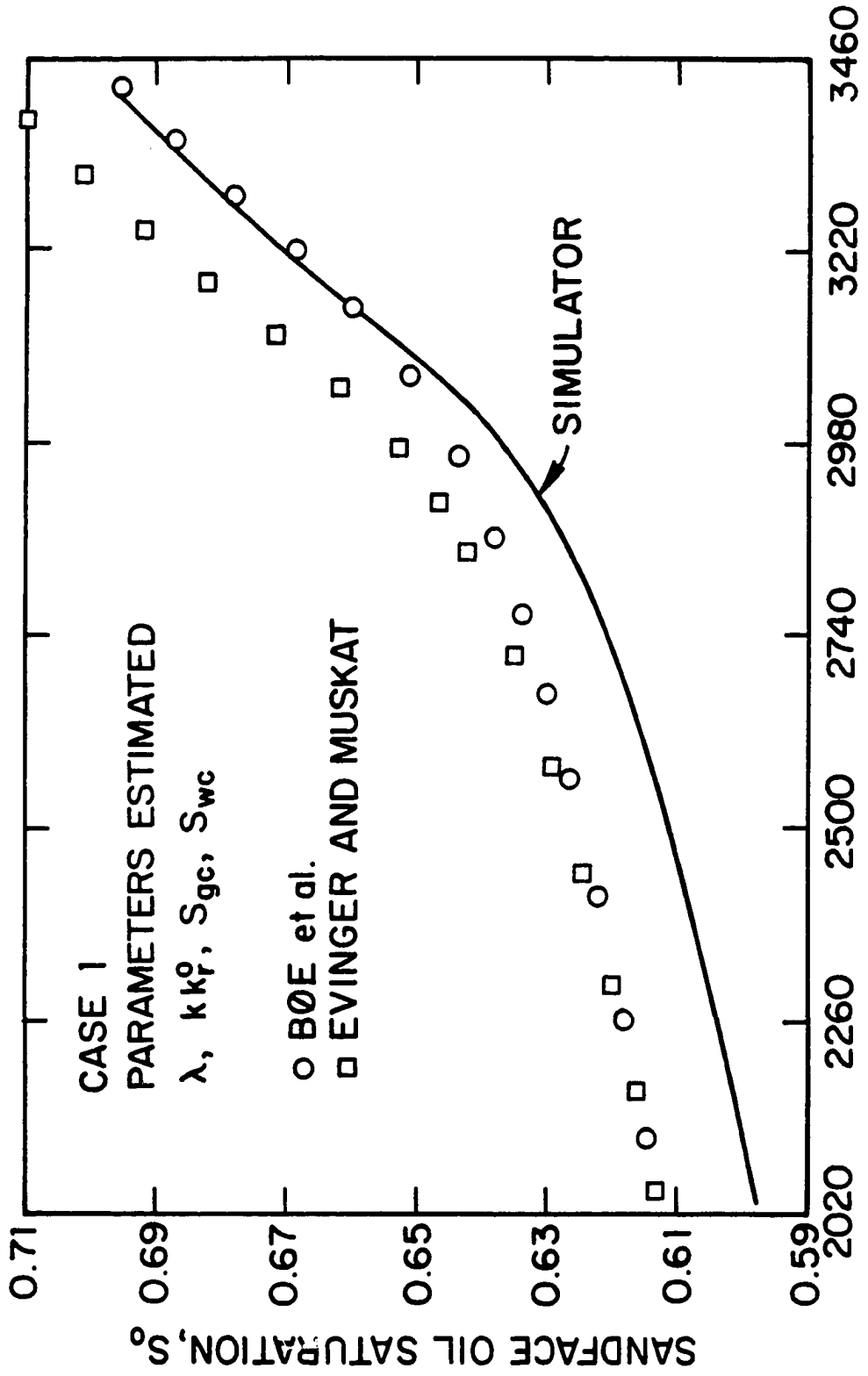

Fig. 3.6.4 - Approximation of oil saturation/wellbore pressure relation; Case 1.

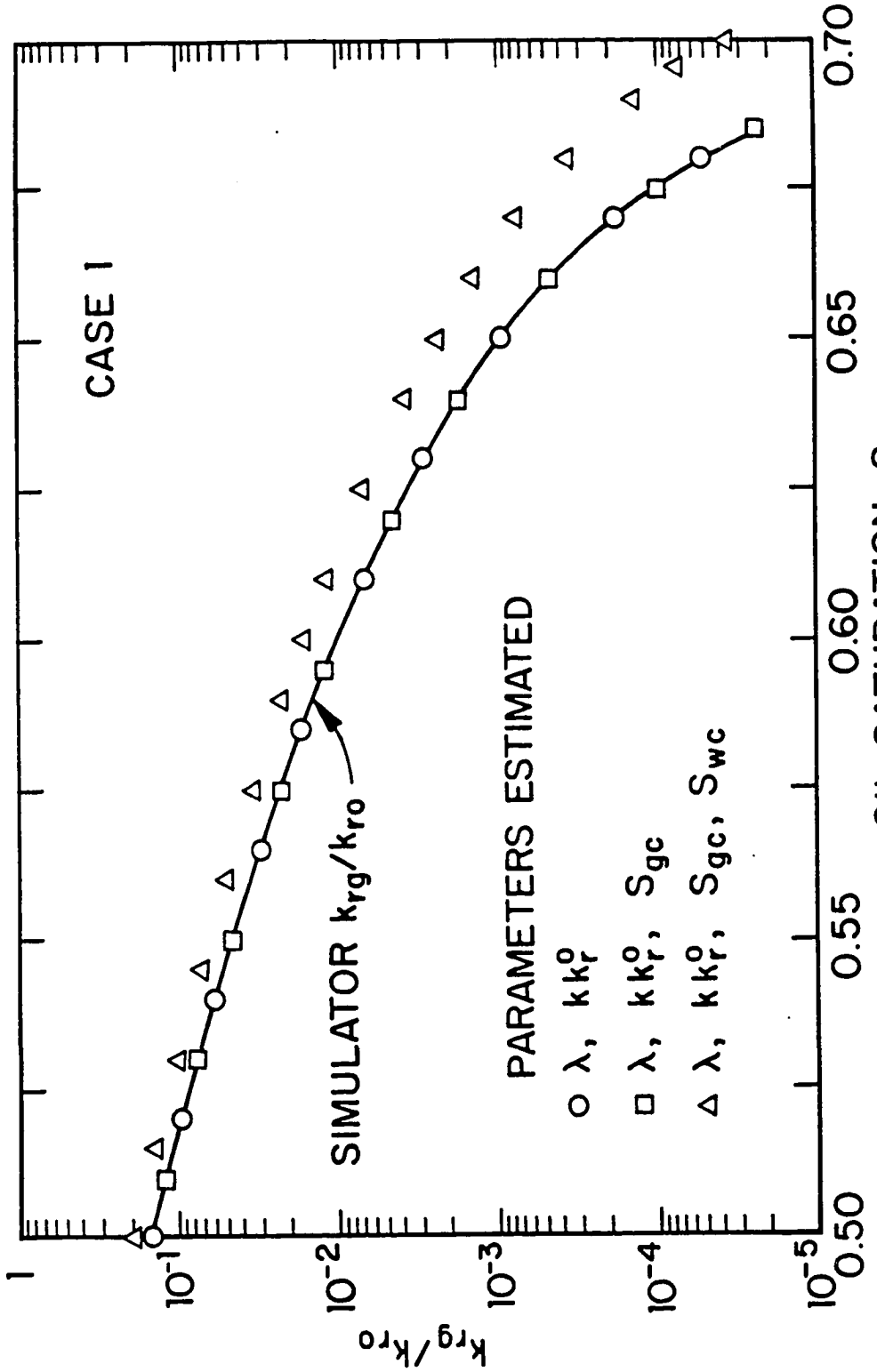

Fig. 3.6.5 - Ratio of oil/gas effective permeability versus oil saturation; Case 1.

3.1.5; and (iii) interpolate to obtain the oil saturation/pressure relationship. From Fig. 3.6.5, we see that the computed k_{rg}/k_{ro} versus oil saturation relationship is very accurate for the cases where two or three parameters were estimated by regression analysis and thus, the Evinger-Muskat[3] method yields a very accurate oil saturation versus pressure relationship (see Fig. 3.6.3). For the case where four parameters were estimated, we do not obtain an accurate k_{rg}/k_{ro} versus oil saturation relationship especially at high values of S_o and therefore, the oil saturation/pressure relationship determined by the above procedure is not accurate either (see Fig. 3.6.4). For all pseudopressure function computations presented in this report, we have used the Bøe et al.[6] method to obtain the oil saturation versus pressure relationship.

Once the sandface oil saturation versus wellbore pressure relation is known, one can compute the p_{pwD} function and then apply Eq. 3.6.4 to estimate the skin factor. To examine this aspect, we have plotted the dimensionless wellbore pseudopressure function, p_{pwD}, computed using the estimated effective permeability curves versus dimensionless time t_D on semilog paper (p_{pwD} and t_D are defined in the standard way (see, for example, Refs. 8-11 and 28-30)). This plot is shown in Fig. 3.6.6. The solid straight line represents the liquid solution, the data points shown by crosses correspond to the p_{pwD} computed using the simulator relative permeability curves, whereas the circular, square, and triangular data points, respectively, correspond to p_{pwD} values computed by using the estimated effective oil and gas effective permeability curves. For the cases where two or three parameters were estimated by regression analysis (circular and square data points) a semilog straight line of slope 1.155 is obtained, but the straight line plot of the triangular data points exhibits a semilog slope of 1.113 compared to the liquid solution semilog slope of 1.151. In all cases, as expected[6,7], the p_{pwD} data lie slightly below the liquid solution. In all cases, if we use p_{pwD} versus t_D data corresponding to $t_D = 10^2$ in Eq. 3.6.4 and solve for s, we obtain $s \approx -0.6$ as compared to the correct value of $s = 0$. Finally, it is important to note that if we obtain accurate effective oil permeability curves by regression analysis, then the resulting p_{pwD} versus t_D semilog plot should yield

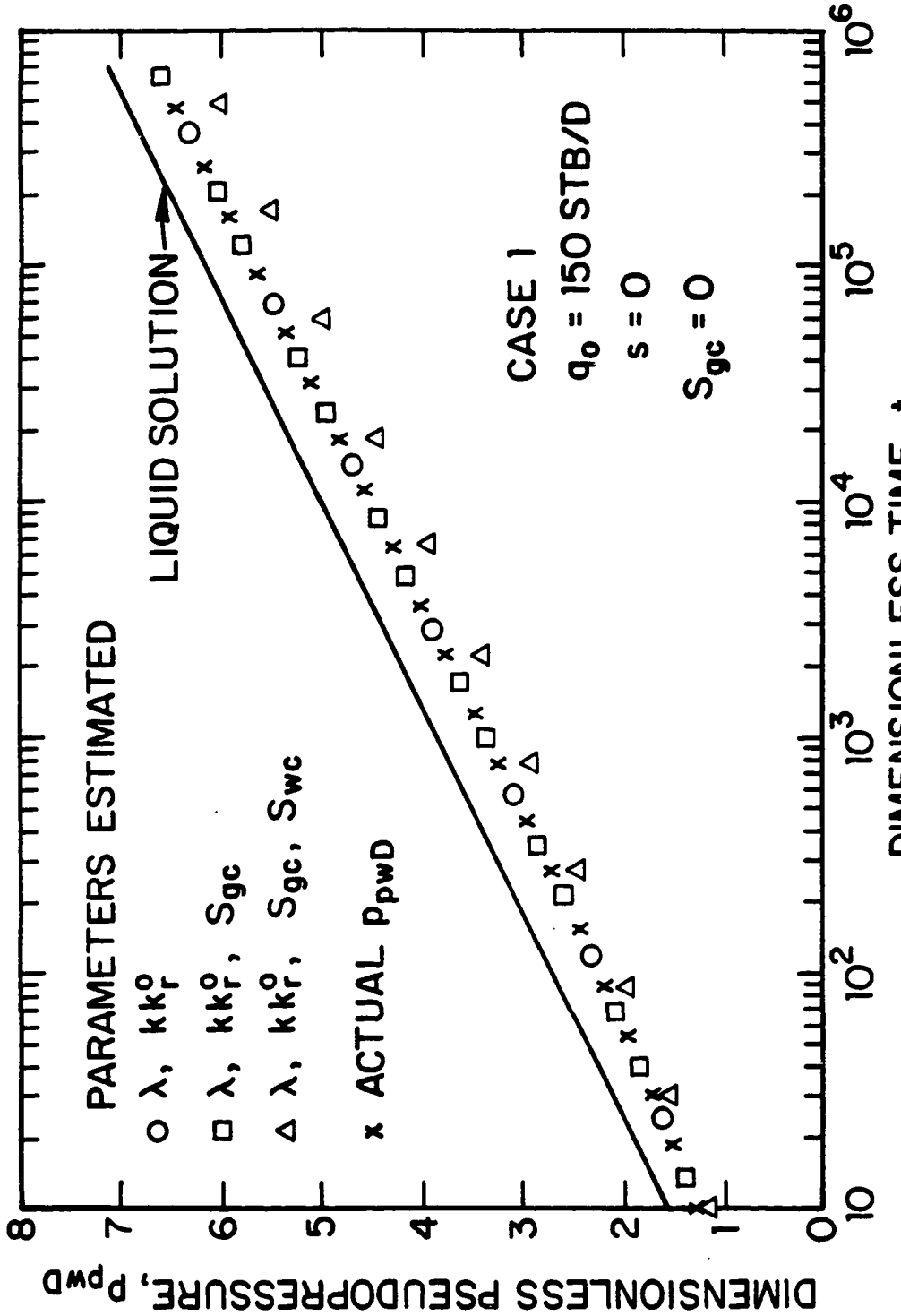

Fig. 3.6.6 - Plot of dimensionless pseudopressure functions versus dimensionless time; Case 1.

a semilog straight line with slope close to 1.151. Even in the case where all four parameters (λ, kk_r^o, S_{gc} and S_{wc}) were estimated by regression analysis (triangular data points of Figs. 3.6.2 and 3.6.6), the resulting p_{pwD} versus t_D plot in Fig. 3.6.6 gives a semilog slope of 1.113 which is not radically different from the theoretical 1.151 value.

3.6.2 Case 2: Non-Zero Critical Gas Saturation, Zero Skin.

In this section, we examine the influence of non-zero critical gas saturation on the computational procedures introduced in this Chapter. The relative permeability data used in this case have been derived using the Honarpour et al.[34] correlations and are given in Table A-4. The Honarpour relative permeability data do not represent Standing's relative permeability correlations. In particular, $k_{ro}(S_o = 1 - S_{wc}) \neq k_{rg}(S_g = 1 - S_{wc})$ for the Honarpour relative permeability set used. Fig. 3.6.7 presents a plot of the kk_{ro} values versus the wellbore pressure computed from Eq. 3.1.1 for Case 2. Results presented pertain to a five-day drawdown test ($t_D \approx 6.02 \times 10^5$) followed by a five-day buildup test. Recall that for this case, the skin factor and wellbore storage coefficient are zero, but the critical gas saturation is 0.07. The oil flow rate is constant and equal to $q_o = 150$ STB/D. The solid curve in Fig. 3.6.7 corresponds to simulator values, the triangular data points represent the kk_{ro} values computed from a drawdown pressure data by using Eq. 3.1.1, and the circular data points represent the kk_{ro} values computed from a buildup pressure data by using Eq. 3.6.1. The results of this figure show that the computed kk_{ro} values at the end of the drawdown test are in good agreement with the simulator kk_{ro} values (see Refs. 8-11, 28 and 29). Using all the computed drawdown values of kk_{ro} and k_{rg}/k_{ro} corresponding to $kk_{ro} \leq 3.3749$ in our nonlinear regression analysis program, we are able to obtain estimates of the unknown parameters λ, kk_r^o, S_{gc} and S_{wc} by using Newton's method. More specifically, we used penalty functions in forming the Hessian matrix, H, modified Cholesky factorization[20] in solving Eq. 2.2.5, and Bard's[16] line search method in updating the solution vector in Eq. 2.2.11.

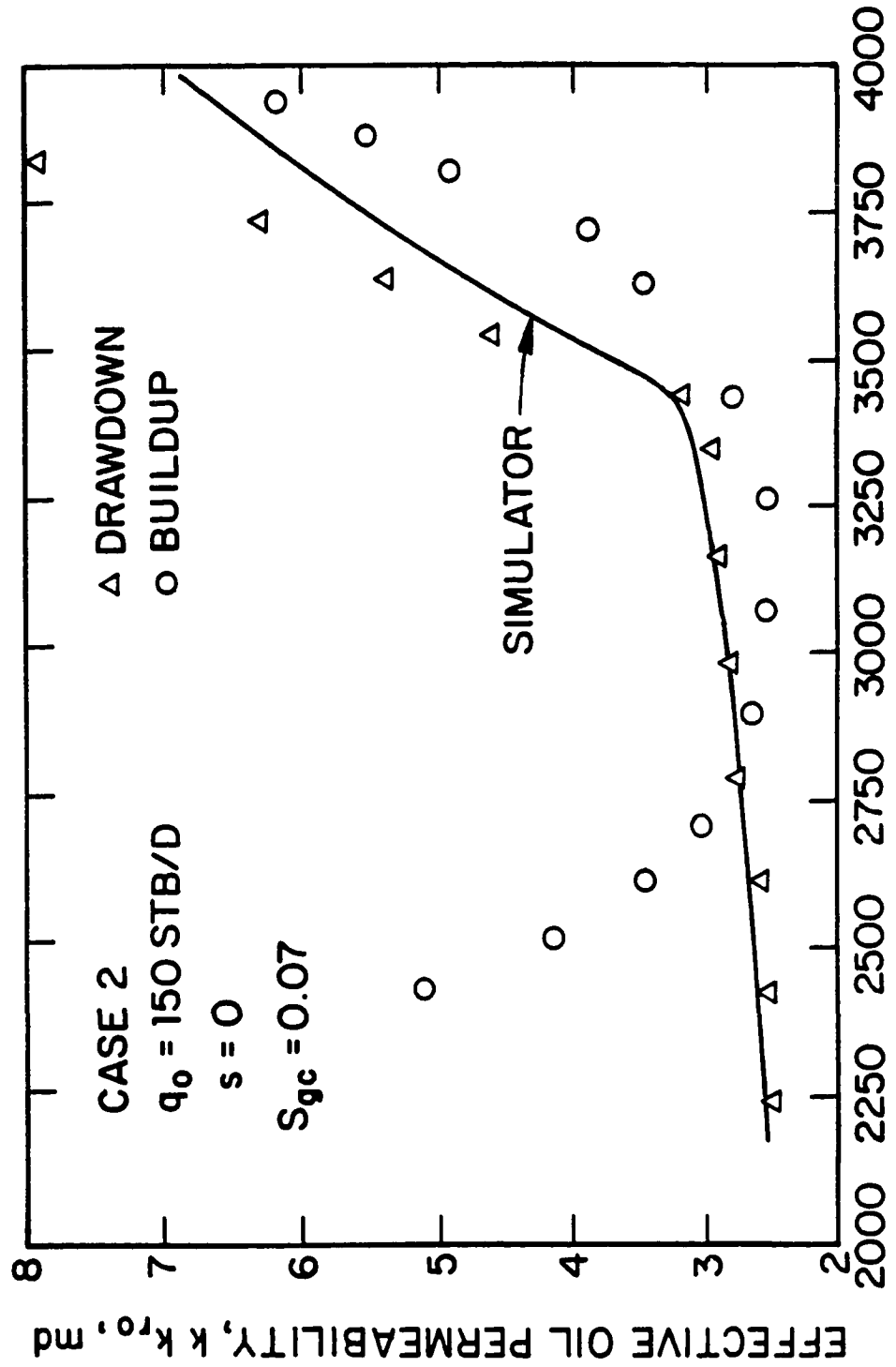

Fig. 3.6.7 - Effective oil permeability as a function of wellbore pressure; Case 2.

Assuming that the values of S_{gc} and S_{wc} are known *a priori* and using $kk_r^o = k_b = 6.3339$ md and $\lambda = 1$ as initial guesses, the values of the estimated parameters obtained by nonlinear regression analysis are $kk_r^o = 6.6645$ md and $\lambda = 1.066$. Unlike Case 1, these estimated values cannot be compared with input kk_r^o and λ values since the input relative permeability are based on Honarpour's et al.[34] correlations. The approximate confidence intervals of the estimated parameters with 95% confidence[22] are: 6.385 md $\leq kk_r^o \leq$ 6.904 md and $0.733 \leq \lambda \leq 1.399$.

Assuming that only the value of S_{wc} is known and using $kk_r^o = k_b = 6.3339$ md, $\lambda = 1$ and $S_{gc} = 1.0 \times 10^{-2}$ as initial guesses, the values of the estimated parameters obtained are $kk_r^o = 6.303$ md, $\lambda = 0.968$ and $S_{gc} = 5.67 \times 10^{-2}$. The computed value of S_{gc} agrees well with the input value $S_{gc} = 0.07$. The approximate confidence intervals of the estimated parameters with 95% confidence[22] are: 6.189 md $\leq kk_r^o \leq$ 6.417 md, $0.854 \leq \lambda \leq 1.707$ and $0.0 \leq S_{gc} \leq 1.707 \times 10^{-1}$.

Assuming none of the four parameters, λ, kk_r^o, S_{wc} and S_{gc}, is known *a priori* and using $kk_r^o = k_b = 6.3339$ md, $\lambda = 1$, $S_{gc} = 1.0 \times 10^{-2}$ and $S_{wc} = 0.2$ as initial guesses, the values of the estimated parameters obtained are $kk_r^o = 6.442$ md, $\lambda = 0.913$, $S_{gc} = 6.67 \times 10^{-2}$ and $S_{wc} = 0.1988$. The computed value of S_{gc} agrees very well with the input value $S_{gc} = 0.07$ but the estimated value of S_{wc} is not very accurate compared with the input value $S_{wc} = 0.3$. The approximate confidence intervals of the estimated parameters with 95% confidence[22] are: 6.179 md $\leq kk_r^o \leq$ 6.704 md, $0.676 \leq \lambda \leq 1.150$, $1.86 \times 10^{-2} \leq S_{gc} \leq 1.15 \times 10^{-1}$ and $0.0 \leq S_{wc} \leq 0.611$.

Using these computed parameter values in Eqs. 3.2.17 and 3.5.9, one can compute the oil and gas effective permeability curves based on Standing's correlations. If the value of the absolute permeability is known, the relative permeability curves can be obtained. Fig. 3.6.8 shows a graph of effective oil and gas permeabilities versus oil saturation. The solid curve represents the correct (simulator) oil and gas effective permeability curves, whereas the data points correspond to the oil and gas effective permeabilities computed using the values of the parameters estimated from the nonlinear regression analysis procedure. The circular data points correspond to

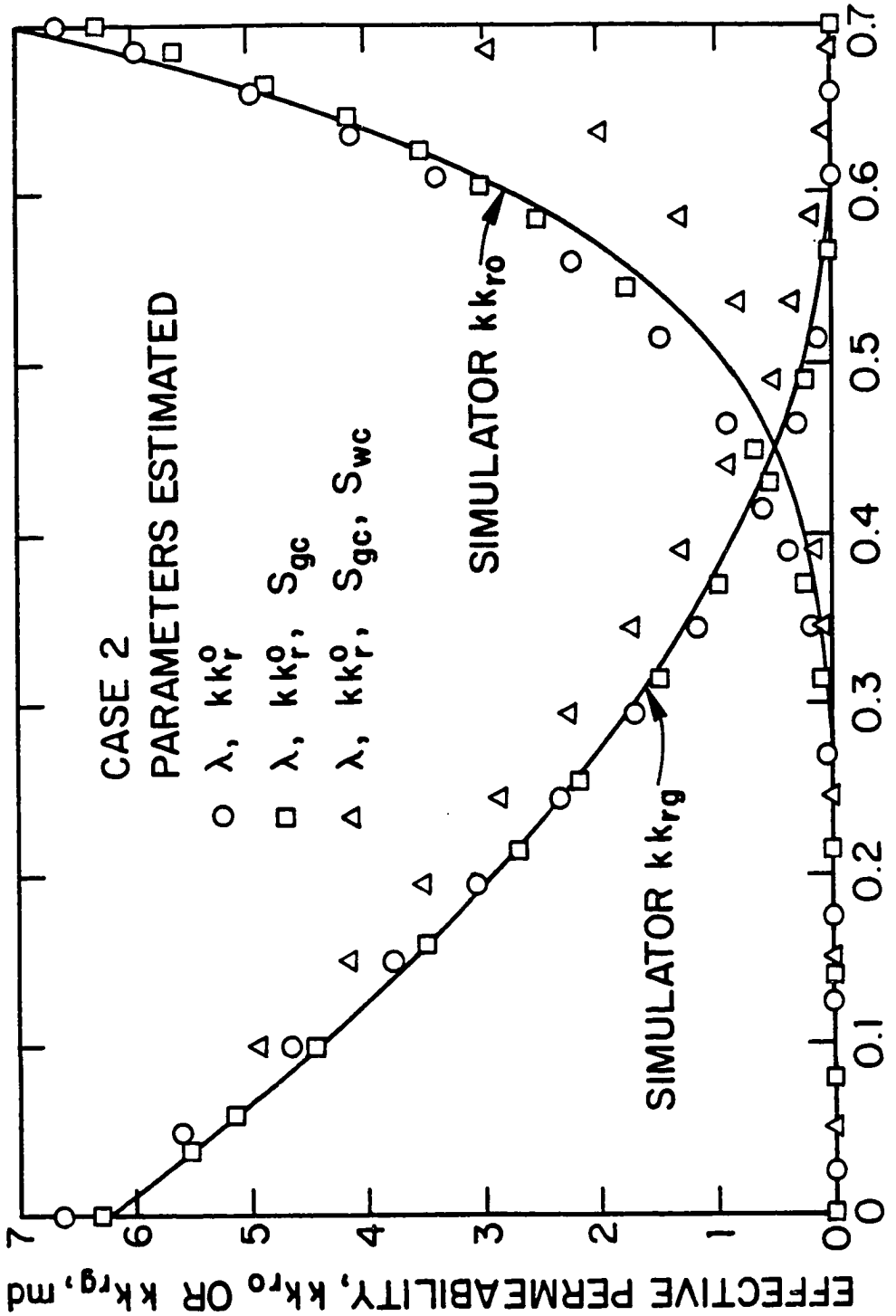

Fig. 3.6.8 - Plot of effective oil and gas permeability curves; Case 2.

kk_{ro} and kk_{rg} values obtained for the case where only λ and kk_r^o are estimated by regression analysis, the square data points correspond to kk_{ro} and kk_{rg} values obtained when λ, kk_r^o, and S_{gc} are estimated by regression analysis, and the triangular data points correspond to kk_{ro} and kk_{rg} values obtained when all four unknown parameters are estimated by regression analysis. The estimated effective permeability curves based on the proposed procedure are in good overall agreement with the input effective permeability curves for the cases where two or three parameters are estimated by regression analysis (S_{wc} known *a priori*), but in the case where four parameters are estimated, there is a significant discrepancy between computed and correct kk_{ro} and kk_{rg} values. This is mainly due to the fact that as the number of estimated parameters increases, nonlinear regression analysis yields less accurate results[25,26]. In particular, the estimate of S_{wc} obtained is inaccurate.

Note that the results obtained in this case are not as good as the ones in Case 1. The confidence intervals for Case 2 are larger than the ones for Case 1 and the final value of λ is very close to its initial value which implies that the confidence in the values of the estimated parameters is not very high. This behavior is due to the fact that during the time interval that the computed kk_{ro} and kk_{rg}/kk_{ro} are accurate, the changes in their values are not significant (see Fig. 3.6.8). During the same time interval the oil saturation S_o does not change significantly either. As a result, we obtain data for only a very limited section of the effective permeability curves which leads to a flat objective function and thus, nonlinear regression analysis methods would have difficulty in obtaining the final minimum point.

As in Case 1, applying the Bøe et al.[6] or Evinger-Muskat[3] method, one can obtain estimates of sandface oil saturation/wellbore pressure relation in order to compute the dimensionless wellbore pseudopressure function, p_{pwD}. Having constructed the p_{pwD} versus t_D relationship, one then can compute the value of the skin factor by applying Eq. 3.6.3. Using the estimated effective permeabilities corresponding to two and three unknown parameters (circular and square data points of Fig. 3.6.8, respectively) to compute the dimensionless pseudopressure function, p_{pwD}, and applying Eq. 3.6.4 at $t_D = 10^4$, we obtain $s \approx -0.5$ as the estimated

value of skin factor, which agrees well with the input value of $s = 0$. However, for the case where we use the constructed permeability curves corresponding to all four estimated unknown parameters (triangular data points of Fig. 3.6.8), the computed value of skin factor from Eq. 3.6.4 at $t_D = 10^4$ is $s = -1.93$, which indicates that the constructed effective permeability curves, in the case of four unknown parameters, are not accurate (see Fig. 3.6.8 and Ref. 7).

3.6.3 Case 3: Zero Critical Gas Saturation, Non-Zero Skin.

In this section we examine the influence of skin effects with zero critical saturation on our computational procedures. According to Refs. 9, 10, 28 and 29, when $s \neq 0$, values of kk_{ro} computed from pressure drawdown data by using Eq. 3.1.1 are not accurate until the skin zone reaches a steady-state behavior. Combining this with the fact that the major change in our sandface oil saturation occurs at the early stages of a drawdown test (Refs. 8-11, 28 and 29), the computational procedure based on Eq. 3.1.1 yields accurate kk_{ro} values only during the time period of our test when the sandface oil saturation is changing very slowly. Therefore, the computed kk_{ro} and k_{rg}/k_{ro} data yield an accurate representation of only a very small portion of the effective permeability curves. When such results are used in the nonlinear regression algorithms, we cannot obtain accurate estimates of the unknown parameters.

An alternative solution to this problem consists of using multirate tests instead of single-rate tests. If the flow period for each rate is short, one may be able to obtain kk_{ro} values corresponding to a significant range of the changes of the sandface oil saturation; see Ref. 8. Here, in multirate tests, the kk_{ro} values were computed using the computational procedures of Ref. 8. Unfortunately, the results we obtained indicate that there are several problems with multirate testing. Specifically, the disadvantages are as follows: (i) Superposition is nonrigorous and the flow period for each test must be long enough so that superposition approximately holds. (The method of Ref. 8 for computing kk_{ro} values from multirate tests assumes that superposition holds.) For cases where the skin factor is not zero, it may be necessary

to maintain the rate of the multirate test for longer times than the cases where $s = 0$ in order to compute reasonably accurate kk_{ro} values by the method of Ref. 8. (ii) Each test usually yields a very small number of accurate kk_{ro} values; in fact, we found that we could not usually obtain sufficiently accurate kk_{ro} values over a wide enough saturation range to obtain reliable estimates of kk_r^o, λ, S_{gc} and S_{wc} by our nonlinear regression analysis techniques. (iii) Buildup tests following multirate tests provide highly inaccurate kk_{ro} values. And, (iv) as the number of flow periods increases (the flow rate increases too), superposition becomes less accurate and thus, the computed kk_{ro} values become less accurate. In general, we found that if we used more than two flow periods, we did not obtain highly accurate kk_{ro} values by the method of Ref. 8. Based on numerous computational experiments, we found that for cases where the skin effect is non-zero, two-rate testing provided the best results for determining parameters in Standing's relative permeability correlation. Unfortunately, two-rate tests only give sufficient data to determine two of the four parameters in Standing's relative permeability correlations. Moreover, we found that one could determine two parameters (λ and kk_r^o) by Powell's[35] method more easily than by nonlinear regression analysis techniques. Thus, our recommended procedure is as follows:

(1) Conduct a two-rate test at rate q_{o1} and q_{o2}, where $q_{o2} > q_{o1}$. Using data at the end of the first flow period, compute one value of kk_{ro} from Eq. 3.1.1 and the corresponding value of k_{rg}/k_{ro} from Eq. 3.1.4. Using data at the end of the second flow period, compute one value of kk_{ro} from

$$kk_{ro} = -\frac{162.6(\mu_o B_o)_{p_{wf}}}{h\left(dp_{wf}/d\left[\sum_{i=1}^{n}(q_i - q_{i-1})\log(t - t_{i-1})\right]\right)}, \qquad (3.6.5)$$

and compute a corresponding value of k_{rg}/k_{ro} from Eq. 3.1.4.

(2) Use the computed kk_{ro} and k_{rg}/k_{ro} in Eq. 3.5.1 to obtain a nonlinear system of two equations in the two unknowns, kk_r^o and λ. Solve this system by Powell's[35] method to obtain estimates of kk_r^o and λ.

Here, we illustrate the computational procedure delineated above. Specifically, we consider a two-rate test with $q_{o1} = 50$ STB/D and $q_{o2} = 100$ STB/D. The first

flow period is of one-half day duration (t_1 = 0.5 day) and the second flow rate is maintained for one day (t_2 = 1.0 day). The relative permeability data for this case are those of Set 1 (see Table A-2) and they were derived using Standing's[15] correlation with $S_{iw} = S_{wc} = 0.3$, $kk_r^o = 7.0$ md, $S_{gc} = 0.0$ and $\lambda = 2.0$. Fig. 3.6.9 shows a plot of the simulated and computed effective oil permeability values versus the wellbore pressure, p_{wf}. The continuous curve represents the kk_{ro} values corresponding to the simulator sandface oil saturation and the circular data points represent the computed kk_{ro} values by applying Eq. 3.6.5. As can be seen from Fig. 3.6.9, the computed and actual effective oil permeability values are in good agreement only for short time intervals at the end of each flow period. This is due to the presence of the skin zone and the assumption that the superposition holds throughout the entire second flow period. Using pressure data at the end of the first flow period, Eqs. 3.1.1 and 3.1.4 give, respectively, $kk_{ro} = 4.595$ md, $k_{rg}/k_{ro} = 0.285 \times 10^{-2}$. Using data at the end of the second flow period, Eqs. 3.6.5 and 3.1.4 give, respectively, $kk_{ro} = 3.981$ md and $k_{rg}/k_{ro} = 0.747 \times 10^{-2}$. The simulated and computed data at the end of the two flow periods, for both kk_{ro} and kk_{rg}, are shown in Tables F-12 and F-13, respectively.

Using the two sets of kk_{ro} and k_{rg}/k_{ro} data in Eq. 3.5.1 gives two nonlinear equations in two unknowns, kk_r^o and λ. In order to solve this system by Powell's[35] method, we need to provide an initial guess. As an initial guess for λ, we used $\lambda = 1$. As an initial guess for kk_r^o, we used the last value of kk_{ro} computed for the first flow period, i.e., $kk_r^o = 4.595$ md. The solution obtained by Powell's[35] method was $\lambda = 2.213$ and $kk_r^o = 6.969$ md. These values compare reasonably well with the correct values of $\lambda = 2.0$ and $kk_r^o = 7.0$ md. (We found that the values of parameters estimated from Powell's[35] method do not depend on the initial guess for λ provided the initial guess satisfies $0.5 \leq \lambda \leq 10$.) Since $S_{wc} = 0.3$ and $S_{gc} = 0.0$ were assumed known, the estimates of $kk_r^o = 6.969$ md and $\lambda = 2.213$ determine the effective permeability curves based on Standing's correlations; see Eqs. 3.2.17 and 3.5.9. The continuous curves in Fig. 3.6.10 represent the correct (simulator) effective permeability curves, whereas the circular data points represent the effective

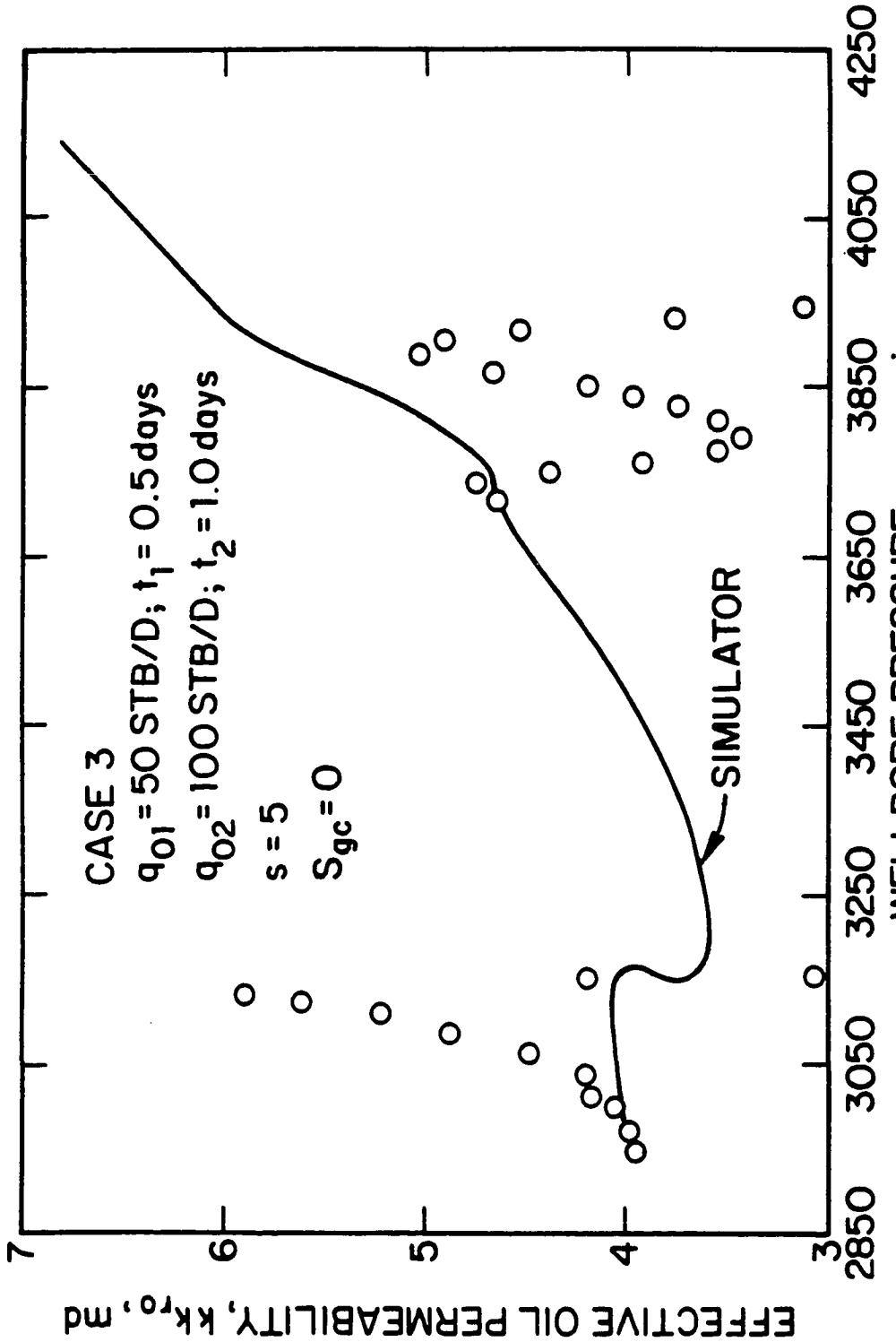

Fig. 3.6.9 - Effective oil permeability as a function of wellbore pressure; Case 3.

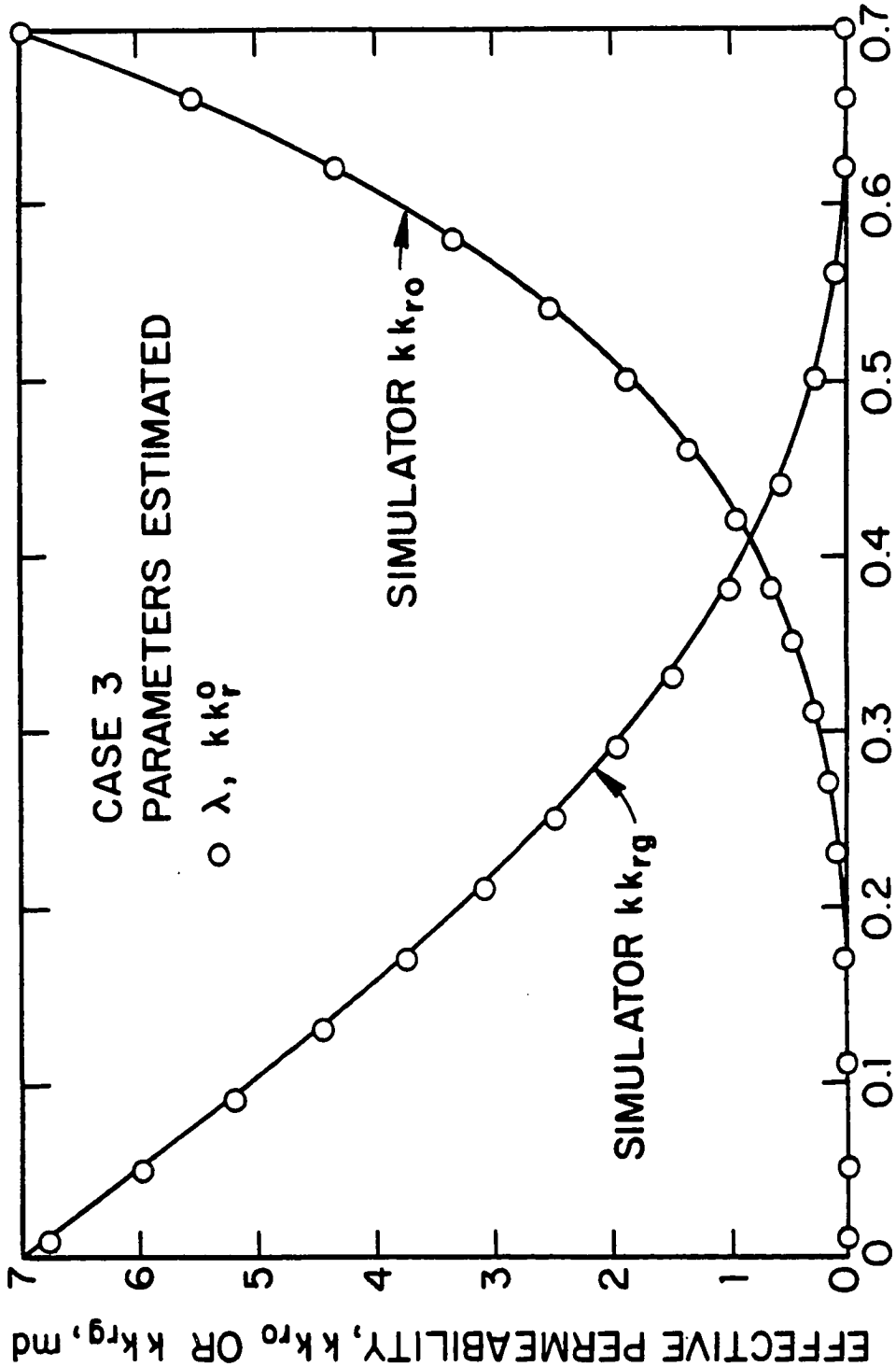

Fig. 3.6.10 - Plot of effective oil and gas permeability curves; Case 3.

permeability curves determined by our computational procedure. Note, our procedure yields excellent estimates of the correct relative permeability curves. Finally, we remark that Newton's method (see Ref. 36) failed to yield reasonable results for the same set of data.

The sandface oil saturation/wellbore pressure relationship was then computed using the estimated effective permeability curves in the Bøe et al.[6] method in order to compute the pseudopressure function. However, due to oscillatory behavior of the pressure solution at the early part of the second rate test, we were unable to obtain a continuous semilog straight line when we plotted the dimensionless pseudopressure function versus the logarithmic convolution time (see Ref. 29). The first rate was long enough, however, to reach the semilog straight line which was in very good agreement with the actual dimensionless pseudopressure solution (see Fig. 3.6.11). Applying Eq. 3.6.4 at $t_D = 10^4$, the value of the skin factor was estimated to be $s \approx 4$ as compared to the correct value of $s = 5$.

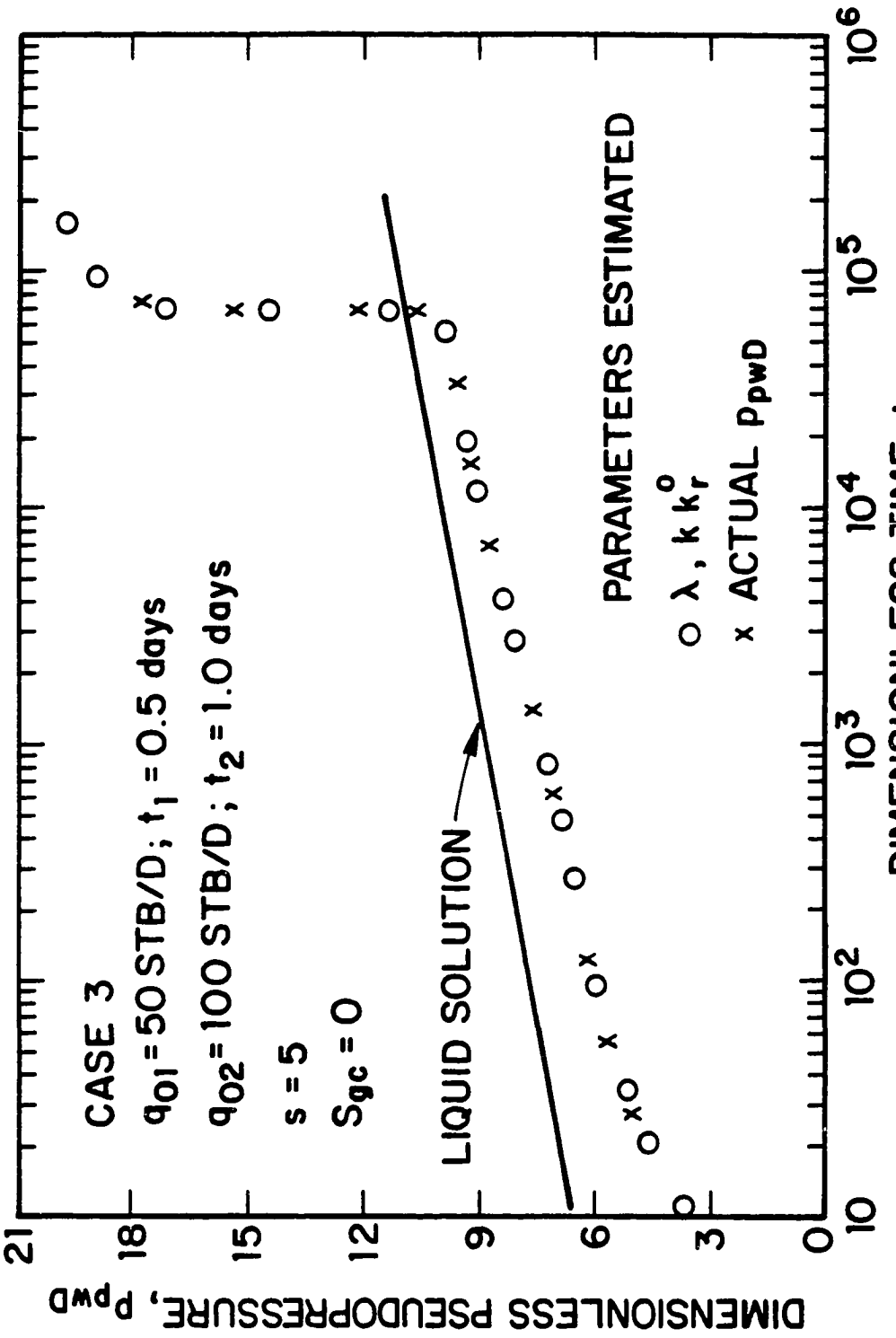

Fig. 3.6.11 - Plot of dimensionless pseudopressure functions versus dimensionless time; Case 3.

CHAPTER IV
ESTIMATION OF EFFECTIVE PERMEABILITIES FOR RESERVOIRS INITIALLY ABOVE BUBBLE-POINT PRESSURE

In this chapter, we investigate the effects of initial reservoir pressure on the computation of effective permeabilities for reservoirs which are initially above the bubble-point pressure. It is shown that the initial effective oil permeability may be estimated from drawdown and buildup pressure data. It is also shown that one can obtain accurate estimates of computed effective permeabilities as pointwise functions of wellbore pressure from drawdown data during the time period that the wellbore pressure is less than the initial bubble-point pressure. Finally, from the estimates of effective permeabilities obtained, it is shown that one can construct approximate effective or relative permeability curves either by nonlinear regression analysis techniques or by solving a system of nonlinear equations.

4.1 INTRODUCTION

In the previous Chapter, we presented an overview of the methods provided by Refs. 8-11 and 28-30 for approximating the oil and gas effective permeability versus wellbore pressure relationship using the pressure drawdown and buildup data. Here, however, we give a summary of these methods for the sake of completeness. The kk_{ro} and kk_{rg} values can be computed from pressure drawdown data by applying the following equations:

$$(kk_{ro})_{p_{wf}} = \frac{-162.6 q_o (\mu_o B_o)_{p_{wf}}}{h dp_{wf}/d\log t}, \tag{4.1.1}$$

and

$$(kk_{rg})_{p_{wf}} = \frac{-162.6 q_g(t) (\mu_g B_g)_{p_{wf}}}{h dp_{wf}/d\log t}, \tag{4.1.2}$$

respectively.

The effective oil and gas permeability values can also be computed from a buildup pressure versus shut-in time data test by using the following equations:

$$(kk_{ro})_{p_{ws}} = \frac{162.6q_o(\mu_o B_o)_{p_{ws}}}{hdp_{ws}/d\log\left(\frac{t\Delta t}{t+\Delta t}\right)} = -\frac{162.6q_o(\mu_o B_o)_{p_{ws}}}{hdp_{ws}/d\log R_{H1}}, \qquad (4.1.3)$$

and

$$(kk_{rg})_{p_{ws}} = \left[R(\Delta t=0) - R_s\right]_{p_{ws}} \left(\frac{\mu_g B_g}{\mu_o B_o}\right)_{p_{ws}} kk_{ro}, \qquad (4.1.4)$$

respectively. Here R_{H1} denotes the primary Horner time ratio, i.e., $R_{H1} = (t + \Delta t)/\Delta t$, and the application of Eq. 4.1.3 requires that the producing GOR at the time of shut-in is measured. Eq. 4.1.3 represents a rearrangement of a basic relationship presented by Evinger and Muskat[3] and Eq. 4.1.3 was used in its original form[3] by Raghavan[5] to construct wellbore pseudopressures.

All the results presented in Refs. 8-11 and 28-30 have assumed that the initial reservoir pressure equals the initial bubble-point pressure. The objective of this Chapter is to investigate the applicability of the computational procedures of these references for cases where the initial reservoir pressure is larger than the initial bubble-point pressure.

4.2 Mathematical Model and Simulator Data

As in Chapter 3, we consider radial flow to a completely penetrating well at the center of a cylindrical solution-gas-drive reservoir. The top, bottom and outer reservoir boundaries are assumed to be sealed, i.e., no flow boundaries. All the results presented, however, are for the infinite-acting period and thus, are not affected by the outer reservoir boundary. Gravity and capillary effects are neglected. Although Refs. 29 and 30 considered wellbore storage effects, all results presented in this Chapter assume that wellbore storage effects are negligible. The pressure and saturation solutions presented were obtained from the black-oil, variable bubble-point simulator described in Ref. 33. For all cases considered, water is immobile and water saturation remains fixed at $S_{wc} = 0.3$.

The skin zone is modeled as a concentric region with absolute permeability, k_s, which is different from the absolute permeability of the reservoir, k. Whenever

the skin factor is nonzero, the permeability of the skin zone is computed using Hawkins'[32] formula.

Table A-3 shows the PVT data and Table A-2 shows the relative permeability data used in this work (Fig. 4.2.1 displays a graph of these relative permeability data). This set of data was derived by using $\lambda = 2$, $k_r^o = k_{ro}(S_o = 1 - S_{wc}) = 0.7$, $S_{gc} = 0.0$, $S_{wc} = 0.3$ and $S_{or} = 0.0$ in Standing's[15] relative permeability correlations. Throughout, the wellbore radius, external reservoir boundary radius, reservoir thickness, porosity, and absolute permeability are specified as $r_w = 0.328$ ft, $r_e = 6600$ ft, $h = 15.547$ ft, $\phi = 0.3$ and $k = 10$ md, respectively, but the values of these parameters have no influence on the validity of the procedures and conclusions presented in this work. All results presented pertain to the infinite-acting period, that is, the closed outer boundary has no influence on the results obtained.

In this Chapter, results are presented for the following cases:

Case 1

$q_o = 150$ STB/D ; s = 0 ; $p_i = 4700$ psi ; $p_{bi} = 4201.6$ psi ;

$c_{ti} = 0.27299 \times 10^{-4}$ psi $^{-1}$; $\mu_{oi} = 0.40147$ cp ; $B_{oi} = 1.50803$ RB/STB.

Case 2

$q_o = 150$ STB/D ; s = 0 ; $p_i = 4500$ psi ; $p_{bi} = 4201.6$ psi ;

$c_{ti} = 0.26822 \times 10^{-4}$ psi $^{-1}$; $\mu_{oi} = 0.39727$ cp ; $B_{oi} = 1.51123$ RB/STB.

Case 3

$q_o = 150$ STB/D ; s = 0 ; $p_i = 5500$ psi ; $p_{bi} = 4201.6$ psi ;

$c_{ti} = 0.40063 \times 10^{-4}$ psi $^{-1}$; $\mu_{oi} = 0.41827$ cp ; $B_{oi} = 1.49523$ RB/STB.

Case 4

$q_o = 50$ STB/D ; s = 5 ; $p_i = 4800$ psi ; $p_{bi} = 4201.6$ psi ;

$c_{ti} = 0.30285 \times 10^{-4}$ psi $^{-1}$; $\mu_{oi} = 0.40357$ cp ; $B_{oi} = 1.50643$ RB/STB.

Case 5

$q_o = 50$ STB/D ; s = 5 ; $p_i = 4600$ psi ; $p_{bi} = 4201.6$ psi ;

$c_{ti} = 0.27105 \times 10^{-4}$ psi $^{-1}$; $\mu_{oi} = 0.39944$ cp ; $B_{oi} = 1.50952$ RB/STB,

where c_{ti}, μ_{oi} and B_{oi} represent the initial values of total compressibility, oil viscosity and oil FVF, respectively.

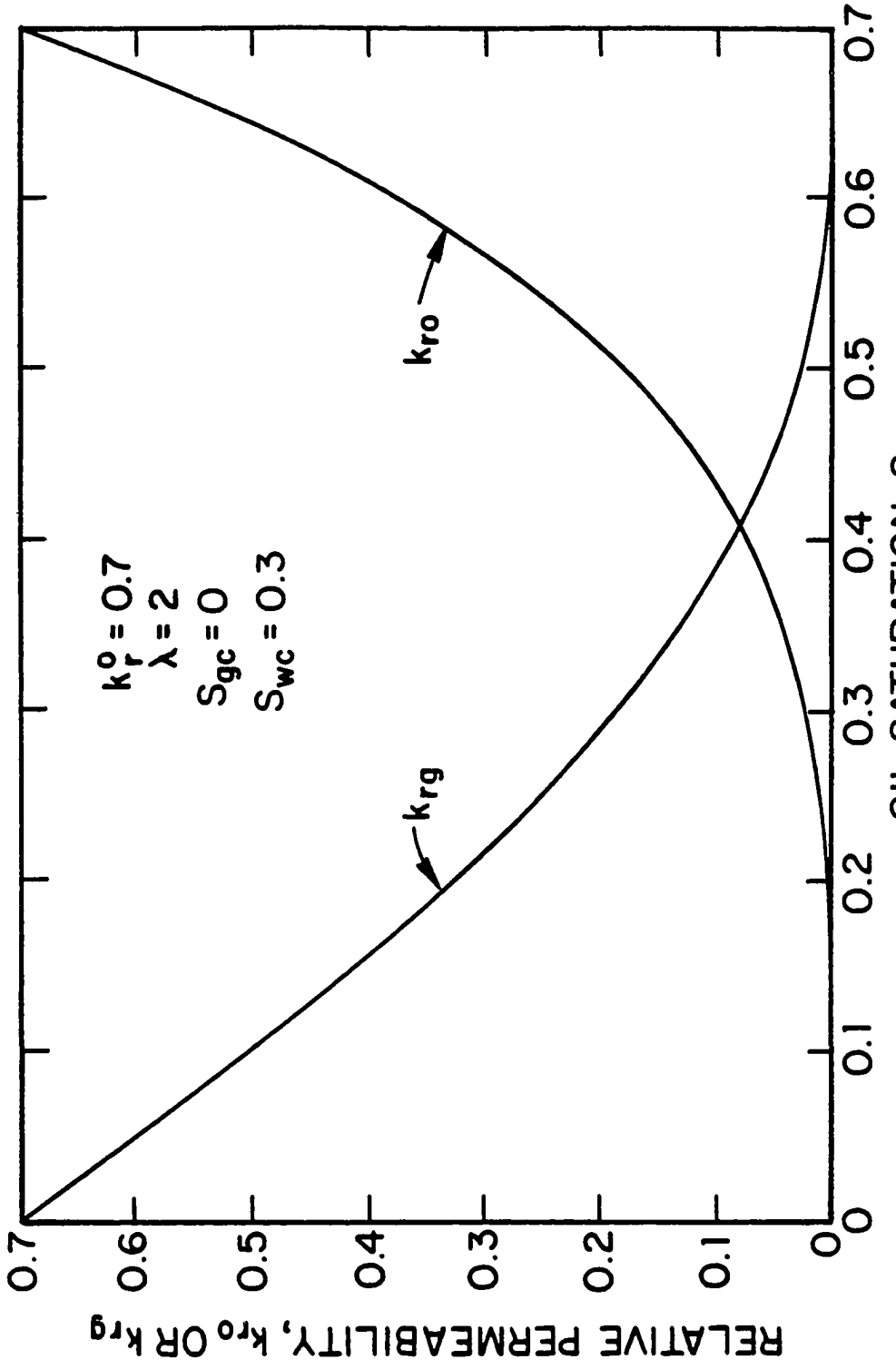

Fig. 4.2.1 - Relative permeability curves; Set 1.

Cases 1-3 consider a problem where the skin effects are negligible and Cases 4 and 5 allow us to examine the effects of a non-zero skin factor on the computation of kk_{ro} for both drawdown and buildup pressure data. All results presented pertain to a three-day drawdown test followed by a three-day buildup test.

4.3 RESULTS

4.3.1 Zero Skin Cases.

We first investigate the results obtained in Case 1, which pertains to the case where the skin factor is zero and the initial reservoir pressure is approximately 500 psi higher than the initial bubble-point pressure. Figs. 4.3.1 and 4.3.2, respectively, show the wellbore pressure and sandface oil saturation plotted versus time for both drawdown and buildup tests for Case 1. From the plot of the drawdown sandface oil saturation versus time shown in Fig. 4.3.2, it can be seen that the reservoir pressure crosses the bubble-point pressure at $t \approx 7 \times 10^{-3}$ days ($t_D \approx 0.87662 \times 10^3$). Prior to this time the sandface oil saturation remains virtually constant and equal to the initial oil saturation, i.e., $S_{oi} = 0.7$. As soon as p_{wf} decreases below p_{bi}, the sandface oil saturation decreases rapidly with the major drop occurring from time $t = 7 \times 10^{-3}$ days to $t = 1 \times 10^{-1}$ days ($0.64506 \leq S_o \leq 0.6996$). For times $t > 1 \times 10^{-1}$ days until the end of the test, i.e. $t = 3$ days, the decrease in the sandface oil saturation is small, from $S_o = 0.64506$ to $S_o = 0.62441$.

The simulated and computed kk_{ro} versus the wellbore pressure p_{wf} are shown in Table F-14. In this table, columns 1 and 2 show the time and flowing wellbore pressure data, columns 3 and 4 show the sandface oil saturation and the effective oil permeability data obtained from the simulator and column 5 shows the kk_{ro} values computed from Eq. 4.1.1. Table F-15 shows the simulated and computed kk_{ro} values for the buildup test of Case 1. Columns 1 and 2 show the shut-in time and shut-in wellbore pressure data, columns 3 and 4 show the sandface oil saturation and the effective oil permeability data corresponding to the drawdown simulator results and column 5 shows the kk_{ro} values computed from Eq. 4.1.3. Effective oil permeability plotted versus the wellbore pressure is shown in Fig. 4.3.3. The solid

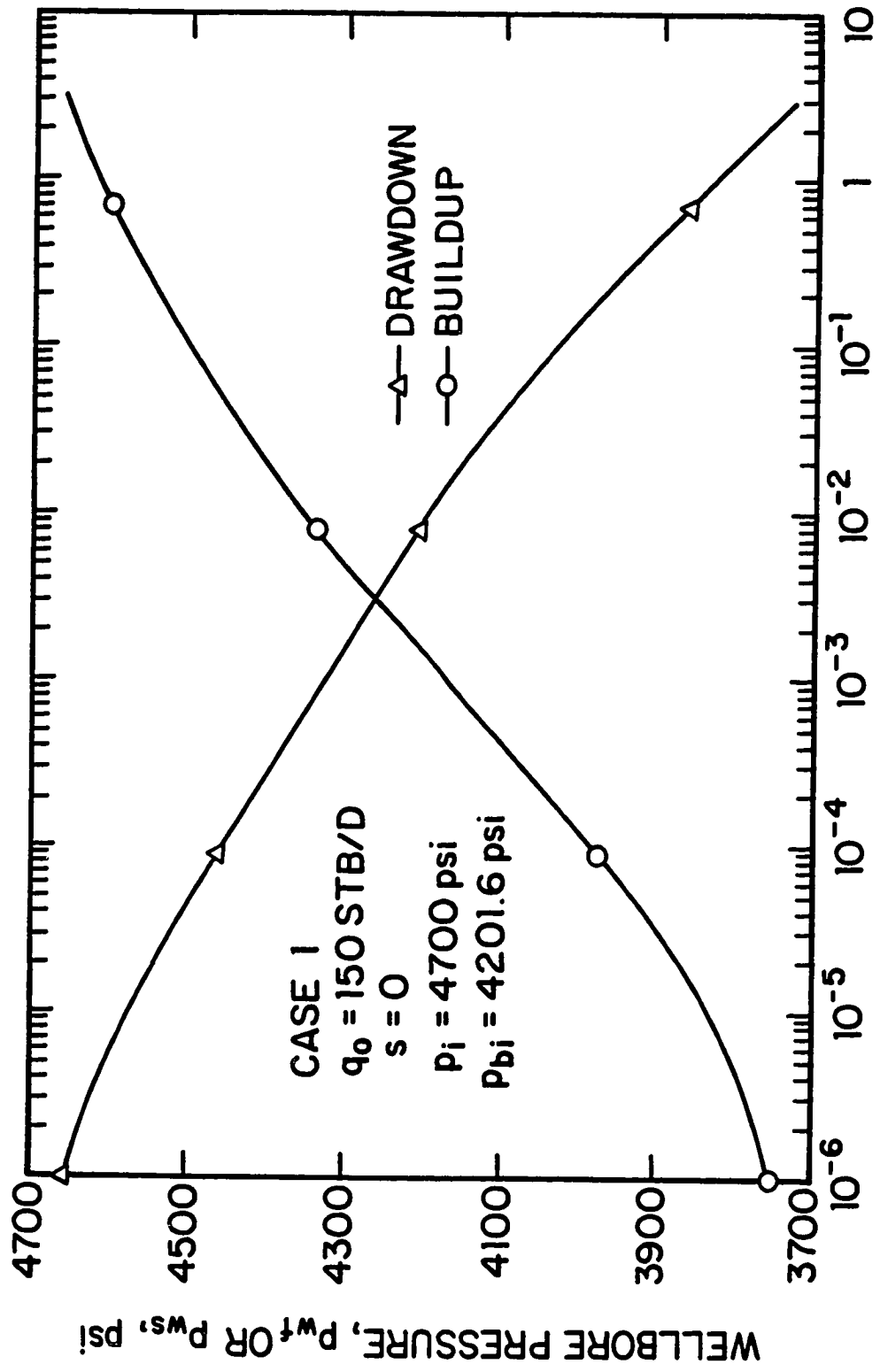

Fig. 4.3.1 - Drawdown and buildup wellbore pressures; Case 1.

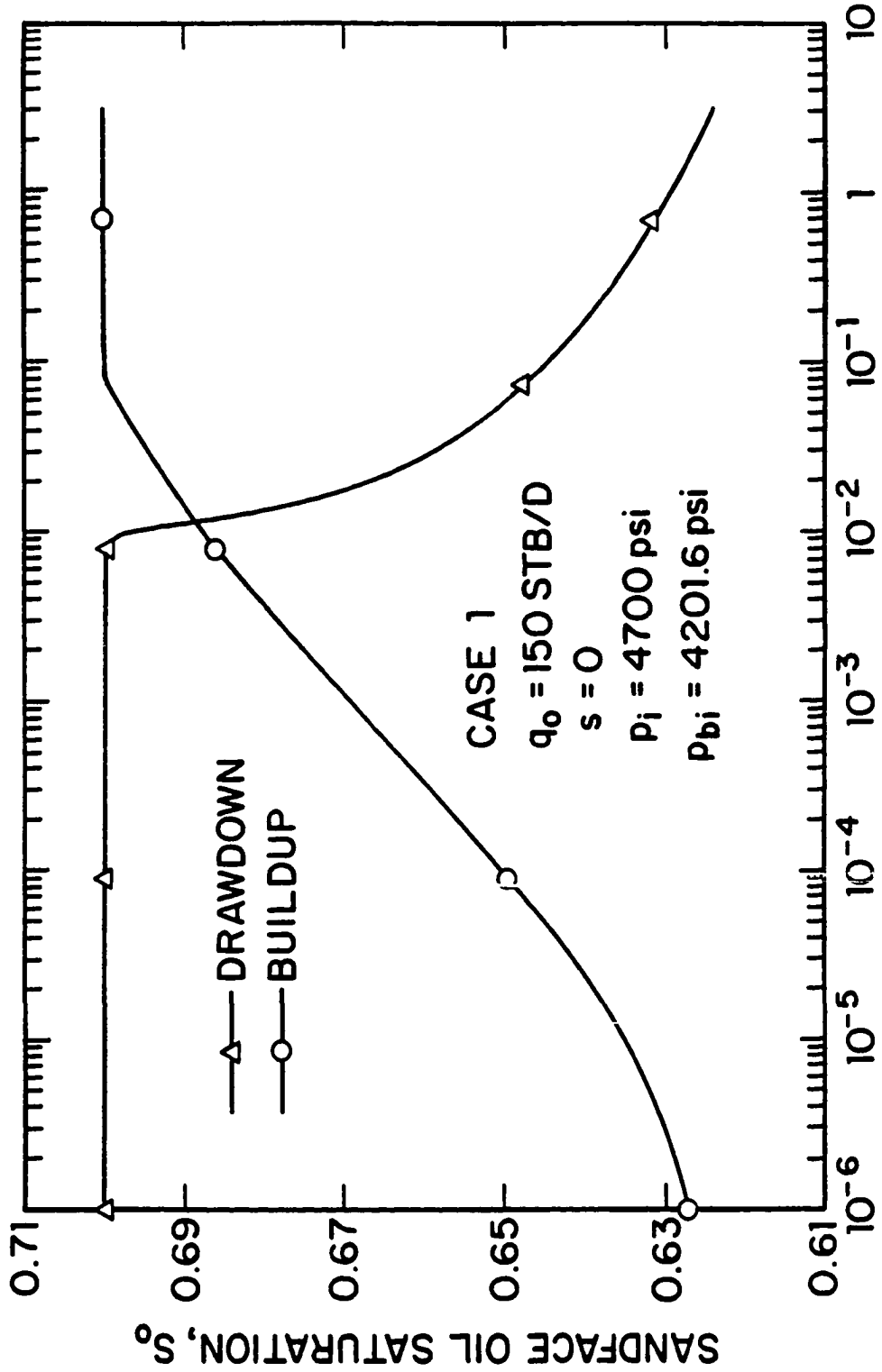

Fig. 4.3.2 - Drawdown and buildup sandface oil saturation; Case 1.

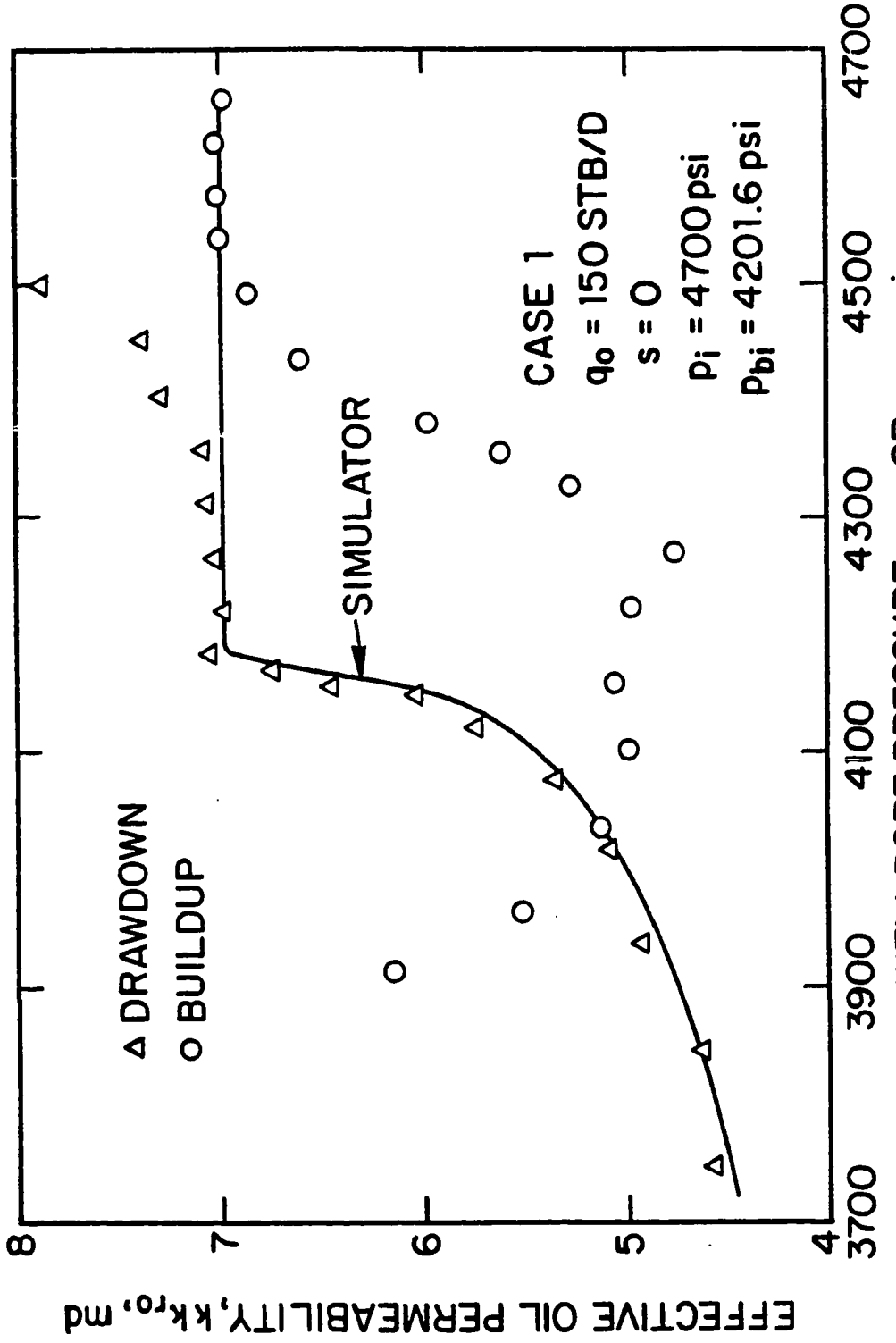

Fig. 4.3.3 - Effective oil permeability as a function of wellbore pressure; Case 1.

curve represents the sandface kk_{ro} values obtained from the simulator, the triangular data points correspond to drawdown kk_{ro} values computed by applying Eq. 4.1.1 and the circular data points correspond to buildup kk_{ro} values computed from Eq. 4.1.3. As in Refs. 8-11 and 28-30 which assumed $p_i = p_{bi}$, Eq. 4.1.1 does not yield accurate computed kk_{ro} values during the very early times of the drawdown test. However, for wellbore pressures such that $p_{bi} \leq p_{wf} \leq 4338$ psi, Eq. 4.1.1 provides kk_{ro} values which are in very good agreement with the initial value of $kk_{roi} = 7.0$ md. Immediately after the bubble-point pressure is crossed, Eq. 4.1.1 yields inaccurate kk_{ro} values, but at all subsequent times, yields good estimates of effective oil permeability. As shown in Fig. 4.3.3, the computed buildup kk_{ro} values provide good estimates of kk_{roi} during the late times of the buildup test, i.e., for times 0.33 days $< \Delta t <$ 3 days (4565 psi $< p_{ws} <$ 4659.4 psi). Note the results of Fig. 4.3.3 indicate that the initial value of effective oil permeability, kk_{roi}, can be distinguished from the flat part of the kk_{ro} versus wellbore pressure curves during either the drawdown or the buildup test period. Tables F-16 and F-17 show the simulated and computed kk_{rg} values as a function of wellbore pressure for both the drawdown and buildup tests, respectively. Effective gas permeability plotted versus the wellbore pressure is shown in Fig. 4.3.4. The solid curve represents the sandface kk_{rg} values obtained from the simulator, the triangular data points correspond to drawdown kk_{rg} values computed by applying Eq. 4.1.2 and the circular data points correspond to buildup kk_{rg} values computed from Eq. 4.1.4. Fig. 4.3.4 implies that the kk_{rg} values computed from drawdown pressure data, i.e., by applying Eq. 4.1.2, yield very accurate estimates of the effective gas permeabilities throughout the entire flow period. The kk_{rg} values computed from buildup pressure data, i.e., by applying Eq. 4.1.4, yield good estimates of the effective gas permeabilities only for $p_{ws} > 3981.9$ psi ($\Delta t > 1.0 \times 10^{-4}$ days). Note that if the wellbore pressure, p_{wf}, is larger than the initial bubble-point pressure, p_{bi}, Eq. 4.1.2 gives $kk_{rg} = 0$ because the sandface flow rate of free gas, $q_g(t)$, is zero.

Case 2 is similar to Case 1, i.e., the skin factor is zero and the wellbore pressure drops below the bubble-point pressure during the drawdown test, but its initial

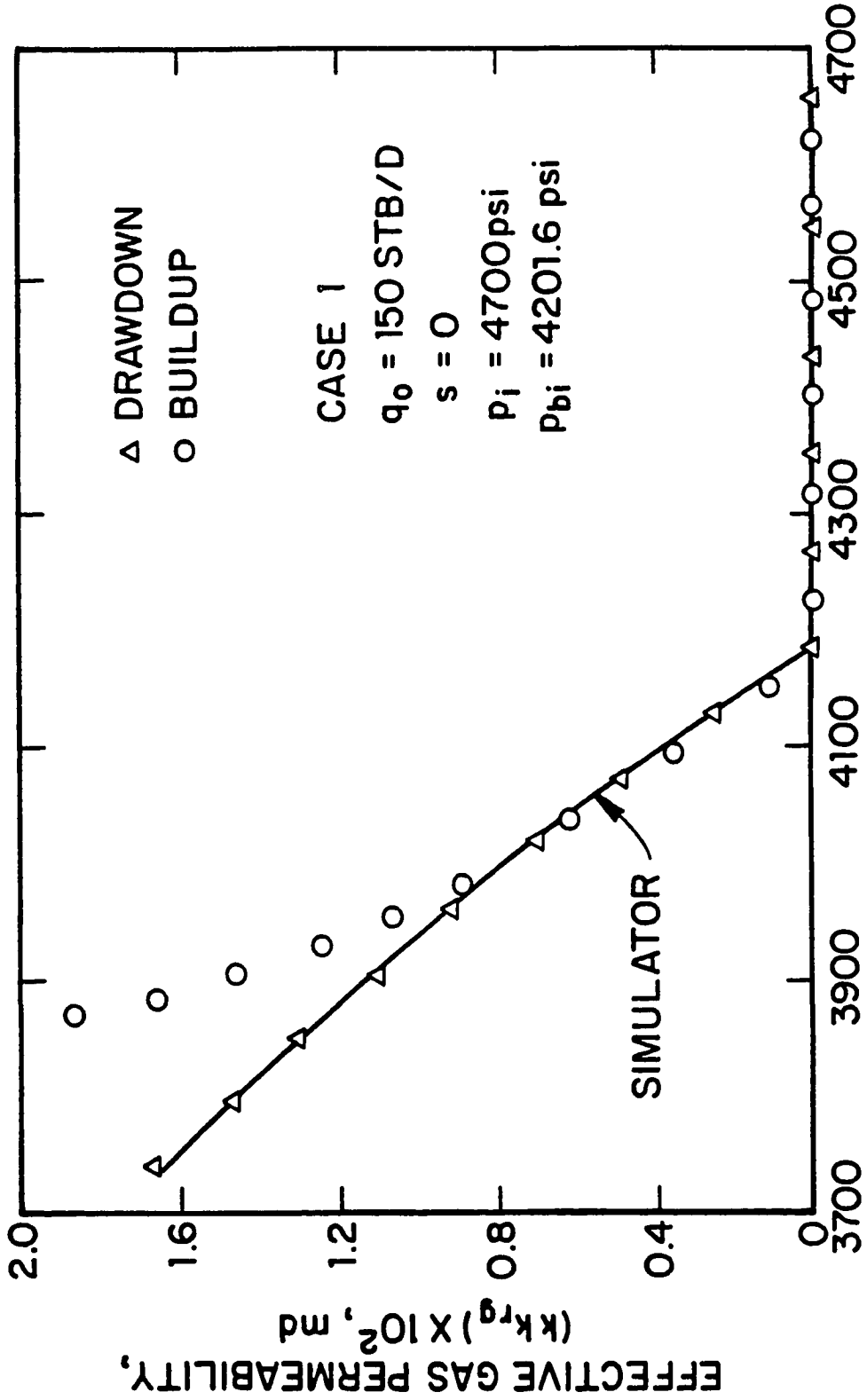

Fig. 4.3.4 - Effective gas permeability as a function of wellbore pressure; Case 1.

pressure is 200 psi closer to the initial bubble-point than in Case 2. Figs. 4.3.5 and 4.3.6, respectively, show the wellbore pressure and sandface oil saturation plotted versus time for both the drawdown and buildup tests for Case 2 (q_o = 150 STB/D, s = 0, p_i = 4500 psi and p_{bi} = 4201.6 psi). From the results of Figs. 4.3.5 and 4.3.6, it can be seen that the reservoir pressure crosses the bubble-point pressure at $t \approx 2.5 \times 10^{-4}$ days. Prior to this time, the sandface oil saturation remains constant (Fig. 4.3.6) and equal to the initial oil saturation, i.e., $S_{oi} = 0.7$. As soon as the p_{wf} decreases below p_{bi}, the sandface oil saturation drops very fast with the major drop occurring from time $t = 2.5 \times 10^{-4}$ days to $t = 1 \times 10^{-1}$ days ($0.63433 \leq S_o \leq 0.69974$). For times $t > 1 \times 10^{-1}$ days until the end of the test (t = 3 days), the sandface oil saturation only decreases slightly, from $S_o = 0.63433$ to $S_o = 0.61887$.

The results of computed effective oil permeability plotted versus the wellbore pressure for this case are shown in Fig. 4.3.7. The solid curve represents the sandface values of kk_{ro} obtained from the simulator, the triangular data points correspond to drawdown kk_{ro} values computed by applying Eq. 4.1.1 and the circular data points correspond to buildup kk_{ro} values computed from Eq. 4.1.3. This figure shows that the computed kk_{ro} values for $p_{wf} > 3995$ psi ($t < 6.5 \times 10^{-2}$ days) are not accurate. Unlike the results from Case 1, the initial pressure was not far enough from the initial bubble-point pressure to allow us to estimate kk_{roi} from the pressure drawdown data. When the wellbore pressure crosses the bubble-point pressure, the kk_{ro} values computed from Eq. 4.1.1 exhibit a hump which is probably due to discontinuities in the derivatives of PVT data, especially system compressibility, at the bubble-point pressure. After the wellbore pressure has dropped below the bubble-point pressure, Fig. 4.3.7 shows that the computed kk_{ro} values from Eq. 4.1.1 are reasonably accurate, i.e., agree with the correct (simulator) kk_{ro} values, for 3434 psi $< p_{wf} <$ 3995 psi (6.5×10^{-2} days $< t <$ 3.0 days). The kk_{ro} values computed from buildup pressure data exhibit the same behavior as the one described in Refs. 10, 28, and 30 as long as the wellbore pressure is below the initial bubble-point pressure. However, as shown in Fig. 4.3.7, the kk_{ro} values computed from buildup pressure data give good estimates of kk_{roi} at late times, i.e., for times 0.94

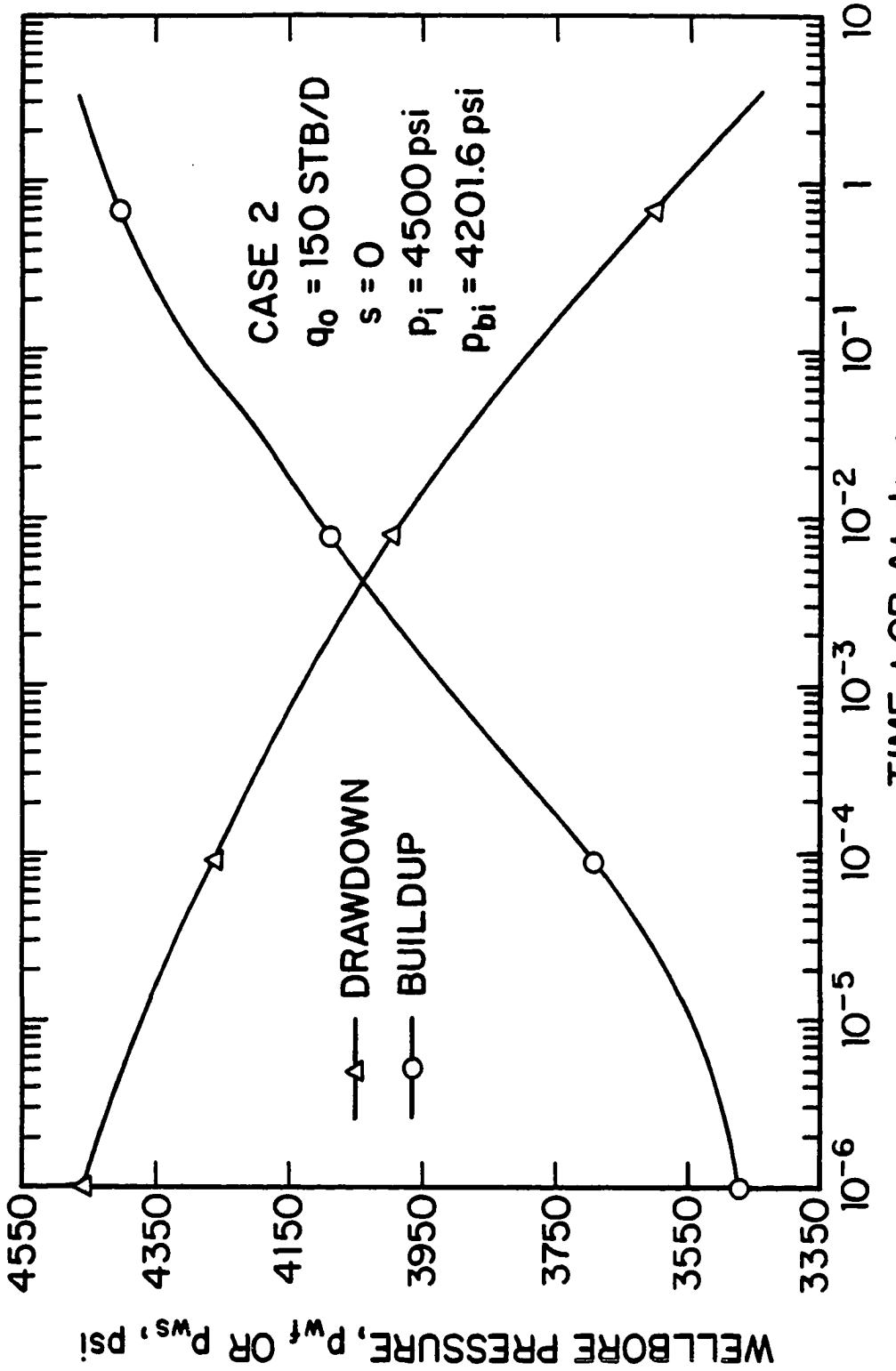

Fig. 4.3.5 - Drawdown and buildup wellbore pressures; Case 2.

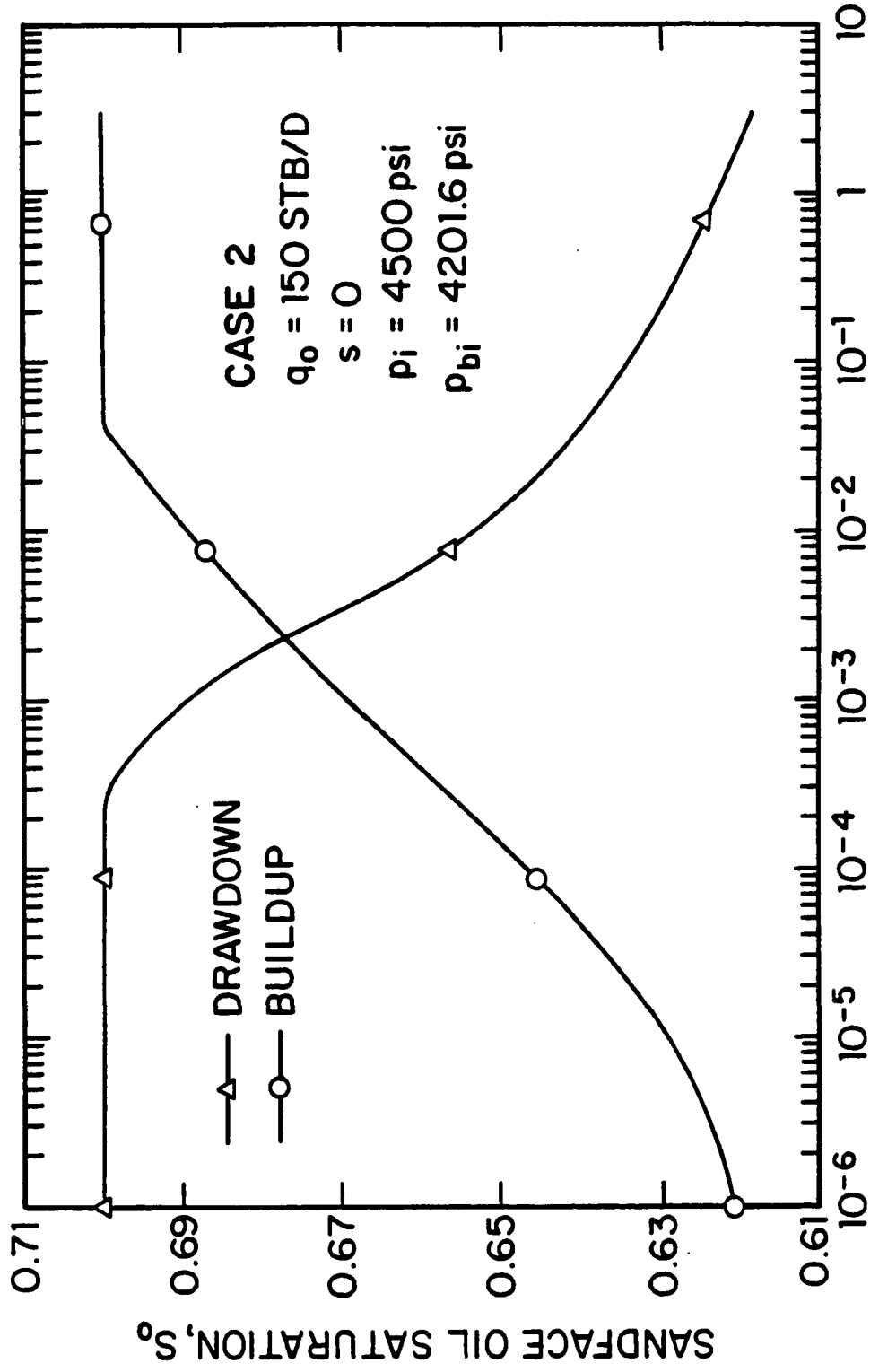

Fig. 4.3.6 - Drawdown and buildup sandface oil saturation; Case 2.

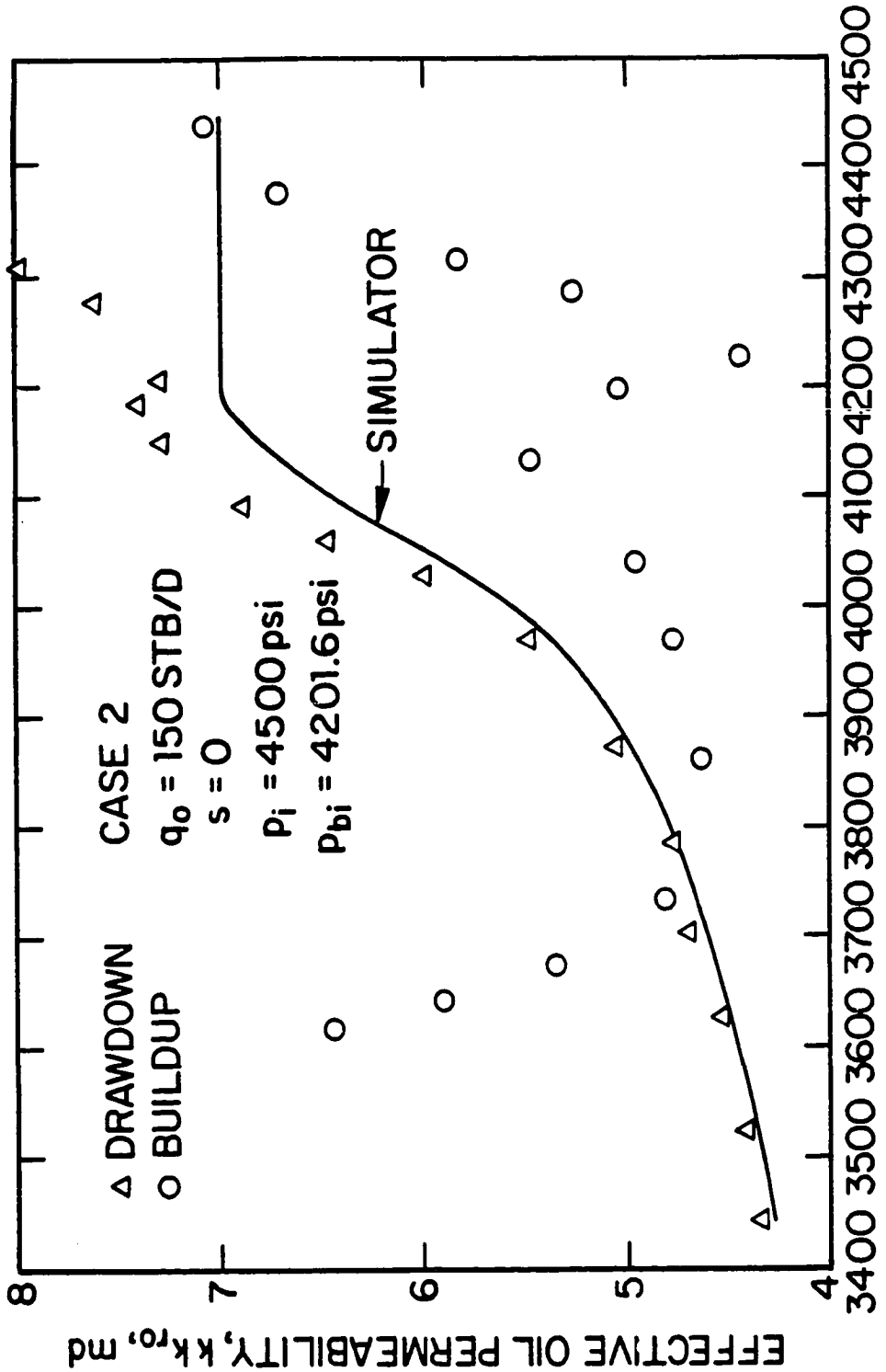

Fig. 4.3.7 - Effective oil permeability as a function of wellbore pressure; Case 2.

days $< \Delta t <$ 3 days (4417 psi $< p_{wf} <$ 4460 psi). Fig. 4.3.8 presents a plot of effective gas permeability versus the wellbore pressure for Case 2. The solid curve represents the sandface kk_{rg} values obtained from the simulator, the triangular data points correspond to drawdown kk_{rg} values computed by applying Eq. 4.1.2 and the circular data points correspond to buildup kk_{ro} values computed from Eq. 4.1.4. As in Case 1, the kk_{rg} values computed from drawdown pressure data in this case (Case 2) yield very accurate estimates of the effective gas permeabilities throughout the entire flow period. Fig. 4.3.8 shows that the kk_{rg} values computed from buildup pressure data yield good estimates of the effective gas permeabilities only for $p_{wf} >$ 3700.9 psi ($\Delta t > 1.0 \times 10^{-4}$ days).

Case 3, the last case considered in this subsection, pertains to the case where the skin factor is zero and the initial reservoir is much higher than the initial bubble-point pressure so that the reservoir remains undersaturated during the entire drawdown test period. The wellbore pressure and sandface oil saturation plotted versus time for the Case 3 drawdown and buildup tests is shown in Figs. 4.3.9 and 4.3.10, respectively. Recall that for this case, the oil flow rate is $q_o = 150$ STB/D, the skin factor $s = 0$, the initial reservoir pressure is $p_i = 5500$ psi and the initial bubble-point pressure is $p_{bi} = 4201.6$ psi. From the results of Figs. 4.3.9 and 4.3.10, it can be seen that the reservoir pressure never crosses the bubble-point pressure. (The very small saturation changes shown in Fig. 4.3.10 are due to numerical problems in the simulator.) In the results obtained from the simulator, the sandface oil saturation varies in the interval $0.69923 < S_o < 0.7$.

The results of computed effective oil permeability plotted versus the wellbore pressure for this case are shown in Fig. 4.3.11. The solid curve represents the sandface kk_{ro} values obtained from the simulator, the triangular data points correspond to drawdown kk_{ro} values computed by applying Eq. 4.1.1 and the circular data points correspond to buildup kk_{ro} values computed from Eq. 4.1.3. This figure shows that the computed kk_{ro} values are not accurate at the beginning of the drawdown test or at early shut-in times. However, for wellbore pressures such that 4641 psi $\leq p_{wf} \leq$ 5050 psi (3.0×10^{-3} days $\leq t \leq$ 3.0 days) Eq. 4.1.11 yields accurate

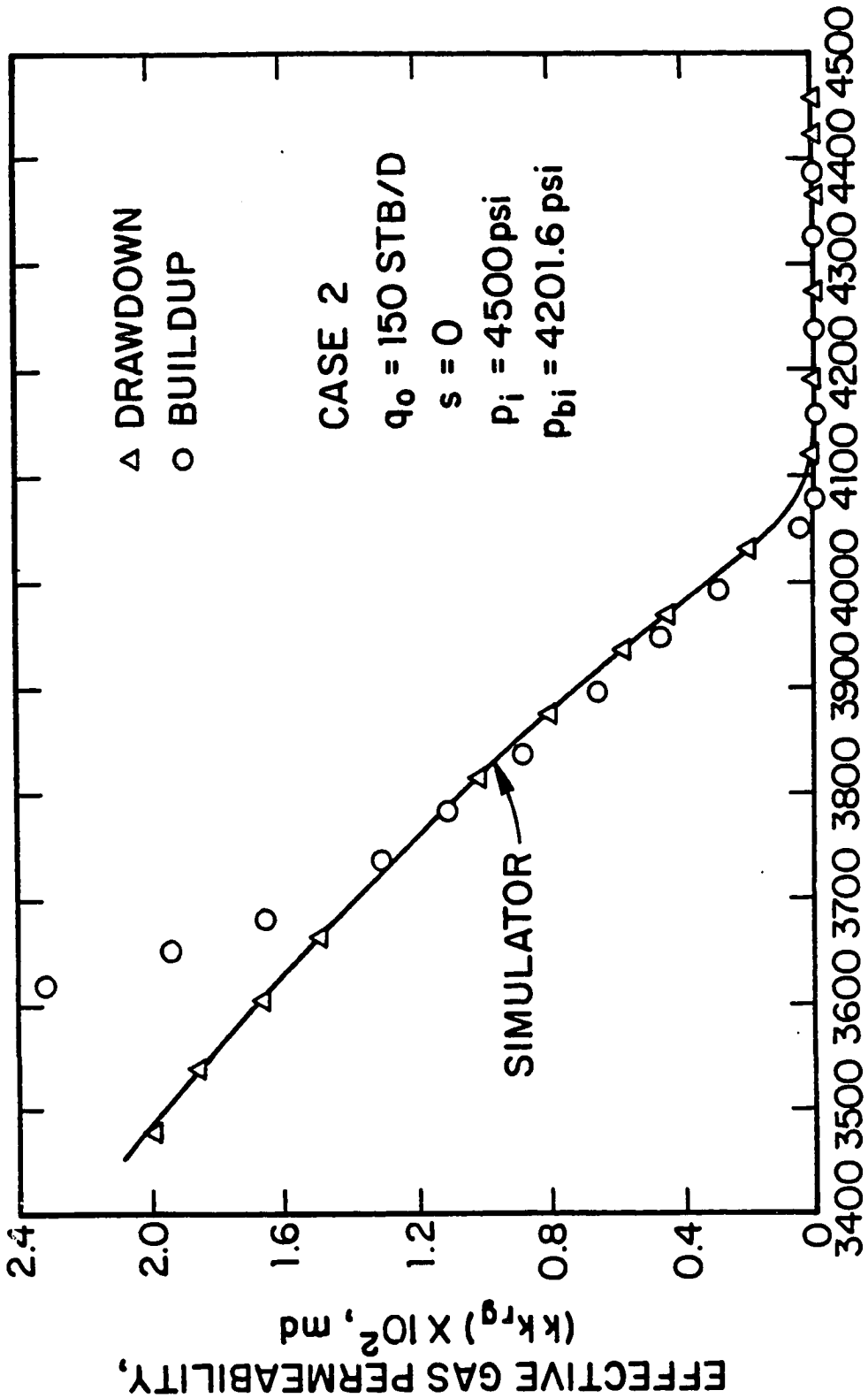

Fig. 4.3.8 - Effective gas permeability as a function of wellbore pressure; Case 2.

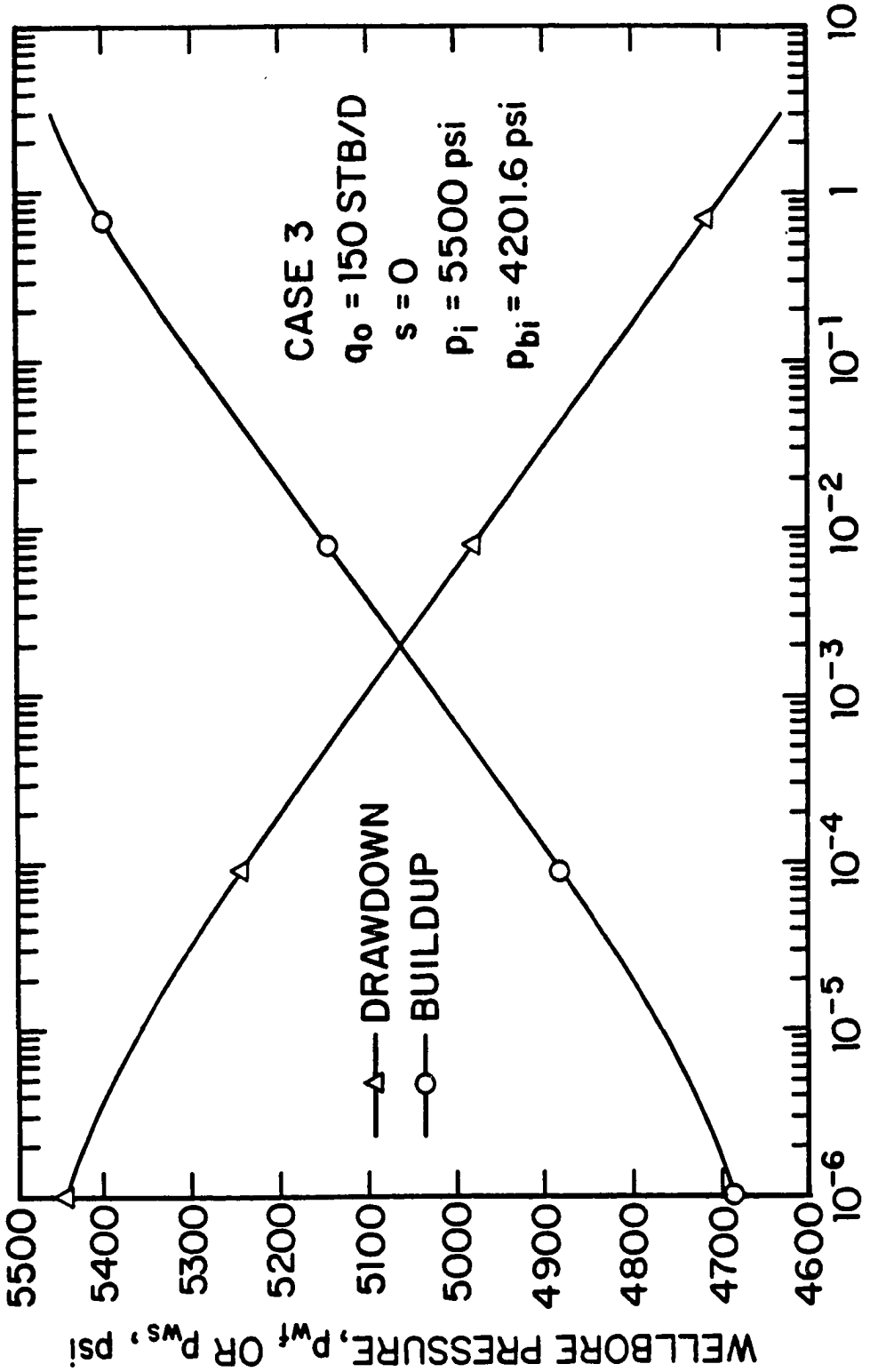

Fig. 4.3.9 - Drawdown and buildup wellbore pressures; Case 3.

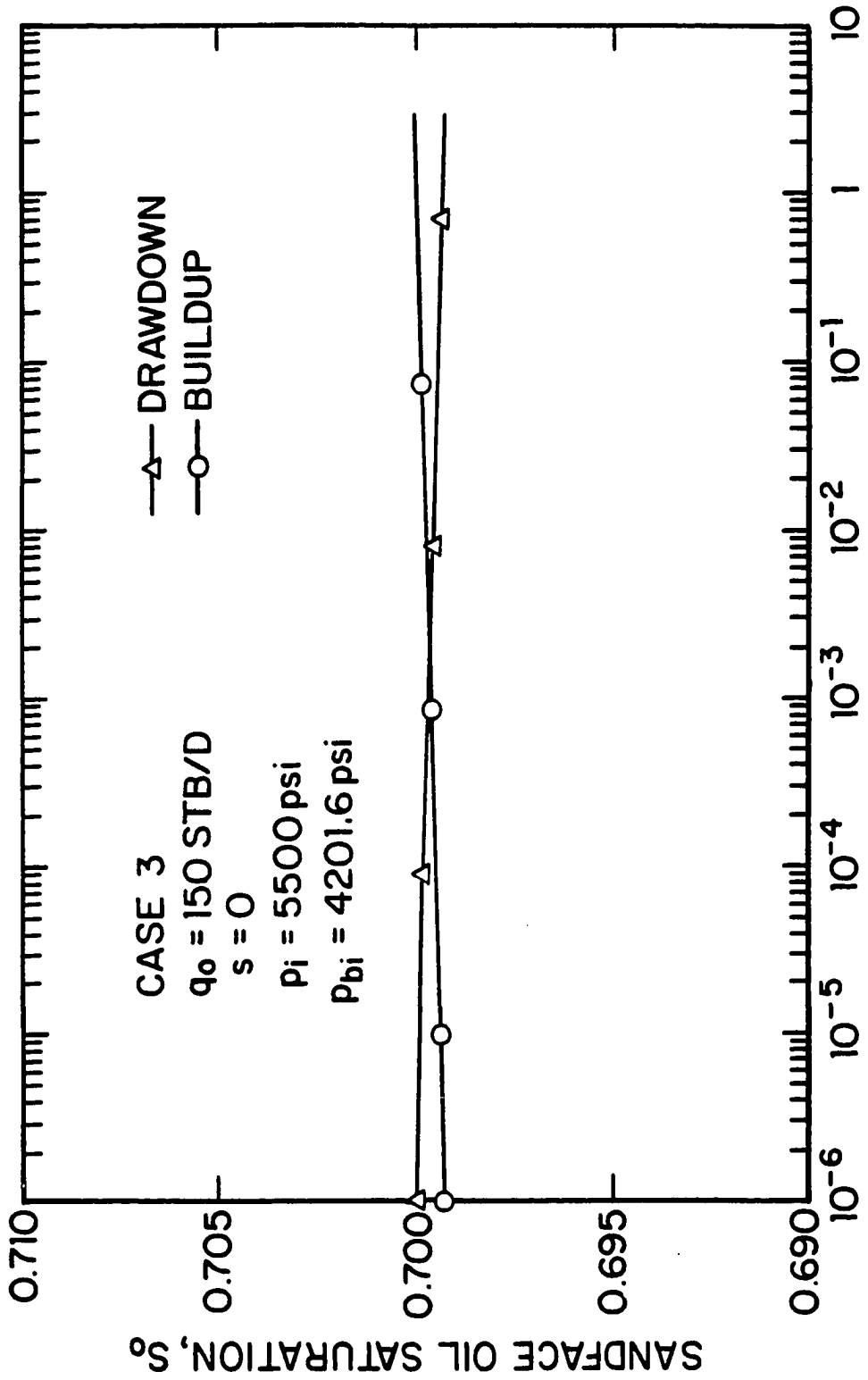

Fig. 4.3.10 - Drawdown and buildup sandface oil saturation; Case 3.

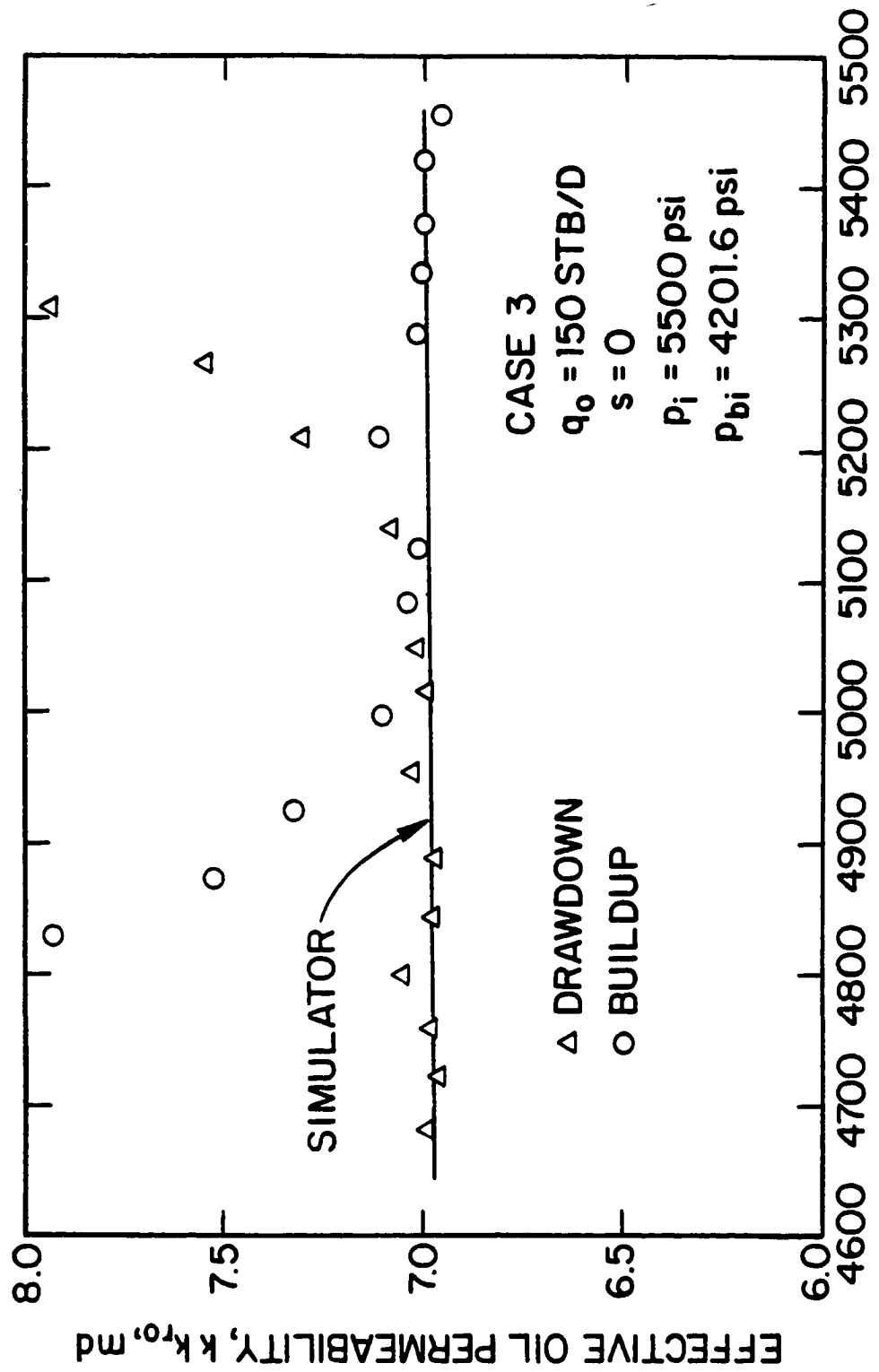

Fig. 4.3.11 - Effective oil permeability as a function of wellbore pressure; Case 3.

results from drawdown data. For 5085 psi $\leq p_{wf} \leq$ 5458 psi (3.0×10^{-3} days $< \Delta t \leq$ 3.0 days) good estimates of kk_{roi} are obtained from buildup data by application of Eq. 4.1.3. The initial value of effective oil permeability, kk_{roi}, corresponds to the flat part of the kk_{ro} versus wellbore pressure curves of Fig. 4.3.11 during both the drawdown and the buildup test periods. Since the reservoir remains undersaturated during the flow period, the computed kk_{rg} values from both drawdown and buildup pressure data tests are zero and agree with the actual (simulator) kk_{rg} values.

Comparing the computed effective oil permeabilities for Cases 1-3, one can conclude that accurate estimates of the initial effective oil permeability kk_{roi} can be obtained from buildup pressure-time data. If p_i is sufficiently greater than p_{bi} or the flow rate is low enough so that p_{wf} remains above p_{bi} for a sufficiently long time, kk_{roi} can also be obtained from drawdown pressure data.

4.3.2 Non-Zero Skin Cases.

In this subsection, we investigate the accuracy of Eqs. 4.1.1 and 4.1.3 for cases where the skin factor is non-zero.

We first consider Case 4 which is similar to Case 3 in that the wellbore pressure remains above the initial bubble-point pressure for all times considered. The wellbore pressure and sandface oil saturation plotted versus time for Case 4 drawdown and buildup tests are shown in Figs. 4.3.12 and 4.3.13, respectively. Recall that for this case, the oil flow rate is q_o = 50 STB/D, the skin factor s = 5, the initial reservoir pressure p_i = 4800 psi and the initial bubble-point pressure is p_{bi} = 4201.6 psi. Note that in the results obtained from the simulator (Fig. 4.3.13), the sandface oil saturation varies in the interval $0.69959 < S_o < 0.7$. The very small saturation changes shown in Fig. 4.3.13 are due to numerical problems in the simulator.

Effective oil permeability plotted versus the wellbore pressure for Case 4 are shown in Fig. 4.3.14. The solid curve represents the kk_{ro} values from the simulator, the triangular data points correspond to drawdown kk_{ro} values computed by applying Eq. 4.1.1 and the circular data points correspond to kk_{ro} values computed from buildup pressure data with Eq. 4.1.3. This figure shows that the computed kk_{ro}

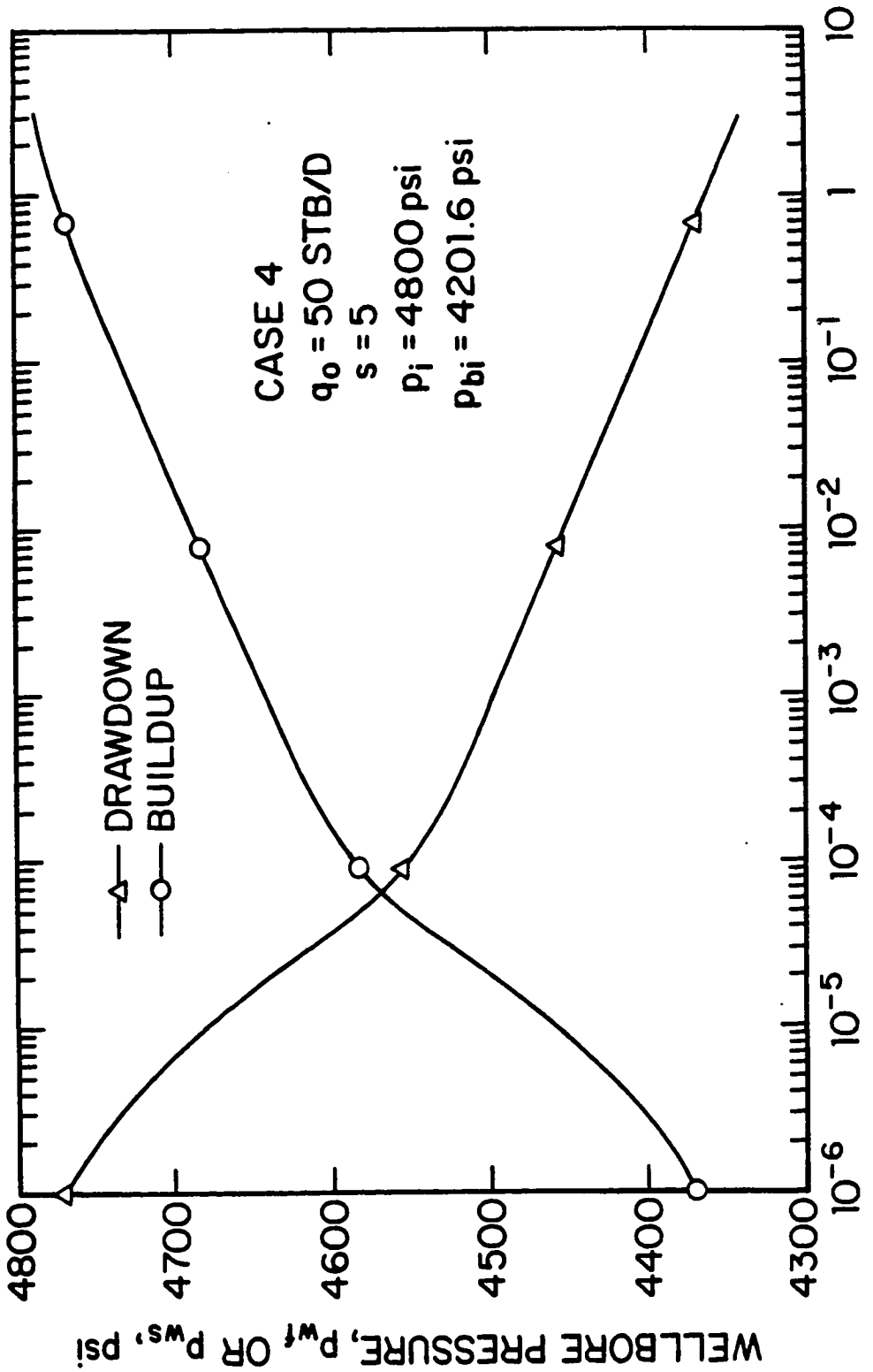

Fig. 4.3.12 - Drawdown and buildup wellbore pressures; Case 4.

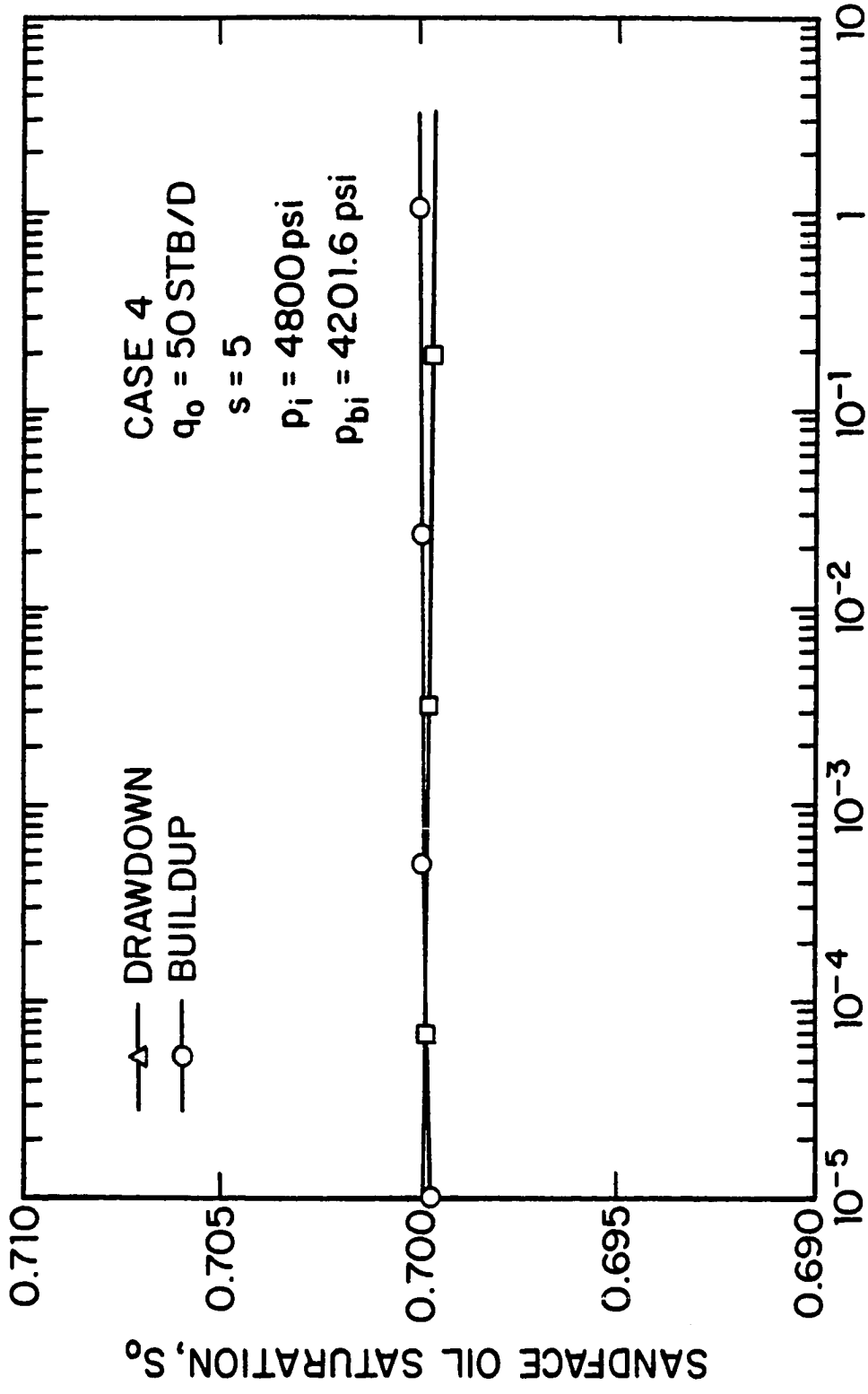

Fig. 4.3.13 - Drawdown and buildup sandface oil saturation; Case 4.

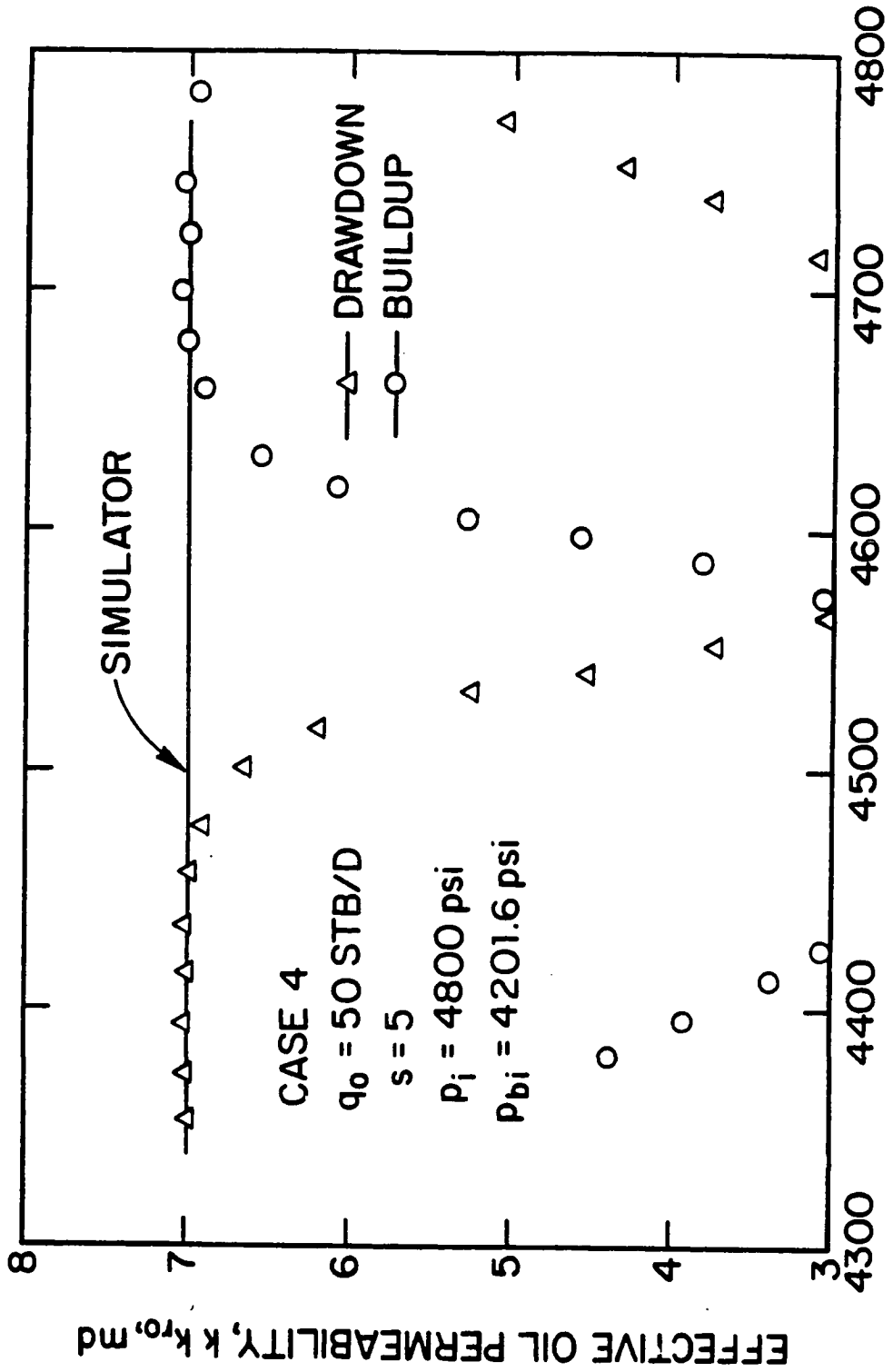

Fig. 4.3.14 - Effective oil permeability as a function of wellbore pressure; Case 4.

values at the early times of the drawdown and buildup tests are very inaccurate. This behavior has also been observed in Refs. 8-11 and 28-30 and is due to the altered permeability in the skin zone. More specifically, Eqs. 4.1.1 and 4.1.3 will not yield accurate estimates of kk_{ro} until the skin zone reaches a steady-state behavior. However, for wellbore pressures 4340.44 psi $\leq p_{wf} \leq$ 4476 psi (2.8×10^{-3} days $\leq t \leq$ 3.0 days) for drawdown data, and 4663 psi $\leq p_{ws} \leq$ 4786 psi (2.8×10^{-3} days $< \Delta t \leq$ 3.0 days) for buildup data, Eqs. 4.1.1 and 4.1.3 provide kk_{ro} values which are in very good agreement with the correct value of $kk_{roi} = 7.0$ md. The value of kk_{roi} can be distinguished from the flat part of the kk_{ro} versus wellbore pressure curves during both the drawdown and the buildup test period. The results of Fig. 4.3.14 illustrate that if a drawdown or buildup test is long enough for the skin zone to reach a steady-state behavior, Eqs. 4.1.1 and 4.1.3 will yield accurate estimates of the initial effective oil permeability in the case where the reservoir remains undersaturated throughout the test period. The kk_{rg} values computed from drawdown and buildup pressure data exhibit the same behavior as the ones in Case 3.

Case 5 pertains to the case where the skin factor is not zero, $p_i = 4600$ psi $> p_{bi} = 4201.6$ psi, but p_{wf} drops below the initial bubble-point pressure during the flow period. In Case 5, the oil flow rate is $q_o = 50$ STB/D, and $s = 5$. Figs. 4.3.15 and 4.3.16, respectively, show the wellbore pressure and sandface oil saturation plotted versus time for both the drawdown and buildup tests. It can be seen that the flowing wellbore pressure crosses the bubble-point pressure at about $t = 0.154$ days. Prior to this time, the sandface oil saturation remains constant and equal to the initial oil saturation, i.e., $S_{oi} = 0.7$. As soon as p_{wf} decreases below p_{bi}, the sandface oil saturation drops rapidly with the major drop occurring from $t = 0.154$ days to $t = 0.298$ days ($0.67394 \leq S_o \leq 0.69945$). For times $t > 0.298$ days until the end of the test, i.e. $t = 3$ days, the sandface oil saturation decreases from $S_o = 0.67394$ to $S_o = 0.65690$.

Effective oil permeability plotted versus the wellbore pressure for Case 5 are shown in Fig. 4.3.17. The solid curve represents the sandface kk_{ro} values from the

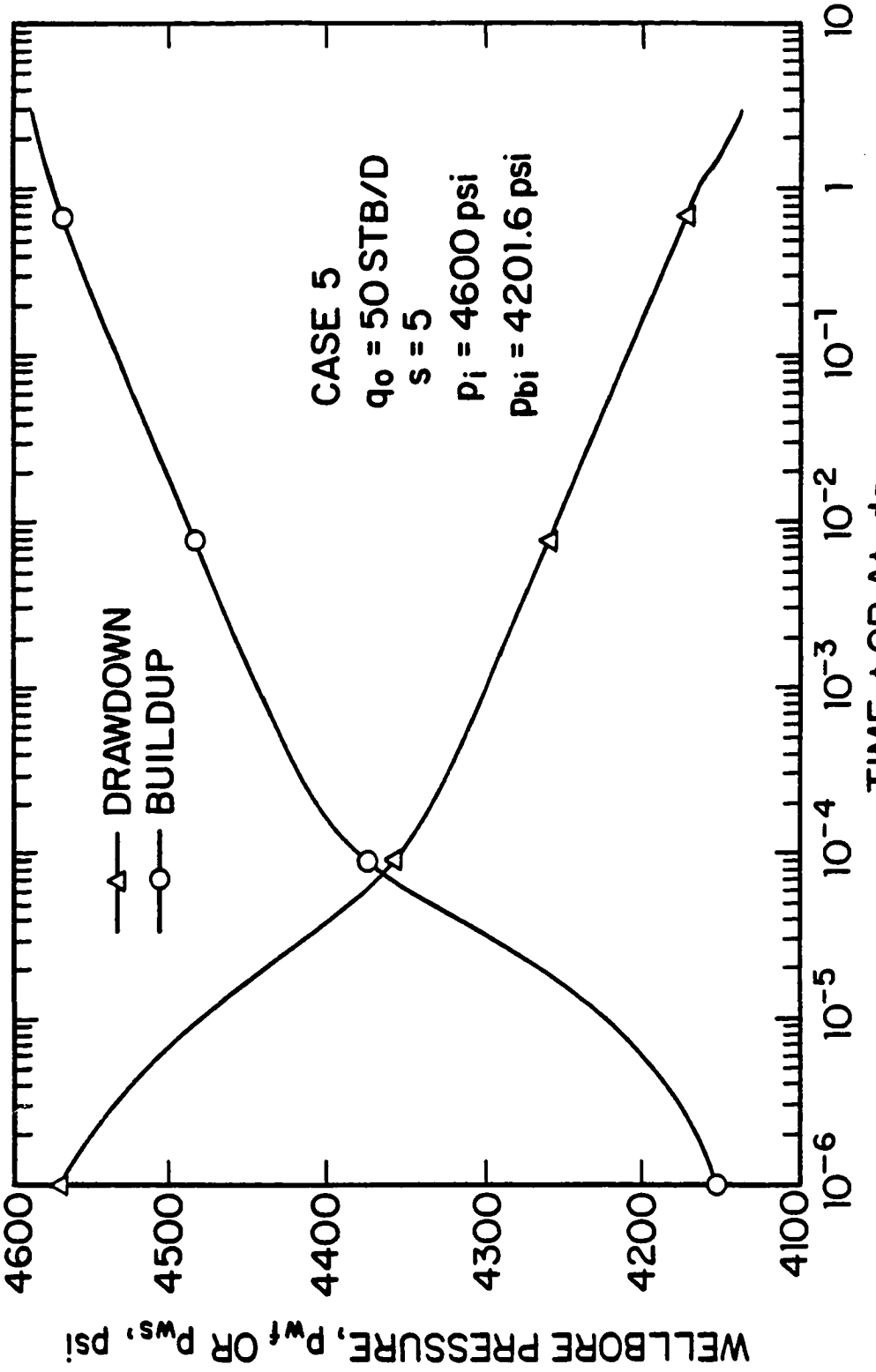

Fig. 4.3.15 - Drawdown and buildup wellbore pressures; Case 5.

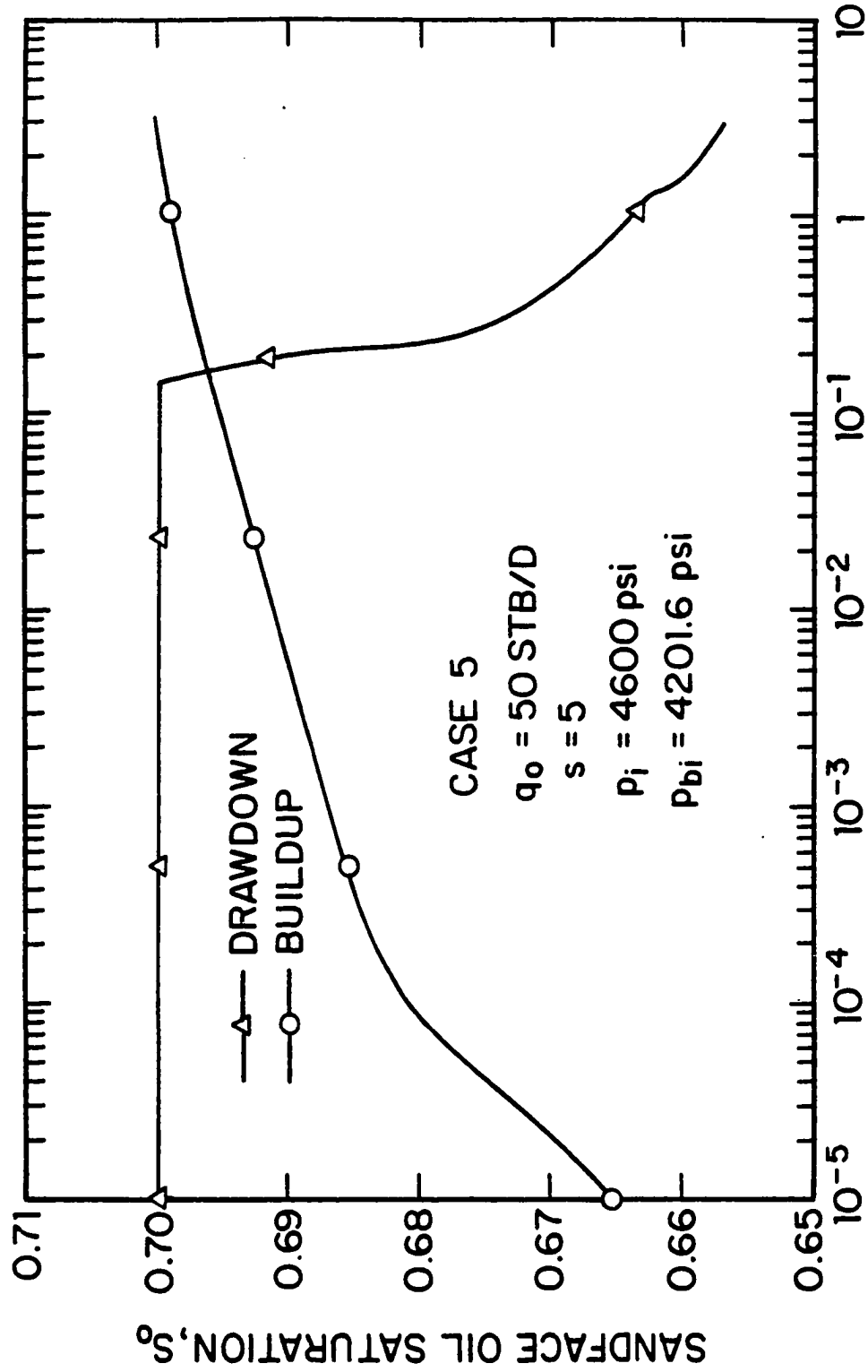

Fig. 4.3.16 - Drawdown and buildup sandface oil saturation; Case 5.

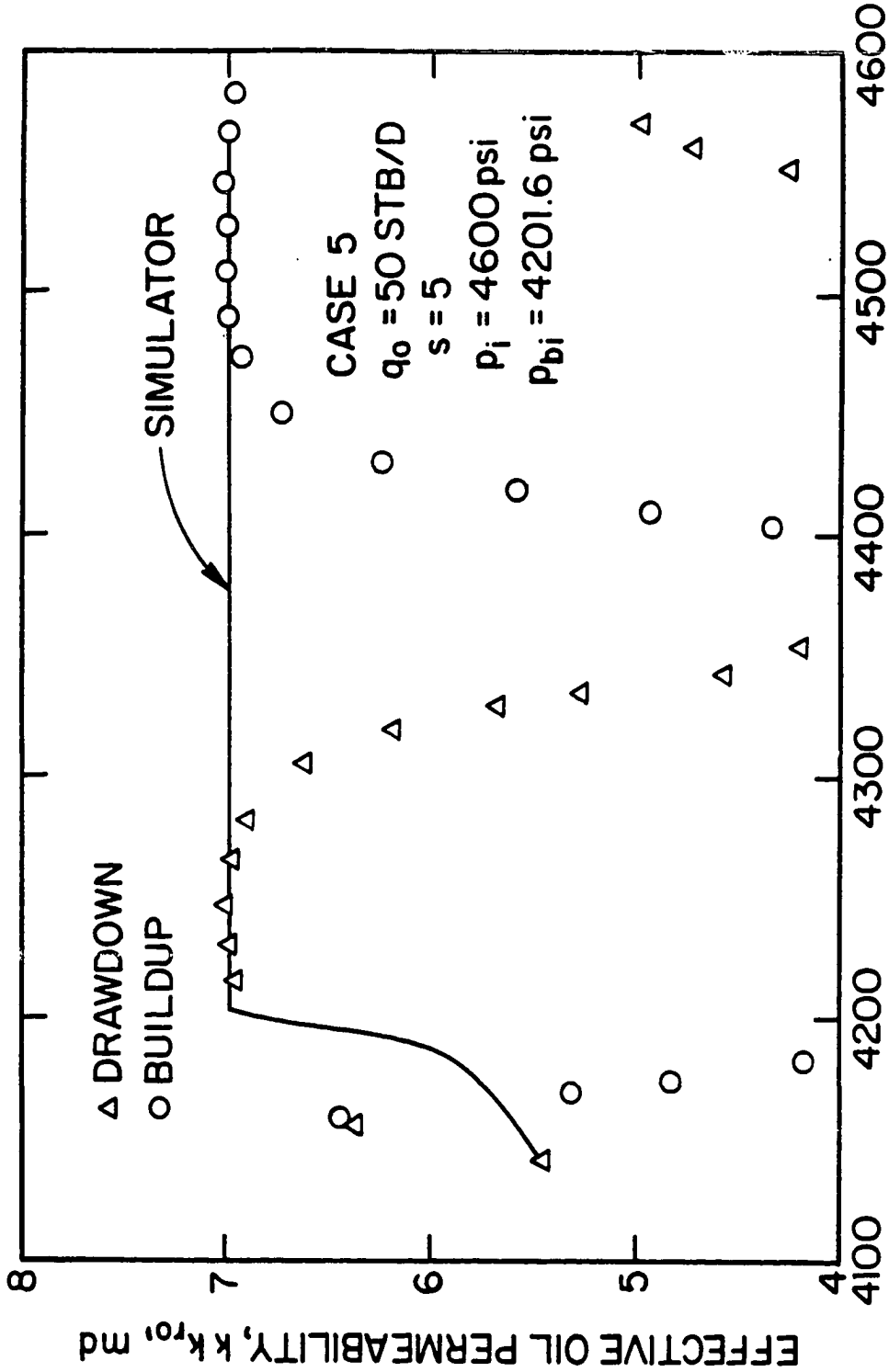

Fig. 4.3.17 - Effective oil permeability as a function of wellbore pressure; Case 5.

simulator, the triangular data points correspond to drawdown kk_{ro} values computed by applying Eq. 4.1.1 and the circular data points correspond to buildup kk_{ro} values computed from Eq. 4.1.3. This figure shows that the computed kk_{ro} values at the early times of the drawdown test are not accurate. As in Case 4, this is due to the presence of the skin zone. However, for wellbore pressures $p_{bi} \leq p_{wf} \leq 4273$ psi ($3.7 \times 10^{-3} \leq t$ days) Eq. 4.1.1 provides kk_{ro} values which are in very good agreement with the correct value of the initial effective oil permeability, $kk_{roi} = 7.0$ md. After the wellbore pressure has dropped below the bubble-point pressure the simulator wellbore pressure is not a smooth function as shown in Fig. 4.3.15; for example, see data at $t \approx 1.5$ days. Results not shown indicate that the pressure derivative with respect to the logarithm of time (see Eq. 4.1.1) is quite noisy for $t > 0.154$ days. To improve the quality of pressure derivatives computed from the pressure data below bubble-point, we smoothed the pressure data by averaging them using a window of a quarter of a log cycle. By doing so, we obtained only two kk_{ro} values during the times that the pressure was below the initial bubble-point pressure and they are shown in Fig. 4.3.17. Only the second of these kk_{ro} values is in good agreement with the simulator data. The kk_{ro} values computed from buildup pressure data exhibit the same behavior as the one described in Refs. 10, 28, and 30 as long as the wellbore pressure is below the initial bubble-point pressure. However, as is shown in Fig. 4.3.17 the computed buildup kk_{ro} values yield good estimates of kk_{roi} values during the late times of the test, i.e., for times 8.2×10^{-3} days $< \Delta t < 3$ days (4485 psi $< p_{ws} <$ 4586 psi). Therefore, the value of kk_{roi} can be distinguished from the flat part of the kk_{ro} versus wellbore pressure curves during either the drawdown or the buildup test period.

4.4 Estimation of kk_{ro} and kk_{rg} Curves

In this section we use the methods presented in Chapter 3 (see also Hatzignatiou and Reynolds[37]) to construct the effective (or relative) permeability curves. These methods apply either a nonlinear regression analysis technique or Powell's method for solving a system of nonlinear equations to kk_{ro} and k_{rg}/k_{ro} values computed

from pressure drawdown data to estimate the effective (or relative) permeability curves based on Standing's[15] correlations.

We first apply the nonlinear regression analysis technique to the *simulated* kk_{ro} and k_{rg}/k_{ro} values for Case 1. Using all the simulated effective oil permeability values, kk_{ro}, and k_{rg}/k_{ro} corresponding to $kk_{ro} \leq 6.9822$ md in our nonlinear regression analysis program, we were able to obtain estimates of the unknown parameters λ, kk_r^o, S_{gc} and S_{wc} by using the Gauss method. We used penalty functions in forming the Hessian matrix, H, Cholesky factorization in solving the matrix problem, and Bard's[16] line search method in updating the solution vector. Throughout, kk_r^o represents the values of effective oil permeability at irreducible water saturation. For all cases considered in this Chapter, $kk_r^o = kk_{roi}$.

Assuming that the values of S_{gc} and S_{wc} are known and using $kk_r^o = 6.9826$ md and $\lambda = 1$ as initial guesses, the values of the estimated parameters obtained are $kk_r^o = 7.007$ md and $\lambda = 1.958$. These values are essentially identical to the correct values of $kk_r^o = 7.0$ md and $\lambda = 2.0$. The variation of the estimated parameters as a function of iteration number is shown in Table F-18. The approximate confidence intervals of the estimated parameters with 95% confidence are: 6.9999 md $\leq kk_r^o \leq$ 7.015 md and $1.950 \leq \lambda \leq 1.966$.

Assuming that only the value of S_{wc} is known and using $kk_r^o = 6.9826$ md, $\lambda = 1$ and $S_{gc} = 1.0 \times 10^{-20}$ as initial guesses, the values of the estimated parameters obtained are $kk_r^o = 7.010$ md, $\lambda = 1.938$ and $S_{gc} = 2.37 \times 10^{-20}$. These values are in excellent agreement with the correct values of $kk_r^o = 7.0$ md, $\lambda = 2.0$ and $S_{gc} = 0.0$. The variation of the estimated parameters as a function of iteration number is shown in Table F-19. The approximate confidence intervals of the estimated parameters with 95% confidence are: 7.002 md $\leq kk_r^o \leq$ 7.019 md, $1.93 \leq \lambda \leq 1.946$ and $-8.313 \times 10^{-3} \leq S_{gc} \leq 8.131 \times 10^{-3}$.

Assuming none of the four parameters is known a priori, and using $kk_r^o = 6.9826$ md, $\lambda = 1$, $S_{gc} = 1.0 \times 10^{-20}$ and $S_{wc} = 0.1$ as initial guesses, the values of the estimated parameters obtained are $kk_r^o = 7.007$ md, $\lambda = 1.974$, $S_{gc} = 1.07 \times 10^{-19}$ and $S_{wc} = 0.3109$. These values agree very well with the correct values of $kk_r^o = 7.0$

md, $\lambda = 2.0$, $S_{gc} = 0.0$ and $S_{wc} = 0.3$. The variation of the estimated parameters as a function of iteration number is shown in Table F-20. The approximate confidence intervals of the estimated parameters with 95% confidence are: 6.997 md $\leq kk_r^o \leq$ 7.017 md, $1.963 \leq \lambda \leq 1.984$, $-1.03 \times 10^{-2} \leq S_{gc} \leq 1.03 \times 10^{-2}$ and $0.301 \leq S_{wc} \leq$ 0.321.

As in Chapter 3, using these computed parameter values, one can compute the oil and gas effective permeability curves based on Standing's correlations (see also Ref. 37). If the value of the absolute permeability is known, the relative permeability curves can be obtained. Alternatively, one can obtain relative permeability curves by normalizing (dividing) effective permeability curves by the value of $kk_r^o = kk_{roi}$ obtained. Fig. 4.4.1 shows a graph of effective oil and gas permeabilities versus oil saturation. The solid curve represents the correct (simulator) oil and gas effective permeability curves, whereas the data points correspond to the oil and gas effective permeabilities computed using the values of the parameters estimated from nonlinear regression analysis. The circular data points correspond to the case where only λ and kk_r^o were estimated by regression analysis and S_{wc} and S_{gc} were assumed known. The square data points correspond to the case where the three parameters, λ, kk_r^o and S_{wc}, were obtained from regression analysis. The triangular data points correspond to the case where all four parameters were estimated by regression analysis. The results shown in this figure imply that one can use nonlinear regression analysis to construct effective (or relative) permeability curves for the cases where the initial reservoir pressure is larger than the initial bubble-point pressure.

However, when we applied nonlinear regression analysis techniques to the kk_{ro} and k_{rg}/k_{ro} values computed from pressure drawdown data for Case 1, we did not obtain accurate estimates of the unknown parameters kk_r^o, λ, S_{gc} and S_{wc}. For example, for the case of two unknown parameters, kk_r^o and λ, the estimated values were $kk_r^o = 7.45$ md and $\lambda = 0.844$ which do not agree well with the simulator values of $kk_r^o = 7.0$ md and $\lambda = 2.0$.

Alternately, as in Chapter 3 and Ref. 37, we can use computed values of kk_{ro}

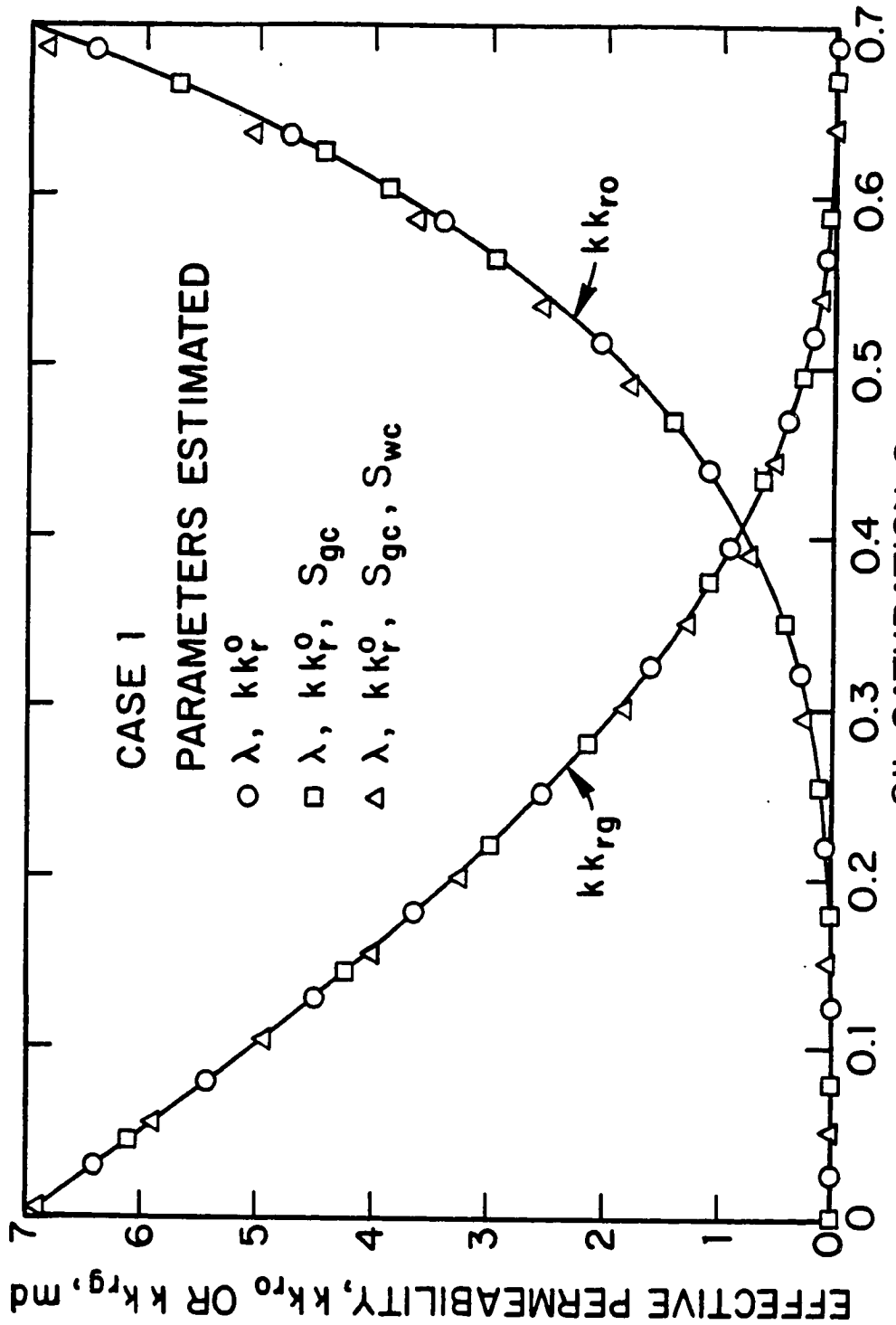

Fig. 4.4.1 - Plot of effective oil and gas permeability curves; Case 1.

and k_{rg}/k_{ro} to obtain a system of nonlinear equations which can be solved by using Powell's method. Assuming that the values of S_{gc} and S_{wc} are known *a priori*, we used the computed sets of data kk_r^o = 7.0095 md, k_{rg}/k_{ro} = 0.0 and kk_r^o = 4.4682 md, $k_{rg}/k_{ro} = 0.38730 \times 10^{-2}$ with kk_r^o = 4.4682 md and $\lambda = 0.5$ as initial guesses to obtain kk_r^o = 7.073 md and $\lambda = 2.11$ as the values of the estimated parameters. These values are in good agreement with the correct values of kk_r^o = 7.0 md and $\lambda = 2.0$. Fig. 4.4.2 shows a plot of the actual (simulator) effective permeability curves (solid curves) and the effective permeability curves (circular data points) constructed by using the estimated parameter values in Standing's relative permeability correlations. The results shown in this figure suggest that one can apply Powell's method to solve a nonlinear system of equations in order to construct effective (or relative) permeability curves for the cases where the initial reservoir pressure is larger than the initial bubble-point pressure. Note, however, that by using this technique the accuracy of the estimated parameters depends heavily on the accuracy of the data used to obtain the system of nonlinear equations. To illustrate this point we used the computed sets of data kk_r^o = 7.0095 md, k_{rg}/k_{ro} = 0.0 and kk_r^o = 4.5291 md, $k_{rg}/k_{ro} = 0.39443 \times 10^{-2}$ with kk_r^o = 4.4682 md and $\lambda = 0.5$ as initial guesses and we obtained kk_r^o = 7.073 md and $\lambda = 4.75$ as the values of the estimated parameters as compared to the correct values of kk_r^o = 7.0 md and λ = 2.0.

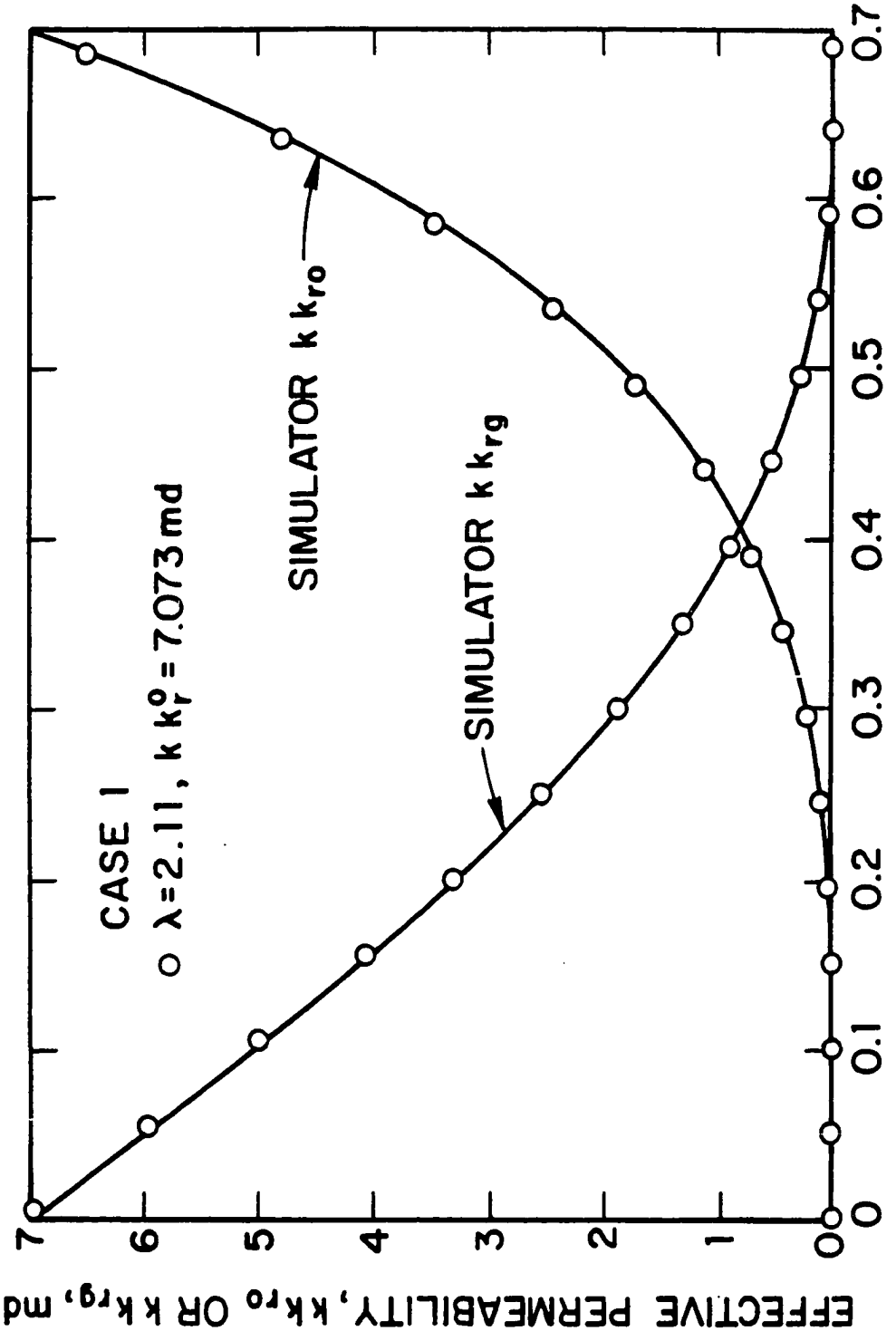

Fig. 4.4.2 - Plot of effective oil and gas permeability curves; Case 1

CHAPTER V
ESTIMATION OF EFFECTIVE PERMEABILITIES FOR HETEROGENEOUS RESERVOIRS

This Chapter investigates the effects of heterogeneities on the estimates of effective or relative permeabilities. The heterogeneous system considered in this Chapter is that of a two-zone composite reservoir with different absolute permeability and/or relative permeability curves in the two regions. It is shown that the effective permeabilities estimated from pressure drawdown or buildup data reflect, at early times, the inner zone effective permeability data, and at later times reflect the outer zone effective permeability data for the oil phase. In general, the effective gas permeability of the outer zone cannot be obtained.

5.1 INTRODUCTION

In the last few years, the estimation of effective (relative) permeability curves from well-test pressure data has been the subject of several studies. Refs. 8, 9 and 28 have presented methods for estimating effective permeability as a pointwise function of the wellbore pressure. Ref. 8 used drawdown pressure data obtained from multirate tests, whereas Refs. 9 and 28 used drawdown pressure data obtained from single-rate constant oil rate production tests. In addition, Refs. 10 and 28 presented computational methods of estimating effective permeability values as a pointwise function of shut-in wellbore pressure from pressure buildup data. Refs. 29 and 30 extended the ideas of Refs. 9, 10 and 28 to present computational procedures for estimating effective permeability values in the presence of wellbore storage effects.

Furthermore, Al-Khalifah et al.[11] (also see Refs. 8-10, and 28-30) showed that one can compute effective (relative) permeability versus oil saturation data provided

accurate estimates of the sandface oil saturation/wellbore pressure relationship can be estimated. In Chapter 3 (also see Hatzignatiou and Reynolds[37]) we circumvented the problem of the estimation of sandface oil saturation versus wellbore pressure. We presented a new method for estimating effective or relative permeability curves, based on Standing's[15] correlations and the application of nonlinear regression analysis techniques. The results of Refs. 8-11, 28-30 and 37 assumed that the initial reservoir pressure was equal to the initial bubble-point pressure. In Chapter 4 (also see Hatzignatiou and Reynolds[38]) we presented results which show that the computation procedures of estimating effective (relative) permeability values as a pointwise function of pressure (Refs. 8-10 and 28) can also be applied to the cases where the initial reservoir pressure is larger than the initial bubble-point pressure. Ref. 38 also showed that accurate estimates of the initial oil effective (relative) permeability can be computed provided the initial reservoir pressure is sufficiently larger than the initial bubble-point pressure (for the case of a drawdown test) or the test is long enough (buildup test).

Al-Khalifah et al.[8] showed that one can use pressure drawdown data obtained from a multirate test to obtain estimates of effective (relative) permeability values for heterogeneous systems. The authors presented results for a system which consisted of a small region, concentric with the wellbore, with relative permeability curves different from the relative permeability curves for the main part of the reservoir. This model represents a two-zone composite reservoir with different relative permeability curves in the two zones. In our work, we sometimes refer to the inner zone as the skin zone and allow the inner zone absolute permeability, k_s, to be different from the reservoir (outer zone) absolute permeability, k. Ref. 8 concluded that the computed effective or relative permeability values obtained from well-test pressure data, reflect the outer zone effective or relative permeability curves.

From the ideas of Ref. 8, the objectives of this work are: (i) to study the applicability of the computational procedures of Refs. 9, 10 and 28 for estimating effective (relative) permeability values in a two-zone composite solution-gas-drive reservoir; (ii) to study the effects of the inner zone radius on the computed effec-

tive (relative) permeability data; (iii) to investigate the effects of different absolute permeabilities in the two zones.

5.2 Mathematical Model

As in the previous Chapters, we consider radial flow to a completely penetrating well at the center of a cylindrical solution-gas-drive reservoir. The top, bottom and outer reservoir boundaries are assumed to be sealed, i.e., no flow boundaries. All the results presented, however, are for the infinite-acting period and thus, are not affected by the outer reservoir boundary. Gravity, capillary and wellbore storage effects are neglected. For all cases considered, water is immobile and water saturation remains fixed at $S_{wc} = 0.3$.

All results presented pertain to the infinite-acting period, that is, the closed outer boundary has no influence on the results obtained. The drawdown and buildup pressure and saturation solutions considered here were generated from a variation of the variable bubble-point, black-oil simulator under radial flow conditions described in Ref. 28. For all cases considered, the external reservoir radius is $r_e = 6600$ ft, which is sufficiently large such that the pressure and saturation changes in the near wellbore region are not affected by outer boundary effects.

Finally, in the results presented in this Chapter, the inner zone absolute permeability equals the outer zone absolute permeability for all the cases that skin effects are not present in the system, i.e., whenever $s = 0$. For the cases that $s \neq 0$ the inner zone radius r_{iz} was specified and the inner zone absolute permeability, k_s, was computed using Hawkins'[32] formula, i.e.,

$$s = \left(\frac{k}{k_s} - 1\right) \ln\left(\frac{r_{iz}}{r_w}\right), \tag{5.2.1}$$

where r_{iz} denotes the radius of the inner zone.

5.3 Simulator Data

For all results presented in this Chapter, except for absolute and relative permeability, the rock and fluid properties are identical in both zones of the reservoir

and represent properties used in Chapters 3 and 4. Table A-1 gives the set of PVT data for both reservoir zones and Figs. 5.3.1 and 4.2.1 present the two sets of relative permeability data used. The "Set 3" relative permeabilities shown in Fig. 5.3.1 (also see Table A-5) were derived by using $\lambda = 3$, $k_r^o = 0.9$, $S_{iw} = 0.3$ and $S_{gc} = 0.0$ in Standing's[15] relative permeability correlations. The "Set 1" relative permeabilities shown in Fig. 4.2.1 were derived by using $\lambda = 2$, $k_r^o = 0.7$, $S_{iw} = 0.3$ and $S_{gc} = 0.0$ in Standing's[15] relative permeability correlations. For both sets of data, the value of residual oil saturation is held fixed with $S_{or} = 0.0$. Throughout, the wellbore radius, external reservoir boundary radius, reservoir thickness, porosity and absolute permeability are specified as $r_w = 0.328$ ft, $r_e = 6600$ ft, $h = 15.547$ ft, $\phi = 0.3$ and $k = 10$ md, respectively, but the values of these parameters have no influence on the validity of the procedures and conclusions presented in this Chapter. The initial reservoir pressure and bubble-point pressure values are equal and given by $p_i = p_{bi} = 3460$ psi. The initial values of total compressibility, oil viscosity and oil FVF are specified as $c_{ti} = 0.23564 \times 10^{-4}$ psi $^{-1}$, $\mu_{oi} = 0.43059$ cp and $B_{oi} = 1.5882$ RB/STB, respectively.

In this Chapter, results are presented for the following nine cases:

Case 1 :

$q_o = 200$ STB/D; s = 0; $S_{gc} = 0.0$; $r_{iz} = 3.91$ ft; $k_s = k = 10$ md; $t_p = 5$ days;

Set 3 (Fig. 5.3.1) describes the inner zone relative permeabilities and Set 1 (Fig. 4.2.1) represents the outer zone relative permeabilities where, throughout, r_{iz} represents the radius of the inner zone and t_p represents the producing time, i.e., the length of the flow period.

Case 1a :

$q_o = 200$ STB/D; s = 0; $S_{gc} = 0.0$; $r_{iz} = 3.91$ ft; $k_s = k = 10$ md; $t_p = 5$ days;

Set 1 (Fig. 4.2.1) describes the outer zone relative permeabilities and Set 3 (Fig. 5.3.1) gives the inner zone oil relative permeability, and the inner zone gas relative permeability is given by $(k_{rg})_{iz} = (k_{ro})_{iz}(k_{rg}/k_{ro})_{oz}$, where, throughout, the subscript iz refers to the inner zone and the subscript oz refers to the outer zone.

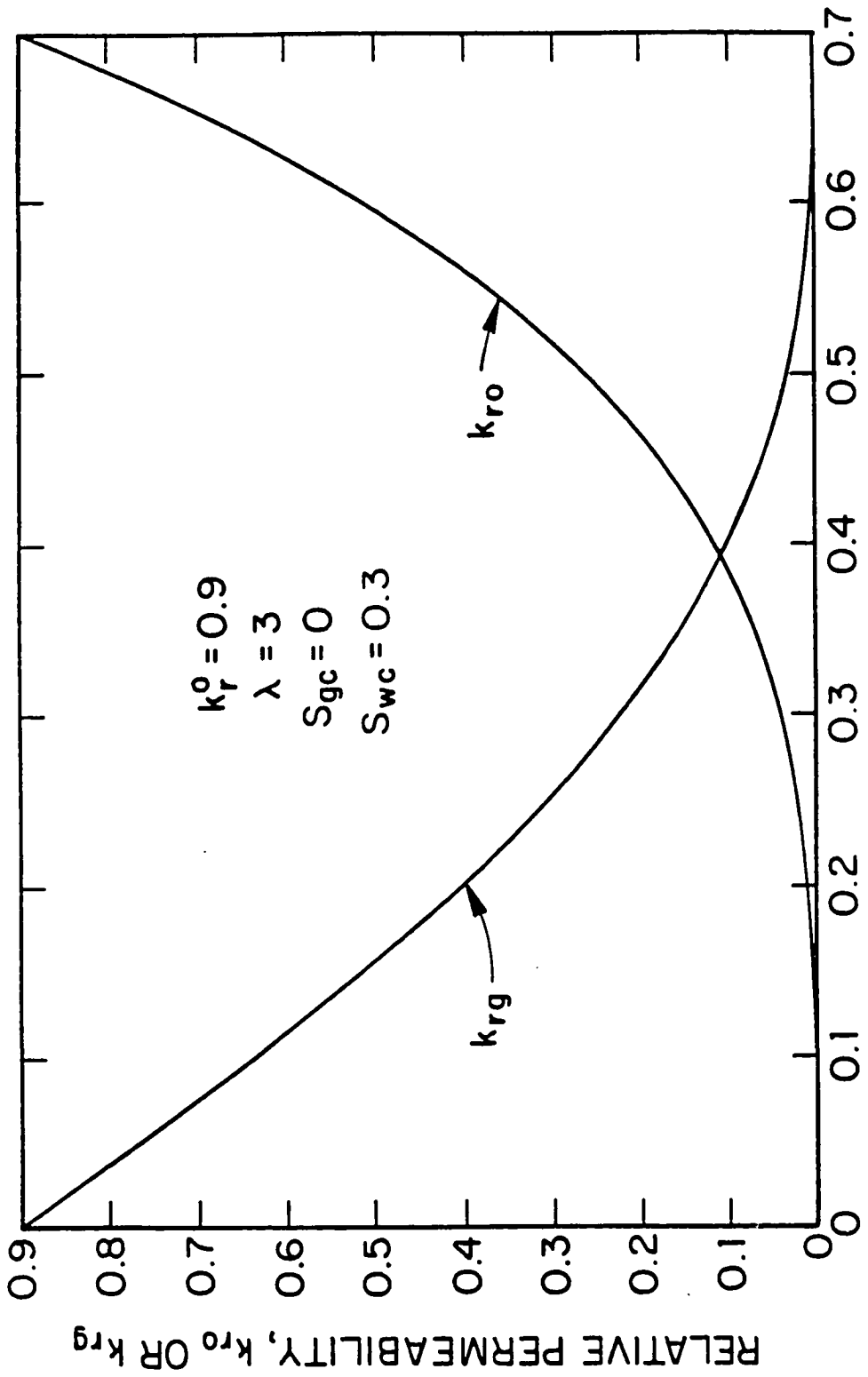

Fig. 5.3.1 - Relative permeability curves; Set 3.

Case 2 :

q_o = 200 STB/D; s = 0; S_{gc} = 0.0; r_{iz} = 46.53 ft; $k_s = k$ = 10 md; t_p = 10 days;

Set 3 (Fig. 5.3.1) describes the inner zone relative permeabilities and Set 1 (Fig. 4.2.1) represents the outer zone relative permeabilities.

Case 3 :

q_o = 200 STB/D; s = 0; S_{gc} = 0.0; r_{iz} = 1436.95 ft; $k_s = k$ = 10 md; t_p = 5 days;

Set 3 (Fig. 5.3.1) describes the inner zone relative permeabilities and Set 1 (Fig. 4.2.1) represents the outer zone relative permeabilities.

Case 4 :

q_o = 200 STB/D; s = 0; S_{gc} = 0.0; r_{iz} = 3.91 ft; $k_s = k$ = 10 md; t_p = 5 days;

Relative permeability curves for the two zones are the inverse of the ones for Case 1, i.e., Set 1 (Fig. 4.2.1) describes the inner zone relative permeabilities and Set 3 (Fig. 5.3.1) represents the outer zone relative permeabilities.

Case 5 :

q_o = 200 STB/D; s = 0; S_{gc} = 0.0; r_{iz} = 46.53 ft; $k_s = k$ = 10 md; t_p = 10 days;

Relative permeability curves for the two zones are the inverse of the ones for Case 2, i.e., Set 1 (Fig. 4.2.1) describes the inner zone relative permeabilities and Set 3 (Fig. 5.3.1) represents the outer zone relative permeabilities.

Case 6 :

q_o = 50 STB/D; s = 5; S_{gc} = 0.0; r_{iz} = 3.91 ft; k_s = 3.313 md; k = 10 md; t_p = 5 days;

Set 3 (Fig. 5.3.1) describes the inner zone relative permeabilities and Set 1 (Fig. 4.2.1) represents the outer zone relative permeabilities.

Case 7 :

q_o = 50 STB/D; s = 10; S_{gc} = 0.0; r_{iz} = 46.53 ft; k_s = 3.313 md; k = 10 md; t_p = 5 days;

Set 3 (Fig. 5.3.1) describes the inner zone relative permeabilities and Set 1 (Fig. 4.2.1) represents the outer zone relative permeabilities.

Case 8 :

q_o = 50 STB/D; s = 20; S_{gc} = 0.0; r_{iz} = 1436.95 ft; k_s = 2.954 md; k = 10 md; t_p = 5 days;

Set 3 (Fig. 5.3.1) describes the inner zone relative permeabilities and Set 1 (Fig. 4.2.1) represents the outer zone relative permeabilities.

For all cases, the duration of the drawdown test (flow period) is given by the value of the producing time, t_p, and the duration of the subsequent buildup test is always equal to the duration of the drawdown test.

Each figure presented contains information which identifies the case presented in the figure. Cases 1-5 allow us to examine the effect of heterogeneities, in the form of different relative permeability curves in the two regions of the system, without the presence of altered absolute reservoir permeability in the inner region. Cases 6-8 consider the problem in which, in addition to the presence of different relative permeability curves in the two regions, the absolute reservoir permeability in the inner region is less than the outer zone one, i.e., the skin factor is non-zero.

5.4 RESULTS

The equations used to compute effective permeabilities as pointwise functions of sandface oil saturation are described in Refs. 9, 10 and 28-30 and are presented here for the sake of completeness. The effective oil and gas permeability values are estimated from pressure drawdown data by applying the following equations:

$$(kk_{ro})_{p_{wf}} = \frac{-162.6 q_o (\mu_o B_o)_{p_{wf}}}{h dp_{wf}/d\log t}, \tag{5.4.1}$$

and

$$(kk_{rg})_{p_{wf}} = (R - R_s)_{p_{wf}} \left(\frac{\mu_g B_g}{\mu_o B_o}\right)_{p_{wf}} (kk_{ro})_{p_{wf}}. \tag{5.4.2}$$

Eq. 5.4.2 is equivalent to computing $(kk_{rg})_{p_{wf}}$ by the gas analogue of Eq. 5.4.1; see Refs. 8 and 28. In applying Eq. 5.4.2, we always use the $(kk_{ro})_{p_{wf}}$ values computed from Eq. 5.4.1.

The effective oil and gas permeability values are estimated from pressure versus shut-in time buildup data by applying the following equations:

$$(kk_{ro})_{p_{ws}} = \frac{162.6q_o(\mu_o B_o)_{p_{ws}}}{hdp_{ws}/d\log\left(\frac{t\Delta t}{t+\Delta t}\right)} = -\frac{162.6q_o(\mu_o B_o)_{p_{ws}}}{hdp_{ws}/d\log R_{H1}}, \qquad (5.4.3)$$

and

$$(kk_{rg})_{p_{ws}} = \left[R(\Delta t = 0) - R_s\right]_{p_{ws}} \left(\frac{\mu_g B_g}{\mu_o B_o}\right)_{p_{ws}} kk_{ro}, \qquad (5.4.4)$$

respectively. R_{H1} denotes the standard Horner time ratio, i.e., $R_{H1} = (t + \Delta t)/\Delta t$, and the application of Eq. 5.4.4 requires that the producing GOR at the time of shut-in is measured. Eq. 5.4.2 represents a rearrangement of a basic relationship presented by Evinger and Muskat[3] and a rearrangement of Eq. 5.4.4 was used by Raghavan[5] to compute k_{rg}/k_{ro} in order to construct wellbore pseudopressures.

Before proceeding with the presentation of the results, we need to make clear at this point that in all cases the kk_{ro} and kk_{rg} values are plotted versus the drawdown sandface oil saturation obtained from the simulator. More specifically, we compute the kk_{ro} and kk_{rg} values as functions of the wellbore pressure, p_{wf} or p_{ws}, and then we use the simulator drawdown sandface oil saturation/wellbore pressure relationship in order to estimate kk_{ro} and kk_{rg} as functions of the drawdown sandface oil saturation.

5.4.1 Zero Skin Cases.

In this subsection, we present the results for the cases where skin effects are not present in the system and therefore, the inner and outer zone absolute permeabilities are equal, i.e., $k_s = k$.

Case 1.

Figs. 5.4.1 and 5.4.2, respectively, show the wellbore pressure and the sandface oil saturation variation with respect to time for the drawdown and buildup tests for Case 1. In Case 1, relative permeability Set 3 (see Fig. 5.3.1) describes the inner zone relative permeabilities and Set 1 (see Fig. 4.2.1) represents the outer zone relative permeabilities. The simulated and computed kk_{ro} values versus the flowing wellbore pressure, p_{wf}, are shown in Table F-21. In this table, columns 1 and 2

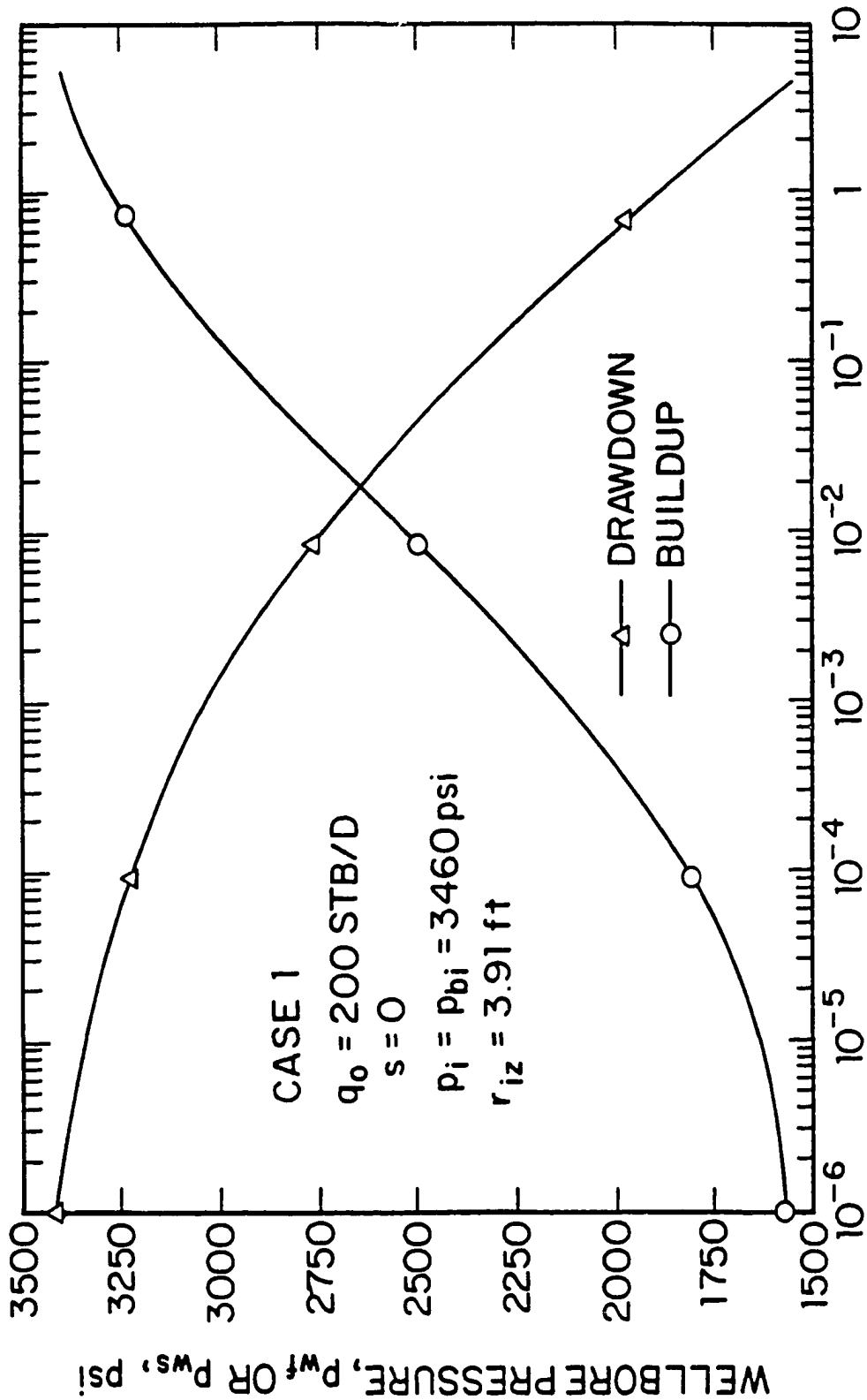

Fig. 5.4.1 - Drawdown and buildup wellbore pressures; Case 1.

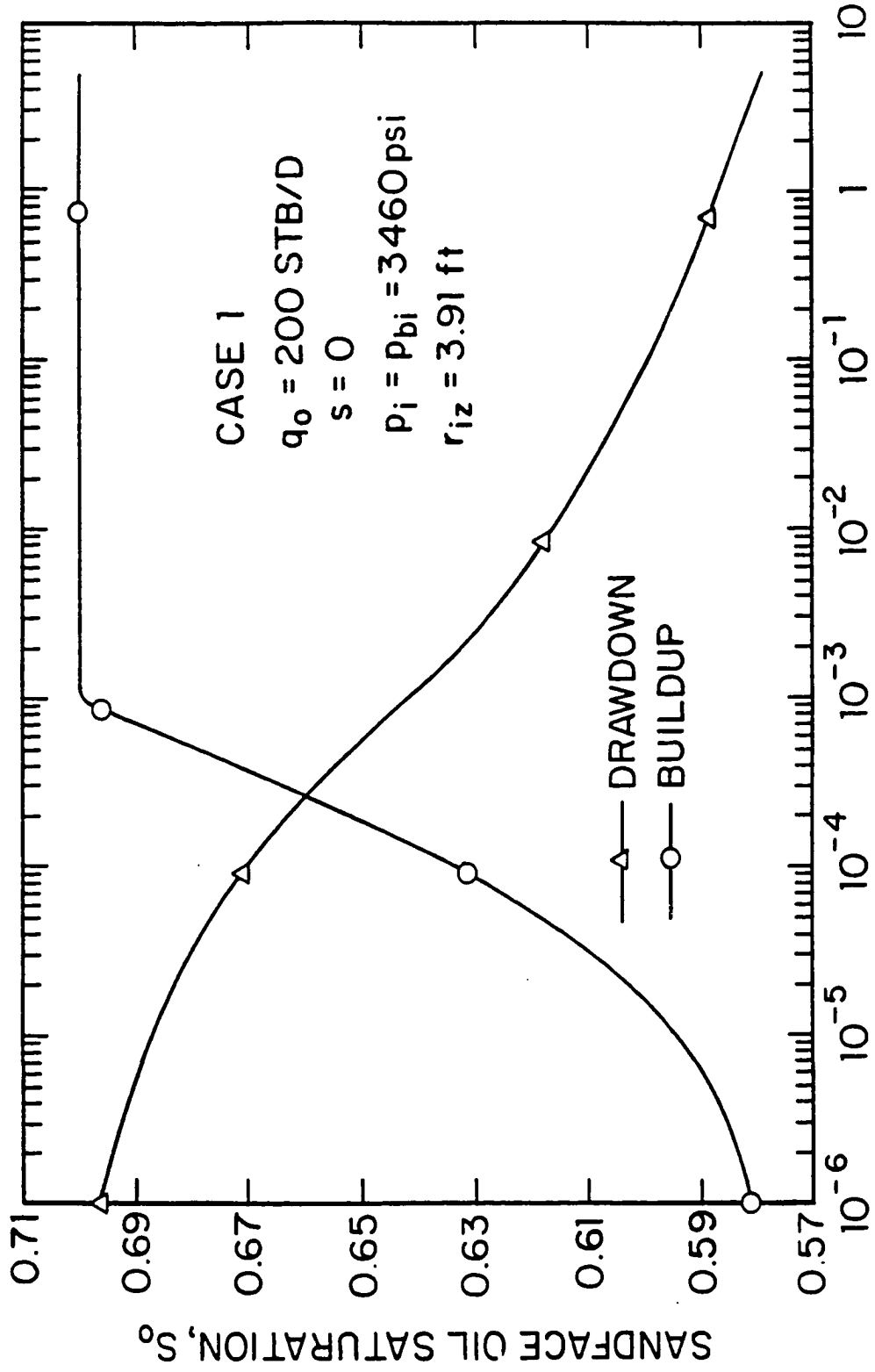

Fig. 5.4.2 - Drawdown and buildup sandface oil saturation; Case 1.

show the time and wellbore pressure data, columns 3 and 4 show the sandface oil saturation and the effective oil permeability data obtained from the simulator and column 5 shows the kk_{ro} values computed from Eq. 5.4.1. Table F-22 shows the simulated and computed kk_{ro} values for the buildup test of Case 1. Columns 1 and 2 show the shut-in time and shut-in wellbore pressure data, columns 3 and 4 show the sandface oil saturation and the effective oil permeability data corresponding to the drawdown simulator results and column 5 shows the kk_{ro} values computed from Eq. 5.4.3. The triangular data points in Fig. 5.4.3 represent a plot of effective oil permeability values obtained from drawdown pressure data by applying Eq. 5.4.1. The circular data points represent kk_{ro} values obtained by applying Eq. 5.4.3 to buildup pressure data. The continuous curve corresponds to the inner zone input (simulator) effective oil permeability curve and the dashed curve corresponds to the outer zone input (simulator) effective oil permeability curve. In all cases, kk_{ro} is plotted versus the simulator drawdown sandface oil saturation values. From Fig. 5.4.3, it can be seen that the kk_{ro} values computed from pressure drawdown data, by applying Eq. 5.4.1, cross the input inner zone kk_{ro} data and for $S_o \leq 0.60403$ ($p_{wf} \leq 2472.1$ psi or $t \geq 5.18 \times 10^{-2}$ days) approximate the outer zone kk_{ro} data. The buildup kk_{ro} values computed by applying Eq. 5.4.3 never yield estimates of the inner zone kk_{ro} data, but yield rough estimates of the outer kk_{ro} data at later shut-in times.

Tables F-23 and F-24 show the simulated and computed kk_{rg} values as a function of wellbore pressure for both the drawdown and buildup tests, respectively. The computed effective gas permeabilities plotted versus the simulator drawdown sandface oil saturation, for Case 1, are shown in Fig. 5.4.4. The continuous curve corresponds to the inner zone input effective gas permeability curve, the dashed curve corresponds to the outer zone input effective gas permeability curve, the triangular data points represent the effective gas permeability values computed from drawdown pressure data obtained from Eq. 5.4.2, and the circular data points represent the computed effective gas permeability values from buildup pressure data obtained with Eq. 5.4.4. From Fig. 5.4.4, it is unclear whether the computed values

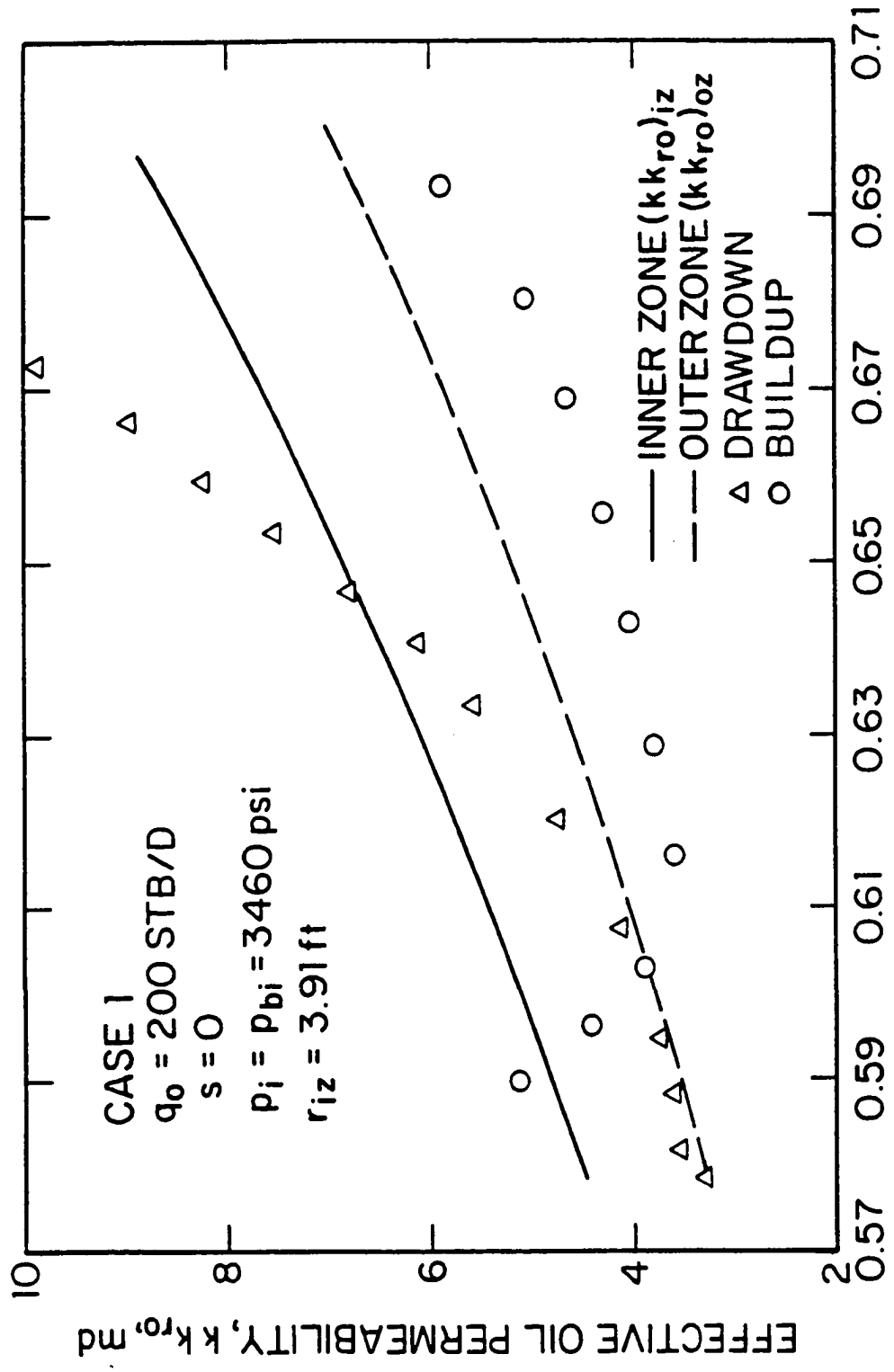

Fig. 5.4.3 - Effective oil permeability as a function of sandface oil saturation; Case 1.

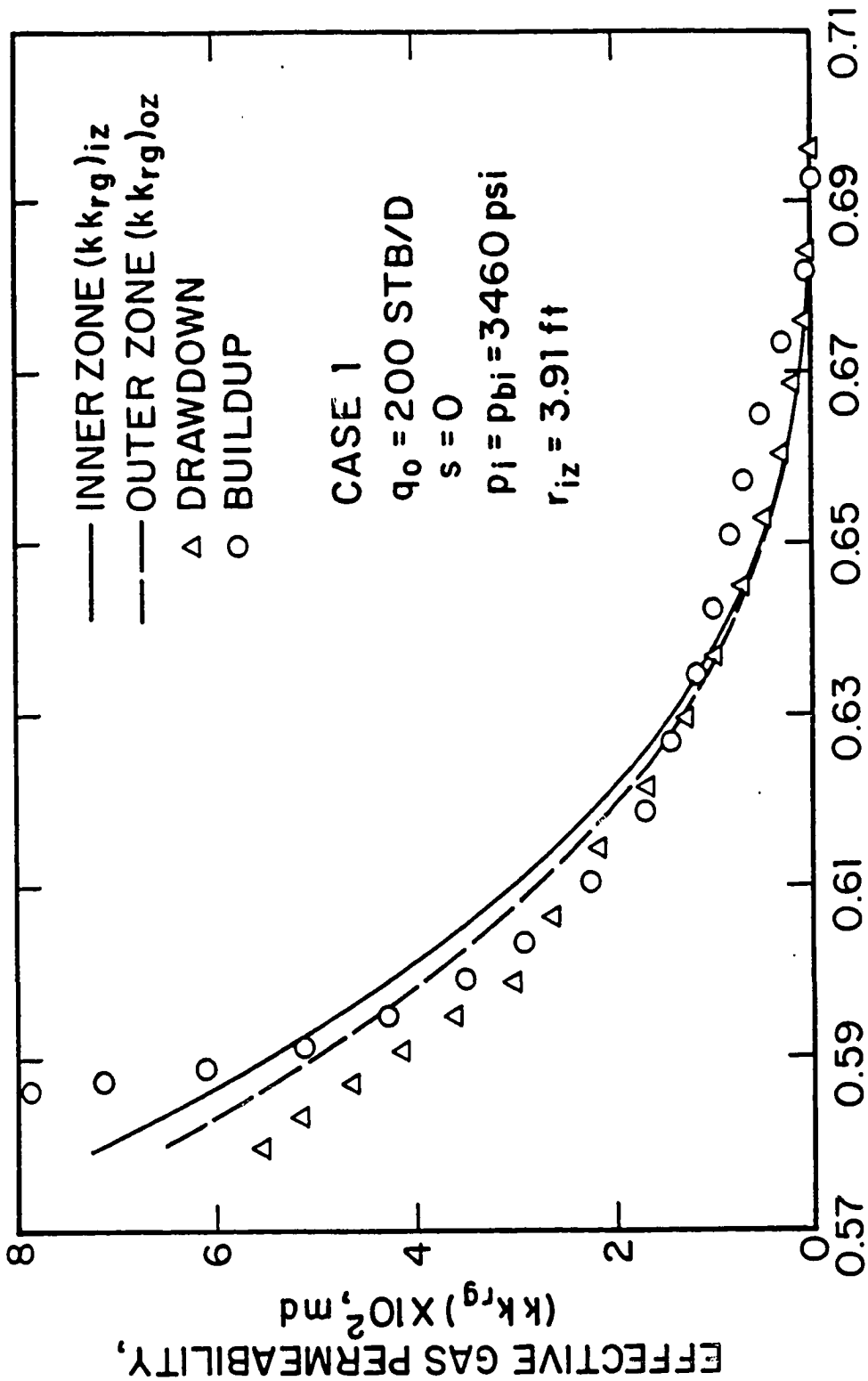

Fig. 5.4.4 - Effective gas permeability as a function of sandface oil saturation; Case 1.

of effective gas permeability reflect the inner or outer zone effective gas permeability values. Note that for $S_o > 0.635$ the kk_{rg} values computed from buildup data lie above both the inner and the outer zone input effective gas permeability data. Furthermore, Fig. 5.4.4 shows that at early times the effective gas permeability values computed from drawdown data are very close to zero and are close to both the inner and outer zone input effective gas permeability curves. At later times, unlike the computed effective oil permeability values, the effective gas permeabilities computed from drawdown data do not yield a good approximation to the outer zone input effective gas permeability curve.

As has been seen earlier (see Fig. 5.4.3) the effective oil permeability values computed from Eq. 5.4.1 reflect the outer zone input effective oil permeability curve at later times. From Darcy's law, the inner boundary condition is given by

$$q_o = 1.127 \times 10^{-3} \frac{2\pi h}{(\mu_o B_o)_{p_{wf}}} (kk_{ro})_{iz} \left(r \frac{\partial p}{\partial r} \right)_{r_w}$$

$$= 1.127 \times 10^{-3} \frac{2\pi h}{(\mu_o B_o)_{p_{wf}}} (kk_{ro})_{iz} \frac{(kk_{ro})_{oz}}{(kk_{ro})_{oz}} \left(r \frac{\partial p}{\partial r} \right)_{r_w}, \qquad (5.4.5)$$

where $(kk_{ro})_{iz}$ denotes effective oil permeability in the inner zone and $(kk_{ro})_{oz}$ denotes effective oil permeability in the outer zone.

Note that during the times that the kk_{ro} values computed from Eq. 5.4.1 reflect the effective oil permeability data of the outer zone, Eq. 5.4.1 must be equivalent to

$$q_o = 1.127 \times 10^{-3} \frac{2\pi h}{(\mu_o B_o)_{p_{wf}}} (kk_{ro})_{oz} (-2t) \frac{\partial p_{wf}}{\partial t}. \qquad (5.4.6)$$

Comparing Eqs. 5.4.5 and 5.4.6, one can see that the following expression is valid:

$$-2t \frac{\partial p_{wf}}{\partial t} = \frac{(kk_{ro})_{iz}}{(kk_{ro})_{oz}} \left(r \frac{\partial p}{\partial r} \right)_{r_w}. \qquad (5.4.7)$$

The sandface flow rate of free gas is given by

$$q_g(t) = 1.127 \times 10^{-3} \frac{2\pi h}{(\mu_g B_g)_{p_{wf}}} (kk_{rg})_{iz} \left(r \frac{\partial p}{\partial r} \right)_{r_w}. \qquad (5.4.8)$$

The free gas flow rate is related to the total gas flow rate by

$$q_g(t) = q_{gt} - R_s q_o, \qquad (5.4.9)$$

where q_{gt} is the total gas flow rate (free gas plus solution gas) at surface conditions.

Substituting Eqs. 5.4.7 and 5.4.9 into Eq. 5.4.8 yields

$$q_{gt} - R_s q_o = 1.127 \times 10^{-3} \frac{2\pi h}{(\mu_g B_g)_{p_{wf}}} (kk_{rg})_{iz} \frac{(kk_{ro})_{oz}}{(kk_{ro})_{iz}} (-2t) \frac{\partial p_{wf}}{\partial t}. \tag{5.4.10}$$

Dividing Eq. 5.4.10 by Eq. 5.4.6, we obtain

$$\frac{q_{gt}}{q_o} - R_s = \frac{1.127 \times 10^{-3} \frac{2\pi h}{(\mu_g B_g)_{p_{wf}}} (kk_{rg})_{iz} \frac{(kk_{ro})_{oz}}{(kk_{ro})_{iz}} (-2t) \frac{\partial p_{wf}}{\partial t}}{1.127 \times 10^{-3} \frac{2\pi h}{(\mu_o B_o)_{p_{wf}}} (kk_{ro})_{oz} (-2t) \frac{\partial p_{wf}}{\partial t}}, \tag{5.4.11}$$

which after simplification yields

$$R - R_s = \frac{(kk_{rg})_{iz}/(\mu_g B_g)_{p_{wf}}}{(kk_{ro})_{iz}/(\mu_o B_o)_{p_{wf}}}, \tag{5.4.12}$$

or equivalently,

$$(kk_{rg})_{iz} = (R - R_s)_{p_{wf}} \left(\frac{\mu_g B_g}{\mu_o B_o} \right)_{p_{wf}} (kk_{ro})_{iz}. \tag{5.4.13}$$

We now consider the equation:

$$(kk_{rg})_{oz} = (R - R_s)_{p_{wf}} \left(\frac{\mu_g B_g}{\mu_o B_o} \right)_{p_{wf}} (kk_{ro})_{oz}. \tag{5.4.14}$$

Note that Eq. 5.4.14 is equivalent to using the outer zone values of effective oil permeability for $(kk_{ro})_{p_{wf}}$ in Eq. 5.4.2. Since Eq. 5.4.13 is correct, it follows that Eq. 5.4.14 is valid if and only if

$$\left(\frac{k_{rg}}{k_{ro}} \right)_{iz} = \left(\frac{k_{rg}}{k_{ro}} \right)_{oz}. \tag{5.4.15}$$

If Eq. 5.4.15 does not hold, it follows that $(kk_{rg})_{oz}$ cannot be computed by using outer zone $(kk_{ro})_{oz}$ values for $(kk_{ro})_{p_{wf}}$ in Eq. 5.4.2. Based on these theoretical arguments and the computed results of this Chapter, the claim of Ref. 8 that one can obtain estimates of outer zone values of both kk_{ro} and kk_{rg} is incorrect. Similarly, one should not expect Eq. 5.4.4 to yield estimates of the outer zone kk_{rg} values.

Case 1a.

Motivated by the previous discussion, we present here results for a case where the permeability curves in the two regions satisfy Eq. 5.4.15. To generate these results, we used Set 1 relative permeability curves in the outer zone and the oil relative permeability curve of Set 3 to describe the inner zone kk_{ro} data. We then used Eq. 5.4.15 to generate the gas relative permeability data for the inner zone. Except for the relative permeability data, the input data for Case 1a are identical to those for Case 1, i.e., the constant oil production rate is $q_o = 200$ STB/D, the inner zone radius is $r_{is} = 3.91$ ft and the duration of both the drawdown and buildup tests is 5 days.

The wellbore pressure and the sandface oil saturation variation with respect to time for Case 1a drawdown and buildup tests are shown in Figs. 5.4.5 and 5.4.6, respectively. The simulated and computed kk_{ro} values for both the drawdown and buildup tests are shown in Tables F-25 and F-26, respectively. Fig. 5.4.7 presents a plot of effective oil permeability values computed from drawdown pressure data (triangular data points) by applying Eq. 5.4.1, and from buildup pressure data (circular data points) by applying Eq. 5.4.3, plotted versus the simulator drawdown sandface oil saturation. In Fig. 5.4.7, the continuous curve corresponds to the inner zone input effective oil permeability curve and the dashed curve corresponds to the outer zone input effective oil permeability curve. It can be seen that, as in Case 1, the kk_{ro} values computed from pressure drawdown data reflect the outer zone kk_{ro} data for $S_o \leq 0.61550$ ($p_{wf} \leq 2648.3$ psi or $t \geq 1.814 \times 10^{-2}$ days). Similarly, as in Case 1, the kk_{ro} values computed from buildup pressure data are closest to the outer zone kk_{ro} data.

The Case 1a effective gas permeabilities are plotted versus the simulator drawdown sandface oil saturation in Fig. 5.4.8. The simulated and computed kk_{rg} values as a function of wellbore pressure for both the drawdown and buildup tests are shown in Tables F-27 and F-28, respectively. The continuous curve corresponds to the inner zone input effective gas permeability curve, the dashed curve corresponds to the outer zone input effective gas permeability curve, the triangular data points

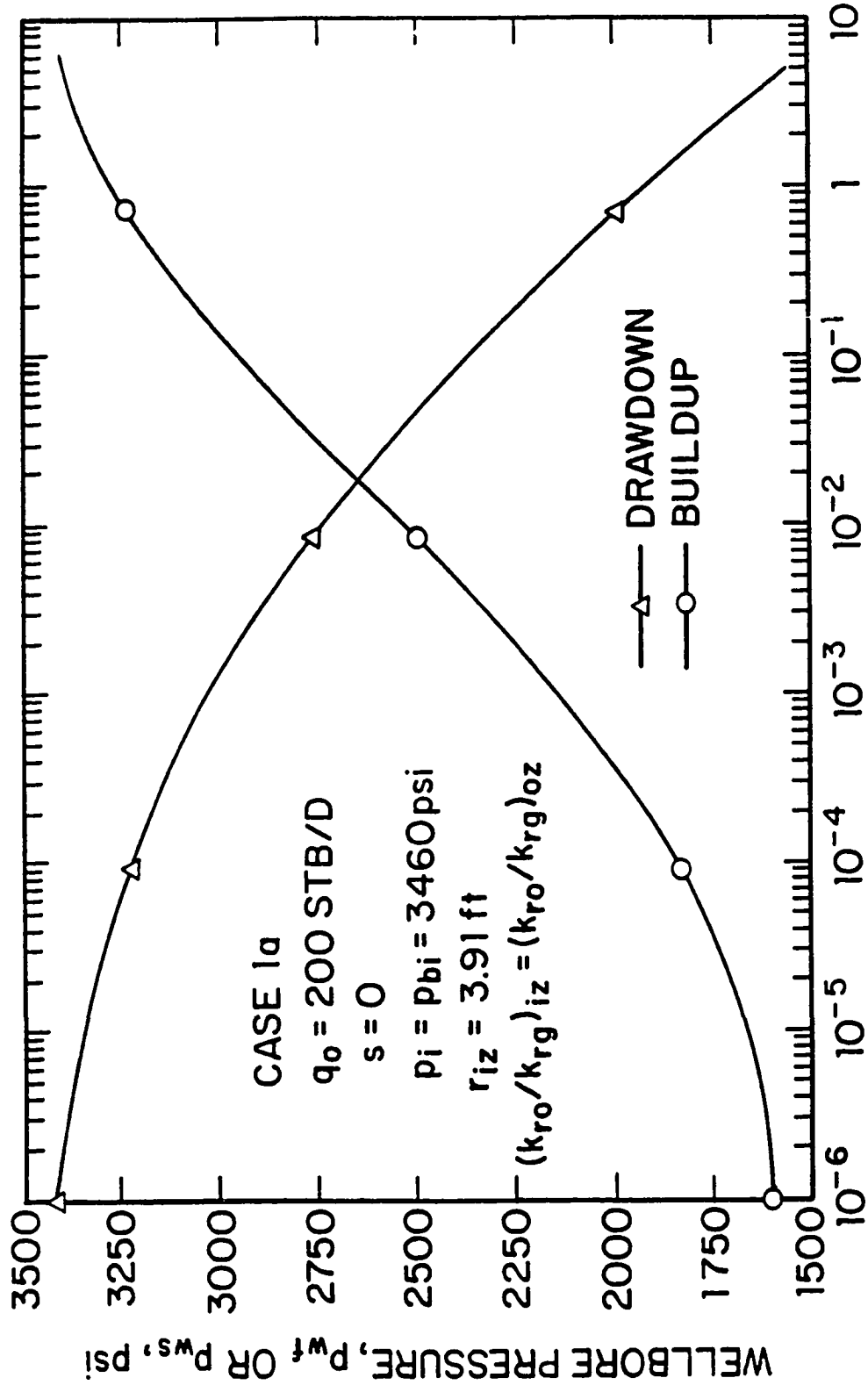

Fig. 5.4.5 - Drawdown and buildup wellbore pressures; Case 1a.

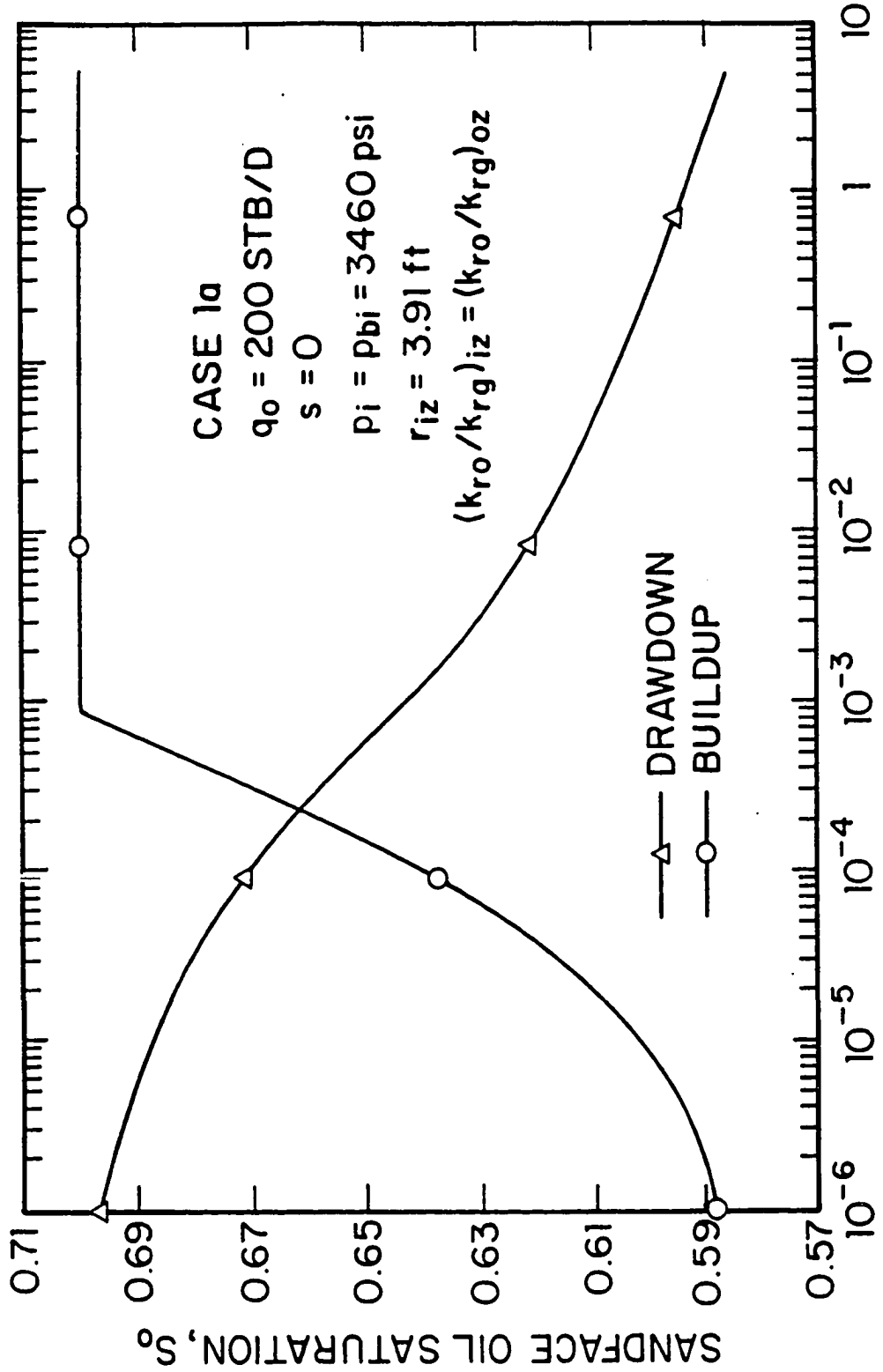

Fig. 5.4.6 - Drawdown and buildup sandface oil saturation; Case 1a.

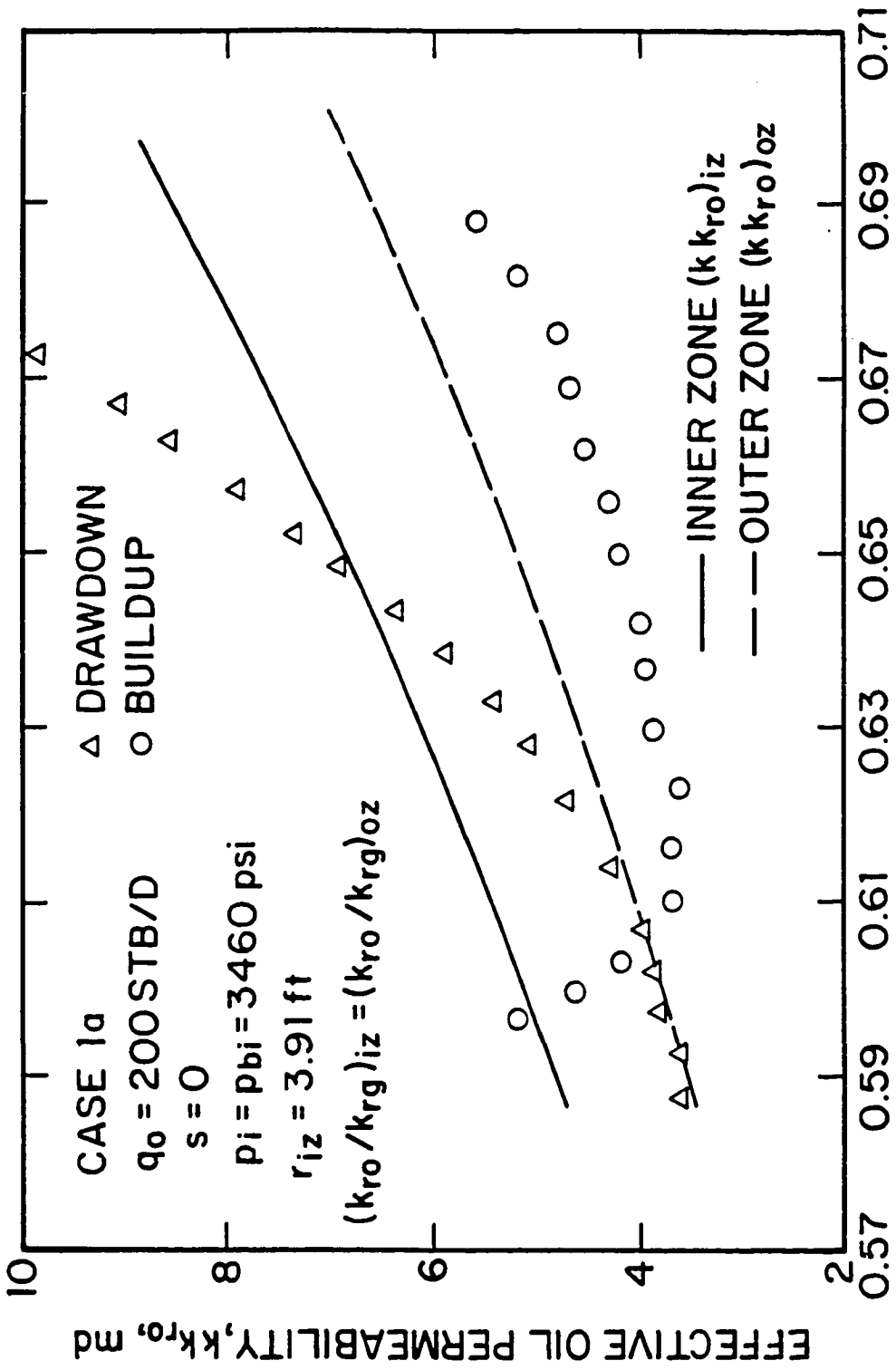

Fig. 5.4.7 - Effective oil permeability as a function of sandface oil saturation; Case 1a.

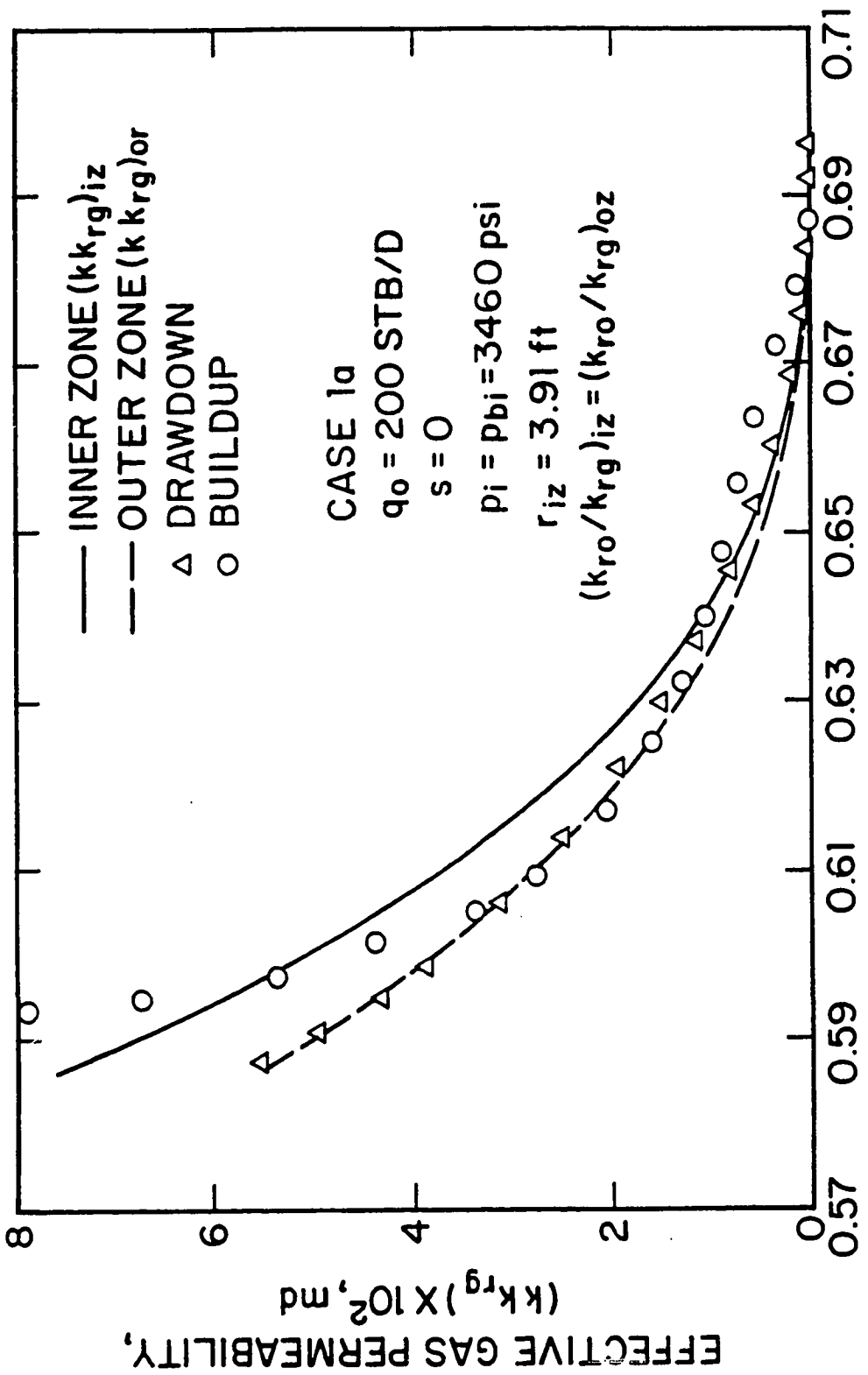

Fig. 5.4.8 - Effective gas permeability as a function of sandface oil saturation; Case 1a.

represent the effective gas permeability values computed from drawdown pressure data by applying Eq. 5.4.2 and the circular data points represent the effective gas permeability values computed from buildup pressure data by applying Eq. 5.4.4. It can be seen that the effective gas permeability values computed from drawdown pressure data, unlike the ones in Case 1, accurately reflect the outer zone input effective gas permeability curve during the time interval that the computed kk_{ro} values (see Fig. 5.4.7) reflect the outer zone input effective oil permeability curve, i.e., for $S_o \leq 0.61550$ ($p_{wf} \leq 2648.3$ psi or $t \geq 1.814 \times 10^{-2}$ days). This result is in agreement with the theoretical conclusion presented earlier in this Chapter. Fig. 5.4.8 also shows that the effective gas permeability values computed from buildup pressure versus shut-in time data are not highly accurate.

Important Remark:

Since we cannot estimate kk_{rg} for the outer zone, we cannot apply the nonlinear regression procedures, presented in Chapters 2 and 3, to estimate effective (relative) permeability curves for the outer zone.

Case 2.

The wellbore pressure and the sandface oil saturation variation, respectively, obtained for the Case 2 drawdown and buildup tests are shown in Figs. 5.4.9 and 5.4.10. In this case, the constant oil production rate is $q_o = 200$ STB/D, the inner zone radius is $r_{iz} = 46.53$ ft and the duration of both drawdown and buildup tests is 10 days. Furthermore, Fig. 5.3.1 represents the inner zone relative permeabilities and Fig. 4.2.1 gives the outer zone relative permeabilities. Fig. 5.4.11 presents a plot of effective oil permeability values computed from drawdown pressure data (triangular data points) by applying Eq. 5.4.1, and computed from buildup pressure data (circular data points) by applying Eq. 5.4.3, versus the simulator drawdown sandface oil saturation. The continuous curve corresponds to the inner zone input effective oil permeability curve and the dashed curve corresponds to the outer zone input effective oil permeability curve. It can be seen that, at early times, the kk_{ro} values computed from pressure drawdown data reflect the inner zone input effective

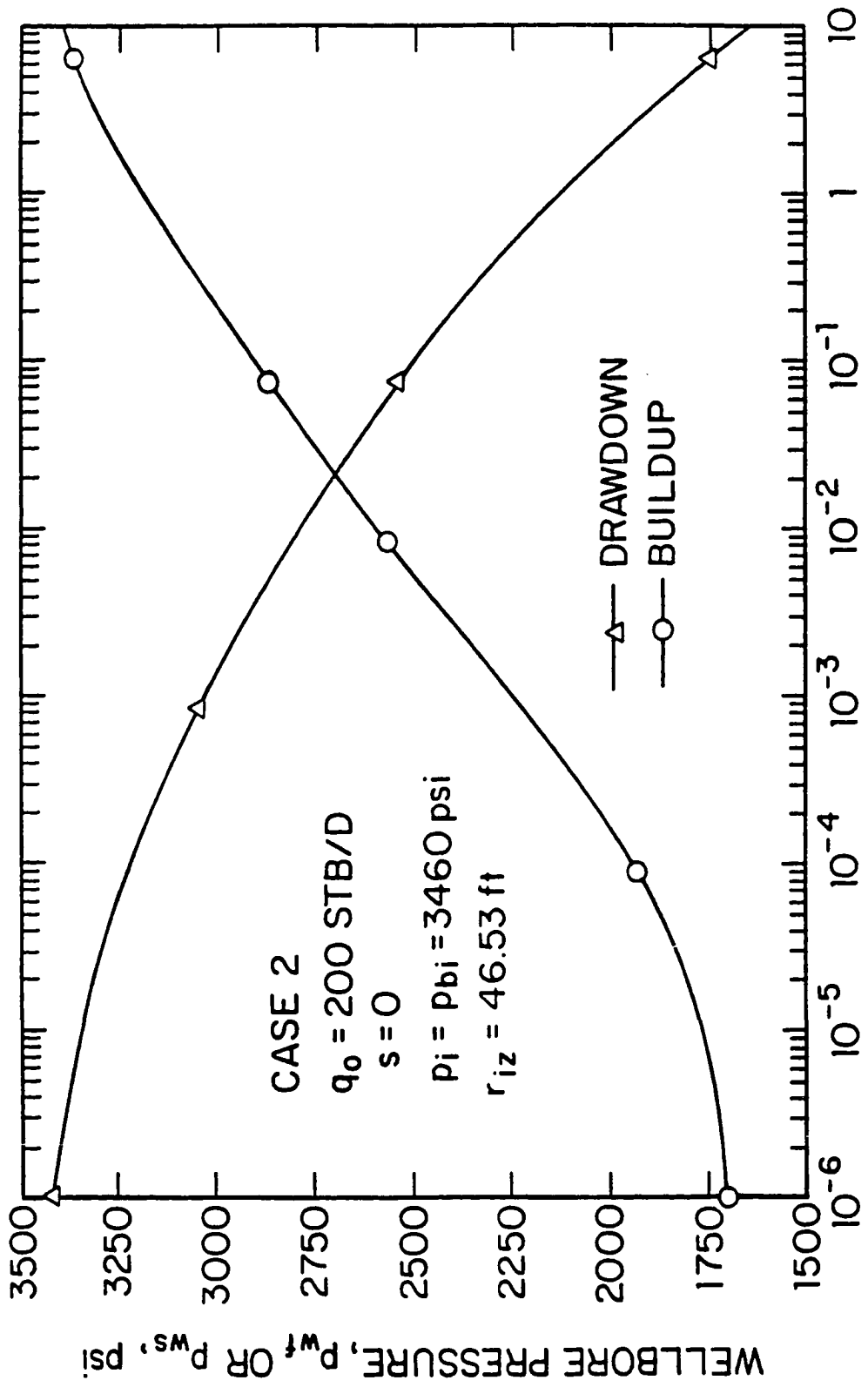

Fig. 5.4.9 - Drawdown and buildup wellbore pressures; Case 2.

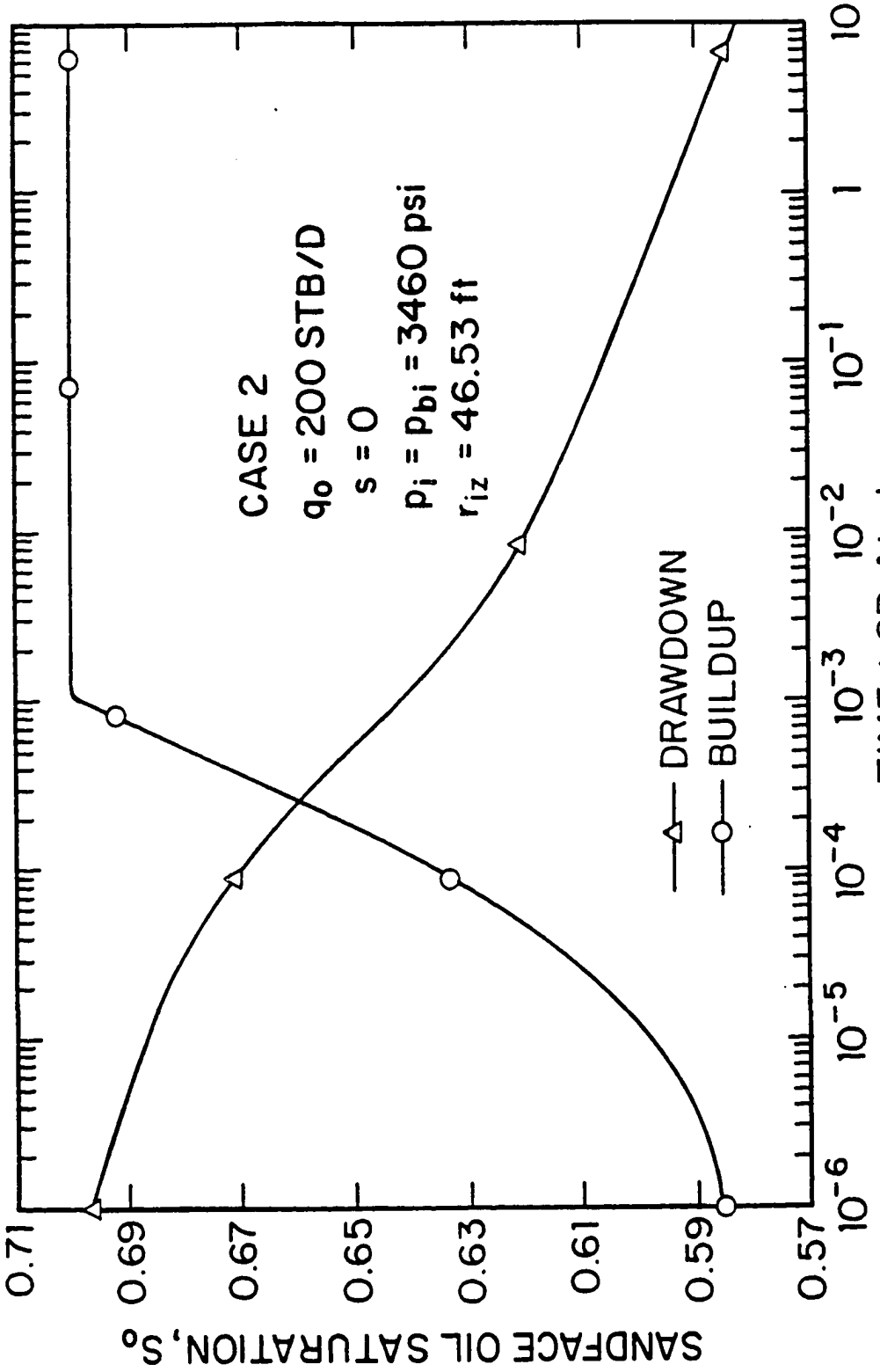

Fig. 5.4.10 - Drawdown and buildup sandface oil saturation; Case 2.

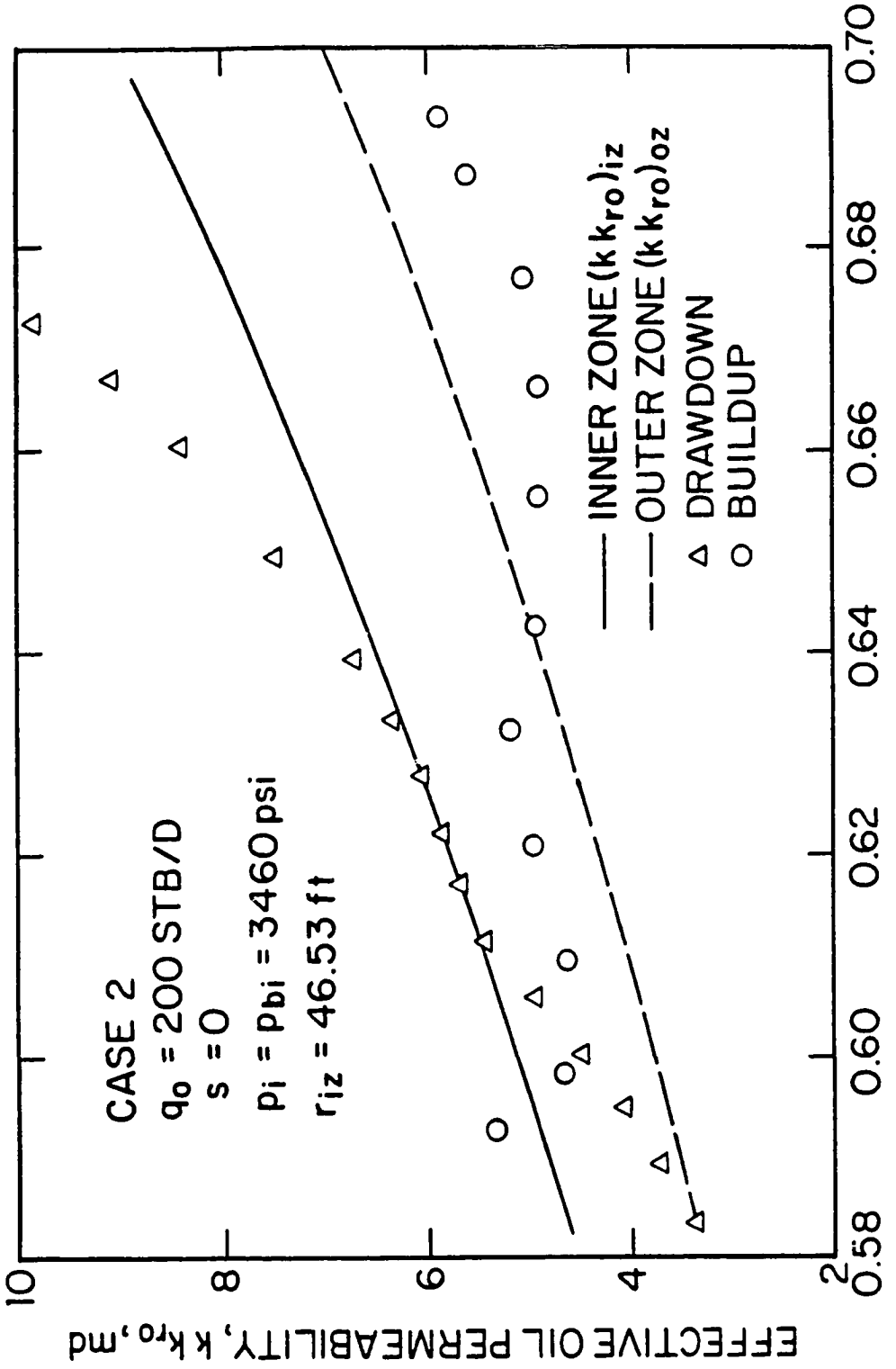

Fig. 5.4.11 - Effective oil permeability as a function of sandface oil saturation; Case 2.

oil permeability data for $0.61549 \leq S_o \leq 0.63069$ (2709.9 psi $\leq p_{wf} \leq$ 2935.9 psi or 2.69×10^{-3} days $\leq t \leq 1.996 \times 10^{-2}$ days). Following this behavior, there is a transition period during which the kk_{ro} values computed from drawdown pressure data do not reflect either the inner or the outer zone input kk_{ro} data. Finally, at very late times the computed kk_{ro} values approach the input kk_{ro} data of the outer zone. The buildup kk_{ro} values obtained from Eq. 5.4.3, at early shut-in times, apparently tend to reflect the inner zone kk_{ro} data, but at later shut-in times they approach the outer zone kk_{ro} data. However, the values of effective oil permeability computed from buildup data are not sufficiently accurate to determine which effective oil permeability curve is reflected by these values.

As is shown in Fig. 5.4.12, the effective gas permeability values computed from drawdown pressure versus time data for Case 2 reflect the inner zone input effective gas permeability data during the times the computed effective oil permeability values reflect the inner zone input effective oil permeability data. However, as in Case 1 and for the reasons explained earlier, the effective gas permeability values computed from drawdown pressure data do not reflect the outer zone effective gas permeability.

Case 3.

The Case 3 wellbore pressure and the sandface oil saturation variation with respect to time for the drawdown and buildup tests are shown in Figs. 5.4.13 and 5.4.14, respectively. Recall that in this case, the constant oil production rate is q_o = 200 STB/D, the inner zone radius is r_{iz} = 1436.95 ft and the duration of both drawdown and buildup tests is 5 days. Furthermore, Set 3 (Fig. 5.3.1) describes the inner zone relative permeabilities and Set 1 (Fig. 4.2.1), the outer zone relative permeabilities. Fig. 5.4.15 presents a plot of effective oil permeability values computed from drawdown pressure data (triangular data points) by applying Eq. 5.4.1, and computed from buildup pressure data (circular data points) by applying Eq. 5.4.3, plotted versus the simulator drawdown sandface oil saturation. The continuous curve corresponds to the inner zone input effective oil permeability curve

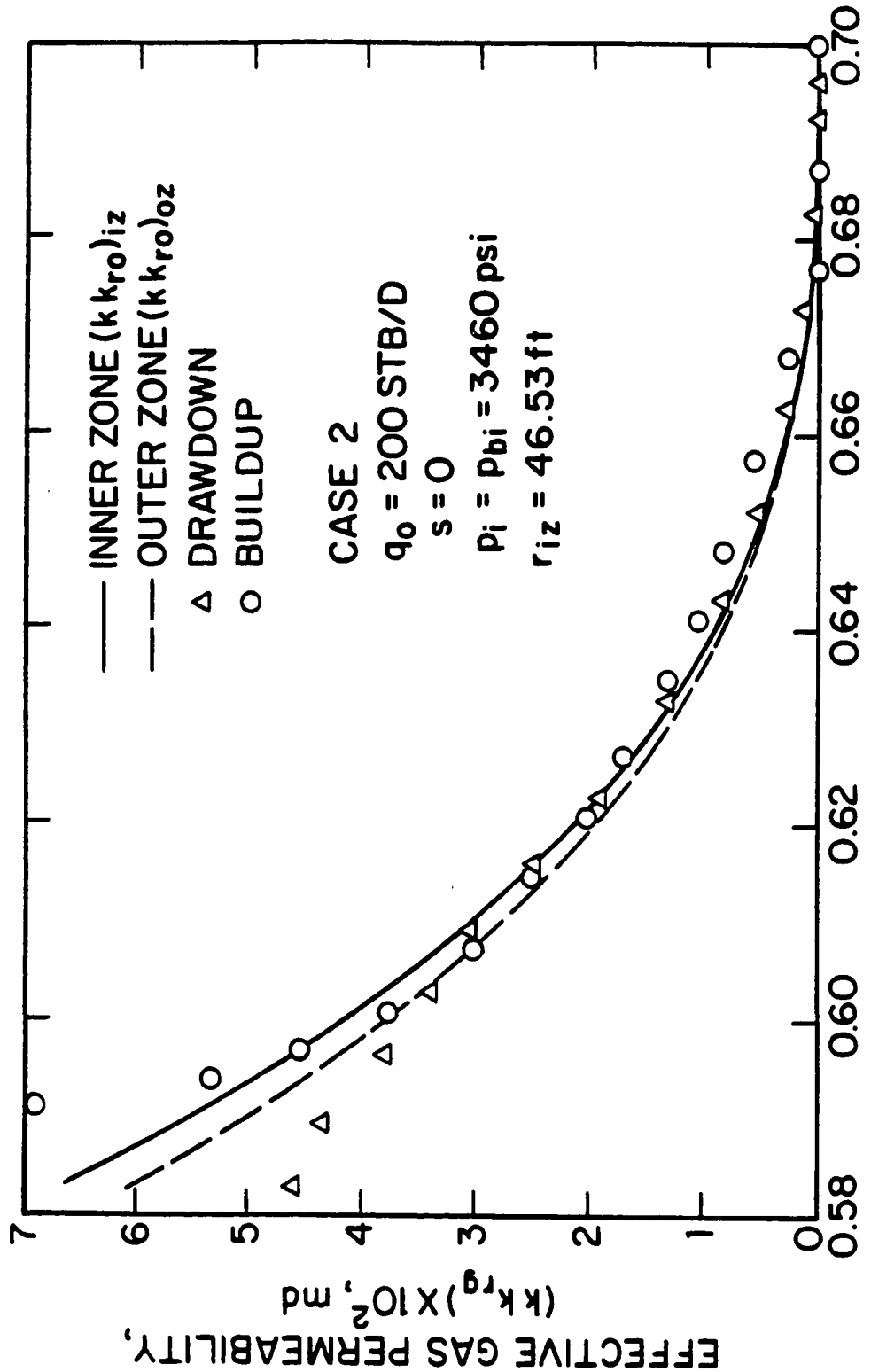

Fig. 5.4.12 - Effective gas permeability as a function of sandface oil saturation; Case 2.

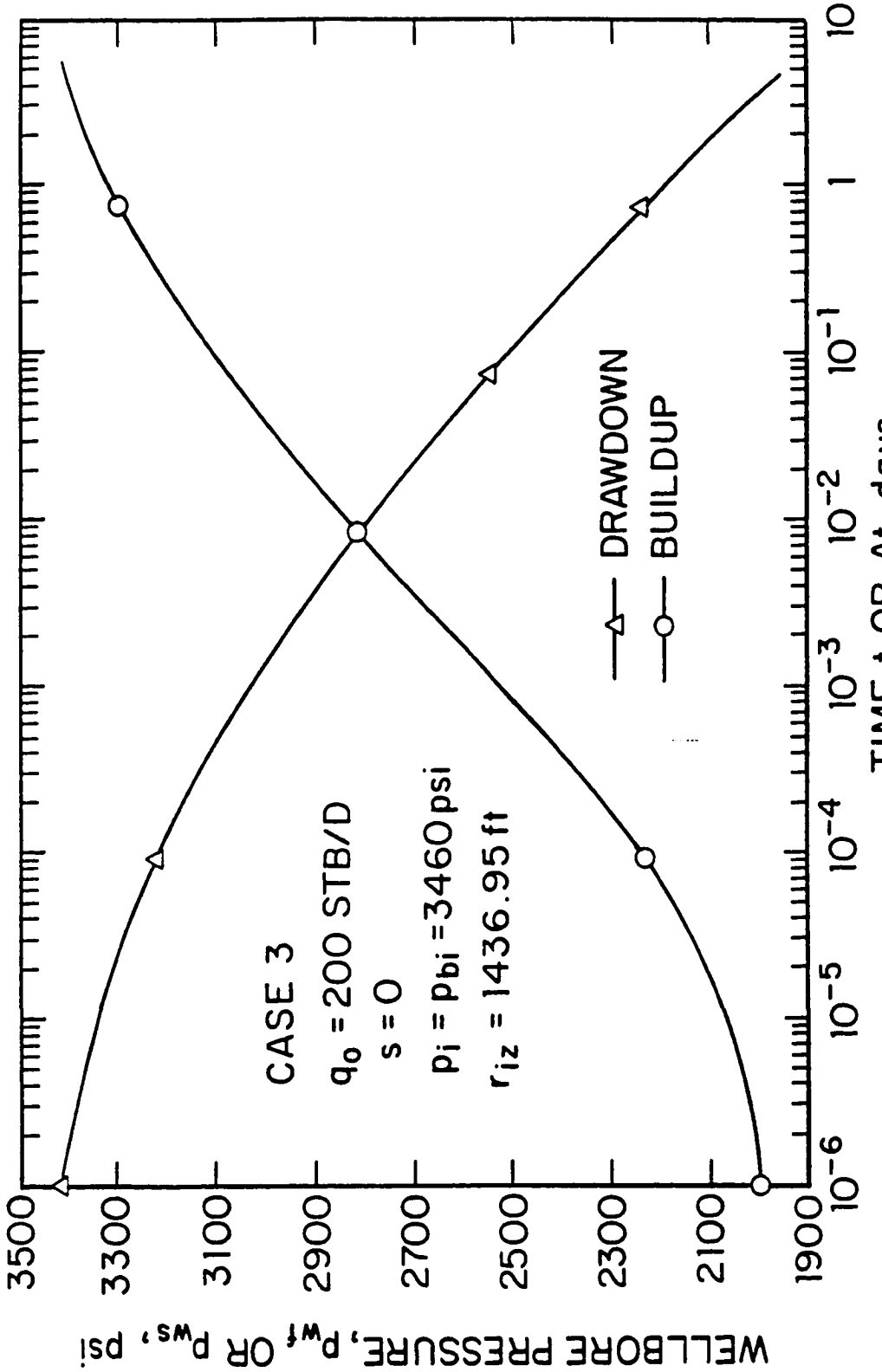

Fig. 5.4.13 - Drawdown and buildup wellbore pressures; Case 3.

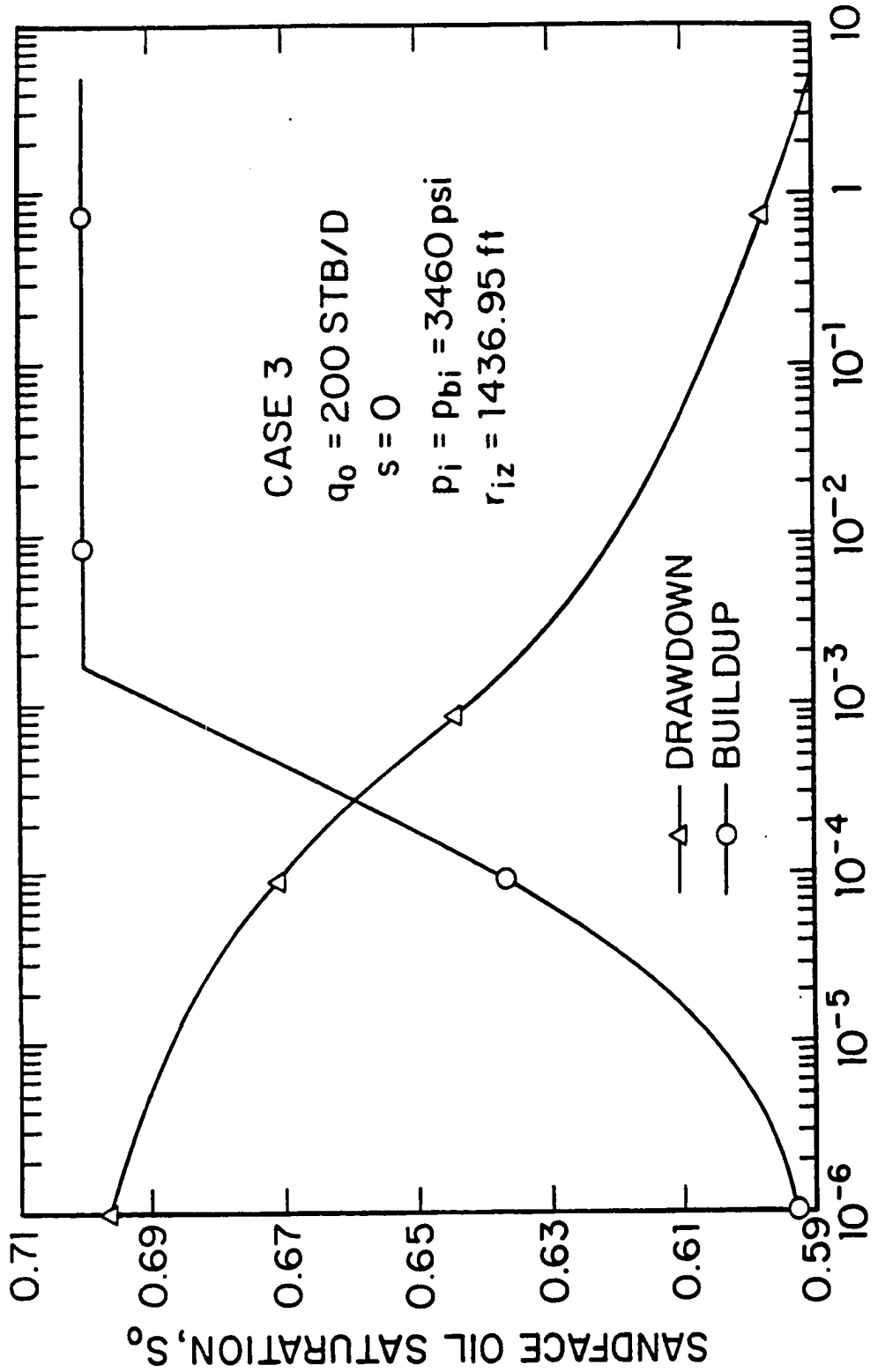

Fig. 5.4.14 - Drawdown and buildup sandface oil saturation; Case 3.

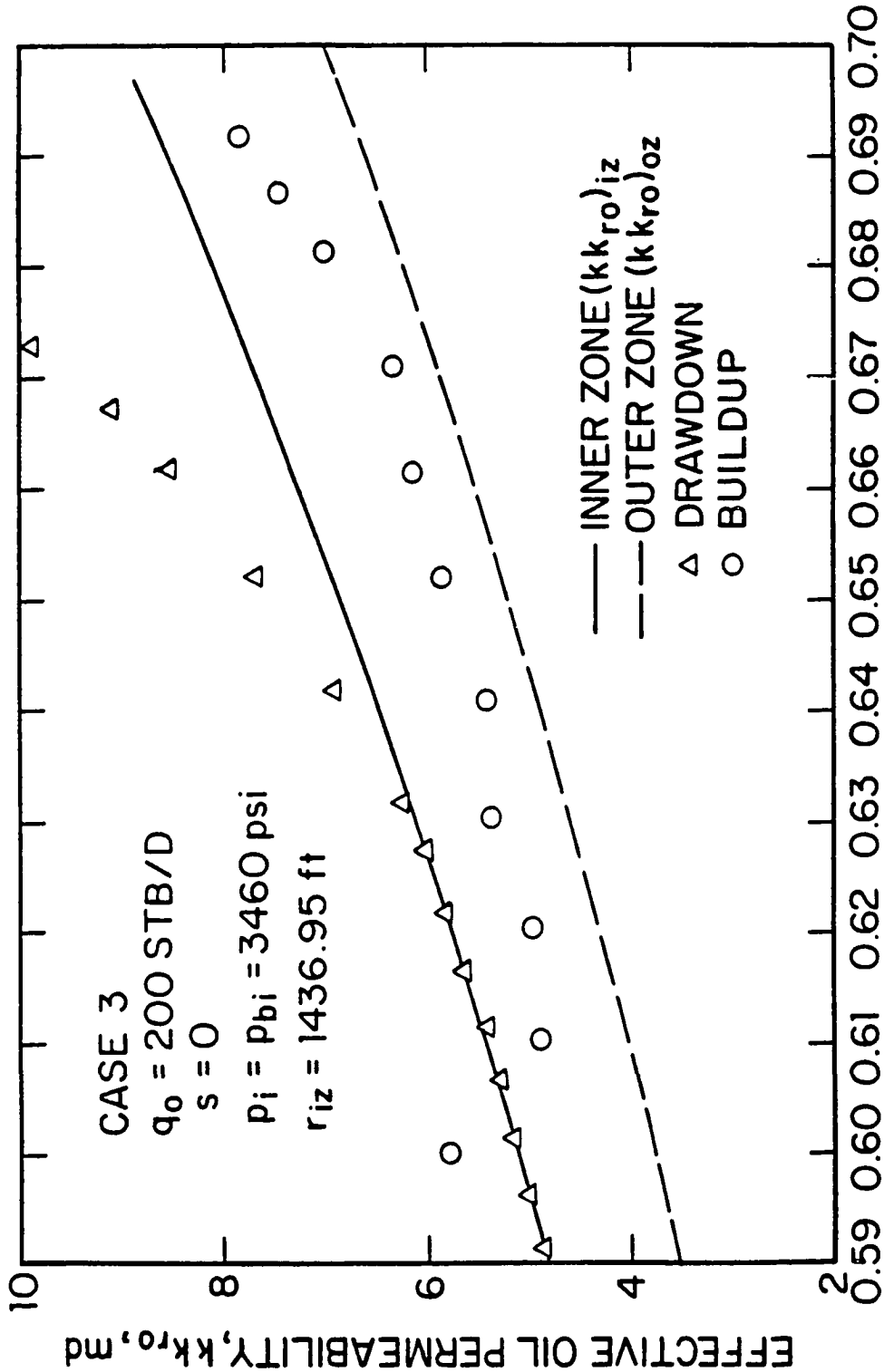

Fig. 5.4.15 - Effective oil permeability as a function of sandface oil saturation; Case 3.

and the dashed curve corresponds to the outer zone input effective oil permeability curve. It can be seen that the kk_{ro} values computed from pressure drawdown data for $0.59014 \leq S_o \leq 0.62792$ (1953.8 psi $\leq p_{wf} \leq$ 2905.5 psi or 3.586×10^{-3} days $\leq t \leq$ 5 days) give an accurate estimate of the inner zone input effective oil permeability data. The radius of the inner zone is sufficiently large such that the computed kk_{ro} values from the pressure drawdown data never see the presence of the outer zone. The buildup kk_{ro} values computed with Eq. 5.4.3 are not very accurate but also tend to reflect only the inner zone kk_{ro} data.

The Case 3 computed effective gas permeabilities plotted versus the simulator drawdown sandface oil saturation are shown in Fig. 5.4.16. In Fig. 5.4.16, the continuous curve corresponds to the inner zone input effective gas permeability curve, the dashed curve corresponds to the outer zone input effective gas permeability curve, the triangular data points represent the effective gas permeability values computed from drawdown pressure data by applying Eq. 5.4.2 and the circular data points represent the effective gas permeability values computed from buildup pressure data by applying Eq. 5.4.4. This figure shows that the computed effective gas permeability values from drawdown data are in very good agreement with the inner zone input effective gas permeability curve throughout the duration of the drawdown test. As in the previous cases, the kk_{rg} values for this case computed from pressure buildup data (circular data points) are not very accurate.

We have presented results for heterogeneous solution-gas-drive systems with small, medium, and large inner zone radii. It is interesting to note that the kk_{ro} values computed from pressure drawdown data follow the same pattern as the pressure for a composite single-phase system. For single-phase flow in a composite reservoir, a semilog plot of the wellbore pressure reflects the properties of the inner zone at early times and the properties of the outer zone at later times; see Ref. 39.

Case 4.

Except for the relative permeability curves, the input data for Case 4 are identical to those for Case 1. In Case 4, Set 1 (Fig. 4.2.1) describes the inner zone relative

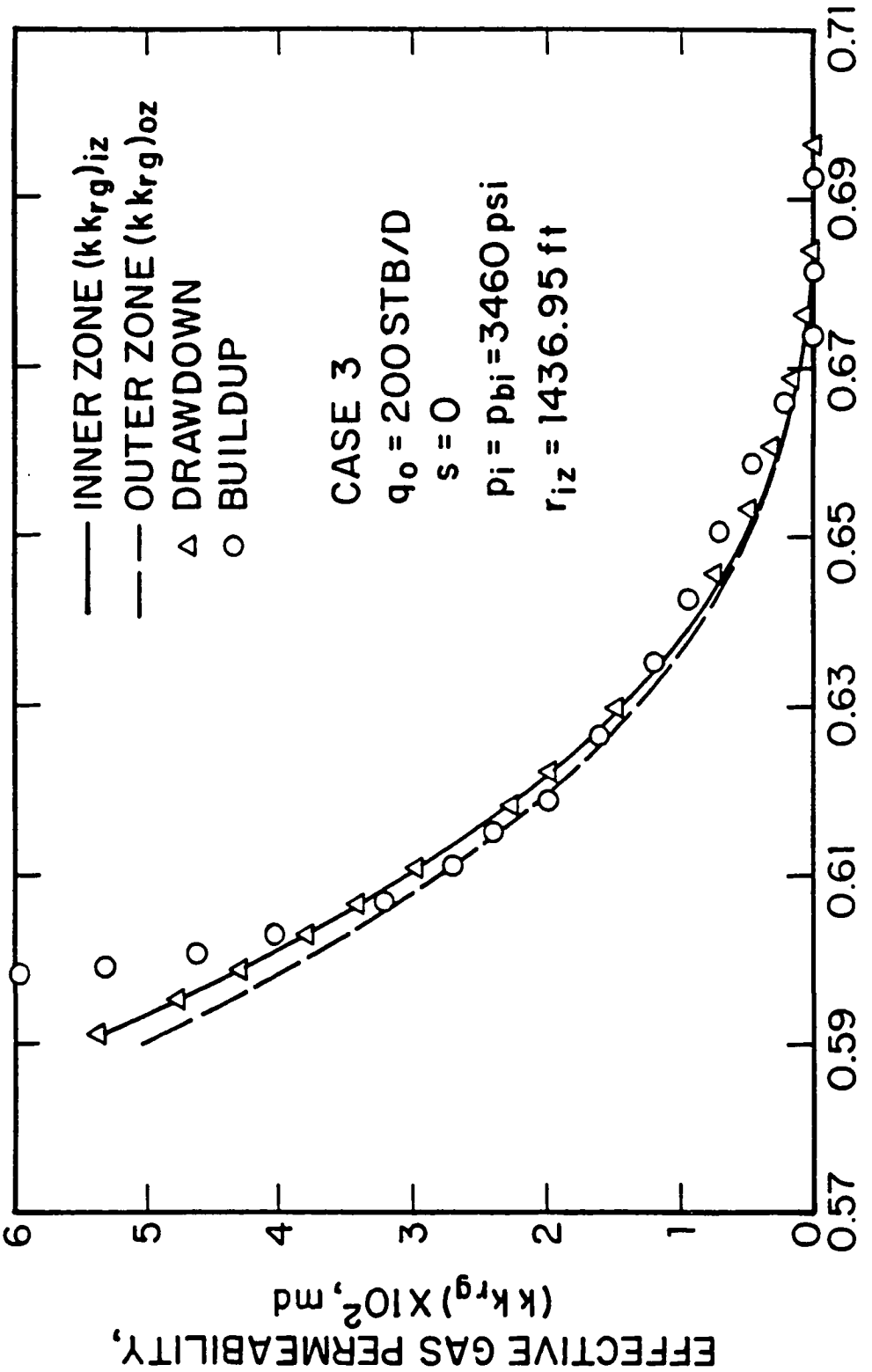

Fig. 5.4.16 - Effective gas permeability as a function of sandface oil saturation; Case 3.

permeabilities and Set 3 (Fig. 5.3.1) represents the outer zone relative permeability curves. Figs. 5.4.17 and 5.4.18, respectively, show the wellbore pressure and the sandface oil saturation variation with respect to time for the Case 4 drawdown and buildup tests. Recall that for this case, the constant oil production rate is $q_o = 200$ STB/D, the inner zone radius is $r_{iz} = 3.91$ ft and the duration of both the drawdown and buildup tests is 5 days. Fig. 5.4.19 presents a plot of effective oil permeability values computed from drawdown pressure data (triangular data points) and from buildup pressure data (circular data points) plotted versus the simulator drawdown sandface oil saturation. The continuous curve corresponds to the inner zone input effective oil permeability curve and the dashed curve corresponds to the outer zone input effective oil permeability curve. It can be seen that, at early times, the kk_{ro} values computed from pressure drawdown data (Eq. 5.4.1) decrease and cross the input outer zone kk_{ro} data, but at later times start increasing and eventually yield a good approximation of the outer zone input kk_{ro} data. Specifically, for $S_o \leq 0.60978$ ($p_{wf} \leq 3266.3$ psi or $t \geq 2.415 \times 10^{-2}$ days), the values of kk_{ro} computed from pressure drawdown data accurately reflect the outer zone kk_{ro} curve. Again the kk_{ro} values computed from buildup data (Eq. 5.4.3) are less accurate, but tend to reflect the outer zone kk_{ro} data. Although, not presented here, the behavior of computed kk_{rg} values is similar to the behavior exhibited by cases discussed earlier.

Case 5.

The input data for this case are identical to the ones for Case 2 except that in Case 5, Set 1 (Fig. 4.2.1) relative permeability curves are used in the inner zone and Set 3 (Fig. 5.3.1) relative permeability curves are used in the outer zone. In Case 5, the constant oil production rate is $q_o = 200$ STB/D, the inner zone radius is $r_{iz} = 46.53$ ft and the duration of both the drawdown and buildup tests is 10 days. The wellbore pressure and the sandface oil saturation variation with respect to time for both drawdown and buildup tests for Case 5 are shown in Figs. 5.4.20 and 5.4.21. Fig. 5.4.22 presents a plot of effective oil permeability values computed from drawdown pressure data (triangular data points) by applying Eq.

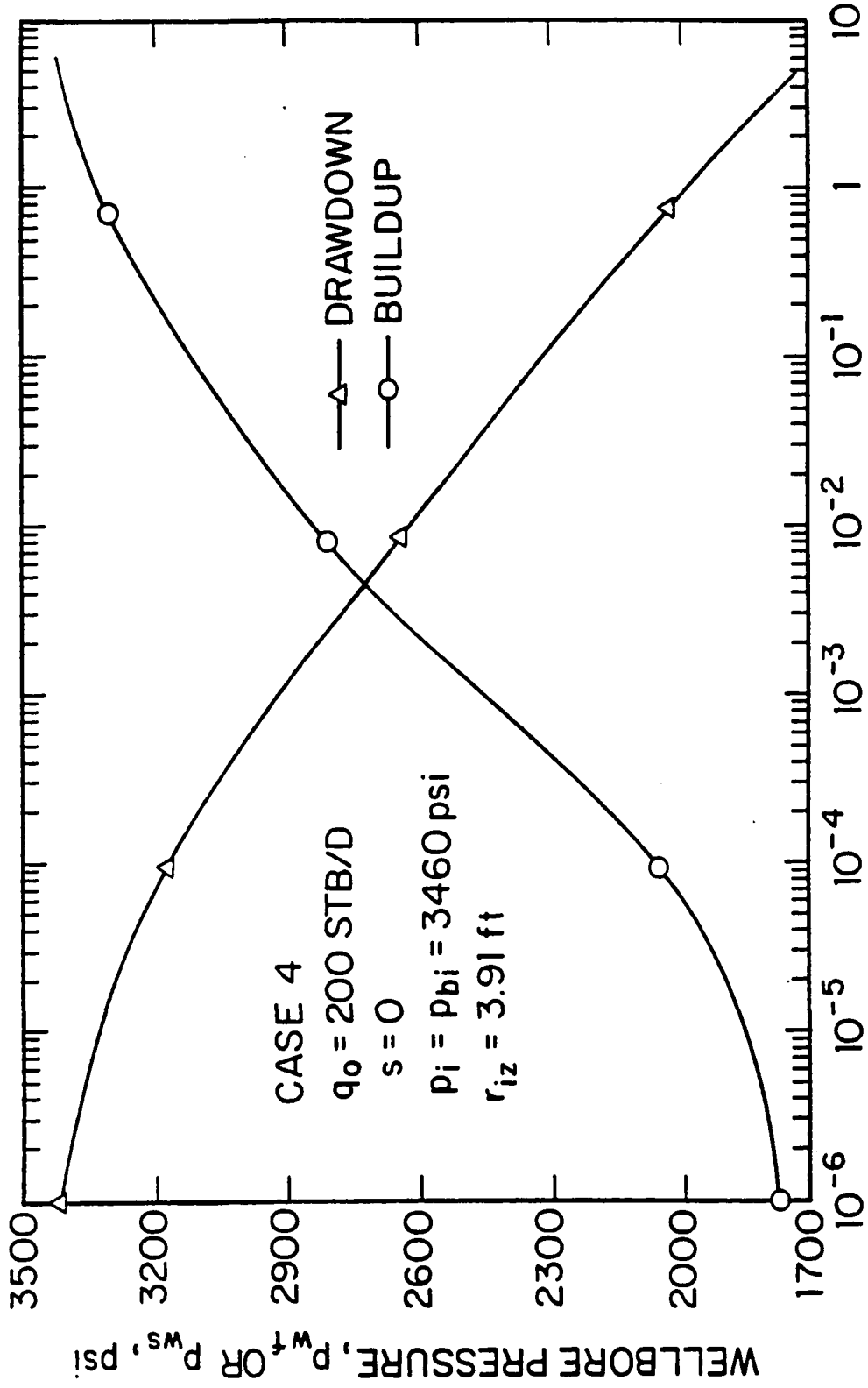

Fig. 5.4.17 - Drawdown and buildup wellbore pressures; Case 4.

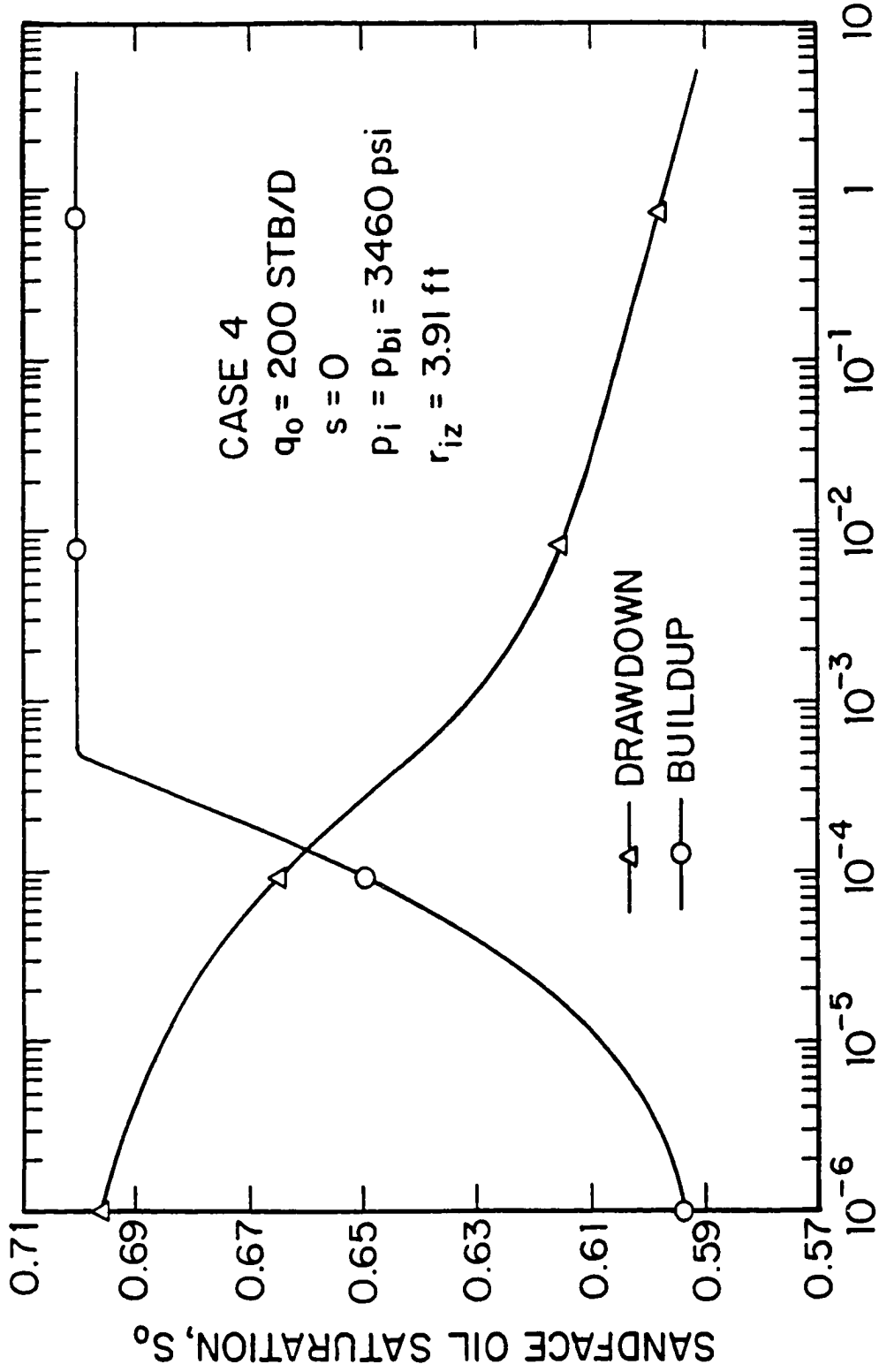

Fig. 5.4.18 - Drawdown and buildup sandface oil saturation; Case 4.

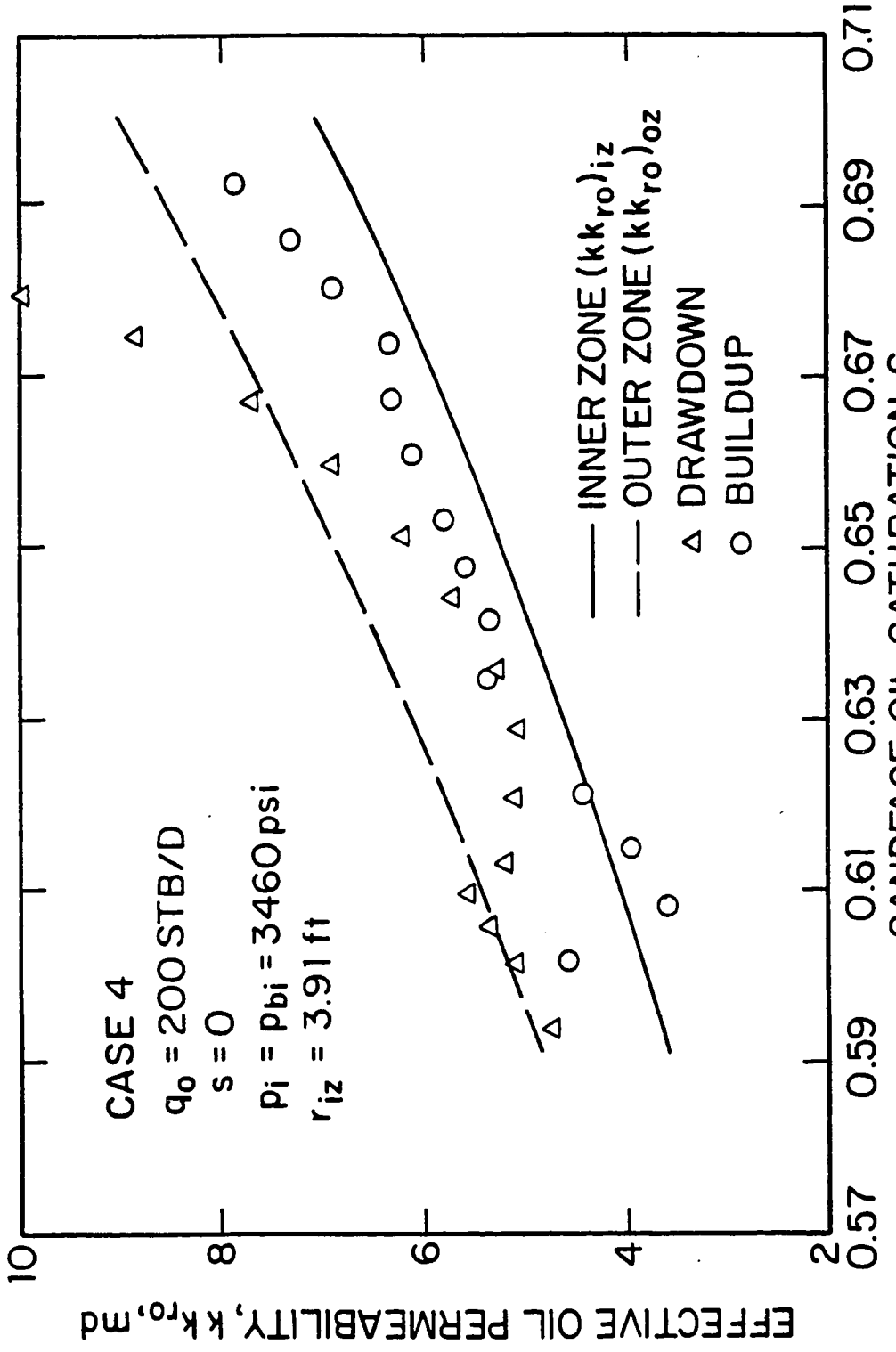

Fig. 5.4.19 - Effective oil permeability as a function of sandface oil saturation; Case 4.

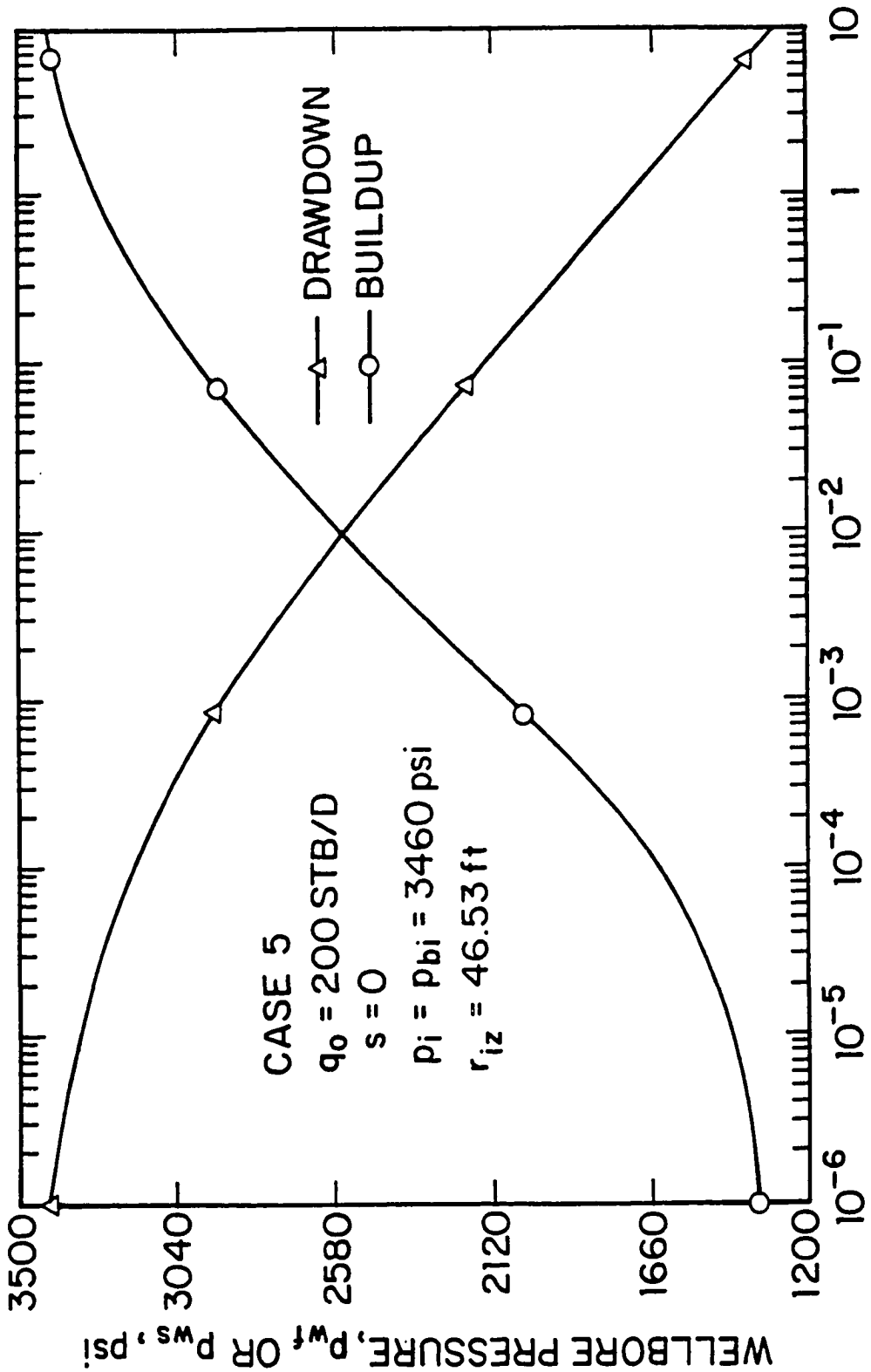

Fig. 5.4.20 - Drawdown and buildup wellbore pressures; Case 5.

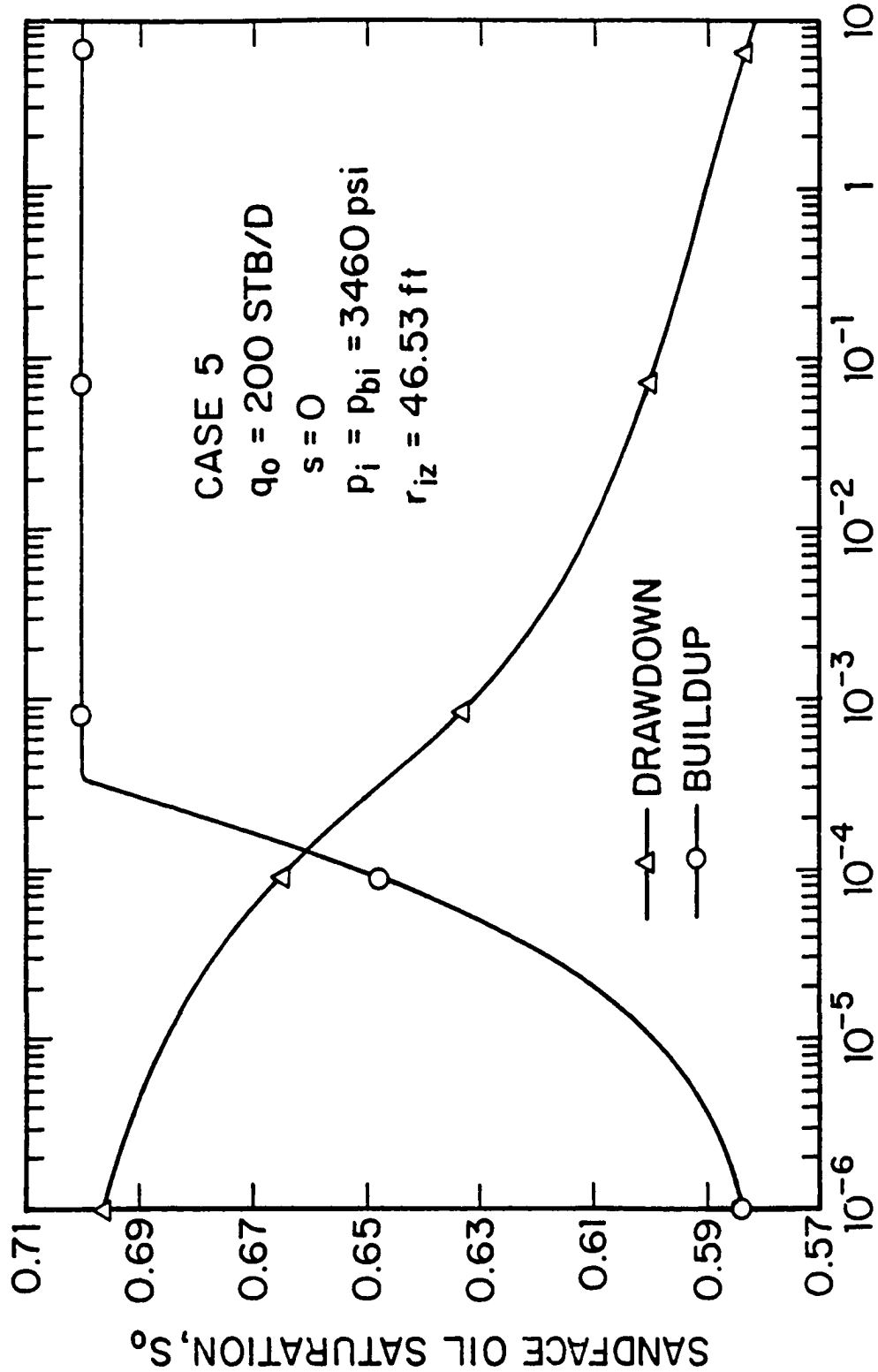

Fig. 5.4.21 - Drawdown and buildup sandface oil saturation; Case 5.

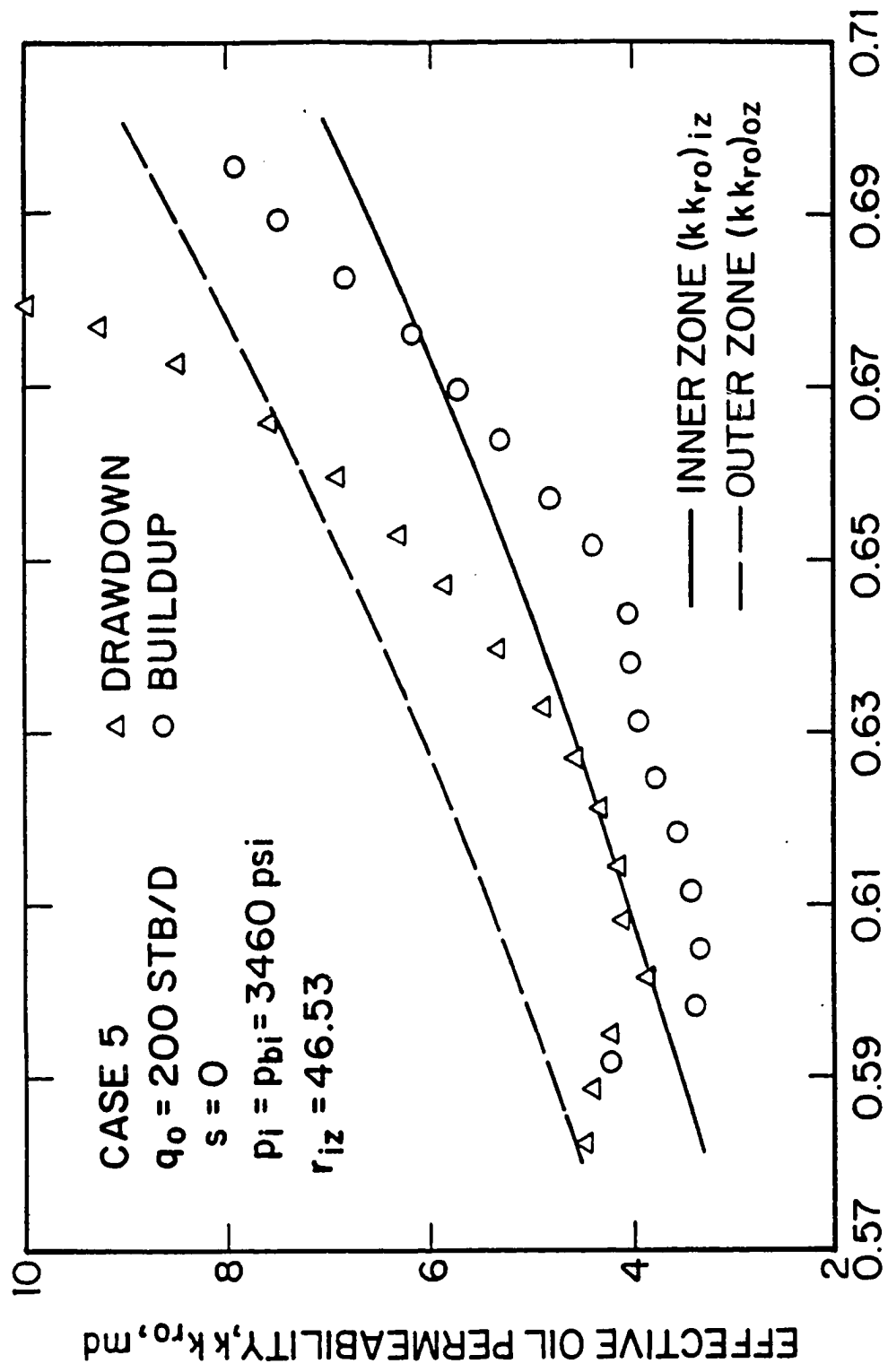

Fig. 5.4.22 - Effective oil permeability as a function of sandface oil saturation; Case 5.

5.4.1, and computed from buildup pressure data (circular data points) by applying Eq. 5.4.3, versus the simulator drawdown sandface oil saturation. The continuous curve corresponds to the inner zone input effective oil permeability curve and the dashed curve corresponds to the outer zone input effective oil permeability curve. It can be seen that the kk_{ro} values computed from pressure drawdown data reflect the inner zone input effective oil permeability data at times corresponding to 4.34×10^{-3} days $\leq t \leq 4.66 \times 10^{-2}$ days (i.e., for $0.60238 \leq S_o \leq 0.61651$ or 2279.2 psi $\leq p_{wf} \leq$ 2689.5 psi). Following this there is a transition period during which the computed kk_{ro} values from drawdown pressure data do not reflect either the inner or the outer zone input kk_{ro} data. Finally, at very late times the computed kk_{ro} values approach the input kk_{ro} data of the outer zone. The buildup computed kk_{ro} values obtained by applying Eq. 5.4.3, tend to reflect the inner zone kk_{ro} data at early times, but at later times they tend to approach the outer zone kk_{ro} data.

The Case 5 effective gas permeabilities computed from Eq. 5.4.4 are not shown, but behave similarly to the ones presented in Case 2, i.e., they reflect the inner zone input effective gas permeability curve as long as the computed kk_{ro} values are accurate estimates of the inner zone input effective oil permeability data, but at later times computed kk_{rg} values do not reflect the outer zone input effective gas permeability curve.

5.4.2 Non-Zero Skin Cases.

In this subsection, we present the results for the cases where skin effects are present in the system and therefore, the inner and outer zone absolute permeabilities are not equal. In these cases the inner zone absolute permeability was computed from Eq. 5.2.1 using the input inner zone radius and skin factor values.

Case 6.

Recall that for Case 6, the constant oil production rate is $q_o = 50$ STB/D, the inner zone radius is $r_{iz} = 3.91$ ft, the skin factor value is $s = 5$ and the duration of both drawdown and buildup tests is 5 days. Using these data, the inner zone absolute permeability values computed from Eq. 5.2.1 is $k_a = 3.313$ md. Finally,

Set 3 (Fig. 5.3.1) describes the inner zone relative permeabilities and Set 1 (Fig. 4.2.1) represents the outer zone relative permeabilities. Figs. 5.4.23 and 5.4.24 show the wellbore pressure and the sandface oil saturation variation with respect to time for both drawdown and buildup tests for Case 6. The simulated and computed kk_{ro} values for both the drawdown and buildup tests are shown in Tables F-29 and F-30, respectively. Similarly, Tables F-31 and F-32 show the simulated and computed kk_{rg} values as a function of wellbore pressure for both the drawdown and buildup tests, respectively. Fig. 5.4.25 presents a plot of effective oil permeability values computed from drawdown pressure data with Eq. 5.4.1 (triangular data points) and computed from buildup pressure data with Eq. 5.4.3 (circular data points) versus the simulator drawdown sandface oil saturation. The continuous curve corresponds to the inner zone input effective oil permeability curve $(kk_{ro})_{iz}$ and the dashed curve corresponds to the outer zone input effective oil permeability curve $(kk_{ro})_{oz}$. Fig. 5.4.25 shows that the kk_{ro} values computed from pressure drawdown data follow the same behavior as in homogeneous systems (see Refs. 9, 10 and 28-30) and yield highly inaccurate results until the skin zone reaches a steady-state behavior. Unlike a homogeneous system, however, after the skin zone reaches a steady-state behavior, there is a transitional period during which the computed kk_{ro} values are located below and parallel to the outer zone effective oil permeability curve. At very late flowing times the computed kk_{ro} values approach the outer zone effective oil permeability data. The kk_{ro} values computed from pressure buildup data are very inaccurate, but seem to approach the outer zone kk_{ro} data as in homogeneous systems (see Refs. 10, 28, and 30) at very late shut-in times.

Case 7.

In Case 7, the constant oil production rate is $q_o = 50$ STB/D, the inner zone radius is $r_{iz} = 46.53$ ft, the skin factor value is $s = 10$ and the duration of both drawdown and buildup tests is 5 days. Using these data, the inner zone absolute permeability value computed from Eq. 5.2.1 is $k_a = 3.313$ md. As in Case 6, Set 3 (Fig. 5.3.1) describes the inner zone relative permeabilities and Set 1 (Fig.

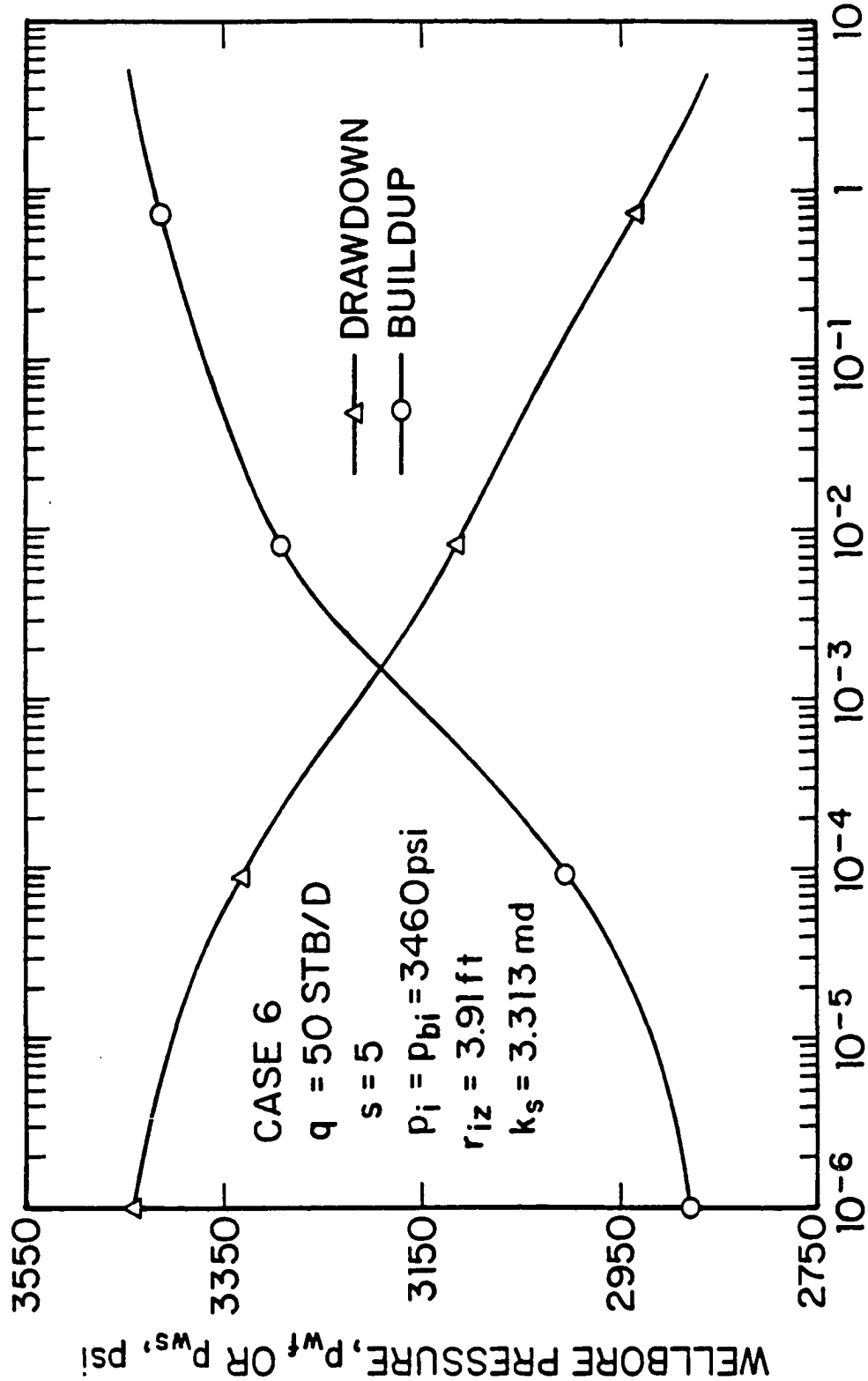

Fig. 5.4.23 - Drawdown and buildup wellbore pressures; Case 6.

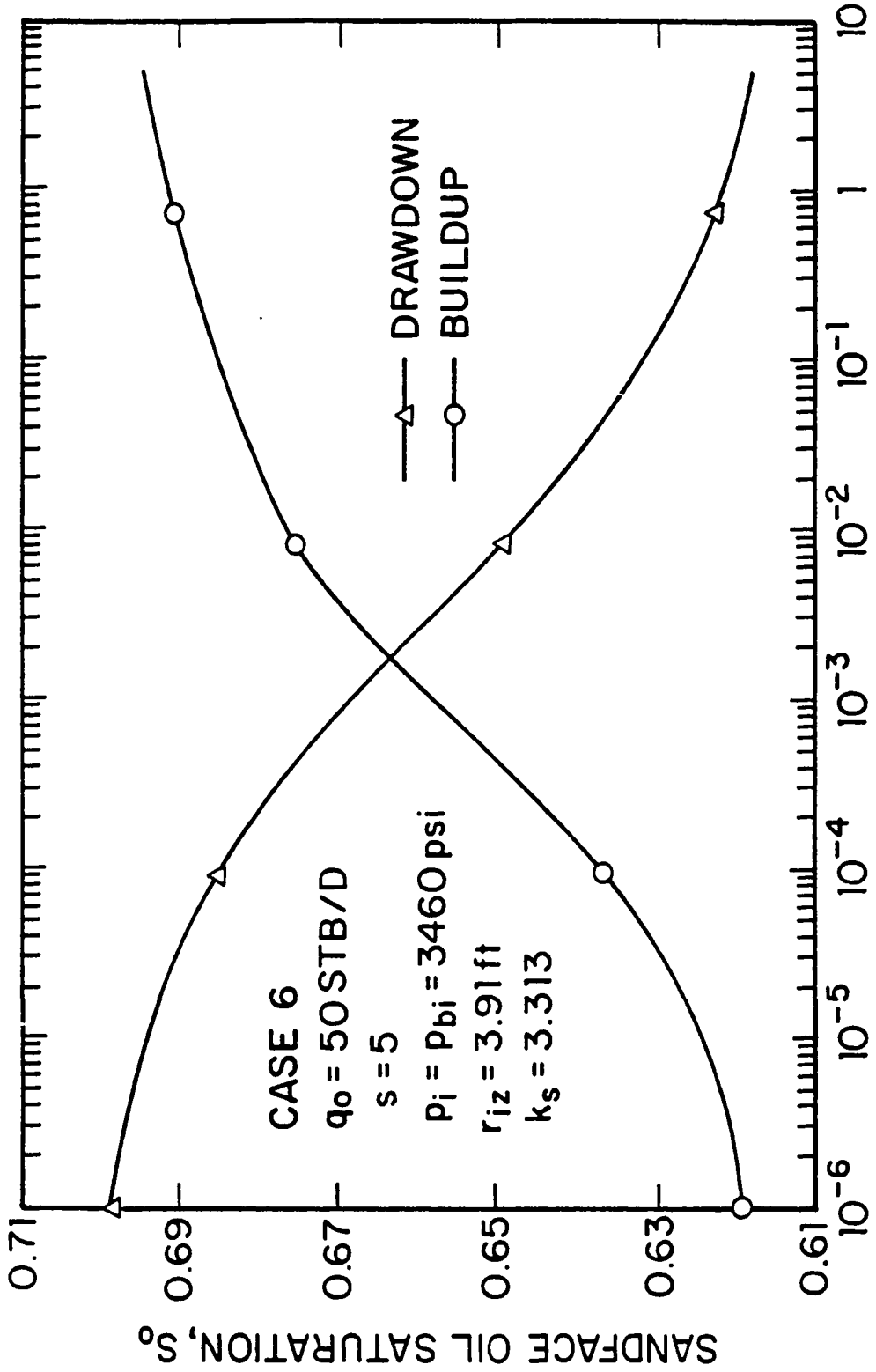

Fig. 5.4.24 - Drawdown and buildup sandface oil saturation; Case 6.

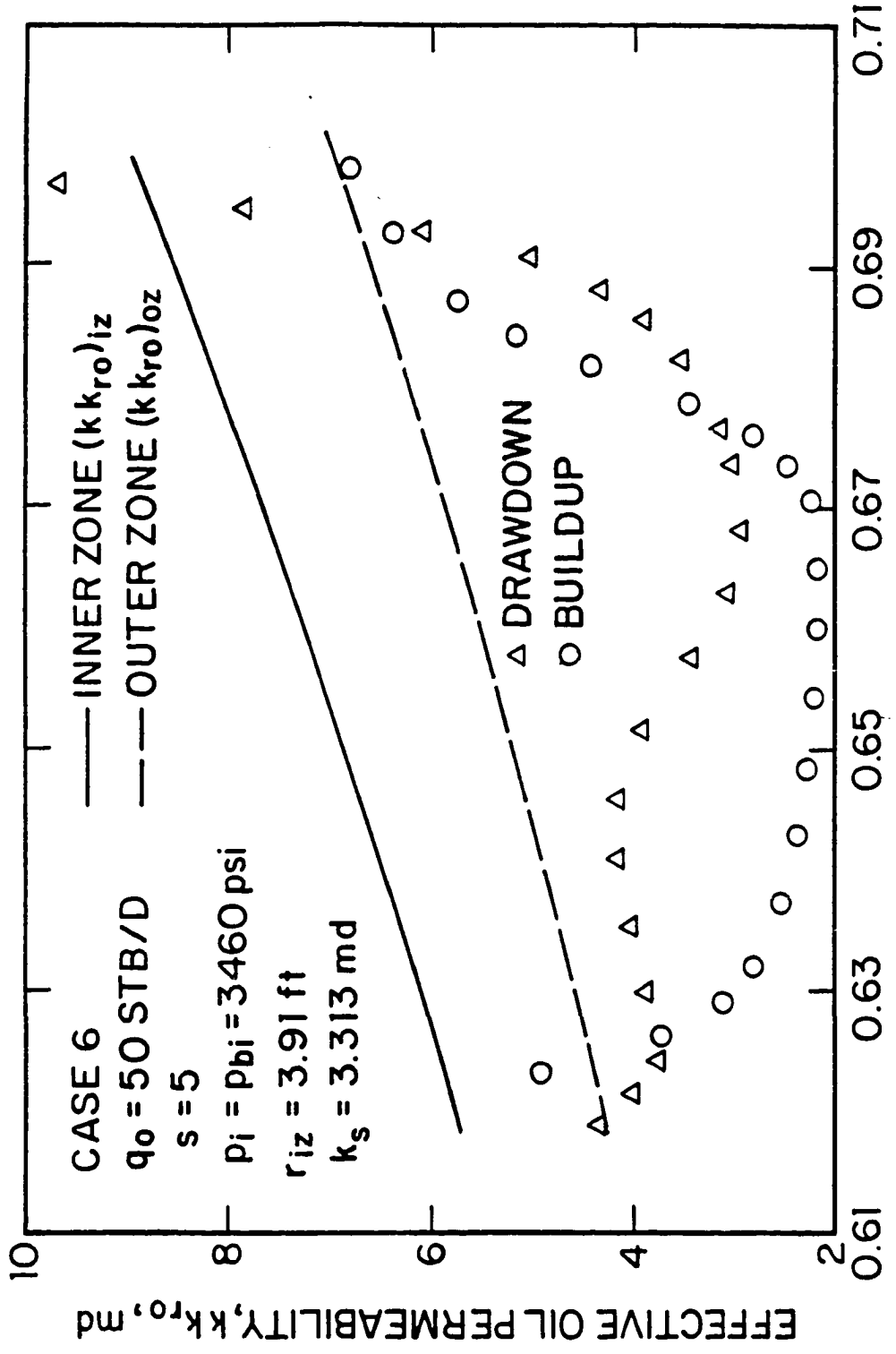

Fig. 5.4.25 - Effective oil permeability as a function of sandface oil saturation; Case 6.

4.2.1) represents the outer zone relative permeabilities. The wellbore pressure and the sandface oil saturation variation with respect to time for both drawdown and buildup tests for Case 7 are shown in Figs. 5.4.26 and 5.4.27, respectively. Fig. 5.4.28 presents a plot of effective oil permeability values computed from drawdown pressure data (triangular data points) and from buildup pressure data (circular data points) versus the simulator drawdown sandface oil saturation. The continuous curve corresponds to the inner zone input effective oil permeability curve $(kk_{ro})_{iz}$, the dashed curve corresponds to the outer zone input effective oil permeability curve $(kk_{ro})_{oz}$ and the broken curve corresponds to the inner zone input effective oil permeability curve $(k_s k_{ro})_{iz}$. This figure shows that the kk_{ro} values computed from pressure drawdown data reflect the relative oil permeability data of the inner zone times the absolute permeability of the same zone, i.e. $(k_s k_{ro})_{iz}$, for $0.62664 \leq S_o \leq 0.64990$ (2903.8 psi $\leq p_{wf} \leq$ 3106.6 psi or 5.777×10^{-3} days $\leq t \leq 8.337 \times 10^{-2}$ days). Unlike Case 6, the computed kk_{ro} results never reflect the outer zone effective oil permeability data during the drawdown flow period. This is due to the fact that the inner zone radius in Case 7 is much larger than the inner zone radius in Case 6. The results of Fig. 5.4.28 indicate that the kk_{ro} values computed from pressure buildup data yield reasonably accurate estimates of the $(k_s k_{ro})_{iz}$ for $0.63 \leq S_o \leq 0.69$, but yield inaccurate values outside of this range. The kk_{rg} values computed from pressure drawdown data, which are not shown, represent a good approximation to the $(k_s k_{rg})_{iz}$ data for $0.63 \leq S_o \leq 0.7$. The kk_{rg} values computed from pressure buildup data also give a reasonably good approximation of the $(k_s k_{rg})_{iz}$ data for the same saturation range.

Case 8.

In Case 8, the constant oil production rate is $q_o = 50$ STB/D, the inner zone radius is $r_{iz} = 1436.95$ ft, the skin factor value is $s = 20$ and the duration of both drawdown and buildup tests is 5 days. Using these data, the inner zone absolute permeability value computed from Eq. 5.2.1 is $k_s = 2.954$ md. As in Cases 6 and 7, Set 3 (Fig. 5.3.1) describes the inner zone relative permeabilities and Set 1 (Fig.

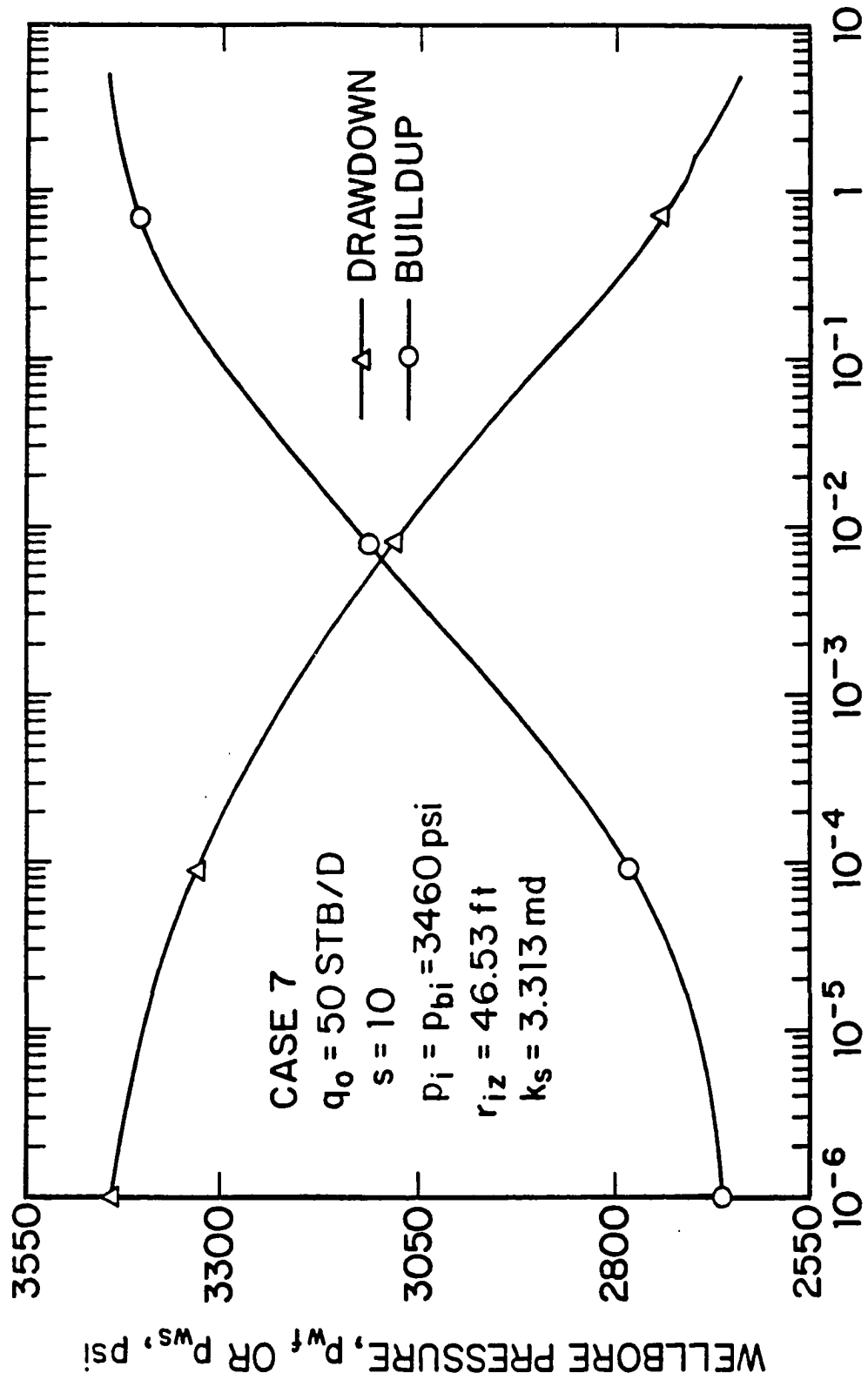

Fig. 5.4.26 - Drawdown and buildup wellbore pressures; Case 7.

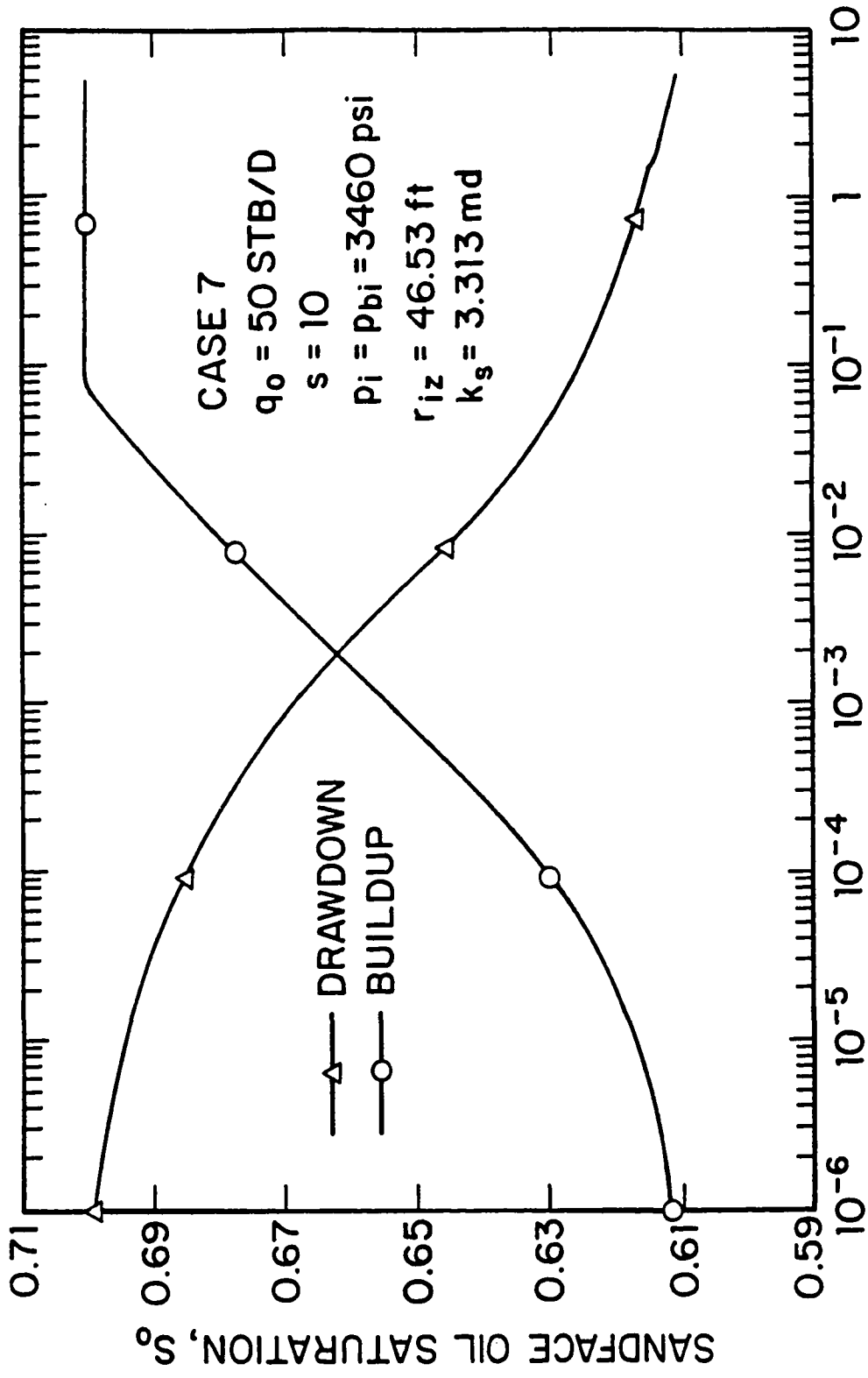

Fig. 5.4.27 - Drawdown and buildup sandface oil saturation; Case 7.

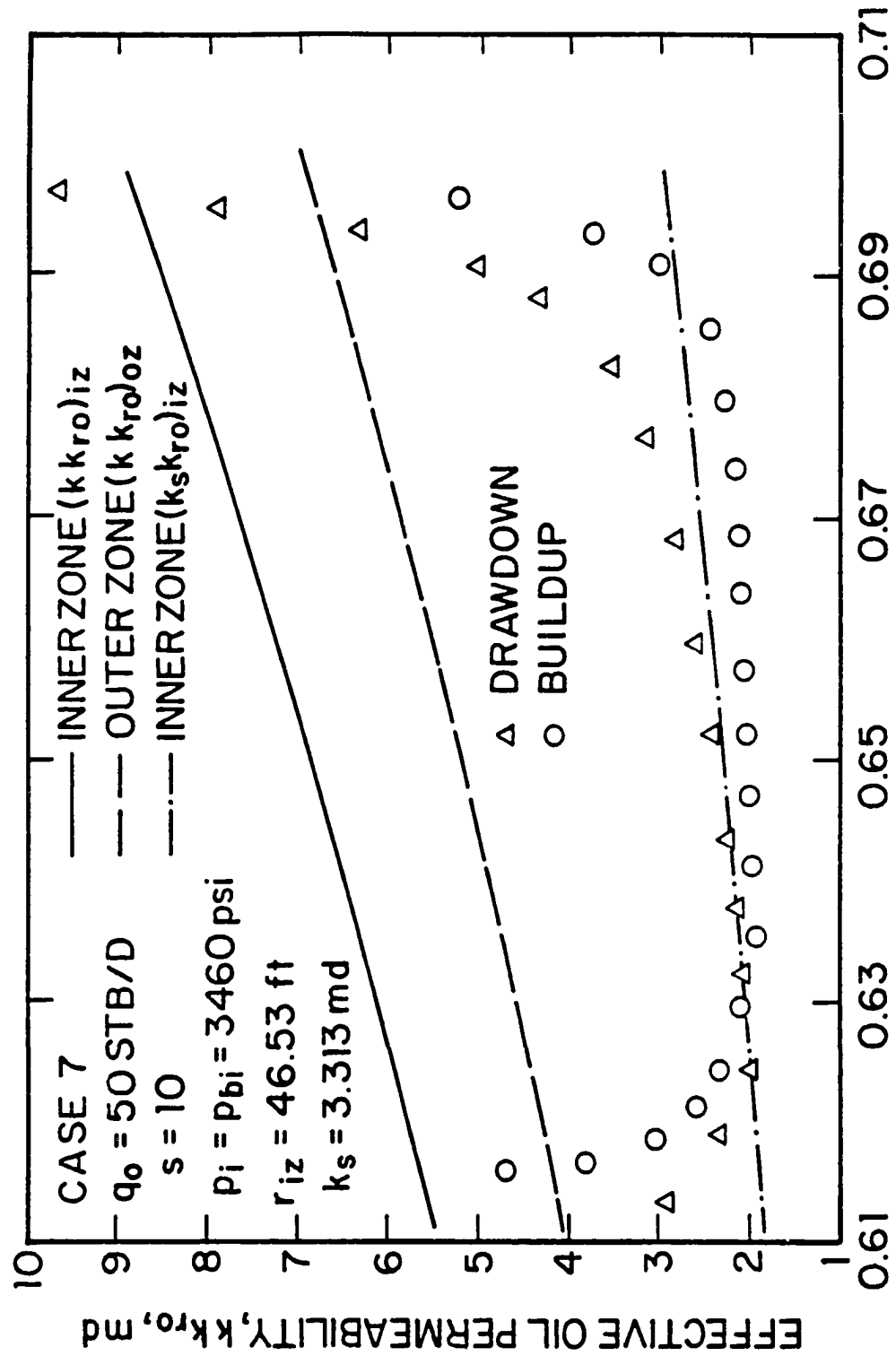

Fig. 5.4.28 - Effective oil permeability as a function of sandface oil saturation; Case 7.

4.2.1) represents the outer zone relative permeabilities. The wellbore pressure and the sandface oil saturation variation with respect to time for both drawdown and buildup tests for Case 7 are shown in Figs. 5.4.29 and 5.4.30, respectively. Fig. 5.4.31 presents a plot of effective oil permeability values computed from drawdown pressure data (triangular data points) and from buildup pressure data (circular data points) versus the simulator drawdown sandface oil saturation. The continuous curve corresponds to the inner zone input effective oil permeability curve $(kk_{ro})_{iz}$, the dashed curve corresponds to the outer zone input effective oil permeability curve $(kk_{ro})_{oz}$ and the broken curve corresponds to the inner zone input effective oil permeability curve $(k_s k_{ro})_{iz}$. This figure shows that the kk_{ro} values computed from pressure drawdown data reflects the relative oil permeability data of the inner zone times the absolute permeability of the same zone, i.e. $(k_s k_{ro})_{iz}$, for $0.60302 \leq S_o \leq 0.65089$ (2403.6 psi $\leq p_{wf} \leq$ 3102.9 psi or 3.586×10^{-3} days $\leq t \leq 5$ days). The computed kk_{ro} values from pressure buildup data also provide reasonably accurate estimates of the $(k_s k_{ro})_{iz}$ data for $0.616 \leq S_c$. In Case 8 the inner zone radius is very large and the outer zone has no influence on the results shown. Thus, Case 8 effectively represents a homogeneous reservoir and the results obtained are similar to those obtained in Refs. 8-10 and 28.

Finally, the computed kk_{rg} values for Case 8 are shown in Fig. 5.4.32. It can be seen that the kk_{rg} values computed from pressure drawdown data provide accurate estimates of the $(k_s k_{rg})_{iz}$ data throughout the drawdown test. Note that the kk_{rg} values computed from pressure buildup data also provide good estimates of the $(k_s k_{rg})_{iz}$ data.

In this Chapter, we have shown that the effective permeabilities estimated from pressure drawdown or buildup data reflect, at early times, the inner zone effective permeability data, and at later times reflect the outer zone effective permeability data for the oil phase. The effective gas permeability of the outer zone cannot be obtained unless the ratios of gas to oil relative permeabilities for both zones are equal. We have also shown that for the cases where $s \neq 0$ the kk_{ro} and kk_{rg} values computed from pressure drawdown data reflect, respectively, the $(k_s k_{ro})_{iz}$

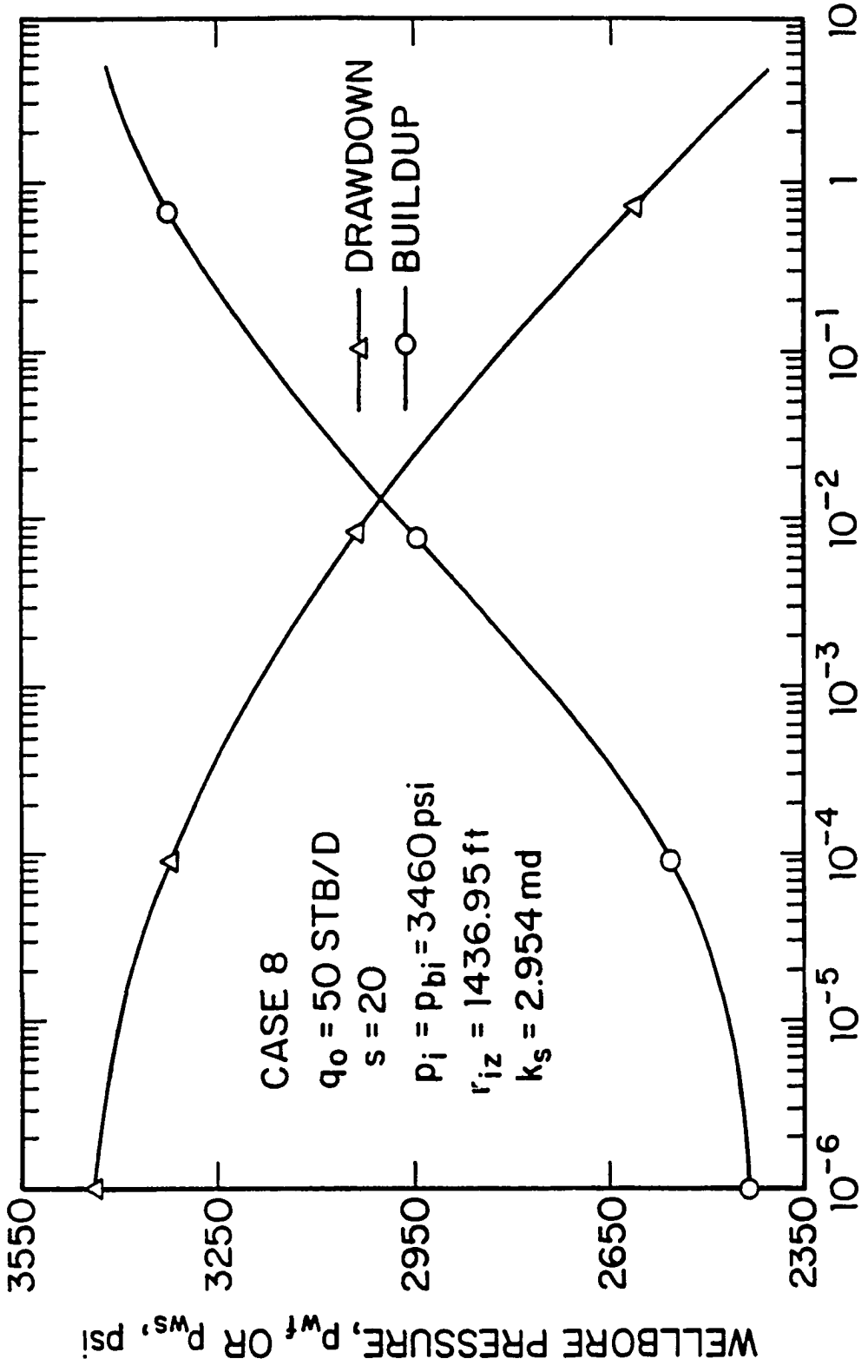

Fig. 5.4.29 - Drawdown and buildup wellbore pressures; Case 8.

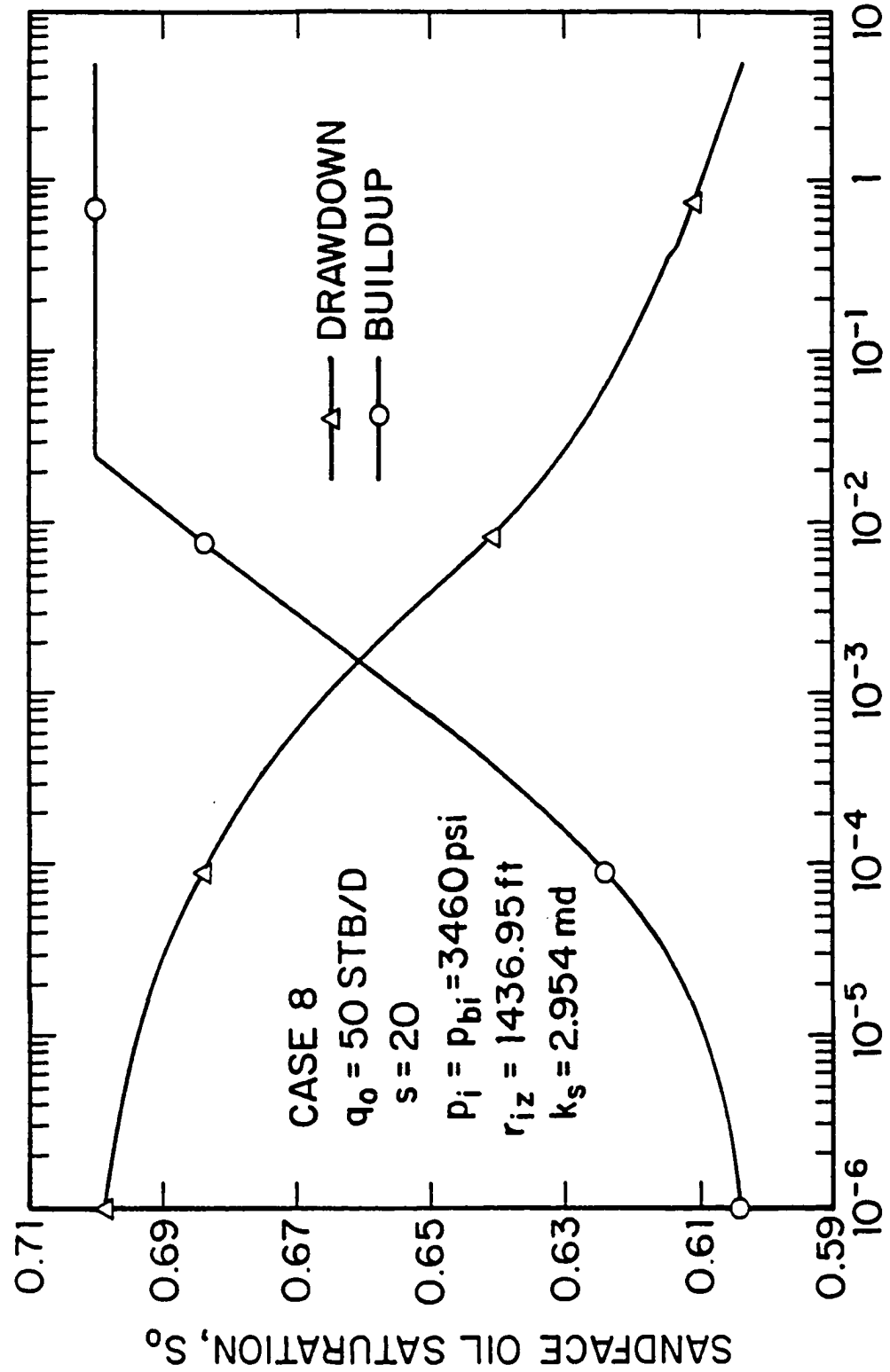

Fig. 5.4.30 - Drawdown and buildup sandface oil saturation; Case 8.

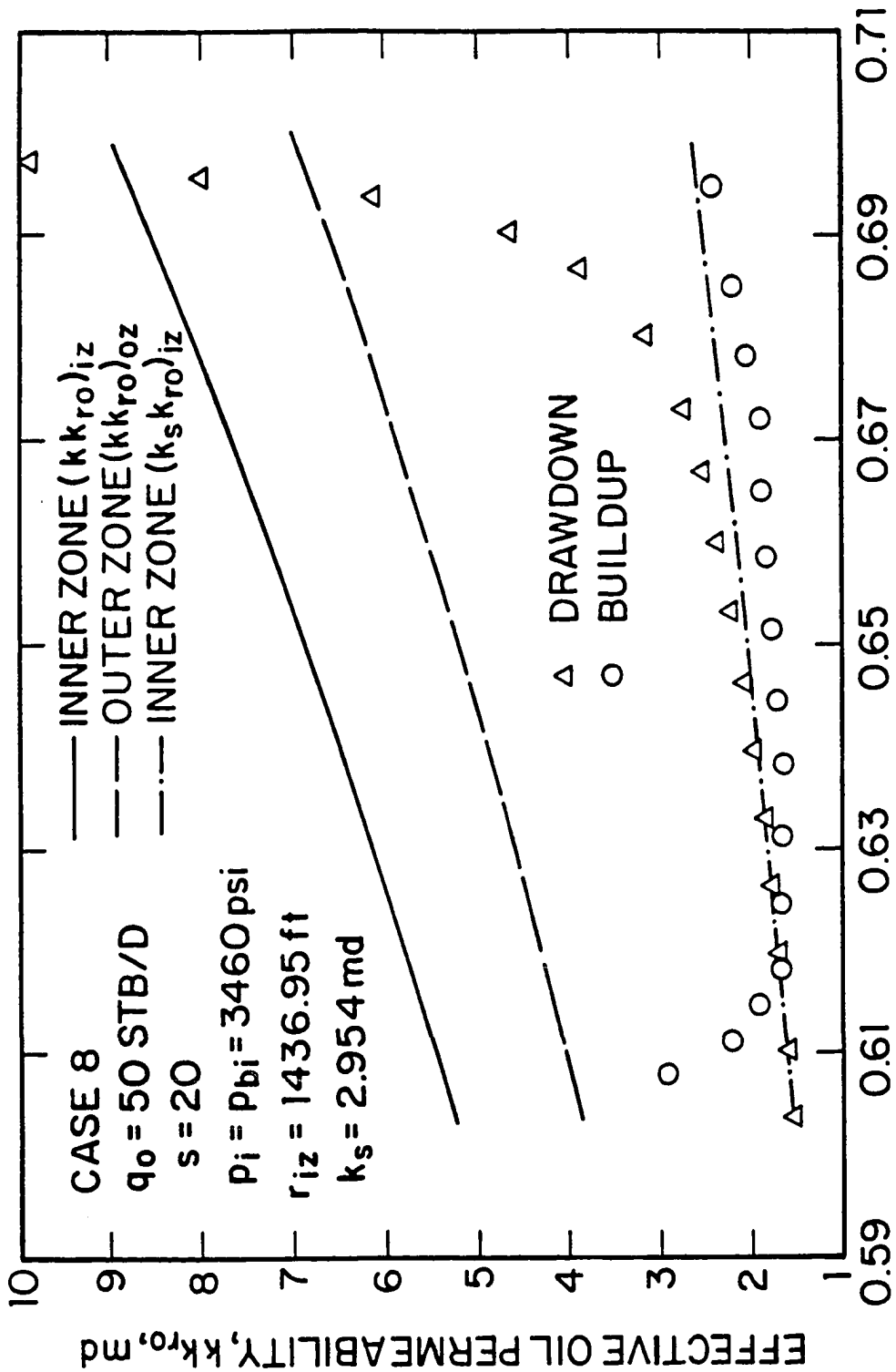

Fig. 5.4.31 - Effective oil permeability as a function of sandface oil saturation; Case 8.

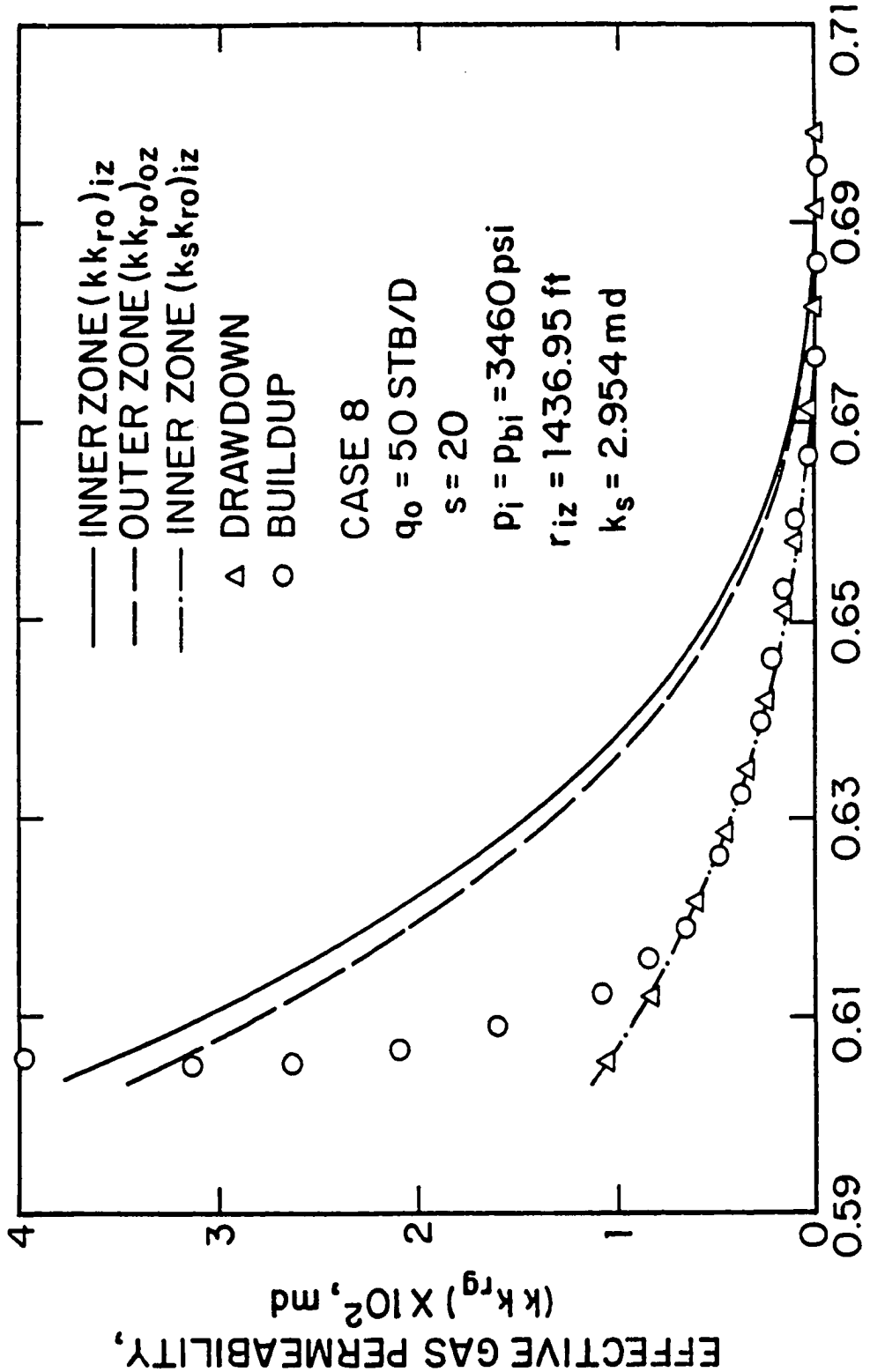

Fig. 5.4.32 - Effective gas permeability as a function of sandface oil saturation; Case 8.

and $(k_s k_{rg})_{iz}$ data of the inner zone.

CHAPTER VI
EFFECT OF WELLBORE STORAGE ON THE ANALYSIS OF MULTIPHASE FLOW PRESSURE DATA

In this Chapter, we investigate the effect of wellbore storage on the analysis of pressure drawdown data obtained at a well producing a solution-gas-drive reservoir. Using new computational equations derived in this Chapter, it is shown that effective oil permeability as a pointwise function of pressure can be computed directly from the measured values of the flowing wellbore pressure provided the sandface oil flow rate is measured and incorporated into the analysis. It is also shown that a semilog plot of wellbore pressure-squared versus time represents a viable method for obtaining estimates of the effective oil permeability at initial conditions, the effective oil permeability at the final value of flowing wellbore pressure and the mechanical skin factor. Finally, for cases where the sandface flow rate is measured we present a new computational procedure for estimating oil saturation as a function of pressure.

6.1 INTRODUCTION

While studies in the reservoir engineering aspects of multiphase flow were conducted at least as early as 1942 (see Evinger and Muskat[3]), the impetus for recent well-testing work in this important area was provided mainly by the work of Bøe et al.[6] and Aanonsen[7]. These works provided some theoretical basis for the use of pseudofunctions to approximately correlate multiphase flow solutions with the corresponding single-phase liquid solution and also provided computational equations for computing oil saturation as a function of pressure. Motivated by the theoretical ideas of Refs. 6 and 7, Peres et al.[40] derived an analytical solution for the oil pseudopressure function and used this solution to generate type curves for analyzing interference pressure data obtained in a solution-gas-drive system.

Recently two major results were achieved on the analysis of well-testing pressure data obtained under multiphase flow conditions. First, Al-Khalifah et al.[8] and Serra et al.[9] showed that one could compute effective permeability as a function of pressure directly from the measured flowing wellbore pressure. Second, Al-Khalifah et al.[11] and Serra et al.[9] showed that one can analyze data by using a semilog plot of the wellbore pressure-squared versus time. The analysis can be used to obtain estimates of the initial value of effective oil permeability, the values of effective permeability at the last measured values of flowing wellbore pressure and the mechanical skin factor. These results were extended to the analysis of buildup data in Refs. 10 and 12. The results of Refs. 8, 9 and 11 pertain to radial flow in solution-gas-drive reservoirs. However, Ref. 9 predicted that the basic computational ideas should extend to gas condensate systems and Thompson and Vo[41] extended the pressure drawdown results of Refs. 8 and 9 to gas condensate reservoirs. Finally, Al-Khalifah et al.[14] presented an overview of the pressure-squared semilog analysis method vis-a-vis semilog analysis based on a plot of pressure versus time. Ref. 14 also showed that, given a specified total flow rate, one could use a semilog plot of the change in pressure-squared divided by the oil flow rate to obtain a rough estimate of the initial oil permeability.

Refs. 5-12 and 14 neglect wellbore storage effects. The objectives of this work are: i) to study the effect of wellbore storage on the analysis of drawdown pressure data obtained at a well producing a solution-gas-drive reservoir; ii) to present new procedures for computing effective permeability as a function of pressure from well-testing pressure data influenced by wellbore storage effects; iii) to present algorithms for computing effective or relative permeability as a function of oil saturation from data influenced by wellbore storage; and iv) to provide methods to estimate the initial effective oil permeability, the effective oil permeability at the last measured values of wellbore pressure and the mechanical skin factor using pressure-squared semilog analysis which does not require *a priori* knowledge of relative permeability data.

6.2 Mathematical Model

The mathematical model considered in this Chapter is similar to the one described in Chapter 3. More specifically, we consider radial flow to a fully penetrating well in a cylindrical, homogeneous solution-gas-drive reservoir of constant thickness. The well is produced at a constant surface oil rate; the porosity and absolute permeability of the system are assumed to be independent of pressure and position, and gravitational and capillary effects are considered to be negligible. The upper, lower and outer reservoir boundaries are considered to be no-flow (sealed) boundaries. The reservoir pressure is assumed to be initially uniform throughout the reservoir and equal to the bubble-point pressure.

The presence of wellbore storage is incorporated in our model by using the exponential decay model of van Everdingen[42] and Hurst[43] where the sandface oil flow rate is related to the oil surface flow rate by

$$q_{osf}(t) = q_o\left(1 - \exp\left(-\alpha^* t\right)\right). \tag{6.2.1}$$

Throughout, q_{osf} denotes the sandface oil flow rate in STB/D, q_o is the constant oil surface rate in STB/D and α^* is a constant with units 1/D which can be adjusted to match field data. This simplified model, which allows the sandface rate to gradually increase from zero to the surface rate during a drawdown test, has been used previously to model wellbore storage effects; see Refs. 42-45.

Absolute permeability is assumed to be constant in the reservoir, but the model allows a different value of absolute permeability in the skin zone. The skin zone is modeled as a concentric region with absolute permeability, k_s, which is different from the absolute permeability of the reservoir, k. Whenever the skin factor is nonzero, the permeability of the skin zone is computed using Hawkins'[32] formula, i.e., Eq. 3.3.1.

The results presented in this study were obtained from a semi-implicit, one-dimensional (radial), variable bubble-point, black-oil reservoir simulator; see Refs. 9, 10, 12 and 28. Although connate water is present in the reservoir, all the results

presented here assume that the water is immobile and incompressible so that the water saturation remains constant throughout the producing period. Thus, only oil and gas flow in the reservoir.

6.3 General Notation and Definitions

This section summarizes much of the general notation and definitions used throughout this Chapter. The parameters α, a, β and b, respectively, are defined by

$$\alpha = \frac{k_{ro}}{\mu_o B_o}, \tag{6.3.1}$$

$$a = \frac{R_s k_{ro}}{\mu_o B_o} + \frac{k_{rg}}{\mu_g B_g}, \tag{6.3.2}$$

$$\beta = \frac{S_o}{B_o}, \tag{6.3.3}$$

and

$$b = \frac{R_s S_o}{B_o} + \frac{S_g}{B_g}. \tag{6.3.4}$$

The insitu gas-oil ratio is defined as follows:

$$R_r = R_s + \left(\frac{k_{rg}}{k_{ro}}\right)\left(\frac{\mu_o B_o}{\mu_g B_g}\right). \tag{6.3.5}$$

The producing GOR is denoted by R and can be computed by evaluating Eq. 6.3.5 at $r = r_w$. The total mobility is defined by the following equation:

$$\lambda_t = \lambda_o + \lambda_g = \frac{k_{ro}}{\mu_o} + \frac{k_{rg}}{\mu_g}. \tag{6.3.6}$$

Using the definition of total mobility, Eq. 6.3.5 can be rewritten as

$$R_r - \left(R_s - \frac{B_o}{B_g}\right) = \frac{\lambda_t}{\lambda_o}\frac{B_o}{B_g}. \tag{6.3.7}$$

Assuming that rock and water compressibility are negligible, we define the total or system compressibility by

$$c_t = -\frac{S_g}{B_g}\frac{dB_g}{dp} + \frac{S_o B_g}{B_o}\frac{dR_s}{dp} - \frac{S_o}{B_o}\frac{dB_o}{dp}, \tag{6.3.8}$$

which is equivalent to the definition of total compressibility presented in the literature by Martin[2]; also see Ramey[46].

The pseudopressure function at the wellbore is defined by

$$p_p(p_{wf}) = p_{p_{wf}} = \int_{p_{wf}}^{p_i} \left(\frac{k_{ro}}{\mu_o B_o}\right) dp, \tag{6.3.9}$$

where p_{wf} denotes the flowing wellbore pressure. Note that $p_p(p_{wf})$ can be computed only if oil relative permeability data *as a function of pressure* are known. The dimensionless pseudopressure drop at the wellbore is defined by

$$p_{pwD} = \frac{khp_p(p_{wf})}{141.2q_o} = \frac{kh\int_{p_{wf}}^{p_i}\left(\frac{k_{ro}}{\mu_o B_o}\right)dp}{141.2q_o}. \tag{6.3.10}$$

Dimensionless time is defined by

$$t_D = \frac{6.328\times 10^{-3}k\lambda_{ti}t}{\phi c_{ti}r_w^2}, \tag{6.3.11}$$

where the subscript i denotes initial conditions, time, t, is in days, and λ_{ti} denotes the initial value of total mobility. For cases considered here, the initial pressure is equal to the bubble-point pressure and $\lambda_{ti} = \lambda_{oi}$.

Finally, the dimensionless sandface oil flow rate is obtained by dividing Eq. 6.2.1 by the surface oil flow rate q_o and is given by

$$q_{osfD} = \frac{q_{osf}}{q_o} = 1 - \exp(-\beta^* t_D), \tag{6.3.12}$$

where the first equality of Eq. 6.3.12 serves to define q_{osfD} and

$$\beta^* = \frac{\alpha^*\phi\mu_{oi}c_{ti}r_w^2}{6.328\times 10^{-3}(kk_{ro})_i}, \tag{6.3.13}$$

is the dimensionless analogue of the wellbore storage parameter α^*. It is difficult to find a unique relation between the wellbore storage model of Eq. 6.3.12 and the standard constant wellbore storage coefficient model commonly used in well testing theory[47] because Eq. 6.3.12 represents a wellbore storage model where the wellbore storage coefficient can change with time. According to Ref. 47, the

effects of wellbore storage become negligible at $t_D = 60C_D$ if $s = 0$. If we set the dimensionless sandface rate of Eq. 6.3.12 equal to the dimensionless sandface rate predicted by the model of Ref. 47 at $t_D = 60C_D$ and solve the resulting equation for C_D, we find

$$C_D = \frac{1}{12.53\beta^*}. \tag{6.3.14}$$

While Eq. 6.3.14 is only approximate, when it holds, the dimensionless sandface rate predicted by Eq. 6.3.12 is not significantly different from the dimensionless sandface rate predicted by the constant wellbore storage coefficient model of Ref. 47.

6.4 Simulator Data

The PVT and relative permeability data used are given in Tables A-1 and A-2, respectively. For all results presented in this Chapter, the value of connate water saturation is held fixed with $S_{wc} = 0.3$, and the critical gas saturation is given by $S_{gc} = 0.0$. The initial reservoir pressure and bubble-point pressure values are equal and given by $p_i = p_{bi} = 3460$ psi. The initial values of total compressibility, oil viscosity and oil FVF, respectively, are specified as $c_{ti} = 0.23564 \times 10^{-4}$ psi $^{-1}$, $\mu_{oi} = 0.43059$ cp and $B_{oi} = 1.5882$ RB/STB. Throughout, the wellbore radius, external reservoir boundary radius, reservoir thickness, porosity and absolute permeability, respectively, are specified as $r_w = 0.328$ ft, $r_e = 6600$ ft, $h = 15.547$ ft, $\phi = 0.3$ and $k = 10$ md, but the values of these parameters have no influence on the validity of the procedures and conclusions presented in this Chapter. For all cases considered, the well is produced at a constant surface oil flow rate, but the sandface oil rate varies according to the wellbore model described by Eq. 6.2.1. All results presented pertain to the infinite-acting period, that is, the closed outer boundary has no influence on the results obtained. Throughout, the dimensionless sandface rate is specified by Eq. 6.3.12. The corresponding values of C_D, as predicted by Eq. 6.3.14, are recorded for each case.

In this Chapter, results are presented for the following six cases:

Case 1 : $q_o = 150$ STB/D; s = 0; No wellbore storage ($\beta^* \rightarrow \infty$);

Case 2 : q_o = 150 STB/D; s = 0; $\beta^* = 6.8 \times 10^{-4}$ ($C_D \approx 117.4$);

Case 3 : q_o = 150 STB/D; s = 0; $\beta^* = 6.8 \times 10^{-5}$ ($C_D \approx 1174$);

Case 4 : q_o = 100 STB/D; s = 5; $\beta^* = 6.8 \times 10^{-5}$ ($C_D \approx 1174$);

Case 5 : q_o = 100 STB/D; s = 5; $\beta^* = 6.8 \times 10^{-4}$ ($C_D \approx 117.4$);

Case 6 : q_o = 100 STB/D; s = 5; No wellbore storage ($\beta^* \rightarrow \infty$).

Each figure presented contains information which identifies the case(s) presented in the figure. Cases 2-5 allow us to examine the effect of wellbore storage with and without a skin effect. Case 1 considers a problem where both wellbore and skin effects are completely negligible and Case 6 refers to a problem where the skin factor is positive, but wellbore storage effects do not exist, that is, $q_{osf} = q_o$ at all times.

6.5 Theoretical Results

6.5.1 Effect of Wellbore Storage on Pressure and Saturation.

In this subsection, we illustrate the effect of wellbore storage on the sandface values of pressure and saturation obtained from our simulator. In Figs. 6.5.1 - 6.5.4, 6.5.6, 6.5.8 and 6.5.9, curves through open triangular data points represent the zero wellbore storage case with $s = 0$ (Case 1), curves through open square data points correspond to the case where $s = 0$ and $\beta^* = 6.8 \times 10^{-4}$ (Case 2) and curves through open circular data points represent results obtained for the case where $s = 0$ and $\beta^* = 6.8 \times 10^{-5}$ (Case 3).

It is important to recall that our wellbore storage model (see Eq. 6.2.1 or Eq. 6.3.12) indicates that, at early times, the rate of production from the reservoir into the wellbore is much less than the specified value of the surface oil rate. Thus, for a given value of the surface oil flow rate, decreasing β^*, i.e., increasing the effect of wellbore storage, should increase the sandface values of pressure and saturation obtained at a given time. Figs. 6.5.1 and 6.5.2, respectively, display semilog plots of wellbore pressure and oil saturation at the sandface versus time, t. As expected, the presence of wellbore storage delays the time at which pressure and oil saturation decrease significantly. The bottom curves on both figures represent the results

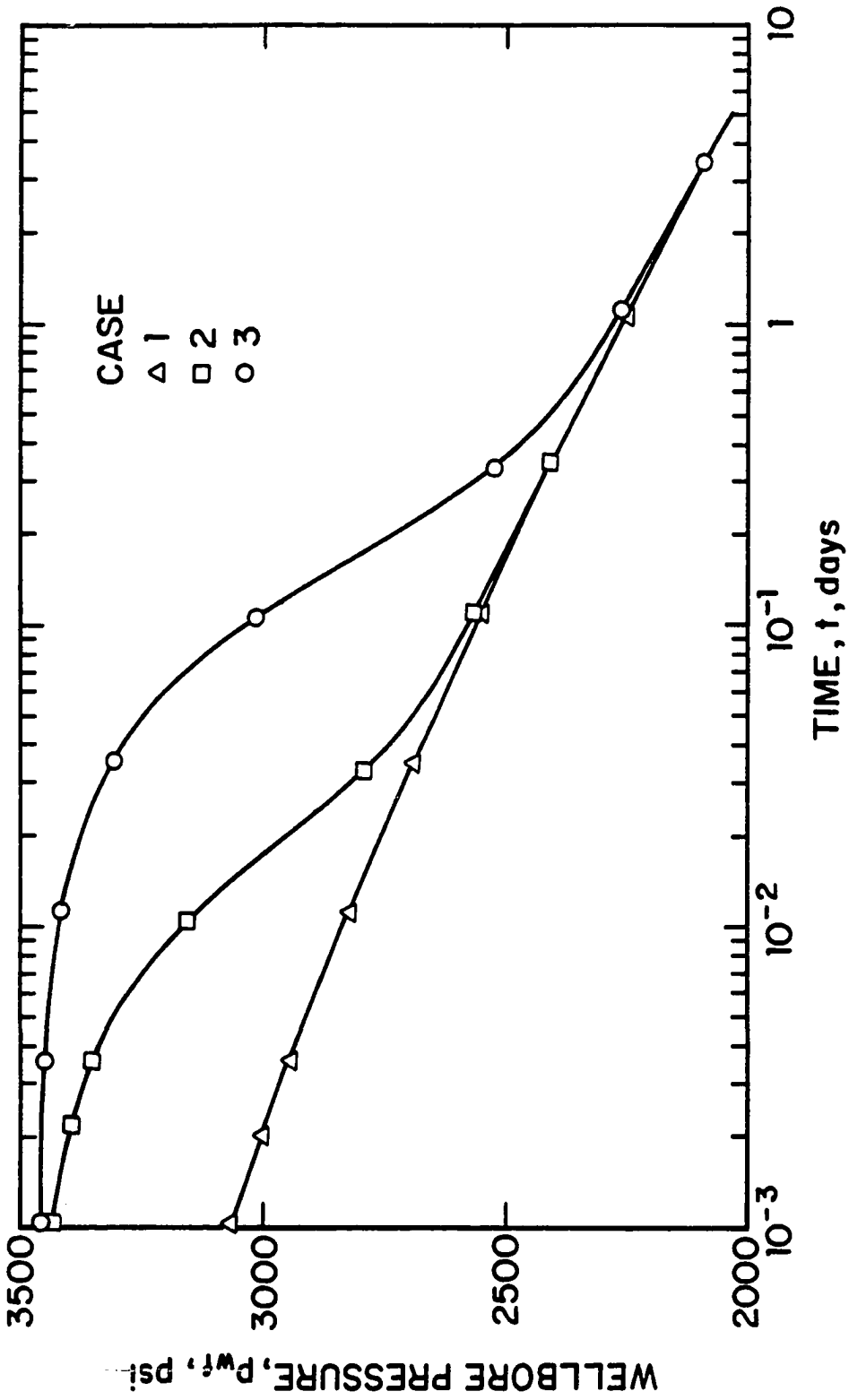

Fig. 6.5.1 - Effect of wellbore storage on the flowing wellbore pressure; Cases 1, 2 and 3.

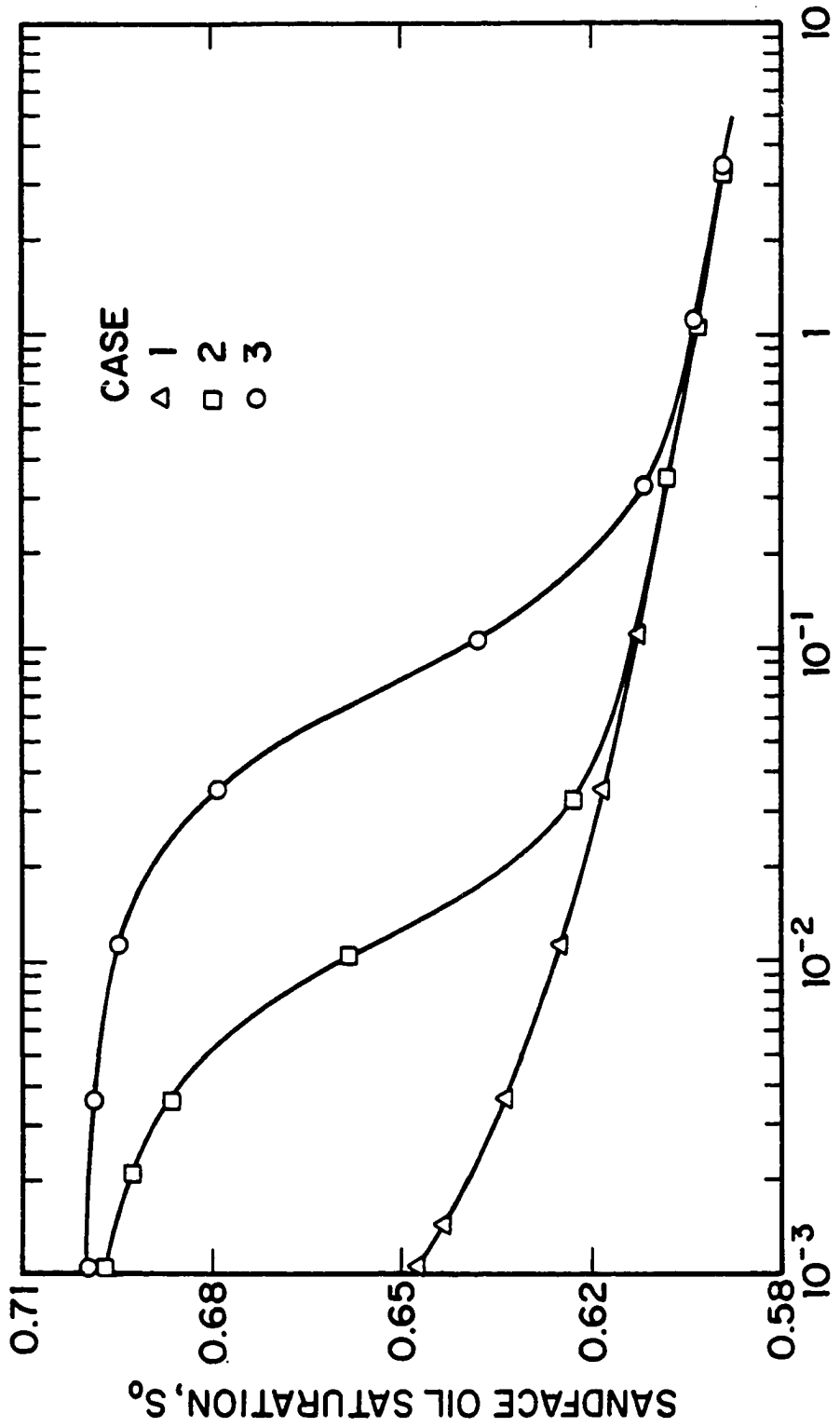

Fig. 6.5.2 - Effect of wellbore storage on the sandface oil saturation; Cases 1, 2 and 3.

obtained for the zero wellbore storage case. Note that as time increases the effects of wellbore storage diminish (that is, $q_{osf} \rightarrow q_o$) and the sandface values obtained for the wellbore storage cases approach the corresponding values obtained for the no wellbore storage case, Case 1.

Fig. 6.5.3 presents a Cartesian plot of sandface oil saturation versus wellbore pressure for Cases 1, 2 and 3, i.e., for the same cases considered in Figs. 6.5.1 and 6.5.2. The results are remarkable in that they illustrate that the basic sandface oil saturation/pressure relation is almost independent of wellbore storage, that is, the effect of an increasing sandface oil flow rate on the pressure/saturation relation is almost negligible even though wellbore storage has a pronounced effect on the individual values of pressure and saturation obtained; see Figs. 6.5.1 and 6.5.2. For $p_{wf} > 2900$ psi, however, the small difference in the S_o versus p_{wf} relation will cause the k_{ro} versus p_{wf} relation to vary slightly from case to case and thus, $p_p(p_{wf})$ and p_{pwD} will vary slightly from case to case. Fig. 6.5.4 shows a Cartesian plot of the producing GOR versus the wellbore pressure. Similar to Fig. 6.5.3, the results of Fig. 6.5.4 indicate that the producing GOR versus pressure relation is only slightly affected by the presence of wellbore storage effects.

The curve through circular data points in Fig. 6.5.5 represents the dimensionless sandface oil rate predicted by Eq. 6.3.12 when $\beta^* = 6.8 \times 10^{-5}$. The curve through triangular data points and the curve through square data points represent the dimensionless sandface flow rate predicted by the single-phase flow constant wellbore storage model of Ref. 47 for $C_D = 1174$ and $C_D = 4184$, respectively. Note that the dimensionless sandface rate for the $C_D = 4184$ solution of Ref. 47 provides a good approximation of the rate predicted by Eq. 6.3.12 at all times. However, for the $C_D = 4184$ case the dimensionless sandface rate becomes equal to one at $t_D \approx 6 \times 10^5$, whereas the sandface rate predicted by Eq. 6.3.12 becomes equal to one ($q_{osf} = q_o$) at $t_D \approx 10^5$. On the other hand, the sandface rate for the $C_D = 1174$ solution of Ref. 47 becomes equal to the rate predicted by Eq. 6.3.12 when $t_D = 60C_D = 7 \times 10^4$ as predicted by the discussion of Eq. 6.3.14.

Fig. 6.5.6 shows a log-log plot of the dimensionless wellbore pseudopressure

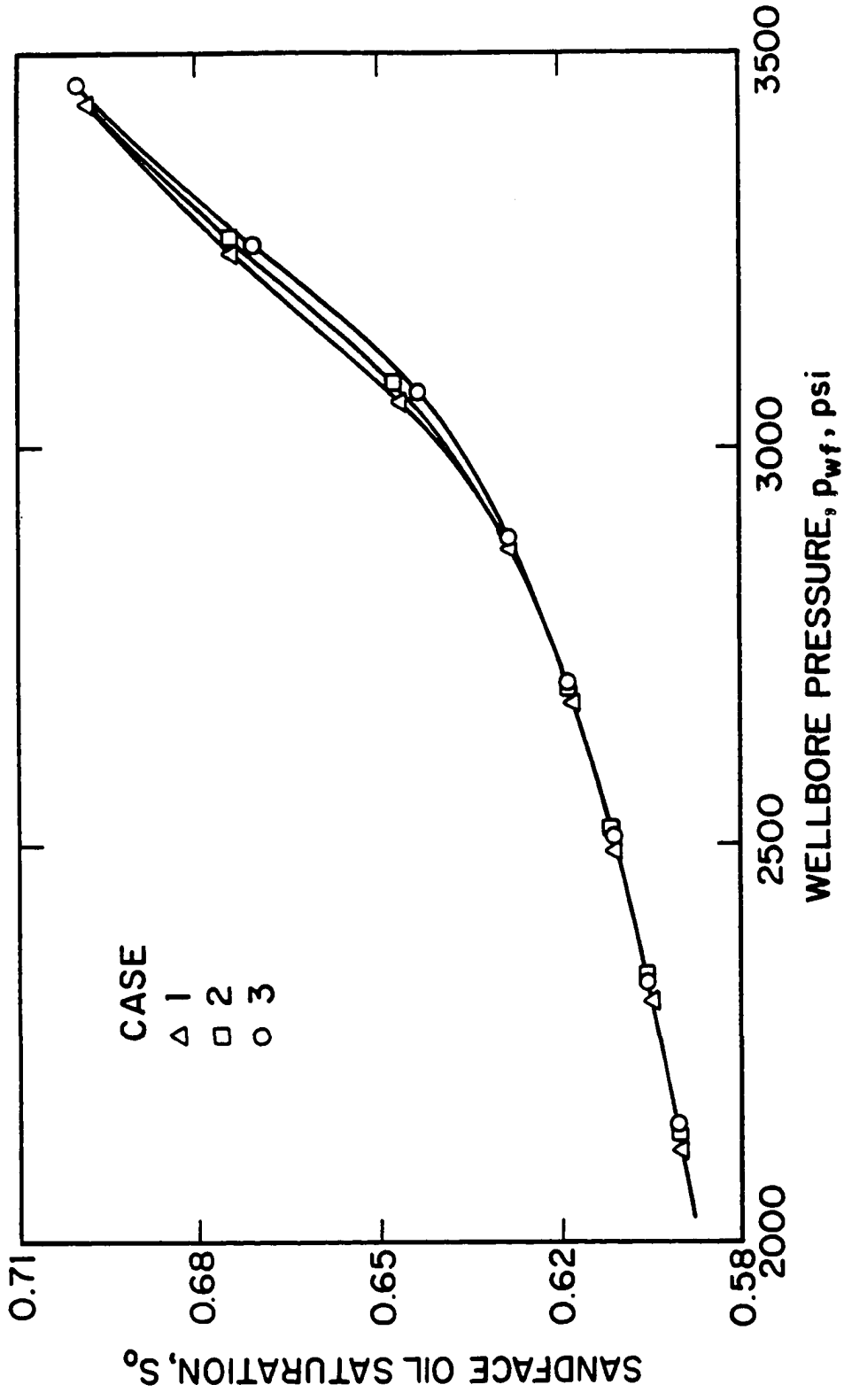

Fig. 6.5.3 - Sandface oil saturation as a function of flowing wellbore pressure; Cases 1, 2 and 3.

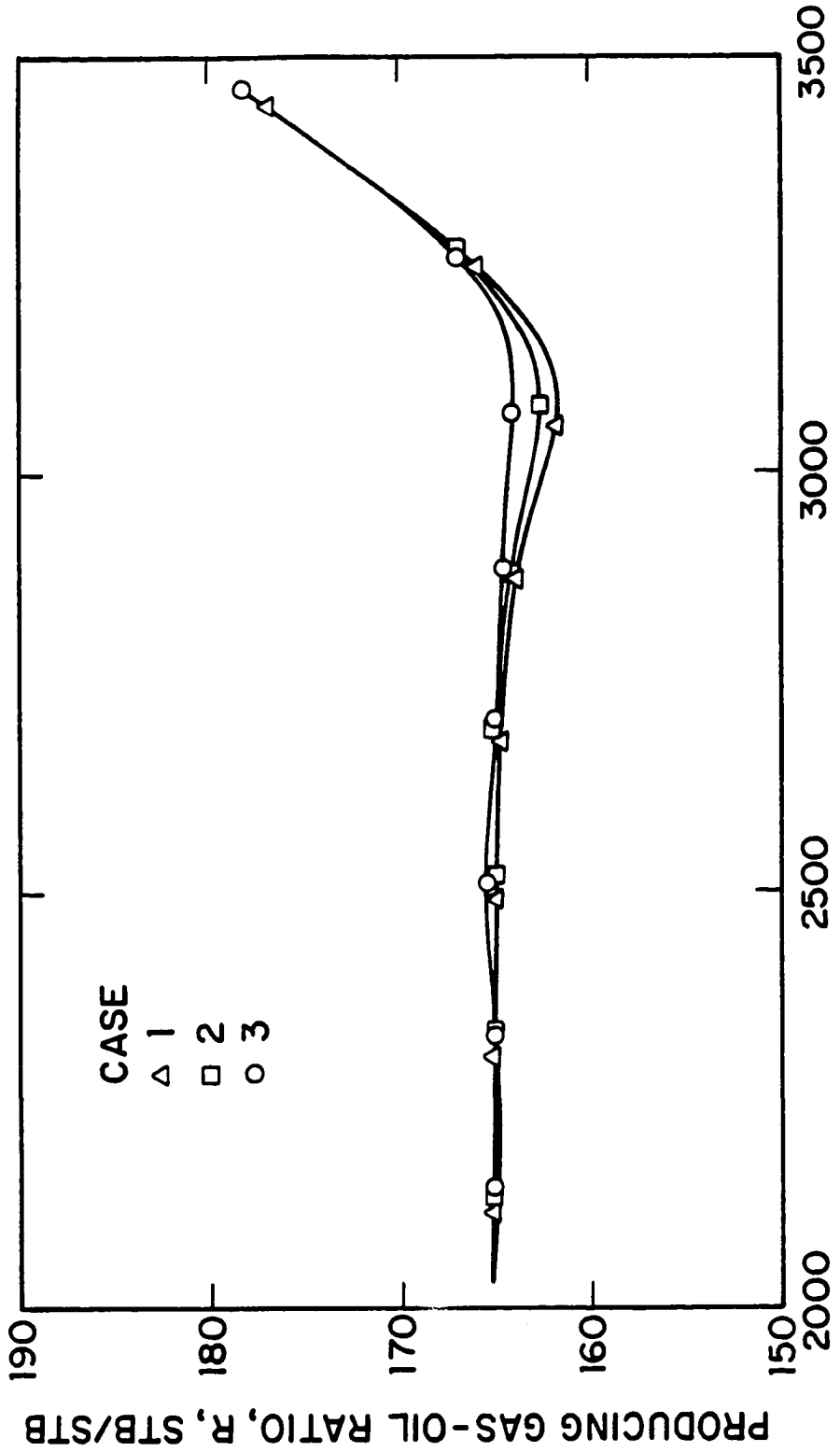

Fig. 6.5.4 - Producing GOR versus flowing wellbore pressure for Cases 1, 2 and 3.

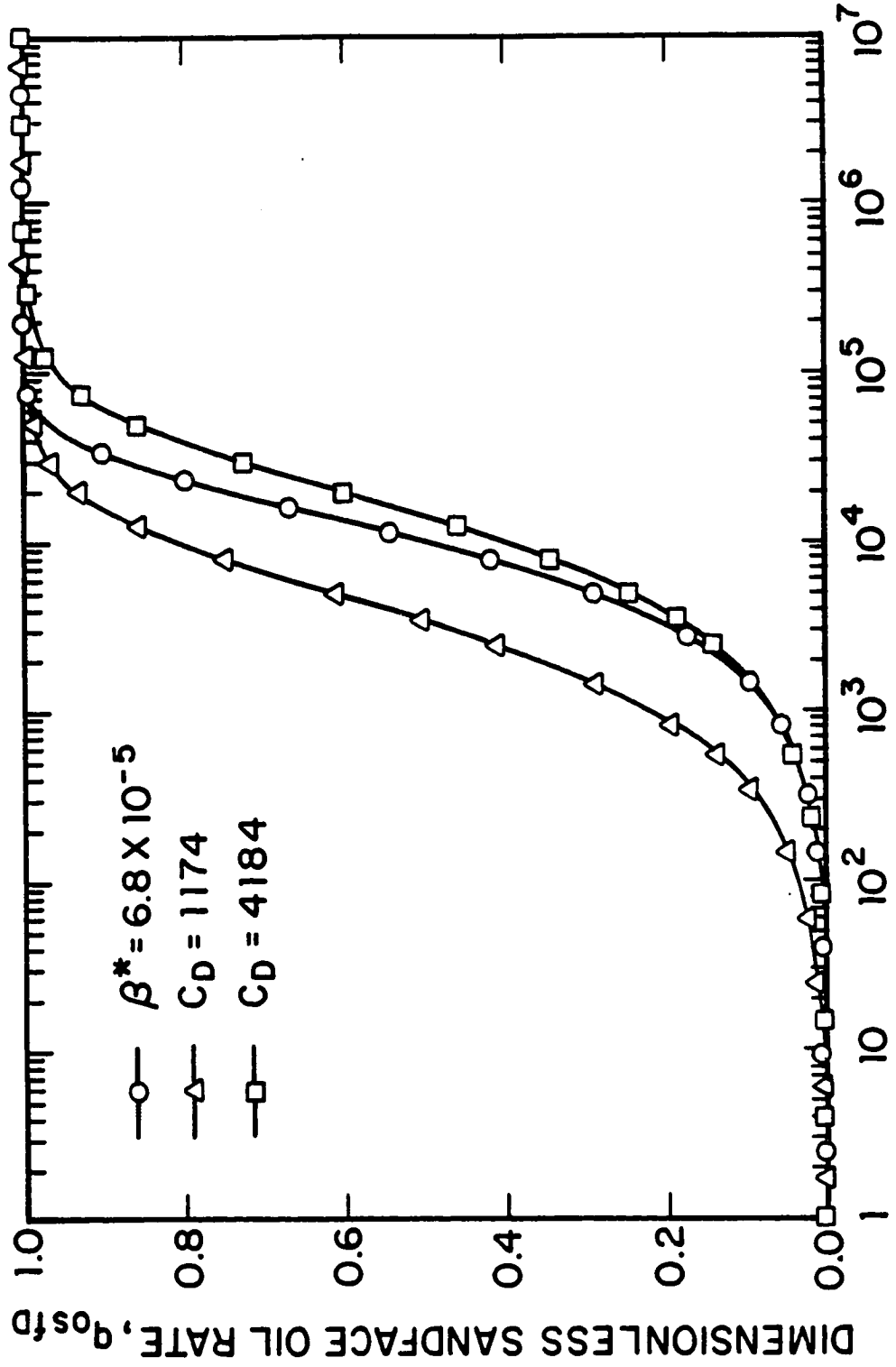

Fig. 6.5.5 - Comparison of sandface flow rates for two wellbore storage models.

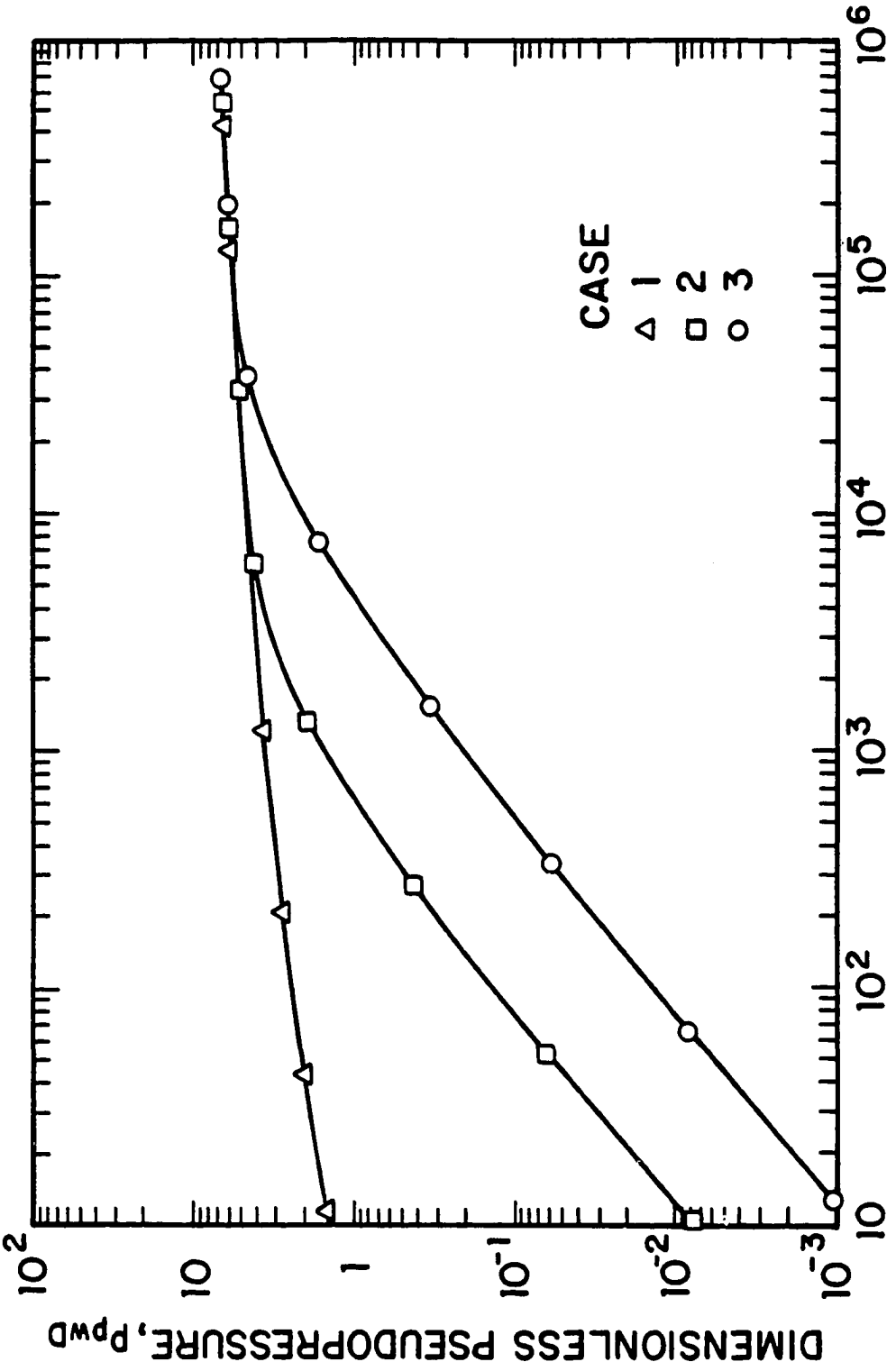

Fig. 6.5.6 - Log-log plot of dimensionless pseudopressure versus dimensionless time; Cases 1, 2 and 3.

versus dimensionless time for Cases 1, 2 and 3. Superficially it appears that the behavior of dimensionless pseudopressure is similar to the behavior of the dimensionless pressure solution obtained for the single-phase flow wellbore storage problem; see Ref. 47. However, the results of Fig. 6.5.7 indicate that the preudopressure solution (circular data points) and its logarithmic derivative (square data points) cannot be type-curve matched with any of the constant wellbore storage type curves. The solid curves in Fig. 6.5.7 represent the single-phase flow constant wellbore storage coefficient type curve solution of Bourdet et al.[48]. This result is expected since, as noted previously, Eq. 6.3.12 represents a wellbore storage model where the wellbore storage coefficient changes with time.

6.5.2 Rate-Normalization and Multirate Pseudopressure Analysis.

Numerous researchers have shown that

$$p_{pwD} = \frac{1}{2}\ln\left(\frac{4t_D}{e^{\gamma}}\right) + s, \tag{6.5.1}$$

if production is at a constant sandface flow rate, i.e., if $q_{osf}(t) = q_o$ at all times. In Eq. 6.5.1, γ denotes Euler's constant, i.e., $\gamma = 0.57722$. To the best of our knowledge, Eq. 6.5.1 was first recorded (in a slightly different form) by Fetkovich[4]. For the problem considered here, the sandface flow rate is variable and Eq. 6.5.1 cannot be expected to apply until wellbore storage effects become negligible, i.e., until $q_{osf} \approx q_o$. This is illustrated by the results of Fig. 6.5.6 which shows a log-log plot of dimensionless pseudopressure versus dimensionless time obtained for Cases 1, 2 and 3. As expected from the results of Figs. 6.5.1, 6.5.2 and 6.5.3, the wellbore storage results for Case 2 become indistinguishable from the zero wellbore storage case at $t_D \approx 7 \times 10^3$ which corresponds to $t \approx 0.052$ days or $t \approx 1.24$ hours. At this time $q_{osf} = 148.8$ STB/D as compared to a surface rate of $q_o = 150$ STB/D. The pseudopressure function results obtained for Case 3 merge with the zero wellbore storage case approximately one log cycle later. Once wellbore storage effects become negligible, parameters could be determined by standard semilog analysis based on a semilog plot of $p_p(p_{wf})$ versus time. However, as noted previously, analysis based on pseudopressure requires one to have accurate oil relative permeability data available.

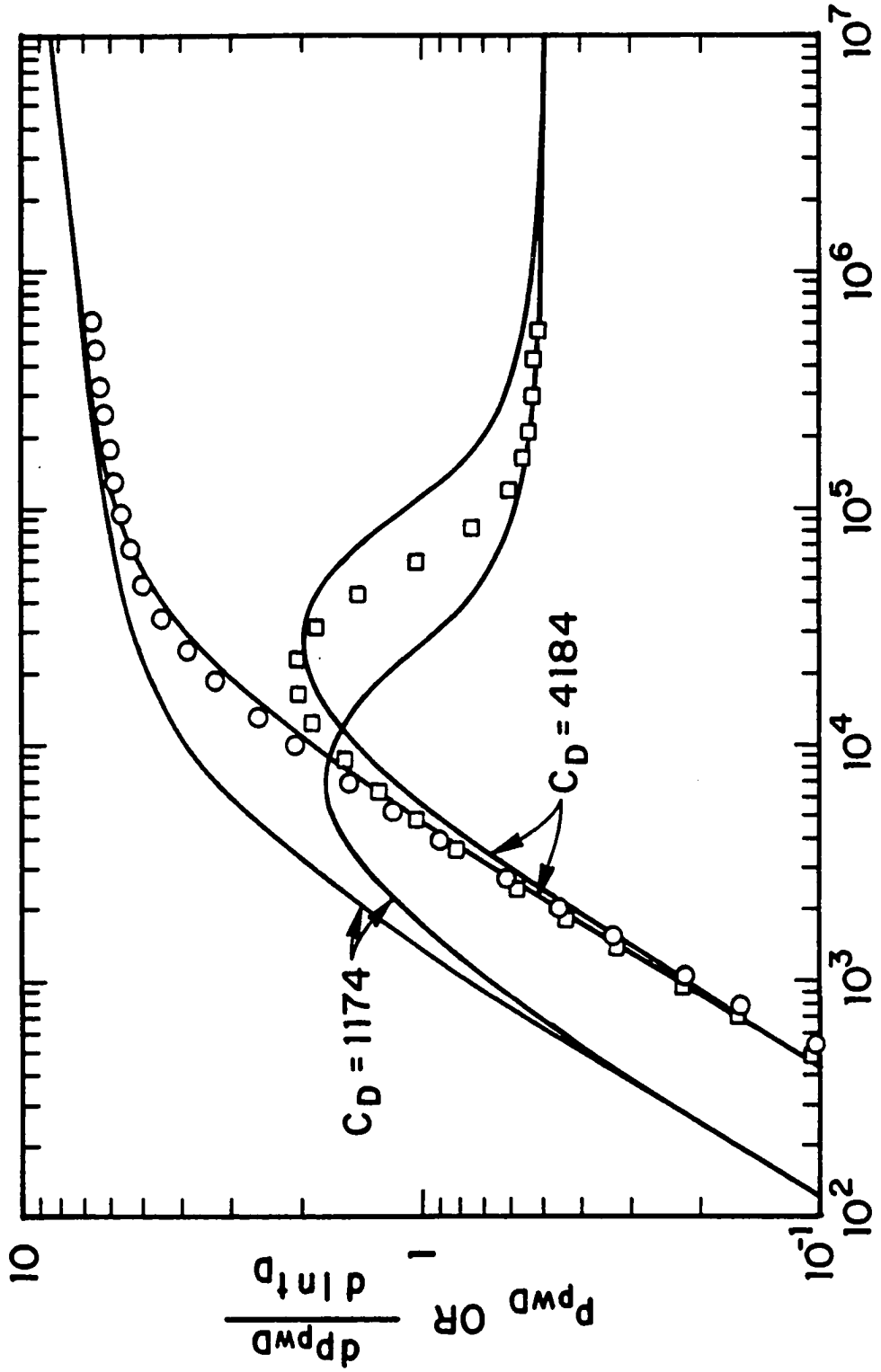

Fig. 6.5.7 - Comparison of pseudopressure solution with liquid wellbore storage solution.

In the remainder of this section, we explore the possibility of incorporating the effect of a variable sandface oil flow rate into the pseudopressure analysis. Al-Khalifah et al.[8] illustrated that semilog analysis based on an Odeh-Jones[49] plot is applicable for an increasing sequence of constant sandface oil flow rates. Here we explore the applicability of this method for a continuously increasing sandface flow rate. We should note that the Odeh-Jones method assumes the validity of superposition and the theoretical validity of superposition for the nonlinear problem considered here has not been established. However, the results of Refs. 8, 9 and 12, as well as results presented here, indicate that from a practical point of view superposition is applicable. From a more rigorous point of view, the analytical solution constructed in Ref. 40 indicates that the effect of nonlinearities are small especially for lower values of the flow rate, and hence, one should expect that superposition can be applied.

We define the sandface logarithmic convolution time by

$$t_{lc} = \sum_{i=0}^{n} \frac{q_{osf}(t_{n+1}) - q_{osf}(t_i)}{q_{osf}(t_{n+1})} \log\left(t_{n+1} - t_i\right), \tag{6.5.2}$$

and define t_{lcD} by

$$t_{lcD} = \sum_{i=0}^{n} \left(\frac{q_{osf}(t_{i+1}) - q_{osf}(t_i)}{q_{osf}(t_{n+1})}\right) \log\left(t_{n+1,D} - t_{i,D}\right). \tag{6.5.3}$$

Both t_{lc} and t_{lcD} are dimensionless. Throughout, we define $t_0 = 0$ and $q_{osf}(t_0) = q_{osf}(0) = 0$. With these definitions, the applicable variable rate multiphase flow analogue of the Odeh-Jones[49] method is given by

$$\frac{p_{pwD}}{q_{osfD}} = \frac{khp_p(p_{wf})}{141.2q_{osf}(t)} = 1.151(t_{lcD} + 0.351) + s = 1.151(t_{lc} + \tilde{s}), \tag{6.5.4}$$

where in Eqs. 6.5.2 and 6.5.3, t_{n+1} is the flowing time, that is, $t_{n+1} = t$ and $\tilde{s}$ in Eq. 6.5.4 is given by

$$\tilde{s} = \log\left(\frac{kk_{roi}}{\phi\mu_{oi}c_{ti}r_w^2}\right) - 1.847 + 0.87s, \tag{6.5.5}$$

The constant 1.847 arises in Eq. 6.5.5 because we perform our analysis with time in days instead of hours. If time in hours is used in the analysis, then 1.847 should be replaced by 3.23 in Eq. 6.5.5.

Fig. 6.5.8 illustrates that Eq. 6.5.4 is reasonably accurate. In Fig. 6.5.8, the solid straight line represents the single-phase liquid solution, i.e., Eq. 6.5.4, and the open data points represent values of p_{pwD}/q_{osfD} obtained from our simulator for Cases 1, 2 and 3 plotted versus t_{lcD}. Fig. 6.5.9 illustrates the accuracy of Eq. 6.5.4 for Cases 4, 5, and 6. In Fig. 6.5.9, the solid straight line represents Eq. 6.5.4 and the data points represent a plot of simulator values of p_{pwD}/q_{osfD} versus t_{lcD} for Cases 4, 5 and 6. For all cases shown in Figs. 6.5.8 and 6.5.9, the plots of simulator data fall slightly below the liquid solution, but all solutions display a straight line with slope approximately equal to 1.151 for $t_{lcD} \geq 3$. Ref. 40 has shown previously by analytical means that the multiphase flow solution will typically be slightly less than the corresponding liquid solution.

The validity of Eq. 6.5.4 indicates that a Cartesian plot of $p_p(p_{wf})/q_{osf}(t)$ versus logarithmic convolution time, t_{lc}, will be a straight line with slope given by

$$m_1 = \frac{162.6}{kh}. \tag{6.5.6}$$

The value of absolute permeability can be computed from the value of this slope via the following equation:

$$k = \frac{162.6}{m_1 h}. \tag{6.5.7}$$

By extrapolating the Cartesian straight line on a plot of $p_p(p_{wf})/q_{osf}(t)$ versus t_{lc} to $t_{lc} = 0$, one obtains the extrapolated value of $p_p(p_{wf})/q_{osf}$ which is denoted by $(p_p(p_{wf})/q_{osf})_{ext}$. From Eqs. 6.5.4 and 6.5.5, it then follows that the mechanical skin factor can be estimated from the following equation:

$$s = 1.151\left(\frac{(p_p(p_{wf})/q_{osf})_{ext}}{m_1} - \log\left(\frac{kk_{roi}}{\phi\mu_{oi}c_{ti}r_w^2}\right) + 1.847\right). \tag{6.5.8}$$

For the single-phase flow wellbore storage and skin problem[47], Ramey[50] established the approximate applicability of the rate-normalization procedure of Gladfelter et al.[51]; also see Winestock and Colpitts[52]. Thompson and Reynolds[53] discussed

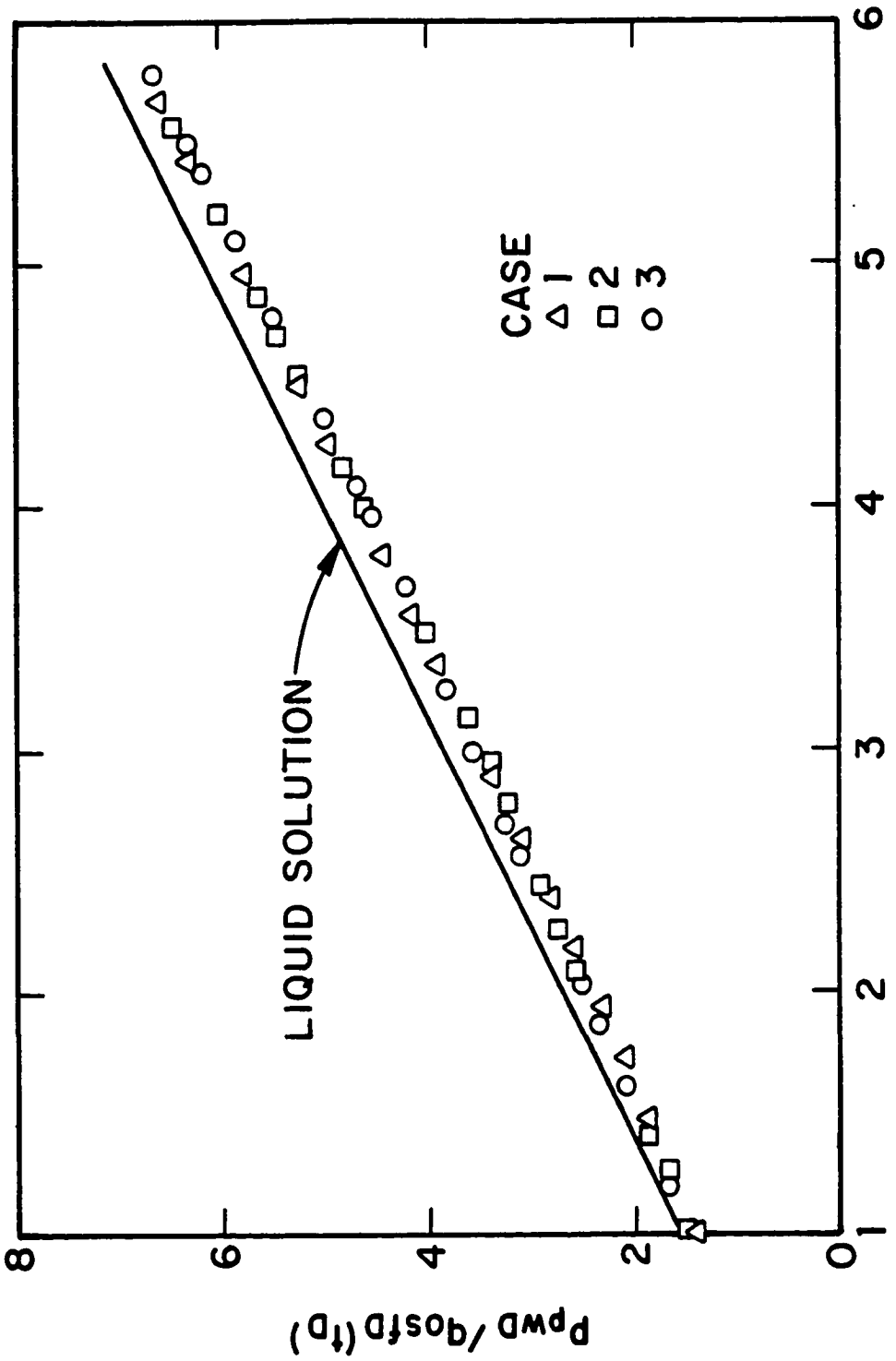

Fig. 6.5.8 - Dimensionless Odeh-Jones plot in terms of pseudopressure; Cases 1, 2 and 3.

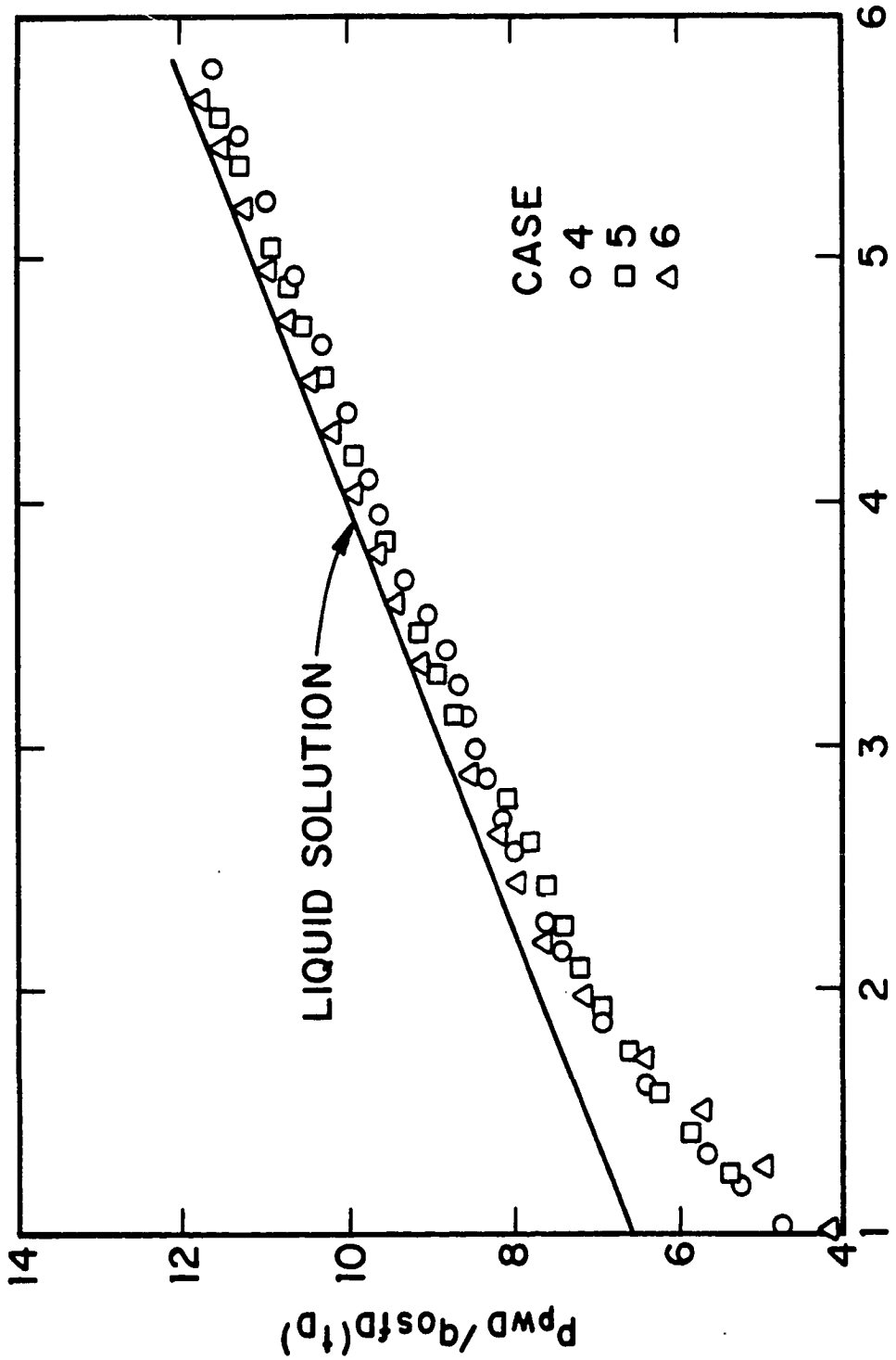

Fig. 6.5.9 - Dimensionless Odeh-Jones plot in terms of pseudopressure; Cases 4, 5 and 6.

the general applicability of rate-normalization vis-a-vis more rigorous deconvolution procedures for a variety of single-phase flow problems, and Peres et al.[54] presented the proper procedure for applying rate-normalization to slug test data.

The multiphase flow analogue of rate-normalization is given by

$$\frac{p_{pwD}}{q_{osfD}(t_D)} = \frac{khp_p(p_{wf})}{141.2q_{osf}(t)} = 1.151\log\left(\frac{4t_D}{e^{\gamma}}\right) + s. \tag{6.5.9}$$

The results of Fig. 6.5.10 illustrate that Eq. 6.5.9 is approximately valid. The results of Fig. 6.5.10 are qualitatively and quantitatively similar to the analogous single-phase flow results established by Ramey[50]. Specifically, at early times, the rate-normalized solutions for the two wellbore storage cases are parallel to the zero wellbore storage solution (Case 1) which exhibits a semilog straight line with slope approximately equal to 1.151 at all times, then there is a transition period lasting approximately one and one-half log cycles, and then the wellbore storage cases again exhibit a semilog slope approximately equal to 1.151 but displaced very slightly below the zero wellbore storage solution. The small differences between the three cases at late times are due to the fact that the three cases have slightly different k_{ro} versus p_{wf} relations; see the discussion of Fig. 6.5.3.

Eq. 6.5.9 can be rearranged to obtain

$$\frac{p_p(p_{wf})}{q_{osf}(t)} = \frac{\int_{p_{wf}}^{p_i}\left(\frac{k_{ro}}{\mu_o B_o}\right)dp}{q_{osf}(t)} = m_1\log t + m_1\left(\log\left(\frac{kk_{ro_i}}{\phi\mu_o c_{ti}r_w^2}\right) - 1.847 + 0.87s\right), \tag{6.5.10}$$

where m_1 is given by Eq. 6.5.6. The value of k can be estimated from this semilog slope using Eq. 6.5.7 and the value of the mechanical skin factor can be estimated as

$$s = 1.151\left(\frac{\left(p_p(p_{wf})/q_{osf}\right)_{1hr}}{m_1} - \log\left(\frac{kk_{roi}}{\phi\mu_{oi}c_{ti}r_w^2}\right) + 3.23\right), \tag{6.5.11}$$

where $\left(p_p(p_{wf})/q_{osf}\right)_{1hr}$ denotes the value of rate-normalized pseudopressure obtained by extrapolating the semilog straight line of Eq. 6.5.10 to $t = 1$ hour. If data corresponding to $t_D < 10^5$ in Fig. 6.5.10 is used in the analysis, then results based on Eqs. 6.5.6, 6.5.7, 6.5.10 and 6.5.11 will be only approximate of course because the results of Fig. 6.5.10 indicate that Eqs. 6.5.10 and 6.5.11 are only approximately correct at earlier times.

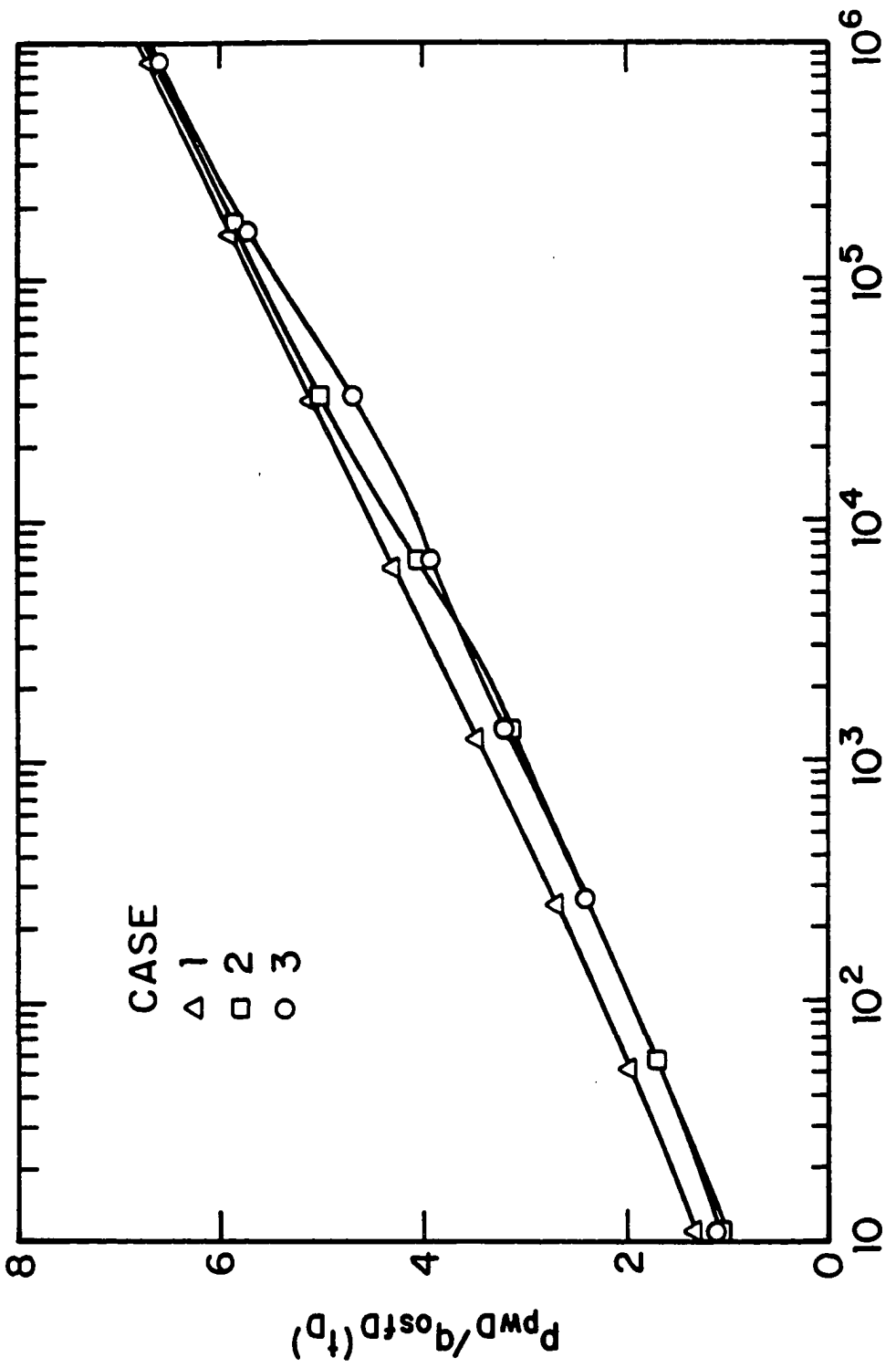

Fig. 6.5.10 - Semilog plot of rate-normalized dimensionless pseudopressure versus dimensionless time; Cases 1-3.

6.6 Computation of Oil Saturation

For the $s = 0$ case, Bøe et al.[6] showed that pressure and saturation are unique functions of the Boltzmann variable, z, which is defined by

$$z = \frac{r^2}{t}. \tag{6.6.1}$$

Using this result, they were able to derive a differential equation for computing S_o as a function of p_{wf}. (Refs. 9 and 10 were able to show that the same differential equation could be used to approximately compute oil saturation as a function of pressure for the case where the skin factor is nonzero.) The equation presented in Ref. 6 can be written as[9]

$$\frac{dS_o}{dp_{wf}} = \left(\frac{\frac{2t}{r}\frac{Q_D}{\alpha}\left(\alpha\frac{\partial a}{\partial p} - a\frac{\partial \alpha}{\partial p}\right) + \left(\alpha\frac{\partial b}{\partial p} - a\frac{\partial \beta}{\partial p}\right)}{\frac{2t}{r}\frac{Q_D}{\alpha}\left(-\alpha\frac{\partial a}{\partial S_o} + a\frac{\partial \alpha}{\partial S_o}\right) + \left(-\alpha\frac{\partial b}{\partial S_o} + a\frac{\partial \beta}{\partial S_o}\right)} \right)_{r=r_w}, \tag{6.6.2}$$

where the definition of Q_D is given by

$$Q_D = \frac{5.615 q_o}{2\pi r_w \phi h}. \tag{6.6.3}$$

Eq. 6.6.2 can be solved numerically to obtain the sandface value of S_o as a function of p_{wf}.

By assuming that pressure is a strictly monotonic function of radius and time (this assumption is valid for the problem considered in this work), and that saturation is a function of pressure, Aanonsen[7] derived the following differential equation:

$$\frac{dS_o}{dp} = \frac{c_1\left(\alpha\frac{\partial a}{\partial p} - a\frac{\partial \alpha}{\partial p}\right)\left(\frac{\partial p}{\partial r}\right)^2 - \left(\alpha\frac{\partial b}{\partial p} - a\frac{\partial \beta}{\partial p}\right)\frac{\phi}{k}\frac{\partial p}{\partial t}}{c_1\left(-\alpha\frac{\partial a}{\partial S_o} + a\frac{\partial \alpha}{\partial S_o}\right)\left(\frac{\partial p}{\partial r}\right)^2 - \left(a\frac{\partial \beta}{\partial S_o} - \alpha\frac{\partial b}{\partial S_o}\right)\frac{\phi}{k}\frac{\partial p}{\partial t}}, \tag{6.6.4}$$

where $c_1 = 0.006328$ and α, a, β and b, respectively, are defined by Eqs. 6.3.1, 6.3.2, 6.3.3 and 6.3.4. If one assumes that the Boltzmann transformation is valid, Eq. 6.6.2 can be obtained from Eq. 6.6.4. The results of Refs. 6 and 7 assume $s = 0$.

Under the same assumptions used by Aanonsen, it can be shown that

$$\frac{dS_o}{dp_{wf}} = \left(\frac{Q_{sD}(t)\left(\alpha\frac{\partial a}{\partial p} - a\frac{\partial \alpha}{\partial p}\right) - \left(\alpha\frac{\partial b}{\partial p} - a\frac{\partial \beta}{\partial p}\right)\left(\frac{dp_{wf}}{dt}\right)}{Q_{sD}(t)\left(-\alpha\frac{\partial a}{\partial S_o} + a\frac{\partial \alpha}{\partial S_o}\right) - \left(-\alpha\frac{\partial b}{\partial S_o} + a\frac{\partial \beta}{\partial S_o}\right)\left(\frac{dp_{wf}}{dt}\right)} \right)_{r=r_w}, \quad (6.6.5)$$

where

$$Q_{sD}(t) = \left(\frac{5.615 q_{osf}(t)}{2\pi r_w h}\right)^2 \frac{1}{k\phi}\frac{1}{c_1\alpha^2}. \quad (6.6.6)$$

The derivation of Eq. 6.6.5, which is outlined in Appendix B, rearranges Eq. 6.6.4 in the same way as done in Ref. 9 and rewrites $\partial p/\partial r$ terms in Eq. 6.6.4 in terms of the sandface oil flow rate using Darcy's Law. In the presence of an altered permeability in the skin zone, as shown in Appendix B, Eq. 6.6.6 should be replaced by

$$Q_{sD}(t) = \left(\frac{5.615 q_{osf}(t)}{2\pi r_w h}\right)^2 \frac{1}{k_s\phi}\frac{1}{c_1\alpha^2}. \quad (6.6.7)$$

If the sandface oil flow rate can be measured or estimated, Eq. 6.6.5 can be numerically integrated to obtain the sandface oil saturation, S_o, as a function of the wellbore flowing pressure, p_{wf}. While Eq. 6.6.5 is convenient from the viewpoint of presentation, its form is misleading in that Eqs. 6.6.6 and 6.6.7 suggest that an estimate of absolute permeability is needed to solve Eq. 6.6.5. However, this is incorrect because one can multiply the numerator and denominator of Eq. 6.6.5 by k and rearrange the resulting equation in a form that involves only kk_{ro}, kk_{rg} and k/k_s. In practice, k/k_s will be unknown and we will be forced to assume this ratio is unity, but this does not cause great errors in our computed values of S_o. With $k/k_s = 1$, solution of the rearranged form of Eq. 6.6.5 utilizes computed values of oil and gas effective permeabilities which can be obtained by the procedures discussed later, but does not require an estimate of absolute permeability.

In Appendix C we show that Eq. 6.6.2 can be written in terms of the ratio of the gas to oil relative permeabilities, i.e., k_{rg}/k_{ro} and therefore, the sandface oil saturation, S_o, as a function of wellbore pressure, p_{wf}, can be estimated by using measured oil and gas flow rate data (see also Ref. 41). However, in the same Appendix we show that in the presence of wellbore storage effects Eq. 6.6.5 cannot

be written in terms of the k_{rg}/k_{ro} ratio and therefore, one needs accurate estimates of kk_{ro} and kk_{rg} in order to estimate the S_o versus p_{wf} relationship.

Essentially, as discussed in Refs. 6 and 9, at early times the terms of Eq. 6.6.5 which involve Q_{sD} are negligible compared to the other terms and, by neglecting these terms and rearranging the resulting equation, one can obtain Martin's equation[2] which is given by

$$\frac{dS_o}{dp_{wf}} = \frac{S_o}{B_o}\frac{dB_o}{dp_{wf}} + c_t\frac{\lambda_o}{\lambda_t}. \tag{6.6.8}$$

Table F-33 shows the simulated and computed S_o values as a function of time, t, and flowing wellbore pressure, p_{wf}, for Case 2. Columns 1 and 2 show the time and wellbore pressure, column 3 shows the simulator oil saturation at the first grid block and column 4 shows the oil saturation computed from Eq. 6.6.5. Figs. 6.6.1, 6.6.2 and 6.6.3 present results that illustrate the applicability of Eq. 6.6.5 and compare the results obtained from Eq. 6.6.5 with those obtained by solving Eqs. 6.6.2 and 6.6.8 for the sandface value of S_o as a function of the flowing wellbore pressure. In generating these results, we used the correct (simulator) values of relative permeabilities when solving Eqs. 6.6.2, 6.6.5 and 6.6.8.

Fig. 6.6.1 presents a graph of sandface oil saturation versus the flowing wellbore pressure. The solid curve with no data points on it represents a plot of S_o versus p_{wf} obtained from the simulator for Case 2. All other results shown also pertain to Case 2. These other results were obtained by solving Eq. 6.6.2, Eq. 6.6.5 or Eq. 6.6.8 numerically. In these numerical computations, the simulator values of p_{wf}, relative permeabilities and PVT data were used when solving these equations numerically for S_o. Note that the results obtained from Eq. 6.6.5 (curve through solid circles) agree most closely with the correct (simulator) S_o versus p_{wf} results. Martin's equation yields accurate results only at early times, i.e., for $p_{wf} > 2900$ psi which corresponds to $t < 0.023$ days or $t < 0.552$ hours. The curve through solid triangular data points represents results obtained from Eq. 6.6.2 and the curve through solid square data points represents values obtained by solving Eq. 6.6.2 with q_o replaced by $q_{osf}(t)$. The derivation of Eq. 6.6.2 given in Ref. 6 assumes

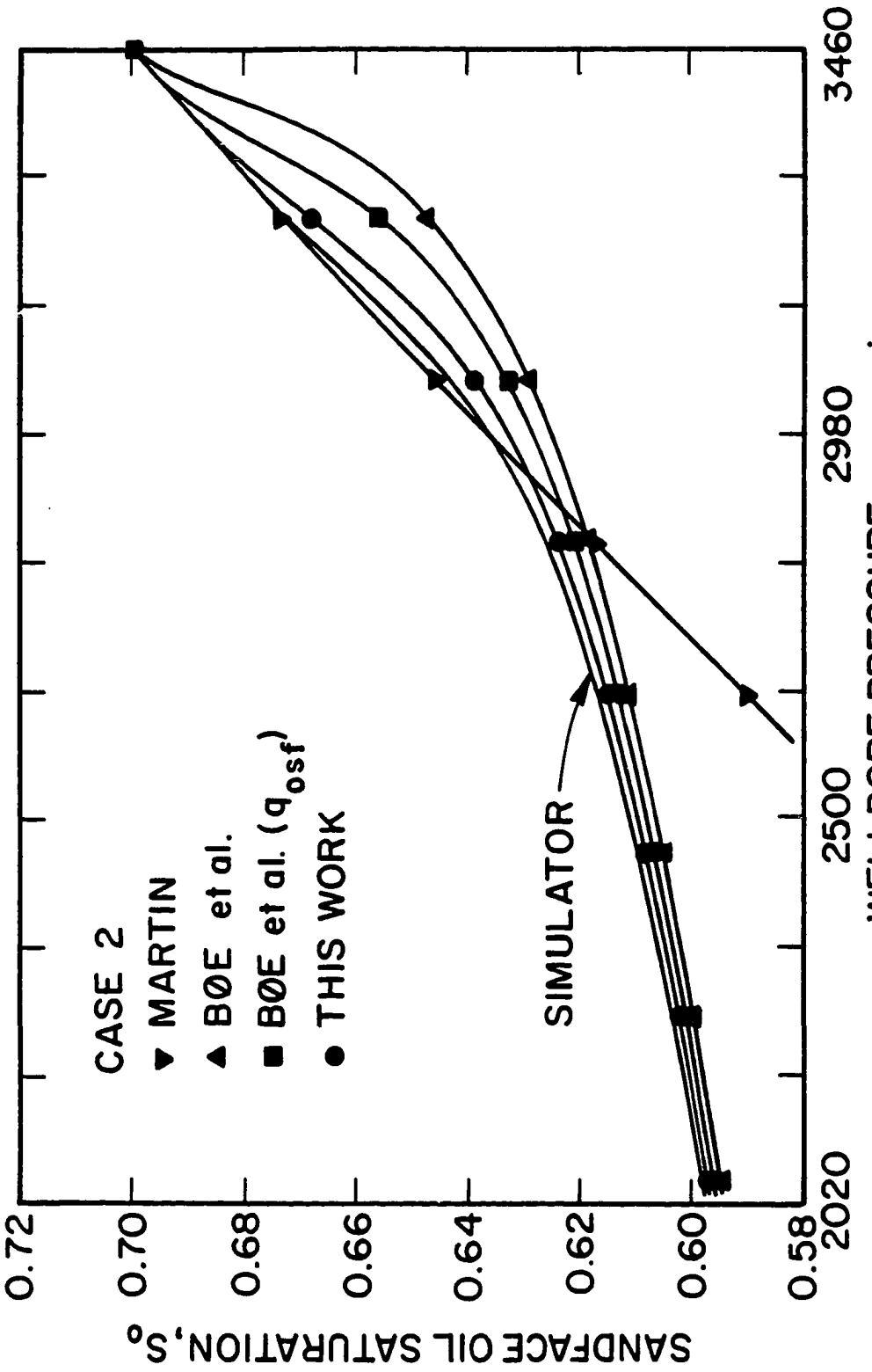

Fig. 6.6.1 - Plot of actual or computed sandface oil saturation versus flowing wellbore pressure; Case 2.

production at a constant sandface rate, but can be generalized to the variable rate case by replacing q_o by q_{osf} in Eq. 6.6.2 provided the assumptions of Ref. 6 remain valid. Aanonsen's equation, Eq. 6.6.4, and our modification (Eq. 6.6.5) of his equation do not assume a constant sandface rate of production. The results of Fig. 6.6.2, which pertain to Case 3, yield similar conclusions to those presented in Fig. 6.6.1.

The results of Fig. 6.6.3 pertain to Case 4. Recall that for this case, both wellbore storage and skin effects exist and $s = 5$. In solving Eq. 6.6.5 to obtain S_o as a function of p_{wf}, Eq. 6.6.6 was used in Eq. 6.6.5, since the value of the skin zone permeability, k_s, will not be available in practice. Fig. 6.6.3 shows that at early times the computed S_o values obtained from Eq. 6.6.5 using Eq. 6.6.6 lie slightly above the simulator results but at later times become parallel and slightly below the simulator S_o versus p_{wf} curve.

Important Remarks:

The results presented in this major section provide a useful means of analyzing data by semilog methods only if relative permeabilities as a function of saturation are known *a priori*. In this case, the pseudopressure function, $p_p(p_{wf})$, can be constructed directly from measured pressure data[6]. If sandface flow rates are known, Eqs. 6.5.4 and 6.5.9 provide a theoretical basis for the analysis of data. If sandface flow rates are unknown, then semilog analysis based on the dimensionless form of Eq. 6.5.1 can be applied after the effects of wellbore storage have become negligible. The computation of oil saturation (see Eq. 6.6.5) also requires knowledge of relative or effective permeability data as well as rock and fluid properties and the sandface flow rate.

6.7 Computation of Effective Permeabilities

In this major section, we present algorithms for computing effective permeabilities as a function of pressure directly from measured values of the flowing wellbore pressure. Using these computed values of effective permeabilities in Eq. 6.6.5, then under ideal conditions one can approximately compute the sandface oil saturation

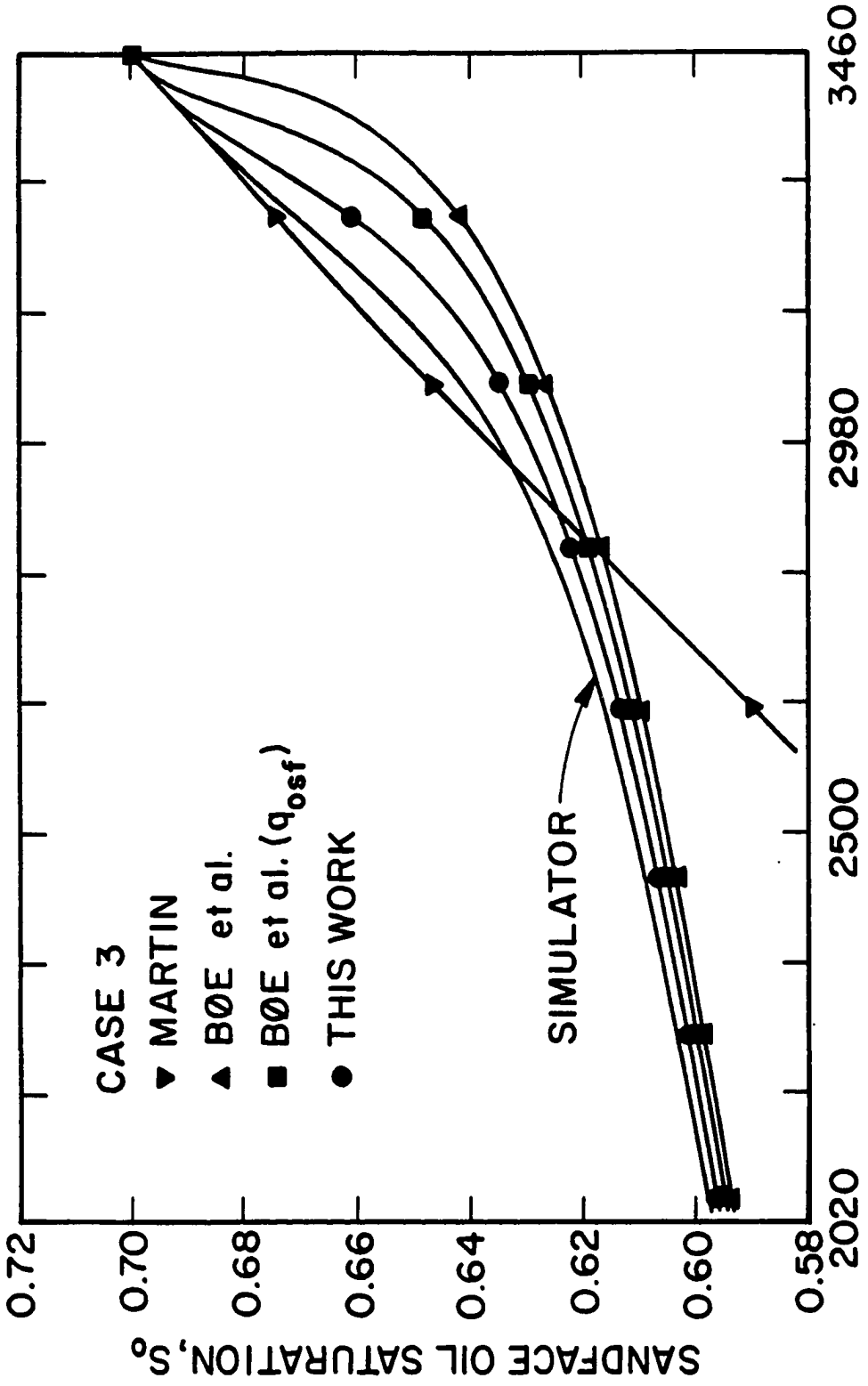

Fig. 6.6.2 - Plot of actual or computed sandface oil saturation versus flowing wellbore pressure; Case 3.

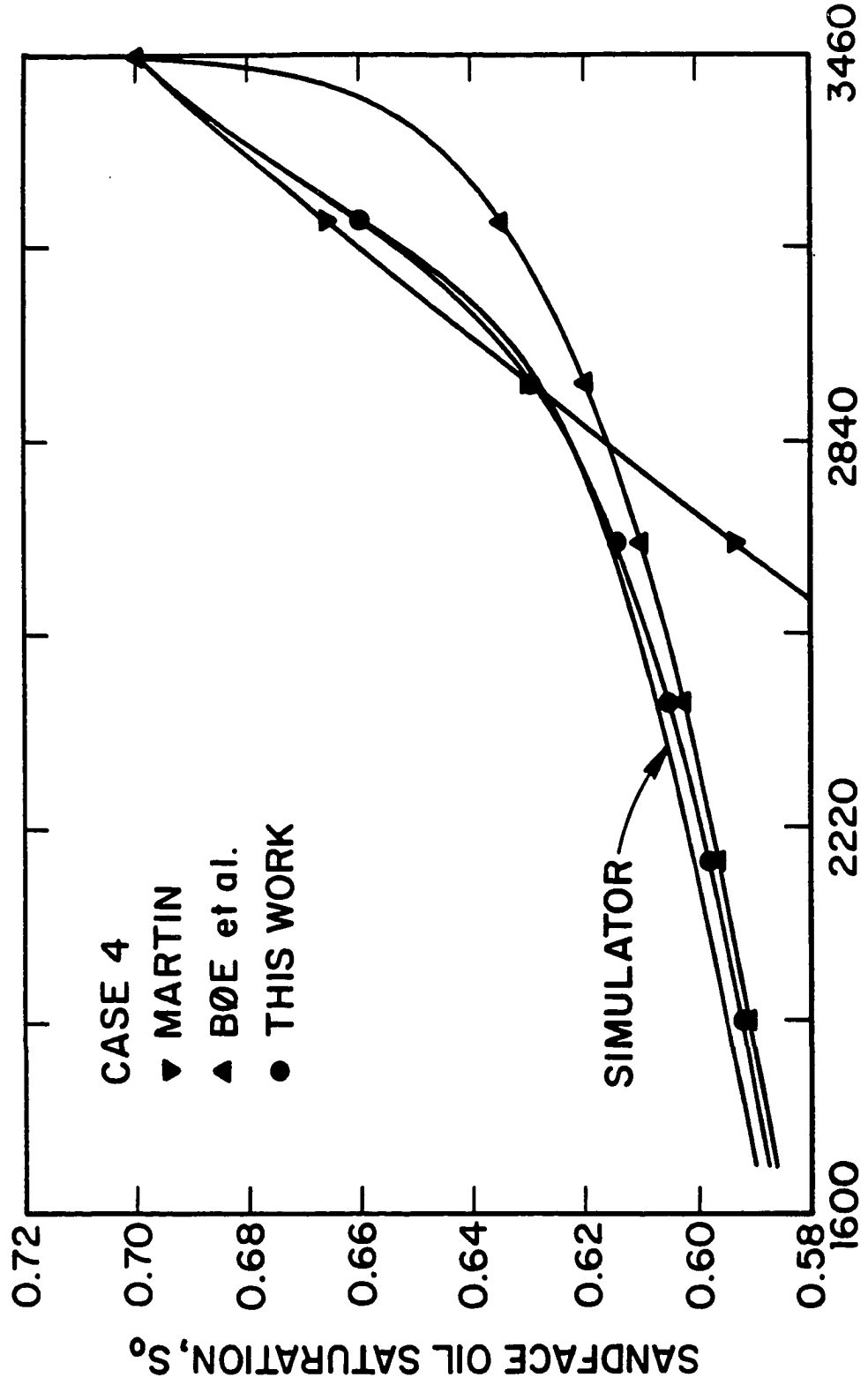

Fig. 6.6.3 - Plot of actual or computed sandface oil saturation versus flowing wellbore pressure; Case 4.

as a function of p_{wf}. Combining the two sets of results yields effective permeabilities as a function of oil saturation. If absolute permeability is known, or can be approximated by the pressure-squared method discussed later, then one can obtain relative permeability curves as a function of oil saturation. The main disadvantage of these procedures is that one must be able to accurately measure the sandface oil flow rate. If the sandface flow rate is unknown, the pressure-squared method of analysis discussed later appears to represent the only practical means of analyzing data.

6.7.1 Effective Permeability as a Function of Pressure.

In Appendix D, we derive the following equation:

$$(kk_{ro})_{p_{wf}} = \frac{-162.6q_{osf}(t)(\mu_o B_o)_{p_{wf}}}{h\frac{dp_{wf}}{dt}}\frac{dt_{lc}}{dt} - \left[\frac{kp_p(p_{wf})(\mu_o B_o)_{p_{wf}}}{\frac{dp_{wf}}{dt}}\frac{d\ln q_{osf}(t)}{dt}\right], \tag{6.7.1}$$

where t_{lc} is the logarithmic convolution time defined by Eq. 6.5.2. As shown in Appendix D, Eq. 6.7.1 is obtained by differentiating Eq. 6.5.4 with respect to time and rearranging the resulting equation.

The term of Eq. 6.7.1 within square brackets, which involves the derivative of the sandface flow rate, represents the effect of wellbore storage on our computational procedure. As the effects of wellbore storage become negligible, i.e., as the sandface flow rate becomes equal to q_o, the derivative of the sandface flow rate becomes equal to zero and Eq. 6.7.1 reduces to the computational equation of Ref. 9. However, at early times the term of Eq. 6.7.1 within square brackets has a dominant influence on the values of effective oil permeability obtained from Eq. 6.7.1.

At each time, i.e., at each value of $p_{wf}(t)$, Eq. 6.7.1 is used to estimate the corresponding value of kk_{ro}. Note that the application of Eq. 6.7.1 requires knowledge of

$$kp_p(p_{wf}) = k\int_{p_{wf}(t)}^{p_i}\frac{k_{ro}}{\mu_o B_o}dp = k\sum_{j=1}^{n+1}\left(\int_{p_{wf}(t_j)}^{p_{wf}(t_{j-1})}\frac{k_{ro}}{\mu_o B_o}dp\right), \tag{6.7.2}$$

where $t_0 = 0$, $p_{wf}(0) = p_i$ and $t_{n+1} = t$. Thus, in order to apply Eq. 6.7.1 to compute kk_{ro} at $t = t_{n+1}$, we must be able to estimate the last integral ($j = n + 1$

term) in the summation of Eq. 6.7.2. This is accomplished by using the following approximation:

$$k\int_{p_{wf}(t_{n+1})}^{p_{wf}(t_n)} \frac{k_{ro}}{\mu_o B_o} dp = \left(\frac{kk_{ro}}{\mu_o B_o}\right)_{p_{wf}(t_n)} \times (p_{wf}(t_n) - p_{wf}(t_{n+1})), \qquad (6.7.3)$$

so that Eq. 6.7.2 reduces to

$$kp_p(p_{wf}) = \sum_{j=1}^{n} \left(\int_{p_{wf}(t_j)}^{p_{wf}(t_{j-1})} \frac{kk_{ro}}{\mu_o B_o} dp\right) + \left(\frac{kk_{ro}}{\mu_o B_o}\right)_{p_{wf}(t_n)} \times (p_{wf}(t_n) - p_{wf}(t_{n+1})). \qquad (6.7.4)$$

By using Eq. 6.7.4 in our computational algorithm, Eq. 6.7.1, we obtain a procedure that can be applied to estimate kk_{ro} as a function of the measured wellbore pressure. At the very first time step, i.e., at the first application of Eq. 6.7.1, the term in square brackets is ignored, i.e., set equal to zero.

Once the effective oil permeability is computed from Eq. 6.7.1, the effective gas permeability can be estimated from the following equation:

$$kk_{rg} = (R - R_s)_{p_{wf}} \left(\frac{\mu_g B_g}{\mu_o B_o}\right)_{p_{wf}} kk_{ro}. \qquad (6.7.5)$$

Note that the application of Eq. 6.7.5 requires that the producing GOR is measured. In our computational procedure, we used the sandface oil and gas flow rates to obtain R.

The simulated and computed kk_{ro} versus the wellbore pressure p_{wf} are shown in Table F-34. In this table, columns 1 and 2 show the time and wellbore pressure data, columns 3 and 4 show the sandface oil saturation and the effective oil permeability data obtained from the simulator, column 5 shows the kk_{ro} values computed from Eq. 6.7.1 and column 6 shows the kk_{ro} values computed from Eq. 6.7.1 by using the constant surface oil rate in place of the sandface oil flow rate in the computational procedure given in Ref. 9. Fig. 6.7.1 presents results obtained from the computational algorithm of Eq. 6.7.1 based on the approximation of Eq. 6.7.4. The results pertain to Case 2, i.e., q_o = 150 STB/D, $s = 0$ and nonzero wellbore storage. In Fig. 6.7.1, the effective oil permeability is plotted as a function of dimensionless time. The solid curve represents the correct (simulator) values of effective oil

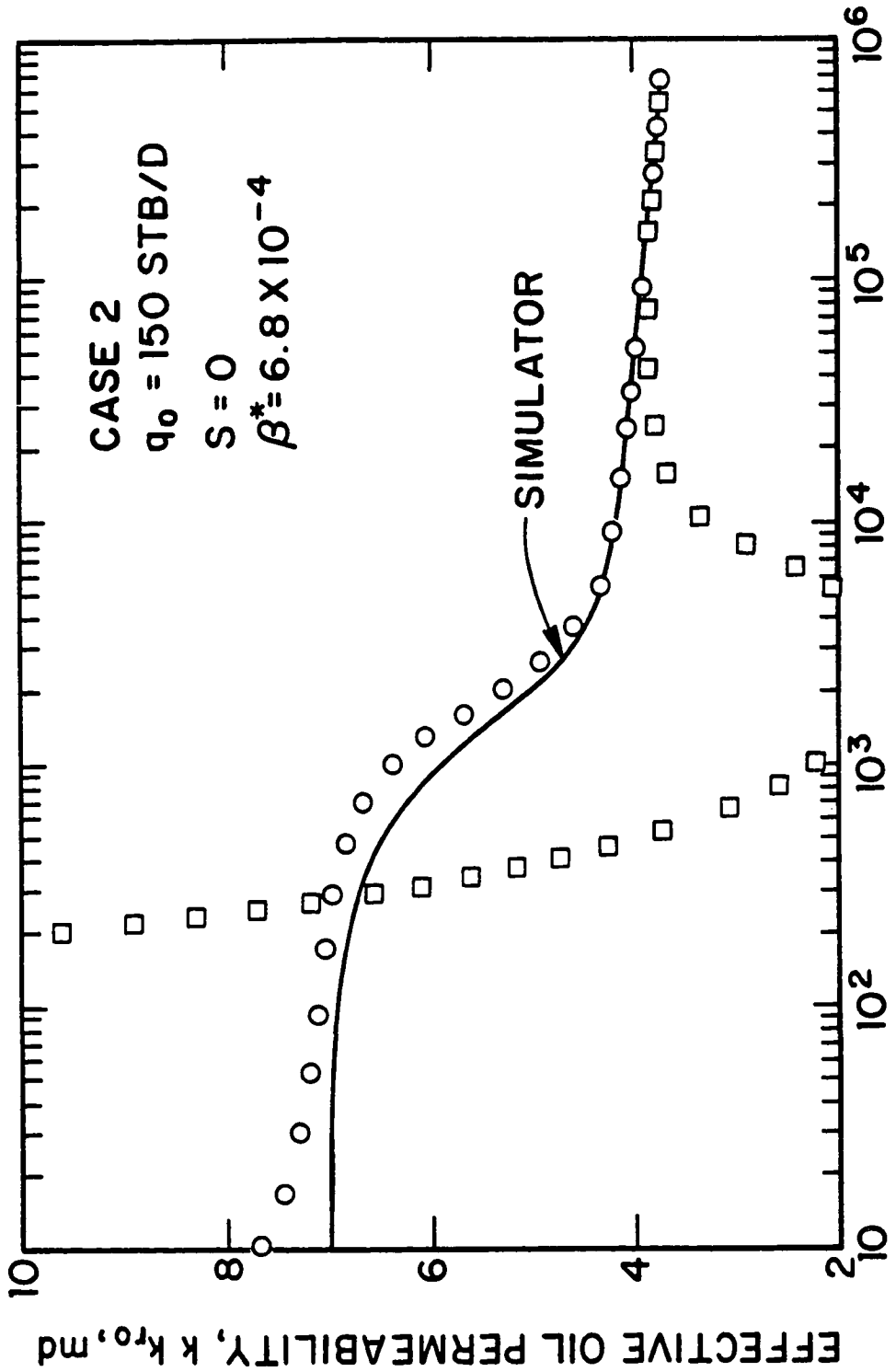

Fig. 6.7.1 - Semilog plot of effective oil permeability versus dimensionless time; Case 2.

permeability and the circular data points represent the values of effective oil permeability obtained from Eq. 6.7.1. Note that Eq. 6.7.1 yields excellent results at all times and at later times yields practically exact values. In Fig. 6.7.1, the square data points represent effective oil permeability computed using the constant surface oil rate in place of the sandface oil flow rate in the computational procedure given in Ref. 9. This is equivalent to setting $q_{osf}(t) = q_o$ at all times in Eq. 6.7.1 so $d \ln q_{osf}(t)/dt = d \ln q_o/dt = 0$. Note that replacing $q_{osf}(t)$ by q_o at all times in the computational procedure gives accurate estimates of kk_{ro} only for $t_D > 10^4$, i.e., only at times when the effect of wellbore storage becomes small; see Fig. 6.5.6. For the cases considered in this work, $t_D = 10^4$ is equivalent to $t = 0.074$ days or $t = 1.77$ hours.

Fig. 6.7.2 shows the same results presented in Fig. 6.7.1, except that in Fig. 6.7.2 we have plotted effective oil permeability versus p_{wf}. In Fig. 6.7.2, the solid curve corresponds to simulator values, the circular data points represent values obtained from Eq. 6.7.1 and the square data points represent values obtained from the procedure given in Ref. 9, i.e., from Eq. 6.7.1 with the sandface flow rate replaced by q_o at all times.

The simulated and computed kk_{rg} versus the wellbore pressure p_{wf} are shown in Table F-35. In this table, column 1 shows the wellbore pressure data, column 2 shows the effective gas permeability data obtained from the simulator, column 3 shows the kk_{rg} values computed from Eq. 6.7.5 and column 4 shows the kk_{rg} values computed from Eq. 6.7.5 by using the computed kk_{ro} values given in column 6 of Table F-34. Fig. 6.7.3 shows a Cartesian plot of the sandface values of kk_{rg} versus the flowing wellbore pressure for Case 2. The solid curve represents simulator values. The circular data points represent values obtained from Eq. 6.7.5. In applying Eq. 6.7.5, the values of kk_{ro} as a function of p_{wf} obtained from Eq. 6.7.1 (circular data points of Fig. 6.7.2) were used. Note this procedure yields excellent estimates of kk_{rg} at all times. The values of kk_{rg} computed from Eq. 6.7.5, using the kk_{ro} values from Eq. 6.7.1 with the sandface flow rate replaced by q_o at all times, are also shown in Fig. 6.7.3 as square data points. Note that the effective gas permeability

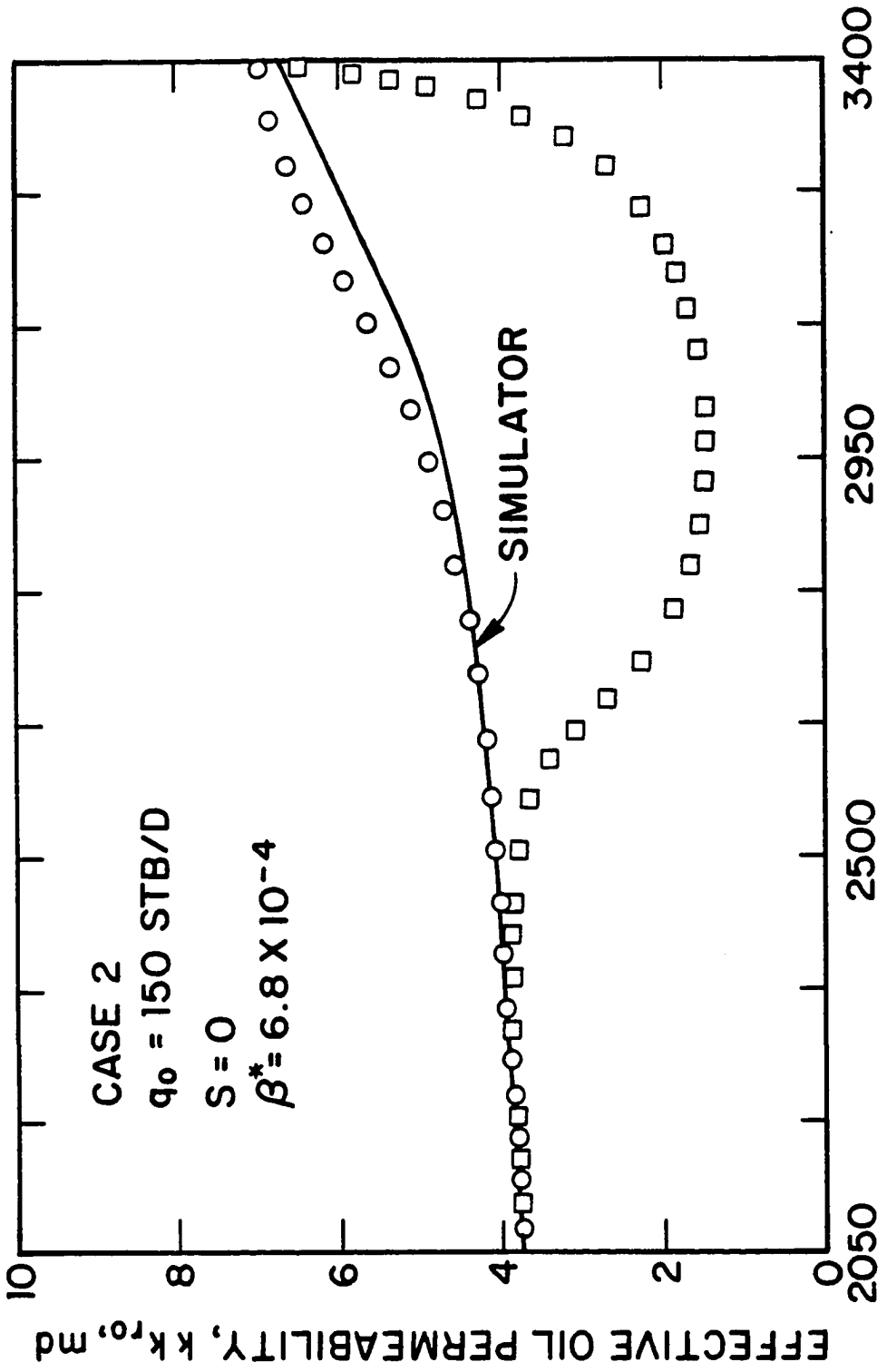

Fig. 6.7.2 - Plot of effective oil permeability versus flowing wellbore pressure; Case 2.

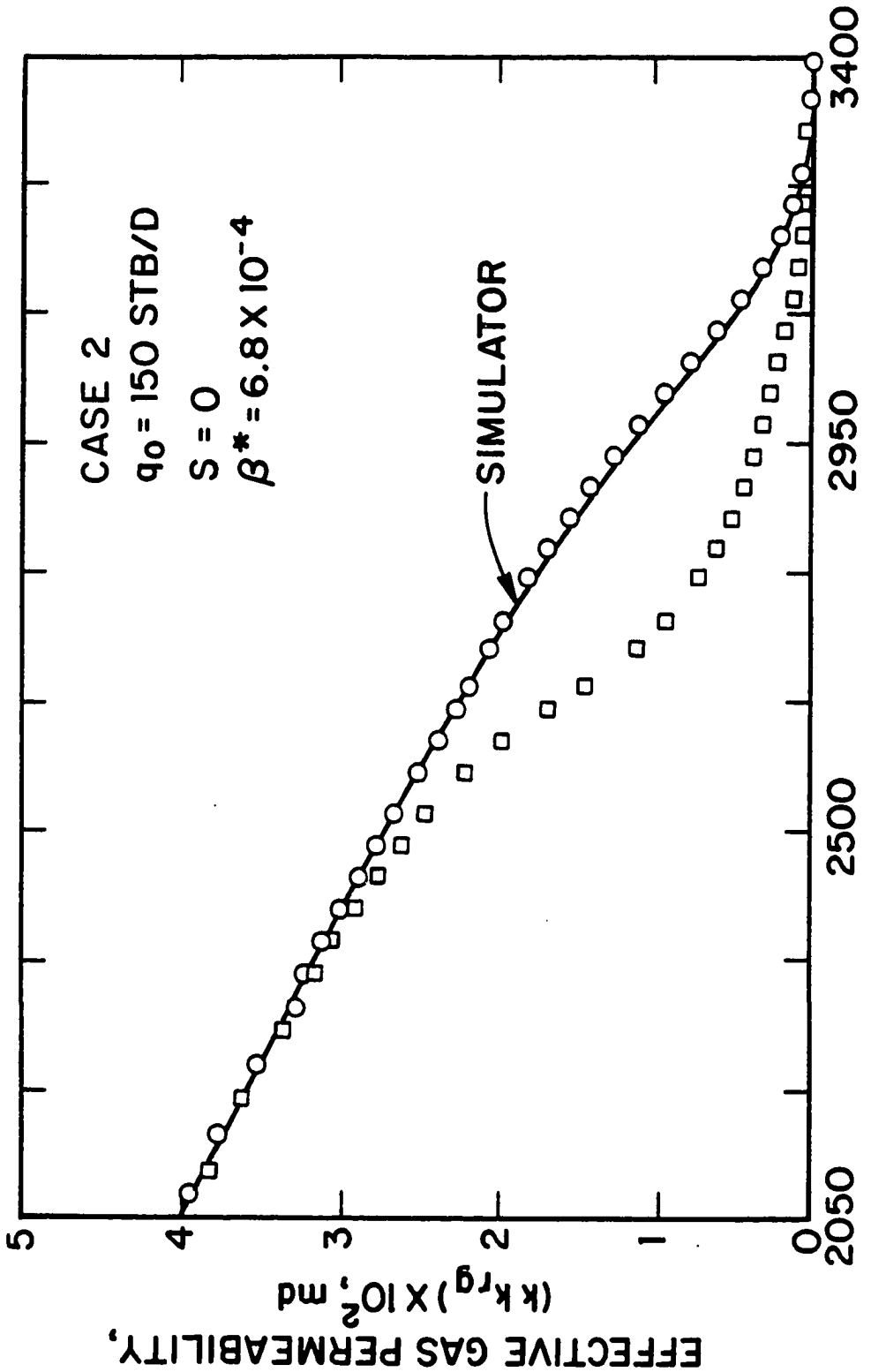

Fig. 6.7.3 - Plot of effective gas permeability versus flowing wellbore pressure; Case 2.

computed by this method is accurate after wellbore storage becomes negligible.

Fig. 6.7.4 shows the effective oil permeabilities of Figs. 6.7.1 and 6.7.2 plotted versus the corresponding *simulator* values of oil saturation. The solid curve in Fig. 6.7.4 represents a plot of the correct (simulator) values of effective oil permeability at the sandface versus the sandface value of oil saturation. As expected from the results of Figs. 6.7.1 and 6.7.2, the plot of kk_{ro} obtained from Eq. 6.7.1 versus S_o (circular data points) is in excellent agreement with the correct effective permeability curve, whereas values obtained using q_o in place of q_{osf} do not agree with the correct effective oil permeability curve until the effects of wellbore storage are diminished considerably.

The results of Fig. 6.7.4 suggest that if Eq. 6.6.5 can be applied to compute accurate values of S_o (at the sandface) as a function of p_{wf}, then these results can be combined with the computed values of kk_{ro} as a function of p_{wf} to obtain kk_{ro} as a function of S_o. Note that if this computation of S_o is successful, then one can compute effective oil permeability as a function of oil saturation directly from measured values of p_{wf}.

Figs. 6.7.5 and 6.7.6 present results obtained for Case 3; $q_o = 150$ STB/D, $s = 0$ and $\beta^* = 6.8 \times 10^{-5}$. As the results of Fig. 6.7.5 are similar to those of Fig. 6.7.1 and the results of Fig. 6.7.6 are analogous to those of Fig. 6.7.2, Figs. 6.7.5 and 6.7.6 are self explanatory.

Fig. 6.7.7 represents a plot of simulated or computed oil saturation values plotted against the wellbore pressure for Case 3. The solid curve represents the simulator sandface oil saturation values plotted versus the wellbore pressure. The circular data points represent the oil saturation values obtained by solving Eq. 6.6.5 numerically. The values of S_o computed by solving Eq. 6.6.5 numerically follow the correct trend but fall below the correct (simulator) curve. This is due to the sensitivity of the numerical solution of Eq. 6.6.5. Similar problems were encountered in Ref. 9. Note that we have used a very sensitive ordinate scale in Fig. 6.7.7; in reality, the results are quite good in that the value of S_o computed from Eq. 6.6.5 is always within 0.03 of the correct value.

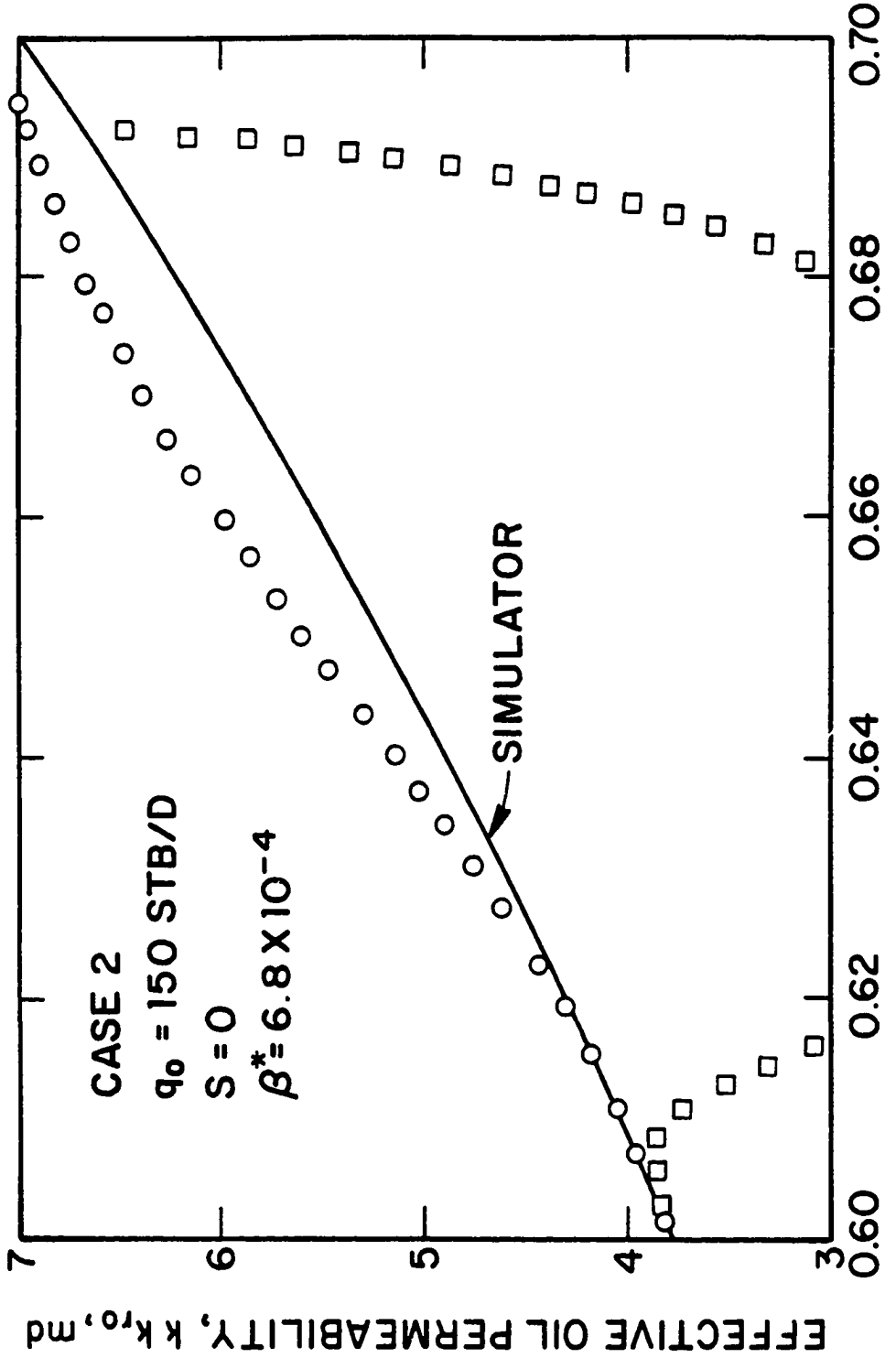

Fig. 6.7.4 - Plot of effective oil permeability versus oil saturation; Case 2.

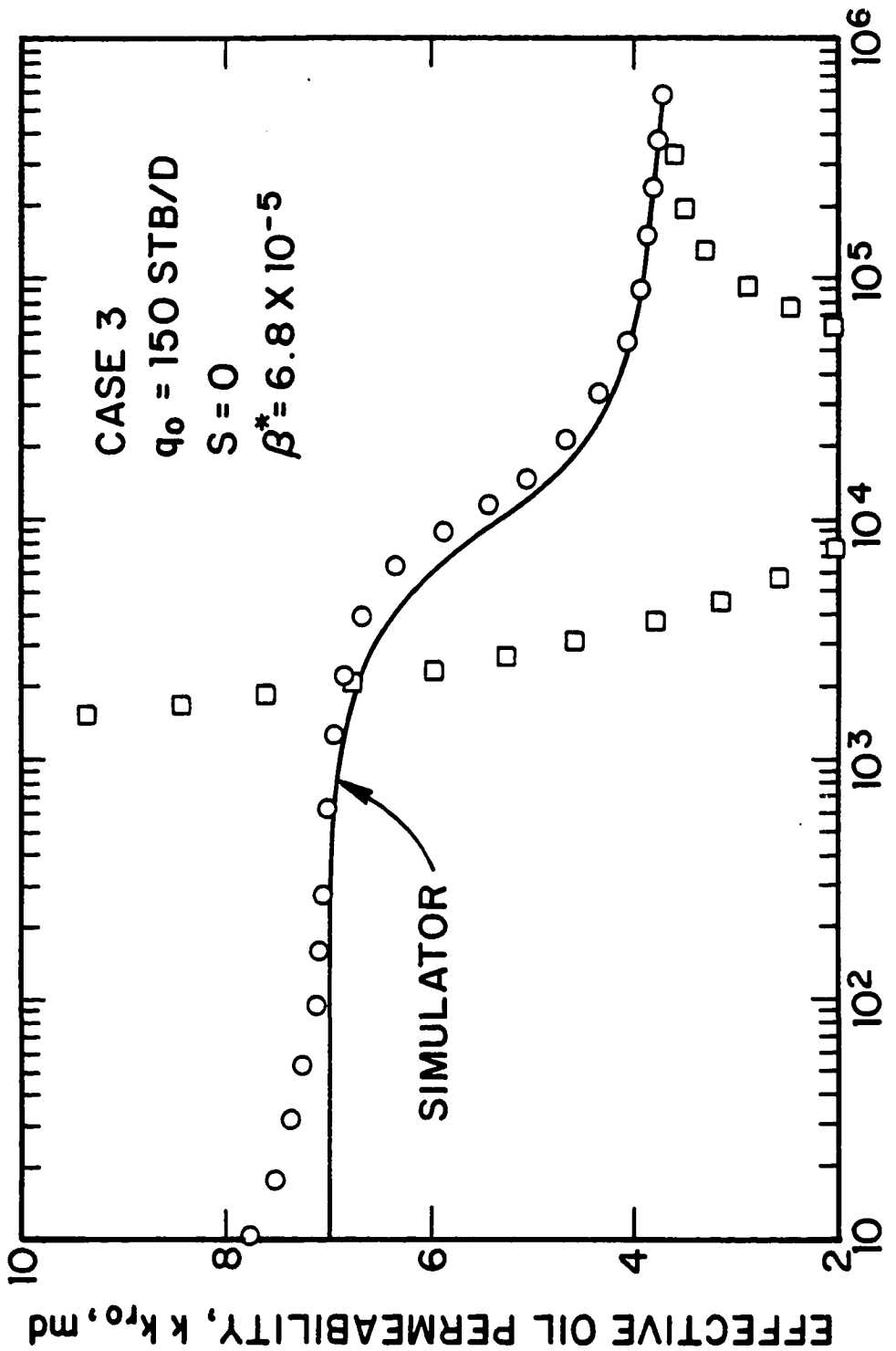

Fig. 6.7.5 - Semilog plot of effective oil permeability versus dimensionless time; Case 3.

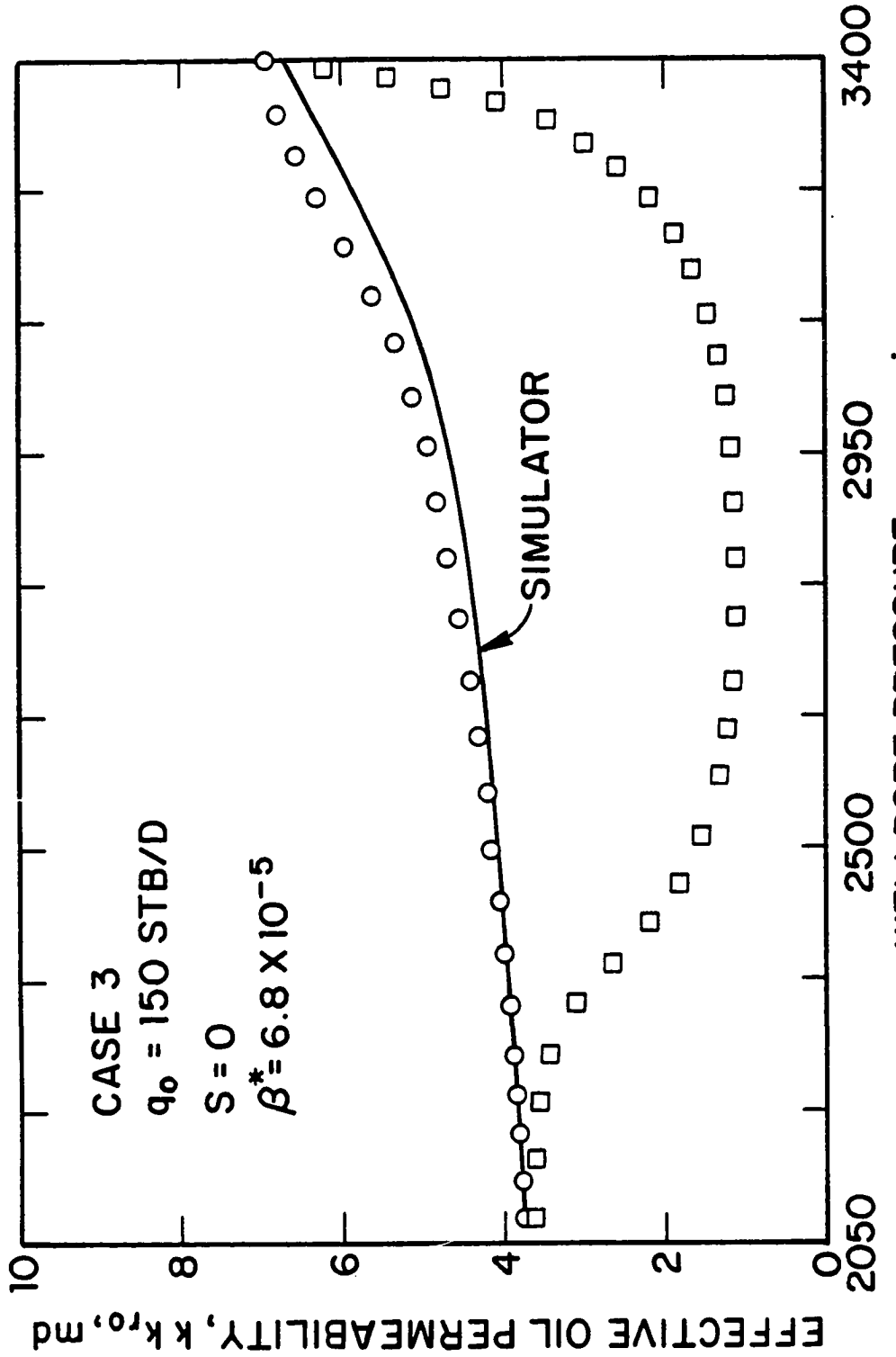

Fig. 6.7.6 - Effective oil permeability versus flowing wellbore pressure; Case 3.

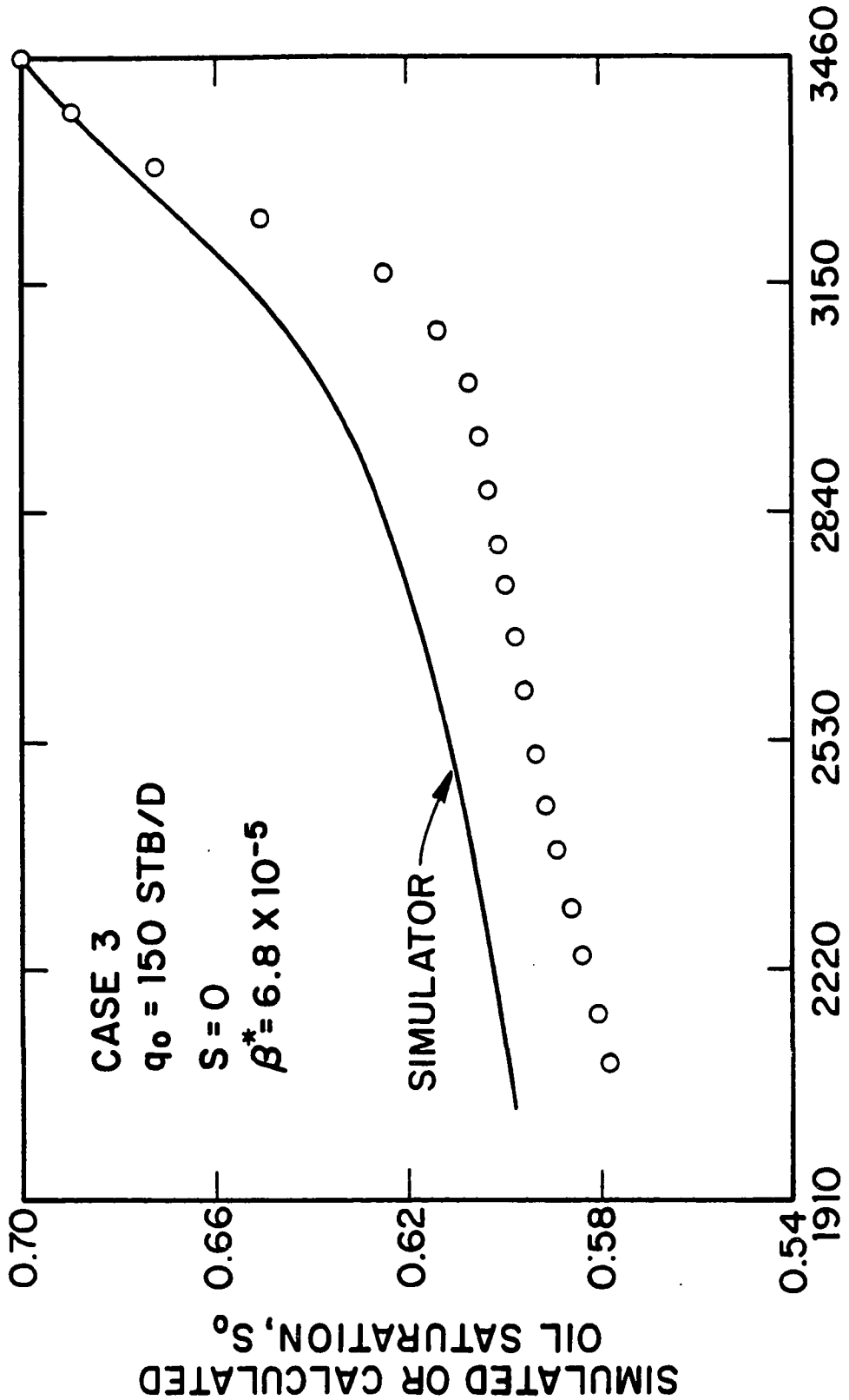

Fig. 6.7.7 - Plot of simulated or computed oil saturation versus flowing wellbore pressure; Case 3.

Fig. 6.7.8 presents a plot of the effective oil permeability versus oil saturation. The solid curve represents the simulator values of kk_{ro} at the sandface plotted versus the sandface simulator values of oil saturation, whereas the circular data points represent the effective oil permeability obtained from Eq. 6.7.1 plotted as a function of the values of oil saturation computed from Eq. 6.6.5. In solving Eq. 6.6.5, we used the values of effective permeabilities computed from Eqs. 6.7.1 and 6.7.5. Since Eqs. 6.7.1 and 6.7.5 do not yield exact values and the solution of Eq. 6.6.5 is numerically sensitive, the plot of k_{ro} versus S_o computed directly from the flowing wellbore pressure does not match the exact value. Nevertheless, the computed results yield good rough estimates of the effective oil permeability curve.

6.7.2 Influence of the Skin Factor.

The results presented in the previous subsection are for cases where $s = 0$. In this subsection, we consider results for Case 4 so that data are influenced by both wellbore storage and skin effects. Recall that for Case 4, $s = 5$, $q_o = 100$ STB/D and $\beta^* = 6.8 \times 10^{-5}$ ($C_D \approx 1174$).

In Fig. 6.7.9, the solid curve represents the simulator value of effective oil permeability plotted versus dimensionless time. The inverted triangular data points correspond to kk_{ro} values obtained from Eq. 6.7.1 using the approximation of Eq. 6.7.4. These values of kk_{ro} fall below the correct (simulator) values at early times because the values obtained from Eq. 6.7.1 actually attempt to reflect $k_s k_{ro}$ instead of kk_{ro} at very early times as explained in Ref. 9. Since this results in inaccurate estimates of kk_{ro} and these estimates are used in successive computations of effective oil permeability (see Eqs. 6.7.1 and 6.7.4), Eq. 6.7.1 cannot yield good results until wellbore storage effects become negligible, i.e., until the term of Eq. 6.7.1 in square brackets becomes negligible. For damaged cases ($s > 0$), the combined effects of near wellbore damage and wellbore storage are such that q_{osf} remains close to zero at early times, i.e., k times the sandface value of k_{ro} remains close to kk_{roi} at early times as illustrated by the simulator values shown in Fig. 6.7.9. Thus, it is

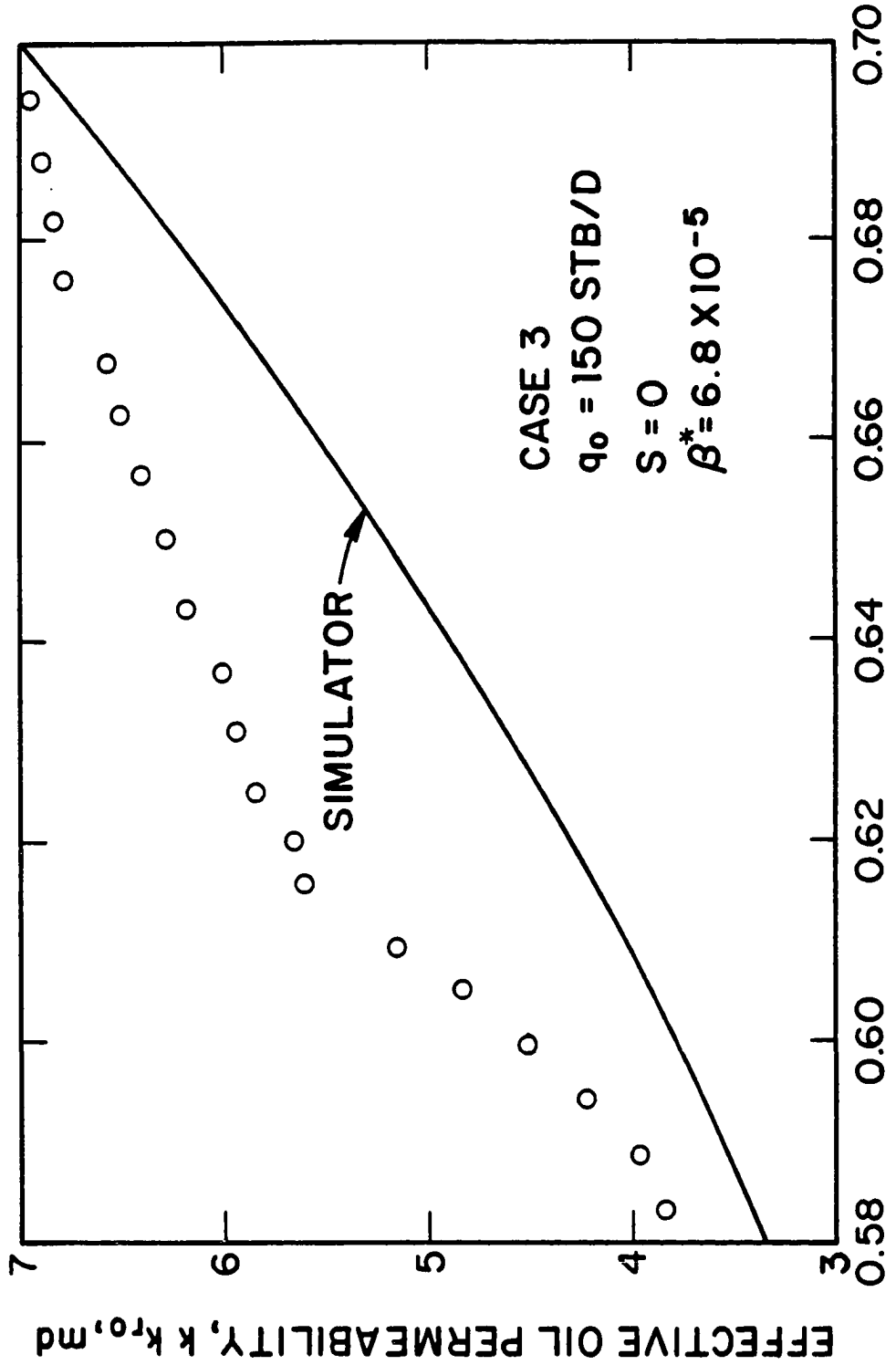

Fig. 6.7.8 - Effective oil permeability versus oil saturation; Case 3.

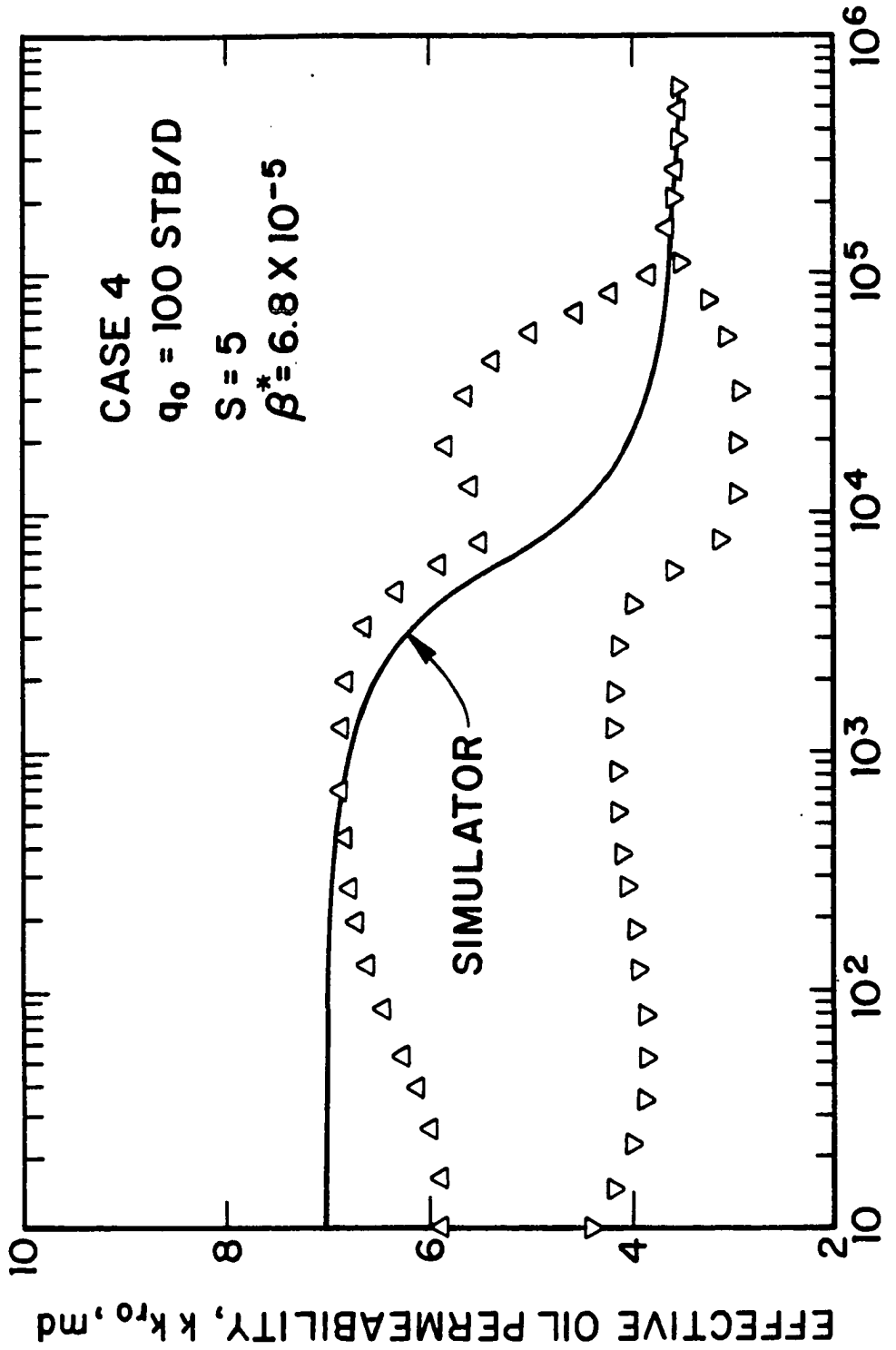

Fig. 6.7.9 - Effective oil permeability versus dimensionless time; Case 4.

reasonable to use the approximation

$$kp_p\,(p_{wf}) \approx k\left(\frac{k_{ro}}{\mu_o B_o}\right)_i (p_i - p_{wf}), \tag{6.7.6}$$

at least at early times. Note that in order to apply the approximation of Eq. 6.7.6, one must have available an estimate of kk_{roi}. The triangular data points of Fig. 6.7.9 represent the values of effective oil permeability computed from Eq. 6.7.1 using the approximation of Eq. 6.7.6. Note this procedure improves the estimate of kk_{ro} at early times but for $t_D > 10^4$ the results are no better than those obtained from Eq. 6.7.1 using the approximation of Eq. 6.7.4. When q_{osf} becomes approximately equal to q_o, the effect of the term of Eq. 6.7.1 in square brackets is negligible and both procedures yield excellent estimates of effective oil permeability.

Fig. 6.7.10 shows a plot of effective oil permeability versus flowing wellbore pressure. The simulator values of kk_{ro} plotted versus the corresponding simulator values of p_{wf} are represented by the solid curve. As in Fig. 6.7.9, kk_{ro} values obtained from Eq. 6.7.1 using the approximation of Eq. 6.7.4 are shown by the inverted triangular data points and results obtained from Eq. 6.7.1 using the approximation of Eq. 6.7.6 are shown by triangular data points. The square data points in Fig. 6.7.10 represent results obtained from the pressure-squared method which is discussed later.

As shown in Figs. 6.7.9 and 6.7.10, computations based on the approximation of Eq. 6.7.6 yield good estimates of kk_{ro} at early times. On the other hand, based on the nonzero skin constant rate cases considered in Ref. 9, one would expect that Eq. 6.7.1 with the approximation of Eq. 6.7.4 will yield good kk_{ro} estimates once the skin zone achieves a steady-state behavior provided one uses the correct $p_p(p_{wf})$ values in Eq. 6.7.1. Based on these intuitive ideas, we generated results using a combination of these two approximations (Eq. 6.7.4 and Eq. 6.7.6). The circular data points shown in Fig. 6.7.11 show the effective values of oil permeability obtained by using this combined approach. Note that these values agree very well with the simulator values at all times. Unfortunately, at this point in time these results are only of theoretical value; in practice it would be difficult to decide when

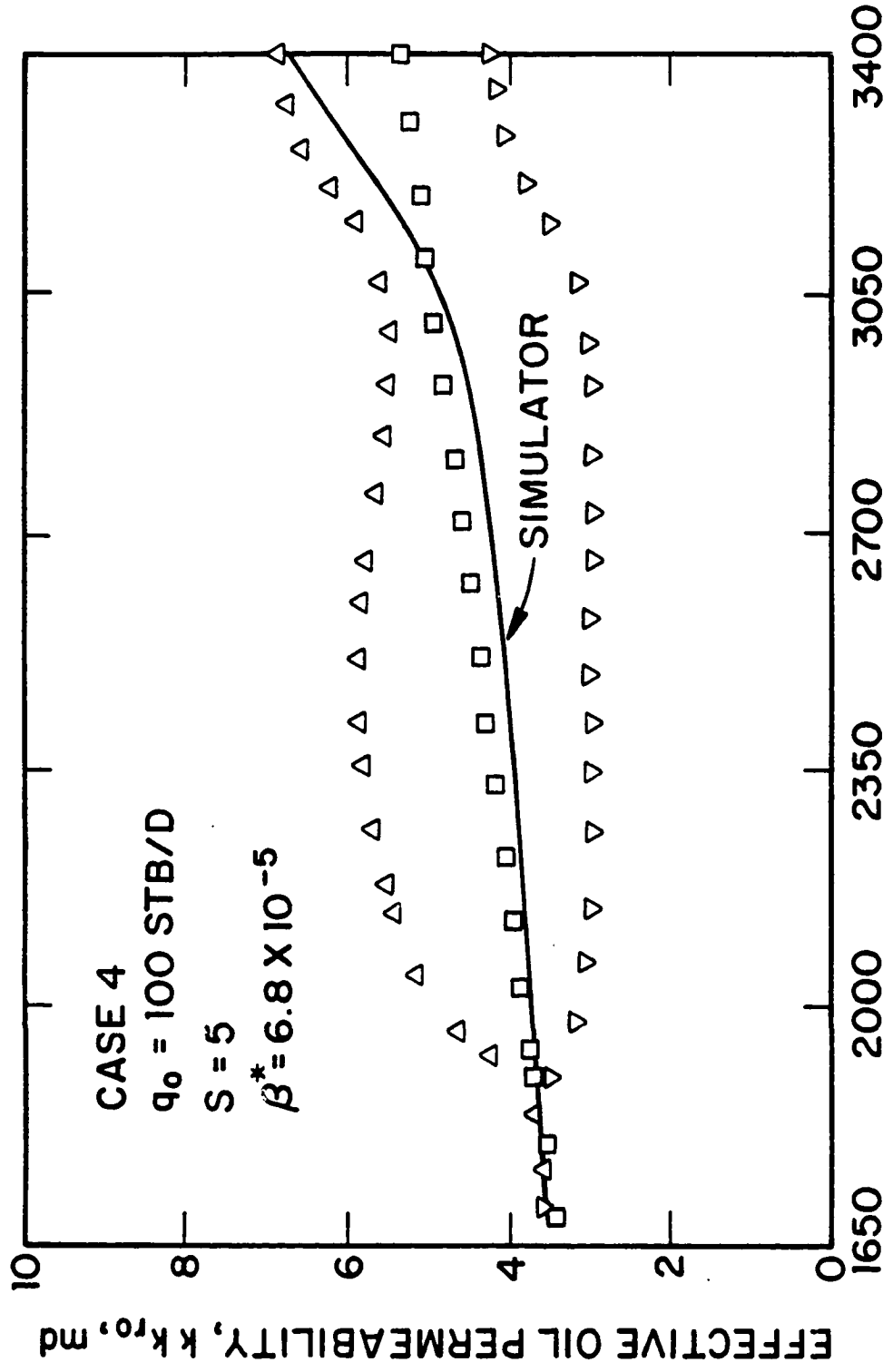

Fig. 6.7.10 - Effective oil permeability versus flowing wellbore pressure; Case 4.

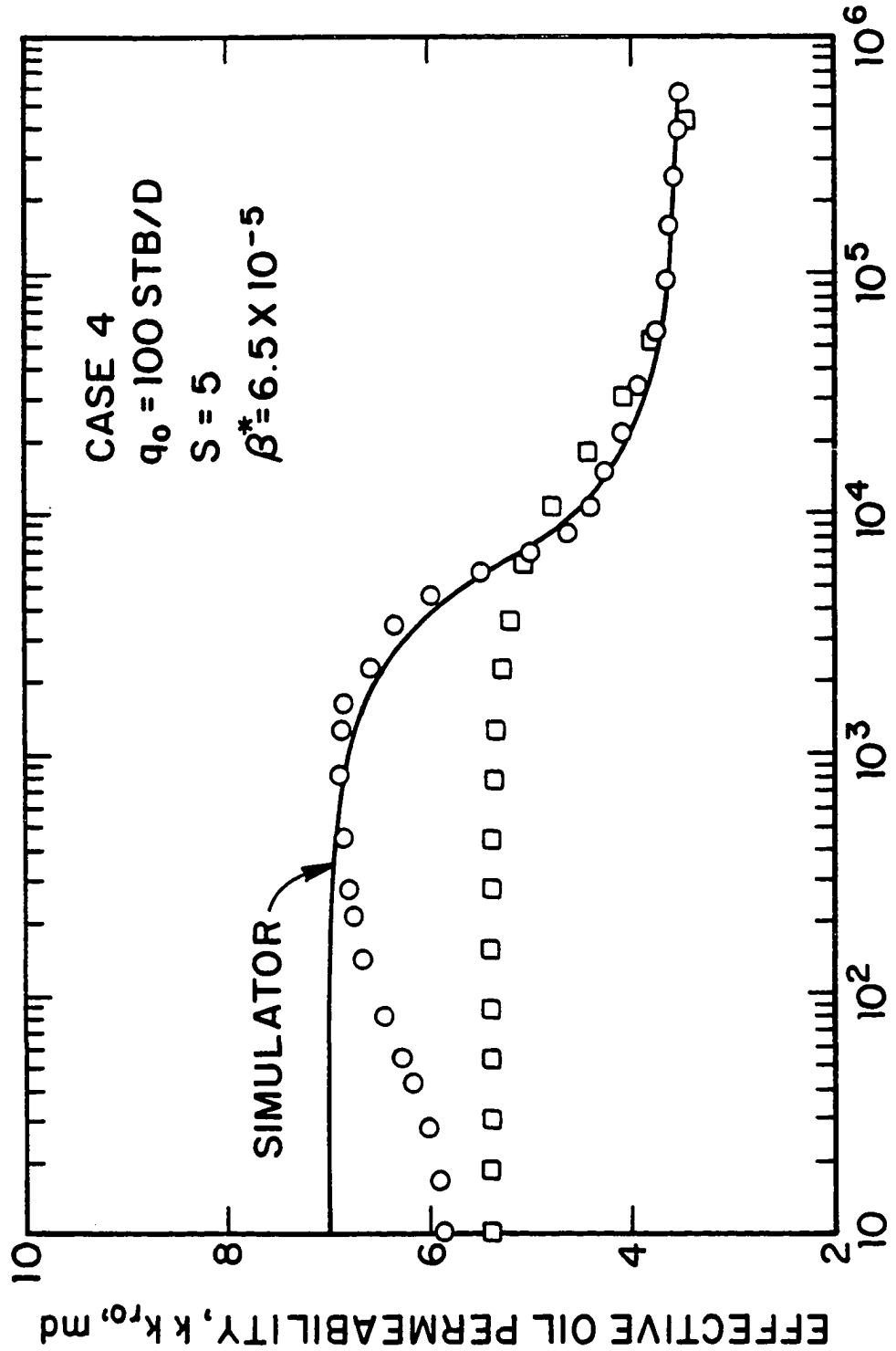

Fig. 6.7.11 - Effective oil permeability versus dimensionless time; Case 4.

to switch from the approximation of Eq. 6.7.6 to the approximation of Eq. 6.7.4. The square data points in Fig. 6.7.11 represent results obtained from the pressure-squared method and is discussed later.

Fig. 6.7.12 shows a Cartesian plot of the Case 4 sandface values of kk_{rg} versus the flowing wellbore pressure. The solid curve represents simulator values and the circular data points represent values of effective gas permeability obtained from Eq. 6.7.5. In applying Eq. 6.7.5, the values of kk_{ro} obtained from Eq. 6.7.1 (inverted triangular data points of Fig. 6.7.10) were used. As expected, Eq. 6.7.5 gives accurate values of kk_{rg} at early times when $R - R_s \approx 0$ and at times when Eq. 6.7.1 yields accurate estimates of kk_{ro}.

The circular data points in Fig. 6.7.13 represent the values of effective oil permeability obtained in Fig. 6.7.11 (circular data points of Fig. 6.7.11) graphed versus the simulator sandface values of S_o. The solid curve in Fig. 6.7.13 represents k times the simulator value of k_{ro} obtained at the sandface plotted versus the corresponding value of the sandface oil saturation. Note that we obtain a good approximation to the correct effective oil permeability versus oil saturation curve. The square data points shown in Figs. 6.7.12 and 6.7.13 represent the effective oil permeability computed using the pressure-squared method which is discussed later.

Fig. 6.7.14 shows plots of oil saturation versus the simulator value of wellbore pressure. The solid curve represents values obtained from the simulator. The solid circular data points represent the oil saturation obtained by solving Eq. 6.6.5 using Q_{sD} given by Eq. 6.6.6, i.e., by ignoring the presence of the skin zone in the computations, whereas the open circular data points represent values obtained by solving Eq. 6.6.6 with Q_{sD} given by Eq. 6.6.7. In solving Eq. 6.6.5 for S_o, the values of effective permeabilities computed from Eqs. 6.7.1 and 6.7.5 were used. The values of kk_{ro} used in this computation are represented by the circular data points of Fig. 6.7.11, i.e., were obtained by switching from the approximation of Eq. 6.7.4 to the approximation of Eq. 6.7.6 at the appropriate time. Note that at early times ($p_{wf} > 3250$) the influence of Q_{sD} (Eq. 6.6.6 or Eq. 6.6.7) on the solution of Eq. 6.6.5 is small because, as discussed previously, Eq. 6.6.5 is well approximated

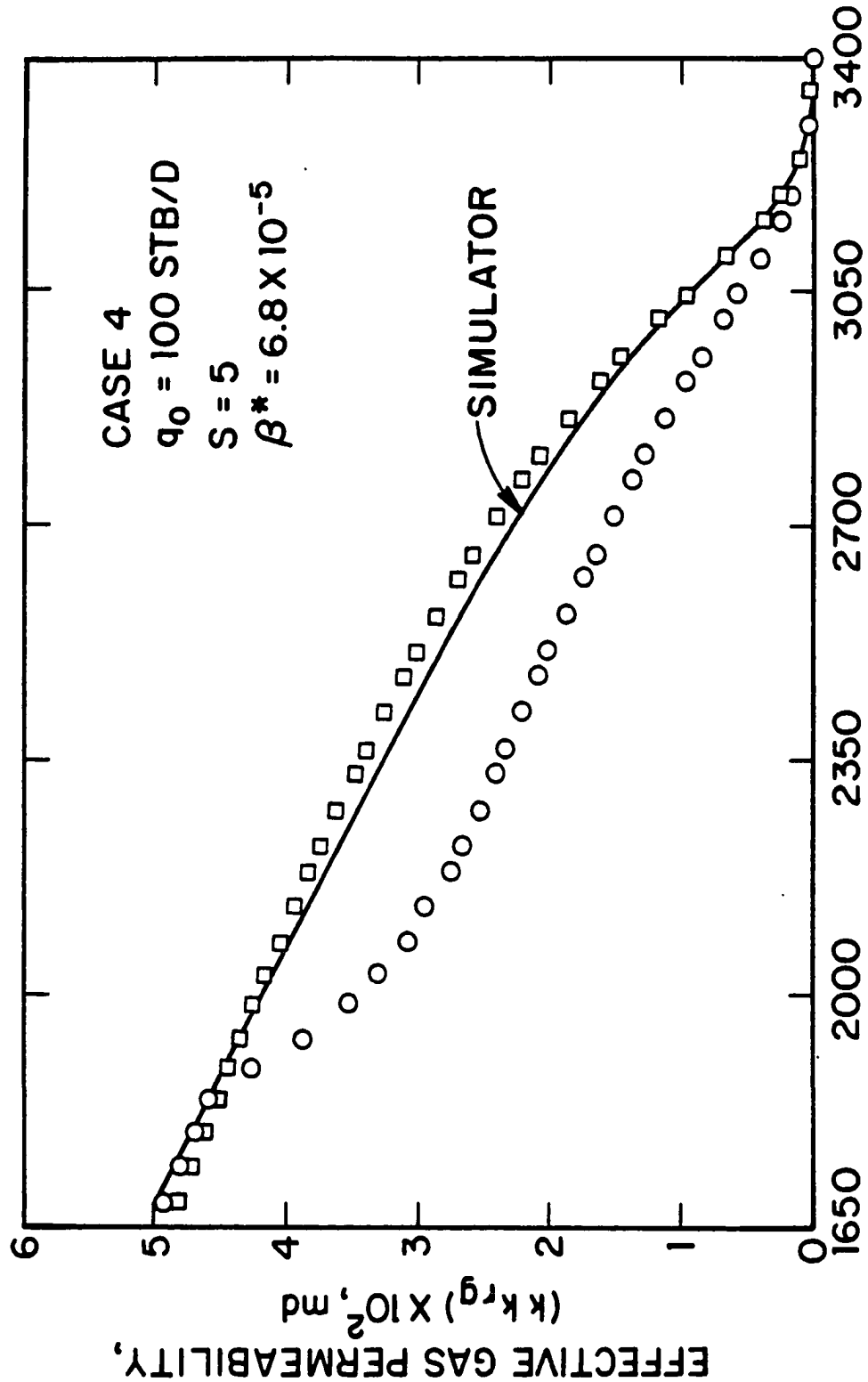

Fig. 6.7.12 - Plot of effective gas permeability versus flowing wellbore pressure; Case 4.

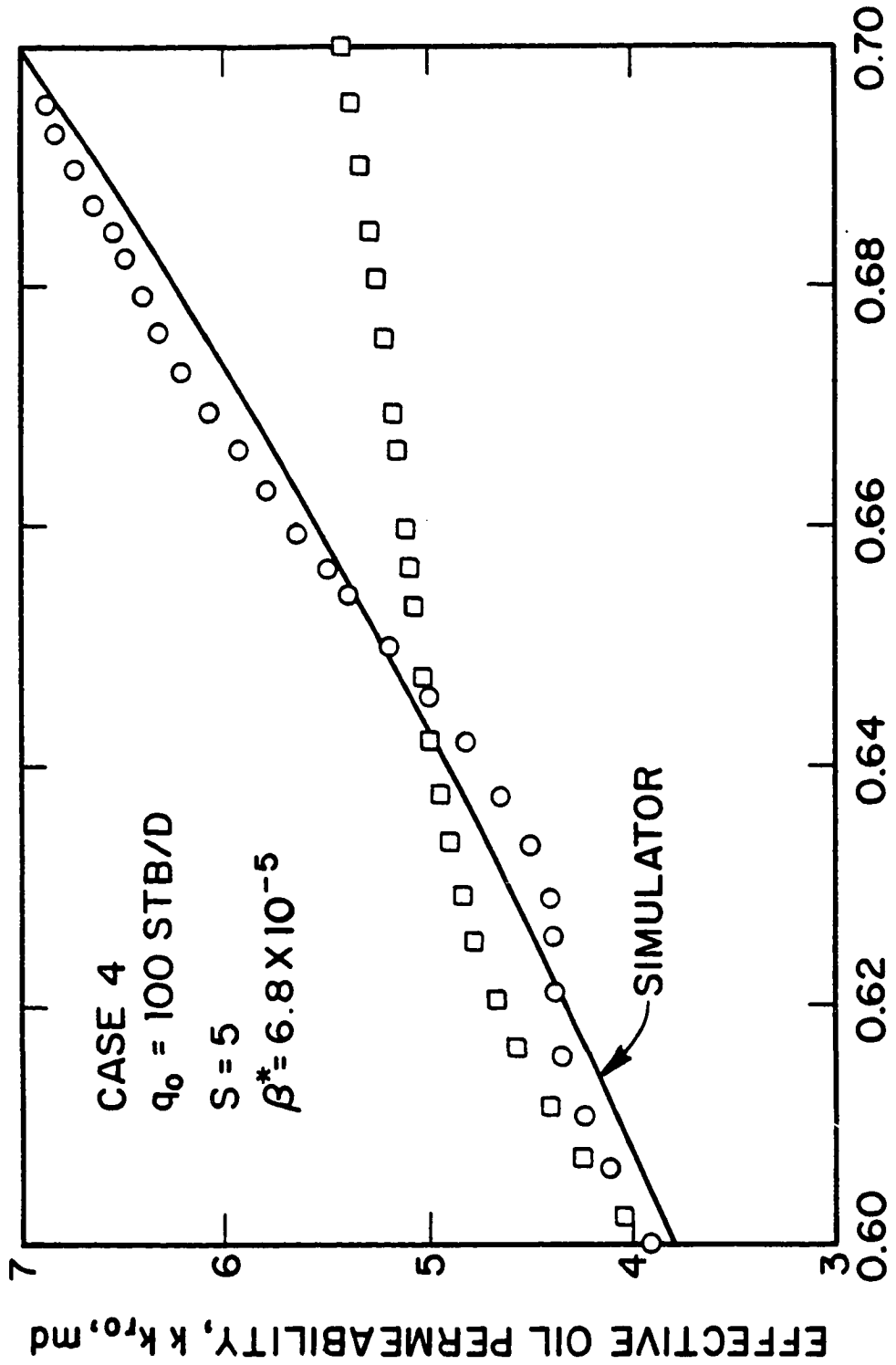

Fig. 6.7.13 - Effective oil permeability versus oil saturation; Case 4.

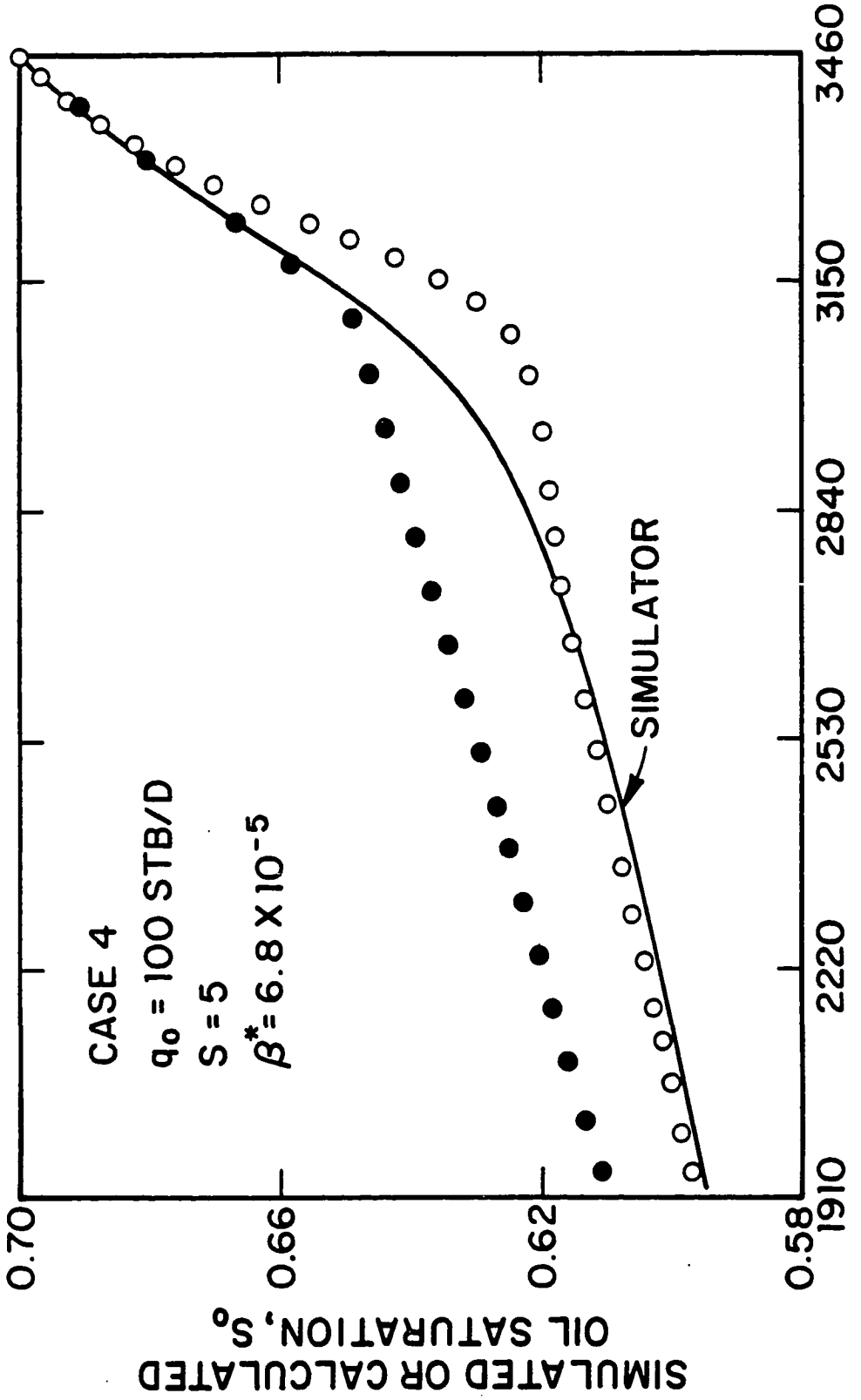

Fig. 6.7.14 - Oil saturation versus flowing wellbore pressure; Case 4.

by Martin's equation at early times. At lower values of pressure, solving Eq. 6.6.5 by using Eq. 6.6.6 which ignores the skin zone gives less accurate oil saturations than solving Eq. 6.6.5 using Eq. 6.6.7. However, in practice the value of k_s will be unknown and thus, Eq. 6.6.6 will need to be used. The main conclusion that should be drawn from the results of Fig. 6.7.14 is as follows: *if* accurate estimates of effective permeabilities can be obtained from Eqs. 6.7.1 and 6.7.5, then reasonable estimates of S_o as a function of p_{wf} can be obtained by solving Eq. 6.6.5 numerically using the expression for Q_{sD} which ignores the presence of a skin zone, Eq. 6.6.6.

The circular data points of Fiq. 6.7.15 represent the values of kk_{ro} obtained from Eq. 6.7.1 (using the approximation of Eq. 6.7.6 at early times and then switching to Eq. 6.7.4 at later times) plotted versus S_o computed by solving Eq. 6.6.5 (using Eq. 6.6.7) numerically; see the open circular data points of Fig. 6.7.14. The solid curve of Fig. 6.7.15 represents the simulator values of effective oil permeabilities plotted versus the sandface oil saturation. Note that the computed values of kk_{ro} as a function of the computed values of S_o are in good agreement with the simulator results. As noted previously, we do not have a practical way for switching from Eq. 6.7.6 to Eq. 6.7.4 therefore, at this point in time the results of Fig. 6.7.15 are only of theoretical interest.

6.8 Pressure-Squared Method

6.8.1 Constant Rate Production.

For the case where production is at a constant sandface oil rate ($q_{osf}(t) = q_o$ at all times), Refs. 9, 11, 12 and 14 suggested that data can be analyzed by a semilog plot of pressure-squared versus time. In terms of providing both a theoretical and practical basis, Ref. 12 is the most complete and we summarize its results here. For all cases considered in Ref. 12 (also see Ref. 28), it was found that the sandface value of $\alpha = k_{ro}/(\mu_o B_o)$ versus p_{wf} could be approximated well by piecewise linear function, i.e., by two straight lines. Mathematically, this result can be expressed as

$$\alpha = \frac{k_{ro}}{\mu_o B_o} = a p_{wf} + d; \qquad for \quad p \leq p_1, \tag{6.8.1}$$

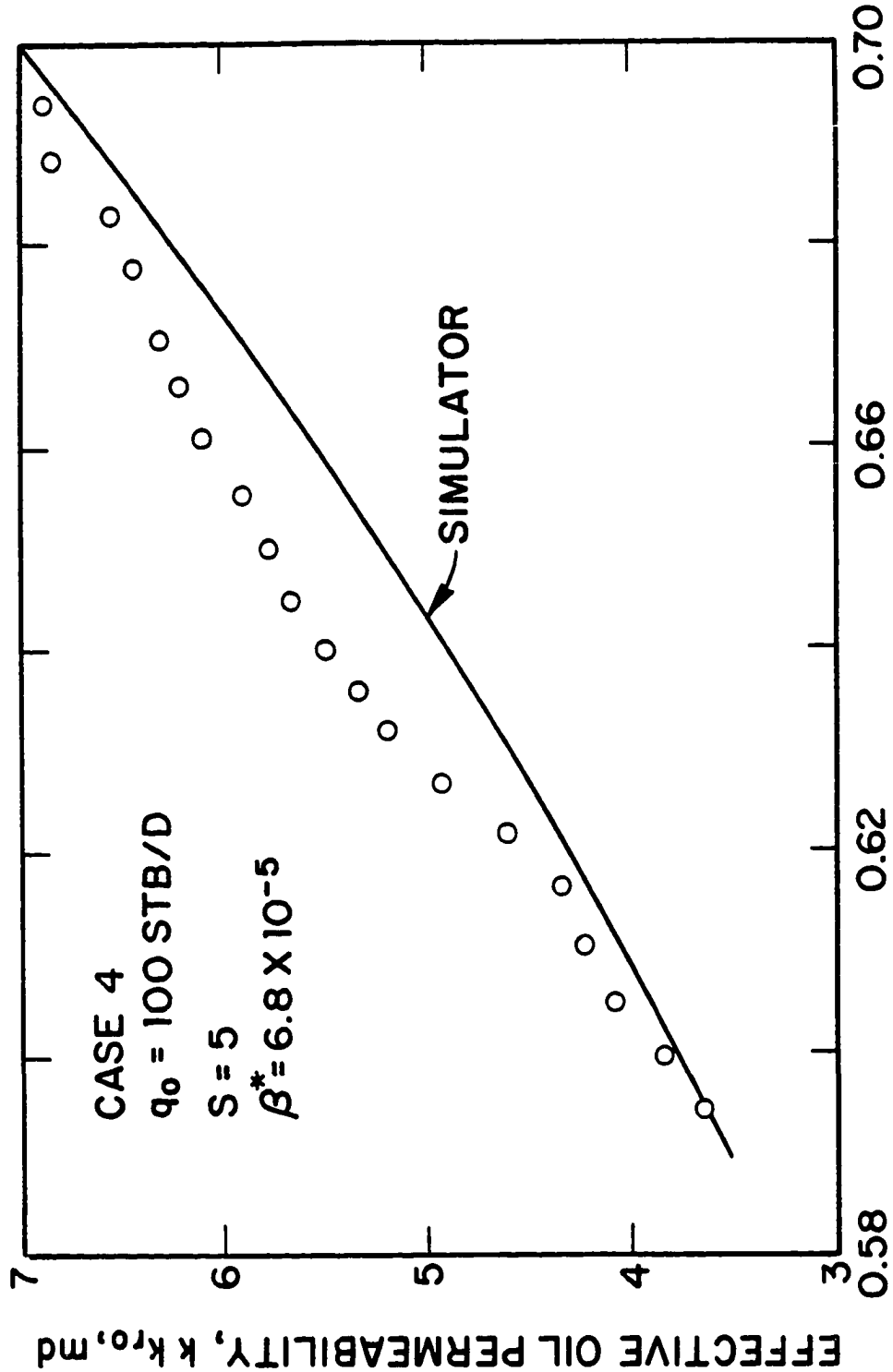

Fig. 6.7.15 - Effective oil permeability versus oil saturation; Case 4.

and

$$\alpha = \frac{k_{ro}}{\mu_o B_o} = bp_{wf} + c; \qquad for \quad p_1 \le p \le p_i, \tag{6.8.2}$$

where p_1 is the pressure at which these two straight lines intersect. In Eqs. 6.8.1 and 6.8.2, a, b, c and d are constants. Fig. 6.8.1 illustrates the validity of this "two straight line" model for the data of Case 4. The solid curve in Fig. 6.8.1 represents a Cartesian plot of the sandface value of $k_{ro}/(\mu_o B_o)$ obtained from the simulator versus the corresponding value of the flowing wellbore pressure. The two dashed lines represent Eqs. 6.8.1 and 6.8.2.

By using Eqs. 6.8.1 and 6.8.2 in Eq. 6.5.1, integrating and rearranging the resulting equation, Ref. 12 obtained the following result:

$$\frac{\hat{a}kh\left(p_i^2 - p_{wf}^2\right)}{141.2\,(2q_o)} = 1.151\log\left(\frac{4t_D}{e^{\gamma}}\right) + s - \frac{\left(\hat{b} - \hat{a}\right)kh\left(p_i^2 - p_1^2\right)}{141.2\,(2q_o)}, \tag{6.8.3}$$

where

$$\hat{a} = a + \frac{2d}{p_1 + p_{wf}}, \tag{6.8.4}$$

and

$$\hat{b} = b + \frac{2c}{p_i + p_1}. \tag{6.8.5}$$

Eq. 6.8.3 applies for $p_{wf} < p_1$ and as shown in Ref. 12 this inequality applies except at early times. For the results of Fig. 6.8.1, $p_1 = 2947$ psi and this pressure is reached at $t = 0.074$ days, $t = 1.8$ hours. Note that Eq. 6.8.4 indicates that $\hat{a}$ is not a constant unless $d = 0$ and in most cases[9,28] d is nonzero; see Fig. 6.8.1. However, Ref. 12 showed that there exists a time period where the variation in $\hat{a}$ is not great and during this time period, Eq. 6.8.3 applies with $\hat{a}$ replaced by its average value. Throughout, we do not distinguish between $\hat{a}$ and its average value.

Eq. 6.8.3 indicates that a semilog plot of $p_i^2 - p_{wf}^2$ versus t will be a straight line of slope

$$m_2 = \frac{162.6(2q_o)}{\hat{a}kh}, \tag{6.8.6}$$

and $\hat{a}k$ can be computed from this semilog slope by the following equation:

$$\hat{a}k = \frac{162.6(2q_o)}{m_2 h}. \tag{6.8.7}$$

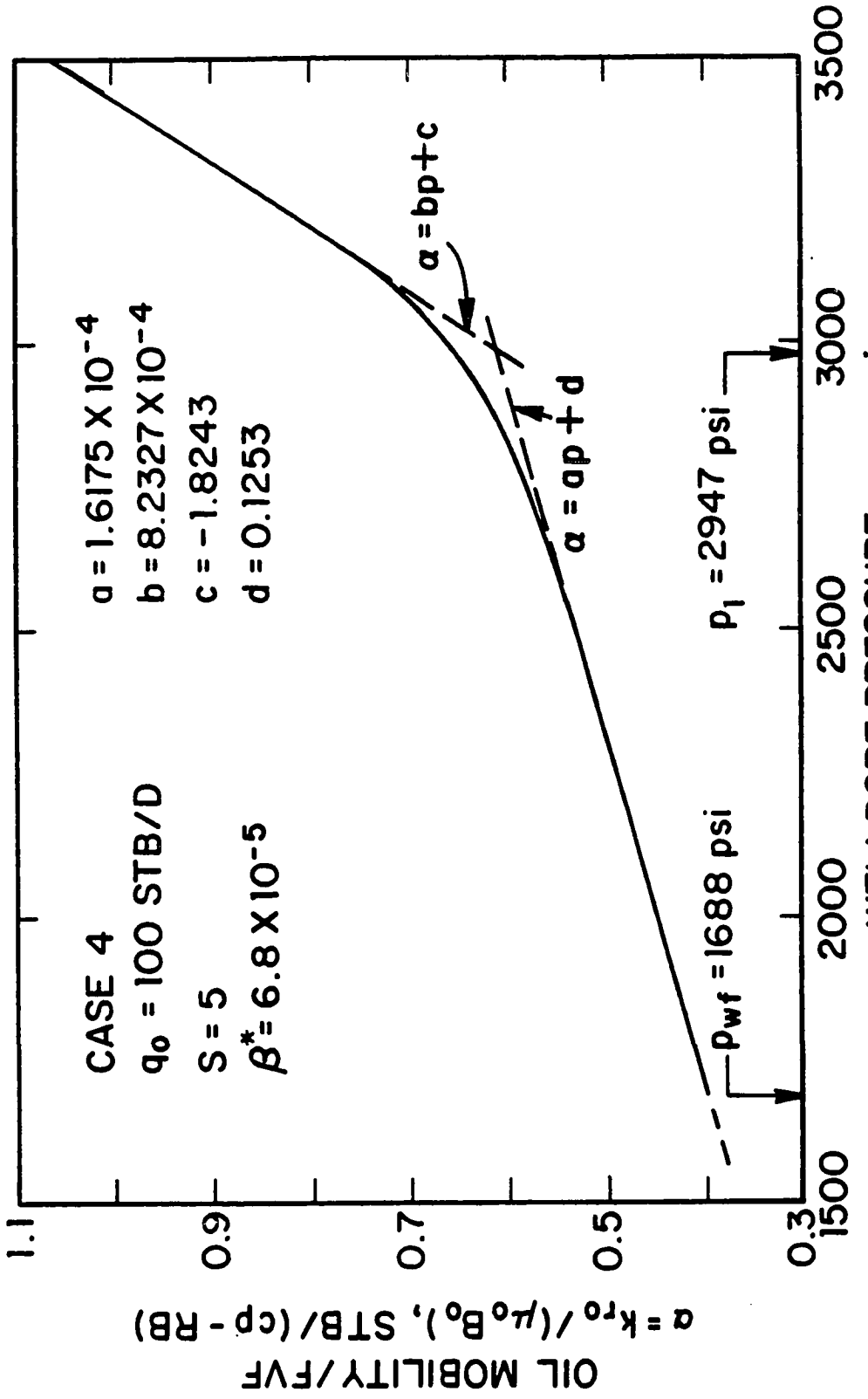

Fig. 6.8.1 - Oil mobility/FVF as a function of flowing wellbore pressure; Case 4.

Ref. 12 also showed that effective oil permeability could then be approximated by

$$\left(kk_{ro}\right)_{p_{wf}} = (\hat{a}k)\left(\mu_o B_o\right)_{p_{wf}} p_{wf}, \tag{6.8.8}$$

where $\hat{a}k$ denotes the value computed from Eq. 6.8.7. As shown in Ref. 12, the approximation of Eq. 6.8.8 can be obtained by multiplying Eq. 6.8.2 by $k\mu_o B_o$ and approximating $k(ap_{wf} + d)$ by $\hat{a}kp_{wf}$. Since the value of $\hat{a}k$ is computed from the semilog slope, Eq. 6.8.8 will yield good estimates of the effective oil permeability only at times when pressure-squared data lie on or almost on the semilog straight line. However, if we extrapolate Eq. 6.8.8 to initial pressure, we can obtain a rough estimate of the initial effective oil permeability from the following equation:

$$kk_{roi} = \left(kk_{ro}\right)_{p_i} = (\hat{a}k)\left(\mu_o B_o\right)_{p_i} p_i, \tag{6.8.9}$$

As shown in Refs. 9, 11, 12 and 28, an equation for estimating the skin factor can also be derived directly from Eq. 6.8.3. The relevant equation is given by

$$s = 1.151\left(\frac{\left(p_i^2 - p_{wf}^2\right)_{1hr}}{m_2} - \log\left(\frac{kk_{roi}}{\phi\mu_{oi}c_{ti}r_w^2}\right) + 3.23\right), \tag{6.8.10}$$

where $\left(p_i^2 - p_{wf}^2\right)_{1hr}$ denotes the value of $p_i^2 - p_{wf}^2$ obtained by extrapolating the pressure-squared semilog straight line to a flowing time of $t = 1$ hour. Since Eq. 6.8.10 ignores the terms of Eq. 6.8.3 which involve $\hat{b} - \hat{a}$, Eq. 6.8.10 is only approximate. Moreover, for all cases considered in Refs. 12 and 28, $\hat{b} - \hat{a} > 0$ and thus, Eq. 6.8.3 indicates that Eq. 6.8.10 will yield an underestimate of the skin factor. However, if rock and fluid properties are such that $\hat{b} - \hat{a} < 0$, then Eq. 6.8.10 will yield an overestimate of the skin factor. Based on the results presented in Refs. 9, 12 and 28 and results presented later in this Chapter, the value of s obtained from Eq. 6.8.10 should differ from the correct value of s by no more than one or two units.

For the wellbore storage problem considered in this Chapter, the analysis methods presented in this subsection should be applicable once the effects of wellbore storage become negligible, i.e., once $q_{osf}(t) \approx q_o$, where q_o is the constant surface

rate of production. In the following two subsections, we present the working equation for pressure-squared analysis based on logarithmic convolution time and rate normalization.

6.8.2 Pressure-Squared Analysis With Logarithmic Convolution Time.

Starting from Eq. 6.5.4 and using the same approximations (Eqs. 6.8.1 and 6.8.2) that led to Eq. 6.8.3, one can show that

$$\frac{\hat{a}kh\left(p_i^2-p_{wf}^2\right)}{141.2\left(2q_{osf}(t)\right)}=1.151t_{lcD}+s-\left[\frac{\left(\hat{b}-\hat{a}\right)kh\left(p_i^2-p_1^2\right)}{141.2\left(2q_{osf}(t)\right)}\right]. \tag{6.8.11}$$

As in the constant rate production case of the last section, the terms of Eq. 6.8.11 which involve $\hat{b}-\hat{a}$ will cause a small error in the computed value of the mechanical skin factor. Ignoring the terms involving $\hat{b}-\hat{a}$, we can rewrite Eq. 6.8.11 as

$$\frac{p_i{}^2-p_{wf}^2}{q_{osf}(t)}=m_3\left(t_{lc}+\tilde{s}\right), \tag{6.8.12}$$

where

$$m_3=\frac{325.2}{\hat{a}kh}, \tag{6.8.13}$$

and

$$\tilde{s}=\left(\log\left(\frac{kk_{roi}}{\phi\mu_{oi}c_{ti}r_w^2}\right)-1.847+0.87s\right). \tag{6.8.14}$$

Eq. 6.8.12 indicates that a plot of $(p_i^2-p_{wf}^2)/q_{osf}(t)$ versus the logarithmic convolution time, t_{lc}, will exhibit a Cartesian straight line with slope equal to m_3. The corresponding value of $\hat{a}k$ can be obtained from the following rearrangement of Eq. 6.8.13:

$$\hat{a}k=\frac{325.2}{m_3h}. \tag{6.8.15}$$

Using this value of $\hat{a}k$, one can compute effective oil permeability as a function of the flowing wellbore pressure from

$$\left(kk_{ro}\right)_{p_{wf}}=(\hat{a}k)\left(\mu_oB_o\right)_{p_{wf}}p_{wf}. \tag{6.8.16}$$

Since the value of $\hat{a}k$ is computed from the Cartesian slope, m_3, Eq. 6.8.16 will yield good estimates of the effective oil permeability only at times when data lie

on or almost on the straight line of Eq. 6.8.12. However, if we extrapolate Eq. 6.8.16 to initial pressure, we can obtain a rough estimate of the initial effective oil permeability from the following equation:

$$kk_{roi} = \left(kk_{ro}\right)_{p_i} = (\hat{a}k)\left(\mu_o B_o\right)_{p_i} p_i. \tag{6.8.17}$$

By extrapolating Eq. 6.8.12 to $t_{lc} = 0$ to obtain $\left((p_i^2 - p_{wf}^2)/q_{osf}(t)\right)_{ext}$ and rearranging the resulting equation, one obtains the following equation:

$$s = 1.151\left(\frac{\left((p_i^2 - p_{wf}^2)/q_{osf}(t)\right)_{ext}}{m_3} - \log\left(\frac{kk_{roi}}{\phi\mu_{oi}c_{ti}r_w^2}\right) + 1.847\right). \tag{6.8.18}$$

Note our derivation of Eq. 6.8.18 ignored the term in square brackets in Eq. 6.8.11. As this term involves $q_{osf}(t)$ which changes with time, a straight line cannot be obtained unless the variation of the term of Eq. 6.8.11 within square brackets is small or negligible compared to the other terms in Eq. 6.8.11. Since Eq. 6.8.12 ignores the terms of Eq. 6.8.11 which involve $\hat{b} - \hat{a}$, Eq. 6.8.18 is only approximate. As in the pressure-squared method, Eq. 6.8.18 will yield an underestimate of the skin factor if $\hat{b} - \hat{a} > 0$ and an overestimate of the skin factor if $\hat{b} - \hat{a} < 0$.

6.8.3 Rate Normalization for Pressure-Squared Method.

In this subsection, we present the working equation for performing analysis based on the rate-normalized change in pressure-squared.

For rate-normalization the analogue of Eq. 6.8.3 is given by

$$\frac{\hat{a}kh\left(p_i^2 - p_{wf}^2\right)}{141.2\left(2q_{osf}(t)\right)} = 1.151\log\left(\frac{4t_D}{e^{\gamma}}\right) + s - \left[\frac{\left(\hat{b} - \hat{a}\right)kh\left(p_i^2 - p_1^2\right)}{141.2\left(2q_{osf}(t)\right)}\right], \tag{6.8.19}$$

where $\hat{a}$ and $\hat{b}$, respectively, are still given by Eqs. 6.8.4 and 6.8.5 and, similar to Eq. 6.8.3, Eq. 6.8.19 applies for $p_{wf} < p_1$.

When Eq. 6.8.19 applies, a semilog plot of $(p_i^2 - p_{wf}^2)/q_{osf}(t)$ versus t will be a semilog straight line of slope m_3, where m_3 is given by Eq. 6.8.13, i.e.,

$$m_3 = \frac{325.2}{\hat{a}kh}, \tag{6.8.20}$$

and $\hat{a}k$ can be computed from this semilog slope by the following equation:

$$\hat{a}k = \frac{325.2}{m_3 h}. \tag{6.8.21}$$

As in the standard pressure-squared method, effective oil permeability can then be approximated by

$$(kk_{ro})_{p_{wf}} = (\hat{a}k)(\mu_o B_o)_{p_{wf}} p_{wf}, \tag{6.8.22}$$

where $\hat{a}k$ denotes the value computed from Eq. 6.8.21. Since the value of $\hat{a}k$ used in Eq. 6.8.22 is computed from the semilog slope, Eq. 6.8.22 will yield good estimates of the effective oil permeability only at times when pressure-squared data lie on or almost on the semilog straight line. However, if we extrapolate Eq. 6.8.22 to initial pressure, we can obtain a rough estimate of the initial effective oil permeability from the following equation:

$$kk_{roi} = (kk_{ro})_{p_i} = (\hat{a}k)(\mu_o B_o)_{p_i} p_i. \tag{6.8.23}$$

Letting $\left((p_i^2 - p_{wf}^2)/q_{osf}(t)\right)_{1hr}$ denote the value of the rate-normalized change in pressure-squared obtained by extrapolating the semilog straight line to $t = 1$ hour, the skin factor can be estimated from the following equation:

$$s = 1.151\left(\frac{\left((p_i^2 - p_{1hr}^2)/q_{osf}(t)\right)_{1hr}}{m_3} - \log\left(\frac{kk_{roi}}{\phi\mu_{oi}c_{ti}r_w^2}\right) + 3.23\right). \tag{6.8.24}$$

As in the pressure-squared method, Eq. 6.8.24 is only approximate because the term involving $\hat{b} - \hat{a}$ in Eq. 6.8.19 is neglected. Moreover, this same term also involves $q_{osf}(t)$ and thus, a straight line cannot be obtained until the variation of the term of Eq. 6.8.19 within square brackets is small or the term in square brackets is negligible compared to the other terms in Eq. 6.8.19. As in the pressure-squared method, Eq. 6.8.24 will yield an underestimate of the skin factor if $\hat{b} - \hat{a} > 0$ and an overestimate of the skin factor if $\hat{b} - \hat{a} < 0$.

6.9 Pressure-Squared Analysis Results

In this major section, we present computational results obtained for Cases 1-6 by analyzing the resulting pressure data using the various forms of pressure-squared analysis.

Cases 1, 2 and 3.

Fig. 6.9.1 presents log-log plots of $p_i^2 - p_{wf}^2$ versus t for Cases 1, 2 and 3. Recall that no wellbore storage effects exist for Case 1, i.e., $q_{osf} = q_o = 150$ STB/D for all times. For Case 2, $\beta^* = 6.8 \times 10^{-4}$ ($C_D \approx 117.4$) and for Case 3, $\beta^* = 6.8 \times 10^{-5}$ ($C_D \approx 1174$). For Cases 2 and 3, as in the constant wellbore storage case, one approximately obtains a unit slope line at early times. However, as noted previously our wellbore storage model is one where the wellbore storage coefficient varies with time and is not uniquely related to a constant C_D value. When we tried to type curve match the data of Fig. 6.9.1 with the constant wellbore storage coefficient type curves of Bourdet et al.[48], a match could not obtained.

Fig. 6.9.2 shows semilog plots of the same data considered in Fig. 6.9.1. For the zero wellbore storage case, Case 1, a well-defined semilog straight line exists at all times corresponding to $t > 4 \times 10^{-3}$ days. The slope of this semilog straight line is 1.441×10^6 psi^2 per log cycle. In Case 2, we obtain the same semilog straight line, but only at times corresponding to $t > 0.4$ days. For the results of Case 3, the semilog straight line does not begin until $t \approx 1.8$ days. Thus, in Case 3 we would need to run a drawdown test for well over two days in order to obtain an easily identifiable semilog straight line. Although our wellbore storage model does not correspond to a constant C_D model, if we use the approximation $C_D = 1174$, then for the corresponding liquid case the semilog straight line will begin at $t \approx 0.52$ days based on the approximate starting time of $t_D/C_D = 60$.

Using the semilog slope obtained in Fig. 6.9.2, $m_2 = 1.441 \times 10^6$ psi^2 per log cycle, in Eq. 6.8.7, one obtains $\hat{a}k = 2.18 \times 10^{-3}$. Eq. 6.8.8 evaluated at the final value of flowing pressure $p_{wf} = 2050$ psi gives $kk_{ro} = 3.65$ md as compared to the correct (simulator) value of $kk_{ro} = 3.73$ md. Eq. 6.8.9 yields $kk_{roi} = 5.15$ md as compared to the correct value of $kk_{roi} = 7.00$ md. Applying Eq. 6.8.10, one obtains $s = -0.68$ as compared to the correct value of $s = 0$.

Fig. 6.9.3 shows Cartesian plots of $(p_i^2 - p_{wf}^2)/q_{osf}(t)$ versus logarithmic convolution time, t_{lc}, for Cases 1, 2 and 3. In Case 1, a well-defined straight line of slope $m_3 = 9.64 \times 10^3$ psi^2/(STB/D) exists for $t_{lc} > -2.7$ ($t > 4.4 \times 10^{-3}$ days). For Case

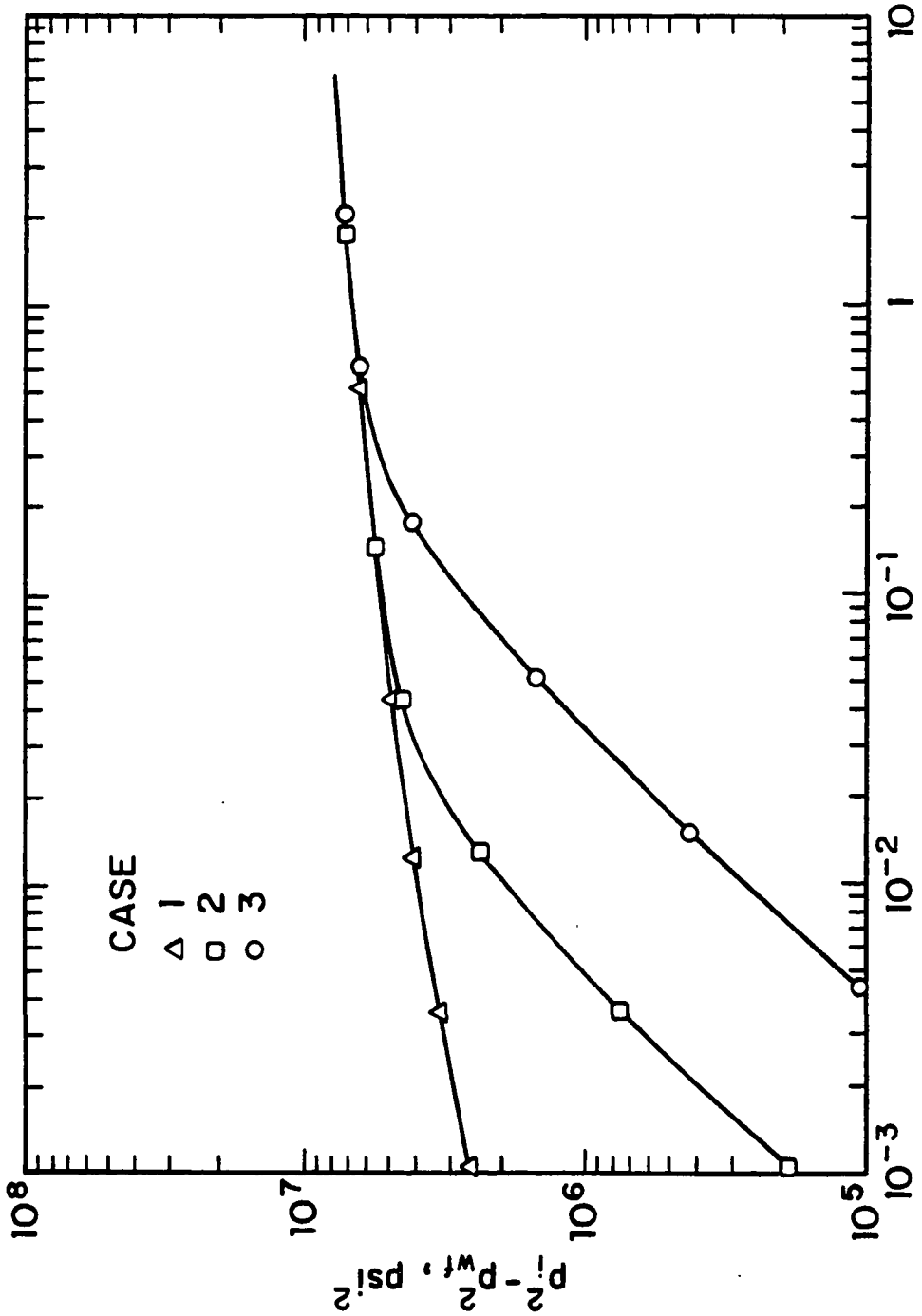

Fig. 6.9.1 - Log-log plot of change in pressure-squared versus time; Cases 1, 2 and 3.

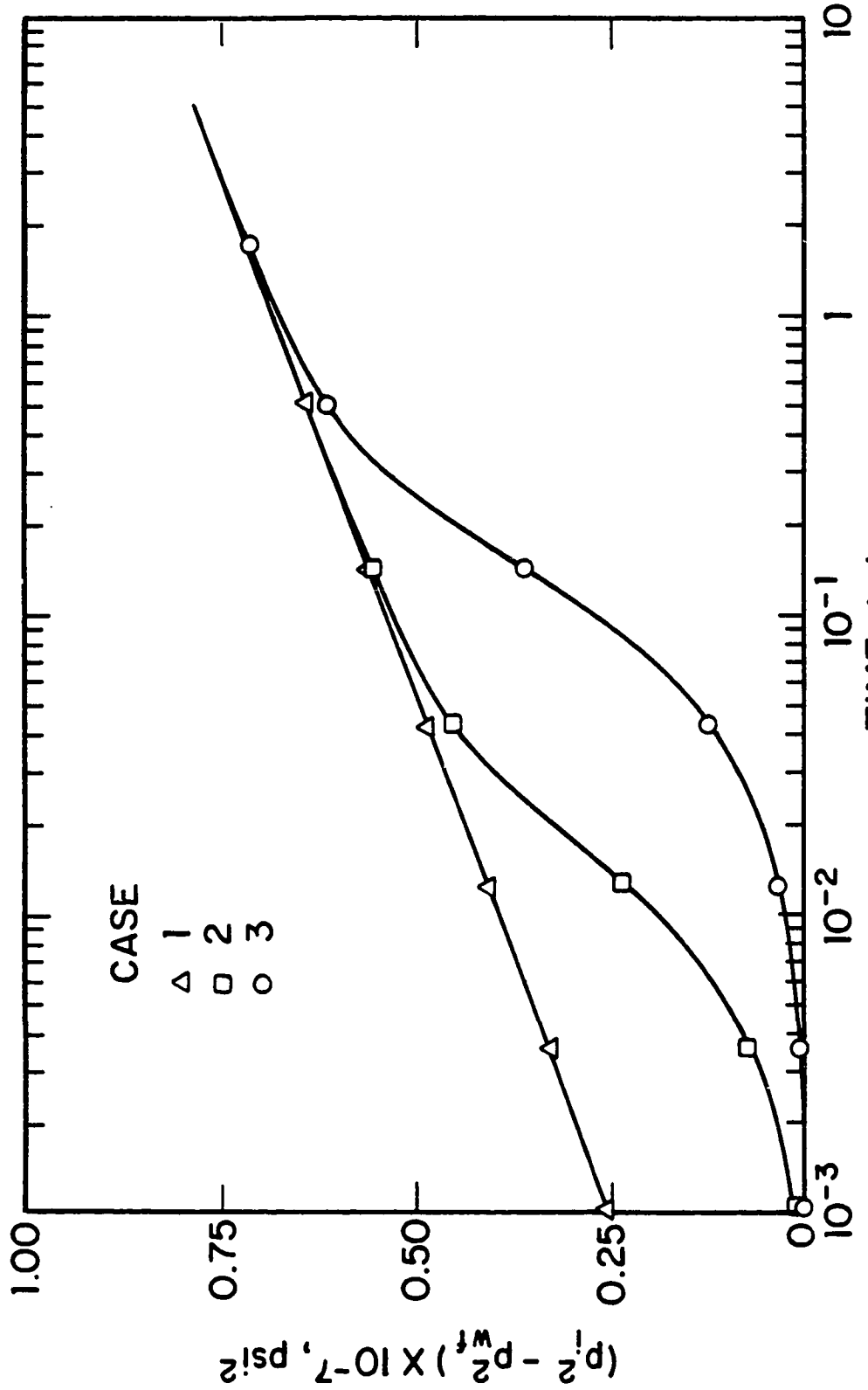

Fig. 6.9.2 - Semilog plot of change in pressure-squared versus time; Cases 1, 2 and 3.

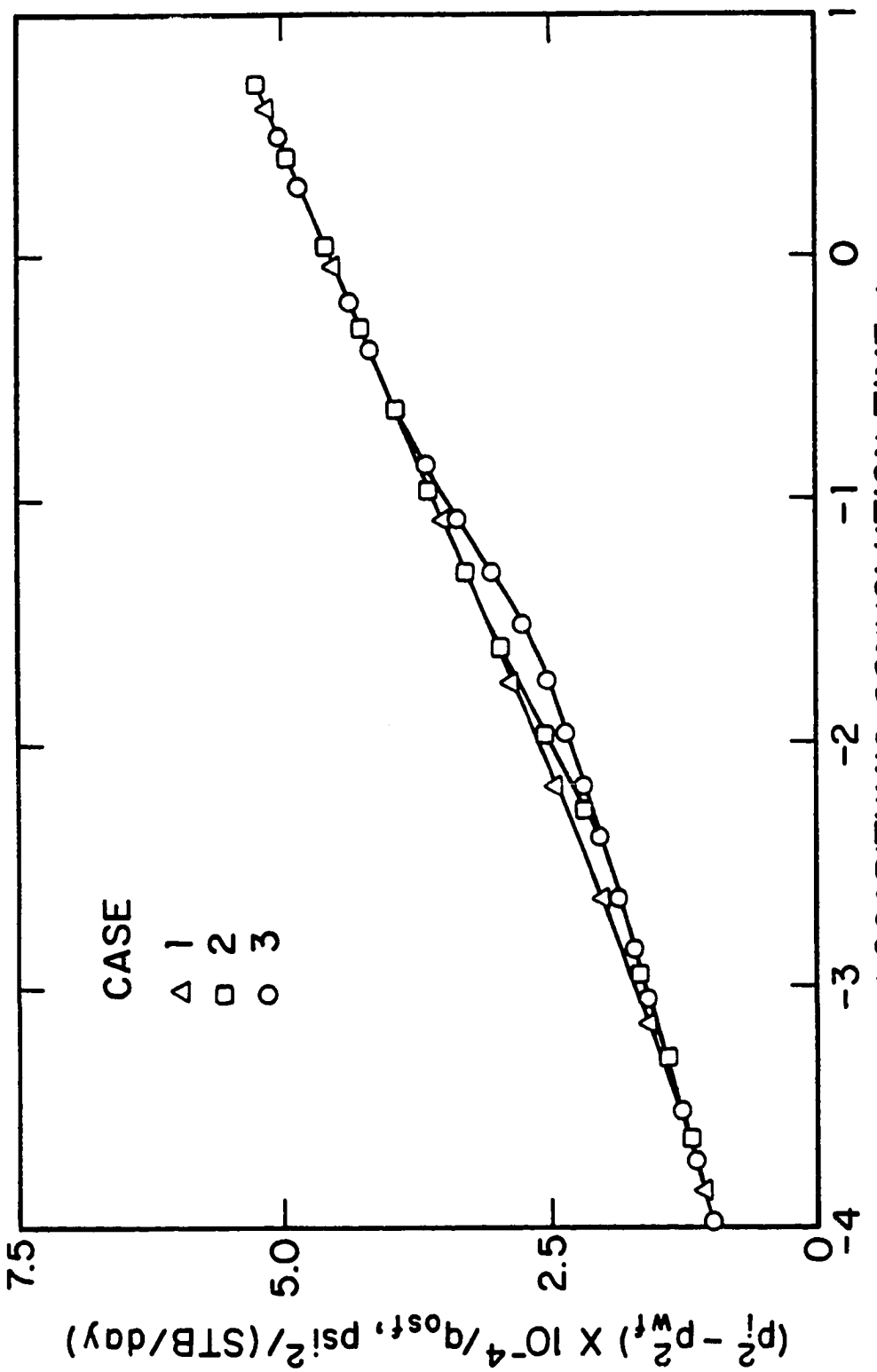

Fig. 6.9.3 - Rate-normalized change in pressure-squared versus logarithmic convolution time; Cases 1, 2 and 3.

2, this straight line begins at $t_{lc} \approx -1.4$ which corresponds to $t = 8.3 \times 10^{-2}$ days. For Case 3, this straight line begins at $t_{lc} \approx -0.7$ which corresponds to $t = 0.3$ days. Recall that when we used the standard pressure-squared method (see Fig. 6.9.2), the semilog straight line began at $t = 0.4$ days for Case 2 and at $t \approx 1.8$ days in Case 3. Thus, the log-convolution time based on measured sandface rates is useful in that one can analyze data at earlier times than is possible using the standard pressure-squared semilog plot of Fig. 6.9.2.

Using the slope of $m_3 = 9.64 \times 10^3$ obtained from the results of Fig. 6.9.3, Eq. 6.8.15 gives $\hat{a}k = 2.17 \times 10^{-3}$. Eq. 6.8.16 evaluated at the final value of flowing pressure $p_{wf} = 2050$ psi gives $kk_{ro} = 3.64$ md as compared to the correct (simulator) value of $kk_{ro} = 3.73$ md. Eq. 6.8.17 yields $kk_{roi} = 5.13$ md as compared to the correct value of $kk_{roi} = 7.00$ md. Applying Eq. 6.8.18, one obtains $s = -0.71$ as compared to the correct value of $s = 0$. Note that the accuracy of these results is essentially the same as that obtained using the pressure-squared method as expected. The advantage of the logarithmic convolution time is that proper straight lines start earlier because t_{lc} accounts for the changing sandface rate, whereas on a semilog plot of the change in pressure-squared versus time, the proper semilog straight line does not begin until $q_{osf} \approx q_o$.

Fig. 6.9.4 shows semilog plots of the rate-normalized change in pressure-squared versus time. As shown, all cases eventually show a well-defined semilog straight line of slope $m_3 = 9.83 \times 10^3$ psi^2/ (STB/D). For Case 2, the semilog straight line begins at $t \approx 0.23$ days compared to a beginning time of $t \approx 0.4$ for the analogous pressure-squared plot of Fig. 6.9.2. For Case 3, the semilog straight line begins at $t \approx 1.5$ days compared to a beginning time of $t \approx 1.8$ for the analogous pressure-squared plot of Fig. 6.9.2. Thus, rate-normalization causes only a small decrease in the beginning time of the semilog straight line. In this regard, plotting data in terms of logarithmic convolution time is preferable. Using the semilog slope of $m_3 = 9.83 \times 10^3$ psi^2/(STB/D) per log cycle in Eq. 6.8.21, one obtains $\hat{a}k = 2.13 \times 10^{-3}$. Eq. 6.8.22 evaluated at the final value of flowing pressure, $p_{wf} = 2050$ psi, gives $kk_{ro} = 3.57$ md as compared to the correct (simulator) value

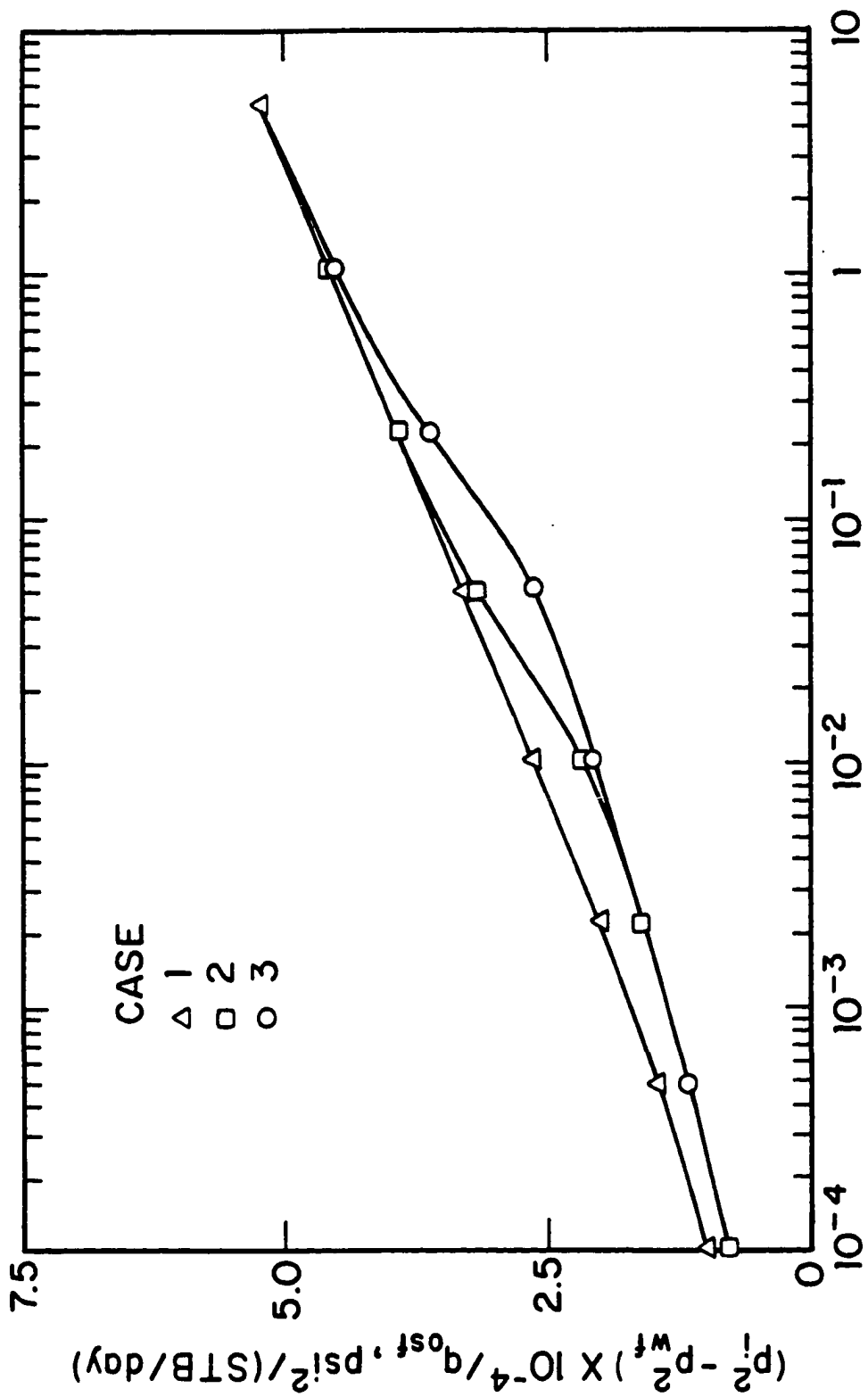

Fig. 6.9.4 - Semilog plot of rate-normalized change in pressure-squared versus time; Cases 1, 2 and 3.

of $kk_{ro} = 3.73$ md. Eq. 6.8.23 yields $kk_{roi} = 5.03$ md as compared to the correct value of $kk_{roi} = 7.00$ md. Applying Eq. 6.8.24, one obtains $s = -0.84$ as compared to the correct value of $s = 0$. Note that these results should be and are essentially identical to those obtained from the other two methods.

Cases 4, 5 and 6.

Fig. 6.9.5 presents log-log plots of $p_i^2 - p_{wf}^2$ versus t for for Cases 4, 5 and 6. Recall that no wellbore storage effects exist for Case 6, i.e., $q_{osf} = q_o = 100$ STB/D for all times. For Case 4, $\beta^* = 6.8 \times 10^{-5}$ ($C_D \approx 1174$) and for Case 5, $\beta^* = 6.8 \times 10^{-4}$ ($C_D \approx 117.4$). In all cases, $s = 5$. The results of Fig. 6.9.5 are qualitatively similar to those of Fig. 6.9.1 and thus, are self explanatory.

Fig. 6.9.6 shows semilog plots of the same data considered in Fig. 6.9.5. For the zero wellbore storage case, Case 6, a well-defined semilog straight line exists at all times corresponding to $t > 2.5 \times 10^{-2}$ days. The slope of this semilog straight line is 0.913×10^6 psi^2 per log cycle. Note that this semilog straight line starts slightly later than the no wellbore storage, $s = 0$ case of Fig. 6.9.2, because, as explained in Ref. 9, proper straight lines cannot exist until the skin zone approaches a steady-state behavior. In Case 5, we obtain the same semilog straight line, but only at times corresponding to $t > 0.4$ days. For the results of Case 4, the semilog straight line does not begin until $t \approx 2$ days. Thus, in Case 4, we would need to run a drawdown test for well over two days in order to obtain an easily identifiable semilog straight line.

Using the semilog slope obtained from Fig. 6.9.6, $m_2 = 0.913 \times 10^6$ psi^2 per log cycle, in Eq. 6.8.7, one obtains $\hat{a}k = 2.29 \times 10^{-3}$. Eq. 6.8.8 evaluated at the final value of flowing pressure $p_{wf} = 1688$ psi gives $kk_{ro} = 3.43$ md as compared to the correct (simulator) value of $kk_{ro} = 3.53$ md. Eq. 6.8.9 yields $kk_{roi} = 5.42$ md as compared to the correct value of $kk_{roi} = 7.00$ md. Applying Eq. 6.8.10, one obtains $s = 4.62$ as compared to the correct value of $s = 5$.

As noted earlier, Eq. 6.8.8 can be used to compute effective oil permeability as a function of pressure during the time period when the pressure-squared plot

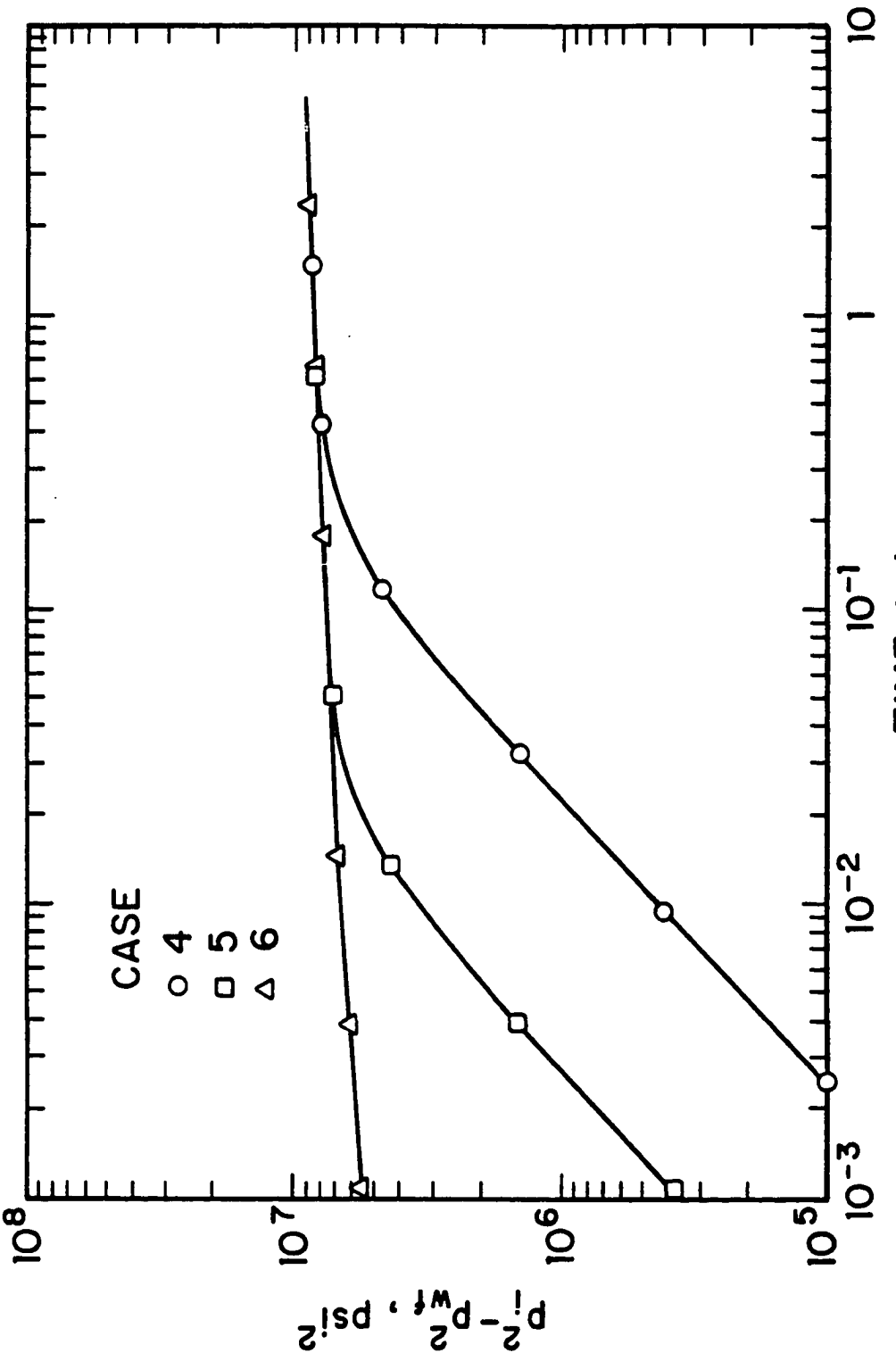

Fig. 6.9.5 - Log-log plot of change in pressure-squared versus time; Cases 4, 5 and 6.

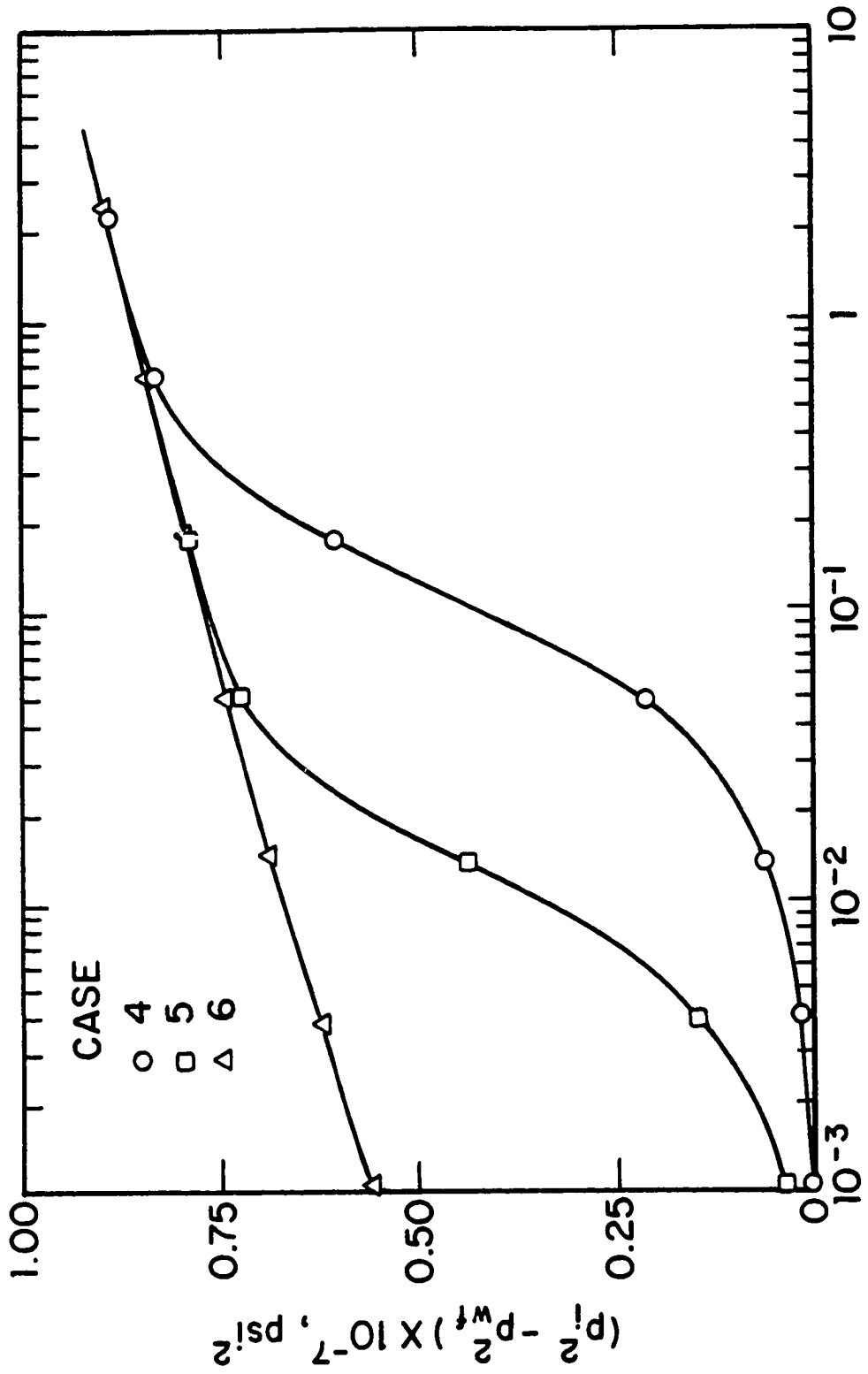

Fig. 6.9.6 - Semilog plot of change in pressure-squared versus time; Cases 4, 5 and 6.

exhibits a semilog straight line. The square data points of Fig. 6.7.11 show the values of kk_{ro} computed via Eq. 6.8.8 for Case 4 of Fig. 6.9.6. Note that for $t_D > 5 \times 10^3$, i.e., for $t > 3.7 \times 10^{-2}$ days and $p_{wf} < 3210$ psi, we obtain excellent estimates of effective permeability as a function of pressure. Also note that for $t_D > 5 \times 10^3$, the estimates of kk_{ro} obtained from Eq. 6.8.8 are in good agreement with the estimates obtained from Eq. 6.7.1. Thus, in practice one should attempt to apply both Eqs. 6.7.1 and 6.8.8 to estimate effective oil permeability. When these two equations give similar results, it should be expected that we have obtained good estimates of effective oil permeability. The square data points in Figs. 6.7.10 and 6.7.12 represent, respectively, the kk_{ro} values computed from Eq. 6.8.8 and the kk_{rg} values computed from Eq. 6.7.5 by using the kk_{ro} values computed from Eq. 6.8.8. Note that the pressure-squared method yields good estimates of the effective gas permeability. The square data points of Fig. 6.7.13 represent a plot of kk_{ro} values obtained from Eq. 6.8.8 for Case 4 versus the simulator oil sandface saturation. As indicated by the results of Fig. 6.7.11, the pressure-squared method gives good estimates of effective oil permeability as a function of S_o for values corresponding to $S_o < 0.66$ ($t > 3.7 \times 10^{-2}$ days).

Fig. 6.9.7 shows Cartesian plots of $(p_i^2 - p_{wf}^2)/q_{osf}(t)$ versus logarithmic convolution time, t_{lc}, for Cases 4, 5 and 6. In Case 6, a well-defined straight line of slope $m_3 = 0.9165 \times 10^4$ psi^2/(STB/D) exists for $t_{lc} > -2$ ($t > 2.2 \times 10^{-2}$ days). Note that this straight line starts later than for the corresponding $s = 0$ case (Case 1 of Fig. 6.9.2) because of the thick skin zone. As explained in Ref. 9, one cannot obtain proper straight lines until the skin zone approaches a steady-state behavior. For Case 5, the proper straight line begins at $t_{lc} \approx -1.7$ ($t \approx 4.5 \times 10^{-2}$ days). For Case 4, wellbore storage effects delay the beginning time of the straight line until $t_{lc} \approx -0.7$ days which corresponds to $t = 0.3$ days. Note this beginning time is approximately the same as the one obtained for Case 3 of Fig. 6.9.3.

Using the slope of $m_3 = 0.9165 \times 10^4$ obtained from Fig. 6.9.7, Eq. 6.8.15 gives $\hat{a}k = 2.28 \times 10^{-3}$. Eq. 6.8.16 evaluated at the final value of flowing pressure $p_{wf} = 1688$ psi gives $kk_{ro} = 3.46$ md as compared to the correct (simulator) value

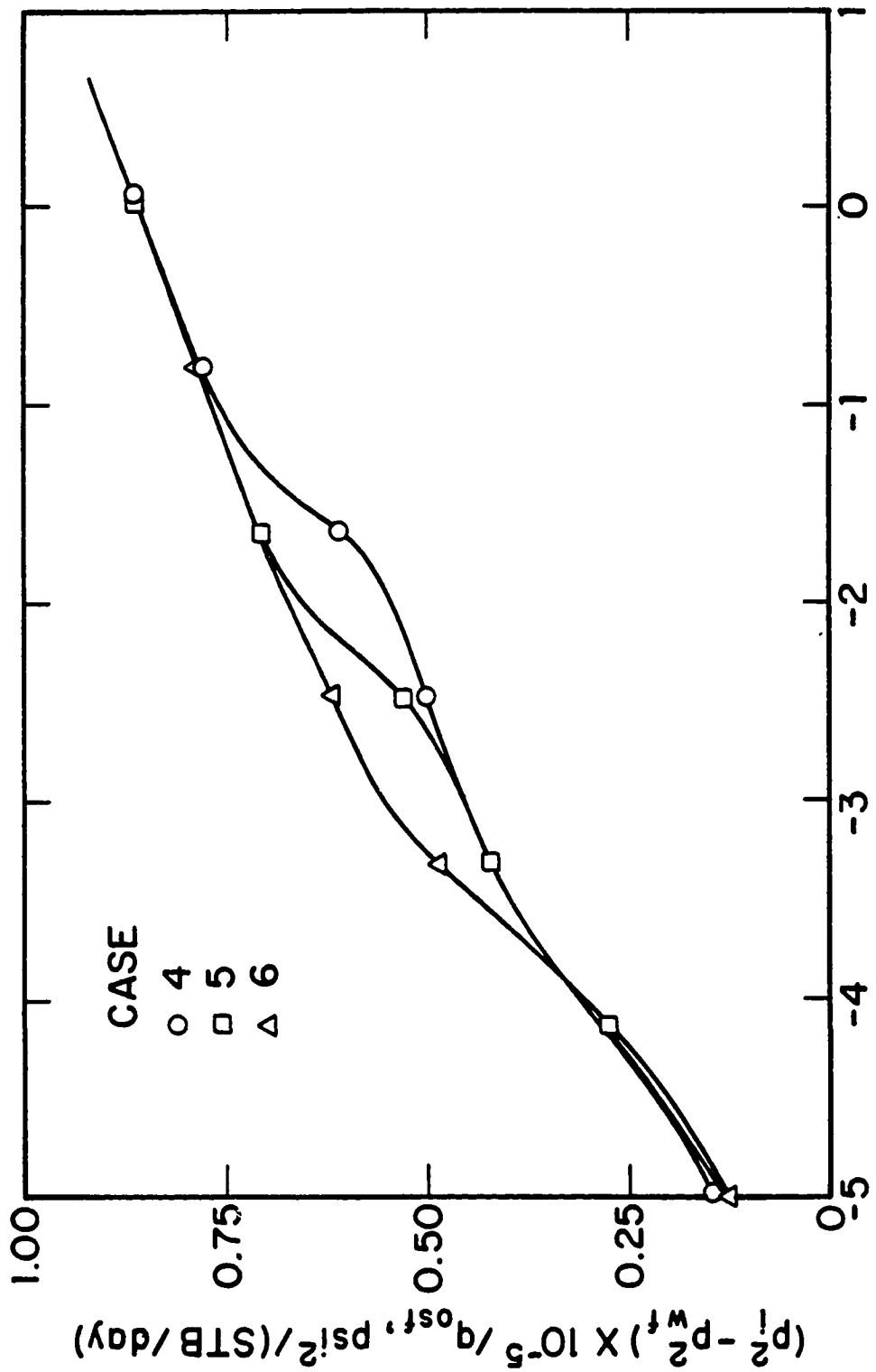

Fig. 6.9.7 - Rate-normalized change in pressure-squared versus logarithmic convolution time; Cases 4, 5 and 6.

of $kk_{ro} = 3.53$ md. Eq. 6.8.17 yields $kk_{roi} = 5.40$ md as compared to the correct value of $kk_{roi} = 7.00$ md. Applying Eq. 6.8.18, one obtains $s = 4.57$ as compared to the correct value of $s = 5$.

Note that for the $s = 0$ results of Fig. 6.9.3, the differences in the results obtained for Cases 1, 2 and 3 are small when $(p_i^2 - p_{wf}^2)$ is plotted versus logarithmic convolution time. However, as shown in Fig. 6.9.7, the differences for Cases 4, 5 and 6 are significant at intermediate times. This is due to the effect of a thick skin zone.

Fig. 6.9.8 shows semilog plots of the rate-normalized change in pressure-squared versus time. As shown, all cases eventually show a well-defined semilog straight line of slope $m_3 = 0.938 \times 10^4$ psi^2/ (STB/D) per log cycle. For Case 5, the semilog straight line begins at $t \approx 0.23$ days compared to a beginning time of $t \approx 0.4$ days for the analogous pressure-squared plot of Fig. 6.9.6. For Case 4, the semilog straight line begins at $t \approx 1.5$ days compared to a beginning time of $t \approx 1.8$ days for the analogous pressure-squared plot of Fig. 6.9.6. Note that these times of the onset of the semilog straight line are the same as the ones obtained for the $s = 0$ cases of Fig. 6.9.4. As for the $s = 0$ cases, rate-normalization results in only a slight decrease in the time at which the proper semilog straight line begins. However, plotting the rate-normalized change in pressure-squared versus logarithmic convolution time causes the proper straight line to begin much earlier; thus, the use of t_{lc} in the analysis will significantly decrease the test time required to obtain analyzable data. Using the semilog slope of $m_3 = 0.938 \times 10^4$ psi^2/ (STB/D) per log cycle in Eq. 6.8.21, one obtains $\hat{a}k = 2.23 \times 10^{-3}$. Eq. 6.8.22 evaluated at the final value of flowing pressure ($p_{wf} = 1688$ psi) gives $kk_{ro} = 3.34$ md as compared to the correct (simulator) value of $kk_{ro} = 3.53$ md. Eq. 6.8.23 yields $kk_{roi} = 5.27$ md as compared to the correct value of $kk_{roi} = 7.00$ md. Applying Eq. 6.8.24, one obtains $s = 4.29$ as compared to the correct value of $s = 5$. As expected, the results obtained from rate-normalized pressure-squared analysis are essentially the same as the results obtained from standard pressure-squared analysis and analysis based on a plot of pressure-squared versus logarithmic convolution time.

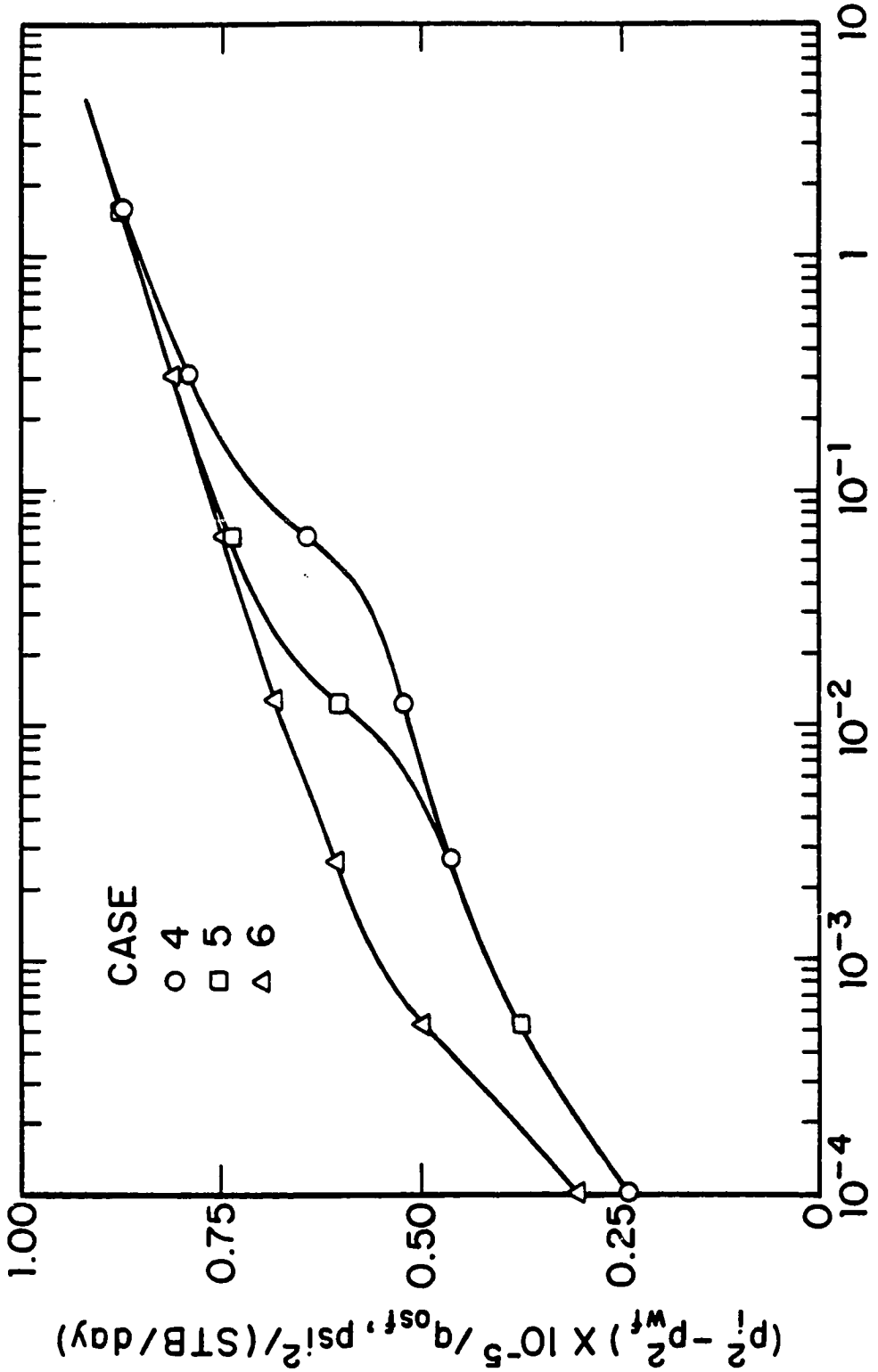

Fig. 6.9.8 - Semilog plot of rate-normalized change in pressure-squared versus time; Cases 4, 5 and 6.

6.10 Pressure Method

Here we examine the results obtained by ignoring the effects of multiphase flow when performing semilog analysis, that is, by using semilog analysis based on single-phase flow theory. Since we wish to consider the effects of wellbore storage, we plot results in terms of the rate-normalized pressure drop, $\Delta p/q_{osf}$, where $\Delta p = p_i - p_{wf}$. According to single-phase flow theory, a semilog plot of $\Delta p/q_{osf}(t)$ versus t should yield a semilog slope of

$$m_4 = \frac{162.6 B_o \mu_o}{k k_{ro} h}. \tag{6.10.1}$$

Eq. 6.10.1 in and of itself indicates there is a problem because the slope cannot be constant unless $B_o\mu_o/k_{ro}$ is constant. However, rearranging Eq. 6.10.1 gives

$$\frac{k k_{ro}}{\mu_o B_o} = \frac{162.6}{m_4 h}. \tag{6.10.2}$$

In the following computations, we fit a semilog straight line through the last few data points on a semilog plot of $\Delta p/q_{osf}(t)$ versus t and use Eq. 6.10.2 to compute values of $kk_{ro}/(\mu_o B_o)$ at the final value of p_{wf}. We also evaluate Eq. 6.10.2 at p_i and rearrange the resulting equation to obtain an estimate of kk_{roi}/μ_{oi}. Then we extrapolate the "semilog straight line" obtained to $t = 1$ hour and estimate the skin factor from

$$s = 1.151\left(\frac{\left((p_i - p_{wf})/q_{osf}(t)\right)_{1hr}}{m_4} - \log\left(\frac{k k_{roi}}{\phi \mu_{oi} c_{ti} r_w^2}\right) + 3.23\right). \tag{6.10.3}$$

Fig. 6.10.1 shows semilog plots of $\Delta p/q_{osf}(t)$ versus time for data obtained for Cases 1, 2 and 3. At times corresponding to $t > 2$ days, the data for all cases appear to fall on a semilog straight line of slope $m_4 = 2.3366$ psi/(STB/D) per log cycle. The final value of flowing wellbore pressure is $p_{wf} = 2050$ psi. This value is denoted by $p_{wf,s}$. Following the computational procedure of the preceding paragraph, we obtain $kk_{ro}/(\mu_o B_o) = 4.48$ md/(cp-(RB/STB)) at $p_{wf,s}$ as compared to the correct value of $kk_{ro}/(\mu_o B_o) = 4.57$ md/(cp-(RB/STB)). The initial estimate obtained for kk_{roi}/μ_{oi} is 7.11 md/cp as compared to the correct value of $kk_{roi}/\mu_{oi} = 16.26$ md/cp. Eq. 6.10.3 then yields $s = -2.02$ as compared to the correct value of $s = 0$.

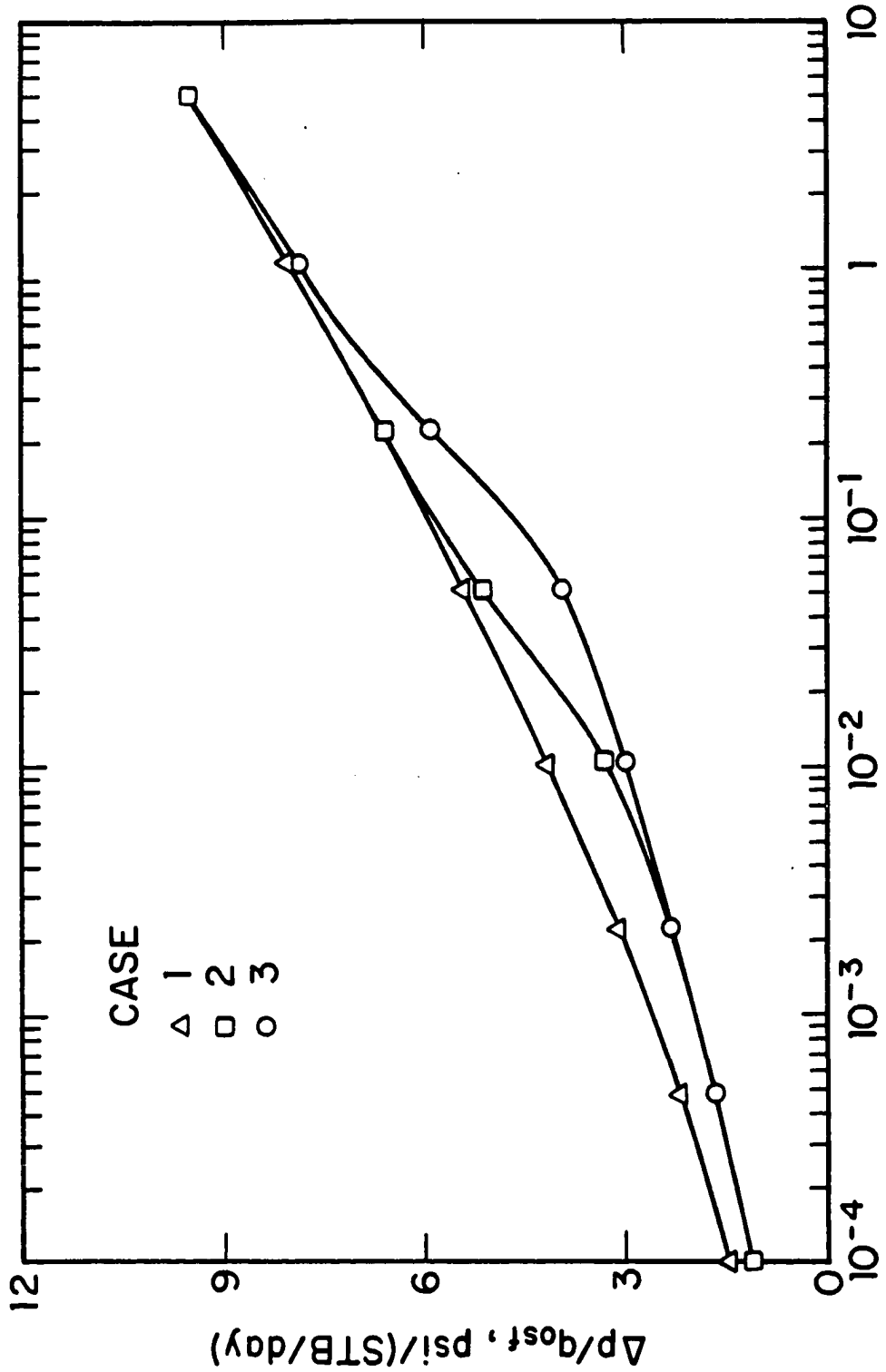

Fig. 6.10.1 - Semilog plot of rate-normalized pressure drop versus time; Cases 1, 2 and 3.

Fig. 6.10.2 shows semilog plots of $\Delta p/q_{osf}(t)$ versus time for data obtained for Cases 4, 5 and 6. At times corresponding to $t > 2$ days, the data appear to lie on a semilog straight line of slope $m_4 = 2.7217$ psi/(STB/D) per log cycle. The final value of flowing wellbore pressure is $p_{wf} = 1688$ psi. This value is denoted by $p_{wf,s}$. Following the computational procedure of the preceding paragraph, we obtain $kk_{ro}/(\mu_o B_o) = 3.84$ md/(cp-(RB/STB)) at $p_{wf,s}$ as compared to the correct value of $kk_{ro}/(\mu_o B_o) = 3.98$ md/(cp-(RB/STB)). The initial estimate obtained for kk_{roi}/μ_{oi} is 6.1 md/cp as compared to the correct value of $kk_{roi}/\mu_{oi} = 16.26$ md/cp. Eq. 6.10.3 then yields $s = 0.96$ as compared to the correct value of $s = 5$.

The results obtained from Figs. 6.10.1 and 6.10.2 indicate that semilog analysis based on a semilog plot of pressure versus time can yield highly inaccurate values of kk_{roi} and s. Moreover, the "semilog straight lines" we selected in Figs. 6.10.1 and 6.10.2 last for only a very short period of time. The fact that we obtained good estimates of $(kk_{ro})/(\mu_o B_o)$ values, or equivalently good estimates of kk_{ro}, at $p_{wf,s}$ is simply due to the fact that Eq. 6.7.1 gives the correct estimate of kk_{ro}. By fitting a semilog straight line through the last few data points in Figs. 6.10.1 and 6.10.2, we determined the correct value of dp_{wf}/dt that should be used in Eq. 6.7.1. During the times when the "semilog lines" of Figs. 6.10.1 and 6.10.2 occur, $q_{osf} = q_o$ and the term within square brackets in Eq. 6.7.1 is zero.

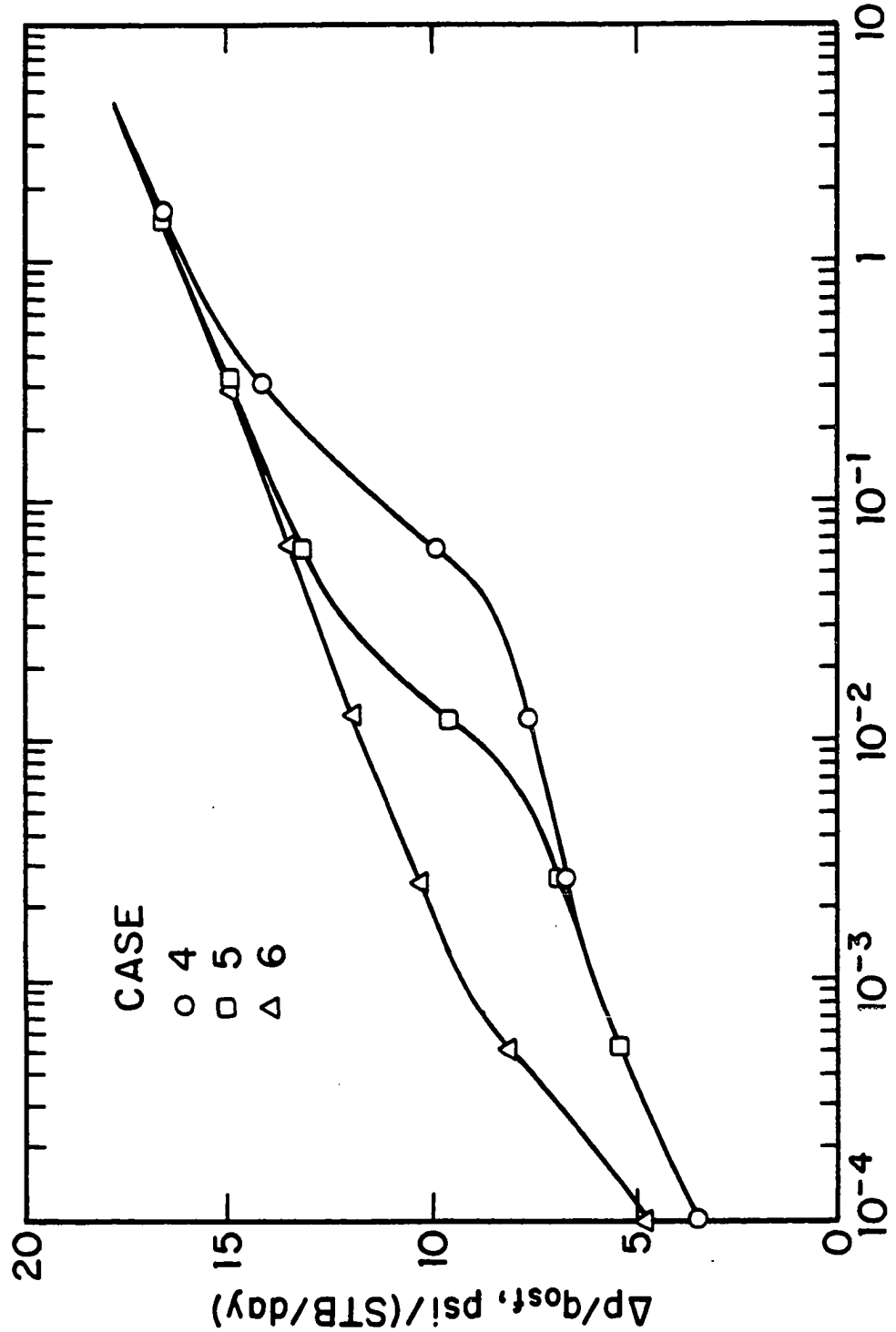

Fig. 6.10.2 - Semilog plot of rate-normalized pressure drop versus time; Cases 4, 5 and 6.

CHAPTER VII
EFFECT OF AFTERFLOW ON THE ANALYSIS OF PRESSURE BUILDUP DATA FROM SOLUTION-GAS-DRIVE RESERVOIRS

In this Chapter, we extend the methods presented in Chapter 6 and investigate the effect of wellbore storage on the analysis of pressure buildup data obtained in a solution-gas-drive reservoir. Based on a superposition equation, we present new computational equations for computing effective oil and gas permeabilities as pointwise functions of pressure from the measured values of the shut-in wellbore pressure. The computational equations require that the sandface oil flow rate is measured and incorporated into the analysis. It is also shown that a semilog plot of shut-in pressure-squared versus Horner time represents a viable method for obtaining estimates of the effective oil permeability at the final value of shut-in wellbore pressure and the mechanical skin factor.

7.1 INTRODUCTION

As we have discussed in the previous Chapters, Al-Khalifah et al.[8] and Serra et al.[9] achieved two major results in the analysis of well-testing pressure data obtained under multiphase flow conditions and showed that one could compute effective permeability as a function of pressure directly from the measured flowing wellbore pressure. Al-Khalifah et al.[11] and Serra et al.[9,10,12] also showed that one can analyze data by using a semilog plot of the wellbore pressure-squared versus time. Finally, Al-Khalifah et al.[14] presented an overview of the pressure-squared semilog analysis method vis-a-vis semilog analysis based on a plot of pressure versus time.

The results of Refs. 8 and 9 consider only drawdown analysis. These results were extended to the analysis of buildup data in Refs. 10 and 12. Serra et al.[10,12] showed that a generalized form of superposition applies provided the same pressure

saturation relationship is used in all pseudopressure functions. The authors extended their drawdown method for estimating oil and gas relative permeabilities to pressure buildup data and showed that the mechanical skin factor can be computed by using the pressure-squared method.

Refs. 1-14 neglect wellbore storage effects. In a recent work (also see Chapter 6) for pressure drawdown, Hatzignatiou et al.[29] extended the ideas of Refs. 8 and 9 to multiphase systems which are influenced by the presence of wellbore storage effects at the producing well. The authors showed that oil and gas relative permeabilities can be estimated during the wellbore storage dominated flow period provided the sandface oil flow rate can be measured or estimated. They also showed that estimates of the initial value of effective oil permeability, the values of effective permeability at the last measured values of flowing wellbore pressure and the mechanical skin factor can be computed by using pressure-squared semilog analysis, rate-normalization-pressure-squared semilog analysis or a pressure-squared logarithmic-convolution-time analysis method. Finally, Hatzignatiou et al.[29] derived theoretical equations for estimating the sandface oil saturation as a function of the wellbore pressure during wellbore storage dominated flow. Fetkovich and Vienot[55] presented an analysis method where the rate normalized pressure buildup versus time data were type-curve matched to identify the $p_D - t_D$ model which describes the transient behavior of a well. Ref. 55 stated that in a multiphase flow pressure buildup test the normalization of pressure data should be based, as Perrine[1] suggested, on the total fluid flow rate.

The objectives of this Chapter are: i) to study the afterflow effects on the analysis of buildup pressure data obtained at a shut-in well in a solution-gas-drive reservoir; ii) to present new procedures for computing effective permeability as a function of pressure from well-testing pressure data influenced by wellbore storage effects; iii) to present algorithms for computing effective or relative permeability as a function of oil saturation from buildup data influenced by wellbore storage; and iv) to provide methods to estimate the effective oil permeability at the last measured values of shut-in pressure and the mechanical skin factor using pressure-squared

semilog analysis which does not require *a priori* knowledge of relative permeability data.

7.2 Mathematical Model

We consider radial flow to a fully-penetrating well in a cylindrical, homogeneous solution-gas-drive reservoir of constant thickness. Prior to shut-in, the well is produced at a constant surface oil rate; the porosity and absolute permeability of the system are assumed to be independent of pressure and position and gravitational and capillary effects are considered to be negligible. The upper, lower and outer reservoir boundaries are considered to be no-flow (sealed) boundaries, but all results presented are for an infinite-acting reservoir. The reservoir pressure is initially assumed to be uniform throughout the reservoir and equal to the bubble-point pressure. Whenever the skin factor is nonzero, the permeability of the skin zone is computed using Hawkins'[32] formula, i.e., Eq. 3.3.1.

The presence of wellbore storage is incorporated in our model by using the exponential decay model of van Everdingen[42] and Hurst[43] where the sandface oil flow rate after shut-in is related to the oil surface flow rate by

$$q_{osf}(\Delta t) = q_{osf}(\Delta t = 0)\exp(-\alpha^* \Delta t). \tag{7.2.1}$$

Throughout, q_{osf} denotes the sandface oil flow rate in STB/D, q_o is the constant oil surface rate in STB/D during production and α^* is a constant with units 1/D, which can be adjusted to match field data. This simplified model, which allows the sandface rate to gradually decrease from the stabilized surface rate at the instant of shut-in to zero during a buildup test, has been used previously to model afterflow effects; see Refs. 29 and 42-45. For all the cases we present in this Chapter, wellbore storage effects are not considered during the producing time period, i.e., $q_{osf}(\Delta t = 0) = q_o$. However, the basic methods presented in this work apply to cases where wellbore storage effects exist during production[29] provided that the oil sandface flow rate becomes equal to the constant surface oil flow rate prior to shut-in.

The results presented in this study were obtained from a semi-implicit, one-dimensional (radial), variable bubble-point, black-oil reservoir simulator; see Ref. 28. Although connate water is present in the reservoir, all the results presented here assume that the water is immobile and incompressible so that the water saturation remains constant throughout the producing period. Thus, only oil and gas flow in the reservoir.

7.3 General Notation and Definitions

The basic general notation and definitions used throughout this Chapter are given in Chapter 6. For the buildup analysis, however, we consider the following dimensionless pseudopressure function:

$$p_{psD} = \frac{khp_p\left(p_{ws}\right)}{141.2q_o} = \frac{kh\int_{p_{wf}}^{p_i}\left(\frac{k_{ro}}{\mu_o B_o}\right)dp}{141.2q_o}, \tag{7.3.1}$$

and

$$\tilde{p}_{psD} = \frac{kh[p_p(p_{ws}) - p_p(p_{wf,s})]}{141.2q_o} = \frac{kh\int_{p_{wf,s}}^{p_{ws}}\left(\frac{k_{ro}}{\mu_o B_o}\right)dp}{141.2q_o}, \tag{7.3.2}$$

where p_{ws} denotes the shut-in pressure and $p_{wf,s}$ denotes the wellbore pressure at the instant of shut-in.

Dimensionless shut-in time and dimensionless normalized time are defined, respectively, by

$$\Delta t_D = \frac{6.328\times10^{-3}k\lambda_{ti}\Delta t}{\phi c_{ti}r_w^2}, \tag{7.3.3}$$

and

$$\Delta t_{nD} = \frac{6.328\times10^{-3}kk_{roi}\Delta t}{\phi\mu_o c_t r_w^2}, \tag{7.3.4}$$

where the subscript i denotes initial conditions, Δt denotes the shut-in time in days and λ_{ti} denotes the initial value of total mobility. For cases considered here, the initial pressure is equal to the bubble-point pressure and $\lambda_{ti} = \lambda_{oi} = k_{roi}/\mu_{oi}$. In Eq. 7.3.4, instantaneous values of μ_o and c_t are used. Specifically, at each value of Δt, μ_o is evaluated at the corresponding value of p_{ws}, whereas at each value of

Δt, c_t is evaluated from Eq. 6.3.8 using the corresponding value of p_{wa} and the corresponding estimate of oil saturation obtained by a method discussed later.

Finally, the dimensionless sandface oil flow rate is obtained by dividing Eq. 7.2.1 by the constant surface oil flow rate $q_o = q_{osf}(\Delta t = 0)$ and is given by

$$q_{osfD} = \frac{q_{osf}(\Delta t)}{q_{osf}(\Delta t = 0)} = \frac{q_{osf}(\Delta t)}{q_o} = \exp(-\beta^* \Delta t_D), \tag{7.3.5}$$

where the first equality of Eq. 7.3.5 serves to define q_{osfD} and

$$\beta^* = \frac{\alpha^* \phi \mu_{oi} c_{ti} r_w^2}{6.328 \times 10^{-3} (k k_{ro})_i}, \tag{7.3.6}$$

is the dimensionless analogue of the wellbore storage parameter α^*. It is difficult to find a unique relation between the wellbore storage model of Eq. 7.3.5 and the standard constant wellbore storage coefficient model commonly used in well testing theory[47] because Eq. 7.3.5 represents a wellbore storage model where the wellbore storage coefficient changes with time. However, in the previous Chapter (also see Ref. 29) we derived the following approximate relationship between the two models

$$C_D = \frac{1}{12.53 \beta^*}. \tag{7.3.7}$$

While Eq. 7.3.7 is only approximate, when it holds the dimensionless sandface rate predicted by Eq. 7.3.7 is not radically different from the dimensionless sandface rate predicted by the constant wellbore storage coefficient model of Ref. 47. Moreover, Eq. 7.3.7 gives us a convenient way to relate the wellbore storage problem considered here with the analogous single-phase flow solution[47].

We now discuss how the sandface oil flow rate predicted by Eq. 7.3.5 changes with respect to shut-in time and present results which indicate that single-phase type curves cannot be used to type-curve match the multiphase flow dimensionless buildup pseudopressure solution. The curve through circular data points in Fig. 7.3.1 represents the dimensionless sandface oil rate change, i.e., $1 - q_{osfD}$ plotted versus the dimensionless shut-in time Δt_D when $\beta^* = 6.8 \times 10^{-5}$. The curve through triangular data points and the curve through square data points,

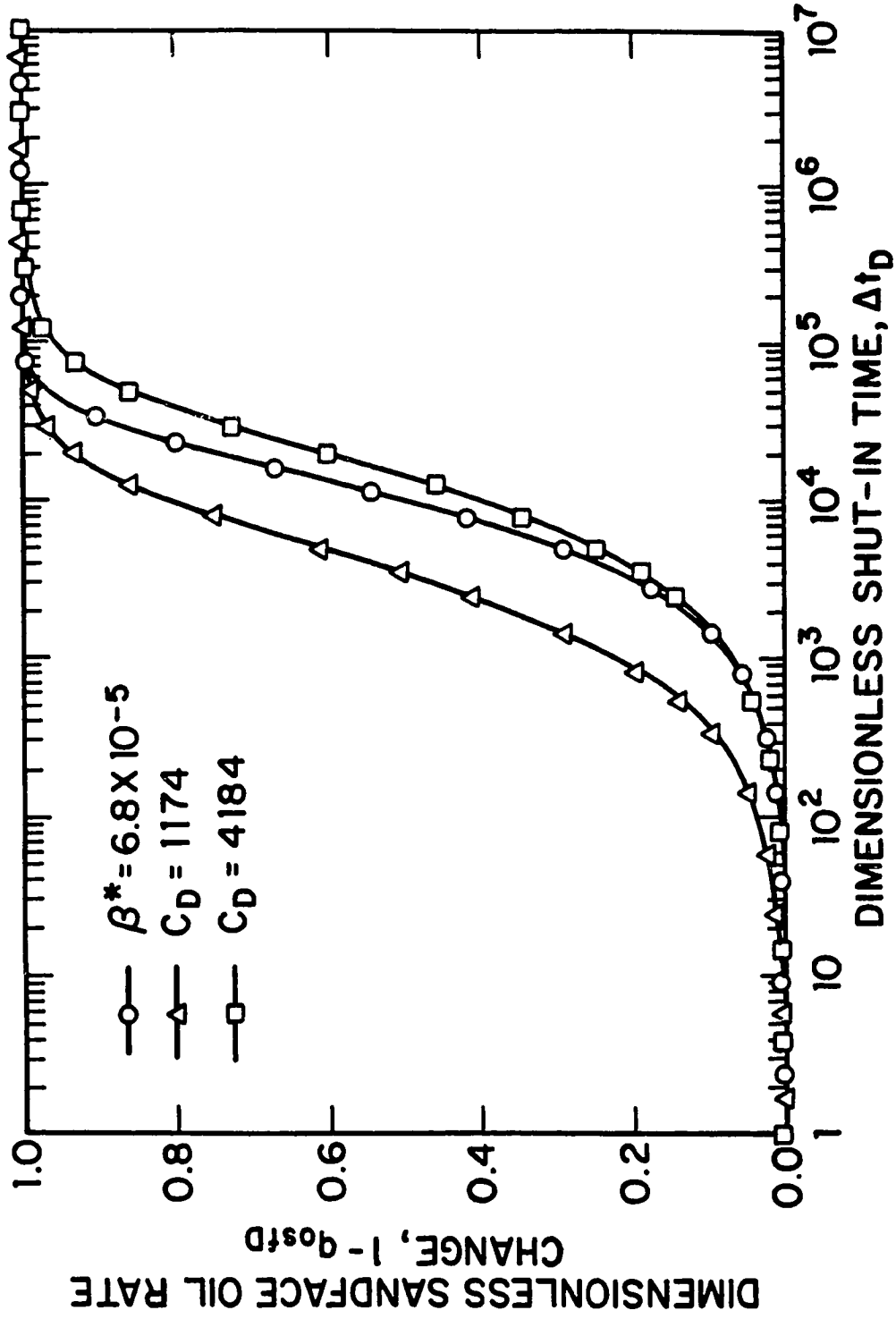

Fig. 7.3.1 - Comparison of dimensionless sandface flow rate change for two wellbore storage models.

respectively, represent the dimensionless sandface flow rate change predicted by the single-phase flow constant wellbore storage model of Ref. 47 for $C_D = 1174$ and $C_D = 4184$. Note that the dimensionless sandface rate change for $C_D = 4184$ solution of Ref. 47 provides a good approximation of the rate change predicted by Eq. 7.3.5 at all times. However, for the $C_D = 4184$ case the dimensionless sandface rate change becomes equal to one at $\Delta t_D \approx 6 \times 10^5$, whereas the sandface rate change predicted by Eq. 7.3.5 becomes equal to one ($q_{osf} = 0$) at $\Delta t_D \approx 10^5$. The sandface rate change for the $C_D = 1174$ solution of Ref. 47 becomes equal to the rate predicted by Eq. 7.3.5 when $\Delta t_D = 60 C_D = 7 \times 10^4$. This is the expected result since the relation between C_D and β^* given by Eq. 7.3.7 was derived from this equation; see Chapter 6 and Ref. 29.

The behavior of dimensionless pseudopressure is similar to the behavior of the dimensionless pressure solution obtained for the single-phase flow wellbore storage problem. However, the results of Fig. 7.3.2 indicate that the preudopressure solution (circular data points) and its logarithmic derivative with respect to equivalent time (square data points) cannot be type-curve matched with any of the constant wellbore storage type curves. The result illustrated in Fig. 7.3.2 is expected since Eq. 7.3.5 represents a wellbore storage model where the wellbore storage coefficient changes with time. The solid curves in Fig. 7.3.2 represent the single-phase flow constant wellbore storage coefficient type curve solution of Bourdet et al.[48] for two cases, $C_D = 1174$ and $C_D = 4184$.

7.4 Simulator Data

For all results presented in this Chapter, the basic rock and fluid properties are given in Tables A-1, A-2, A-3 and A-4. Tables A-1 and A-2, respectively, give "Set 1" PVT and relative permeability data and Tables A-3 and A-4, respectively, give "Set 2" PVT and relative permeability data. Throughout, the wellbore radius, external reservoir boundary radius, reservoir thickness, porosity and absolute permeability, respectively, are specified as $r_w = 0.328$ ft, $r_e = 6600$ ft, $h = 15.547$ ft, $\phi = 0.3$ and $k = 10$ md, but the values of these parameters have no influence on the validity

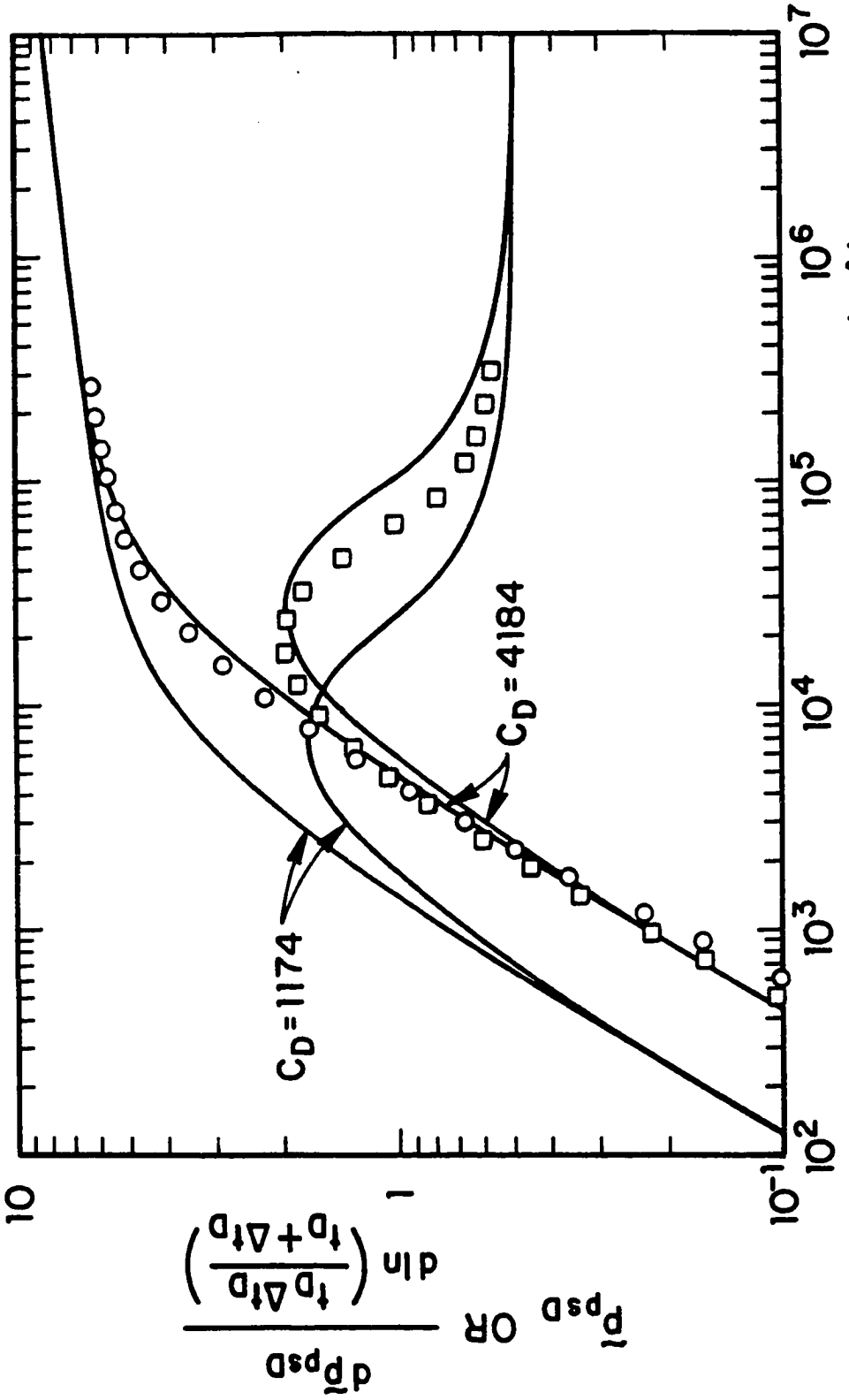

Fig. 7.3.2 - Comparison of pseudopressure solution with liquid wellbore storage solution.

of the procedures and conclusions presented in this Chapter. All results presented pertain to the infinite-acting period, that is, the closed outer boundary has no influence on the results obtained. Throughout, the dimensionless sandface rate is specified by Eq. 7.3.5. The corresponding values of C_D as predicted by Eq. 7.3.7 are recorded for each case.

In this Chapter, results are presented for the following nine cases:

Data Set 1

Case 1 : q_o = 150 STB/D; s = 0; S_{gc} = 0.0; No wellbore storage ($\beta^* \rightarrow \infty$);

Case 2 : q_o = 150 STB/D; s = 0; S_{gc} = 0.0; $\beta^* = 6.8 \times 10^{-4}$ ($C_D \approx 117.4$);

Case 3 : q_o = 150 STB/D; s = 0; S_{gc} = 0.0; $\beta^* = 6.8 \times 10^{-5}$ ($C_D \approx 1174$);

Case 4 : q_o = 50 STB/D; s = 5; S_{gc} = 0.0; $\beta^* = 6.8 \times 10^{-5}$ ($C_D \approx 1174$);

Case 5 : q_o = 50 STB/D; s = 5; S_{gc} = 0.0; $\beta^* = 6.8 \times 10^{-4}$ ($C_D \approx 117.4$);

Case 6 : q_o = 50 STB/D; s = 5; S_{gc} = 0.0; No wellbore storage ($\beta^* \rightarrow \infty$).

Data Set 2

Case 7 : q_o = 150 STB/D; s = 0; S_{gc} = 0.07; No wellbore storage ($\beta^* \rightarrow \infty$);

Case 8 : q_o = 150 STB/D; s = 0; S_{gc} = 0.07; $\beta^* = 6.8 \times 10^{-4}$ ($C_D \approx 117.4$);

Case 9 : q_o = 150 STB/D; s = 0; S_{gc} = 0.07; $\beta^* = 6.8 \times 10^{-5}$ ($C_D \approx 1174$).

For Cases 1 through 6, the PVT and relative permeability data are given in Tables A-1 and A-2, respectively. For this set of data (Set 1) the critical gas saturation is S_{gc} = 0.0, the initial reservoir pressure and bubble-point pressure values are equal and given by $p_i = p_{bi}$ = 3460 psi. The initial values of total compressibility, oil viscosity and oil FVF, respectively, are specified as $c_{ti} = 0.23564 \times 10^{-4}$ psi $^{-1}$, μ_{oi} = 0.43059 cp and B_{oi} = 1.5882 RB/STB. The PVT and relative permeability data, Set 2, for Cases 7-9 are shown in Tables A-3 and A-4, respectively. For this set of data, the critical gas saturation is S_{gc} = 0.07, the initial reservoir pressure and bubble-point pressure values are equal and given by $p_i = p_{bi}$ = 4000 psi. The initial values of total compressibility, oil viscosity and oil FVF, respectively, are specified as $c_{ti} = 0.27604 \times 10^{-4}$ psi $^{-1}$, μ_{oi} = 0.41313 cp and B_{oi} = 1.48301 RB/STB. For both set of data, the values of connate water saturation and residual oil saturation are held fixed with S_{wc} = 0.3 and S_{or} = 0.0 respectively. For all cases considered,

the well is produced for $t = 5$ days ($t_D \approx 6.76 \times 10^5$ for Set 1 and $t_D \approx 6.02 \times 10^5$ for Set 2) at a constant surface oil flow rate prior to shut-in, but after the well is shut-in the sandface oil rate varies according to the wellbore model described by Eq. 7.2.1. The buildup test for all cases considered in this report lasts for 5 days.

As mentioned previously, the drawdown and buildup pressure data considered here were generated from a variable bubble-point, black-oil simulator under radial flow conditions. For all cases considered, the external reservoir radius is $r_e = 6600$ ft which is sufficiently large such that the pressure and saturation changes in the near wellbore region are not affected by outer boundary effects.

Each figure presented contains information which identifies the case(s) presented in the figure. Cases 2-5 allow us to examine the effect of wellbore storage with and without a skin effect. Case 1 considers a problem where both wellbore and skin effects are completely negligible and Case 6 refers to a problem where the skin factor is positive, but wellbore storage effects do not exist, that is, $q_{osf} = 0.0$ STB/D throughout the buildup period. Finally, Cases 7-9 consider the effects of a nonzero critical gas saturation with and without afterflow during the pressure buildup.

7.5 Theoretical Results

7.5.1 Rate-Normalization and Multirate Pseudopressure Analysis.

The superposition equations considered in this Chapter are

$$p_{psD} = p_{pwD}(t_D + \Delta t_D) - p_{pwD}(\Delta t_D), \tag{7.5.1}$$

and

$$\tilde{p}_{psD} = p_{pwD}(t_D) - p_{pwD}(t_D + \Delta t_D) + p_{pwD}(\Delta t_D). \tag{7.5.2}$$

Serra et al.[10,12], based on theoretical and numerical results, concluded that these superposition equations approximately hold for the solution-gas-drive problem provided the same saturation/pressure relationship is used for both drawdown and buildup when constructing the pseudopressure functions.

Numerous researchers (see Refs. 5-9) have shown that for drawdown single-phase flow in an infinite-acting system,

$$p_{pwD} = \frac{1}{2}\ln\left(\frac{4t_D}{e^{\gamma}}\right) + s, \tag{7.5.3}$$

if production is at a constant sandface flow rate, i.e., if $q_{osf}(t) = q_o$ at all times. In Eq. 7.5.3, γ denotes Euler's constant, i.e., $\gamma = 0.57722$. Using the semilog approximation for all drawdown solutions, the superposition scheme of Eq. 7.5.2 yields

$$\tilde{p}_{psD} = -1.151\log(R_{H1}) + 1.151\log\left(\frac{4t_D}{e^{\gamma}}\right) + s, \tag{7.5.4}$$

where R_{H1} represents the primary Horner ratio and is defined as

$$R_{H1} = \frac{t_D + \Delta t_D}{\Delta t_D} = \frac{t + \Delta t}{\Delta t}. \tag{7.5.5}$$

For the problem considered here, the sandface flow rate is variable during buildup and Eq. 7.5.4 cannot be expected to apply until wellbore storage effects become negligible, i.e., until $q_{osf}(\Delta t) \approx 0$.

In the previous Chapter (also see Ref. 29), we used the Odeh-Jones[49] method for an increasing sequence of constant sandface oil flow rates to derive the drawdown variable rate solution for multiphase flow. Here, we use the same idea to derive the buildup variable rate solution for a decreasing sequence of constant sandface oil flow rates during buildup. Note that the Odeh-Jones method assumes the validity of superposition and the theoretical validity of superposition for the nonlinear problem considered here has not been established. However, the results of Refs. 8, 10, 12, 28 and 29, as well as results presented here, indicate that from a practical point of view superposition is applicable. From a more rigorous point of view, the analytical solution constructed in Ref. 40 indicates that the effect of nonlinearities are small especially for lower values of the flow rate, and hence, one should expect that superposition can be approximately applied.

We define the following two dimensionless sandface logarithmic convolution shut-in times:

$$\Delta t_{lc} = \left[\log\left(\frac{t}{t+\Delta t}\right) - \sum_{i=0}^{n}\left\{\left(q_{osfD}(t_D + \Delta t_{i+1,D}) - q_{osfD}(t_D + \Delta t_{i,D})\right)\right.\right.$$

$$\log\left(\Delta t_{n+1} - \Delta t_i\right)\Big\}\Big]/(1 - q_{osfD}(t_D + \Delta t_{n+1,D})), \tag{7.5.6}$$

and

$$\Delta t_{lcD} = \Big[\log\left(\frac{t_D}{t_D + \Delta t_D}\right) - \sum_{i=0}^{n}\Big\{\Big(q_{osfD}(t_D + \Delta t_{i+1,D}) - q_{osfD}(t_D + \Delta t_{i,D})\Big)$$

$$\log\left(\Delta t_{n+1,D} - \Delta t_{i,D}\right)\Big\}\Big]/(1 - q_{osfD}(t_D + \Delta t_{n+1,D})). \tag{7.5.7}$$

Throughout, we define $\Delta t_0 = 0$. Note that $q_{osf}(\Delta t_0) = q_o$. Eqs. 7.5.6 and 7.5.7 are the direct analogues of the corresponding superposition equations for the single-phase flow case. In these equations, a value of Δt_{lc} is computed for each value of Δt and $\Delta t_{n+1} = \Delta t$. For each value of Δt, $0 = \Delta t_0 < \Delta t_1 < \ldots < \Delta t_{n+1} = \Delta t$ represents a partition of the interval $[0, \Delta t]$. With these definitions, the applicable variable rate multiphase flow analogue of the Odeh-Jones[49] method is given by

$$\frac{\tilde{p}_{psD}}{(1 - q_{osfD}(t_D + \Delta t_D))} = \frac{kh[p_p(p_{ws}) - p_p(p_{wf,s})]}{141.2q_o(1 - q_{osfD}(t_D + \Delta t_D))} =$$

$$\frac{kh[p_p(p_{ws}) - p_p(p_{wf,s})]}{141.2\Delta q(\Delta t)} = 1.151(\Delta t_{lcD} + 0.351) + s = 1.151(\Delta t_{lc} + \tilde{s}), \tag{7.5.8}$$

where $\tilde{s}$ is given by

$$\tilde{s} = \log\left(\frac{kk_{roi}}{\phi\mu_{oi}c_{ti}r_w^2}\right) - 1.847 + 0.87s, \tag{7.5.9}$$

and

$$\Delta q(\Delta t) = q_o - q_{osf}(\Delta t). \tag{7.5.10}$$

The constant 1.847 arises in Eq. 7.5.9 because we perform our analysis with time in days instead of hours. If time in hours is used in the analysis, then 1.847 should be replaced by 3.23 in Eq. 7.5.9. If $q_{osf}(\Delta t) = 0$ for all Δt, i.e., if no afterflow exists, then it is easy to see that $\Delta t_{lcD} = \log[(t_D\Delta t_D)/(t_D + \Delta t_D)]$. Note $(t_D\Delta t_D)/(t_D + \Delta t_D)$ represents Agarwal's[56] equivalent time.

Fig. 7.5.1 illustrates that Eq. 7.5.8 is reasonably accurate. In Fig. 7.5.1, the solid straight line represents the single-phase liquid solution, i.e., Eq. 7.5.8, and the open data points represent values of $\tilde{p}_{psD}/(1 - q_{osfD})$ obtained from our

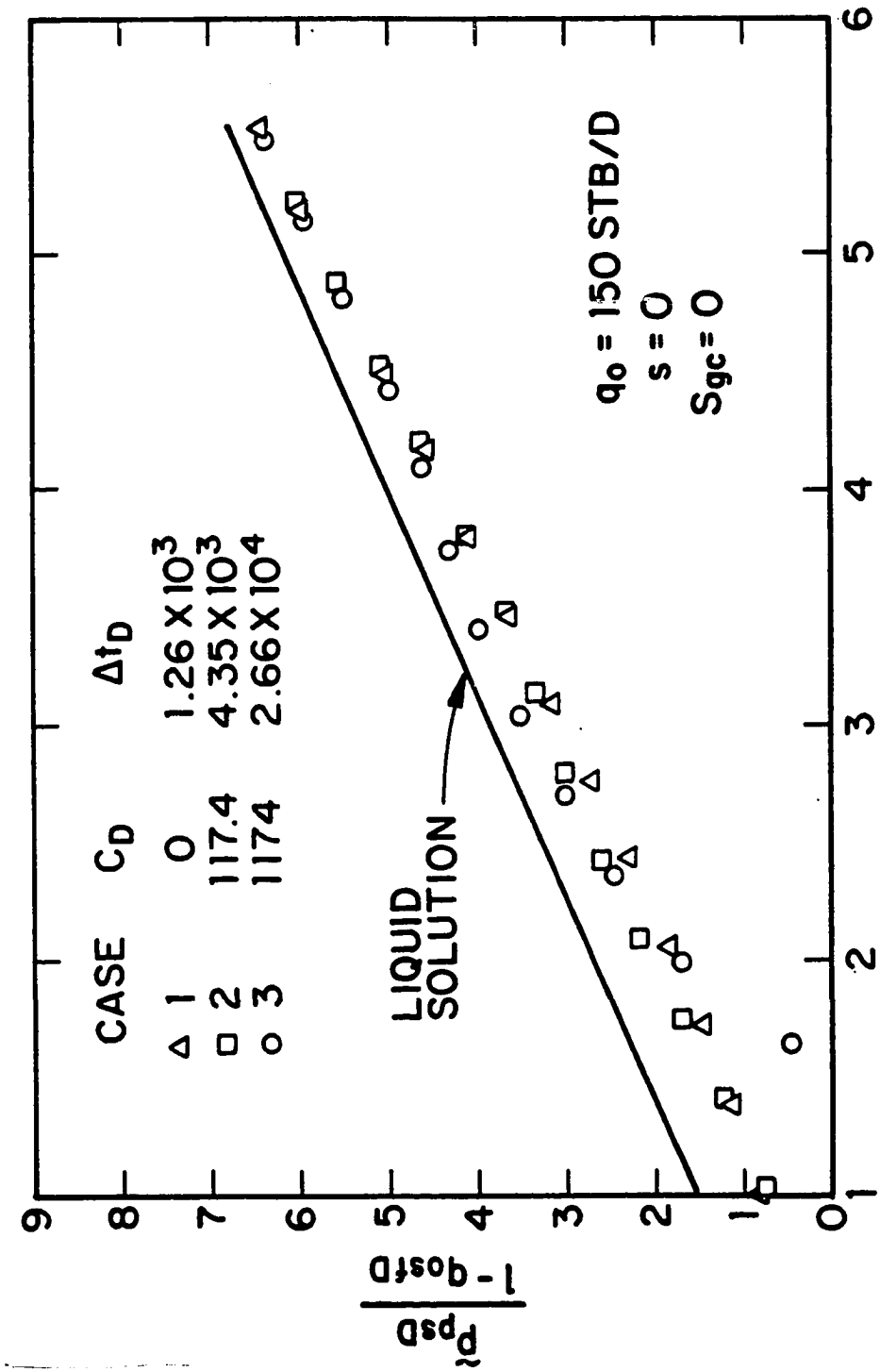

Fig. 7.5.1 - Dimensionless Odeh-Jones plot in terms of dimensionless pseudopressure; Cases 1-3.

simulator for Cases 1, 2 and 3 plotted versus Δt_{lcD}. In generating these results, we used drawdown simulator values of $(kk_{ro})/(\mu_o B_o)$ to calculate $\tilde{p}_{pwD}$ from Eq. 7.3.2. In Case 1, a well-defined Cartesian straight line exists for $\Delta t_{lcD} > 3.09$ ($R_{H1} < 5.38 \times 10^2$ and $\Delta t_D > 1.26 \times 10^3$). In Case 2, the same straight line begins at $\Delta t_{lcD} \approx 3.6$ ($R_{H1} \approx 1.57 \times 10^2$ and $\Delta t_D \approx 4.35 \times 10^3$), whereas in Case 3, the straight line does not begin until $\Delta t_{lcD} \approx 4.4$ ($R_{H1} \approx 26.4$ and $\Delta t_D \approx 2.66 \times 10^4$). Notice that for all cases the multiphase flow solutions are located under the liquid solution and they exhibit a Cartesian straight line with slope 1.256 which is 9% higher than the "theoretical" value of 1.151 predicted by Eq. 7.5.8. For each case, the value of Δt_D recorded in Fig. 7.5.1 represents the time at which the Cartesian straight line (slope = 1.256) begins. Note, the fact that the slope is higher than the "theoretical" 1.151 value indicates that if we apply the analysis procedure discussed below to corresponding field data, the estimate of kh obtained will be approximately 9% less than the correct value. Refs. 7 and 10 have noted a similar result for the zero wellbore storage case. In Fig. 7.5.1, and throughout this Chapter, the starting time for a straight line was determined visually and then the slope was determined by regression analysis.

The approximate validity of Eq. 7.5.8 indicates that a Cartesian plot of $[p_p(p_{ws}) - p_p(p_{wf,s})]/\Delta q$ versus logarithmic convolution shut-in time, Δt_{lc}, will be a straight line with slope approximately equal to

$$m_1 = \frac{162.6}{kh}. \tag{7.5.11}$$

The value of absolute permeability can be estimated from the value of this slope via the following equation:

$$k = \frac{162.6}{m_1 h}. \tag{7.5.12}$$

Based on the results of Fig. 7.5.1 and Refs. 9 and 10, Eq. 7.5.12 will usually yield a low estimate of k. By extrapolating the Cartesian straight line on a plot of $[p_p(p_{ws}) - p_p(p_{wf,s})]/\Delta q$ versus Δt_{lc} to $\Delta t_{lc} = 0$, one obtains the extrapolated value of $[p_p(p_{ws}) - p_p(p_{wf,s})]/\Delta q$ which is denoted by $\left[[p_p(p_{ws}) - p_p(p_{wf,s})]/\Delta q\right]_{ext}$.

From Eqs. 7.5.8 and 7.5.9, it then follows that the mechanical skin factor can be estimated from the following equation:

$$s = 1.151\left(\frac{[\left(p_p(p_{ws}) - p_p(p_{wf,s})\right)/\Delta q(\Delta t)]_{ext}}{m_1} - \log\left(\frac{kk_{roi}}{\phi\mu_{oi}c_{ti}r_w^2}\right) + 1.847\right). \tag{7.5.13}$$

The multiphase flow analogue of rate-normalization is given by

$$\frac{\tilde{p}_{psD}}{(1 - q_{osfD}(t_D + \Delta t_D))} = \frac{kh[p_p(p_{ws}) - p_p(p_{wf,s})]}{141.2\Delta q(\Delta t)} =$$

$$-1.151\log(R_{H1}) + 1.151\log\left(\frac{4t_D}{e^\gamma}\right) + s. \tag{7.5.14}$$

The results of Fig. 7.5.2 illustrate that Eq. 7.5.14 is approximately valid. In Case 1, a well-defined semilog straight line exists for $R_{H1} < 4.88 \times 10^2$ ($\Delta t_D > 1.26 \times 10^3$). In Case 2, the same straight line begins at $R_{H1} \approx 1.54 \times 10^1$ ($\Delta t_D \approx 4.71 \times 10^4$), whereas in Case 3, the straight line does not begin until $R_{H1} \approx 4.1$ ($\Delta t_D \approx 2.20 \times 10^5$). Like the results of Fig. 7.5.1, the multiphase flow solutions fall below the liquid solution. The slope of the semilog straight line is approximately 1.256, the same value as the Cartesian slope of Fig. 7.5.1. The shut-in times at which the semilog straight line begins for each case are recorded in Fig. 7.5.2. Note, for each case the straight line begins somewhat earlier when pseudopressure data are plotted versus Δt_{lcD} than when pseudopressure data are plotted versus the Horner time ratio. This illustrates the advantage of logarithmic convolution time over standard rate normalization. However, from a practical viewpoint the results of Fig. 7.5.2 indicate that if one fits any single log cycle of data corresponding to $R_{H1} < 10^3$ ($\Delta t_D > 0.68 \times 10^4$) with a semilog straight line, then Eq. 7.5.12 will yield a reasonably good approximation of k.

Eq. 7.5.14 can be rearranged to obtain

$$\frac{p_p(p_{ws}) - p_p(p_{wf,s})}{\Delta q(\Delta t)} = \frac{\int_{p_{wf,s}}^{p_{ws}}\left(\frac{k_{ro}}{\mu_o B_o}\right)dp}{\Delta q(\Delta t)}$$

$$= -m_1\log\left(\frac{t+\Delta t}{\Delta t}\right) + m_1\log t + m_1\left(\log\left(\frac{kk_{ro_i}}{\phi\mu_o c_{ti}r_w^2}\right) - 1.847 + 0.87s\right), \tag{7.5.15}$$

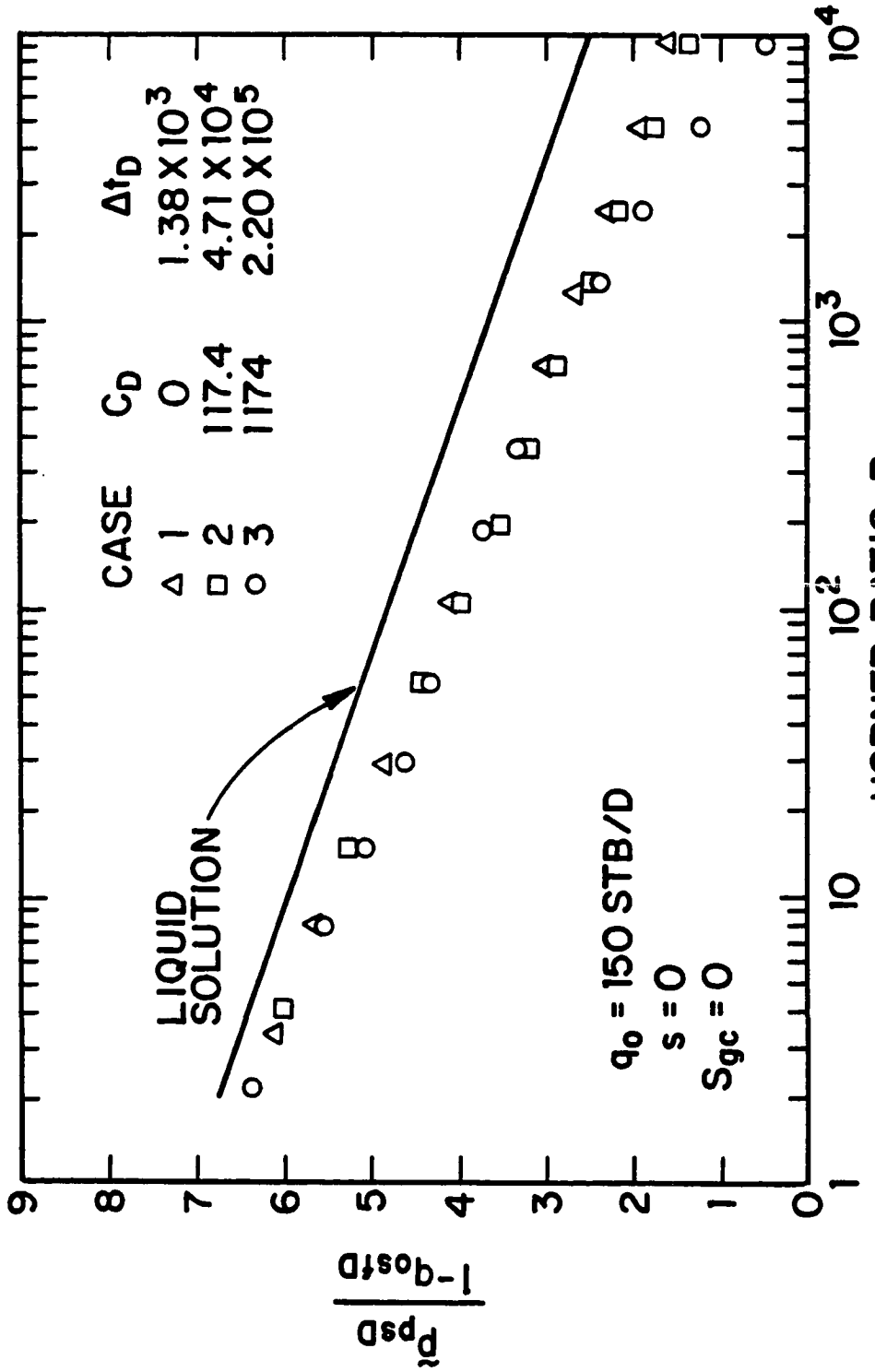

Fig. 7.5.2 - Semilog plot of rate-normalized dimensionless pseudopressure versus Horner time; Cases 1-3.

where m_1 is given by Eq. 7.5.11. The value of k can be estimated from this semilog slope using Eq. 7.5.12 and the value of the mechanical skin factor can be estimated as

$$s = 1.151\left(\frac{\left([p_p(p_{ws}) - p_p(p_{wf,s})]/\Delta q(\Delta t)\right)_{1hr}}{m_1} - \log\left(\frac{kk_{roi}}{\phi\mu_{oi}c_{ti}r_w^2}\right) + 3.23\right), \tag{7.5.16}$$

where $\left([p_p(p_{ws}) - p_p(p_{wf,s})]/\Delta q(\Delta t)\right)_{1hr}$ denotes the value of rate-normalized pseudopressure obtained by extrapolating the semilog straight line of Eq. 7.5.15 to $\Delta t = 1$ hour.

Fig. 7.5.3 shows the same pseudopressure solutions considered in Figs. 7.5.1 and 7.5.2 except Fig. 7.5.3 shows a semilog plot of $\tilde{p}_{psD}$ versus the Horner time ratio. Again, for sufficiently large values of shut-in time we obtain a semilog straight line of slope 1.256. More specifically, in Case 1 a well-defined semilog straight line exists for $R_{H1} < 4.88 \times 10^2$ ($\Delta t_D > 1.26 \times 10^3$). In Case 2 and Case 3, the same straight line begins at $R_{H1} \approx 0.99 \times 10^1$ ($\Delta t_D \approx 7.6 \times 10^4$) and $R_{H1} \approx 3.84$ ($\Delta t_D \approx 2.38 \times 10^5$), respectively. For each case, the values of Δt_D recorded on Fig. 7.5.3 denotes the time at which the semilog straight line begins. Comparing the results of Figs. 7.5.2 and 7.5.3, we see that the semilog straight line begins earlier when rate-normalization is used.

7.6 Computation of Oil Saturation

Based on conclusions presented in the literature by Serra et al.[10,28], superposition for the solution-gas-drive problem approximately holds provided that the same saturation/pressure relationship is used for both drawdown and buildup. This implies that relative or effective oil and gas permeabilities computed from a buildup test correspond to drawdown values. Therefore, if one wishes to compute the relative or effective oil and gas permeabilities as a function of sandface oil saturation, one needs to compute accurately the oil saturation/pressure profile for the drawdown part of the test.

Refs. 6, 7 and 9 have presented equations which can be used to compute the sandface oil saturation versus pressure relationship if wellbore storage effects are

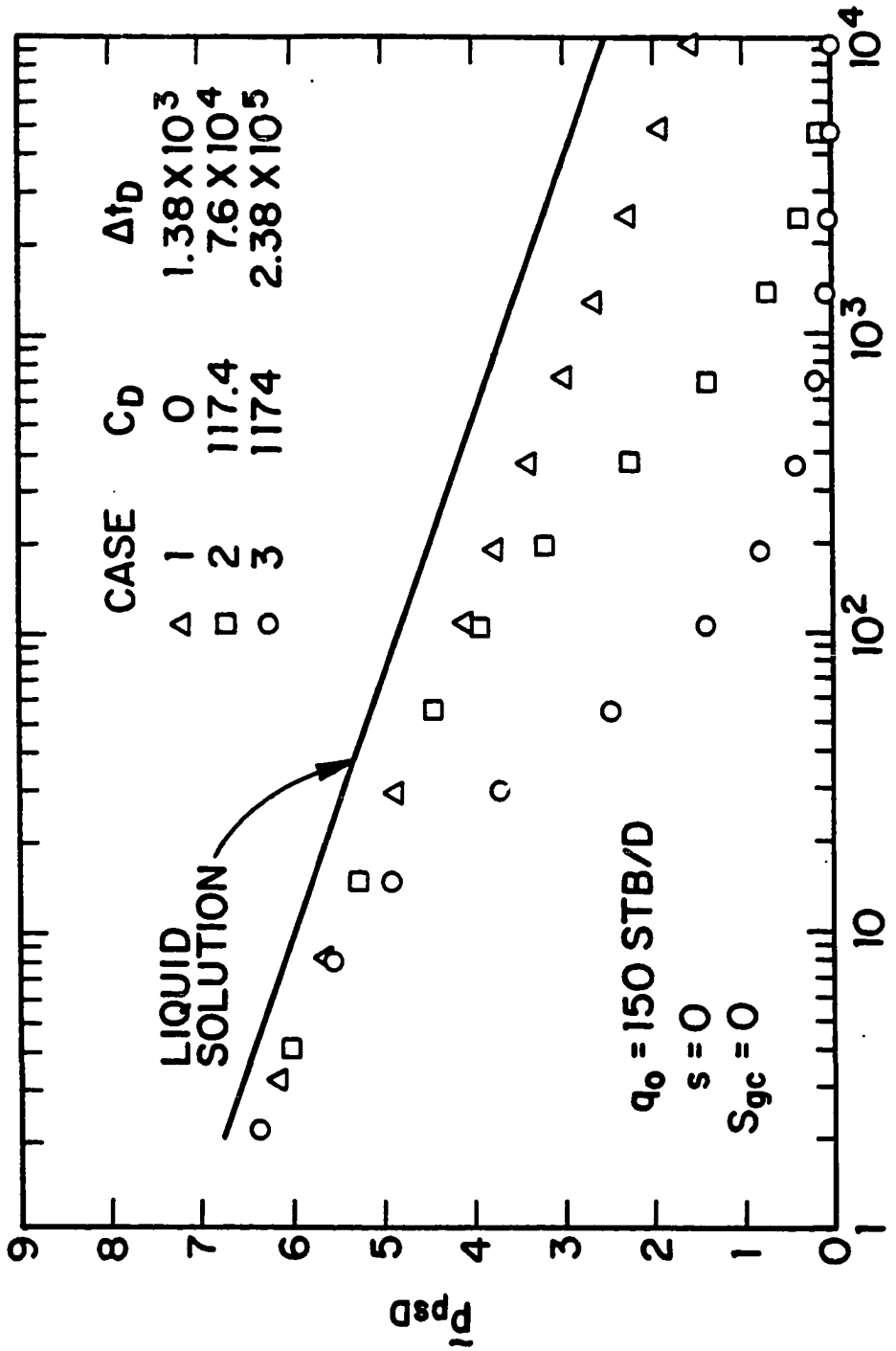

Fig. 7.5.3 - Semilog plot of dimensionless pseudopressure versus Horner time; Cases 1-3.

not considered. Chapter 6 (also see Hatzignatiou et al.[29]) extended these ideas to derive the sandface oil saturation/wellbore pressure profile when wellbore storage effects are present provided the sandface oil flow rate can be measured or estimated. However, the numerical computation of S_o versus p_{wf} relationship based on the above methods is very sensitive and the resulting saturation values are not always highly accurate.

Serra et al.[10] have presented an approximate method for computing the sandface oil saturation versus wellbore pressure based on a material balance calculation. Starting from the equation that gives the dissolved GOR at bubble-point pressure, i.e.,

$$R_{sb} = R_s + \frac{S_g B_o}{S_o B_g}, \tag{7.6.1}$$

and solving for S_o one obtains

$$S_o = \frac{(1 - S_w)B_o}{B_o + (R_{sb} - R_s)B_g}, \tag{7.6.2}$$

where R_{sb} represents the value of the dissolved GOR at the grid block bubble-point pressure and R_s represents the grid block value of dissolved GOR. Assuming S_w is known (in our case $S_w = S_{wc}$) and the variation in the bubble-point is not large, i.e., $R_{sb} \approx R_{sbi}$, Eq. 7.6.2 yields

$$S_o = \frac{(1 - S_{wc})B_o}{B_o + (R_{sbi} - R_s)B_g}, \tag{7.6.3}$$

where R_{sbi} denotes the dissolved GOR evaluated at the initial bubble-point pressure.

Fig. 7.6.1 shows the variation of the bubble-point pressure in terms of the flowing or shut-in wellbore pressure for Case 2, i.e., when $\beta^* = 6.8 \times 10^{-4}$. The solid curve represents the drawdown bubble-point pressure at the sandface, whereas the dashed curve corresponds to the buildup bubble-point pressure at the sandface. Unlike the zero wellbore storage cases considered in Refs. 10 and 45, note that the bubble-point pressure changes significantly during pressure buildup. This change is caused by afterflow effects. Note that Eq. 7.6.3 depends only on the value of pressure and does not depend on whether we consider drawdown or buildup pressures. Since

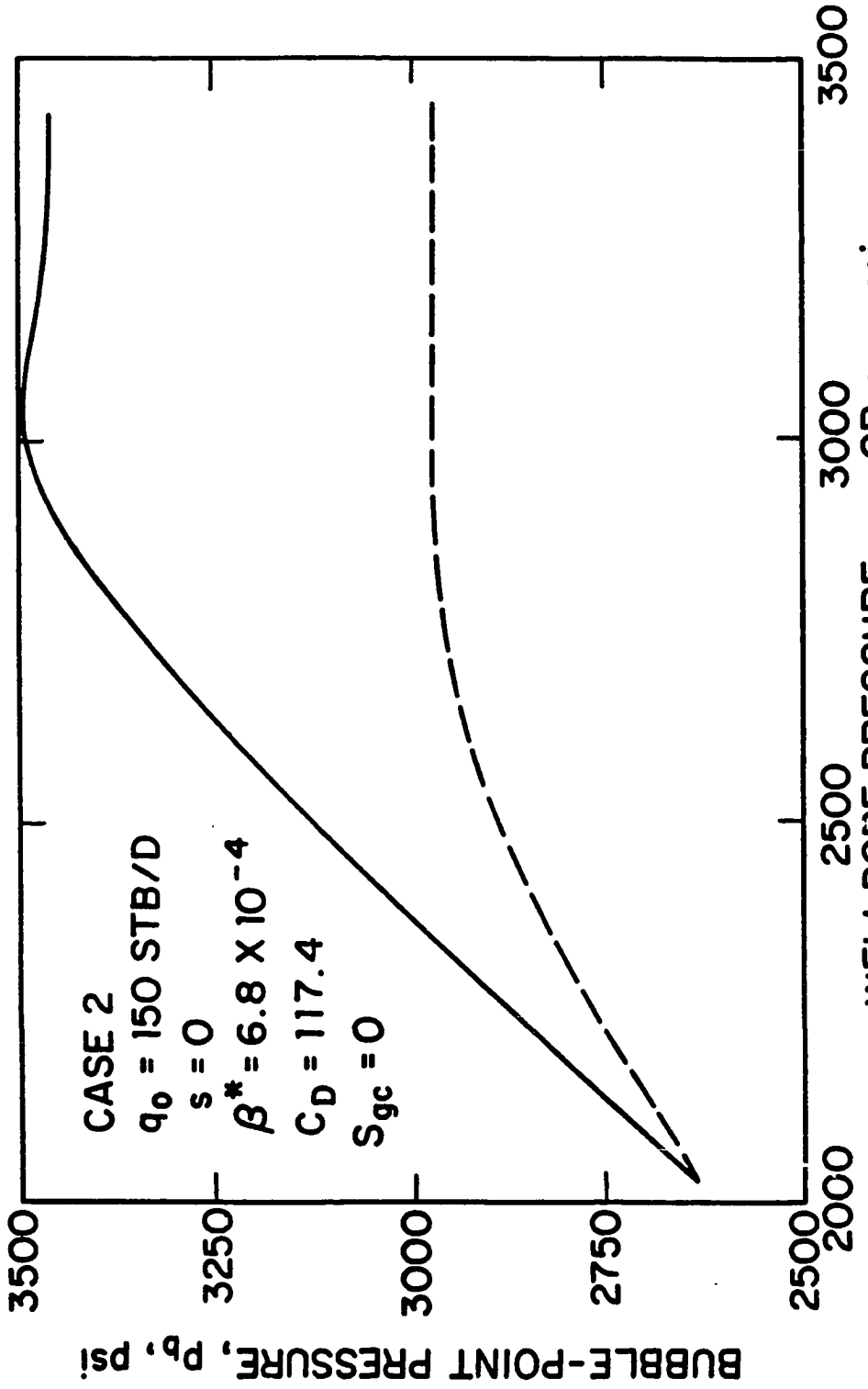

Fig. 7.6.1 - Variation of drawdown or buildup bubble-point pressure as a function of the wellbore pressure; Case 2.

we are interested in obtaining the drawdown S_o versus p relation at the sandface, we want Eq. 7.6.3 to yield the drawdown S_o versus p values. During drawdown, the bubble-point pressure remains approximately equal to $p_{bi} = 3460$ psi until the wellbore pressure decreases below $p_{wf} = 2900$ psi which occurs at $t = 5.5 \times 10^{-3}$ days. Therefore, one expects Eq. 7.6.3 to yield excellent estimates of the drawdown sandface oil saturation at wells of $p \geq 2900$ psi. For times $t > 5.5 \times 10^{-3}$ days, the drawdown bubble-point pressure decreases continuously and therefore, results obtained from Eq. 7.6.3 should become less accurate when evaluated at values of $p < 2900$ psi. Fig. 7.6.2 represents a plot of simulated or computed oil saturation values plotted against the wellbore pressure for Case 2. The solid curve represents the simulator sandface oil saturation values plotted versus the flowing wellbore pressure. The circular data points represent the oil saturation values obtained from Eq. 7.6.3. The results shown on this figure support the conclusion drawn by examining Fig. 7.6.1. As can be seen from the results of Fig. 7.6.2, Eq. 7.6.3 yields highly accurate results for $p_{wf} \geq 2900$ psi but at smaller wellbore pressures the S_o values computed from Eq. 7.6.3 become less accurate.

7.6.1 Influence of Skin Factor.

The variation of the bubble point pressure in terms of the flowing or shut-in wellbore pressure for Case 5, i.e., when $s = 5$ and $\beta^* = 6.8 \times 10^{-4}$ is shown in Fig. 7.6.3. The solid curve represents the drawdown bubble-point pressure behavior, whereas the dashed curve corresponds to the buildup bubble-point pressure variation. The drawdown bubble-point remains fairly constant for $p_{wf} \geq 3100$ psi which corresponds to $t = 7.0 \times 10^{-4}$ days. Fig. 7.6.4 is a plot of simulated or computed oil saturation values plotted versus the wellbore pressure for Case 5. The solid curve represents the drawdown simulator sandface oil saturation values plotted versus the flowing wellbore pressure. The circular data points represent the oil saturation values obtained from Eq. 7.6.3. As expected, Eq. 7.6.3 yields reasonably accurate estimates of S_o for $p_{wf} \geq 3100$ psi, however, in this case the values of S_o obtained from Eq. 7.6.3 are not highly inaccurate even at lower values of pressure. This

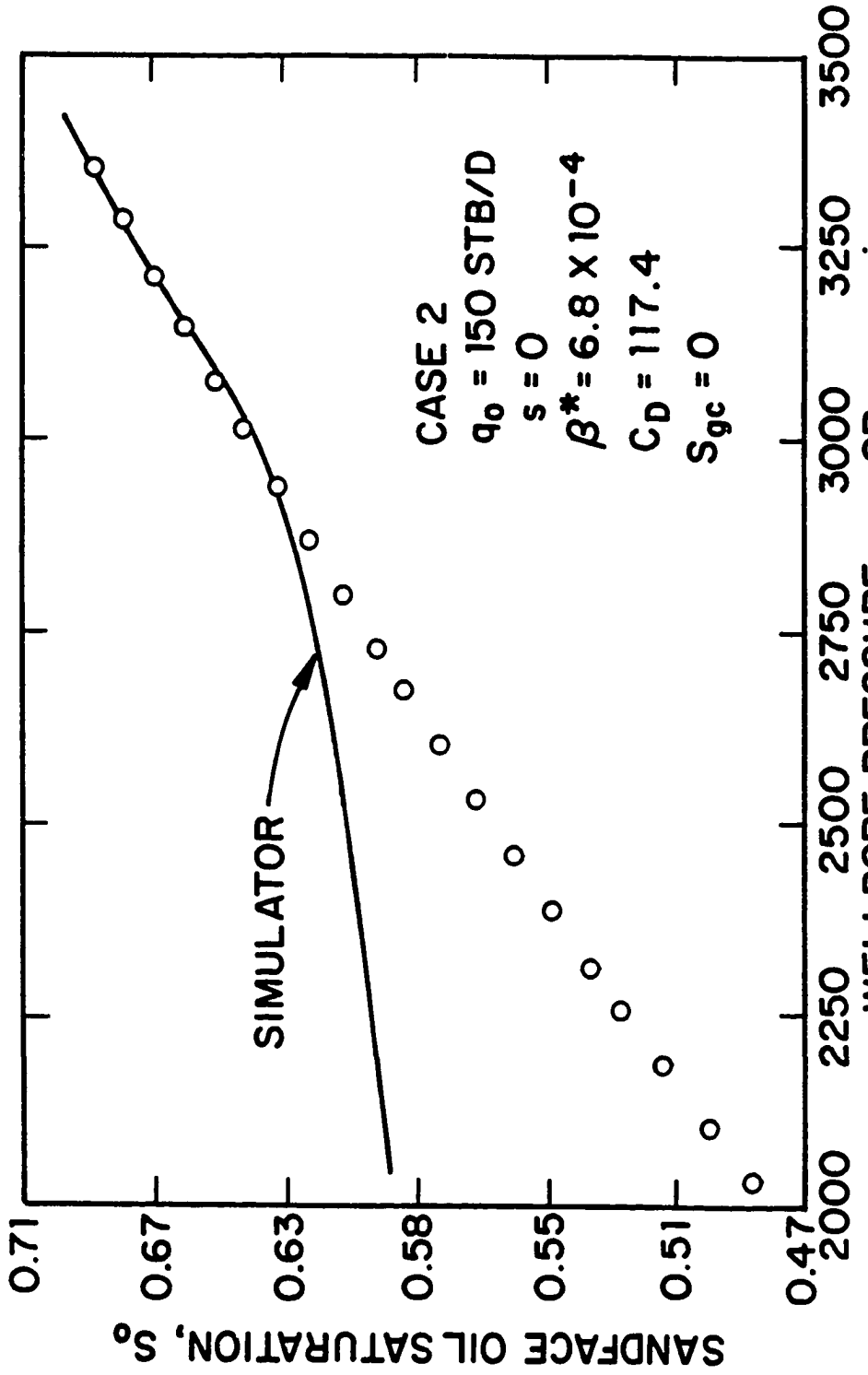

Fig. 7.6.2 - Approximation of sandface oil saturation/pressure relation; Case 2.

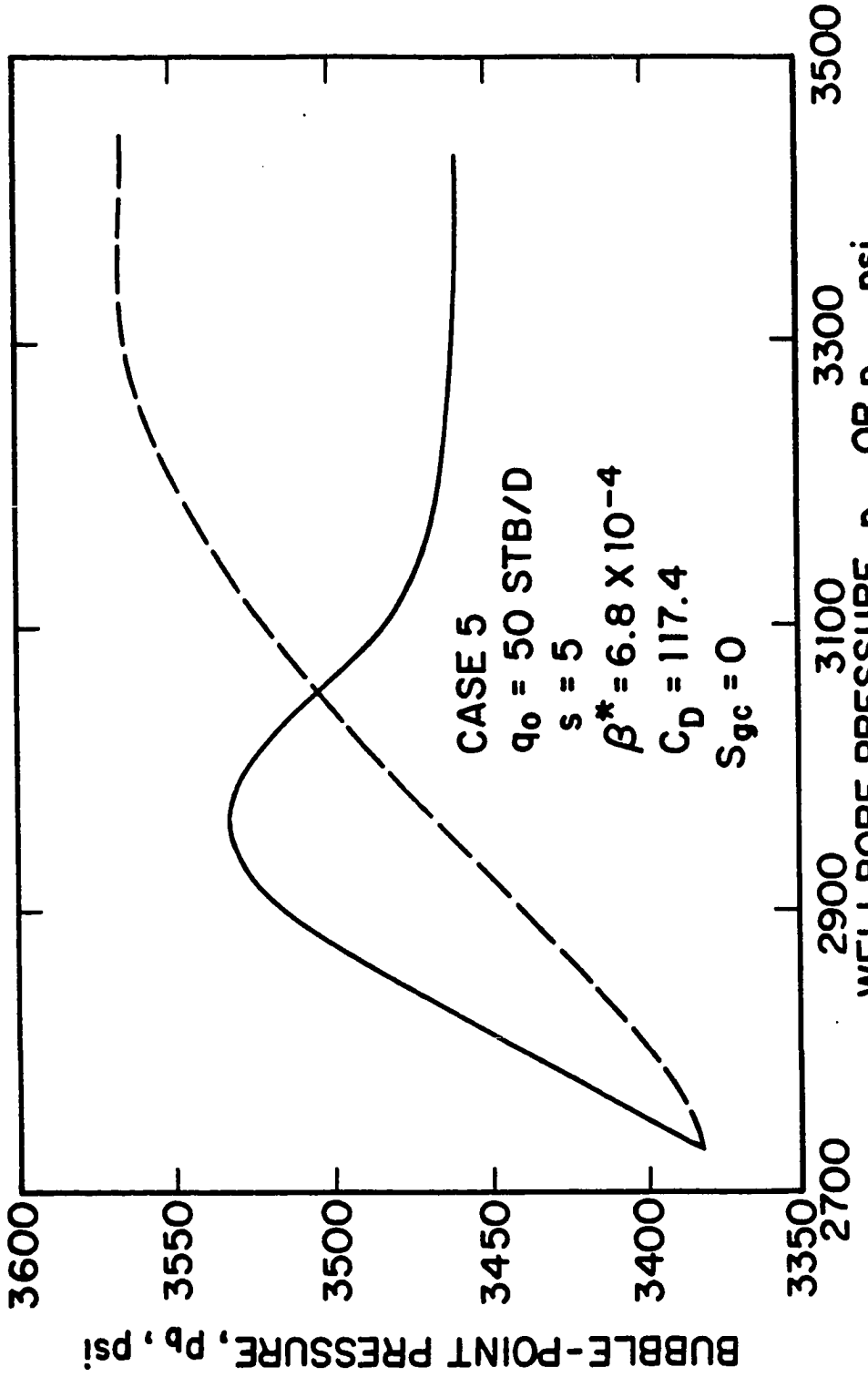

Fig. 7.6.3 - Variation of drawdown or buildup bubble-point pressure as a function of the wellbore pressure; Case 5.

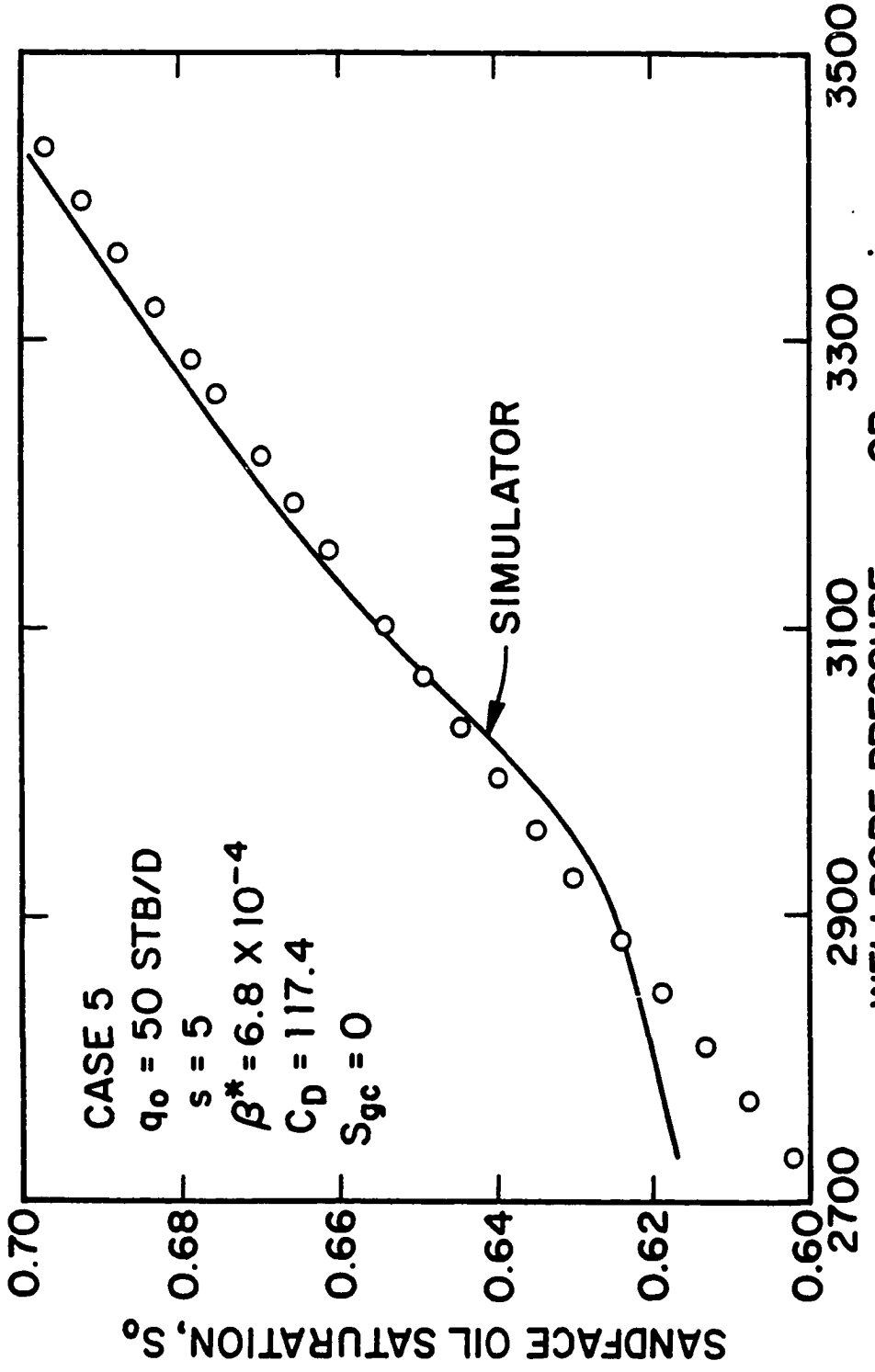

Fig. 7.6.4 - Approximation of sandface oil saturation/pressure relation; Case 5.

is mainly due to the low oil flow rate which results in small bubble-point pressure variations; see Fig. 7.6.3. The sandface value of bubble-point pressure at the time of shut-in is $p_b \approx 2620$ psi for Case 2 and $p_b \approx 3380$ psi for Case 5. Since the initial value of bubble-point pressure for both cases is $p_{bi} = 3460$ psi, the error introduced in Eq. 7.6.3 by assuming $R \approx R_{si}$ is not nearly as significant for Case 5 as it is for Case 2.

7.6.2 Influence of Critical Gas Saturation.

Figs. 7.6.5 and 7.6.6 show, respectively, the variation of the bubble point pressure in terms of the flowing or shut-in wellbore pressure and the simulated or computed oil saturation values plotted against the wellbore pressure for Case 8, i.e., when $s = 0$, $S_{gc} = 0.07$ and $\beta^* = 6.8 \times 10^{-4}$. As shown in Fig. 7.6.5 the bubble-point pressure remains fairly constant for $p_{wf} \geq 3680$ psi ($t = 4.5 \times 10^{-4}$ days). As shown in Fig. 7.6.6, Eq. 7.6.3 yields accurate values for $p \geq 3680$ psi, i.e., only for a short period of time.

7.7 Computation of Effective Permeabilities

In this major section, we present algorithms for computing effective permeabilities as a function of pressure directly from measured values of the shut-in wellbore pressure. Since the computed values of sandface oil saturation as a function of wellbore pressure can be approximately obtained from the material balance equation (Eq. 7.6.3), combining the two sets of results yields effective permeabilities as a function of oil saturation. If absolute permeability is known or can be approximated, then one can obtain approximately a small segment of the relative permeability curves as a function of oil saturation. The main disadvantage of these procedures is that one must be able to measure accurately the sandface oil flow rate.

7.7.1 Effective Permeability as a Function of Pressure.

In Appendix E, we derive the following equation:

$$kk_{ro} = \frac{162.6\Delta q(\Delta t)(\mu_o B_o)_{p_{ws}}(d\Delta t_{lc}/d\Delta t)}{h(dp_{ws}/d\Delta t)}$$

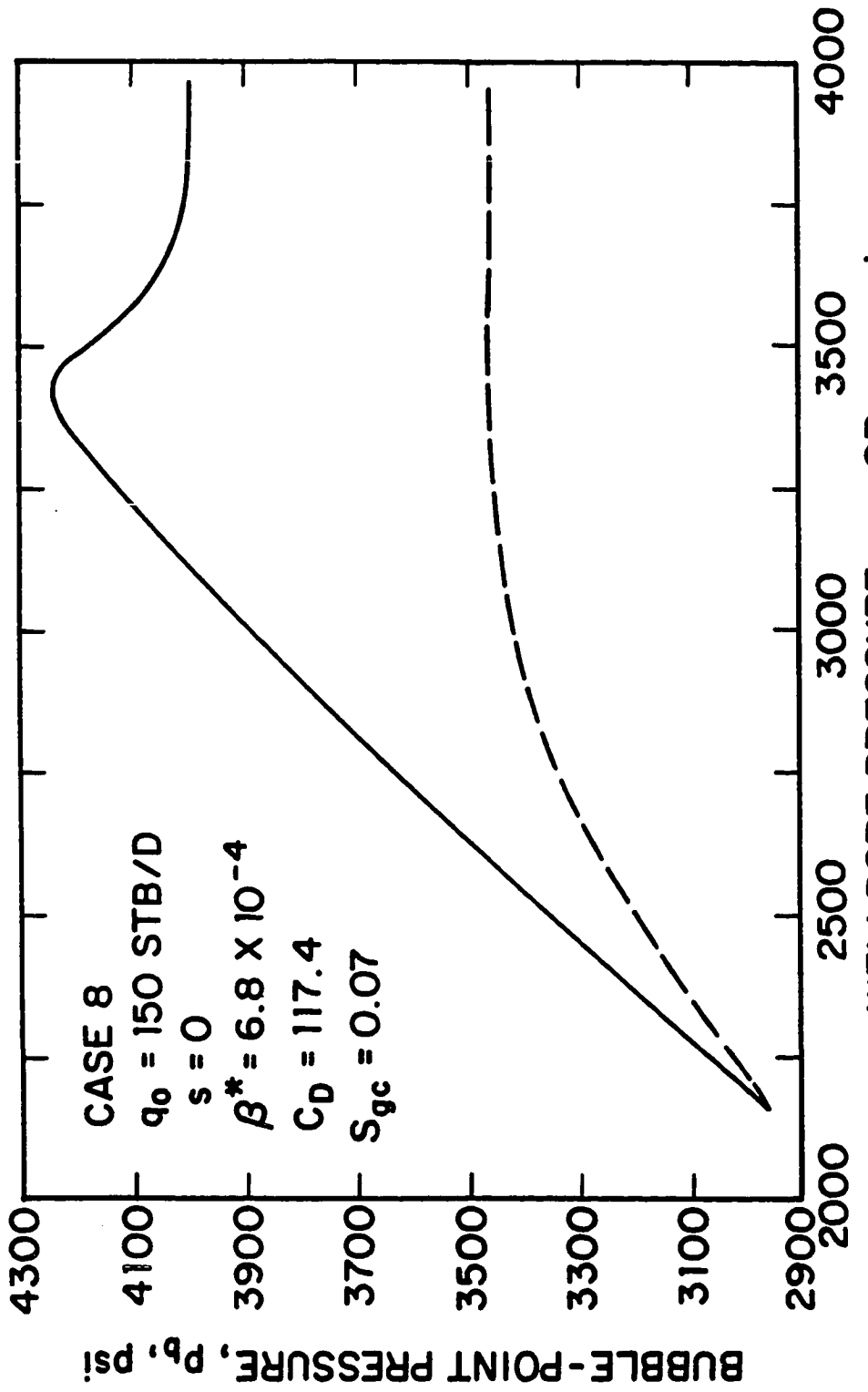

Fig. 7.6.5 - Variation of drawdown or buildup bubble-point pressure as a function of the wellbore pressure; Case 8.

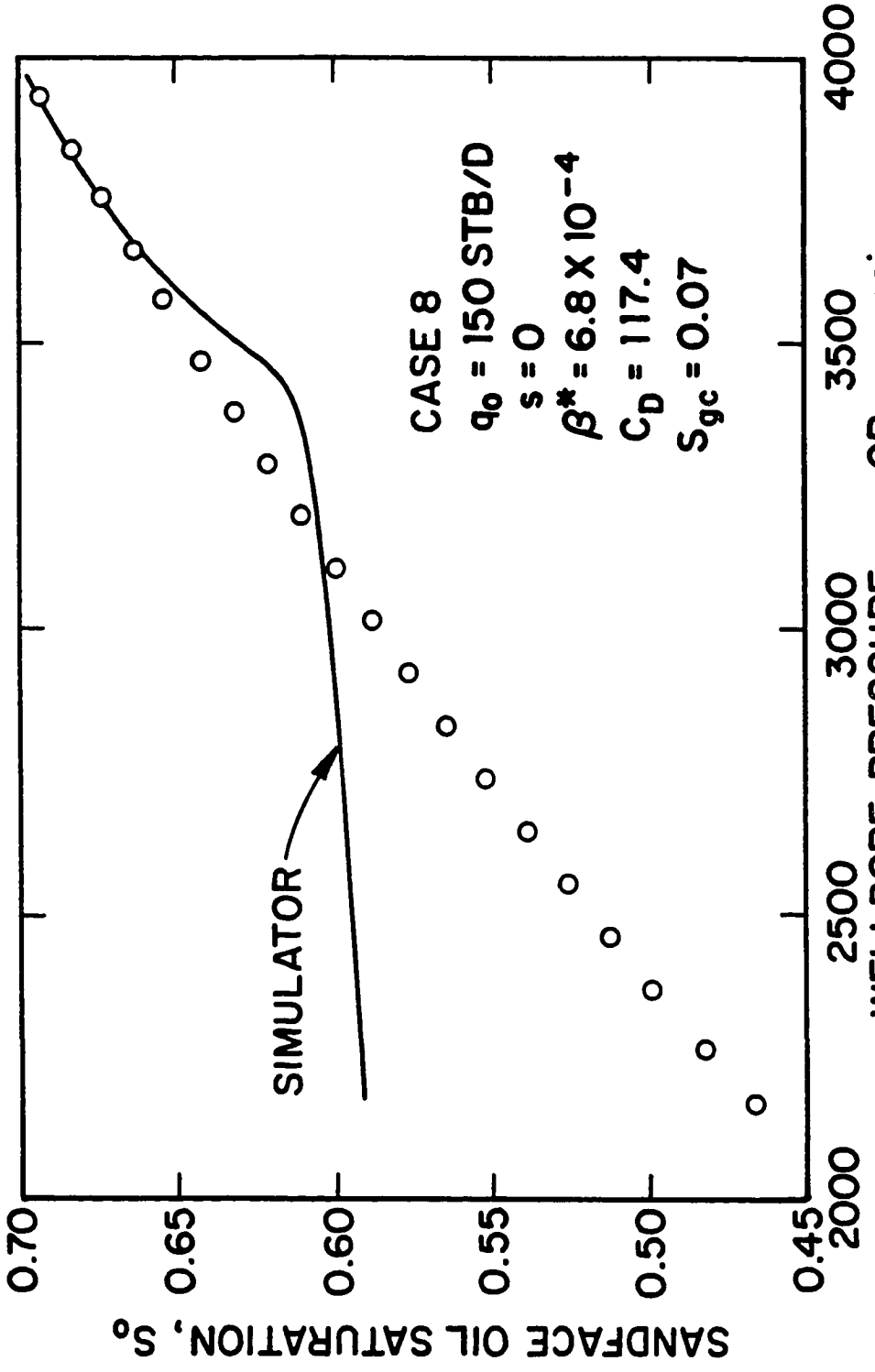

Fig. 7.6.6 - Approximation of sandface oil saturation/pressure relation; Case 8.

$$+\left[\frac{k[p_p(p_{ws}) - p_p(p_{wf,s})](\mu_o B_o)_{p_{ws}}}{(dp_{ws}/d\Delta t)} \frac{d\ln(\Delta q(\Delta t))}{d\Delta t}\right], \qquad (7.7.1)$$

where Δt_{lc} is the logarithmic convolution shut-in time defined by Eq. 7.5.6 and $\Delta q(\Delta t)$ represents the change of the sandface oil flow rate defined by Eq. 7.5.10. As shown in Appendix E, Eq. 7.7.1 is obtained by differentiating Eq. 7.5.8 with respect to shut-in time and rearranging the resulting equation. Note that from the chain rule it follows that

$$\frac{d\Delta t_{lc}/d\Delta t}{dp_{ws}/d\Delta t} = \frac{1}{dp_{ws}/d\Delta t_{lc}}. \qquad (7.7.2)$$

When wellbore storage effects become negligible Δq becomes constant with $\Delta q = q_{osf}(\Delta t = 0) = q_o$ and the term after the plus sign on the right side of Eq. 7.7.1 is zero. If we ignore wellbore storage effects, i.e., assume $C_D = 0$ so $\Delta q = q_o$, then $\Delta t_{lc} = \log[(t\Delta t)/(t + \Delta t)]$ and Eq. 7.7.1 is replaced by

$$kk_{ro} = \frac{162.6 q_o(\mu_o B_o)_{p_{ws}}}{hdp_{ws}/d\log(\frac{t\Delta t}{t+\Delta t})} = -\frac{162.6 q_o(\mu_o B_o)_{p_{ws}}}{hdp_{ws}/d\log R_{H1}}, \qquad (7.7.3)$$

which is the equation presented in Ref. 10 for the zero wellbore storage case. Note that Eq. 7.7.3 is instructive in estimating the errors involved in classical analysis. By classical analysis we mean analysis of buildup data based on a semilog plot of p_{ws} versus $(t + \Delta t)/\Delta t$. Since Eq. 7.7.3 is approximately correct[10], the classical analysis will yield a semilog straight line on a pressure interval $p_1 \leq p_{ws} \leq p_2$ if and only if kro, μ_o and B_o are approximately constant on this pressure interval. Moreover, if this occurs the value of kk_{ro} determined from this semilog slope will represent some type of average value of kk_{ro} on the interval $p_1 \leq p_{ws} \leq p_2$.

The term of Eq. 7.7.1 within square brackets, which involves the derivative of the change in the sandface flow rate, represents the effect of wellbore storage on our computational procedure. As the effects of wellbore storage become negligible, i.e., as the sandface flow rate becomes equal to zero ($\Delta q(\Delta t) \rightarrow q_o$), the derivative of the sandface flow rate becomes equal to zero and Eq. 7.7.1 reduces to the computational equation of Ref. 10, i.e., to Eq. 7.7.3. However, at early times the term of Eq. 7.7.1 within square brackets has a dominant influence on the values of effective oil permeability obtained from Eq. 7.7.1.

At each time, i.e., at each value of $p_p(p_{ws}) - p_p(p_{wf,s})$, Eq. 7.7.1 is used to estimate the corresponding value of kk_{ro}. Note the application of Eq. 7.7.1 requires knowledge of

$$k[p_p(p_{ws}) - p_p(p_{wf,s})] = \int_{p_{wf,s}}^{p_{ws}(\Delta t)} \frac{kk_{ro}}{\mu_o B_o} dp = \sum_{j=1}^{n+1} \left(\int_{p_{ws}(\Delta t_{j-1})}^{p_{ws}(\Delta t_j)} \frac{kk_{ro}}{\mu_o B_o} dp \right), \quad (7.7.4)$$

where $\Delta t_0 = 0$, $p_{ws}(0) = p_{wf,s}$ and $\Delta t_{n+1} = \Delta t$. Thus, in order to apply Eq. 7.7.1 to compute kk_{ro} at $\Delta t = \Delta t_{n+1}$, we must be able to estimate the last integral ($j = n + 1$ term) in the summation of Eq. 7.7.4. This is accomplished by using the following approximation:

$$\int_{p_{ws}(\Delta t_n)}^{p_{ws}(\Delta t_{n+1})} \frac{kk_{ro}}{\mu_o B_o} dp = \left(\frac{kk_{ro}}{\mu_o B_o}\right)_{p_{ws}(\Delta t_n)} \times (p_{ws}(\Delta t_{n+1}) - p_{ws}(\Delta t_n)), \quad (7.7.5)$$

so that Eq. 7.7.4 reduces to

$$k[p_p(p_{ws}) - p_p(p_{wf,s})] = \sum_{j=1}^{n} \left(\int_{p_{ws}(\Delta t_{j-1})}^{p_{ws}(\Delta t_j)} \frac{kk_{ro}}{\mu_o B_o} dp \right)$$

$$+ \left(\frac{kk_{ro}}{\mu_o B_o}\right)_{p_{ws}(\Delta t_n)} \times (p_{ws}(\Delta t_{n+1}) - p_{ws}(\Delta t_n)). \quad (7.7.6)$$

By using Eq. 7.7.6 in our computational algorithm, Eq. 7.7.1, we obtain a procedure that can be applied to estimate kk_{ro} as a function of the measured shut-in wellbore pressure. At the very first time step, i.e., at the first application of Eq. 7.7.1, the term in square brackets is ignored, i.e., set equal to zero. The accuracy of kk_{ro} values computed from Eq. 7.7.1 can be improved by assuming that the value of kk_{ro} at $\Delta t = 0$ is known from the computational procedures of a pressure drawdown test. This estimate of kk_{ro} can be used to compute the value of $k[p_p(p_{ws}) - p_p(p_{wf,s})]$ at the first time step in the computational algorithm presented above.

Once the effective oil permeability is computed from Eq. 7.7.1, the effective gas permeability can be estimated from the following equation:

$$kk_{rg} = \left[R(\Delta t = 0) - R_s\right]_{p_{ws}} \left(\frac{\mu_g B_g}{\mu_o B_o}\right)_{p_{ws}} kk_{ro}. \quad (7.7.7)$$

Note that the application of Eq. 7.7.7 requires that the producing GOR at the time of shut-in is measured. Eq. 7.7.7 follows from the work of Ref. 3 and is essentially the same procedure used by Raghavan[5] for computing k_{rg}/k_{ro} as a function of pressure.

The simulated and computed kk_{ro} versus the shut-in wellbore pressure, p_{ws}, are shown in Table F-36 for Case 2. In this table, columns 1 and 2 show the shut-in time and shut-in wellbore pressure data, columns 3 and 4 show the drawdown simulator sandface oil saturation and the simulator effective oil permeability data and column 5 shows the kk_{ro} values computed from Eq. 7.7.1. Fig. 7.7.1 presents results obtained from the computational algorithm of Eq. 7.7.1 assuming the kk_{ro} value at $\Delta t = 0$ is known. The results pertain to Cases 1-3, i.e., $q_o = 150$ STB/D, $S_{gc} = 0.0$ and $s = 0$ for various wellbore storage values. In Fig. 7.7.1, the effective oil permeability is plotted as a function of p_{wf} or p_{ws}. The solid line corresponds to simulator values and the triangular, square and circular data points represent values obtained from Eq. 7.7.1 from buildup pressure data. The triangular data points represent the computed kk_{ro} values for Case 1 ($C_D = 0$), the square data points represent values of kk_{ro} for Case 2 ($\beta^* = 6.8 \times 10^{-4}$) and the circular data points are the kk_{ro} values computed by Eq. 7.7.1 for Case 3 ($\beta^* = 6.8 \times 10^{-5}$). The x data points represent the effective oil permeability values computed from drawdown pressure versus time data based on computational procedures outlined in Chapter 6 and Refs. 8, 9, 10, 28 and 29. Note that the drawdown data yield essentially exact estimates of kk_{ro} values at low values of the flowing wellbore pressure, whereas the buildup data yield only approximate estimates of kk_{ro} values at all values of shut-in wellbore pressure. At high values of shut-in pressure, Eq. 7.7.1 yields underestimates of the drawdown effective oil permeability (solid curve). Fig. 7.7.1 implies that the computed kk_{ro} values for Cases 2 and 3 are in better overall agreement with the simulator results when wellbore storage effects are present. When the afterflow becomes zero, the kk_{ro} values from all buildup cases are identical.

Fig. 7.7.2 is a plot of the simulator kk_{ro} values plotted against the simulator S_o values (solid line) and the kk_{ro} values computed from Eq. 7.7.1 plotted versus

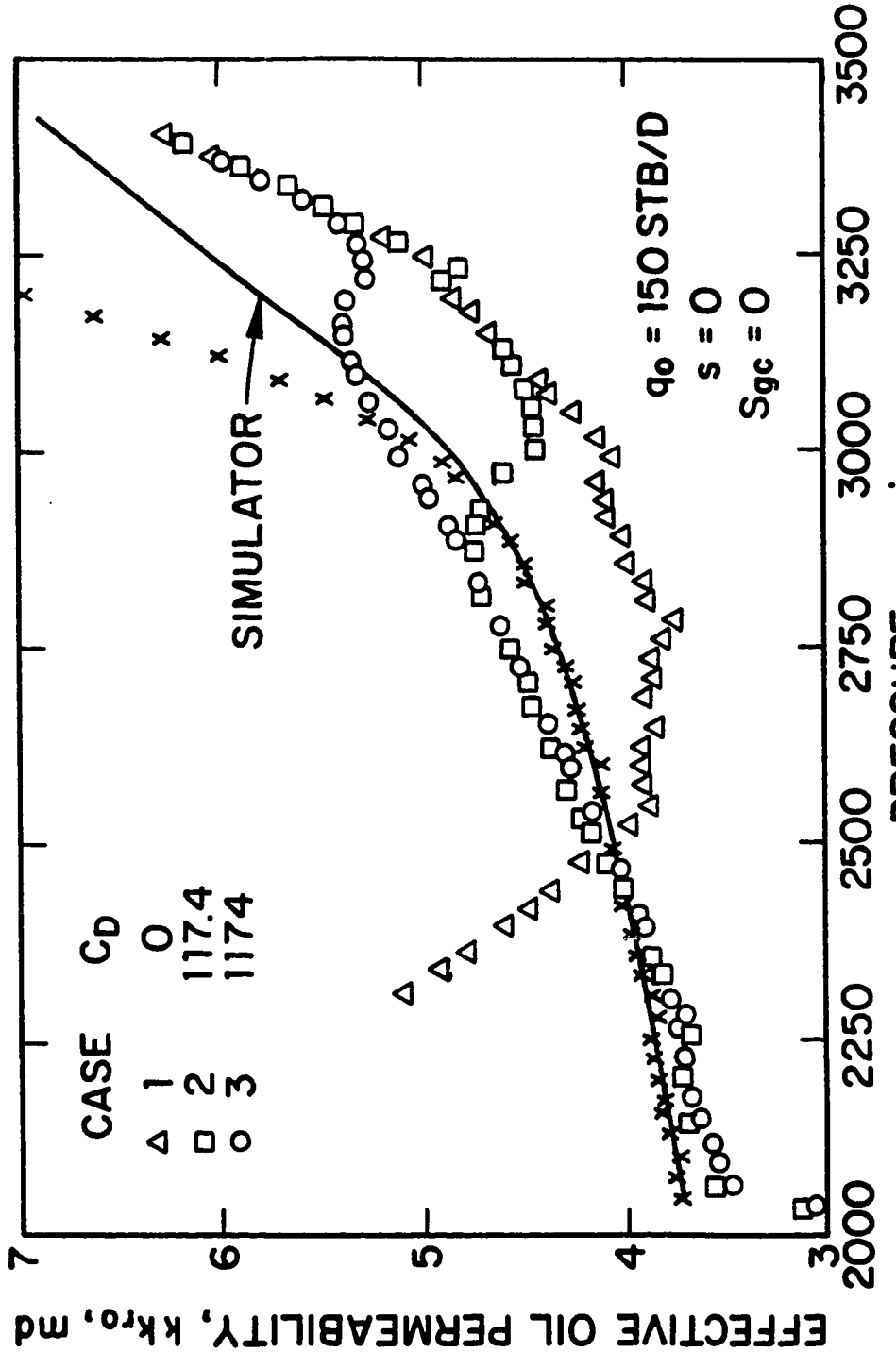

Fig. 7.7.1 - Plot of effective oil permeability versus wellbore pressure; Cases 1-3.

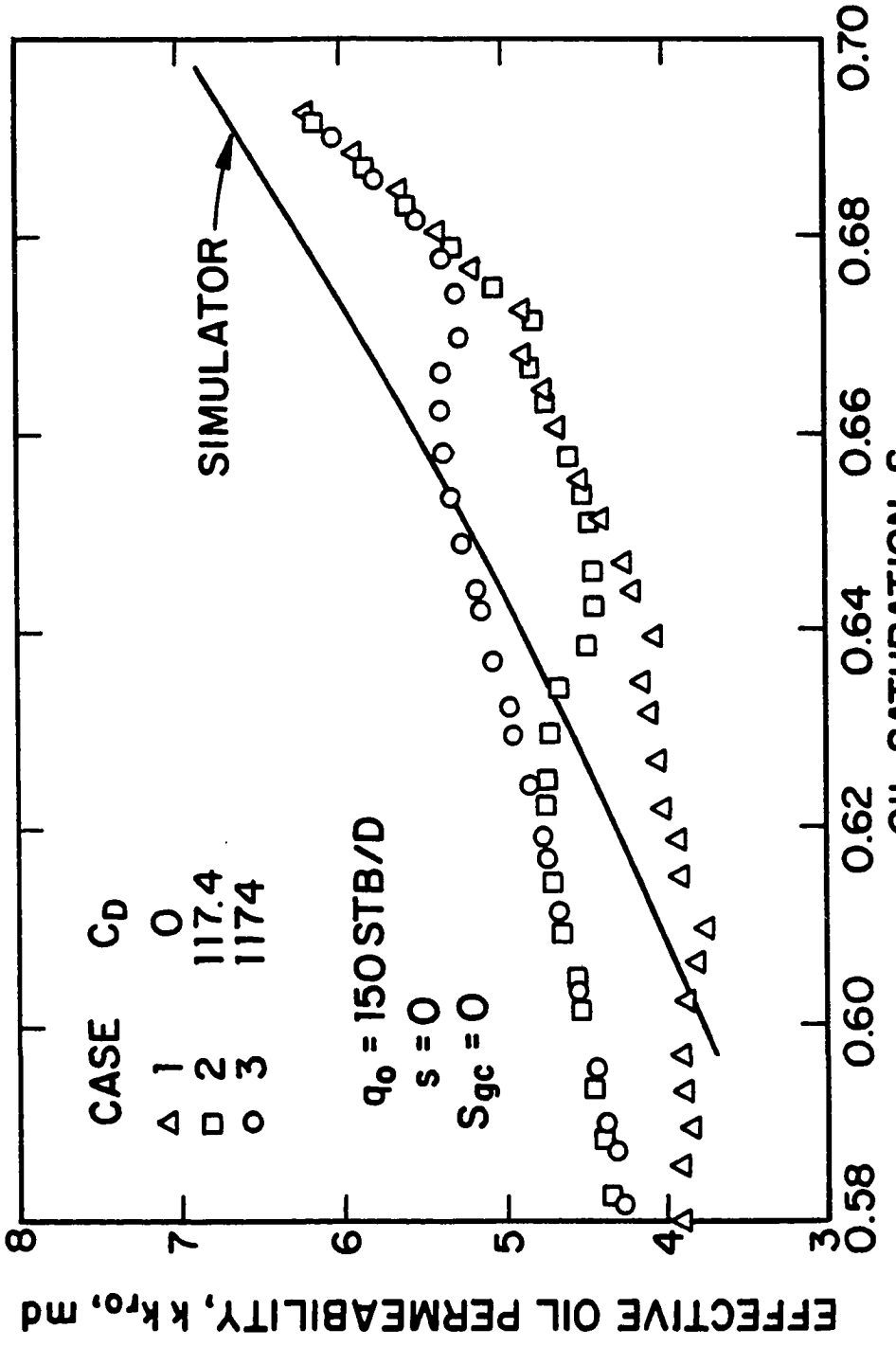

Fig. 7.7.2 - Effective oil permeability as a function of oil saturation; Cases 1-3.

the S_o values computed from Eq. 7.6.3 (data points) for Cases 1-3. Again, the triangular data points represent the computed kk_{ro} values for Case 1 ($C_D = 0$), the square data points represent values of kk_{ro} for Case 2 ($\beta^* = 6.8 \times 10^{-4}$) and the circular data points are the kk_{ro} values computed by Eq. 7.7.1 for Case 3 ($\beta^* = 6.8 \times 10^{-5}$). The computed kk_{ro} versus S_o profile is only in rough agreement with the simulator one.

The simulated and computed kk_{rg} versus the shut-in wellbore pressure, p_{ws}, are shown in Table F-37 for Case 2. In this table, column 1 shows the wellbore pressure data, column 2 shows the drawdown effective gas permeability data obtained from the simulator and column 3 shows the kk_{rg} values computed from Eq. 7.7.7. The effective gas permeability as a function of pressure is presented in Fig. 7.7.3 for the same cases, i.e., Cases 1-3. The solid line corresponds to drawdown simulator values and the data points represent values obtained from Eq. 7.7.7 from buildup pressure data. The triangular data points represent the computed kk_{rg} values for Case 1 ($C_D = 0$), the square data points represent values of kk_{rg} for Case 2 ($\beta^* = 6.8 \times 10^{-4}$) and the circular data points are the kk_{rg} values computed by Eq. 7.7.1 for Case 3 ($\beta^* = 6.8 \times 10^{-5}$). The x data points represent the effective gas permeability values computed from drawdown pressure versus time data based on computational procedures outlined in Chapter 6 and Refs. 9, 10, 28 and 29. Fig. 7.7.3 implies that the computed kk_{rg} values from both drawdown and buildup data are in very good agreement with the simulator values. The only exception is Case 1 which does not yield accurate results for $p_{ws} < 2400$ psi. This occurs because the estimated kk_{ro} values from Eq. 7.7.1 are not accurate for $p_{ws} < 2400$ psi (see Fig. 7.7.1).

The effective gas permeability as a function of sandface oil saturation is shown in Fig. 7.7.4. The solid line represents the simulator results, whereas the data points correspond to the kk_{rg} values computed from Eq. 7.7.7 plotted against the S_o values computed from Eq. 7.6.3. The agreement between computed and simulated results is reasonably good for $S_o > 0.625$. This is due to the fact that Eq. 7.6.3 yields accurate sandface oil saturation/wellbore pressure only for $S_o > 0.625$ and $p > 2823$

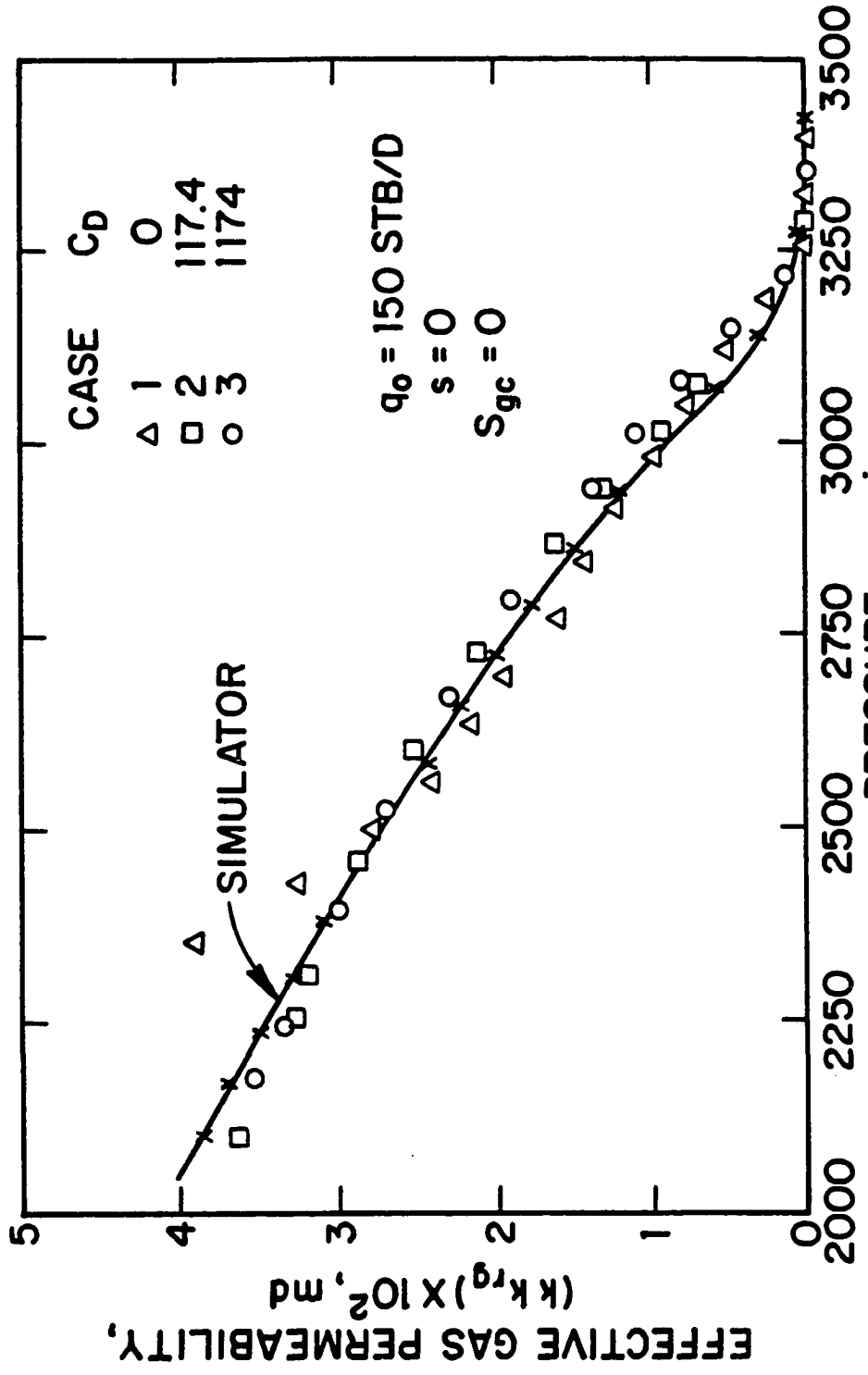

Fig. 7.7.3 - Effective gas permeability as a function of wellbore pressure; Cases 1-3.

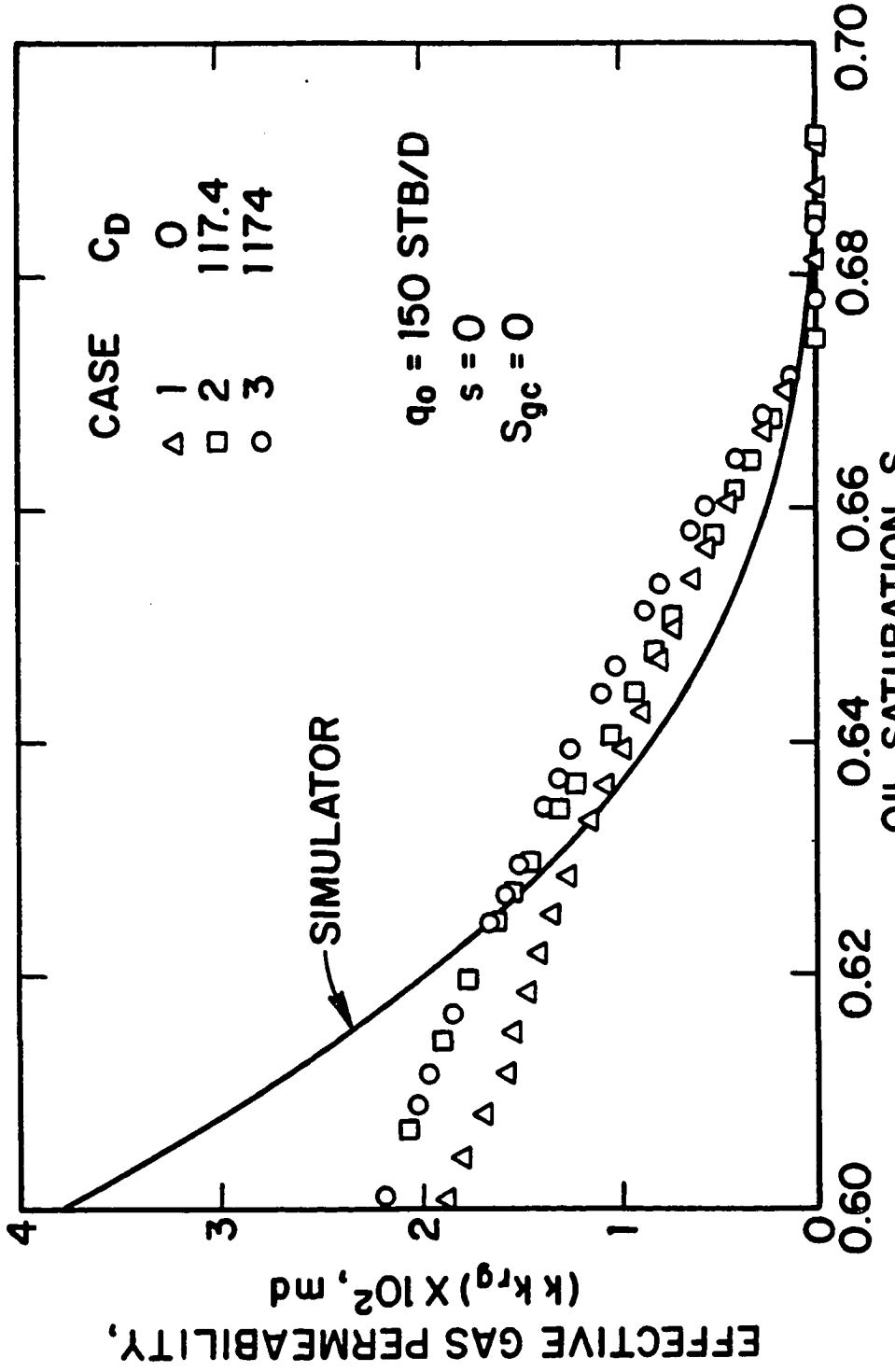

Fig. 7.7.4 - Effective gas permeability as a function of oil saturation; Cases 1-3.

psi, i.e., $\Delta t > 4.0 \times 10^{-5}$ days (see Fig. 7.6.2).

Figs. 7.7.5 through 7.7.8 are the same as Figs. 7.7.1 through 7.7.4 with the only difference being the method of computing the wellbore storage term within the square brackets of Eq. 7.7.1. For the estimation of kk_{ro} and kk_{rg} values shown in Figs. 7.7.5 through 7.7.8 we set the term in square brackets of Eq. 7.7.1 equal to zero at the first iteration, i.e., in applying Eq. 7.7.1 to compute kk_{ro} at the first buildup pressure data point, $p_{ws}(\Delta t_1)$, we ignore the term of Eq. 7.7.1 which is in square brackets. At subsequent data points, we use Eq. 7.7.6 to evaluate this term. This results in lower estimates of oil and gas effective permeabilities for the non-zero wellbore storage cases, i.e., Cases 2 and 3 especially during the early shut-in times when the wellbore storage term of Eq. 7.7.1 has a dominant influence on the computed kk_{ro} values.

Finally, Fig. 7.7.9 shows a plot of kk_{ro} values computed from Eq. 7.7.3 versus the wellbore pressure p_{wf} or p_{ws}. Since Eq. 7.7.3 ignores the wellbore storage effects, one expects it to yield reasonable estimates of kk_{ro} only after the wellbore storage has ceased. From Fig. 7.7.9 one can see that Eq. 7.7.3 provides reasonable estimates of kk_{ro} only for $p > 3120$ psi for Case 2 and $p > 3300$ psi for Case 3.

7.7.2 Influence of Skin Factor.

The results presented in the previous subsection are for cases where $s = 0$. In this subsection, we consider results for Cases 4-6 so that data is influenced by both wellbore storage and skin effects. Recall that for these cases, $s = 5$, $q_o = 50$ STB/D and $S_{gc} = 0.0$.

For all the results shown in this subsection, the solid line corresponds to simulator values, the triangular data points represent the values for Case 6 ($C_D = 0$), the square data points represent values for Case 5 ($\beta^* = 6.8 \times 10^{-4}$, $C_D \approx 117.4$) and the circular data points are the values for Case 4 ($\beta^* = 6.8 \times 10^{-5}$, $C_D \approx 1174$). The x data points represent the results computed from drawdown pressure versus time data based on computational procedures outlined in Refs. 8, 9, 10, 28 and 29.

Fig. 7.7.10 is a plot of simulated or computed effective oil permeability versus

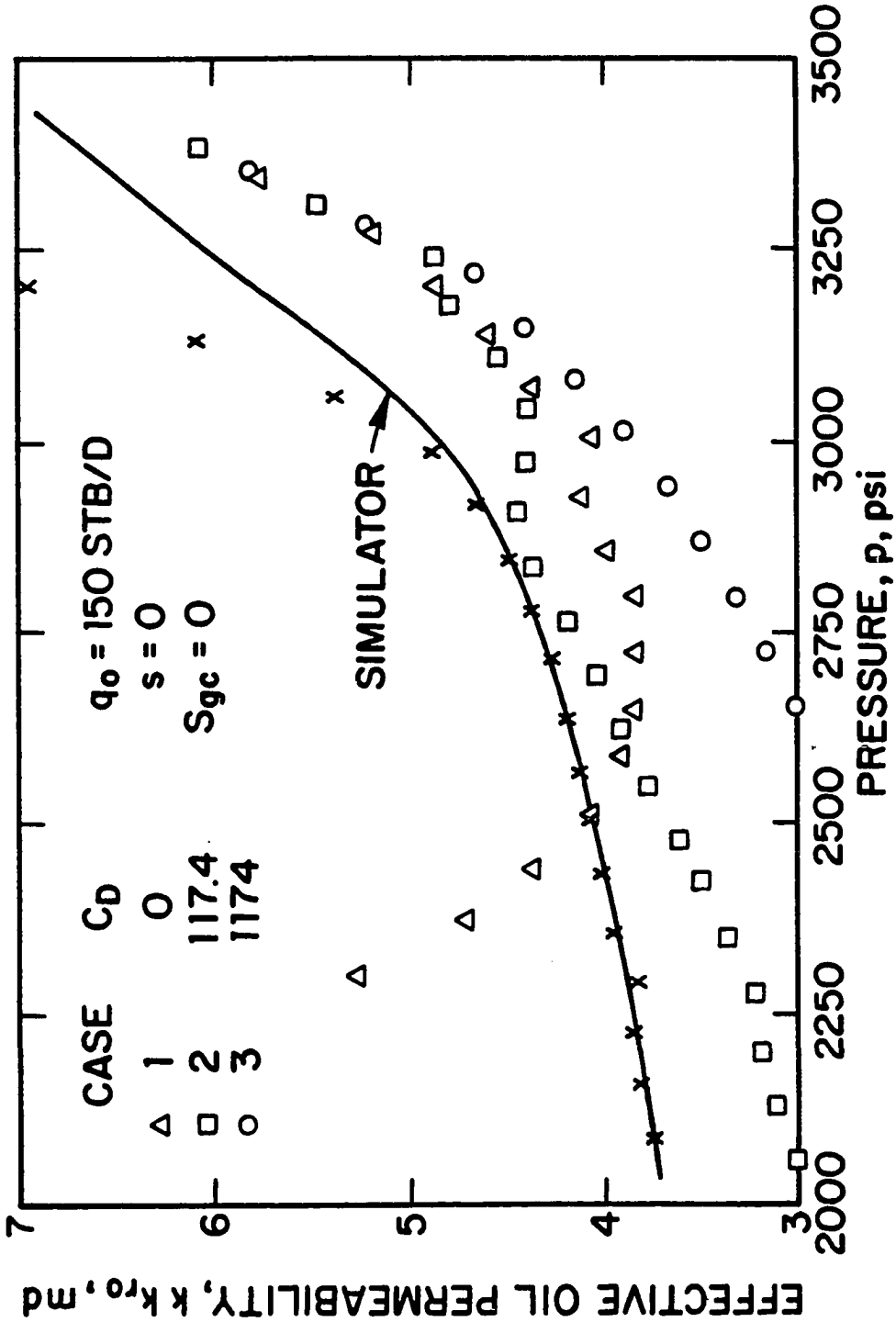

Fig. 7.7.5 - Effective oil permeability as a function of wellbore pressure; Cases 1-3.

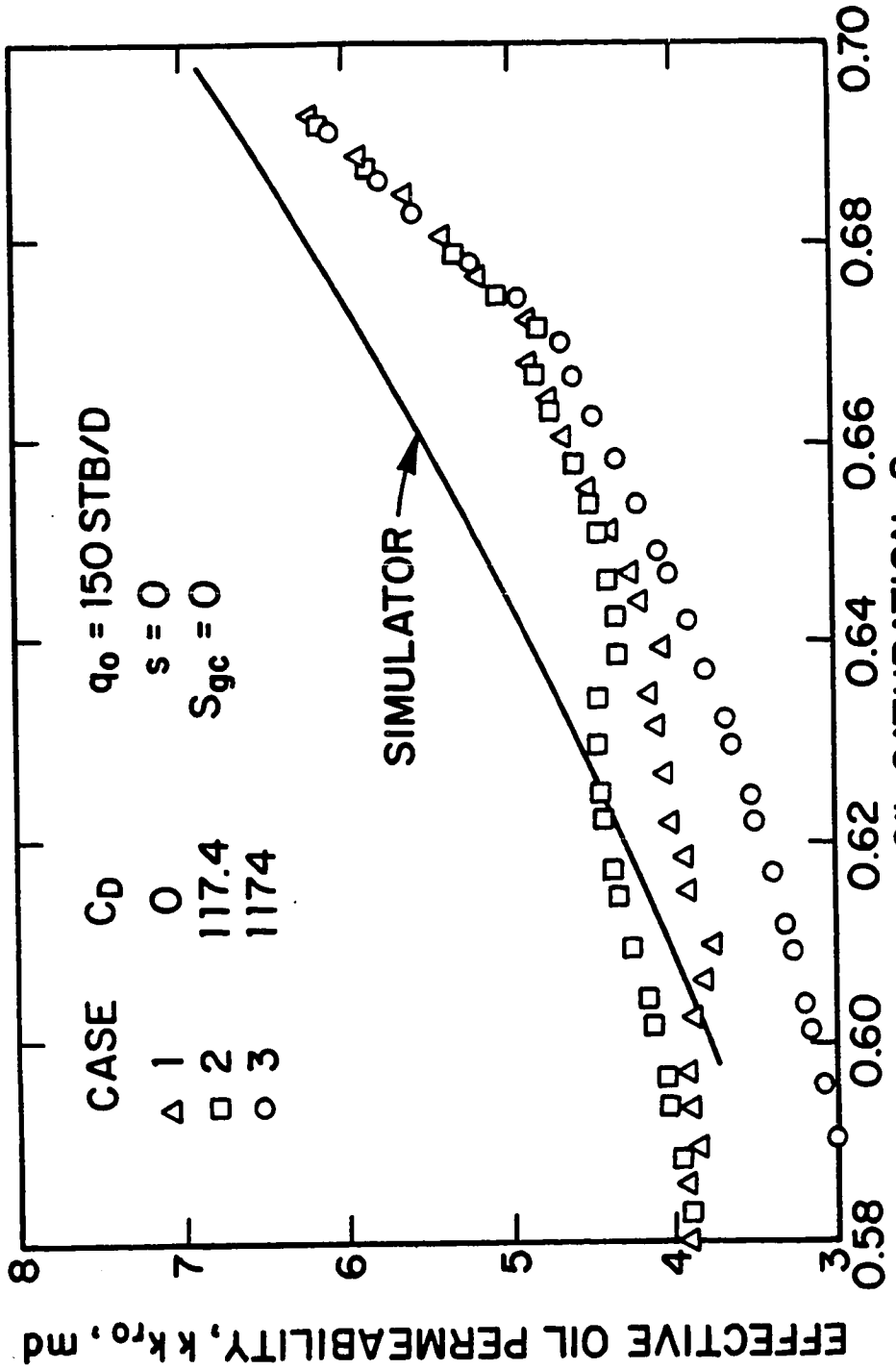

Fig. 7.7.6 - Effective oil permeability as a function of oil saturation; Cases 1-3.

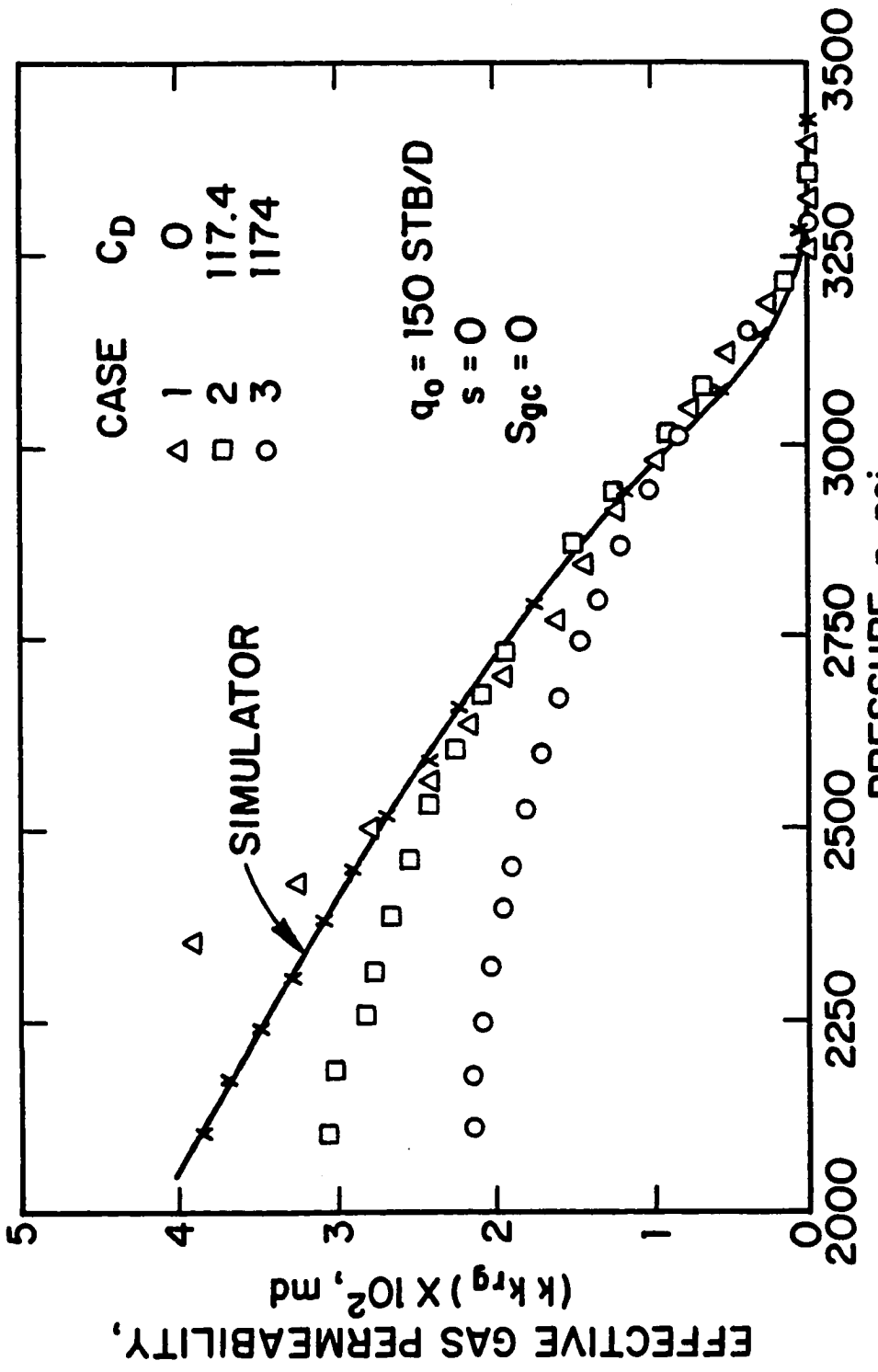

Fig. 7.7.7 - Effective gas permeability as a function of wellbore pressure; Cases 1-3.

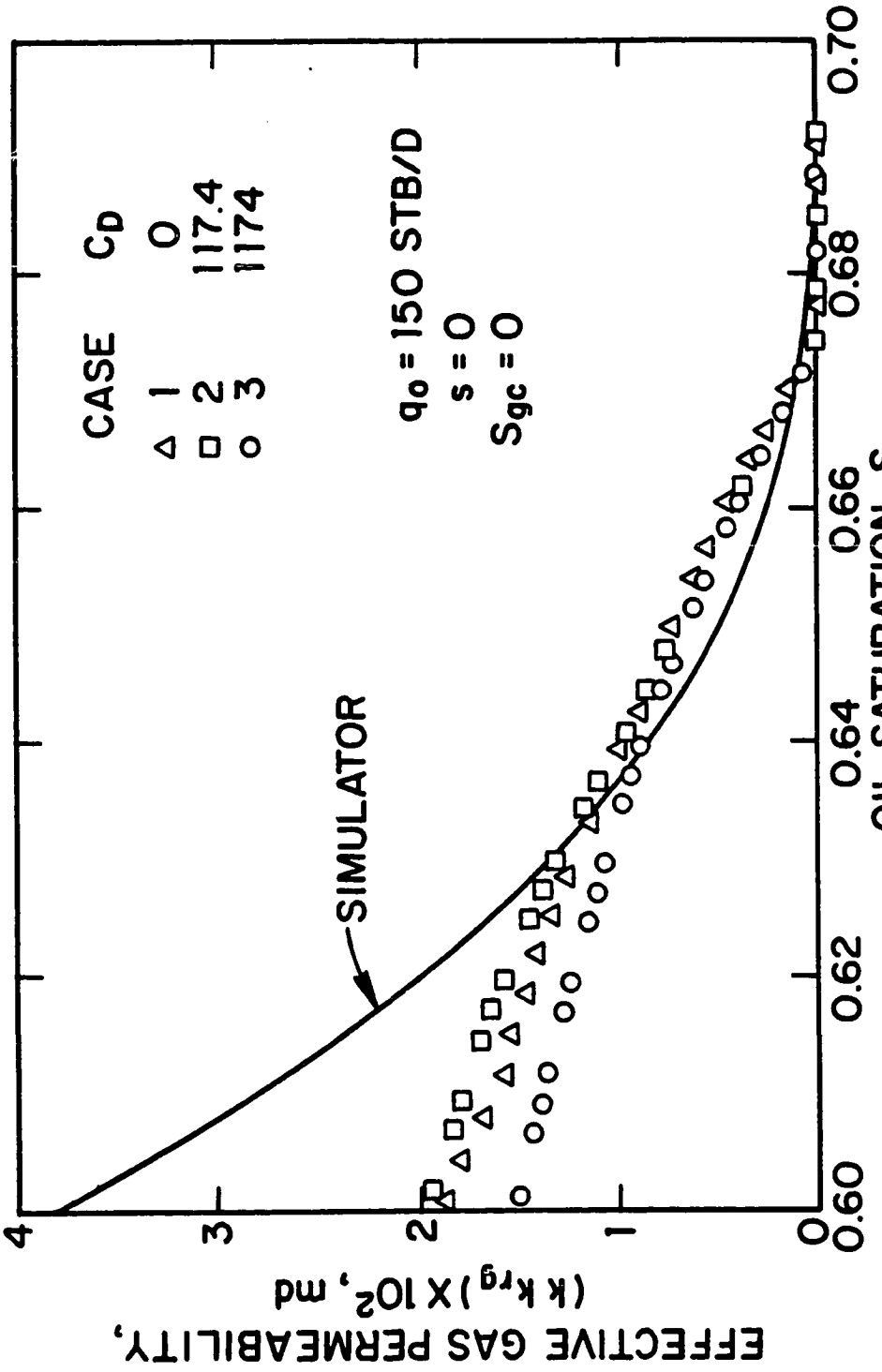

Fig. 7.7.8 - Effective gas permeability as a function of oil saturation; Cases 1-3.

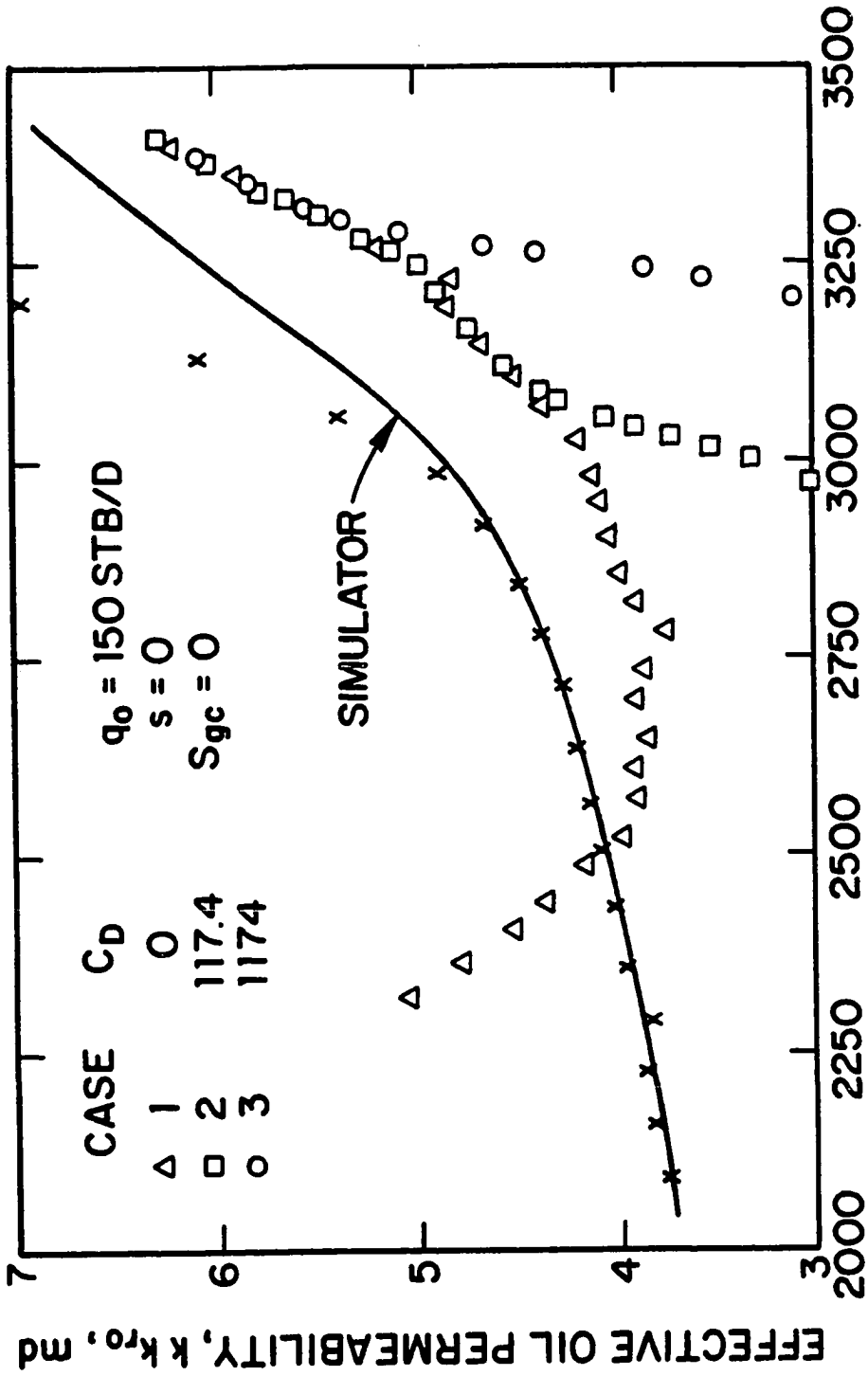

Fig. 7.7.9 - Effective oil permeability as a function of wellbore pressure from Eq. 7.7.3; Cases 1-3.

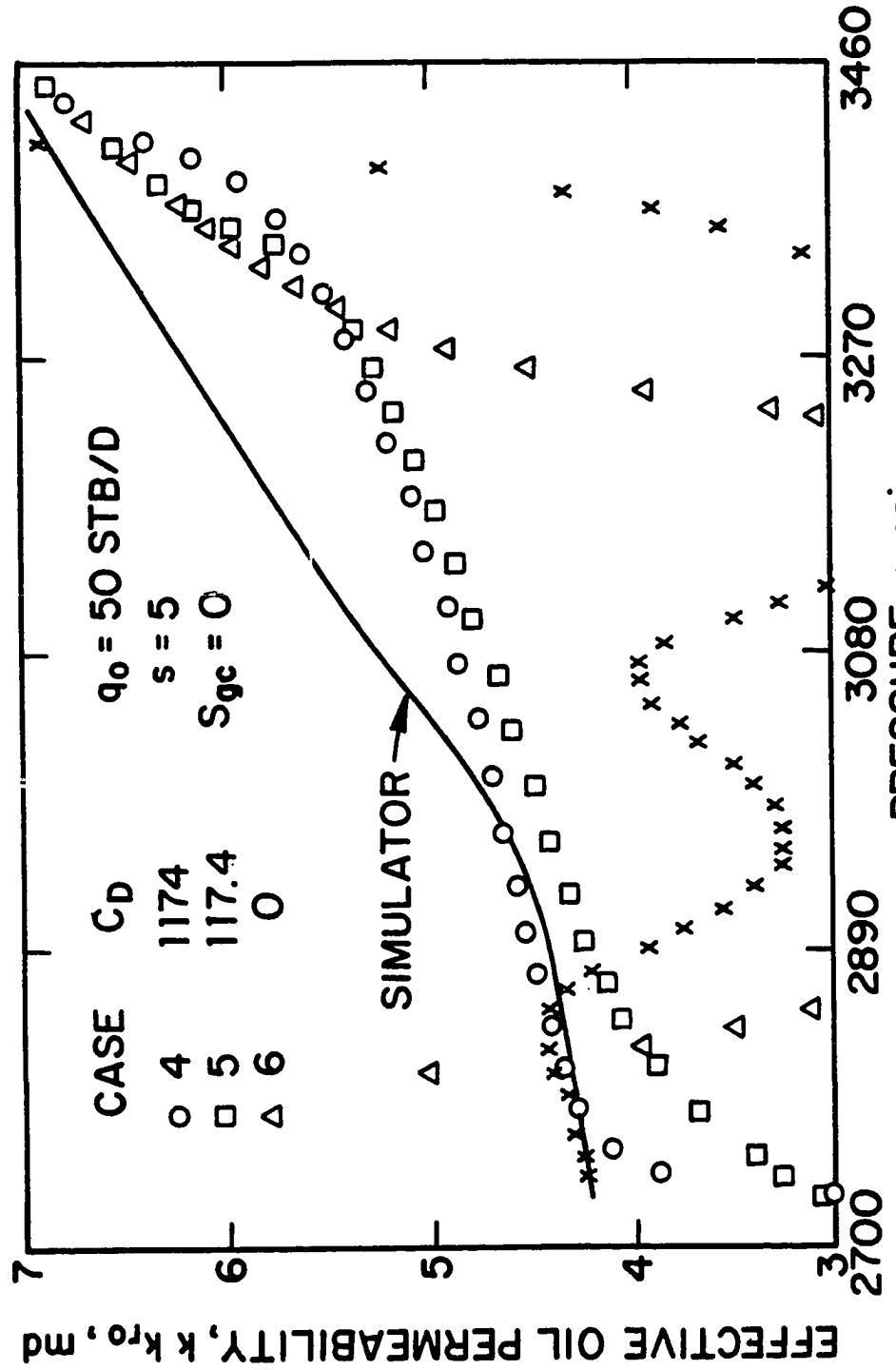

Fig. 7.7.10 - Effective oil permeability as a function of wellbore pressure; Cases 4-6.

wellbore pressure data for Cases 4-6. The computed values of kk_{ro} were obtained from Eq. 7.7.1 using the last drawdown value of effective permeability, $(kk_{ro})_{p_{wf,s}}$ when applying Eq. 7.7.6. The presence of skin effects results in inaccurate results during the time periods when the behavior of the skin zone has not yet stabilized. The presence of wellbore storage tends to balance the skin effects and the computed kk_{ro} values for all the cases are identical after the wellbore storage effects cease.

Fig. 7.7.11 is a plot of the simulator kk_{ro} values plotted against the simulator S_o values (solid line) and the computed kk_{ro} values obtained from Eq. 7.7.1 plotted versus the S_o values computed from Eq. 7.6.3 (data points) for Cases 4-6. The computed kk_{ro} versus S_o profile is in good overall agreement with the simulator one except for Case 6. Since the computed sandface oil saturation from Eq. 7.6.3 is in very good agreement with the simulator values (see Fig. 7.6.3), Fig. 7.7.11, like Fig. 7.7.10, suggests that the presence of afterflow effects during a pressure buildup test tend to balance the effects of the presence of a skin zone.

The effective gas permeability as a function of pressure is presented in Fig. 7.7.12 for the same cases, i.e., Cases 4-6. The kk_{rg} values shown by triangular, square and circular data points were computed from buildup data by using Eq. 7.7.7 and the data points shown by x were obtained from drawdown data using the kk_{ro} values obtained from the drawdown equivalent of Eq. 7.7.1 (see Chapter 6 and Refs. 9, 10, 28 and 29) and Eq. 7.7.7 with $R(\Delta t = 0)$ replaced by the instantaneous producing GOR (R) and p_{ws} replaced by p_{wf}.

The effective gas permeability as a function of sandface oil saturation are shown for the same cases in Fig. 7.7.13. The solid line represents the simulator results, whereas the data points correspond to the kk_{rg} values computed from Eq. 7.7.7 plotted against the S_o values computed from Eq. 7.6.3. Note that the results indicate that we only obtain rough estimates of the actual kk_{rg} versus S_o curve.

The values of kk_{ro} computed from Eq. 7.7.3 by neglecting the afterflow effects for Cases 4 and 5 are plotted versus pressure in Fig. 7.7.14. The estimated kk_{ro} values for Cases 4 and 5 are in good agreement with the simulator ones only at high values of pressure (late shut-in times); compare with Fig. 7.7.10.

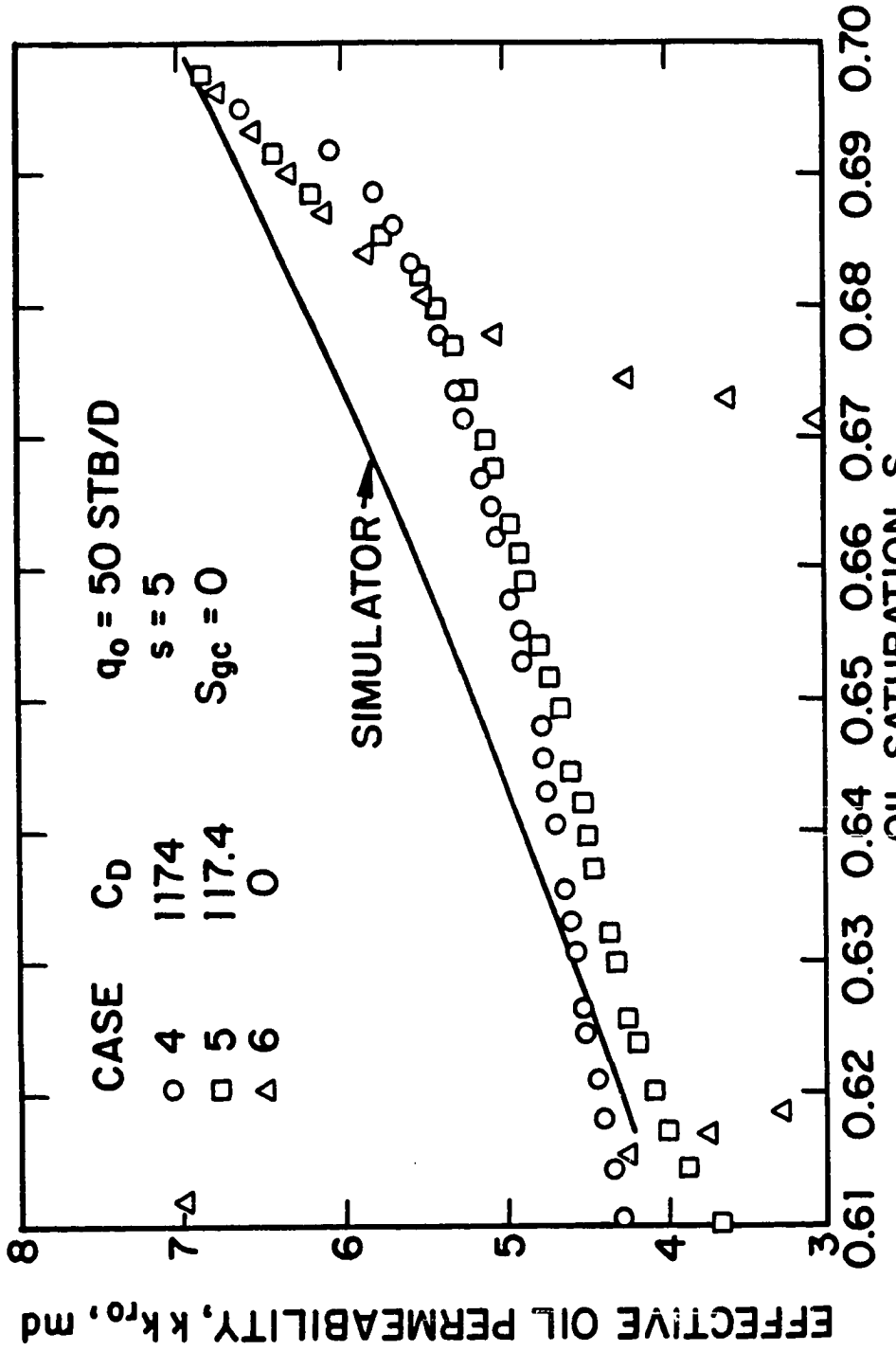

Fig. 7.7.11 - Effective oil permeability as a function of oil saturation; Cases 4-6.

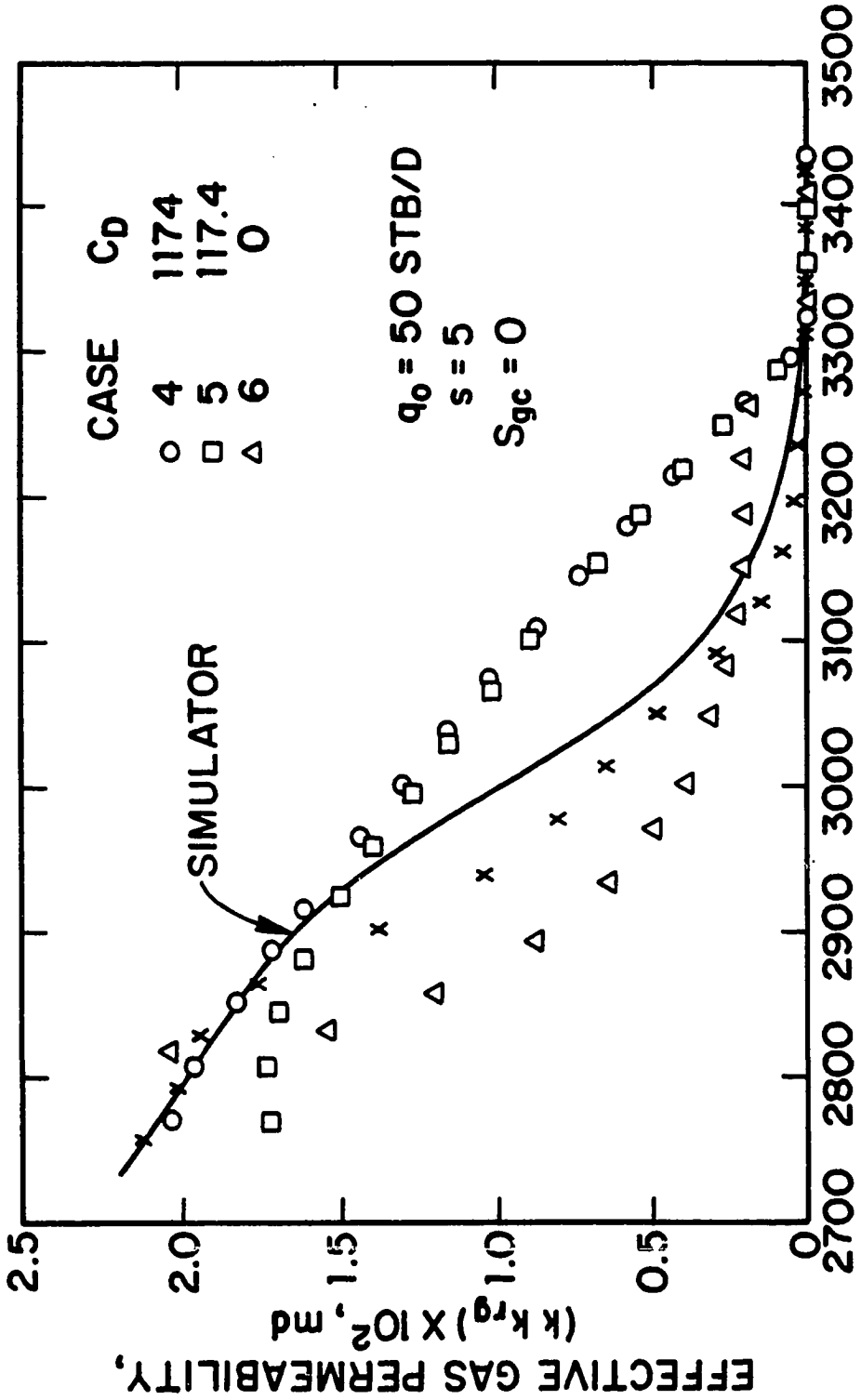

Fig. 7.7.12 - Effective gas permeability as a function of wellbore pressure; Cases 4-6.

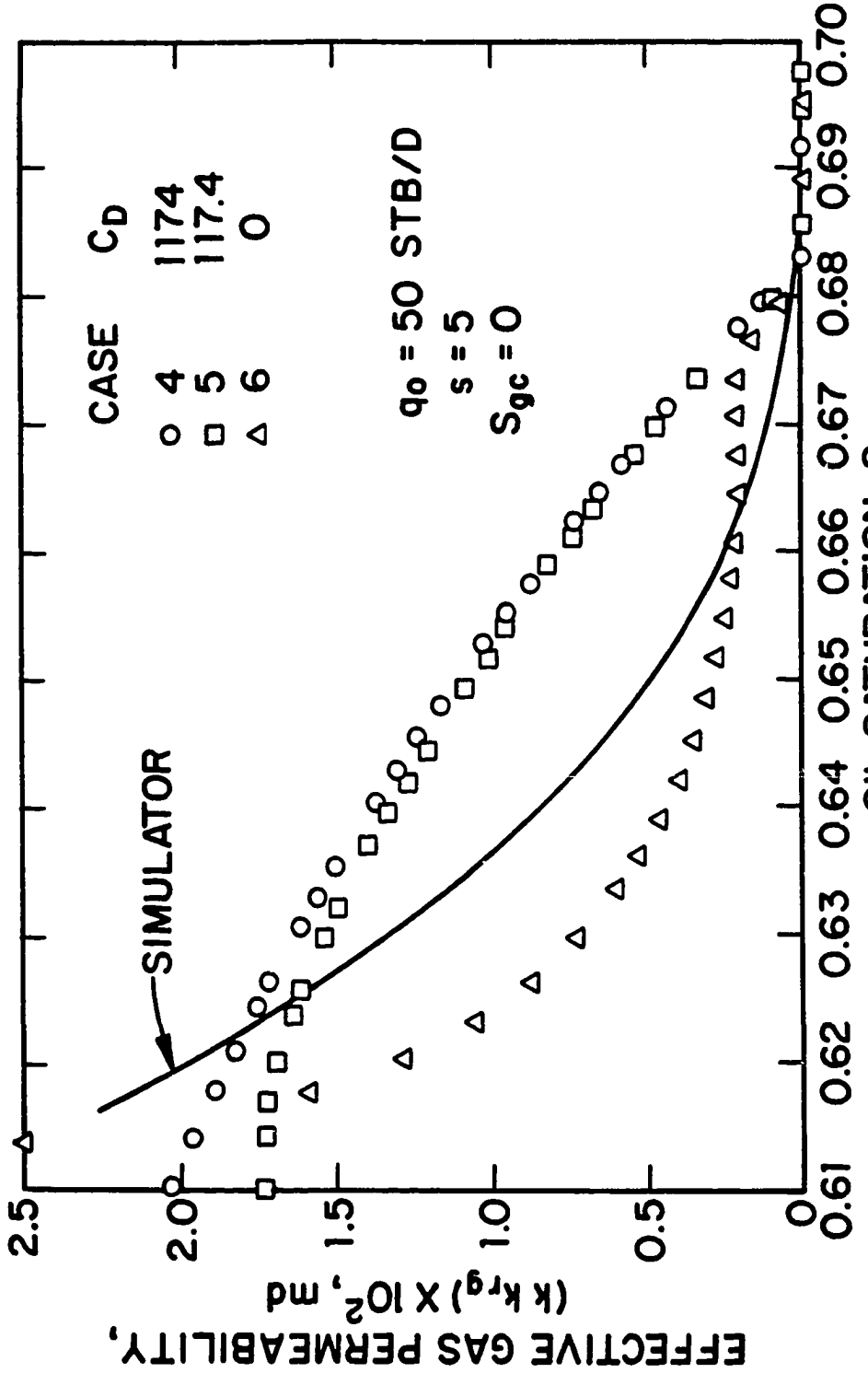

Fig. 7.7.13 - Effective gas permeability as a function of oil saturation; Cases 4-6.

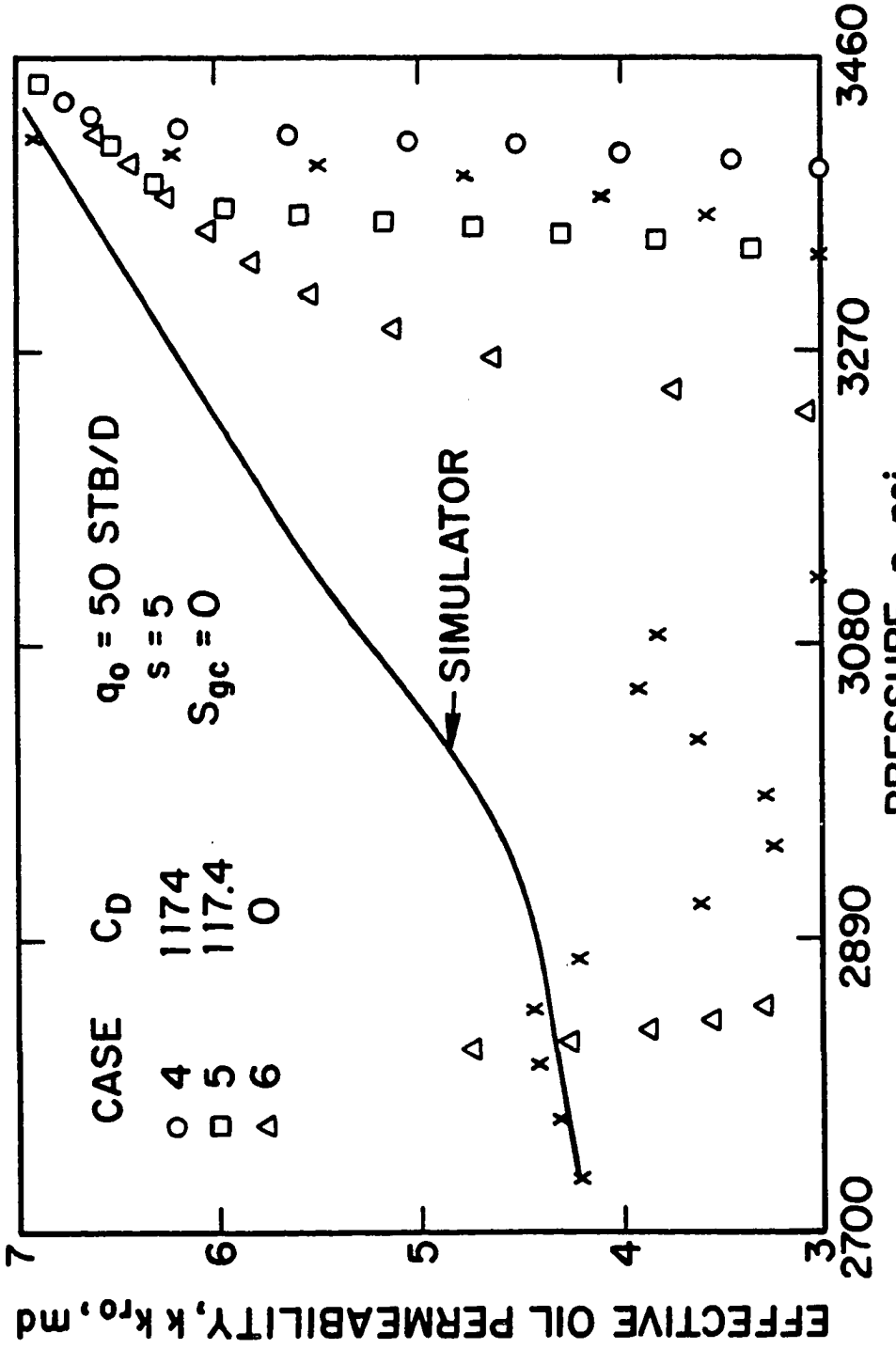

Fig. 7.7.14 - Effective oil permeability as a function of wellbore pressure from Eq. 7.7.3; Cases 4-6.

7.7.3 Influence of Critical Gas Saturation.

The results presented in the previous subsections are for cases where $S_{gc} = 0$. In this subsection, we consider results for Cases 7-9 so that data is influenced by both wellbore storage and critical gas saturation. Recall that for these cases $s = 0$, $q_o = 150$ STB/D and $S_{gc} = 0.07$.

For all the results shown in this subsection, the solid line corresponds to simulator values, the triangular data points represent the values for Case 7 ($C_D = 0$), the square data points represent values for Case 8 ($\beta^* = 6.8 \times 10^{-4}$, $C_D \approx 117.4$) and the circular data points are the values for Case 9 ($\beta^* = 6.8 \times 10^{-5}$, $C_D \approx 117.4$). The x data points represent the results computed from drawdown pressure versus time data (see Chapter 6 and Refs. 8, 9, 10, 28 and 29).

Fig. 7.7.15 is a plot of simulated or computed effective oil permeability versus wellbore pressure data for Cases 7-9. Again, the computed values of kk_{ro} were obtained from Eq. 7.7.1 using the value of $(kk_{ro})_{p_{wf.}}$ obtained from drawdown data when using Eq. 7.7.6. Fig. 7.7.16 is a plot of the simulator kk_{ro} values plotted against the simulator S_o values (solid line) and the computed kk_{ro} obtained from Eq. 7.7.1 plotted versus the S_o values computed from Eq. 7.6.3 (data points) for Cases 7-9. Finally, the effective gas permeability as a function of pressure is presented in Fig. 7.7.17 for the same cases, i.e., Cases 7-9. The kk_{rg} values were computed from buildup data by using Eq. 7.7.7 (triangular, square and circular data points) and from drawdown data based on computational procedures outlined in Refs. 9, 10, 28 and 29. All figures suggest that the presence of critical gas saturation does not greatly affect the computed kk_{ro} values for any of the cases. The computed values of effective permeabilities give rough approximations of the correct (simulated) effective permeability values. The behavior of the computed kk_{ro} and kk_{rg} values for these cases is similar to those shown for Cases 1-3; see Figs. 7.7.1 through 7.7.3.

The effective gas permeabilities as a function of sandface oil saturation are shown for the same cases in Fig. 7.7.18. The solid line represents the simulator results, whereas the data points correspond to the kk_{rg} values computed from

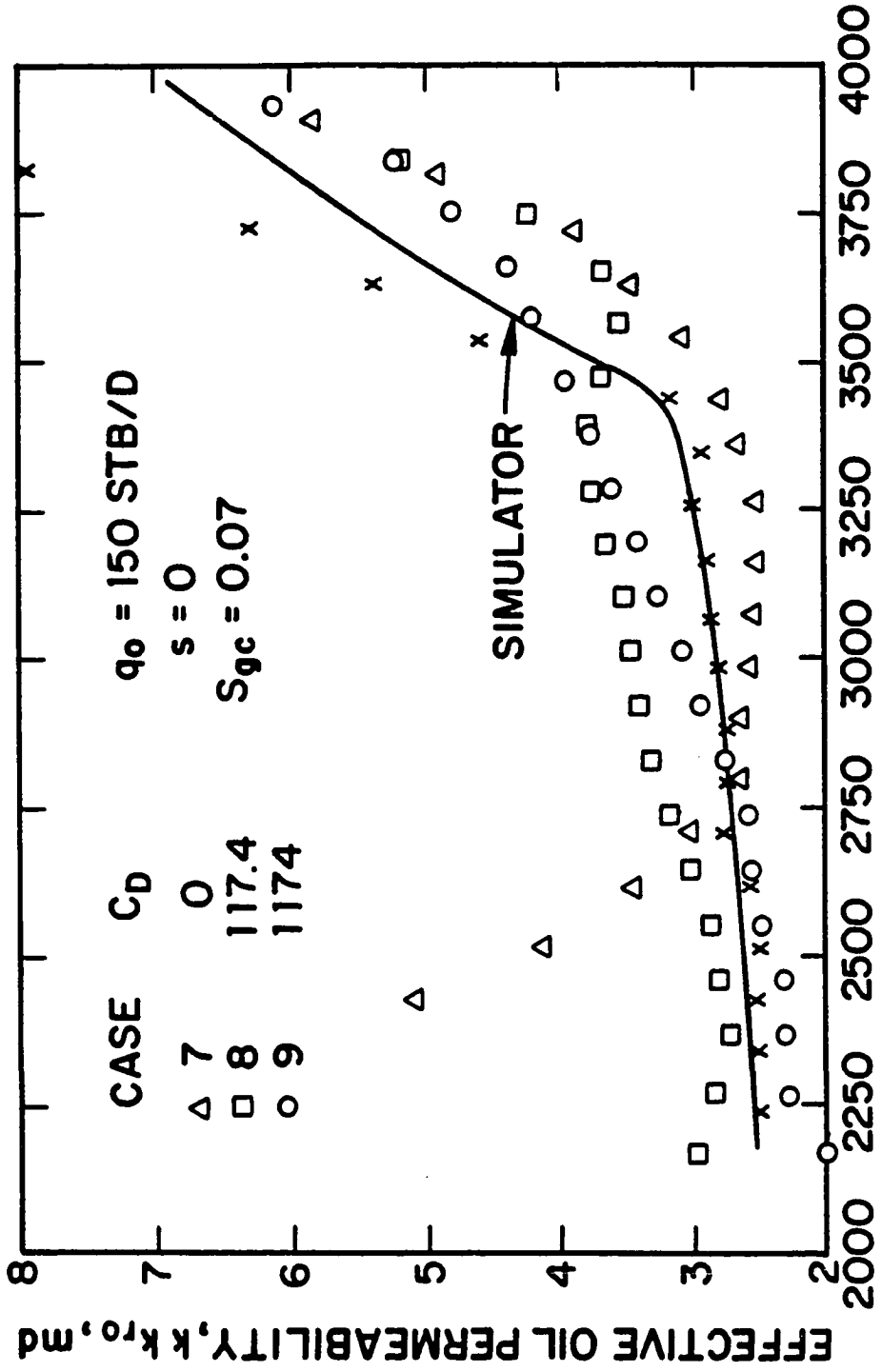

Fig. 7.7.15 - Effective oil permeability as a function of wellbore pressure; Cases 7-9.

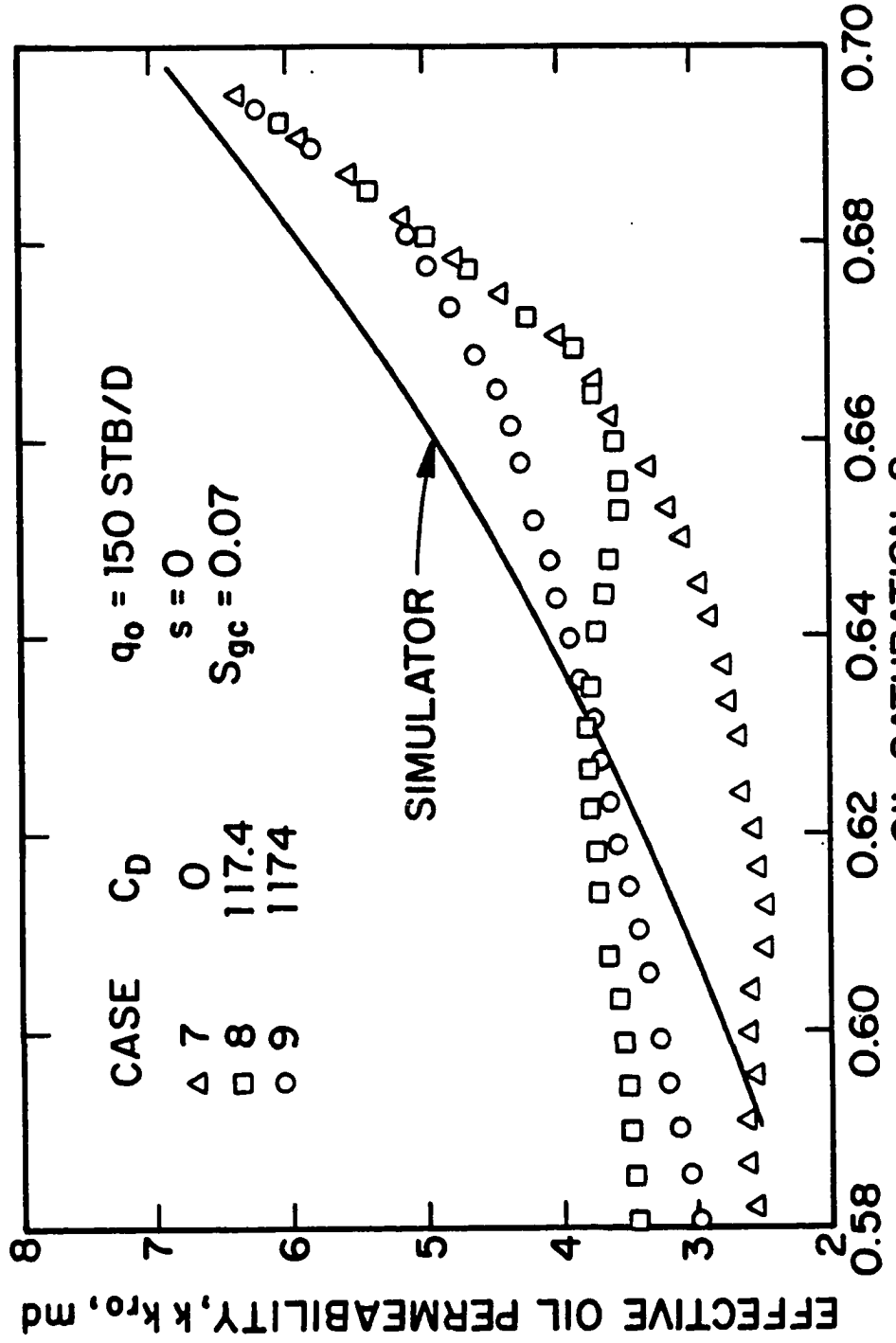

Fig. 7.7.16 - Effective oil permeability as a function of oil saturation; Cases 7-9.

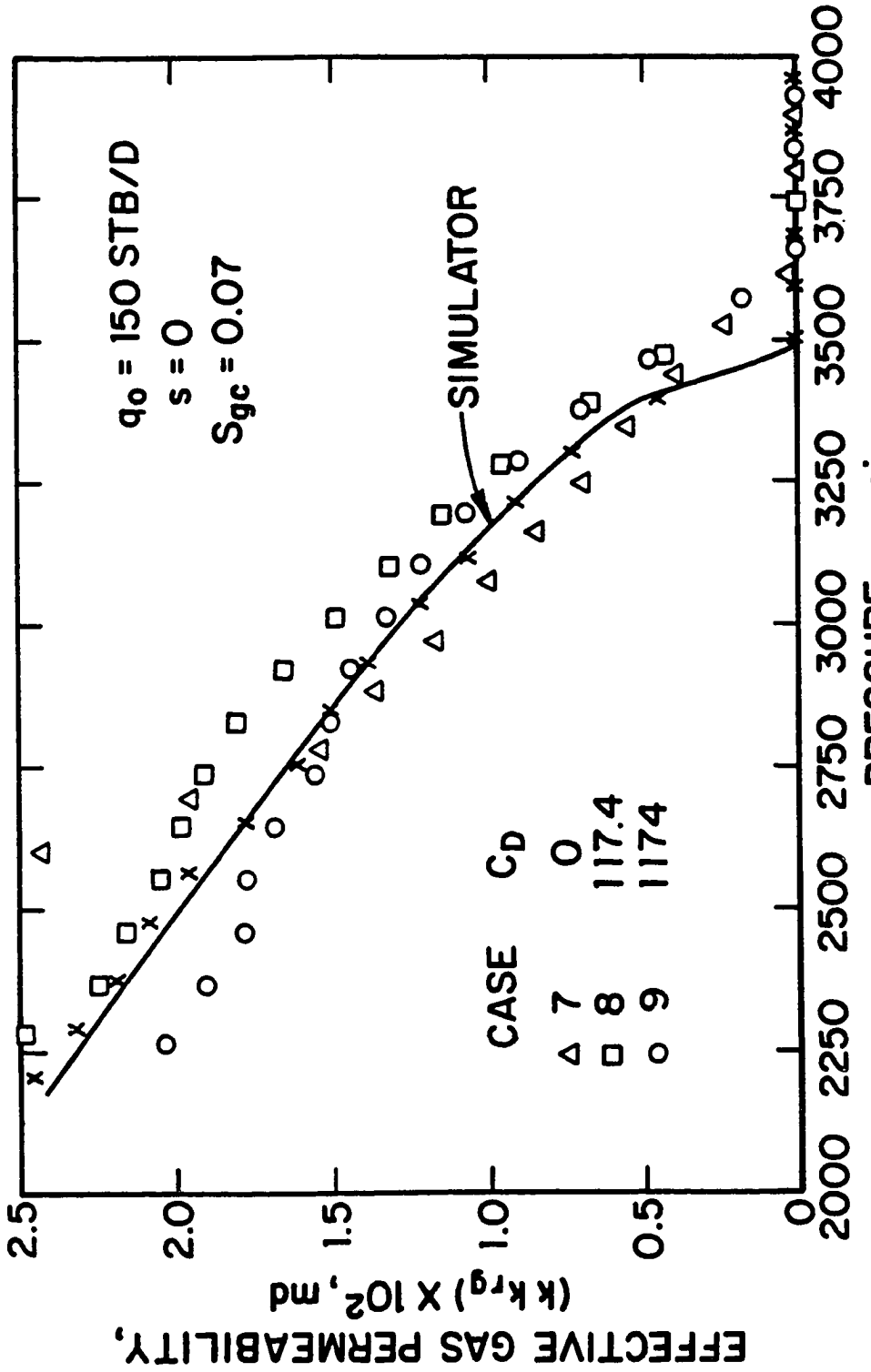

Fig. 7.7.17 - Effective gas permeability as a function of wellbore pressure; Cases 7-9.

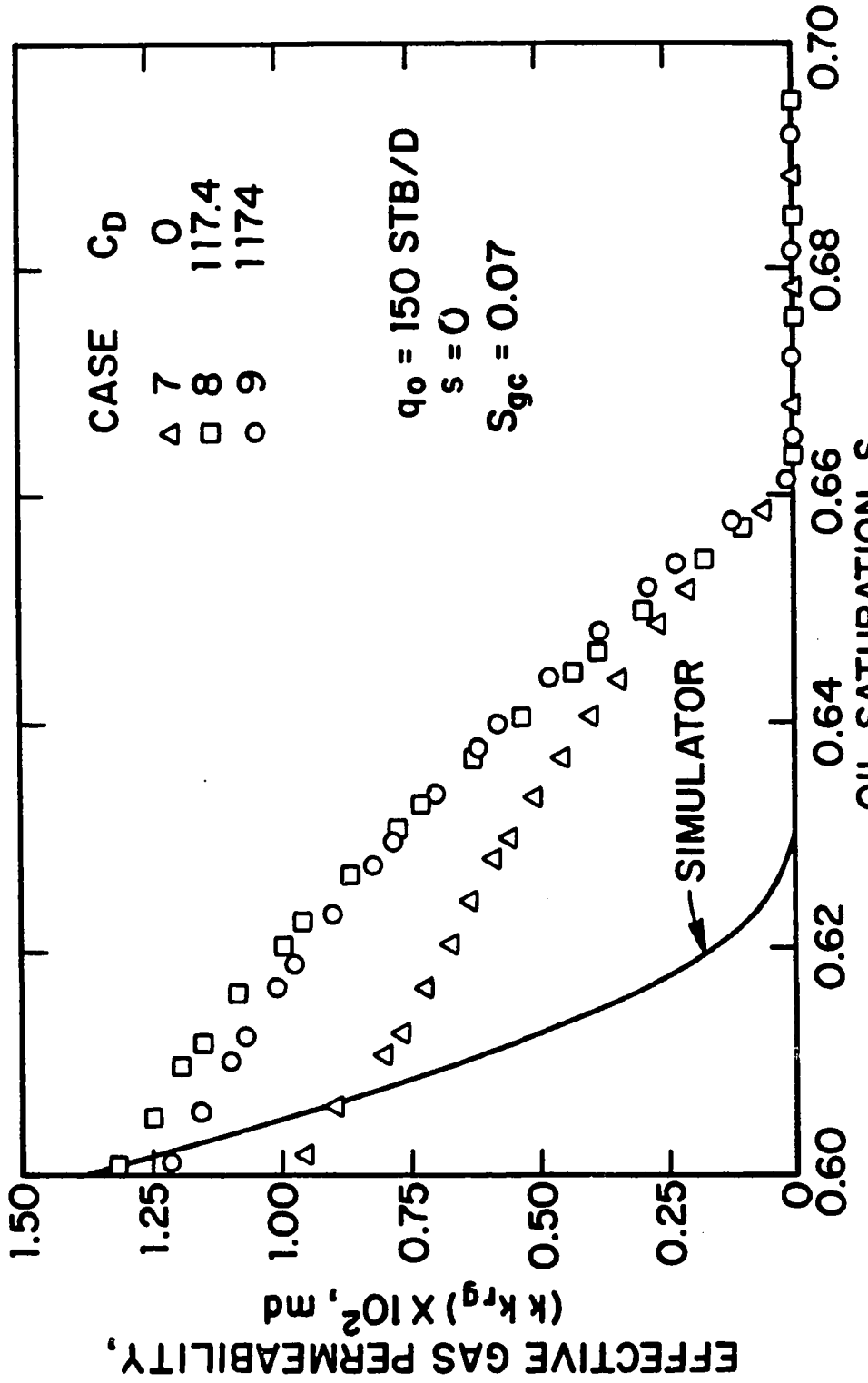

Fig. 7.7.18 - Effective gas permeability as a function of oil saturation; Cases 7-9.

Eq. 7.7.7 plotted against the S_o values computed from Eq. 7.6.3. The agreement between computed and simulated results is good only for $S_o > 0.66$ and in this saturation range $kk_{rg} \approx 0$. The problem here is that Eq. 7.6.3 yields accurate estimates of the drawdown sandface oil saturation/wellbore pressure for $S_o > 0.66$ (see Fig. 7.6.6).

Fig. 7.7.19 shows the computed kk_{ro} values obtained from Eq. 7.7.1 which ignores the afterflow effects for Cases 8 and 9. As in the previous cases, the estimated oil effective permeability based on the computational procedures of Ref. 10 yields good results only when afterflow becomes negligible.

7.8 Pressure-Squared Method

7.8.1 Constant Rate Production.

For all cases considered in Refs. 9, 10, 12, 28, 29 and 45, it was found that the sandface value of $\alpha = k_{ro}/(\mu_o B_o)$ versus p_{ws} could be well approximated by a piecewise linear function, i.e., by two straight lines. Mathematically this result can be expressed as

$$\alpha = \frac{k_{ro}}{\mu_o B_o} = ap_{ws} + d; \qquad for \quad p_{ws} \leq p_1, \tag{7.8.1}$$

and

$$\alpha = \frac{k_{ro}}{\mu_o B_o} = bp_{ws} + c; \qquad for \quad p_1 \leq p_{ws} \leq p_i, \tag{7.8.2}$$

where p_1 is the pressure at which these two straight lines intersect. In Eqs. 7.8.1 and 7.8.2, a, b, c and d are constants.

By using Eqs. 7.8.1 and 7.8.2 in Eq. 7.5.4, integrating and rearranging the resulting equation, Ref. 10 obtained the following result:

$$\frac{\hat{b}kh\left(p_{ws}^2 - p_{wf,s}^2\right)}{141.2\,(2q_o)} = 1.151\log\left(\frac{4t_D}{e^\gamma}\right) + s + \frac{\left(\hat{b} - \hat{a}\right)kh\left(p_1^2 - p_{wf,s}^2\right)}{141.2\,(2q_o)} - 1.151\log\left(R_{H1}\right), \tag{7.8.3}$$

where

$$\hat{a} = a + \frac{2d}{p_1 + p_{wf,s}}, \tag{7.8.4}$$

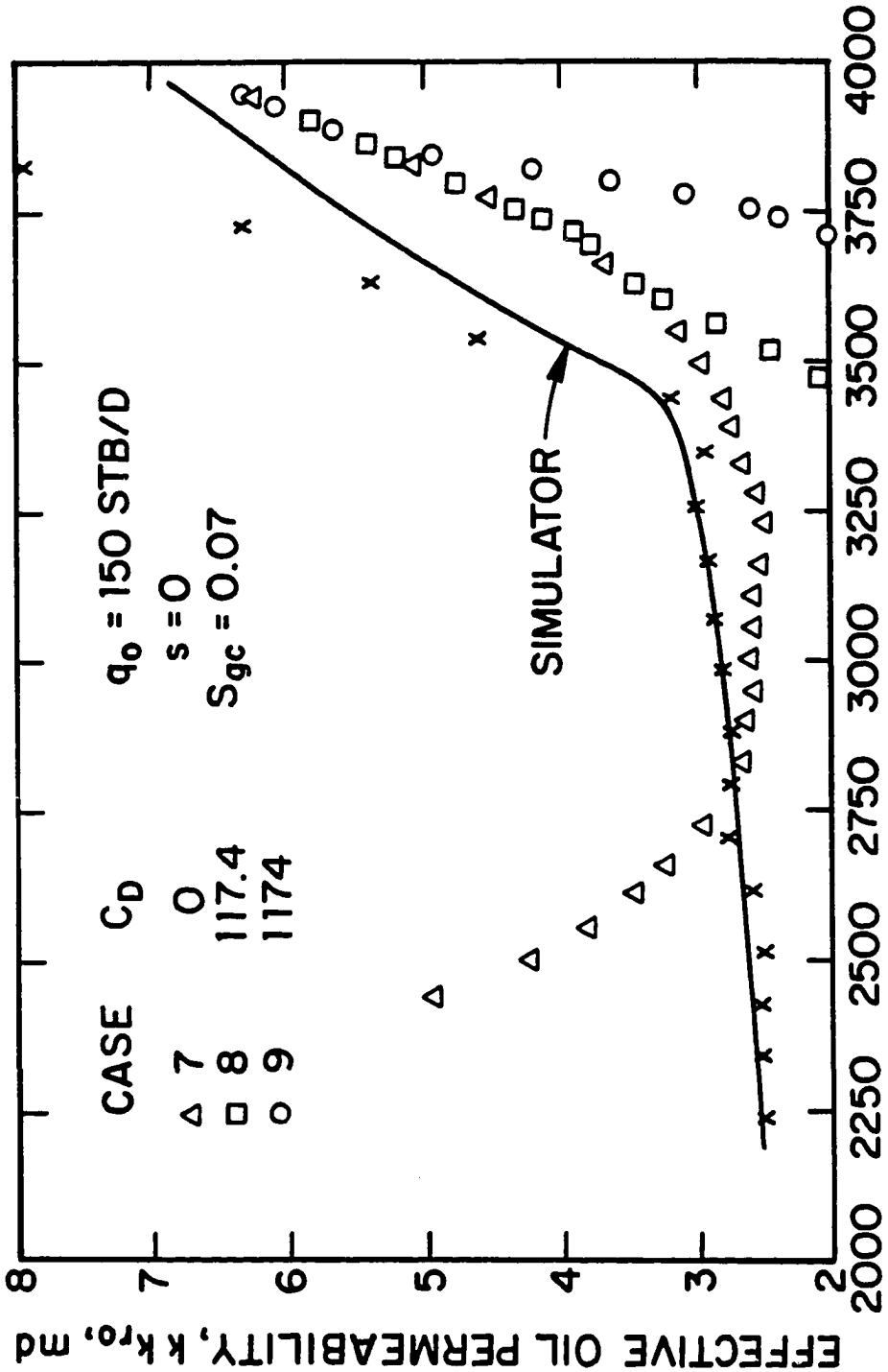

Fig. 7.7.19 - Effective oil permeability as a function of wellbore pressure from Eq. 7.7.3; Cases 7-9.

and

$$\hat{b} = b + \frac{2c}{p_{ws} + p_1}. \tag{7.8.5}$$

Eq. 7.8.3 applies for $p_{ws} > p_1$ and the constants $\hat{a}$ and $\hat{b}$ are defined differently for buildup from drawdown; see Ref. 10. Fig. 7.8.1 shows a plot of the drawdown $\alpha = k_{ro}/(\mu_o B_o)$ versus p_{wf} simulator results (solid curve) for Cases 1-3. The mobility profile can be approximated very well by two straight lines (dashed lines) which intersect at $p_1 = 2902.18$ psi. The wellbore pressure at the instant of shut-in was $p_{wf,s} = 2032.65$ psi. The constants a, b, c and d are given in Fig. 7.8.1 and the values of $\hat{a}$ and $\hat{b}$ computed from Eqs. 7.8.4 and 7.8.5 are $\hat{a} = 2.136 \times 10^{-4}$ and $\hat{b} = 2.525 \times 10^{-4}$.

Eq. 7.8.3 indicates that a semilog plot of $p_{ws}^2 - p_{wf,s}^2$ versus R_{H1} will be a straight line of slope

$$m_2 = \frac{162.6(2q_o)}{\hat{b}kh}, \tag{7.8.6}$$

and $\hat{b}k$ can be computed from this semilog slope by the following equation:

$$\hat{b}k = \frac{162.6(2q_o)}{m_2 h}. \tag{7.8.7}$$

Note that Eq. 7.8.5 indicates $\hat{b}$ depends on the shut-in pressure, p_{ws}, unless the constant c in Eq. 7.8.2 and 7.8.5 is zero which is not usually the case. If $c \neq 0$, $\hat{b}$ varies with shut-in pressure and one does not obtain a true semilog straight line. However, for all cases considered in Refs. 10 and 28, it was found that a semilog plot of $p_{ws}^2 - p_{wf,s}^2$ versus the Horner time ratio exhibited a well-defined apparent semilog straight line for some range of shut-in pressure. Moreover, if this semilog straight line occurs during the interval $p_2 \leq p_{ws} \leq p_3$, then the semilog slope obtained is given by m_2 (Eq. 7.8.6) where

$$\hat{b} \approx b + \frac{2c}{p_3 + p_2}. \tag{7.8.8}$$

As shown in Ref. 10, during the time interval (or pressure interval) where this semilog straight line exists, Eq. 7.8.2 can be roughly approximated by

$$\frac{k_{ro}}{\mu_o B_o} = bp_{ws} + c = \hat{b}p_{ws}, \tag{7.8.9}$$

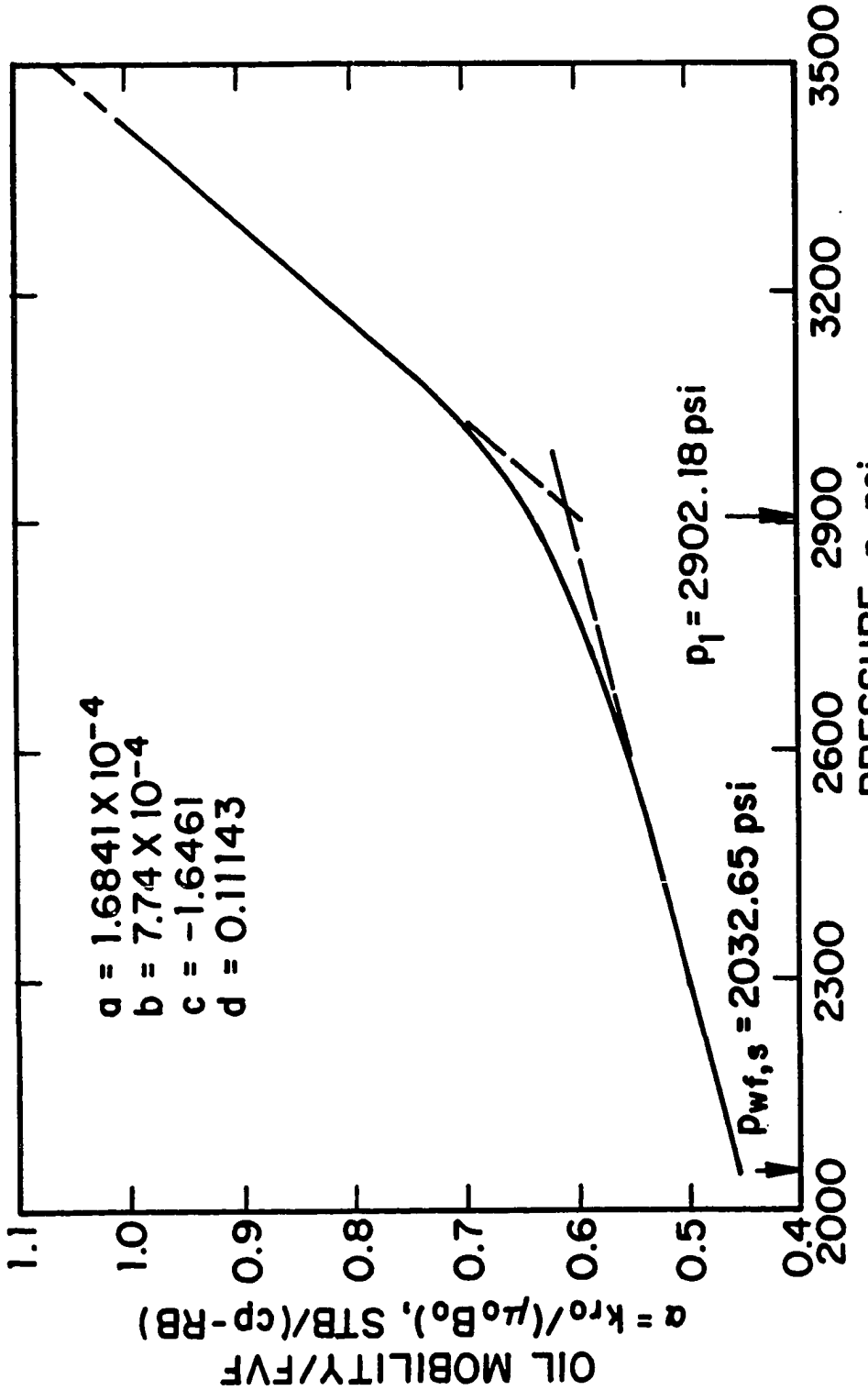

Fig. 7.8.1 - Oil mobility / FVF as a function of wellbore pressure; Cases 1-3.

or

$$\frac{kk_{ro}}{\mu_o B_o} = k(bp_{ws} + c) = \hat{b}kp_{ws}. \tag{7.8.10}$$

A schematic diagram of the approximation of Eq. 7.8.9 is shown in Fig. 7.8.2. The solid curve represents a schematic diagram of the actual drawdown $\alpha = k_{ro}/(\mu_o B_o)$ versus pressure relation and the three dashed lines represent three possible $p_2 \leq p_{ws} \leq p_3$ pressure intervals where an apparent semilog straight line could occur on a Horner plot of $p_{ws}^2 - p_{wf,s}^2$ (or just p_{ws}^2) versus $(t+\Delta t)/\Delta t$. Which of these possibilities actually occurs would depend on the producing time and the length of the buildup period. In fact, it is at least theoretically possible that the Horner plot could exhibit two straight lines and we have found cases where this occurs when using buildup data generated from our simulator. Note that on each $p_2 \leq p_{ws} \leq p_3$ pressure interval shown in Fig. 7.8.2, the actual kk_{ro} curve (solid curve) is well approximated by a straight line of the form given by Eq. 7.8.2.

Also note that the schematic diagram of Fig. 7.8.2 indicates that we need as many as four straight lines to approximate the actual α versus p curve with a piecewise linear function. Even if this is the case, one can still obtain a semilog approximation of the form of Eq. 7.8.3. This can be seen as follows:

If

$$\alpha = bp_{ws} + c; \qquad for \quad p_2 \leq p_{ws} \leq p_3, \tag{7.8.11}$$

then for $p_2 \leq p_{ws} \leq p_3$,

$$\begin{aligned}\int_{p_{wf,s}}^{p_{ws}} \alpha dp &= \int_{p_{wf,s}}^{p_2} \alpha dp + \int_{p_2}^{p_{ws}} (bp_{ws} + c)dp \\ &= \int_{p_{wf,s}}^{p_2} \alpha dp + \frac{b}{2}\left(p_{ws}^2 - p_2^2\right) + c\left(p_{ws} - p_2\right) \\ &\approx \frac{\hat{b}}{2}\left(p_{ws}^2 - p_2^2\right) + \int_{p_{wf,s}}^{p_2} \alpha dp. \end{aligned} \tag{7.8.12}$$

Since the last integral in Eq. 7.8.12 is a constant, using Eq. 7.8.12 in Eq. 7.5.4 and rearranging the resulting equation, one obtains an equation of the form

$$\frac{\hat{b}kh\left(p_{ws}^2 - p_{wf,s}^2\right)}{141.2\,(2q_o)} = 1.151\log\left(\frac{4t_D}{e^{\gamma}}\right) - 1.151\log\left(R_{H1}\right) + s + s_p, \tag{7.8.13}$$

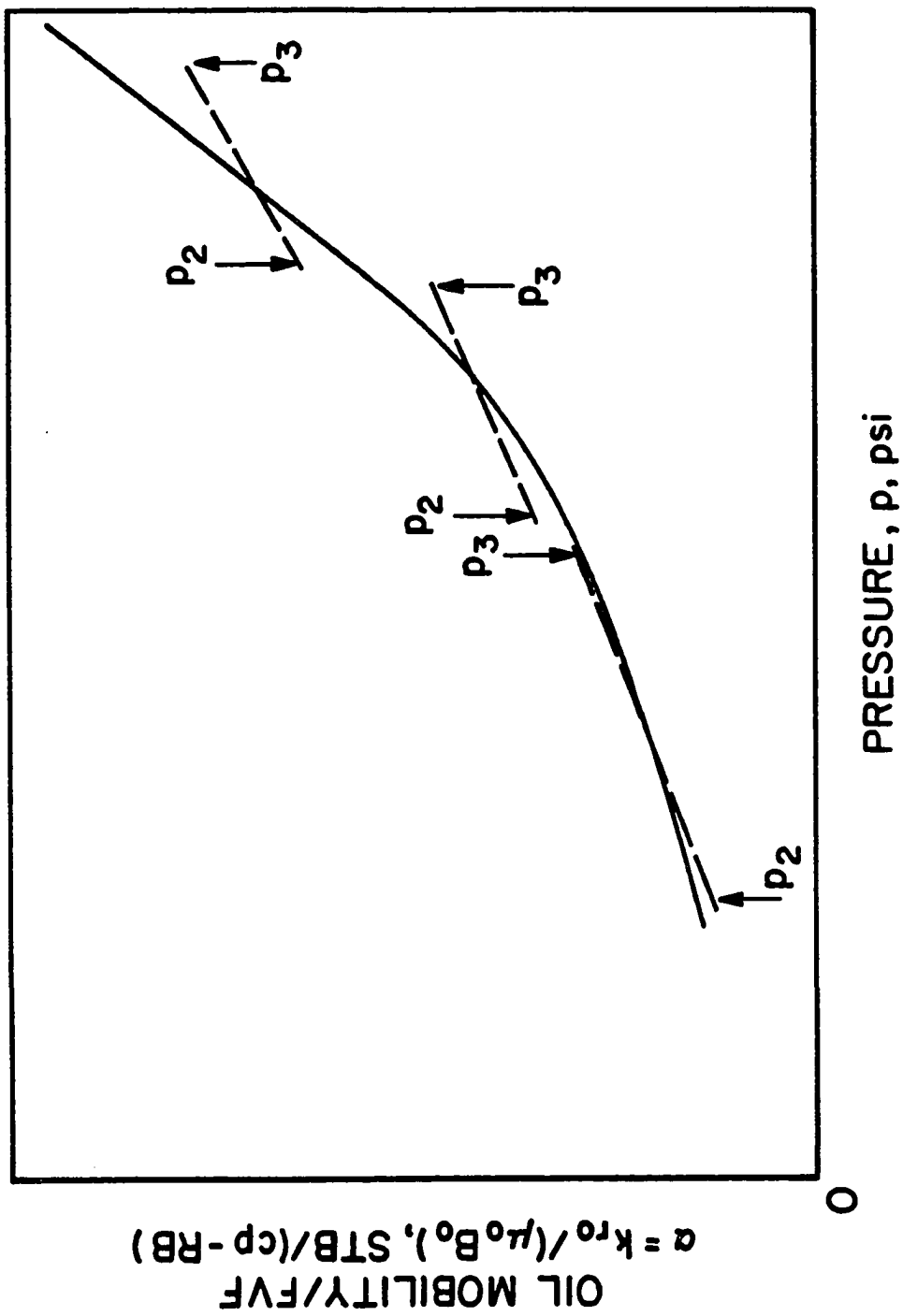

Fig. 7.8.2 - Approximation of oil mobility / FVF for pressure-squared method.

where $\hat{b}$ is given by Eq. 7.8.5 with p_1 replaced by p_2, p_{ws} replaced by p_3 and

$$s_p = \frac{kh}{141.2(2q_o)}\left\{\frac{\hat{b}}{2}(p_2^2 - p_{wf,s}^2) - \int_{p_{wf,s}}^{p_2} \alpha dp\right\}. \tag{7.8.14}$$

When Eq. 7.8.13 applies, we still obtain a semilog straight line of slope m_2 given by Eq. 7.8.6.

By multiplying the approximation of Eq. 7.8.10 by $\mu_o B_o$ one obtains

$$(kk_{ro})_{p_{ws}} = (\hat{b}k)(\mu_o B_o)_{p_{ws}} p_{ws}, \tag{7.8.15}$$

where $\hat{b}k$ denotes the value computed from Eq. 7.8.7. Eq. 7.8.15 provides a means to obtain kk_{ro} as a function of p_{ws}. Note, however, that Eq. 7.8.15 (and Eq. 7.8.10) only makes sense for values of p_{ws} in the range where the semilog straight line of Eq. 7.8.3 (or Eq. 7.8.13) occurs. Moreover, values of kk_{ro} computed from Eq. 7.8.15 will duplicate the values satisfying the approximation $(kk_{ro})/(\mu_o B_o) = \hat{b}kp_{ws}$ instead of the actual α versus p curve, that is, the values obtained from Eq. 7.8.15 will follow one of the dashed lines in Fig. 7.8.2. Thus, the values obtained from Eq. 7.8.15 will fall on a line that crosses the actual kk_{ro} versus pressure curve. The closed square data points in Fig. 7.8.3 represent the kk_{ro} values computed from Eq. 7.8.15 for Case 5. The results of this figure agree with the conclusions derived above based on a theoretical analysis. If we extrapolate Eq. 7.8.15 to initial pressure, we can obtain a rough estimate of the initial effective oil permeability from the following equation:

$$kk_{roi} = (kk_{ro})_{p_i} = (\hat{b}k)(\mu_o B_o)_{p_i} p_i. \tag{7.8.16}$$

As indicated by the dashed line on the schematic diagram of Fig. 7.8.2, Eq. 7.8.16 will usually yield an underestimate of kk_{roi}.

As shown in Ref. 10, an equation for estimating the skin factor can also be derived directly from Eq. 7.8.3. The relevant equation is given by

$$s = 1.151\left(\frac{(p_{ws}^2 - p_{wf,s}^2)_{1hr}}{m_2} - \log\left(\frac{kk_{roi}}{\phi\mu_{oi}c_{ti}r_w^2}\right) + 3.23\right), \tag{7.8.17}$$

where $(p_{ws}^2 - p_{wf,s}^2)_{1hr}$ denotes the value of $p_{ws}^2 - p_{wf,s}^2$ obtained by extrapolating the pressure-squared semilog straight line to a shut-in time of $\Delta t = 1$ hour. Since

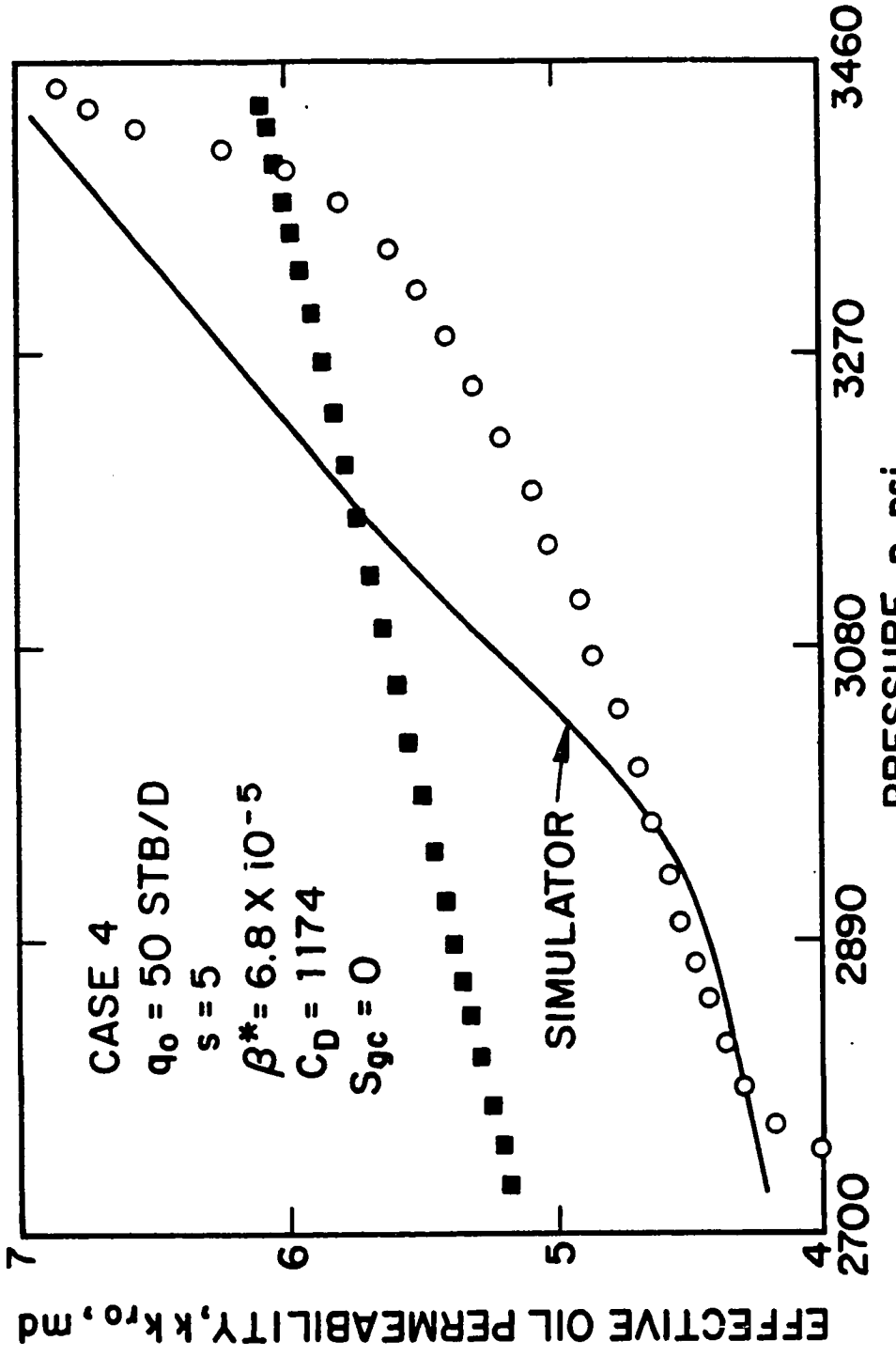

Fig. 7.8.3 - Effective oil permeability as a function of wellbore pressure; Case 4.

Eq. 7.8.17 ignores the terms of Eq. 7.8.3 which involve $\hat{b} - \hat{a}$, Eq. 7.8.17 is only approximate. Moreover, for all cases considered in Refs. 9, 10, 12, 28 and 29, $\hat{b} - \hat{a} > 0$ and thus, Eq. 7.8.3 indicates that Eq. 7.8.17 will yield an overestimate of the skin factor. As shown in Ref. 10 and in Chapter 6 (also see Ref. 29) this is the normal case, however, if one could find rock and fluid properties such that $\hat{b} - \hat{a} < 0$, then Eq. 7.8.17 would yield an underestimate of the skin factor. (On the other hand, the analysis of drawdown pressure data using the pressure-squared method typically underestimates the skin factor; see Refs. 10 and 29.) Based on the results presented in Refs. 9, 10, 12, 28 and 29 and results presented later in this Chapter, the value of s obtained from Eq. 7.8.17 should differ from the correct value of s by no more than one or two units.

In the following two subsections, we present the working equation for pressure-squared analysis based on logarithmic convolution time and rate normalization.

7.8.2 Pressure-Squared Analysis With Logarithmic Convolution Time.

Starting from Eq. 7.5.8 and using the same approximations (Eqs. 7.8.1 and 7.8.2) that led to Eq. 7.8.3, one can show that

$$\frac{\hat{b}kh\left(p_{ws}^2 - p_{wf,s}^2\right)}{141.2 \times 2\Big(q_o - q_{osf}(t+\Delta t)\Big)} = 1.151\Delta t_{lcD} + s + \left[\frac{\left(\hat{b} - \hat{a}\right)kh\left(p_1^2 - p_{wf,s}^2\right)}{141.2 \times 2\Big(q_o - q_{osf}(t+\Delta t)\Big)}\right]. \tag{7.8.18}$$

Ignoring the terms involving $\hat{b} - \hat{a}$ and using Eq. 7.5.10, we can rewrite Eq. 7.8.18 as

$$\frac{p_{ws}^2 - p_{wf,s}^2}{\Delta q\,(\Delta t)} = m_3\left(\Delta t_{lc} + \tilde{s}\right), \tag{7.8.19}$$

where

$$m_3 = \frac{2 \times 162.6}{\hat{b}kh}, \tag{7.8.20}$$

and

$$\tilde{s} = \log\left(\frac{kk_{roi}}{\phi\mu_{oi}c_{ti}r_w^2}\right) - 1.847 + 0.87s. \tag{7.8.21}$$

Eq. 7.8.19 indicates that a plot of $(p_{ws}^2 - p_{wf,s}^2)/\Delta q\,(\Delta t)$ versus the logarithmic convolution shut-in time, Δt_{lc}, will exhibit a Cartesian straight line with slope

equal to m_3. The corresponding value of $\hat{b}k$ can be obtained from the following rearrangement of Eq. 7.8.20:

$$\hat{b}k = \frac{2 \times 162.6}{m_3 h}. \tag{7.8.22}$$

Using this value of $\hat{b}k$, one can compute effective oil permeability as a function of the wellbore pressure from

$$(kk_{ro})_{p_{wf}} = (\hat{b}k)(\mu_o B_o)_{p_{wf}} p_{wf}. \tag{7.8.23}$$

As in the constant rate case, the kk_{ro} versus p_{wf} relation obtained from Eq. 7.8.23 will be a line (curve) that crosses the actual kk_{ro} versus pressure curve; see Fig. 7.8.2. Extrapolating Eq. 7.8.23 to initial pressure, we can obtain a rough estimate of the initial effective oil permeability from the following equation:

$$kk_{roi} = (kk_{ro})_{p_i} = (\hat{b}k)(\mu_o B_o)_{p_i} p_i. \tag{7.8.24}$$

As in the constant rate case, Eq. 7.8.24 will typically yield an underestimate of kk_{roi}. By extrapolating Eq. 7.8.19 to $\Delta t_{lc} = 0$ to obtain $\left[(p_{wf}^2 - p_{wf,s}^2)/\Delta q(\Delta t)\right]_{ext}$ and rearranging the resulting equation, one obtains the following equation:

$$s = 1.151 \left(\frac{\left[(p_{wf}^2 - p_{wf,s}^2)/\Delta q(\Delta t)\right]_{ext}}{m_3} - \log\left(\frac{kk_{roi}}{\phi \mu_{oi} c_{ti} r_w^2}\right) + 1.847 \right). \tag{7.8.25}$$

Note our derivation of Eq. 7.8.25 ignored the term in square brackets in Eq. 7.8.18 and thus, as in the constant rate case, Eq. 7.8.25 is only approximate. As this term involves $\Delta q(\Delta t)$ which changes with time, a straight line cannot be obtained unless the variation of the term of Eq. 7.8.18 within square brackets is small, or is negligible compared to the other terms in Eq. 7.8.18. As in the pressure-squared method, Eq. 7.8.25 will yield an overestimate of the skin factor if $\hat{b} - \hat{a} > 0$ and an underestimate of the skin factor if $\hat{b} - \hat{a} < 0$. In all cases considered in Chapter 6 (also see Ref. 29) and in this Chapter it was always found that $\hat{b} - \hat{a} > 0$.

7.8.3 Rate Normalization for Pressure-Squared Method.

In this subsection, we present the working equation for performing analysis based on the rate-normalized change in pressure-squared.

For rate-normalization the analogue of Eq. 7.8.3 is given by

$$\frac{\hat{b}kh\left(p_{ws}^2 - p_{wf,s}^2\right)}{141.2\,(2\Delta q(\Delta t))} = 1.151\log\left(\frac{4t_D}{e^{\gamma}}\right) + s + \left[\frac{\left(\hat{b}-\hat{a}\right)kh\left(p_1^2 - p_{wf,s}^2\right)}{141.2\,(2\Delta q(\Delta t))}\right] - 1.151\log(R_{H1}), \tag{7.8.26}$$

where $\hat{a}$ and $\hat{b}$, respectively, are still given by Eqs. 7.8.4 and 7.8.5 and, similar to Eq. 7.8.3, Eq. 7.8.26 applies for $p_{ws} > p_1$.

When Eq. 7.8.26 applies, a semilog plot of $(p_{ws}^2 - p_{wf,s}^2)/\Delta q(\Delta t)$ versus Horner time R_{H1} will be a semilog straight line of slope m_3, where m_3 is given by Eq. 7.8.20, i.e., by

$$m_3 = \frac{2 \times 162.6}{\hat{b}kh}, \tag{7.8.27}$$

and $\hat{b}k$ can be computed from this semilog slope by the following equation:

$$\hat{b}k = \frac{2 \times 162.6}{m_3 h}. \tag{7.8.28}$$

As in the standard pressure-squared method, effective oil permeability can then be approximated by

$$(kk_{ro})_{p_{ws}} = (\hat{b}k)(\mu_o B_o)_{p_{ws}} p_{ws}, \tag{7.8.29}$$

where $\hat{b}k$ denotes the value computed from Eq. 7.8.28. As in the previous case, Eq. 7.8.29 will yield a kk_{ro} versus p_{ws} curve that crosses the correct one. Extrapolating Eq. 7.8.29 to initial pressure, we can obtain an estimate of the initial effective oil permeability from the following equation:

$$kk_{roi} = (kk_{ro})_{p_i} = (\hat{b}k)(\mu_o B_o)_{p_i} p_i. \tag{7.8.30}$$

Again Eq. 7.8.30 will typically yield an underestimate of kk_{roi}.

Letting $\left[(p_{ws}^2 - p_{wf,s}^2)/\Delta q(\Delta t)\right]_{1hr}$ denote the value of the rate-normalized change in pressure-squared obtained by extrapolating the semilog straight line to $\Delta t = 1$ hour, the skin factor can be estimated from the following equation:

$$s = 1.151\left(\frac{\left[(p_{ws}^2 - p_{wf,s}^2)/\Delta q(\Delta t)\right]_{1hr}}{m_3} - \log\left(\frac{kk_{roi}}{\phi\mu_{oi}c_{ti}r_w^2}\right) + 3.23\right). \tag{7.8.31}$$

As in the pressure-squared method, Eq. 7.8.31 is only approximate because the term involving $\hat{b} - \hat{a}$ in Eq. 7.8.26 is neglected. Moreover, this same term also involves $\Delta q(\Delta t)$ and thus, a straight line cannot be obtained until the variation of the term of Eq. 7.8.26 within square brackets is small, or when the term in square brackets is negligible compared to the other terms in Eq. 7.8.26. As in the pressure-squared method, Eq. 7.8.31 will yield an overestimate of the skin factor if $\hat{b} - \hat{a} > 0$ and an underestimate of the skin factor if $\hat{b} - \hat{a} < 0$. Again for all cases considered in Chapter 6 (also see Ref. 29) and in this Chapter it was always found that $\hat{b} - \hat{a} > 0$.

7.9 Pressure-Squared Analysis Results

In this major section, we present computational results obtained for Cases 1-9 by analyzing the resulting pressure data using the various forms of pressure-squared analysis.

Cases 1, 2 and 3.

Fig. 7.9.1 presents semilog plots of $p_{ws}^2 - p_{wf,s}^2$ versus R_{H1} for Cases 1, 2 and 3. Recall that no wellbore storage effects exist for Case 1, i.e., $q_{osf} = 0.0$ STB/D at all shut-in times. For Case 2, $\beta^* = 6.8 \times 10^{-4}$ ($C_D \approx 117.4$) and for Case 3, $\beta^* = 6.8 \times 10^{-5}$ ($C_D \approx 1174$). For the zero wellbore storage case, Case 1, a well-defined semilog straight line exists at all times corresponding to $R_{H1} < 12$ ($\Delta t > 4.55 \times 10^{-1}$ days). The slope of this semilog straight line is 1.2524×10^6 psi^2 per log cycle. In Case 2, we obtain the same semilog straight line, but only at times corresponding to $R_{H1} < 9.1$ ($\Delta t > 6.17 \times 10^{-1}$ days). For the results of Case 3, the semilog straight line does not begin until $R_{H1} \approx 3.6$ ($\Delta t \approx 1.923$ days). Thus, in Case 3, we would need to run a buildup test for well over two days in order to obtain an easily identifiable semilog straight line. Although our wellbore storage model does not correspond to a constant C_D model, if we use the approximation $C_D = 1174$, then for the corresponding liquid case, the semilog straight line would begin at $\Delta t \approx 0.52$ days based on the approximate starting time of $\Delta t_D/C_D = 60$.

Using the semilog slope obtained in Fig. 7.9.1, $m_2 = 1.2524 \times 10^6$ psi^2 per

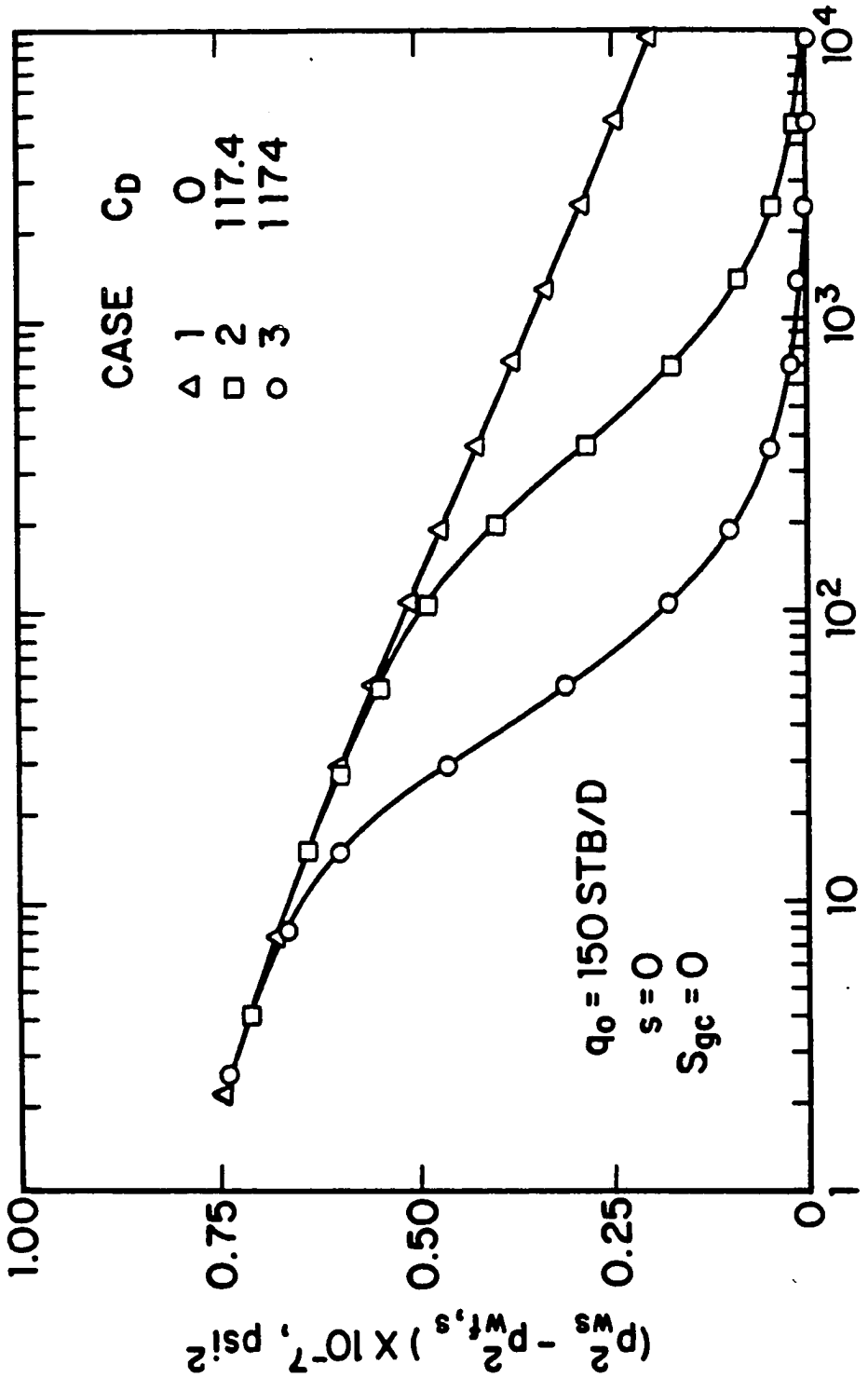

Fig. 7.9.1 - Semilog plot of change in pressure squared versus Horner time; Cases 1-3.

log cycle, in Eq. 7.8.7, one obtains $\hat{b}k = 2.7196 \times 10^{-3}$ as compared to the value of $\hat{b}k = 2.525 \times 10^{-3}$ obtained by computing $\hat{b}$ from Eq. 7.8.5 with $p_{ws} = 3408$ psi and multiplying this value of $\hat{b}$ by k. Eq. 7.8.15 evaluated at the final value of shut-in pressure, $p_{ws} = 3408$ psi, gives $kk_{ro} = 5.91$ md as compared to the correct (simulator) value of $kk_{ro} = 6.81$ md. Eq. 7.8.16 yields $kk_{roi} = 6.44$ md as compared to the correct value of $kk_{roi} = 7.00$ md. Applying Eq. 7.8.17, one obtains $s = 0.454$ as compared to the correct value of $s = 0$.

Fig. 7.9.2 shows Cartesian plots of $(p_{ws}^2 - p_{wf,s}^2)/(q_o - q_{os f}(\Delta t))$ versus logarithmic convolution shut-in time, Δt_{lc}, for Cases 1, 2 and 3. In Case 1, a well-defined straight line of slope $m_3 = 8.4193 \times 10^3$ psi^2/(STB/D) exists for $\Delta t_{lc} > -0.56$ ($R_{H1} < 18.4$ and $\Delta t > 2.87 \times 10^{-1}$ days). For Cases 2 and 3, this straight line begins at about this same time. Recall that when we used the standard pressure-squared method (see Fig. 7.9.1), the semilog straight line began at $R_{H1} \approx 12$ ($\Delta t \approx 4.55 \times 10^{-1}$ days) for Case 1, at $R_{H1} = 9.1$ ($\Delta t = 6.17 \times 10^{-1}$ days) for Case 2 and at $R_{H1} \approx 3.6$ ($\Delta t \approx 1.923$ days) in Case 3. Thus, the logarithmic-convolution shut-in time based on measured sandface rates is useful in that one can analyze data at earlier times than is possible using the standard pressure-squared semilog plot of Fig. 7.9.1.

Using the slope of $m_3 = 8.4193 \times 10^3$ psi^2/(STB/D) obtained for the results of Fig. 7.9.2, Eq. 7.8.22 gives $\hat{b}k = 2.485 \times 10^{-3}$ as compared to the value of $\hat{b}k = 2.525 \times 10^{-3}$ obtained by computing $\hat{b}$ from Eq. 7.8.5 with $p_{ws} = 3408$ psi and multiplying this value of $\hat{b}$ by k. Eq. 7.8.23 evaluated at the final value of shut-in pressure, $p_{ws} = 3408$ psi, gives $kk_{ro} = 5.82$ md as compared to the correct (simulator) value of $kk_{ro} = 6.81$ md. Eq. 7.8.24 yields $kk_{roi} = 5.88$ md as compared to the correct value of $kk_{roi} = 7.00$ md. Applying Eq. 7.8.25, one obtains $s = 0.07$ as compared to the correct value of $s = 0$. Note that the accuracy of these results is essentially the same as those obtained by using the pressure-squared method as one would expect. The advantage of the logarithmic convolution shut-in time is that proper straight lines start earlier because Δt_{lc} accounts for the changing sandface rate, whereas on a semilog plot of the change in pressure-squared versus Horner

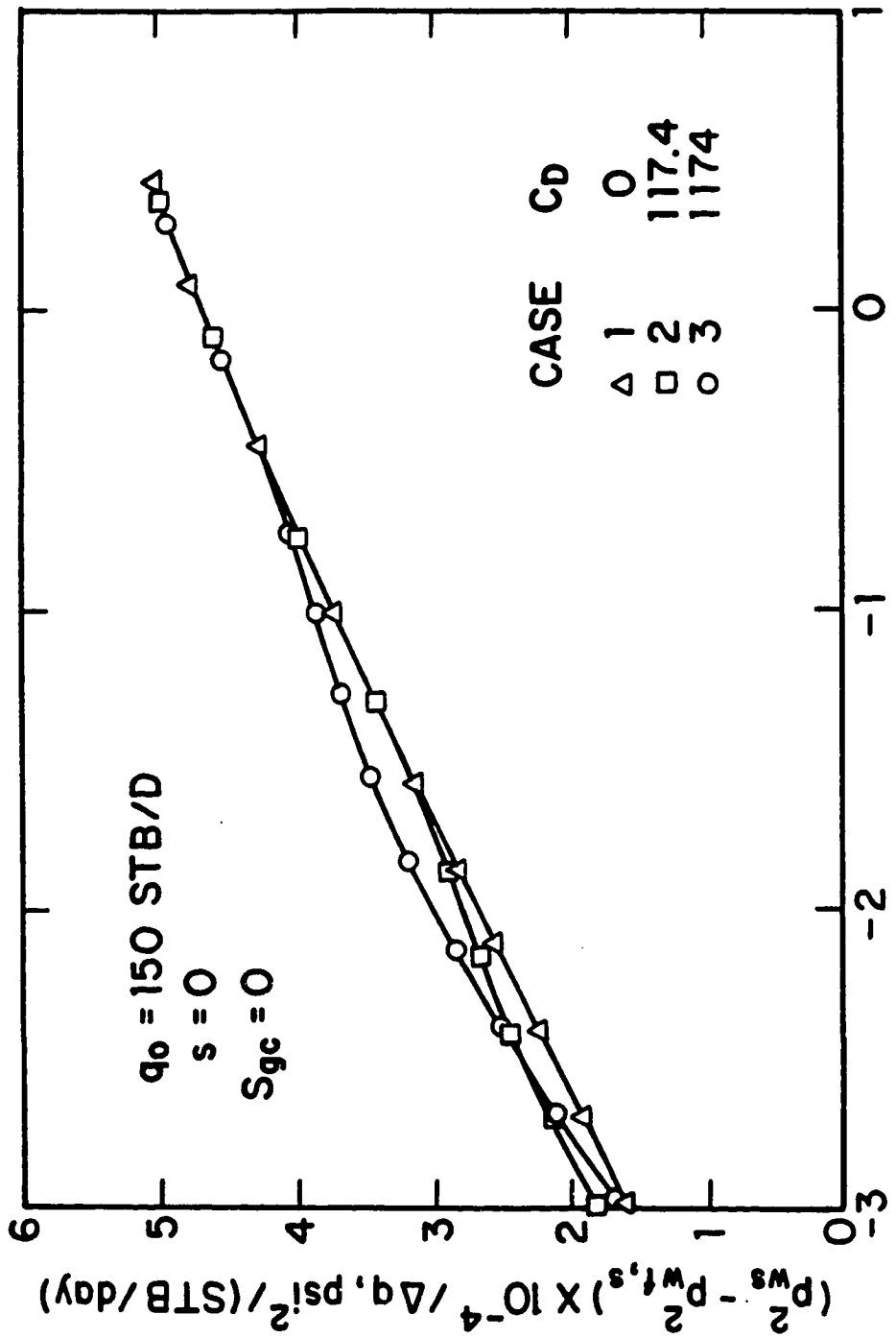

Fig. 7.9.2 - Rate-normalized change in pressure squared versus logarithmic convolution shut-in time; Cases 1-3.

ratio time, the proper semilog straight line will not begin until $q_{osf}(\Delta t) \approx 0.0$.

Fig. 7.9.3 shows semilog plots of the rate-normalized change in pressure-squared versus the primary Horner time. As shown, all cases eventually show a well-defined semilog straight line of slope $m_3 = 8.3151 \times 10^3$ psi^2/ (STB/D) per log cycle. Using the semilog slope of $m_3 = 8.3151 \times 10^3$ psi^2/(STB/D) per log cycle in Eq. 7.8.28, one obtains $\hat{b}k = 2.5156 \times 10^{-3}$ as compared to the value of $\hat{b}k = 2.525 \times 10^{-3}$ computed from Eq. 7.8.5. Eq. 7.8.29 evaluated at the final value of shut-in pressure, $p_{ws} = 3408$ psi, gives $kk_{ro} = 5.89$ md as compared to the correct (simulator) value of $kk_{ro} = 6.81$ md. Eq. 7.8.30 yields $kk_{roi} = 5.95$ md as compared to the correct value of $kk_{roi} = 7.00$ md. Applying Eq. 7.8.31, one obtains $s = 0.162$ as compared to the correct value of $s = 0$. Note these results should be and are essentially identical to those obtained from the other two methods. For all the cases the semilog straight lines begin at about the same time as the ones for the analogous pressure-squared method (see Fig. 7.9.1), i.e., in Case 2 the Horner straight line begins at $R_{H1} = 9.1$ ($\Delta t = 6.17 \times 10^{-1}$ days) and in Case 3 at $R_{H1} \approx 3.6$ ($\Delta t \approx 1.923$ days). In this regard, plotting data in terms of logarithmic convolution shut-in time is preferable.

However, note that in comparing Figs. 7.9.3 and 7.9.1, we see that rate normalization does tend to "straighten" the shut-in pressure data; for example, if one fits a regression analysis semilog straight line to all Case 3 data of Fig. 7.9.3 corresponding to $R_{H1} \leq 100$, one obtains a semilog slope of $m_3 = 9.4454 \times 10^3$ psi^2/(STB/D) per log cycle as opposed to $m_3 = 8.3151 \times 10^3$ psi^2/(STB/D) per log cycle for the semilog straight line actually chosen. Using m_3 in Eq. 7.8.28 gives $\hat{b}k = 2.215 \times 10^{-3}$, Eq. 7.8.29 evaluated at the final shut-in pressure, $p_{ws} = 3408$ psi, gives $kk_{ro} = 5.19$ and Eq. 7.8.30 gives $kk_{roi} = 5.24$. Applying Eq. 7.8.31, one obtains $s = -0.66$ as compared to the correct value of $s = 0$. These values are not substantially different from the values actually obtained from the Horner straight line actually chosen for the Case 3 data of Fig. 7.9.3.

Cases 4, 5 and 6.

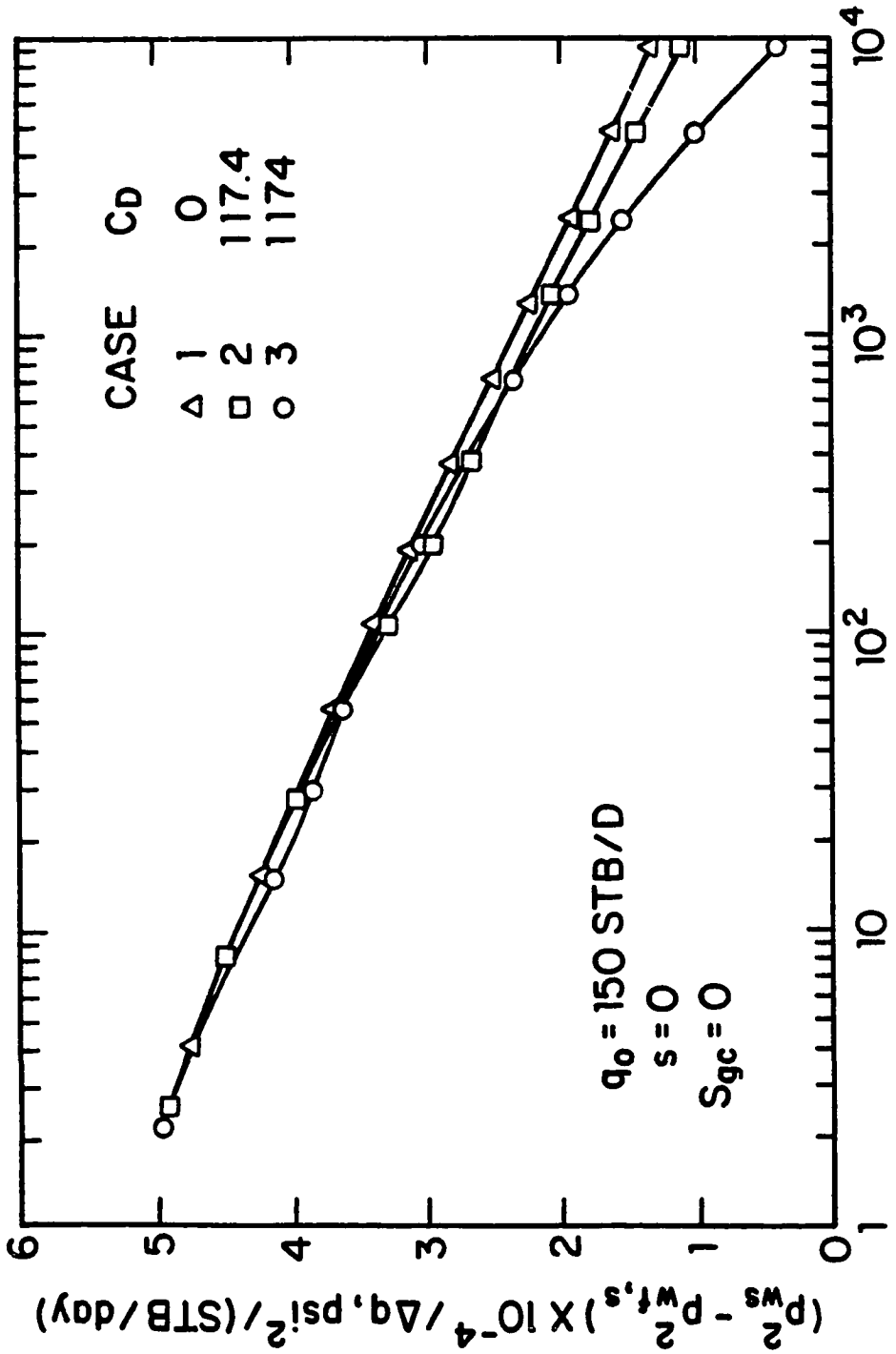

Fig. 7.9.3 - Semilog plot of rate-normalized change in pressure squared versus Horner time; Cases 1-3.

Figs. 7.9.4 and 7.9.5 illustrate that Eq. 7.5.8 is reasonably accurate when skin effects are present. The solid straight line represents the single-phase liquid solution, i.e., Eq. 7.5.8, and the open data points represent values of $\tilde{p}_{pwD}/(1-q_{owfD})$ obtained from our simulator for Cases 4, 5 and 6 plotted versus Δt_{lcD} (Fig. 7.9.4) or R_{H1} (Fig. 7.9.5). Fig. 7.9.4 shows that a well-defined Cartesian straight line exists for $\Delta t_{lcD} > 3.64$ ($R_{H1} < 1.57 \times 10^2$ and $\Delta t_D > 4.35 \times 10^3$) for Cases 5 and 6 and for $\Delta t_{lcD} > 4.61$ ($R_{H1} < 1.68 \times 10^1$ and $\Delta t_D > 4.28 \times 10^4$) for Case 4. The results shown in Fig. 7.9.5 indicate that a well-defined semilog straight line exists for $R_{H1} < 1.296 \times 10^2$ ($\Delta t_D > 5.26 \times 10^3$) for Case 6, for $R_{H1} < 2.9 \times 10^1$ ($\Delta t_D > 2.42 \times 10^4$) for Case 5 and for $R_{H1} < 4.1$ ($\Delta t_D > 2.16 \times 10^5$) for Case 4. Notice that for all cases the multiphase flow solutions are located under the liquid solution and they exhibit a Cartesian or semilog straight line with slope 1.172 which is very close to the "theoretical" value of 1.151 predicted by Eq. 7.5.8. (Recall for the zero storage case, $\Delta t_{lcD} = \log[t_D \Delta t_D/(t_D + \Delta t_D)]$.)

For the zero wellbore storage case, Refs. 10 and 28 showed that Eq. 7.5.4 approximately applies. Fig. 7.9.6 presents a plot of $\tilde{p}_{pwD}$ versus the Horner time ratio, R_{H1}. For all cases shown, a well-defined semilog straight line exists with slope 1.172. This semilog straight line begins at $R_{H1} \approx 1.296 \times 10^2$ ($\Delta t_D \approx 5.26 \times 10^3$) for Case 6, at $R_{H1} \approx 2.01 \times 10^1$ ($\Delta t_D \approx 3.54 \times 10^4$) for Case 5 and at $R_{H1} \approx 3.13$ ($\Delta t_D \approx 3.17 \times 10^5$) for Case 4. For each case, the values of Δt_D recorded in Figs. 7.9.4 through 7.9.6 represent the time at which the Cartesian or semilog straight line begins. The results of these figures imply that incorporating the effect of the variable flow rate into the analysis causes the relevant straight line to begin earlier.

Fig. 7.9.7 presents semilog plots of $p_{ws}^2 - p_{wf,s}^2$ versus the Horner time ratio, R_{H1}, for Cases 4, 5 and 6. Recall that no wellbore storage effects exist for Case 6, i.e., $q_{osf} = 0.0$ STB/D at all shut-in times. For Case 4, $\beta^* = 6.8 \times 10^{-5}$ ($C_D \approx 1174$) and for Case 5, $\beta^* = 6.8 \times 10^{-4}$ ($C_D \approx 117.4$). In all cases, $s = 5$ and $S_{gc} = 0.0$. For the zero wellbore storage case, Case 6, a well-defined semilog straight line exists at all times corresponding to $R_{H1} < 70.0$ ($\Delta t > 7.25 \times 10^{-2}$ days). The slope of this semilog straight line is 0.37369×10^6 psi^2 per log cycle. In Case 5, we obtain

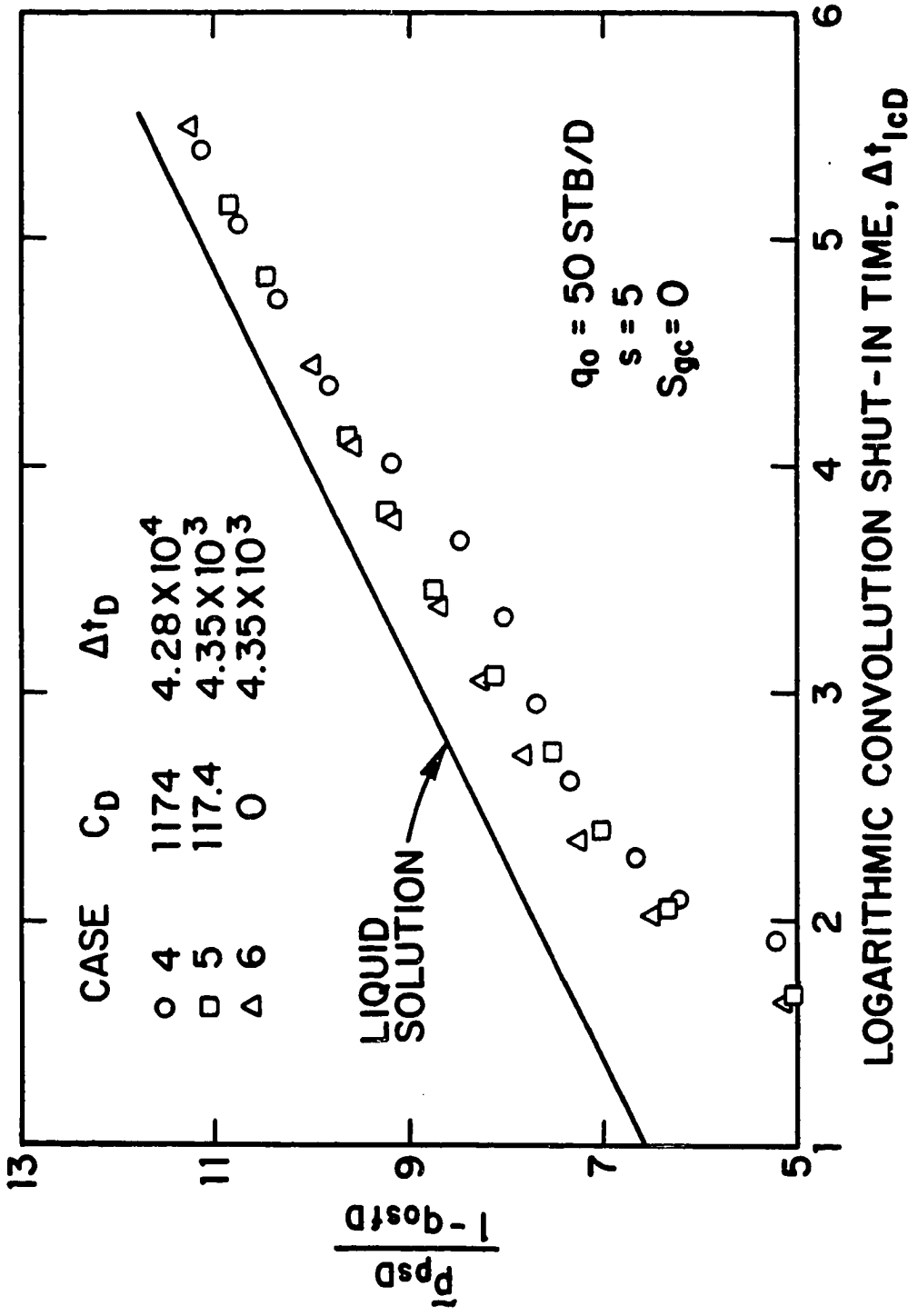

Fig. 7.9.4 - Dimensionless Odeh-Jones plot in terms of dimensionless pseudopressure; Cases 4-6.

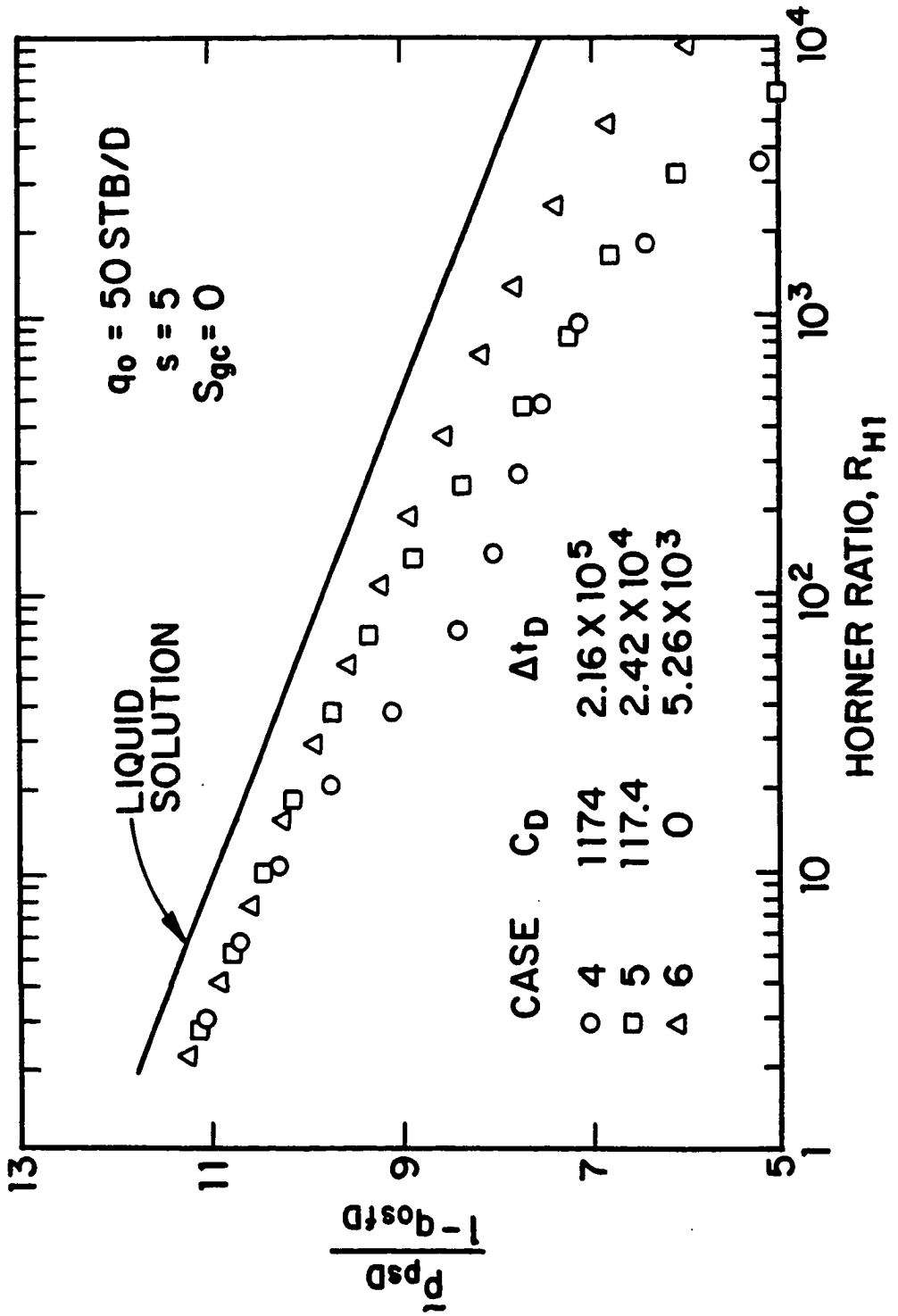

Fig. 7.9.5 - Semilog plot of rate-normalized dimensionless pseudopressure versus Horner time; Cases 4-6.

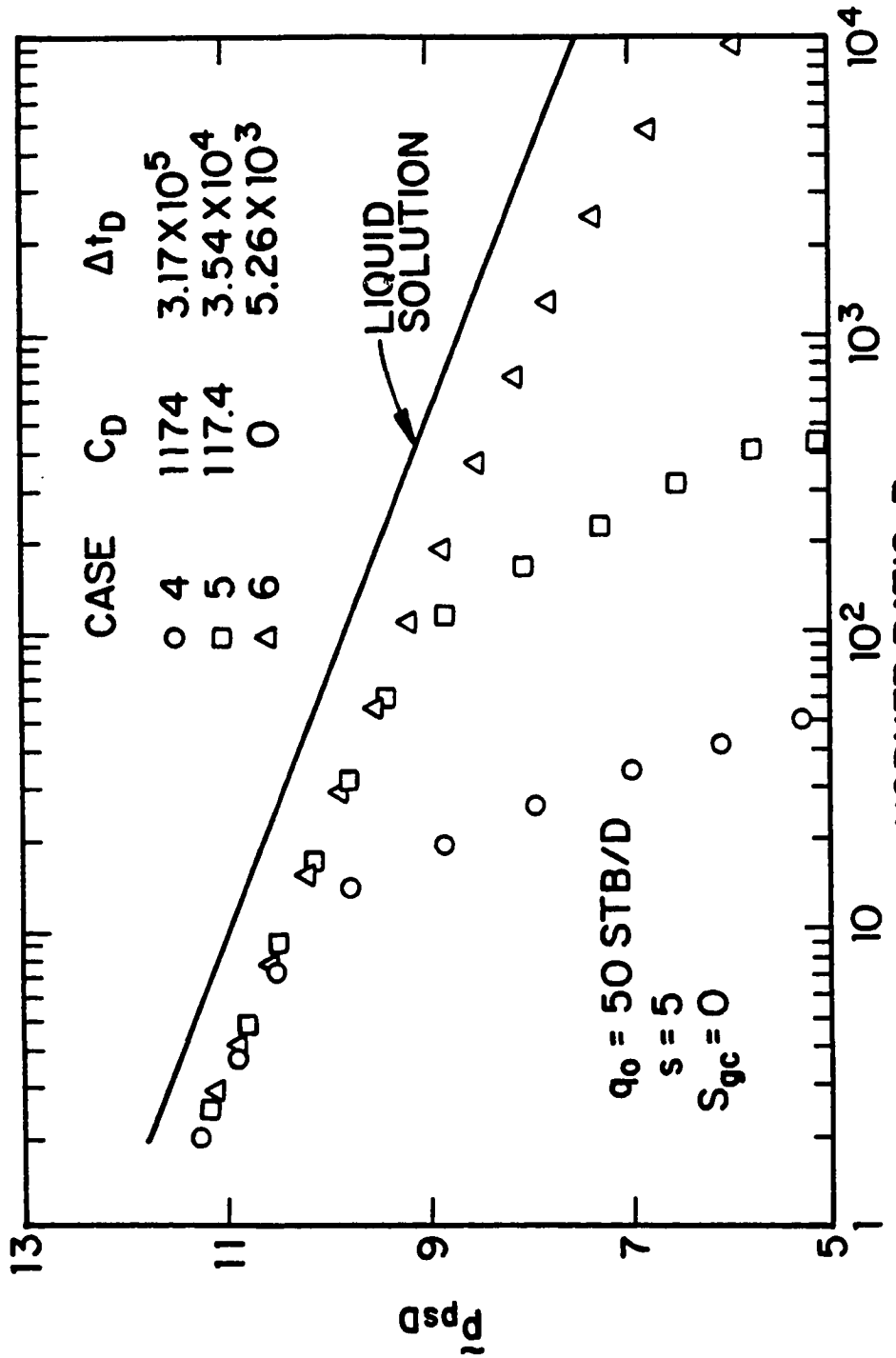

Fig. 7.9.6 - Semilog plot of dimensionless pseudopressure versus Horner time; Cases 4-6.

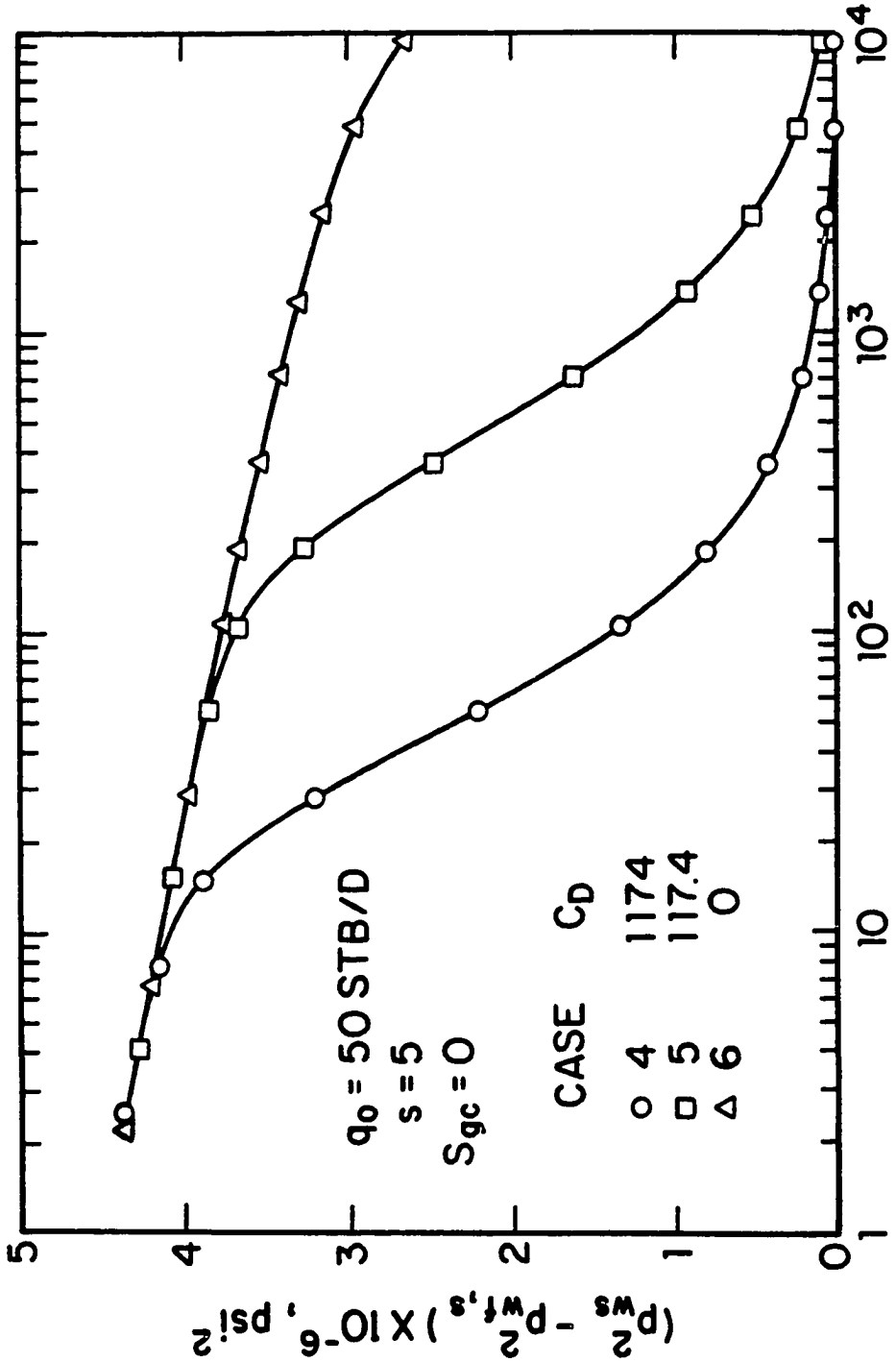

Fig. 7.9.7 - Semilog plot of change in pressure squared versus Horner time; Cases 4-6.

the same semilog straight line, but only at times corresponding to $R_{H1} < 29.0$ ($\Delta t > 1.79 \times 10^{-1}$ days). For the results of Case 4, the semilog straight line does not begin until $R_{H1} \approx 4.8$ ($\Delta t \approx 1.316$ days). Thus, in Case 4 we would need to run a buildup test for well over 1.5 days in order to obtain an easily identifiable semilog straight line.

Using the semilog slope obtained from Fig. 7.9.7, $m_2 = 0.37369 \times 10^6$ psi^2 per log cycle, in Eq. 7.8.7, one obtains $\hat{b}k = 2.7987 \times 10^{-3}$ as compared to the value of $\hat{b}k = 2.586 \times 10^{-3}$ computed from Eq. 7.8.5. Eq. 7.8.15 evaluated at the final value of shut-in pressure, $p_{ws} = 3443$ psi, gives $kk_{ro} = 6.6$ md as compared to the correct (simulator) value of $kk_{ro} = 6.91$ md. Eq. 7.8.16 yields $kk_{roi} = 6.62$ md as compared to the correct value of $kk_{roi} = 7.00$ md. Applying Eq. 7.8.17, one obtains $s = 6.81$ as compared to the correct value of $s = 5$.

As noted earlier, Eq. 7.8.15 can be used to compute effective oil permeability as a function of pressure. The closed square data points of Fig. 7.8.3 show the values of kk_{ro} computed via Eq. 7.8.15 for the Case 4 results of Fig. 7.9.7. Note that based on the discussion of Fig. 7.8.2, Eq. 7.8.15 yields a kk_{ro} versus pressure relation that crosses the actual kk_{ro} versus pressure drawdown relation.

Fig. 7.9.8 shows Cartesian plots of $(p_{ws}^2 - p_{wf,s}^2)/(q_o - q_{osf}(\Delta t))$ versus logarithmic convolution shut-in time, Δt_{lc}, for Cases 4, 5 and 6. In Case 6, a well-defined straight line of slope $m_3 = 0.75703 \times 10^4$ psi^2/(STB/D) exists for $\Delta t_{lc} > -1.2$ ($R_{H1} < 70.0$ and $\Delta t > 7.25 \times 10^{-2}$ days). For Case 5, the proper straight line begins at $\Delta t_{lc} \approx -0.8$ ($R_{H1} \approx 31.0$ and $\Delta t \approx 1.67 \times 10^{-1}$ days). For Case 4, wellbore storage effects delay the beginning time of the straight line until $\Delta t_{lc} \approx -0.56$ days which corresponds to $R_{H1} = 18.0$ and $\Delta t = 2.94 \times 10^{-1}$ days. Note that these beginning times are smaller than the ones obtained for the same cases from the pressure-squared method (see Fig. 7.9.7).

Using the slope of $m_3 = 0.75703 \times 10^4$ psi^2/(STB/D) obtained from Fig. 7.9.8, Eq. 7.8.22 gives $\hat{b}k = 2.76 \times 10^{-3}$ as compared to the value of $\hat{b}k = 2.586 \times 10^{-3}$ computed from Eq. 7.8.5. Eq. 7.8.23 evaluated at the final value of shut-in pressure, $p_{ws} = 3443$ psi, gives $kk_{ro} = 6.51$ md as compared to the correct (simulator) value

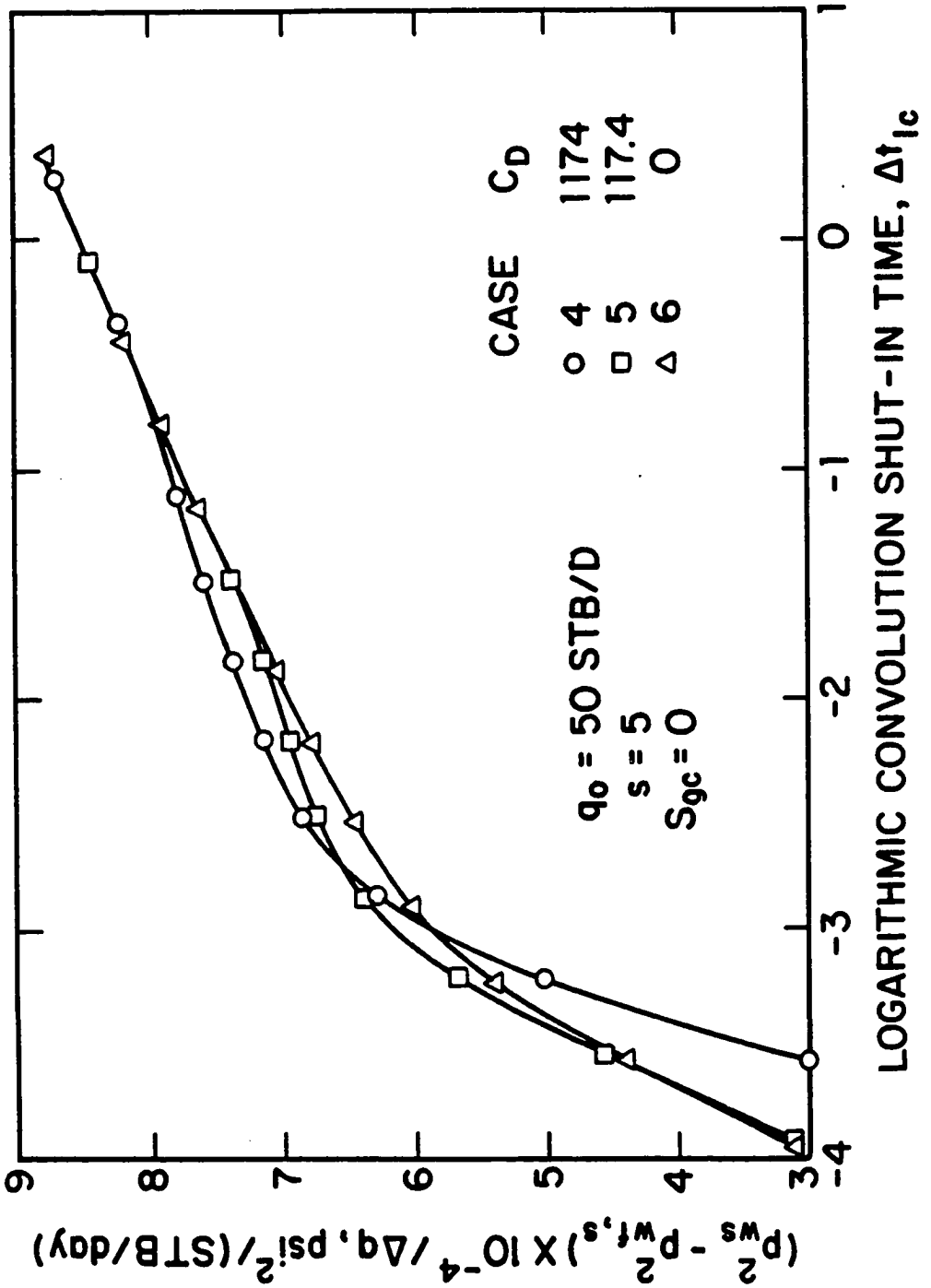

Fig. 7.9.8 - Rate-normalized change in pressure squared versus logarithmic convolution shut-in time; Cases 4-6.

of $kk_{ro} = 6.91$ md. Eq. 7.8.24 yields $kk_{roi} = 6.53$ md as compared to the correct value of $kk_{roi} = 7.00$ md. Applying Eq. 7.8.25, one obtains $s = 6.6$ as compared to the correct value of $s = 5$.

Fig. 7.9.9 shows semilog plots of the rate-normalized change in pressure-squared versus Horner time. As shown, all cases eventually show a well-defined semilog straight line of slope $m_3 = 0.74737 \times 10^4$ psi^2/ (STB/D) per log cycle. For all cases, the semilog straight lines begin approximately at the same shut-in times as the ones from the pressure-squared method, i.e., $R_{H1} < 29.0$ ($\Delta t > 1.79 \times 10^{-1}$ days) for Case 5 and $R_{H1} \approx 4.8$ ($\Delta t \approx 1.316$ days) for Case 4. However, note that all data corresponding to $R_{H1} < 10^3$ could be fit with a reasonably semilog straight line. Using the semilog slope of $m_3 = 0.74737 \times 10^4$ psi^2/ (STB/D) per log cycle in Eq. 7.8.28, one obtains $\hat{b}k = 2.7986 \times 10^{-3}$ as compared to the value of $\hat{b}k = 2.586 \times 10^{-3}$ computed from Eq. 7.8.5 using the value of shut-in pressure $p_{ws} = 3443$ psi. Eq. 7.8.29 evaluated at the final value of shut-in pressure ($p_{ws} = 3443$ psi) gives $kk_{ro} = 6.6$ md as compared to the correct (simulator) value of $kk_{ro} = 6.91$ md. Eq. 7.8.30 yields $kk_{roi} = 6.62$ md as compared to the correct value of $kk_{roi} = 7.00$ md. Applying Eq. 7.8.31, one obtains $s = 6.8$ as compared to the correct value of $s = 5$. As expected, the results obtained from rate-normalized pressure-squared analysis are essentially the same as the results obtained from standard pressure-squared analysis and analysis based on a plot of pressure-squared versus logarithmic convolution shut-in time.

Cases 7, 8 and 9.

Similar to the results of Figs. 7.9.4 through 7.9.6, we found that at later shut-in times Eq. 7.5.8 provides a reasonable approximation in Cases 7, 8 and 9.

Fig. 7.9.10 presents semilog plots of $p_{ws}^2 - p_{wf,s}^2$ versus the Horner time ratio R_{H1} for Cases 7, 8 and 9. Recall that no wellbore storage effects exist for Case 7, i.e., $q_{osf} = 0.0$ STB/D at all shut-in times. For Case 8, $\beta^* = 6.8 \times 10^{-4}$ ($C_D \approx 117.4$) and for Case 9, $\beta^* = 6.8 \times 10^{-5}$ ($C_D \approx 1174$). In all cases, $s = 0$ and $S_{gc} = 0.07$. For the zero wellbore storage case, Case 7, a well-defined semilog straight line exists

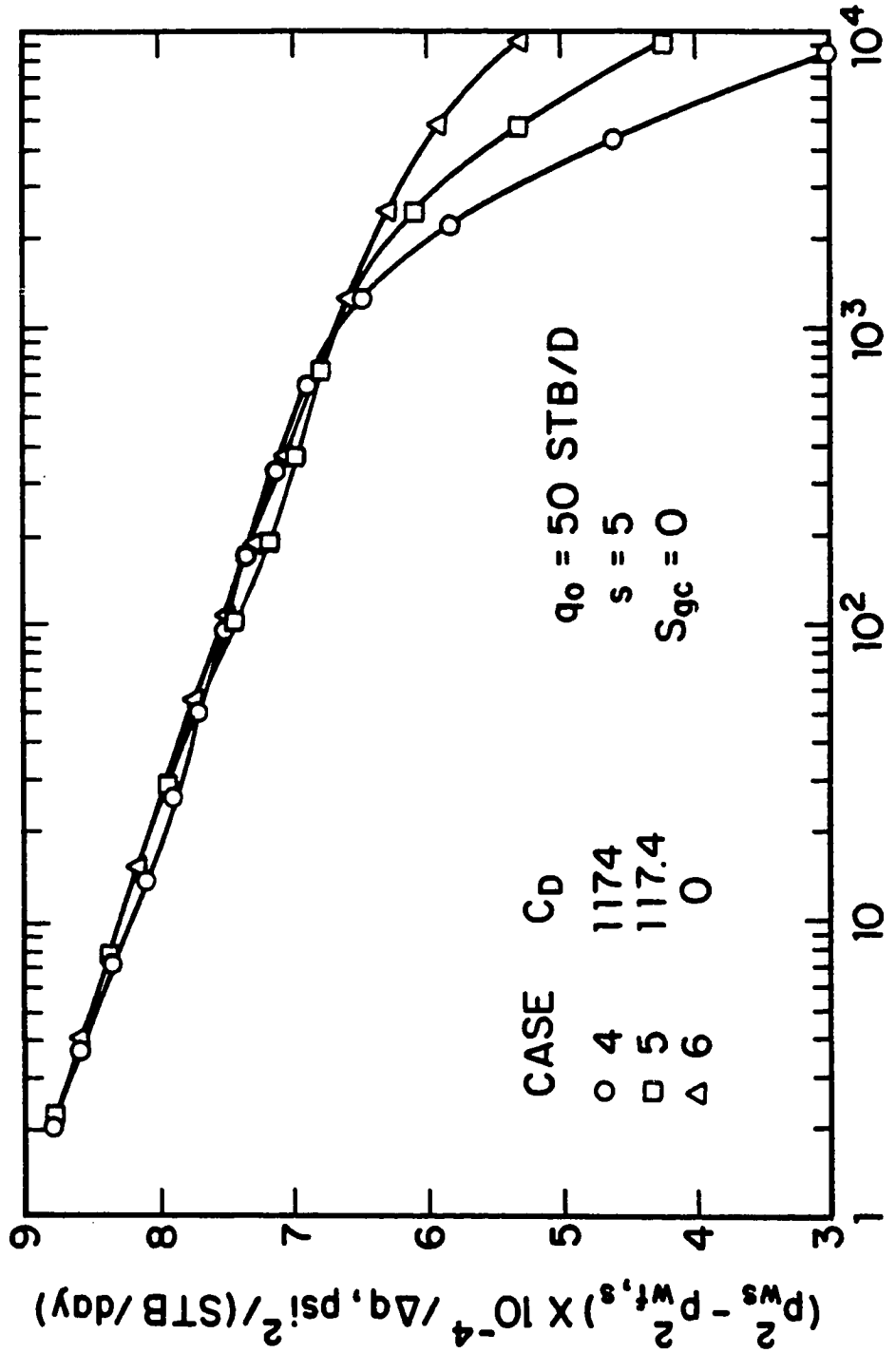

Fig. 7.9.9 - Semilog plot of rate-normalized change in pressure squared versus Horner time; Cases 4-6.

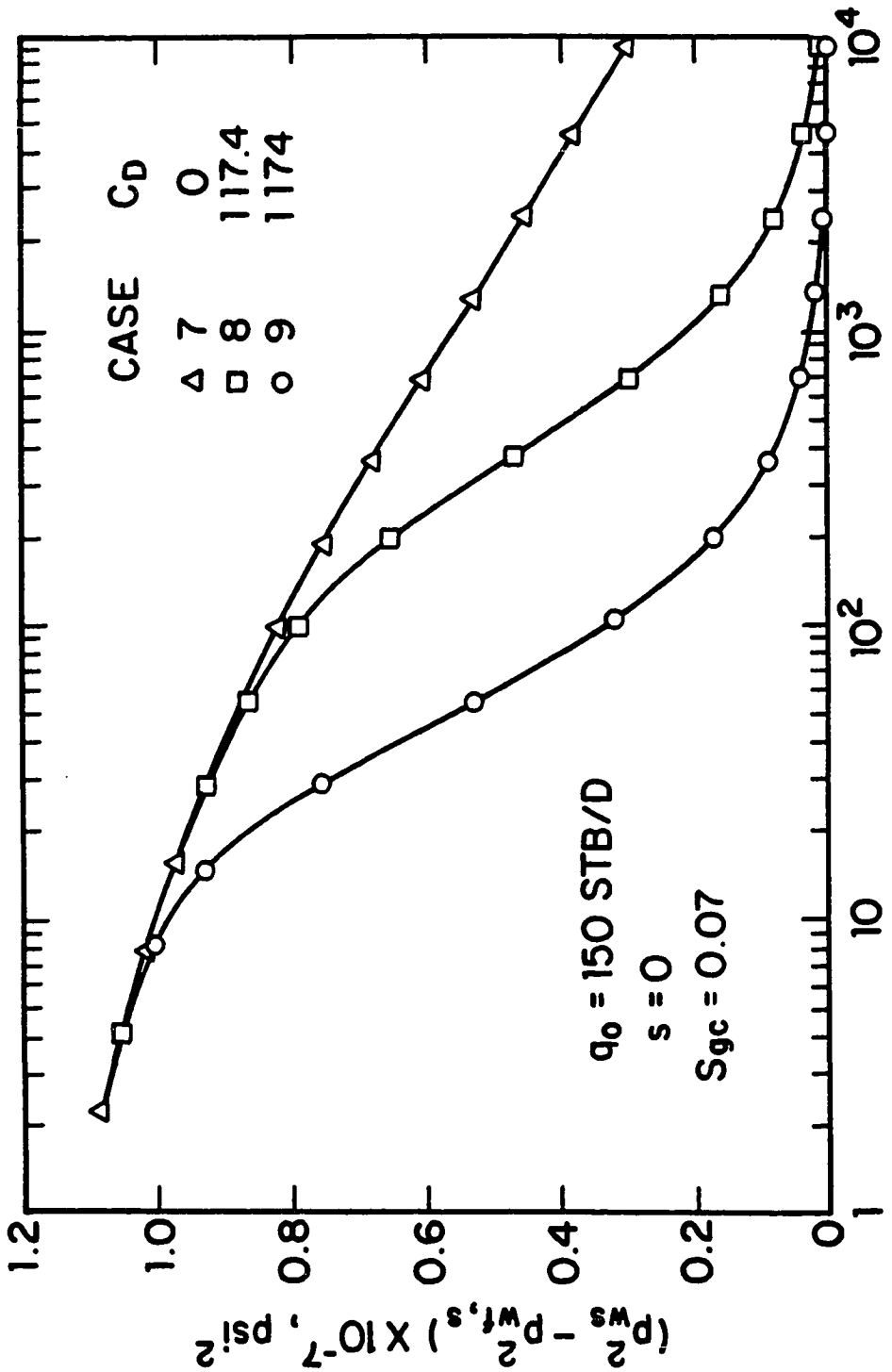

Fig. 7.9.10 - Semilog plot of change in pressure squared versus Horner time; Cases 7-9.

at all times corresponding to $R_{H1} < 17.0$ ($\Delta t > 3.125 \times 10^{-1}$ days). The slope of this semilog straight line is $m_2 = 0.13507 \times 10^7$ psi^2 per log cycle. In Case 8, we obtain the same semilog straight line, but only at times corresponding to $R_{H1} < 15.0$ ($\Delta t > 3.57 \times 10^{-1}$ days). For the results of Case 9, the semilog straight line does not begin until $R_{H1} \approx 4.2$ ($\Delta t \approx 1.563$ days). Thus, in Case 9 we would need to run a buildup test for over two days in order to obtain an easily identifiable semilog straight line.

Using the semilog slope obtained from Fig. 7.9.10, $m_2 = 0.13507 \times 10^7$ psi^2 per log cycle, in Eq. 7.8.7, one obtains $\hat{b}k = 2.323 \times 10^{-3}$ as compared to the value of $\hat{b}k = 2.077 \times 10^{-3}$ computed from Eq. 7.8.5 with $p_{ws} = 3956.2$ psi. Eq. 7.8.15 evaluated at the final value of shut-in pressure, $p_{ws} = 3956.2$ psi, gives $kk_{ro} = 5.67$ md as compared to the correct (simulator) value of $kk_{ro} = 6.8$ md. Eq. 7.8.16 yields $kk_{roi} = 6.69$ md as compared to the correct value of $kk_{roi} = 7.00$ md. Applying Eq. 7.8.17, one obtains $s = 2.64$ as compared to the correct value of $s = 0$.

Fig. 7.9.11 shows Cartesian plots of $(p_{ws}^2 - p_{wf,s}^2)/(q_o - q_{osf}(\Delta t))$ versus logarithmic convolution shut-in time, Δt_{lc}, for Cases 7, 8 and 9. For all cases a well-defined straight line of slope $m_3 = 0.90599 \times 10^4$ psi^2/(STB/D) exists for $\Delta t_{lc} > -0.53$ ($R_{H1} < 17.0$ and $\Delta t > 3.125 \times 10^{-1}$ days). Note that the beginning times for the nonzero wellbore storage cases are smaller than the ones obtained for the same cases from the pressure-squared method (see Fig. 7.9.10).

Using the slope of $m_3 = 0.90599 \times 10^4$ psi^2/(STB/D) obtained from Fig. 7.9.11, Eq. 7.8.22 gives $\hat{b}k = 2.309 \times 10^{-3}$ as compared to the value of $\hat{b}k = 2.077 \times 10^{-3}$ computed from Eq. 7.8.5. Eq. 7.8.23 evaluated at the final value of shut-in pressure, $p_{ws} = 3956.2$ psi, gives $kk_{ro} = 5.634$ md as compared to the correct (simulator) value of $kk_{ro} = 6.8$ md. Eq. 7.8.24 yields $kk_{roi} = 5.66$ md as compared to the correct value of $kk_{roi} = 7.00$ md. Applying Eq. 7.8.25, one obtains $s = 2.58$ as compared to the correct value of $s = 0$.

Fig. 7.9.12 shows semilog plots of the rate-normalized change in pressure-squared versus Horner time. As shown, all cases eventually show a well-defined semilog straight line of slope $m_3 = 0.90599 \times 10^4$ psi^2/ (STB/D) per log cycle.

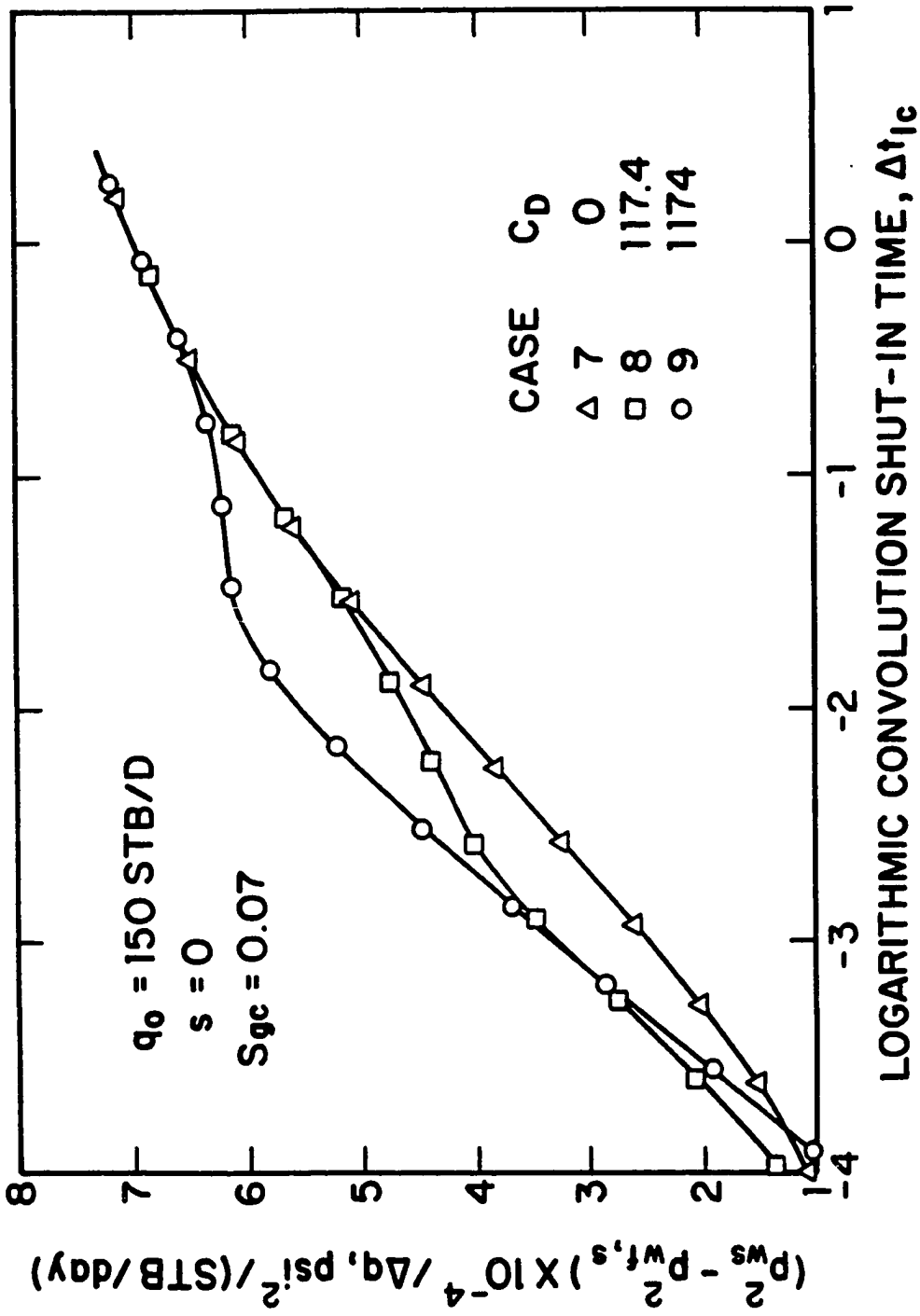

Fig. 7.9.11 - Rate-normalized change in pressure squared versus logarithmic convolution shut-in time; Cases 7-9.

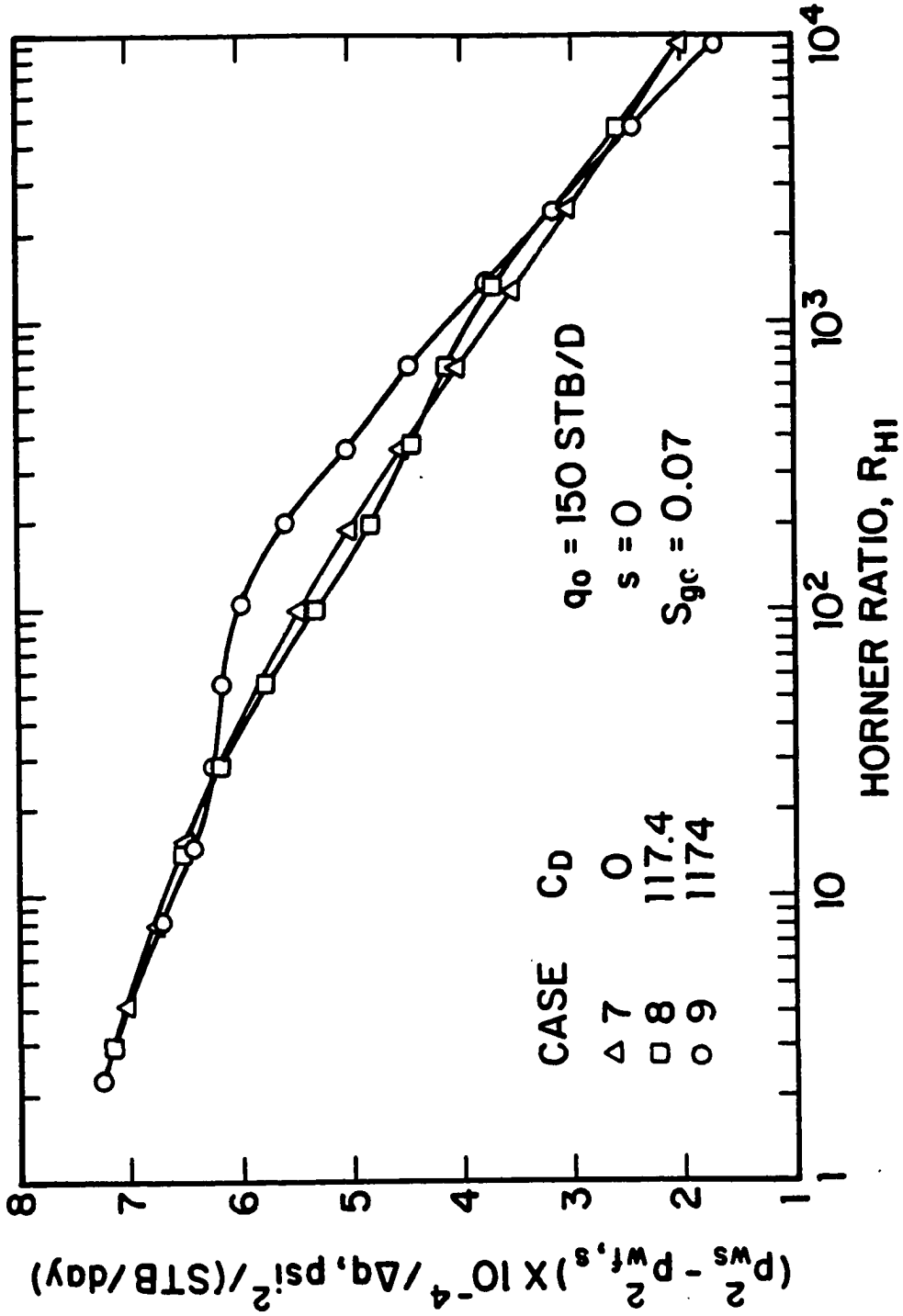

Fig. 7.9.12 - Semilog plot of rate-normalized change in pressure squared versus Horner time; Cases 7-9.

For all cases the semilog straight lines begin approximately at the same shut-in times as the ones from the pressure-squared method. Using the semilog slope of $m_3 = 0.90599 \times 10^4$ psi^2/ (STB/D) per log cycle in Eq. 7.8.28, one obtains $\hat{b}k = 2.309 \times 10^{-3}$ as compared to the value of $\hat{b}k = 2.077 \times 10^{-3}$ computed from Eq. 7.8.5 with $p_{ws} = 3956.2$ psi. Eq. 7.8.29 evaluated at the final value of shut-in pressure ($p_{ws} = 3956.2$ psi) gives $kk_{ro} = 5.634$ md as compared to the correct (simulator) value of $kk_{ro} = 6.8$ md. Eq. 7.8.30 yields $kk_{roi} = 5.66$ md as compared to the correct value of $kk_{roi} = 7.00$ md. Applying Eq. 7.8.31, one obtains $s = 2.58$ as compared to the correct value of $s = 0$. As expected, the results obtained from rate-normalized pressure-squared analysis are essentially the same as the results obtained from standard pressure-squared analysis and analysis based on a plot of pressure-squared versus logarithmic convolution shut-in time.

Comparing the results from Cases 1-3 and 7-9, one can conclude that the presence of critical gas saturation in the relative permeability data of a solution-gas-drive reservoir yields larger values of skin zone damage than its counterpart system with zero critical gas saturation.

From a number of runs we made for systems with $S_{gc} \neq 0$ (see also Ref. 40) we found that the oil saturation decreases faster in a system with $S_{gc} > 0$ than in a system with zero critical gas saturation. Therefore, in order for the system ($S_{gc} \neq 0$) to maintain constant oil production, larger pressure gradients are required. Hence, as soon as the gas saturation reaches its critical value, the pressure declines faster than the pressure in a system with zero critical gas saturation. This fact leads to smaller wellbore pressures at the time of shut-in, $p_{wf,s}$, for systems with $S_{gc} > 0$ than for ones with zero critical gas saturation. Since the pressure for a buildup test becomes the same for both systems during the semilog straight line shut-in period, plotting $p_{ws}^2 - p_{wf,s}^2$ versus R_{H1}, one should obtain the same slopes, but different values of $[p_{ws}^2 - p_{wf,s}^2]_{1hr}$ for the two systems. Specifically, $[p_{ws}^2 - p_{wf,s}^2]_{1hr}(S_{gc} \neq 0) > [p_{ws}^2 - p_{wf,s}^2]_{1hr}(S_{gc} = 0)$. Thus, Eq. 7.8.17 should yield larger skin factor values if the system's critical gas saturation is not zero. In fact, the skin factor computed from Eq. 7.8.17 for the $S_{gc} \neq 0$ case will exceed the value computed for

the corresponding $S_{gc} = 0$ case by $1.151\left\{p^2_{wf,s}(S_{gc}=0) - p^2_{wf,s}(S_{gc}\neq 0)\right\}/m_2$.

7.10 Pressure Method

Here we examine the results obtained by ignoring the effects of multiphase flow when performing semilog analysis, that is, by using semilog analysis based on single-phase flow theory. Since we wish to consider the effects of wellbore storage, we plot results in terms of the rate-normalized pressure change, $\Delta p/\Delta q(\Delta t)$, where $\Delta p = p_{ws} - p_{wf,s}$. According to single-phase flow theory, if rate normalization applies or wellbore storage effects become negligible, then a semilog plot of $\Delta p/\Delta q(\Delta t)$ versus R_{H1} should yield a semilog slope of

$$m_4 = \frac{162.6 B_o \mu_o}{k k_{ro} h}. \tag{7.10.1}$$

Eq. 7.10.1 in and of itself indicates there is a problem because the slope cannot be constant unless $B_o\mu_o/k_{ro}$ is constant. However, rearranging Eq. 7.10.1 gives

$$\frac{k k_{ro}}{\mu_o B_o} = \frac{162.6}{m_4 h}. \tag{7.10.2}$$

In the following, we fit a semilog straight line through the last few data points on a semilog plot of $\Delta p/\Delta q(\Delta t)$ versus R_{H1} and use Eq. 7.10.2 to compute values of $kk_{ro}/(\mu_o B_o)$ at the final value of p_{ws}. We also evaluate Eq. 7.10.2 at p_i and rearrange the resulting equation to obtain an estimate of kk_{roi}/μ_{oi}. Then we extrapolate the "semilog straight line" obtained to $\Delta t = 1$ hour and estimate the skin factor from

$$s = 1.151\left(\frac{\left((p_{ws} - p_{wf,s})/\Delta q(\Delta t)\right)_{1hr}}{m_4} - \log\left(\frac{k k_{roi}}{\phi \mu_{oi} c_{ti} r_w^2}\right) + 3.23\right). \tag{7.10.3}$$

Fig. 7.10.1 shows semilog plots of $\Delta p/\Delta q(\Delta t)$ versus the Horner ratio for data obtained for Cases 1, 2 and 3. At times corresponding to $R_{H1} < 4.124$ ($\Delta t > 1.6$ days), the data for all cases appear to fall on a semilog straight line of slope $m_4 = 1.184$ psi/(STB/D) per log cycle. The final value of shut-in wellbore pressure is $p_{ws,f} = 3408$ psi. Following the computational procedure of the

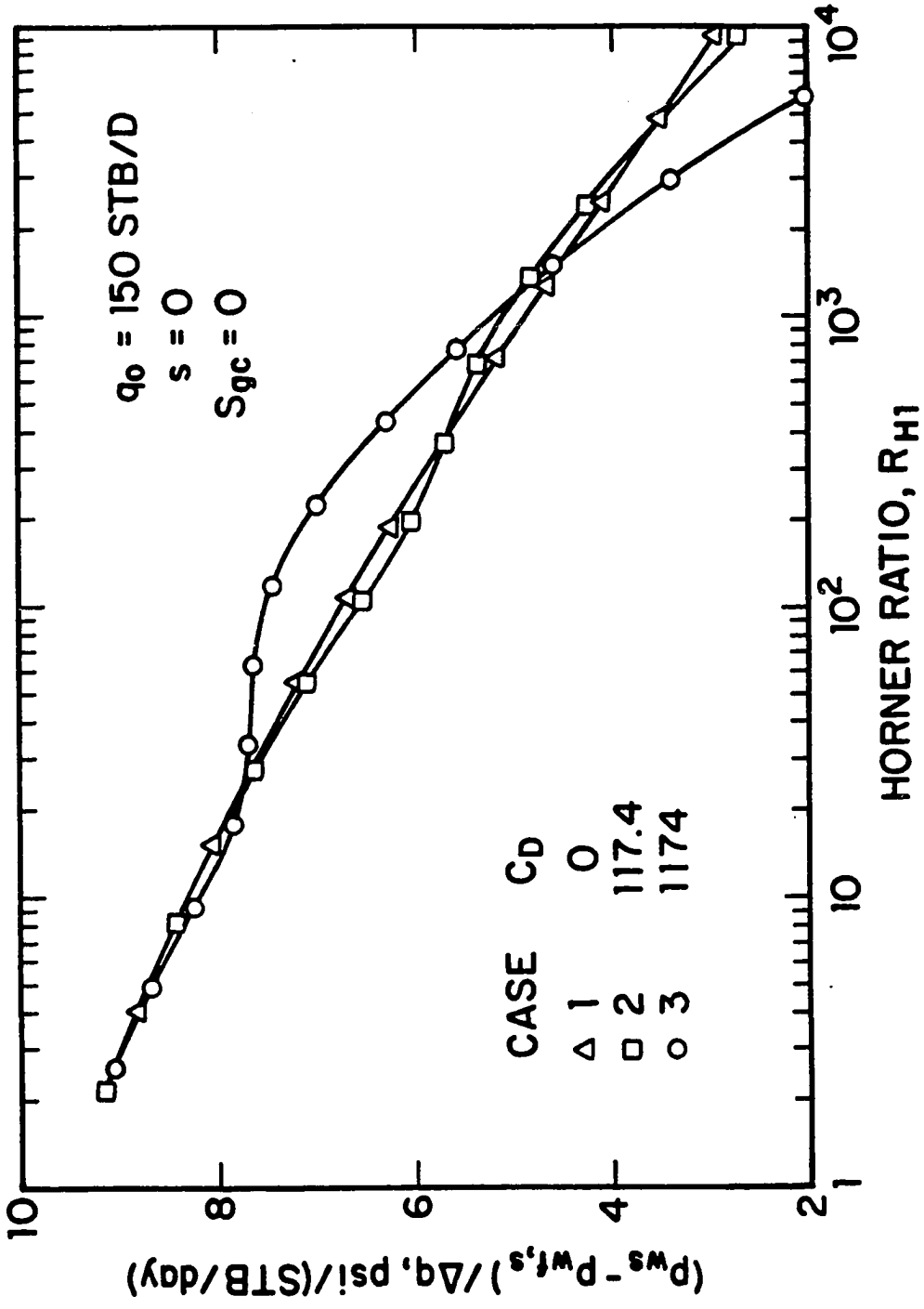

Fig. 7.10.1 - Semilog plot of rate-normalized change in pressure versus Horner time; Cases 1-3.

preceding paragraph, we obtain $kk_{ro}/(\mu_o B_o) = 8.83$ md/(cp-(RB/STB)) at $p_{ws,f}$ as compared to the correct value of $kk_{ro}/(\mu_o B_o) = 9.91$ md/(cp-(RB/STB)). The initial estimate obtained for kk_{roi}/μ_{oi} is 14.03 md/cp as compared to the correct value of $kk_{roi}/\mu_{oi} = 16.26$ md/cp. Eq. 7.10.3 then yields $s = 2.17$ as compared to the correct value of $s = 0$.

Fig. 7.10.2 shows semilog plots of $\Delta p/\Delta q(\Delta t)$ versus Horner time ratio for data obtained for Cases 4, 5 and 6. At times corresponding to $R_{H1} < 20.1$ ($\Delta t > 2.62 \times 10^{-1}$ days), the data for Case 6 appear to lie on a semilog straight line of slope $m_4 = 1.0794$ psi/(STB/D) per log cycle. For Cases 5 and 4 the semilog straight line begins at times $R_{H1} < 15.4$ ($\Delta t > 3.483 \times 10^{-1}$ days) and $R_{H1} < 3.84$ ($\Delta t > 1.76$ days), respectively. The final value of shut-in wellbore pressure is $p_{ws,f} = 3443$ psi. Following the computational procedure of the preceding paragraph, we obtain $kk_{ro}/(\mu_o B_o) = 9.69$ md/(cp-(RB/STB)) at $p_{ws,f}$ as compared to the correct value of $kk_{ro}/(\mu_o B_o) = 10.177$ md/(cp-(RB/STB)). The initial estimate obtained for kk_{roi}/μ_{oi} is 15.39 md/cp as compared to the correct value of $kk_{roi}/\mu_{oi} = 16.26$ md/cp. Eq. 7.10.3 then yields $s = 8.45$ as compared to the correct value of $s = 5$.

The results obtained from Figs. 7.10.1 and 7.10.2 indicate that semilog analysis based on a semilog plot of pressure versus time can yield inaccurate values of kk_{roi} and s. Moreover, the "semilog straight line" we selected in Figs. 7.10.1 and 7.10.2 lasts for only a very short period of time. The fact that we obtained good estimates of $(kk_{ro})/(\mu_o B_o)$ values, or equivalently good estimates of kk_{ro} at $p_{ws,f}$ is simply due to the fact that Eq. 7.7.1 gives the correct estimate of kk_{ro}. By fitting a semilog straight line through the last few data points in Figs. 7.10.1 and 7.10.2, we determined the correct value of $dp_{ws}/d\log R_{H1}$ that should be used in Eq. 7.7.1. During the times when the "semilog lines" of Figs. 7.10.1 and 7.10.2 occur, $q_{osf}(\Delta t) = 0.0$ and the term within square brackets in Eq. 7.7.1 is zero.

Note that the pressure method yields overestimates of the skin value. The explanation of this fact is as follows. Based on the results presented in Figs. 7.5.3 and 7.9.6, Eq. 7.5.4 is approximately correct for multiphase flow once wellbore

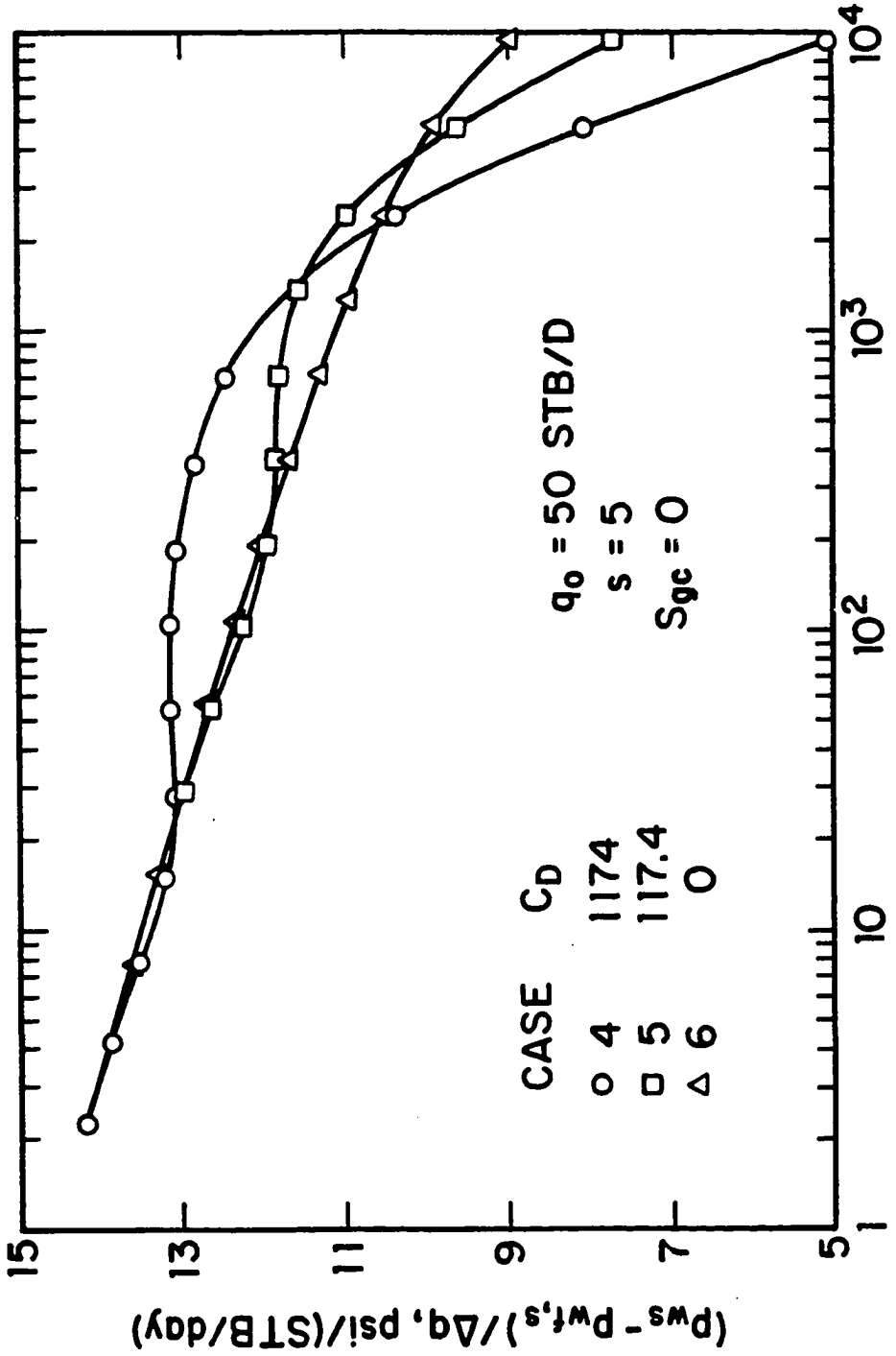

Fig. 7.10.2 - Semilog plot of rate-normalized change in pressure versus Horner time; Cases 4-6.

storage effects become negligible. Substituting Eq. 7.3.2 in Eq. 7.5.4, one obtains

$$\frac{kh\int_{p_{wf,s}}^{p_{ws}}\left(\frac{k_{ro}}{\mu_o B_o}\right)dp}{141.2q_o} = 1.151\log\left(\frac{4t_D}{e^{\gamma}}\frac{\Delta t}{t+\Delta t}\right)+s. \tag{7.10.4}$$

If the semilog straight line occurs during the interval $p_1 \leq p_{ws}$ Eq. 7.10.4 yields

$$\frac{kh}{141.2q_o}\left\{\int_{p_{wf,s}}^{p_1}\alpha dp+\int_{p_1}^{p_{ws}}\alpha dp\right\} = 1.151\log\left(\frac{4t_D}{e^{\gamma}}\frac{\Delta t}{t+\Delta t}\right)+s, \tag{7.10.5}$$

or

$$\frac{kh}{141.2q_o}\left\{\int_{p_{wf,s}}^{p_1}\alpha dp+\alpha_{avg}(p_{ws}-p_{wf,s}+p_{wf,s}-p_1)\right\} = 1.151\log\left(\frac{4t_D}{e^{\gamma}}\frac{\Delta t}{t+\Delta t}\right)+s, \tag{7.10.6}$$

where $\alpha_{avg} = \left[k_{ro}/(\mu_o B_o)\right]_{avg}$ denotes the average value of α in the pressure interval $[p_1, p_{ws}]$.

Rearranging Eq. 7.10.6 provides

$$p_{ws}-p_{wf,s}-\int_{p_{wf,s}}^{p_1}\left[1-\frac{\alpha}{\alpha_{avg}}\right]dp = \frac{162.6q_o}{kh\alpha_{avg}}\left\{\log\left(\frac{4t_D}{e^{\gamma}}\frac{\Delta t}{t+\Delta t}\right)+0.87s\right\}. \tag{7.10.7}$$

If

$$m = \frac{162.6q_o}{kh\alpha_{avg}}, \tag{7.10.8}$$

denotes the slope of the semilog straight line of the plot $p_{ws}-p_{wf,s}$ versus R_{H1}, then by evaluating Eq. 7.10.7 at $\Delta t = 1$ hour and rearranging the resulting equation, one obtains the following equation for the skin factor:

$$s = 1.151\left\{\frac{(p_{ws}-p_{wf,s})_{1hr}}{m}-\log\left(\frac{kk_{roi}}{\phi\mu_{oi}c_{ti}r_w^2}\right)+3.23-\frac{1}{m}\int_{p_{wf,s}}^{p_1}\left[1-\frac{\alpha}{\alpha_{avg}}\right]dp\right\}. \tag{7.10.9}$$

Since $\alpha_{avg} > \alpha$, i.e., $1-\alpha/\alpha_{avg} > 0$ and $p_1 > p_{wf,s}$, Eq. 7.10.9 implies that neglecting the term associated with the integral one will get higher estimates of skin factor.

CHAPTER VIII
CONCLUSIONS

We have presented new procedures for estimating effective or relative permeability curves directly from well-testing pressure data. The procedures use estimates of kk_{ro} and k_{rg}/k_{ro} as a function of pressure obtained from the methods of Refs. 8, 9, 10 and 28 to determine effective or relative permeability curves by nonlinear parameter estimation techniques with Standing's relative permeability correlations as the model function. When the skin factor is non-zero, in general, we can obtain accurate estimates of only two of the four parameters involved in Standing's relative permeability correlations. In such cases, the preferred approach is to obtain two estimates of kk_{ro} and k_{rg}/k_{ro} from a two-rate test and then apply Powell's method to obtain the two unknown parameters necessary to determine Standing's relative permeability curves.

We have shown that the computational procedures of Refs. 8, 9, 10 and 28 can be applied to cases where the initial reservoir pressure is larger than the initial bubble-point pressure. For this situation, the following conclusions are warranted.

(i) If the flowing wellbore pressure remains above bubble-point pressure for a sufficiently long time, then the computational procedures of Refs. 8, 9 and 28, i.e., Eq. 4.4.1, applied to pressure-time drawdown data will yield an accurate estimate of the initial effective oil permeability as well as accurate estimates of kk_{ro} during most of the time period when $p_{wf} < p_{bi}$. In either case, application of the computational procedures of Refs. 9 and 28 to buildup pressure versus shut-in data will only yield accurate estimates of initial oil effective permeability.

(ii) If the initial reservoir pressure is greater than the initial bubble-point pressure, the effective gas permeability values computed from drawdown data by applying Eq. 4.1.2 always yield very accurate estimates of the correct kk_{rg} data. The

kk_{rg} values computed from pressure buildup data by applying Eq. 4.1.4 yield rough estimates of the correct kk_{rg} data except at early shut-in times.

The computational procedures of Refs. 8, 9, 10 and 28 have been extended to study the effects of reservoir heterogeneities on the estimation of the effective or relative permeability data in a composite reservoir. For this problem, the following four conclusions apply.

(i) Generally, the effective or relative oil permeability values computed from pressure drawdown data reflect, at early times, the inner zone effective or relative oil permeability data and, at later times, reflect the outer zone effective or relative oil permeability data. If the radius of the inner zone is small, then one can only obtain estimates of the outer zone effective or relative oil permeability.

(ii) If the absolute permeability of the inner zone, k_s, is different from the outer zone absolute permeability, k, then the computed effective oil or gas permeability values reflect the $(k_s k_{ro})_{iz}$ or $(k_s k_{rg})_{iz}$ data of the inner zone at early times.

(iii) The effective or relative gas permeability values computed from pressure data will not reflect the outer zone effective or relative gas permeability data unless the k_{rg}/k_{ro} ratio is identical in both the inner and outer zones.

(iii) The effective oil permeability values computed from pressure buildup data are not highly accurate but tend to reflect the inner zone effective oil permeability data at early shut-in times, and at later shut-in times, tend to reflect the outer zone effective oil permeability data.

The influence of wellbore storage on transient, radial flow to a well producing a solution-gas-drive reservoir has been considered in this work. For this problem, the results presented in this study lead to the following conclusions.

(i) Given the sandface oil flow rate and the wellbore pressure as a function of time, the oil and gas effective permeabilities as a function of pressure can be computed by the following two procedures: (a) direct computation using the time derivative of the flowing wellbore pressure and the time derivative of the sandface oil flow rate; see Eq. 6.7.1; and (b) by straight line analysis based on plots of rate-normalized pressure-squared versus logarithmic convolution time.

(ii) A good estimate of skin factor, the effective oil permeability at the last measured values of flowing wellbore pressure and the initial effective oil permeability can be obtained using any of the three pressure-squared analysis methods presented.

(iii) Analysis based on a semilog plot of pressure versus time will not yield reasonable estimates of the initial effective permeability and the skin factor.

Finally, the influence of afterflow on transient, radial flow to a shut-in well in a solution-gas-drive reservoir has been considered. The results presented lead to the following conclusions.

(i) Given the sandface oil flow rate and the wellbore pressure as a function of time, the oil and gas effective permeabilities as a function of pressure and oil saturation can be roughly approximated by using the time derivative of the shut-in wellbore pressure and the time derivative of the sandface oil flow rate; see Eqs. 7.7.1 and 7.7.6.

(ii) A reasonably good estimate of skin factor, the effective oil permeability at the last measured values of shut-in wellbore pressure and the initial effective oil permeability can be obtained using any of the three pressure-squared analysis methods presented. However, if the variable flow rate due to afterflow is incorporated into the pressure-squared analysis, then the appropriate straight line will begin earlier.

(iii) Analysis based on a semilog plot of pressure versus time will not yield a highly accurate estimate of the initial effective oil permeability or the skin factor.

NOMENCLATURE

Symbol

a = parameter defined by Eq. 6.3.2, scf/RB-cp.

$\hat{a}$ = parameter defined by Eqs. 6.8.4 and 7.8.4.

b = parameter defined by Eq. 6.3.4.

$\hat{b}$ = parameter defined by Eqs. 6.8.5 and 7.8.5.

B_g = gas formation volume factor, RB/scf.

B_o = oil formation volume factor, RB/STB.

$\vec{c}$ = inequality constraints vector.

C_D = dimensionless wellbore storage coefficient.

c_g = gas compressibility, psi^{-1}.

c_t = total compressibility, psi^{-1}.

D = diagonal matrix.

E = objective function, md^2.

E^* = approximation to E, md^2.

F = model function.

$\vec{g}$ = gradient vector.

h = formation thickness, ft.

H = Hessian matrix.

I = unit matrix.

k = absolute permeability, md.

k_b = last buildup computed effective oil permeability, md.

k_{rg} = relative permeability of gas.

k_r^o = relative permeability of nonwetting phase at S_{iw}.

k_{ro} = relative permeability of oil.

k_s = absolute permeability in the skin zone, md.

kk_{rg} = effective permeability of gas, md.

kk_r^o = effective permeability of nonwetting phase at S_{iw}, md.

kk_{ro} = effective permeability of oil, md.

L = lower triangular matrix.

m = number of data.

n = number of parameters.

nc = number of constraints.

p = pressure, psi.

p_{bi} = initial bubble-point pressure, psi.

p_i = initial reservoir pressure, psi.

$p_p(p)$ = pseudopressure function, STB-psi/RB-cp.

p_{pDs} = dimensionless pseudopressure function.

p_{pwD} = dimensionless wellbore pseudopressure function.

$\tilde{p}_{pwD}$ = dimensionless wellbore pseudopressure function.

p_{wf} = flowing wellbore pressure, psi.

$p_{wf,s}$ = wellbore pressure at the instant of shut-in, psi.

p_{ws} = shut-in wellbore pressure, psi.

$p_p(p)$ = pseudopressure function, STB-psi/RB-cp.

p_{pwD} = dimensionless wellbore pseudopressure function.

$\vec{q}$ = equality constraints vector.

$q_g(t)$ = free gas flow rate, scf/day.

q_{gt} = total gas flow rate, scf/day.

q_o = oil flow rate, STB/day.

q_{osf} = sandface oil flow rate, STB/Day.

q_{osfD} = dimensionless sandface oil flow rate.

Q_{sD} = parameter defined by Eq. 6.6.6 or Eq. 6.6.7.

Q_D = parameter defined by Eq. C-6.

r = residual, md.

R = producing gas-oil ratio, scf/STB.

r_e = external reservoir radius, ft.

R_{H1} = primary Horner time ratio.

r_{iz} = inner zone radius, ft.

R_r = in-situ flowing gas-oil ratio, scf/STB.

r_s = radius of the skin zone, ft.

R_s = dissolved gas-oil ratio, scf/STB.

R_{sb} = dissolved GOR at bubble point pressure, scf/STB.

R_{sbi} = dissolved GOR at initial bubble point pressure, scf/STB.

r_w = wellbore radius, ft.

s = skin factor.

$\tilde{s}$ = apparent skin factor defined by Eqs. 6.5.5, 6.8.14, 7.5.9 and 7.8.21.

S_{iw} = irreducible water saturation, fraction.

S_g = gas saturation, fraction.

S_g^* = normalized gas saturation, fraction.

S_{gc} = critical gas saturation, fraction.

S_L^* = normalized liquid saturation, fraction.

S_o = oil saturation, fraction.

S_{or} = residual oil saturation, fraction.

S_o^* = normalized oil saturation, fraction.

S_w^* = normalized water saturation, fraction.

S_{wc} = connate water saturation, fraction.

t = time, days.

t_{lc} = logarithmic convolution time defined by Eq. 6.5.2.

t_{lcD} = logarithmic convolution time defined by Eq. 6.5.3.

t_D = dimensionless time defined by Eq. 6.3.11.

z = Boltzmann variable.

z_D = dimensionless Boltzmann variable.

Greek Symbols

α = parameter defined by Eq. 6.3.1, STB/RB-cp.

β = parameter defined by Eq. 6.3.3, STB/RB.

α^* = wellbore storage parameter, 1/days.

β^* = dimensionless wellbore storage parameter.

γ = Euler's constant, 0.577221.

Δt = shut-in time, days.

Δt_D = dimensionless shut-in time defined by Eq. 7.3.3.

Δt_{lc} = logarithmic convolution shut-in time defined by Eq. 7.5.6.

Δt_{lcD} = logarithmic convolution shut-in time defined by Eq. 7.5.7.

Δt_{nD} = dimensionless normalized shut-in time defined by Eq. 7.3.4.

ϵ_M = machine precision.

ς = penalty function.

η = mean error square.

$\vec{\theta}$ = vector of unknown parameters.

λ = pore size distribution index.

λ_g = gas mobility, cp^{-1}.

λ_o = oil mobility, cp^{-1}.

λ_t = total mobility, cp^{-1}.

μ_g = gas viscosity, cp.

μ_o = oil viscosity, cp.

μ_{oi} = initial oil viscosity, cp.

ρ = step length.

ϕ = porosity.

Υ = standard error.

Subscripts

D = dimensionless.

g = gas phase.

i = initial conditions.

iz = inner zone.

o = oil phase.

oz = outer zone.

sf = sandface.

t = total.

Superscripts

i = iteration.

T = transpose.

-1 = inverse.

$+$ = modified.

REFERENCES

1. Perrine, R. L.:"Analysis of Pressure Buildup Curves," *Drill. and Prod. Prac.*, API (1956) 482-509.
2. Martin, J. C.: "Simplified Equations of Flow in Gas Drive Reservoirs and the Theoretical Foundation of Multiphase Flow Pressure Buildup Analysis," *J. Pet. Tech.* (Oct. 1959) 321-323; *Trans., AIME,* 216.
3. Evinger, H. H. and Muskat, M.: "Calculation of Theoretical Productivity Factor," *Trans., AIME,* 146 (1942) 126-139.
4. Fetkovich, M.: "The Isochronal Testing of Oil Wells," paper SPE 4529 presented at the 1973 SPE Annual Technical Conference and Exhibition, Las Vegas, Sept. 30 - Oct. 3.
5. Raghavan R.: "Well Test Analysis: Wells Producing by Solution Gas Drive," *Soc. Pet. Eng. J.* (Aug. 1976) 196-208.
6. Bøe, A., Skjaeveland, S. and Whitson, C.: "Two-Phase Pressure Test Analysis," paper SPE 10224, presented at the 1981 SPE Annual Technical Conference and Exhibition, San Antonio, TX, Oct. 5-7.
7. Aanonsen, S.: "Nonlinear Effects During Transient Fluid Flow in Reservoirs as Encountered in Well Test Analysis," Dr. Scient. dissertation, U. of Bergen, Norway (1985).
8. Al-Khalifah, A., Horne, R. and Aziz, K.: "In-Place Determination of Reservoir Relative Permeability Using Well Test Analysis," paper SPE 16774 presented at the 1987 SPE Annual Technical Conference and Exhibition, Dallas, TX, Sept. 27-30.
9. Serra, K., Peres, A. and Reynolds, A.: "Well Test Analysis for Solution-Gas-Drive Reservoirs: Part 1 - Determination of Relative and Absolute Permeabilities," *SPE Formation Evaluation* (June 1990) 124-132.

10. Serra, K., Peres, A. and Reynolds, A.: "Well Test Analysis for Solution-Gas-Drive Reservoirs: Part 2 - Buildup Analysis," *SPE Formation Evaluation* (June 1990) 133-140.

11. Al-Khalifah, A., Aziz, K. and Horne, R.: "A New Approach to Multiphase Well Test Analysis," paper SPE 16743 presented at the 1987 SPE Annual Technical Conference and Exhibition, Dallas, TX, Sept. 27-30.

12. Serra, K., Peres, A. and Reynolds, A.: "Well Test Analysis for Solution-Gas-Drive Reservoirs: Part 3 - A Unified Treatment of the Pressure-Squared Method," *SPE Formation Evaluation* (June 1990) 141-150.

13. Chu, W., Reynolds, A and Raghavan R.: "Pressure Transient Analysis of Two-Phase Flow Problems," *SPE Formation Evaluation* (April 1986) 151-164.

14. Al-Khalifah, A., Horne, R. and Aziz, K.: "Multiphase Well Test Analysis: Pressure and Pressure-Squared Methods," paper SPE 18803 presented at the 1989 SPE California Regional Meeting, Bakersfield, CA, April 5-7.

15. Standing, M. B.: *Notes on Relative Permeability Relationships,* Div. of Pet. Eng. and Appl. Geoph., Norwegian Institute of Technology, University of Trondheim, Trondheim (1974).

16. Bard, Y.: *Nonlinear Parameter Estimation,* Academic Press Inc. Ltd., New York (1974).

17. Greenstadt, J. L.: "On the Relative Efficiency of Greenstadt Methods," *Mathematics of Computation,* (1967) 21, 360-367.

18. Marquardt, D. W.: "Algorithm for Least-Squares Estimation of Nonlinear Parameters," *J. Soc. Indust. Appl. Math.,* (June 1963) 11, No. 2, 434-441.

19. Levenberg, K.: "A Method for the Solution of Certain Problems in Least Squares," *Quart. Appl. Math.,* (1944) 2, 164-168.

20. Gill, P. E., Murray, W., and Wright, M. H.: *Practical Optimization,* Academic Press Inc. Ltd., New York (1983).

21. Fiacco, A. V. and McCormick, G. P.: "The Sequential Unconstrained Minimization Technique for Nonlinear Programming: A Primal-dual Method," *Management Sci.,* (1964) 10, 360-366.

22. Afifi, A. A. and Azen, S. P.: *Statistical Analysis - A Computer Oriented Approach,* (2nd edition), Academic Press, New York (1979).

23. Rosa, A. J. and Horne, R. N.: "Automated Type-Curve Matching in Well Test Analysis Using Laplace Space Determination of Parameter Gradients," paper SPE 12131 presented at the 58th Annual Meeting, San Francisco, CA, Oct. 5-8, 1983.

24. Barua, J. and Horne, R. N.: "Computerized Analysis of Thermal Recovery Well Test Data," *SPE Formation Evaluation* (Dec. 1987) 560-566.

25. Barua, J., Horne, R. N., Greenstadt, J. L. and Lopez, L.: "Improved Estimation Algorithms for Automated Type Curve Analysis of Well Tests," *SPE Formation Evaluation* (March 1988) 186-196.

26. Nanba, T. and Horne, R. N.: "An Improved Regression Algorithm for Automated Well Test Analysis," paper SPE 18161 presented at the 1988 SPE Annual Technical Conference and Exhibition, Houston, TX, Oct. 2-5.

27. Nanba, T. and Horne, R. N.: "Estimation of Water and Oil Relative Permeabilities From Pressure Transient Analysis of Water Injection Well Data," paper SPE 19829 presented at the 1989 SPE Annual Technical Conference and Exhibition, San Antonio, TX, Oct. 8-11.

28. Serra, K.: "Well Testing for Solution-Gas-Drive Reservoirs," PhD dissertation, The University of Tulsa, Tulsa, OK (June 1988).

29. Hatzignatiou, D. G., Peres, A. and Reynolds, A. C.: "Wellbore Storage Effects on the Multiphase Pressure Test Analysis," paper SPE 19841 presented at the 1989 SPE Annual Technical Conference and Exhibition, San Antonio, TX, Oct. 8-11.

30. Hatzignatiou, D. G. and Reynolds, A. C.: "Effect of Afterflow on the Analysis of Pressure Buildup Data From Solution-Gas-Drive Reservoirs," report presented at the 2nd TUPREP meeting (Nov. 1989).

31. Corey, A. T.: "The Interrelation Between Gas and Oil Relative Permeabilities," *Prod. Monthly* (Nov. 1954) 19 (1), 38.

32. Hawkins, M. F., Jr.: "A Note on the Skin Effect," *Trans. AIME* (1956) 356-

357.

33. ECLIPSE: *Reference Manual,* Version 88/09, Exploration Consultants Limited (Sept. 1988).
34. Honarpour, M., Koederitz, L. F. and Harvey, A. H.: "Empirical Equations for Estimating Two-Phase Relative Permeability in Consolidated Rock," *J. Pet. Tech.* (Dec. 1982) 2905-2908.
35. Powell, M. J. D.: "A Fortran Subroutine for Solving Systems of Nonlinear Algebraic Equations," *Numerical Methods for Nonlinear Algebraic Equations,* Rabinowitz, P. Editor, Gordon and Breach Science Publishers, London (1970).
36. Press, W. H., Flannery, B. P., Teukolsky, S. A. and Vetterling, W. T.: *Numerical Recipes - The Art of Scientific Computing,* Cambridge University Press, Cambridge (1987).
37. Hatzignatiou, D. G. and Reynolds, A. C.: "Determination of Effective or Relative Permeability Curves From Well Tests," paper SPE 20537 to be presented at the 1990 SPE Annual Technical Conference and Exhibition, New Orleans, LA, Sept. 23-26.
38. Hatzignatiou, D. G. and Reynolds, A. C.: "Estimation of Effective Permeabilities for Reservoirs Initially Above Bubble-Point Pressure," report presented at the 3rd TUPREP meeting (May 1990).
39. Earlougher, R. C.: *Advances in Well Test Analysis,* Monograph Series, Society of Petroleum Engineers of AIME, Dallas, TX, (1977) *5* .
40. Peres, A., Serra, K., and Reynolds, A.: "Towards a Unified Theory of Well Testing for Nonlinear Radial Flow Problems with Applications to Interference Tests," *SPE Formation Evaluation* (June 1990) 151-160.
41. Thompson, L. G., and Vo, D. T.: "Drawdown Well Test Analysis for Multicomponent Hydrocarbon Systems," paper SPE 18126 presented at the 1988 SPE Annual Technical Conference and Exhibition, Houston, TX, Oct. 2-5.
42. van Everdingen, A.F.: "The Skin Effects and its Influence on the Productive Capacity of a Well," *Trans. AIME* (1958) 171-176.
43. Hurst, W.: "Establishment of the Skin Effect and its Impediment to Fluid

Flow into a Wellbore," *Pet. Eng.* (Oct. 1953) B 6-16.

44. Kucuk, F., and Ayestaran, L.: "Analysis of Simultaneously Measured Pressure and Sandface Flow Rate in Transient Well Testing," *J. Pet. Tech.* (Feb. 1985) 323-334.
45. Peres, A., Macias-Chapa, L., Serra, K. and Reynolds, A.: "Well Conditioning Effects on Bubble-point Pressure of Fluid Samples from Solution-Gas-Drive Reservoirs," paper SPE 18530 presented at the 1988 SPE Eastern Regional Meeting, Charleston WV, Nov. 1-4.
46. Ramey, H. J., Jr.: "Rapid Methods for Estimating Reservoir Compressibilities," *J. Pet. Tech.* (April 1964) 447-454.
47. Agarwal, R. G., Al-Hussainy, R., and Ramey, H.J.,Jr.: "An Investigation of Wellbore Storage and Skin Effects in Unsteady Liquid Flow: I Analytical Treatment," *Soc. Pet. Eng. J.* (Sept. 1970) 270-290; *Trans., AIME* , 249.
48. Bourdet, D., Whittle, T. M., Douglas, A. A., and Pirard, Y. M.: "A New Set of Type Curves Simplifies Well Test Analysis," *World Oil* (May 1983) 95-106.
49. Odeh, A. S., and Jones, L. G.: "Pressure Drawdown Analysis, Variable-Rate Case," *Trans. AIME,* 234 (1965) 960-964.
50. Ramey, H. J., Jr.: "Verification of the Gladfelter-Tracy-Wilsey Concept for Wellbore Storage Dominated Transient Pressures During Production," *J. Cdn. Pet. Tech.* (April-June 1976) 84-85.
51. Gladfelter, R. E., Tracy, G. W., and Wilsey, L. E.: "Selecting Wells which will Respond to Production-stimulation Treatment," *Drill. and Prod. Prac.* , API (1955) 117-128.
52. Winestock, A. G., and Colpitts, G. P.: "Advances in Estimating Gas Well Deliverability," *J. Cdn. Pet. Tech.* (July-Sept. 1965) 111-119.
53. Thompson, L. G., and Reynolds, A. C.: "Analysis of Variable-Rate Well-Test Pressure Data Using Duhamel's Principle," paper SPE 13080 presented at the 1984 SPE Annual Technical Conference and Exhibition, Houston, TX, Sept. 16-19.
54. Peres, A., Onur, M., and Reynolds, A. C.: "A New General Pressure Anal-

ysis Procedure for Slug Tests," paper SPE 18801 presented at the 1989 SPE California Regional Meeting, Bakersfield, CA, April 5-7.

55. Fetkovich, M. J. and Vienot, M. E.: "Rate Normalization of Buildup Pressure by Using Afterflow Data," *J. Pet. Eng.* (Dec. 1984) 2211-2224.

56. Agarwal, R. G.: "A New Method to Account for Producing Time Effects When Drawdown Type Curves Are Used to Analyze Pressure Buildup and Other Test Data," paper SPE 9289 presented at the 1980 SPE Annual Technical Conference and Exhibition, Dallas, TX, Sept. 21-24.

APPENDIX A

ROCK AND FLUID PROPERTIES

Table A-1

PVT DATA

Set 1

Pressure psi	B_o RB/STB	μ_o cp	R_s SCF/STB	B_g RB/SCF	μ_g cp
216.9	1.074	1.744	0.38293E+02	0.13256E-01	0.0120
448.6	1.097	1.408	0.88280E+02	0.63268E-02	0.0125
680.2	1.124	1.177	0.14390E+03	0.40415E-02	0.0131
911.9	1.153	1.013	0.20352E+03	0.29104E-02	0.0138
1143.5	1.184	0.891	0.26630E+03	0.22559E-02	0.0146
1375.2	1.217	0.797	0.33173E+03	0.18374E-02	0.0155
1606.8	1.252	0.723	0.39945E+03	0.15537E-02	0.0165
1838.5	1.289	0.662	0.46918E+03	0.13541E-02	0.0174
2070.1	1.328	0.612	0.54073E+03	0.12077E-02	0.0183
2301.8	1.368	0.570	0.61393E+03	0.10983E-02	0.0192
2533.4	1.409	0.534	0.68865E+03	0.10139E-02	0.0200
2765.1	1.452	0.503	0.76477E+03	0.94728E-03	0.0206
2996.7	1.496	0.476	0.84221E+03	0.89332E-03	0.0212
3228.3	1.542	0.452	0.92088E+03	0.84862E-03	0.0217
3460.0	1.588	0.431	0.99964E+03	0.81086E-03	0.0222
3691.6	1.642	0.414	0.10809E+04	0.78059E-03	0.0226
3923.3	1.692	0.400	0.11631E+04	0.75031E-03	0.0229
4154.9	1.747	0.389	0.12463E+04	0.72378E-03	0.0233
4386.6	1.798	0.378	0.13305E+04	0.70098E-03	0.0236
4618.2	1.853	0.372	0.14156E+04	0.68958E-03	0.0238
4849.9	1.908	0.365	0.15016E+04	0.68210E-03	0.0240

Table A-2

ROCK PROPERTIES

Set 1

So	k_{ro}	k_{rg}
0.000000E+00	0.000000E+00	0.700000E+00
0.400000E+00	0.746356E-01	0.865889E-01
0.500000E+00	0.182216E+00	0.279883E-01
0.530000E+00	0.230043E+00	0.176181E-01
0.560000E+00	0.286720E+00	0.100800E-01
0.580000E+00	0.329927E+00	0.644851E-02
0.590000E+00	0.353276E+00	0.500580E-02
0.595000E+00	0.365405E+00	0.437062E-02
0.600000E+00	0.377843E+00	0.379008E-02
0.605000E+00	0.390596E+00	0.326202E-02
0.615000E+00	0.417068E+00	0.235444E-02
0.620000E+00	0.430797E+00	0.197038E-02
0.625000E+00	0.444863E+00	0.162969E-02
0.630000E+00	0.459270E+00	0.133000E-02
0.635000E+00	0.474025E+00	0.106888E-02
0.640000E+00	0.489132E+00	0.843848E-03
0.645000E+00	0.504597E+00	0.652404E-03
0.650000E+00	0.520426E+00	0.491983E-03
0.655000E+00	0.536625E+00	0.359984E-03
0.660000E+00	0.553199E+00	0.253760E-03
0.665000E+00	0.570154E+00	0.170625E-03
0.670000E+00	0.587496E+00	0.107842E-03
0.675000E+00	0.605231E+00	0.626365E-04
0.680000E+00	0.623364E+00	0.321865E-04
0.685000E+00	0.641901E+00	0.136279E-04
0.690000E+00	0.660849E+00	0.405246E-05
0.695000E+00	0.680213E+00	0.508380E-06
0.700000E+00	0.700000E+00	0.000000E+00

Table A-3

PVT DATA

Set 2

Pressure psi	B_o RB/STB	μ_o cp	R_s SCF/STB	B_g RB/SCF	μ_g cp
14.7	1.0280	1.4000	0.00	0.022725	0.01100
193.0	1.0580	1.3500	44.29	0.016881	0.01130
622.6	1.0880	1.1640	119.14	0.004998	0.01250
1052.1	1.1210	1.0110	196.10	0.002825	0.01380
1481.6	1.1590	0.8810	278.24	0.001929	0.01520
1911.0	1.2020	0.7680	366.52	0.001455	0.01660
2340.5	1.2490	0.6710	461.53	0.001172	0.01810
2770.1	1.3020	0.5870	563.75	0.000991	0.01950
3199.5	1.3600	0.5150	673.74	0.000871	0.02100
3700.5	1.4340	0.4460	812.55	0.000775	0.02280
4201.6	1.5160	0.3910	963.48	0.000712	0.02460
4702.7	1.6050	0.3480	1127.44	0.000659	0.02630
5203.7	1.7020	0.3170	1305.54	0.000623	0.02810
5633.1	1.7910	0.3000	1470.40	0.000606	0.02950
5704.4	1.8060	0.2980	1498.98	0.000588	0.02980

Table A-4

ROCK PROPERTIES

Set 2

So	k_{ro}	k_{rg}
0.000000E+00	0.000000E+00	0.627782E+00
0.100000E+00	0.594990E-05	0.444304E+00
0.200000E+00	0.380794E-03	0.292459E+00
0.300000E+00	0.433748E-02	0.172249E+00
0.400000E+00	0.243708E-01	0.836727E-01
0.420000E+00	0.326592E-01	0.697536E-01
0.450000E+00	0.494066E-01	0.512475E-01
0.470000E+00	0.641353E-01	0.404919E-01
0.500000E+00	0.929672E-01	0.267310E-01
0.510000E+00	0.104696E+00	0.227767E-01
0.520000E+00	0.117633E+00	0.191387E-01
0.530000E+00	0.131876E+00	0.158171E-01
0.540000E+00	0.147527E+00	0.128119E-01
0.550000E+00	0.164697E+00	0.101230E-01
0.560000E+00	0.183501E+00	0.775040E-02
0.570000E+00	0.204060E+00	0.569417E-02
0.580000E+00	0.226505E+00	0.395429E-02
0.590000E+00	0.250970E+00	0.253074E-02
0.595000E+00	0.264005E+00	0.193760E-02
0.600000E+00	0.277599E+00	0.142354E-02
0.605000E+00	0.291771E+00	0.988569E-03
0.615000E+00	0.321929E+00	0.355885E-03
0.620000E+00	0.337956E+00	0.158171E-03
0.625000E+00	0.354642E+00	0.395427E-04
0.630000E+00	0.372009E+00	0.000000E+00
0.635000E+00	0.390079E+00	0.000000E+00
0.640000E+00	0.408874E+00	0.000000E+00
0.645000E+00	0.428418E+00	0.000000E+00
0.650000E+00	0.448735E+00	0.000000E+00
0.655000E+00	0.469848E+00	0.000000E+00
0.660000E+00	0.491783E+00	0.000000E+00
0.665000E+00	0.514564E+00	0.000000E+00
0.670000E+00	0.538219E+00	0.000000E+00
0.675000E+00	0.562772E+00	0.000000E+00
0.680000E+00	0.588252E+00	0.000000E+00
0.685000E+00	0.614686E+00	0.000000E+00
0.690000E+00	0.642103E+00	0.000000E+00
0.695000E+00	0.670531E+00	0.000000E+00
0.700000E+00	0.700000E+00	0.000000E+00

Table A-5

ROCK PROPERTIES

Set 3

So	k_{ro}	k_{rg}
0.00000E+00	0.00000E+00	0.90000E+00
0.40000E+00	0.11564E+00	0.10026E+00
0.50000E+00	0.26208E+00	0.31536E-01
0.53000E+00	0.32451E+00	0.19695E-01
0.56000E+00	0.39711E+00	0.11181E-01
0.58000E+00	0.45163E+00	0.71163E-02
0.59000E+00	0.48085E+00	0.55102E-02
0.59500E+00	0.49596E+00	0.48049E-02
0.60000E+00	0.51141E+00	0.41615E-02
0.60500E+00	0.52721E+00	0.35772E-02
0.61000E+00	0.54337E+00	0.30494E-02
0.62000E+00	0.57675E+00	0.21526E-02
0.62500E+00	0.59399E+00	0.17782E-02
0.63000E+00	0.61160E+00	0.14494E-02
0.63500E+00	0.62958E+00	0.11634E-02
0.64000E+00	0.64795E+00	0.91735E-03
0.64500E+00	0.66671E+00	0.70836E-03
0.65000E+00	0.68585E+00	0.53353E-03
0.65500E+00	0.70540E+00	0.38990E-03
0.66000E+00	0.72534E+00	0.27452E-03
0.66500E+00	0.74570E+00	0.18436E-03
0.67000E+00	0.76646E+00	0.11638E-03
0.67500E+00	0.78764E+00	0.67514E-04
0.68000E+00	0.80925E+00	0.34651E-04
0.68500E+00	0.83128E+00	0.14654E-04
0.69000E+00	0.85375E+00	0.43523E-05
0.69500E+00	0.87665E+00	0.54534E-06
0.70000E+00	0.90000E+00	0.00000E+00

APPENDIX B
SATURATION-PRESSURE RELATIONSHIP DURING DRAWDOWN

Proceeding in a manner similar to that of Ref. 28 and defining $c_1 = 6.328 \times 10^{-3}$, one may combine the oil and gas flow equations to obtain

$$R_r \frac{\partial \beta}{\partial t} - \frac{\partial b}{\partial t} = -\frac{c_1 k_s \alpha}{\phi} \frac{\partial R_r}{\partial r} \frac{\partial p}{\partial r}. \qquad (B-1)$$

The skin zone permeability appears in Eq. B-1 because we have combined the flow equations within the skin zone to obtain Eq. B-1. Assuming that oil saturation is a unique function of pressure and following the same type of derivation used in Ref. 28, one can show that

$$\frac{dS_o}{dp} = \frac{c_1 \frac{k_s}{\phi} \left(\alpha \frac{\partial a}{\partial p} - a \frac{\partial \alpha}{\partial p}\right) \left(\frac{\partial p}{\partial r}\right)^2 + \left(a \frac{\partial \beta}{\partial p} - \alpha \frac{\partial b}{\partial p}\right) \frac{\partial p}{\partial t}}{c_1 \frac{k_s}{\phi} \left(a \frac{\partial \alpha}{\partial S_o} - \alpha \frac{\partial a}{\partial S_o}\right) \left(\frac{\partial p}{\partial r}\right)^2 - \left(a \frac{\partial \beta}{\partial S_o} - \alpha \frac{\partial b}{\partial S_o}\right) \frac{\partial p}{\partial t}}. \qquad (B-2)$$

Eq. B-2 is identical to an equation derived by Aanonsen[7] except that he did not consider a skin zone, i.e., Aanonsen's equation can be obtained from Eq. B-2 by setting $k_s = k$. Bøe et al.[6] assumed that $k_s = k$, i.e., $s = 0$, and also assumed that pressure and saturation are functions of the Boltzmann variable, $z = r^2/t$, so that

$$\frac{\partial p/\partial r}{\partial p/\partial t} = -\frac{2t}{r}. \qquad (B-3)$$

From Darcy's law, it follows that

$$\left(\frac{\partial p}{\partial r}\right)_{r_w} = \frac{5.615 q_{osf}(t)}{c_1 (2\pi r_w k h \alpha)}. \qquad (B-4)$$

Replacing k_s by k in Eq. B-2, evaluating at $r = r_w$, dividing the resulting equation by $-\partial p_{wf}/\partial t$ and using Eqs. B-3 and B-4 in the resulting equation yields

$$\frac{dS_o}{dp_{wf}} = \frac{\frac{2t}{\alpha r_w} Q_D \left(\alpha \frac{\partial a}{\partial p_{wf}} - a \frac{\partial \alpha}{\partial p_{wf}}\right) + \left(\alpha \frac{\partial b}{\partial p_{wf}} - a \frac{\partial \beta}{\partial p_{wf}}\right)}{\frac{2t}{\alpha r_w} Q_D \left(a \frac{\partial \alpha}{\partial S_o} - \alpha \frac{\partial a}{\partial S_o}\right) + \left(a \frac{\partial \beta}{\partial S_o} - \alpha \frac{\partial b}{\partial S_o}\right)}, \qquad (B-5)$$

where

$$Q_D = \frac{5.615 q_{osf}(t)}{2\pi r_w \phi h}, \qquad (B-6)$$

and all terms in Eq. B-5 are evaluated at $r = r_w$. If we also assume $q_{osf}(t) = q_o$, then Eq. B-5 reduces to the dS_o/dp_{wf} equation given in Ref. 6.

As pointed out in Ref. 6, the Boltzmann transformation does not apply if $s \neq 0$. Hence, Eq. B-5 does not apply unless the skin factor is zero. Eq. B-2 is more general in that it does not assume the validity of the Boltzmann transformation. Evaluating Eq. B-2 at $r = r_w$ and using Eq. B-4 gives

$$\frac{dS_o}{dp_{wf}} = \left(\frac{Q_{sD}\left(\alpha \frac{\partial a}{\partial p} - a\frac{\partial \alpha}{\partial p}\right) - \left(\alpha \frac{\partial b}{\partial p} - a\frac{\partial \beta}{\partial p}\right)\left(\frac{dp_{wf}}{dt}\right)}{Q_{sD}\left(-\alpha \frac{\partial a}{\partial S_o} + a\frac{\partial \alpha}{\partial S_o}\right) - \left(-\alpha \frac{\partial b}{\partial S_o} + a\frac{\partial \beta}{\partial S_o}\right)\left(\frac{dp_{wf}}{dt}\right)} \right)_{r=r_w}, \qquad (B-7)$$

where

$$Q_{sD} = \frac{5.615 q_{osf}(t)}{c_1 \alpha 2\pi k_s r_w h}\left(\frac{5.615 q_{osf}(t)}{2\pi \phi r_w h \alpha}\right)$$

$$= \left(\frac{5.615 q_{osf}(t)}{2\pi r_w h}\right)^2 \frac{1}{c_1 \alpha^2 k_s \phi}. \qquad (B-8).$$

Eqs. B-7 and B-8, respectively, are equivalent to Eqs. 6.6.5 and 6.6.7 of the text.

APPENDIX C
SATURATION-PRESSURE RELATIONSHIP IN TERMS OF THE RATIO k_{rg}/k_{ro} DURING DRAWDOWN

Zero Wellbore Storage.

Bøe et al.[6] showed that for the $s = 0$ case, pressure and saturation are unique functions of the Boltzmann variable, z, and they derived an ordinary differential equation for computing S_o as a function of p_{wf}. The equation they presented can be written as

$$\frac{dS_o}{dp_{wf}} = \left(\frac{\frac{2t}{r}\frac{Q_D}{\alpha}\left(\alpha\frac{\partial a}{\partial p} - a\frac{\partial \alpha}{\partial p}\right) + \left(\alpha\frac{\partial b}{\partial p} - a\frac{\partial \beta}{\partial p}\right)}{\frac{2t}{r}\frac{Q_D}{\alpha}\left(-\alpha\frac{\partial a}{\partial S_o} + a\frac{\partial \alpha}{\partial S_o}\right) + \left(-\alpha\frac{\partial b}{\partial S_o} + a\frac{\partial \beta}{\partial S_o}\right)} \right)_{r=r_w}, \qquad (C-1)$$

where

$$\alpha = \frac{k_{ro}}{\mu_o B_o}, \qquad (C-2)$$

$$a = \frac{R_s k_{ro}}{\mu_o B_o} + \frac{k_{rg}}{\mu_g B_g}, \qquad (C-3)$$

$$\beta = \frac{S_o}{B_o}, \qquad (C-4)$$

$$b = \frac{R_s S_o}{B_o} + \frac{S_g}{B_g}, \qquad (C-5)$$

and

$$Q_D = \frac{5.615 q_o}{2\pi r_w \phi h}. \qquad (C-6)$$

Defining

$$f_o = \frac{\frac{kk_{ro}}{\mu_o B_o}}{\frac{kk_{ro}}{\mu_o B_o} + \frac{kk_{rg}}{\mu_g B_g}} = \frac{\frac{k_{ro}}{\mu_o B_o}}{\frac{k_{ro}}{\mu_o B_o} + \frac{k_{rg}}{\mu_g B_g}} = \frac{\alpha}{\lambda_t}, \qquad (C-7)$$

and

$$f_g = \frac{\frac{kk_{rg}}{\mu_g B_g}}{\frac{kk_{ro}}{\mu_o B_o} + \frac{kk_{rg}}{\mu_g B_g}} = \frac{\frac{k_{rg}}{\mu_g B_g}}{\frac{k_{ro}}{\mu_o B_o} + \frac{k_{rg}}{\mu_g B_g}} = \frac{\frac{k_{rg}}{\mu_g B_g}}{\lambda_t}, \qquad (C-8)$$

then

$$f_o + f_g = 1. \qquad (C-9)$$

Using the definitions given by Eqs. C-2, C-3, C-7 and C-8 , one obtains

$$\frac{1}{\alpha}\left(\alpha\frac{\partial a}{\partial p} - a\frac{\partial \alpha}{\partial p}\right) = \frac{\partial a}{\partial p} - \frac{a}{\alpha}\frac{\partial \alpha}{\partial p}$$

$$= \frac{\partial}{\partial p}\left(\alpha R_s + \frac{k_{rg}}{\mu_g B_g}\right) - \frac{\alpha R_s + \frac{k_{rg}}{\mu_g B_g}}{\alpha}\frac{\partial \alpha}{\partial p}, \qquad (C-10)$$

which after cancelation yields

$$\frac{1}{\alpha}\left(\alpha\frac{\partial a}{\partial p} - a\frac{\partial \alpha}{\partial p}\right) = \alpha\frac{\partial R_s}{\partial p} + \frac{\partial(f_g\lambda_t)}{\partial p} - \frac{\frac{kk_{rg}}{\mu_g B_g}}{\frac{kk_{ro}}{\mu_o B_o}}\frac{\partial \alpha}{\partial p}$$

$$= \alpha\frac{\partial R_s}{\partial p} + \frac{\partial(f_g\lambda_t)}{\partial p} - \frac{f_g}{f_o}\frac{\partial(f_o\lambda_t)}{\partial p}. \qquad (C-11)$$

Expanding and rearranging, one can rewrite Eq. C-11 as follows:

$$\frac{1}{\alpha}\left(\alpha\frac{\partial a}{\partial p} - a\frac{\partial \alpha}{\partial p}\right) = f_o\lambda_t\frac{\partial R_s}{\partial p} - \lambda_t\frac{\partial(1-f_o)}{\partial p} - \lambda_t\frac{f_g}{f_o}\frac{\partial(f_o\lambda_t)}{\partial p}$$

$$= \lambda_t\left[f_o\frac{\partial R_s}{\partial p} - \frac{\partial f_o}{\partial p}\left(1 + \frac{f_g}{f_o}\right)\right], \qquad (C-12)$$

which finally yields

$$\frac{1}{\alpha}\left(\alpha\frac{\partial a}{\partial p} - a\frac{\partial \alpha}{\partial p}\right) = \lambda_t\left[f_o\frac{\partial R_s}{\partial p} - \frac{1}{f_o}\frac{\partial f_o}{\partial p}\right], \qquad (C-13)$$

Working in a similar manner, one obtains

$$\alpha\frac{\partial b}{\partial p} - a\frac{\partial \beta}{\partial p} = f_o\lambda_t\frac{\partial b}{\partial p} - f_o\lambda_t R_s\frac{\partial \beta}{\partial p} - f_g\lambda_t\frac{\partial \beta}{\partial p}$$

or

$$\alpha\frac{\partial b}{\partial p} - a\frac{\partial \beta}{\partial p} = \lambda_t\left[f_o\frac{\partial b}{\partial p} - (f_g + f_o R_s)\frac{\partial \beta}{\partial p}\right]. \qquad (C-14)$$

Similarly,

$$\frac{1}{\alpha}\left(-\alpha\frac{\partial a}{\partial S_o} + a\frac{\partial \alpha}{\partial S_o}\right) = \lambda_t\left[-f_o\frac{\partial R_s}{\partial S_o} + \frac{1}{f_o}\frac{\partial f_o}{\partial S_o}\right] = \lambda_t\frac{1}{f_o}\frac{\partial f_o}{\partial S_o}, \qquad (C-15)$$

and

$$-\alpha\frac{\partial b}{\partial S_o}+a\frac{\partial \beta}{\partial S_o}=\lambda_t\left[-f_o\frac{\partial b}{\partial S_o}+(f_g+f_oR_s)\frac{\partial \beta}{\partial S_o}\right]. \qquad (C-16)$$

Substituting Eqs. C-13, C-14, C-15 and C-16, one can rewrite Eq. C-1 as follows:

$$\frac{dS_o}{dp_{wf}}=\left(\frac{\frac{2t}{r}Q_D\left(f_o\frac{\partial R_s}{\partial p}-\frac{1}{f_o}\frac{\partial f_o}{\partial p}\right)+\left(f_o\frac{\partial b}{\partial p}-(f_g+f_oR_s)\frac{\partial \beta}{\partial p}\right)}{\frac{2t}{r}Q_D\left(\frac{1}{f_o}\frac{\partial f_o}{\partial S_o}\right)+\left(-f_o\frac{\partial b}{\partial S_o}+(f_g+f_oR_s)\frac{\partial \beta}{\partial S_o}\right)}\right)_{r=r_w}. \qquad (C-17)$$

Since

$$f_o=\frac{1}{1+\frac{k_{rg}}{k_{ro}}\frac{\mu_oB_o}{\mu_gB_g}}, \qquad (C-18)$$

and

$$f_g=\frac{1}{1+\frac{k_{ro}}{k_{rg}}\frac{\mu_gB_g}{\mu_oB_o}}, \qquad (C-19)$$

Eq. C-17 implies that dS_o/dp_{wf} is a function of k_{rg}/k_{rg} instead of the individual oil and gas effective permeabilities kk_{ro} and kk_{rg}.

Non-Zero Wellbore Storage.

In Chapter 6 (see also Hatzignatiou et al.[29]) we have shown that in the presence of wellbore storage the sandface oil saturation as a function of wellbore pressure can be computed from the following equation:

$$\frac{dS_o}{dp_{wf}}=\left(\frac{Q_{sD}(t)\left(\alpha\frac{\partial a}{\partial p}-a\frac{\partial \alpha}{\partial p}\right)-\left(\alpha\frac{\partial b}{\partial p}-a\frac{\partial \beta}{\partial p}\right)\left(\frac{dp_{wf}}{dt}\right)}{Q_{sD}(t)\left(-\alpha\frac{\partial a}{\partial S_o}+a\frac{\partial \alpha}{\partial S_o}\right)-\left(-\alpha\frac{\partial b}{\partial S_o}+a\frac{\partial \beta}{\partial S_o}\right)\left(\frac{dp_{wf}}{dt}\right)}\right)_{r=r_w}, \qquad (C-20)$$

where

$$Q_{sD}(t)=\left(\frac{5.615q_{osf}(t)}{2\pi r_wh}\right)^2\frac{1}{k\phi}\frac{1}{c_1\alpha^2}. \qquad (C-21)$$

In the presence of an altered permeability in the skin zone, Eq. C-21 should be replaced by

$$Q_{sD}(t)=\left(\frac{5.615q_{osf}(t)}{2\pi r_wh}\right)^2\frac{1}{k_s\phi}\frac{1}{c_1\alpha^2}. \qquad (C-22)$$

Using Eq. C-13, one can obtain

$$\frac{1}{\alpha^2}\left(\alpha\frac{\partial a}{\partial p}-a\frac{\partial \alpha}{\partial p}\right)=\frac{\lambda_t}{\alpha}\left[f_o\frac{\partial R_s}{\partial p}-\frac{1}{f_o}\frac{\partial f_o}{\partial p}\right], \qquad (C-23)$$

which in terms of Eqs. C-7 can be rewritten as follows:

$$\frac{1}{\alpha^2}\left(\alpha\frac{\partial a}{\partial p}-a\frac{\partial \alpha}{\partial p}\right)=\frac{\partial R_s}{\partial p}-\frac{1}{f_o^2}\frac{\partial f_o}{\partial p}. \qquad (C-24)$$

Similarly, Eq. C-14 yields

$$k\left[\alpha\frac{\partial b}{\partial p}-a\frac{\partial \beta}{\partial p}\right]=k\lambda_t\left[f_o\frac{\partial b}{\partial p}-(f_g+f_oR_s)\frac{\partial \beta}{\partial p}\right],$$

or

$$k\left[\alpha\frac{\partial b}{\partial p}-a\frac{\partial \beta}{\partial p}\right]=\tilde{\lambda}_t\left[f_o\frac{\partial b}{\partial p}-(f_g+f_oR_s)\frac{\partial \beta}{\partial p}\right], \qquad (C-25)$$

where

$$\tilde{\lambda}_t=\frac{kk_{ro}}{\mu_oB_o}+\frac{kk_{rg}}{\mu_gB_g}. \qquad (C-26)$$

Using the same methodology, one obtains

$$\frac{1}{\alpha^2}\left(-\alpha\frac{\partial a}{\partial S_o}+a\frac{\partial \alpha}{\partial S_o}\right)=\frac{1}{f_o^2}\frac{\partial f_o}{\partial S_o}, \qquad (C-27)$$

and

$$k\left[-\alpha\frac{\partial b}{\partial S_o}+a\frac{\partial \beta}{\partial S_o}\right]=\tilde{\lambda}_t\left[-f_o\frac{\partial b}{\partial S_o}-(f_g+f_oR_s)\frac{\partial \beta}{\partial S_o}\right]. \qquad (C-28)$$

Substituting Eqs. C-24, C-25, C-26, C-27 and C-28, one can rewrite Eq. C-20 as follows:

$$\frac{dS_o}{dp_{wf}}=\left(\frac{\tilde{Q}_{sD}\left(\frac{\partial R_s}{\partial p}-\frac{1}{f_o^2}\frac{\partial f_o}{\partial p}\right)-\tilde{\lambda}_t\left(f_o\frac{\partial b}{\partial p}-(f_g+f_oR_s)\frac{\partial \beta}{\partial p}\right)\frac{dp_{wf}}{dt}}{\tilde{Q}_{sD}\left(\frac{1}{f_o^2}\frac{\partial f_o}{\partial S_o}\right)-\tilde{\lambda}_t\left(-f_o\frac{\partial b}{\partial S_o}+(f_g+f_oR_s)\frac{\partial \beta}{\partial S_o}\right)\frac{dp_{wf}}{dt}}\right)_{r=r_w}, \qquad (C-29)$$

where

$$\tilde{Q}_{sD}=\left(\frac{5.615q_{osf}}{2\pi r_wh}\right)^2\frac{1}{6.328\times10^{-3}\phi}. \qquad (C-30)$$

Eq. C-29 implies that Eq. C-20, unlike Eq. C-1, cannot be written in terms of the ratio of the gas to oil relative permeabilities, i.e., k_{rg}/k_{ro}.

APPENDIX D
DERIVATION OF EQUATION FOR COMPUTING EFFECTIVE OIL PERMEABILITY DURING DRAWDOWN

Differentiating Eq. 6.6.5 with respect to time gives

$$\frac{kh}{141.2}\left(\frac{1}{q_{osf}(t)}\frac{dp_p(p_{wf})}{dp_{wf}}\frac{dp_{wf}}{dt}-\frac{p_p(p_{wf})}{q_{osf}^2(t)}\frac{dq_{osf}(t)}{dt}\right)=1.151\frac{dt_{lc}}{dt}. \qquad (D-1)$$

Multiplying Eq. D-1 by $q_{osf}(t)/(dp_{wf}/dt)$ and using:

$$\frac{dp_p(p_{wf})}{dp_{wf}}=-\left(\frac{k_{ro}}{\mu_o B_o}\right)_{p_{wf}}, \qquad (D-2)$$

(see Eq. 6.3.9 evaluated at p_{wf}) gives:

$$\frac{kh}{141.2}\left(-\left(\frac{k_{ro}}{\mu_o B_o}\right)_{p_{wf}}-\frac{p_p(p_{wf})}{q_{osf}(t)(dp_{wf}/dt)}\frac{dq_{osf}(t)}{dt}\right)=1.151q_{osf}(t)\frac{dt_{lc}/dt}{dp_{wf}/dt}. \qquad (D-3)$$

Since:

$$\frac{1}{q_{osf}(t)}\frac{dq_{osf}}{dt}=\frac{d\ln q_{osf}(t)}{dt}, \qquad (D-4)$$

rearranging Eq. D-3 yields:

$$-\left(\frac{k_{ro}}{\mu_o B_o}\right)_{p_{wf}}=\frac{162.6q_{osf}(t)(dt_{lc}/dt)}{kh\frac{dp_{wf}}{dt}}+\frac{p_p(p_{wf})}{(dp_{wf}/dt)}\frac{d\ln q_{osf}(t)}{dt}. \qquad (D-5)$$

By multiplying Eq. D-5 by k and rearranging the resulting equation, one can easily obtain the following equation:

$$(kk_{ro})_{p_{wf}}=\frac{-162.6q_{osf}(t)(\mu_o B_o)_{p_{wf}}(dt_{lc}/dt)}{h\frac{dp_{wf}}{dt}}-\frac{kp_p(p_{wf})(\mu_o B_o)_{p_{wf}}}{(dp_{wf}/dt)}\frac{d\ln q_{osf}(t)}{dt}, \qquad (D-6)$$

which is Eq. 6.7.1 of the text.

APPENDIX E
DERIVATION OF EQUATION FOR COMPUTING EFFECTIVE OIL PERMEABILITY DURING BUILDUP

Differentiating Eq. 7.5.8 with respect to time gives

$$\frac{kh}{141.2}\left(\frac{1}{\Delta q(\Delta t)}\frac{d[p_p(p_{ws})-p_p(p_{wf,s})]}{dp_{ws}}\frac{dp_{ws}}{d\Delta t}-\frac{p_p(p_{ws})-p_p(p_{wf,s})}{\Delta q^2(\Delta t)}\frac{d\Delta q(\Delta t)}{d\Delta t}\right)$$
$$=1.151\frac{d\Delta t_{lc}}{d\Delta t}. \qquad (E-1)$$

Multiplying Eq. E-1 by $\Delta q(\Delta t)/(dp_{ws}/d\Delta t)$ and using

$$\frac{d[p_p(p_{ws})-p_p(p_{wf,s})]}{dp_{ws}}=\left(\frac{k_{ro}}{\mu_o B_o}\right)_{p_{ws}}, \qquad (E-2)$$

gives

$$\frac{kh}{141.2}\left(\left(\frac{k_{ro}}{\mu_o B_o}\right)_{p_{ws}}-\frac{p_p(p_{ws})-p_p(p_{wf,s})}{\Delta q(\Delta t)(dp_{ws}/d\Delta t)}\frac{d\Delta q(\Delta t)}{d\Delta t}\right)=1.151\Delta q(\Delta t)\frac{d\Delta t_{lc}/d\Delta t}{dp_{ws}/d\Delta t}. \qquad (E-3)$$

Since

$$\frac{1}{\Delta q(\Delta t)}\frac{d\Delta q(\Delta t)}{d\Delta t}=\frac{d\ln(\Delta q(\Delta t))}{d\Delta t}, \qquad (E-4)$$

rearranging Eq. E-3 yields

$$\left(\frac{k_{ro}}{\mu_o B_o}\right)_{p_{ws}}=\frac{162.6\Delta q(\Delta t)(d\Delta t_{lc}/d\Delta t)}{kh(dp_{ws}/d\Delta t)}+\frac{p_p(p_{ws})-p_p(p_{wf,s})}{(dp_{ws}/d\Delta t)}\frac{d\ln(\Delta q(\Delta t))}{d\Delta t}. \qquad (E-5)$$

By multiplying Eq. E-5 by k and rearranging the resulting equation, one can easily obtain the following equation:

$$(kk_{ro})_{p_{ws}}=\frac{162.6\Delta q(\Delta t)(\mu_o B_o)_{p_{ws}}(d\Delta t_{lc}/d\Delta t)}{h(dp_{ws}/d\Delta t)}$$
$$+\frac{k[p_p(p_{ws})-p_p(p_{wf,s})](\mu_o B_o)_{p_{ws}}}{(dp_{ws}/d\Delta t)}\frac{d\ln(\Delta q(\Delta t))}{d\Delta t}, \qquad (E-6)$$

which is Eq. 7.7.1 of the text.

APPENDIX F
TABLES

Rock and Fluid Properties for Tables F-1 through F-11

$r_w = 0.328$ ft ; $r_e = 6600$ ft

$h = 15.547$ ft ; $\phi = 0.3$

$k = 10$ md

$q_o = 150$ STB/DAY

$s = 0.0$; $S_{gc} = 0.0$

$S_{wc} = S_{iw} = 0.3$; $S_{or} = 0.0$

$C_D = 0.0$ $(\beta^* \rightarrow \infty)$

PVT Data are given by Set 1 (Table A-1)

Relative Permeability Data are given by Set 1 (Table A-2)

$p_i = p_{bi} = 3460$ psi

$c_{ti} = 0.23564 \times 10^{-4}$ psi^{-1}

$\mu_{oi} = 0.43059$ cp

$B_{oi} = 1.5882$ RB/STB

Table F-1

Simulated and Computed kk_{ro} Values
Drawdown Test
Case 1

t days	p_{wf} psi	Sim. So	Sim. kk_{ro} md	Comp. kk_{ro} md
0.10000E-05	0.34233E+04	0.69706E+00	0.68837E+01	0.21431E+02
0.15000E-05	0.34144E+04	0.69600E+00	0.68417E+01	0.20627E+02
0.20500E-05	0.34070E+04	0.69510E+00	0.68061E+01	0.18946E+02
0.26550E-05	0.34003E+04	0.69428E+00	0.67742E+01	0.17570E+02
0.33205E-05	0.33941E+04	0.69352E+00	0.67448E+01	0.16456E+02
0.40525E-05	0.33883E+04	0.69280E+00	0.67169E+01	0.15522E+02
0.48578E-05	0.33827E+04	0.69210E+00	0.66898E+01	0.14725E+02
0.57436E-05	0.33772E+04	0.69142E+00	0.66635E+01	0.14038E+02
0.67179E-05	0.33718E+04	0.69076E+00	0.66379E+01	0.13436E+02
0.77897E-05	0.33665E+04	0.69010E+00	0.66124E+01	0.12900E+02
0.89687E-05	0.33613E+04	0.68944E+00	0.65873E+01	0.12421E+02
0.10266E-04	0.33561E+04	0.68879E+00	0.65626E+01	0.11988E+02
0.11692E-04	0.33509E+04	0.68813E+00	0.65376E+01	0.11595E+02
0.13261E-04	0.33457E+04	0.68748E+00	0.65130E+01	0.11237E+02
0.14987E-04	0.33405E+04	0.68682E+00	0.64880E+01	0.10908E+02
0.16886E-04	0.33353E+04	0.68615E+00	0.64626E+01	0.10604E+02
0.18975E-04	0.33301E+04	0.68548E+00	0.64372E+01	0.10324E+02
0.21272E-04	0.33248E+04	0.68480E+00	0.64116E+01	0.10063E+02
0.23800E-04	0.33194E+04	0.68412E+00	0.63864E+01	0.98181E+01
0.26580E-04	0.33141E+04	0.68342E+00	0.63604E+01	0.95887E+01
0.29637E-04	0.33087E+04	0.68272E+00	0.63345E+01	0.93742E+01
0.33001E-04	0.33032E+04	0.68201E+00	0.63082E+01	0.91723E+01
0.36701E-04	0.32977E+04	0.68128E+00	0.62811E+01	0.89836E+01
0.40772E-04	0.32921E+04	0.68055E+00	0.62540E+01	0.88063E+01
0.45249E-04	0.32864E+04	0.67980E+00	0.62264E+01	0.86381E+01
0.50174E-04	0.32807E+04	0.67904E+00	0.61988E+01	0.84772E+01
0.55591E-04	0.32750E+04	0.67826E+00	0.61705E+01	0.83225E+01
0.61550E-04	0.32691E+04	0.67748E+00	0.61422E+01	0.81769E+01
0.68105E-04	0.32632E+04	0.67668E+00	0.61132E+01	0.80392E+01
0.75315E-04	0.32572E+04	0.67586E+00	0.60835E+01	0.79081E+01
0.83247E-04	0.32512E+04	0.67503E+00	0.60534E+01	0.77854E+01
0.91972E-04	0.32451E+04	0.67419E+00	0.60236E+01	0.76642E+01
0.10157E-03	0.32389E+04	0.67332E+00	0.59927E+01	0.75442E+01
0.11213E-03	0.32326E+04	0.67245E+00	0.59619E+01	0.74311E+01
0.12374E-03	0.32263E+04	0.67155E+00	0.59299E+01	0.73231E+01
0.13651E-03	0.32199E+04	0.67064E+00	0.58977E+01	0.72220E+01
0.15056E-03	0.32134E+04	0.66971E+00	0.58649E+01	0.71482E+01
0.16602E-03	0.32069E+04	0.66876E+00	0.58320E+01	0.70581E+01
0.18302E-03	0.32003E+04	0.66779E+00	0.57983E+01	0.69422E+01
0.20172E-03	0.31935E+04	0.66680E+00	0.57640E+01	0.68444E+01
0.22230E-03	0.31867E+04	0.66579E+00	0.57289E+01	0.67607E+01
0.24493E-03	0.31799E+04	0.66476E+00	0.56934E+01	0.66882E+01
0.26982E-03	0.31729E+04	0.66371E+00	0.56578E+01	0.65978E+01

Table F-1 (Cont'd)

t days	p_{wf} psi	Sim. So	Sim. kk_{ro} md	Comp. kk_{ro} md
0.29720E-03	0.31659E+04	0.66264E+00	0.56215E+01	0.64968E+01
0.32732E-03	0.31587E+04	0.66155E+00	0.55846E+01	0.64076E+01
0.36045E-03	0.31515E+04	0.66044E+00	0.55469E+01	0.63372E+01
0.39690E-03	0.31442E+04	0.65932E+00	0.55094E+01	0.62637E+01
0.43699E-03	0.31368E+04	0.65818E+00	0.54717E+01	0.61693E+01
0.48109E-03	0.31293E+04	0.65702E+00	0.54332E+01	0.60782E+01
0.52959E-03	0.31216E+04	0.65584E+00	0.53941E+01	0.60019E+01
0.58295E-03	0.31139E+04	0.65466E+00	0.53552E+01	0.59322E+01
0.64165E-03	0.31061E+04	0.65346E+00	0.53164E+01	0.58492E+01
0.70621E-03	0.30982E+04	0.65226E+00	0.52775E+01	0.57595E+01
0.77724E-03	0.30901E+04	0.65105E+00	0.52383E+01	0.56805E+01
0.85536E-03	0.30819E+04	0.64984E+00	0.51992E+01	0.56123E+01
0.94130E-03	0.30737E+04	0.64864E+00	0.51612E+01	0.55376E+01
0.10358E-02	0.30653E+04	0.64744E+00	0.51232E+01	0.54545E+01
0.11398E-02	0.30568E+04	0.64625E+00	0.50855E+01	0.53779E+01
0.12542E-02	0.30481E+04	0.64507E+00	0.50482E+01	0.53159E+01
0.13800E-02	0.30394E+04	0.64391E+00	0.50123E+01	0.52511E+01
0.15184E-02	0.30306E+04	0.64277E+00	0.49770E+01	0.51770E+01
0.16706E-02	0.30216E+04	0.64165E+00	0.49424E+01	0.51092E+01
0.18381E-02	0.30125E+04	0.64056E+00	0.49086E+01	0.50551E+01
0.20223E-02	0.30033E+04	0.63950E+00	0.48762E+01	0.50103E+01
0.22250E-02	0.29940E+04	0.63846E+00	0.48448E+01	0.49488E+01
0.24479E-02	0.29846E+04	0.63745E+00	0.48143E+01	0.48841E+01
0.26930E-02	0.29750E+04	0.63647E+00	0.47847E+01	0.48419E+01
0.29627E-02	0.29654E+04	0.63555E+00	0.47569E+01	0.48193E+01
0.32594E-02	0.29557E+04	0.63464E+00	0.47296E+01	0.47894E+01
0.35858E-02	0.29460E+04	0.63374E+00	0.47031E+01	0.47304E+01
0.39447E-02	0.29361E+04	0.63287E+00	0.46774E+01	0.46797E+01
0.43396E-02	0.29261E+04	0.63206E+00	0.46535E+01	0.46621E+01
0.47740E-02	0.29160E+04	0.63128E+00	0.46305E+01	0.46521E+01
0.52518E-02	0.29060E+04	0.63051E+00	0.46078E+01	0.46291E+01
0.57773E-02	0.28958E+04	0.62973E+00	0.45849E+01	0.45920E+01
0.63555E-02	0.28856E+04	0.62898E+00	0.45633E+01	0.45521E+01
0.69914E-02	0.28753E+04	0.62827E+00	0.45429E+01	0.45282E+01
0.76910E-02	0.28649E+04	0.62759E+00	0.45233E+01	0.45109E+01
0.84605E-02	0.28545E+04	0.62691E+00	0.45037E+01	0.44907E+01
0.93069E-02	0.28440E+04	0.62626E+00	0.44849E+01	0.44841E+01
0.10238E-01	0.28335E+04	0.62562E+00	0.44665E+01	0.44798E+01
0.11262E-01	0.28229E+04	0.62498E+00	0.44481E+01	0.44581E+01
0.12389E-01	0.28123E+04	0.62433E+00	0.44298E+01	0.44067E+01
0.13628E-01	0.28015E+04	0.62372E+00	0.44126E+01	0.43759E+01
0.14991E-01	0.27907E+04	0.62314E+00	0.43963E+01	0.43803E+01
0.16491E-01	0.27799E+04	0.62258E+00	0.43806E+01	0.43699E+01

Table F-1 (Cont'd)

t days	p_{wf} psi	Sim. So	Sim. kk_{ro} md	Comp. kk_{ro} md
0.18140E-01	0.27691E+04	0.62201E+00	0.43645E+01	0.43502E+01
0.19955E-01	0.27581E+04	0.62146E+00	0.43490E+01	0.43467E+01
0.21951E-01	0.27472E+04	0.62091E+00	0.43336E+01	0.43425E+01
0.24146E-01	0.27362E+04	0.62036E+00	0.43181E+01	0.43180E+01
0.26561E-01	0.27252E+04	0.61981E+00	0.43028E+01	0.42866E+01
0.29218E-01	0.27140E+04	0.61927E+00	0.42879E+01	0.42573E+01
0.32140E-01	0.27027E+04	0.61876E+00	0.42739E+01	0.42466E+01
0.35354E-01	0.26915E+04	0.61827E+00	0.42605E+01	0.42411E+01
0.38890E-01	0.26801E+04	0.61778E+00	0.42470E+01	0.42303E+01
0.42779E-01	0.26688E+04	0.61730E+00	0.42338E+01	0.42328E+01
0.47058E-01	0.26574E+04	0.61683E+00	0.42209E+01	0.42341E+01
0.51764E-01	0.26461E+04	0.61635E+00	0.42077E+01	0.42143E+01
0.56941E-01	0.26346E+04	0.61587E+00	0.41946E+01	0.41918E+01
0.62635E-01	0.26230E+04	0.61539E+00	0.41814E+01	0.41881E+01
0.68899E-01	0.26115E+04	0.61492E+00	0.41686E+01	0.41792E+01
0.75789E-01	0.25999E+04	0.61444E+00	0.41559E+01	0.41159E+01
0.83369E-01	0.25880E+04	0.61400E+00	0.41442E+01	0.40765E+01
0.91706E-01	0.25761E+04	0.61358E+00	0.41331E+01	0.41051E+01
0.10088E+00	0.25643E+04	0.61318E+00	0.41225E+01	0.41259E+01
0.11097E+00	0.25525E+04	0.61277E+00	0.41116E+01	0.41161E+01
0.12206E+00	0.25406E+04	0.61235E+00	0.41005E+01	0.40945E+01
0.13427E+00	0.25286E+04	0.61195E+00	0.40899E+01	0.40889E+01
0.14770E+00	0.25167E+04	0.61155E+00	0.40794E+01	0.40911E+01
0.16247E+00	0.25047E+04	0.61114E+00	0.40685E+01	0.40755E+01
0.17871E+00	0.24926E+04	0.61073E+00	0.40576E+01	0.40543E+01
0.19658E+00	0.24804E+04	0.61033E+00	0.40471E+01	0.40533E+01
0.21624E+00	0.24683E+04	0.60993E+00	0.40365E+01	0.40562E+01
0.23787E+00	0.24561E+04	0.60953E+00	0.40259E+01	0.40369E+01
0.26166E+00	0.24437E+04	0.60912E+00	0.40150E+01	0.40132E+01
0.28782E+00	0.24314E+04	0.60872E+00	0.40044E+01	0.40116E+01
0.31660E+00	0.24190E+04	0.60832E+00	0.39938E+01	0.40147E+01
0.34826E+00	0.24066E+04	0.60792E+00	0.39833E+01	0.39955E+01
0.38309E+00	0.23940E+04	0.60751E+00	0.39724E+01	0.39714E+01
0.42140E+00	0.23814E+04	0.60712E+00	0.39621E+01	0.39697E+01
0.46354E+00	0.23688E+04	0.60672E+00	0.39515E+01	0.39730E+01
0.50990E+00	0.23562E+04	0.60632E+00	0.39409E+01	0.39538E+01
0.56089E+00	0.23434E+04	0.60592E+00	0.39303E+01	0.39294E+01
0.61697E+00	0.23306E+04	0.60552E+00	0.39197E+01	0.39275E+01
0.67867E+00	0.23178E+04	0.60513E+00	0.39094E+01	0.39312E+01
0.74654E+00	0.23049E+04	0.60472E+00	0.38988E+01	0.38727E+01
0.82119E+00	0.22916E+04	0.60433E+00	0.38889E+01	0.38161E+01
0.90331E+00	0.22783E+04	0.60397E+00	0.38797E+01	0.38425E+01
0.99365E+00	0.22652E+04	0.60362E+00	0.38708E+01	0.38783E+01

Table F-1 (Cont'd)

t days	p_{wf} psi	Sim. So	Sim. kk_{ro} md	Comp. kk_{ro} md
0.10930E+01	0.22520E+04	0.60327E+00	0.38618E+01	0.38713E+01
0.12023E+01	0.22388E+04	0.60290E+00	0.38524E+01	0.38508E+01
0.13225E+01	0.22254E+04	0.60255E+00	0.38435E+01	0.38501E+01
0.14548E+01	0.22121E+04	0.60220E+00	0.38345E+01	0.38546E+01
0.16003E+01	0.21987E+04	0.60185E+00	0.38256E+01	0.38371E+01
0.17603E+01	0.21852E+04	0.60148E+00	0.38162E+01	0.38144E+01
0.19363E+01	0.21716E+04	0.60113E+00	0.38073E+01	0.38138E+01
0.21300E+01	0.21580E+04	0.60078E+00	0.37983E+01	0.38186E+01
0.23430E+01	0.21444E+04	0.60043E+00	0.37894E+01	0.38012E+01
0.25773E+01	0.21306E+04	0.60007E+00	0.37802E+01	0.37782E+01
0.28350E+01	0.21167E+04	0.59971E+00	0.37712E+01	0.37431E+01
0.31185E+01	0.21026E+04	0.59938E+00	0.37630E+01	0.37336E+01
0.34303E+01	0.20886E+04	0.59904E+00	0.37545E+01	0.37470E+01
0.37734E+01	0.20745E+04	0.59871E+00	0.37463E+01	0.37496E+01
0.41507E+01	0.20605E+04	0.59837E+00	0.37379E+01	0.37608E+01
0.45658E+01	0.20464E+04	0.59804E+00	0.37297E+01	0.37224E+01

Table F-2

Simulated and Computed kk_{rg} Values
Drawdown Test
Case 1

p_{wf} psi	Sim. kk_{rg} md	Comp. kk_{rg} md
0.34233E+04	0.29893E-05	0.93764E-05
0.34144E+04	0.40670E-05	0.12325E-04
0.34070E+04	0.49821E-05	0.13893E-04
0.34003E+04	0.10187E-04	0.26461E-04
0.33941E+04	0.15574E-04	0.38034E-04
0.33883E+04	0.20678E-04	0.47787E-04
0.33827E+04	0.25639E-04	0.56351E-04
0.33772E+04	0.30459E-04	0.64141E-04
0.33718E+04	0.35138E-04	0.71178E-04
0.33665E+04	0.39816E-04	0.77674E-04
0.33613E+04	0.51249E-04	0.96518E-04
0.33561E+04	0.63697E-04	0.11640E-03
0.33509E+04	0.76337E-04	0.13527E-03
0.33457E+04	0.88785E-04	0.15329E-03
0.33405E+04	0.10142E-03	0.17060E-03
0.33353E+04	0.11426E-03	0.18732E-03
0.33301E+04	0.12709E-03	0.20377E-03
0.33248E+04	0.14370E-03	0.22526E-03
0.33194E+04	0.16894E-03	0.25977E-03
0.33141E+04	0.19492E-03	0.29363E-03
0.33087E+04	0.22091E-03	0.32689E-03
0.33032E+04	0.24726E-03	0.35975E-03
0.32977E+04	0.27435E-03	0.39235E-03
0.32921E+04	0.30145E-03	0.42469E-03
0.32864E+04	0.33405E-03	0.46360E-03
0.32807E+04	0.38033E-03	0.52030E-03
0.32750E+04	0.42783E-03	0.57667E-03
0.32691E+04	0.47533E-03	0.63304E-03
0.32632E+04	0.52405E-03	0.68943E-03
0.32572E+04	0.57399E-03	0.74597E-03
0.32512E+04	0.62454E-03	0.80301E-03
0.32451E+04	0.69960E-03	0.89049E-03
0.32389E+04	0.77826E-03	0.97919E-03
0.32326E+04	0.85691E-03	0.10686E-02
0.32263E+04	0.93828E-03	0.11587E-02
0.32199E+04	0.10206E-02	0.12499E-02
0.32134E+04	0.11148E-02	0.13588E-02
0.32069E+04	0.12341E-02	0.14935E-02
0.32003E+04	0.13559E-02	0.16236E-02
0.31935E+04	0.14802E-02	0.17581E-02
0.31867E+04	0.16071E-02	0.18969E-02
0.31799E+04	0.17462E-02	0.20511E-02
0.31729E+04	0.19207E-02	0.22394E-02

Table F-2 (Cont'd)

p_{wf} psi	Sim. kk_{rg} md	Comp. kk_{rg} md
0.31659E+04	0.20986E-02	0.24252E-02
0.31587E+04	0.22799E-02	0.26157E-02
0.31515E+04	0.24644E-02	0.28151E-02
0.31442E+04	0.26821E-02	0.30492E-02
0.31368E+04	0.29243E-02	0.32979E-02
0.31293E+04	0.31707E-02	0.35480E-02
0.31216E+04	0.34214E-02	0.38063E-02
0.31139E+04	0.36896E-02	0.40877E-02
0.31061E+04	0.40064E-02	0.44066E-02
0.30982E+04	0.43232E-02	0.47176E-02
0.30901E+04	0.46426E-02	0.50334E-02
0.30819E+04	0.49712E-02	0.53644E-02
0.30737E+04	0.53562E-02	0.57464E-02
0.30653E+04	0.57412E-02	0.61115E-02
0.30568E+04	0.61230E-02	0.64743E-02
0.30481E+04	0.65016E-02	0.68450E-02
0.30394E+04	0.69414E-02	0.72706E-02
0.30306E+04	0.73779E-02	0.76732E-02
0.30216E+04	0.78067E-02	0.80686E-02
0.30125E+04	0.82241E-02	0.84699E-02
0.30033E+04	0.86635E-02	0.89006E-02
0.29940E+04	0.91316E-02	0.93278E-02
0.29846E+04	0.95861E-02	0.97255E-02
0.29750E+04	0.10027E-01	0.10145E-01
0.29654E+04	0.10441E-01	0.10578E-01
0.29557E+04	0.10877E-01	0.11012E-01
0.29460E+04	0.11347E-01	0.11414E-01
0.29361E+04	0.11801E-01	0.11805E-01
0.29261E+04	0.12224E-01	0.12246E-01
0.29160E+04	0.12632E-01	0.12690E-01
0.29060E+04	0.13034E-01	0.13096E-01
0.28958E+04	0.13462E-01	0.13483E-01
0.28856E+04	0.13911E-01	0.13879E-01
0.28753E+04	0.14337E-01	0.14289E-01
0.28649E+04	0.14745E-01	0.14707E-01
0.28545E+04	0.15152E-01	0.15107E-01
0.28440E+04	0.15542E-01	0.15537E-01
0.28335E+04	0.15925E-01	0.15970E-01
0.28229E+04	0.16311E-01	0.16345E-01
0.28123E+04	0.16753E-01	0.16668E-01
0.28015E+04	0.17169E-01	0.17025E-01
0.27907E+04	0.17564E-01	0.17496E-01
0.27799E+04	0.17946E-01	0.17905E-01

Table F-2 (Cont'd)

p_{wf} psi	Sim. kk_{rg} md	Comp. kk_{rg} md
0.27691E+04	0.18334E-01	0.18275E-01
0.27581E+04	0.18709E-01	0.18699E-01
0.27472E+04	0.19084E-01	0.19122E-01
0.27362E+04	0.19459E-01	0.19456E-01
0.27252E+04	0.19850E-01	0.19777E-01
0.27140E+04	0.20265E-01	0.20121E-01
0.27027E+04	0.20656E-01	0.20520E-01
0.26915E+04	0.21033E-01	0.20936E-01
0.26801E+04	0.21409E-01	0.21324E-01
0.26688E+04	0.21778E-01	0.21771E-01
0.26574E+04	0.22139E-01	0.22210E-01
0.26461E+04	0.22507E-01	0.22544E-01
0.26346E+04	0.22876E-01	0.22864E-01
0.26230E+04	0.23245E-01	0.23279E-01
0.26115E+04	0.23617E-01	0.23676E-01
0.25999E+04	0.24053E-01	0.23823E-01
0.25880E+04	0.24452E-01	0.24057E-01
0.25761E+04	0.24833E-01	0.24663E-01
0.25643E+04	0.25196E-01	0.25220E-01
0.25525E+04	0.25568E-01	0.25600E-01
0.25406E+04	0.25949E-01	0.25911E-01
0.25286E+04	0.26313E-01	0.26311E-01
0.25167E+04	0.26676E-01	0.26757E-01
0.25047E+04	0.27048E-01	0.27094E-01
0.24926E+04	0.27420E-01	0.27397E-01
0.24804E+04	0.27783E-01	0.27827E-01
0.24683E+04	0.28146E-01	0.28281E-01
0.24561E+04	0.28509E-01	0.28589E-01
0.24437E+04	0.28881E-01	0.28869E-01
0.24314E+04	0.29244E-01	0.29297E-01
0.24190E+04	0.29607E-01	0.29757E-01
0.24066E+04	0.29970E-01	0.30060E-01
0.23940E+04	0.30342E-01	0.30329E-01
0.23814E+04	0.30696E-01	0.30759E-01
0.23688E+04	0.31059E-01	0.31225E-01
0.23562E+04	0.31422E-01	0.31523E-01
0.23434E+04	0.31785E-01	0.31782E-01
0.23306E+04	0.32148E-01	0.32212E-01
0.23178E+04	0.32502E-01	0.32686E-01
0.23049E+04	0.32916E-01	0.32698E-01
0.22916E+04	0.33328E-01	0.32706E-01
0.22783E+04	0.33708E-01	0.33383E-01
0.22652E+04	0.34078E-01	0.34141E-01

Table F-2 (Cont'd)

p_{wf} psi	Sim. kk_{rg} md	Comp. kk_{rg} md
0.22520E+04	0.34447E-01	0.34536E-01
0.22388E+04	0.34838E-01	0.34817E-01
0.22254E+04	0.35208E-01	0.35265E-01
0.22121E+04	0.35577E-01	0.35758E-01
0.21987E+04	0.35947E-01	0.36060E-01
0.21852E+04	0.36338E-01	0.36315E-01
0.21716E+04	0.36707E-01	0.36767E-01
0.21580E+04	0.37077E-01	0.37270E-01
0.21444E+04	0.37447E-01	0.37567E-01
0.21306E+04	0.37827E-01	0.37812E-01
0.21167E+04	0.38238E-01	0.37955E-01
0.21026E+04	0.38621E-01	0.38326E-01
0.20886E+04	0.39015E-01	0.38932E-01
0.20745E+04	0.39399E-01	0.39434E-01
0.20605E+04	0.39793E-01	0.40032E-01
0.20464E+04	0.40177E-01	0.40103E-01

Table F-3

Parameter Values for the Computation of kk_{ro} and kk_{rg}
Drawdown Test
Case 1

t days	$dp_{wf}/d\log t$ psi	$\mu_o B_o$ cp-RB/STB	$\mu_g B_g$ cp-RB/STB	R STB/STB	R_s STB/STB
0.100000E-05	0.218046E+02	0.685992E+00	0.101352E-03	0.175873E+03	0.175870E+03
0.150000E-05	0.226708E+02	0.686497E+00	0.101451E-03	0.175339E+03	0.175334E+03
0.205000E-05	0.246979E+02	0.686920E+00	0.101533E-03	0.174889E+03	0.174884E+03
0.265500E-05	0.266466E+02	0.687298E+00	0.101607E-03	0.174490E+03	0.174480E+03
0.332050E-05	0.284652E+02	0.687646E+00	0.101675E-03	0.174121E+03	0.174106E+03
0.405255E-05	0.301915E+02	0.687975E+00	0.101740E-03	0.173772E+03	0.173751E+03
0.485780E-05	0.318406E+02	0.688290E+00	0.101802E-03	0.173436E+03	0.173410E+03
0.574359E-05	0.334150E+02	0.688595E+00	0.101862E-03	0.173109E+03	0.173078E+03
0.671794E-05	0.349267E+02	0.688893E+00	0.101921E-03	0.172789E+03	0.172754E+03
0.778974E-05	0.363926E+02	0.689185E+00	0.101979E-03	0.172474E+03	0.172434E+03
0.896871E-05	0.378130E+02	0.689474E+00	0.102036E-03	0.172169E+03	0.172117E+03
0.102656E-04	0.391930E+02	0.689760E+00	0.102093E-03	0.171867E+03	0.171801E+03
0.116921E-04	0.405378E+02	0.690044E+00	0.102150E-03	0.171566E+03	0.171487E+03
0.132614E-04	0.418487E+02	0.690328E+00	0.102206E-03	0.171265E+03	0.171173E+03
0.149875E-04	0.431294E+02	0.690611E+00	0.102263E-03	0.170963E+03	0.170857E+03
0.168862E-04	0.443834E+02	0.690894E+00	0.102319E-03	0.170660E+03	0.170541E+03
0.189749E-04	0.456067E+02	0.691177E+00	0.102376E-03	0.170356E+03	0.170223E+03
0.212724E-04	0.468058E+02	0.691462E+00	0.102433E-03	0.170054E+03	0.169903E+03
0.237996E-04	0.479945E+02	0.691747E+00	0.102491E-03	0.169759E+03	0.169581E+03
0.265795E-04	0.491630E+02	0.692034E+00	0.102548E-03	0.169462E+03	0.169256E+03
0.296375E-04	0.503088E+02	0.692323E+00	0.102607E-03	0.169163E+03	0.168928E+03
0.330012E-04	0.514376E+02	0.692613E+00	0.102665E-03	0.168861E+03	0.168596E+03
0.367014E-04	0.525402E+02	0.692905E+00	0.102725E-03	0.168556E+03	0.168261E+03
0.407715E-04	0.536208E+02	0.693199E+00	0.102784E-03	0.168248E+03	0.167923E+03
0.452487E-04	0.546881E+02	0.693495E+00	0.102844E-03	0.167943E+03	0.167581E+03
0.501735E-04	0.557504E+02	0.693793E+00	0.102905E-03	0.167650E+03	0.167236E+03
0.555909E-04	0.568110E+02	0.694093E+00	0.102967E-03	0.167353E+03	0.166886E+03
0.615500E-04	0.578483E+02	0.694396E+00	0.103028E-03	0.167054E+03	0.166532E+03
0.681050E-04	0.588646E+02	0.694701E+00	0.103091E-03	0.166753E+03	0.166175E+03
0.753155E-04	0.598669E+02	0.695008E+00	0.103154E-03	0.166448E+03	0.165813E+03
0.832470E-04	0.608372E+02	0.695317E+00	0.103218E-03	0.166141E+03	0.165447E+03
0.919717E-04	0.618273E+02	0.695629E+00	0.103282E-03	0.165859E+03	0.165076E+03
0.101569E-03	0.628394E+02	0.695942E+00	0.103347E-03	0.165576E+03	0.164702E+03
0.112126E-03	0.638245E+02	0.696259E+00	0.103413E-03	0.165290E+03	0.164322E+03
0.123738E-03	0.647992E+02	0.696620E+00	0.103485E-03	0.165003E+03	0.163938E+03
0.136512E-03	0.657493E+02	0.697074E+00	0.103571E-03	0.164715E+03	0.163550E+03
0.150563E-03	0.664715E+02	0.697531E+00	0.103658E-03	0.164437E+03	0.163158E+03
0.166020E-03	0.673648E+02	0.697989E+00	0.103745E-03	0.164187E+03	0.162763E+03
0.183022E-03	0.685342E+02	0.698453E+00	0.103833E-03	0.163935E+03	0.162362E+03
0.201724E-03	0.695605E+02	0.698921E+00	0.103922E-03	0.163683E+03	0.161955E+03
0.222296E-03	0.704694E+02	0.699394E+00	0.104012E-03	0.163431E+03	0.161544E+03
0.244926E-03	0.712817E+02	0.699869E+00	0.104103E-03	0.163190E+03	0.161128E+03
0.269818E-03	0.723078E+02	0.700347E+00	0.104195E-03	0.162990E+03	0.160708E+03

Table F-3 (Cont'd)

t days	$dp_{wf}/d\log t$ psi	$\mu_o B_o$ cp-RB/STB	$\mu_g B_g$ cp-RB/STB	R STB/STB	R_v STB/STB
0.297200E-03	0.734821E+02	0.700830E+00	0.104288E-03	0.162790E+03	0.160282E+03
0.327320E-03	0.745568E+02	0.701318E+00	0.104381E-03	0.162592E+03	0.159849E+03
0.360452E-03	0.754388E+02	0.701810E+00	0.104476E-03	0.162395E+03	0.159411E+03
0.396898E-03	0.763772E+02	0.702304E+00	0.104571E-03	0.162239E+03	0.158970E+03
0.436987E-03	0.776013E+02	0.702804E+00	0.104668E-03	0.162111E+03	0.158522E+03
0.481086E-03	0.788210E+02	0.703308E+00	0.104765E-03	0.161985E+03	0.158066E+03
0.529595E-03	0.796803E+02	0.703818E+00	0.104864E-03	0.161861E+03	0.157605E+03
0.582954E-03	0.806783E+02	0.704330E+00	0.104964E-03	0.161762E+03	0.157138E+03
0.641650E-03	0.820862E+02	0.704847E+00	0.105065E-03	0.161720E+03	0.156666E+03
0.706215E-03	0.834265E+02	0.705369E+00	0.105167E-03	0.161679E+03	0.156186E+03
0.777236E-03	0.846490E+02	0.705897E+00	0.105270E-03	0.161640E+03	0.155698E+03
0.855360E-03	0.857435E+02	0.706429E+00	0.105374E-03	0.161612E+03	0.155204E+03
0.941296E-03	0.869658E+02	0.706965E+00	0.105479E-03	0.161660E+03	0.154704E+03
0.103583E-02	0.883581E+02	0.707506E+00	0.105586E-03	0.161705E+03	0.154197E+03
0.113981E-02	0.896857E+02	0.708052E+00	0.105693E-03	0.161746E+03	0.153681E+03
0.125419E-02	0.908020E+02	0.708603E+00	0.105802E-03	0.161783E+03	0.153159E+03
0.138001E-02	0.919949E+02	0.709157E+00	0.105912E-03	0.161902E+03	0.152631E+03
0.151841E-02	0.933847E+02	0.709716E+00	0.106023E-03	0.162016E+03	0.152095E+03
0.167065E-02	0.946998E+02	0.710280E+00	0.106136E-03	0.162120E+03	0.151551E+03
0.183811E-02	0.957883E+02	0.710847E+00	0.106249E-03	0.162210E+03	0.151000E+03
0.202233E-02	0.967235E+02	0.711417E+00	0.106363E-03	0.162326E+03	0.150444E+03
0.222496E-02	0.980135E+02	0.712052E+00	0.106486E-03	0.162489E+03	0.149885E+03
0.244785E-02	0.994227E+02	0.712850E+00	0.106629E-03	0.162635E+03	0.149323E+03
0.269304E-02	0.100401E+03	0.713653E+00	0.106773E-03	0.162758E+03	0.148754E+03
0.296274E-02	0.100986E+03	0.714458E+00	0.106917E-03	0.162848E+03	0.148181E+03
0.325942E-02	0.101732E+03	0.715262E+00	0.107062E-03	0.162968E+03	0.147606E+03
0.358576E-02	0.103116E+03	0.716070E+00	0.107207E-03	0.163141E+03	0.147025E+03
0.394473E-02	0.104353E+03	0.716887E+00	0.107354E-03	0.163280E+03	0.146434E+03
0.433961E-02	0.104866E+03	0.717705E+00	0.107502E-03	0.163376E+03	0.145839E+03
0.477397E-02	0.105210E+03	0.718521E+00	0.107649E-03	0.163450E+03	0.145243E+03
0.525177E-02	0.105852E+03	0.719336E+00	0.107796E-03	0.163522E+03	0.144644E+03
0.577734E-02	0.106830E+03	0.720152E+00	0.107944E-03	0.163629E+03	0.144040E+03
0.635548E-02	0.107890E+03	0.720973E+00	0.108093E-03	0.163766E+03	0.143430E+03
0.699142E-02	0.108583E+03	0.721796E+00	0.108242E-03	0.163857E+03	0.142814E+03
0.769097E-02	0.109124E+03	0.722617E+00	0.108391E-03	0.163932E+03	0.142197E+03
0.846046E-02	0.109737E+03	0.723439E+00	0.108540E-03	0.163997E+03	0.141575E+03
0.930691E-02	0.110025E+03	0.724260E+00	0.108689E-03	0.164040E+03	0.140950E+03
0.102380E-01	0.110255E+03	0.725076E+00	0.108838E-03	0.164075E+03	0.140325E+03
0.112622E-01	0.110914E+03	0.725890E+00	0.108986E-03	0.164117E+03	0.139698E+03
0.123888E-01	0.112334E+03	0.726705E+00	0.109135E-03	0.164252E+03	0.139066E+03
0.136281E-01	0.113255E+03	0.727530E+00	0.109286E-03	0.164323E+03	0.138422E+03
0.149913E-01	0.113268E+03	0.728349E+00	0.109436E-03	0.164364E+03	0.137779E+03
0.164908E-01	0.113664E+03	0.729163E+00	0.109585E-03	0.164400E+03	0.137136E+03

Table F-3 (Cont'd)

t days	$dp_{wf}/d\log t$ psi	$\mu_o B_o$ cp-RB/STB	$\mu_g B_g$ cp-RB/STB	R STB/STB	R_p STB/STB
0.181403E-01	0.114307E+03	0.729977E+00	0.109735E-03	0.164434E+03	0.136489E+03
0.199548E-01	0.114556E+03	0.730981E+00	0.109912E-03	0.164455E+03	0.135845E+03
0.219506E-01	0.114841E+03	0.732089E+00	0.110105E-03	0.164484E+03	0.135206E+03
0.241461E-01	0.115666E+03	0.733198E+00	0.110299E-03	0.164515E+03	0.134563E+03
0.265611E-01	0.116691E+03	0.734309E+00	0.110492E-03	0.164576E+03	0.133915E+03
0.292176E-01	0.117673E+03	0.735425E+00	0.110686E-03	0.164662E+03	0.133261E+03
0.321398E-01	0.118147E+03	0.736543E+00	0.110881E-03	0.164699E+03	0.132601E+03
0.353542E-01	0.118479E+03	0.737656E+00	0.111074E-03	0.164726E+03	0.131942E+03
0.388900E-01	0.118962E+03	0.738767E+00	0.111267E-03	0.164748E+03	0.131279E+03
0.427794E-01	0.119068E+03	0.739876E+00	0.111460E-03	0.164757E+03	0.130614E+03
0.470577E-01	0.119211E+03	0.740977E+00	0.111651E-03	0.164762E+03	0.129950E+03
0.517639E-01	0.119946E+03	0.742075E+00	0.111841E-03	0.164777E+03	0.129283E+03
0.569407E-01	0.120771E+03	0.743177E+00	0.112032E-03	0.164794E+03	0.128611E+03
0.626351E-01	0.121055E+03	0.744277E+00	0.112223E-03	0.164800E+03	0.127936E+03
0.688991E-01	0.121491E+03	0.745370E+00	0.112412E-03	0.164824E+03	0.127260E+03
0.757894E-01	0.123543E+03	0.746465E+00	0.112602E-03	0.164951E+03	0.126580E+03
0.833687E-01	0.124923E+03	0.747582E+00	0.112795E-03	0.164995E+03	0.125881E+03
0.917060E-01	0.124236E+03	0.748687E+00	0.112986E-03	0.164997E+03	0.125185E+03
0.100877E+00	0.123791E+03	0.749777E+00	0.113174E-03	0.164991E+03	0.124495E+03
0.110965E+00	0.124263E+03	0.750861E+00	0.113361E-03	0.164999E+03	0.123804E+03
0.122062E+00	0.125098E+03	0.751946E+00	0.113548E-03	0.165014E+03	0.123108E+03
0.134269E+00	0.125476E+03	0.753186E+00	0.113765E-03	0.165013E+03	0.122413E+03
0.147696E+00	0.125655E+03	0.754651E+00	0.114026E-03	0.165010E+03	0.121726E+03
0.162466E+00	0.126379E+03	0.756113E+00	0.114285E-03	0.165020E+03	0.121036E+03
0.178713E+00	0.127287E+03	0.757580E+00	0.114545E-03	0.165035E+03	0.120341E+03
0.196584E+00	0.127565E+03	0.759046E+00	0.114804E-03	0.165033E+03	0.119642E+03
0.216243E+00	0.127717E+03	0.760502E+00	0.115061E-03	0.165028E+03	0.118944E+03
0.237868E+00	0.128573E+03	0.761956E+00	0.115316E-03	0.165037E+03	0.118243E+03
0.261655E+00	0.129580E+03	0.763415E+00	0.115572E-03	0.165052E+03	0.117535E+03
0.287821E+00	0.129879E+03	0.764874E+00	0.115828E-03	0.165049E+03	0.116824E+03
0.316604E+00	0.130026E+03	0.766323E+00	0.116081E-03	0.165044E+03	0.116113E+03
0.348264E+00	0.130897E+03	0.767769E+00	0.116333E-03	0.165053E+03	0.115399E+03
0.383091E+00	0.131942E+03	0.769219E+00	0.116585E-03	0.165067E+03	0.114679E+03
0.421401E+00	0.132246E+03	0.770670E+00	0.116837E-03	0.165064E+03	0.113954E+03
0.463541E+00	0.132382E+03	0.772110E+00	0.117086E-03	0.165058E+03	0.113230E+03
0.509896E+00	0.133274E+03	0.773546E+00	0.117333E-03	0.165067E+03	0.112504E+03
0.560886E+00	0.134350E+03	0.774987E+00	0.117581E-03	0.165081E+03	0.111770E+03
0.616975E+00	0.134665E+03	0.776428E+00	0.117829E-03	0.165077E+03	0.111032E+03
0.678673E+00	0.134785E+03	0.777858E+00	0.118074E-03	0.165071E+03	0.110295E+03
0.746540E+00	0.137073E+03	0.779283E+00	0.118317E-03	0.165165E+03	0.109556E+03
0.821195E+00	0.139439E+03	0.781145E+00	0.118660E-03	0.165226E+03	0.108806E+03
0.903315E+00	0.138830E+03	0.783130E+00	0.119030E-03	0.165215E+03	0.108056E+03
0.993647E+00	0.137891E+03	0.785077E+00	0.119392E-03	0.165200E+03	0.107316E+03

Table F-3 (Cont'd)

t days	$dp_{wf}/d\log t$ psi	$\mu_o B_o$ cp-RB/STB	$\mu_g B_g$ cp-RB/STB	R STB/STB	R_s STB/STB
0.109301E+01	0.138484E+03	0.787013E+00	0.119751E-03	0.165206E+03	0.106576E+03
0.120231E+01	0.139565E+03	0.788955E+00	0.120110E-03	0.165221E+03	0.105830E+03
0.132254E+01	0.139932E+03	0.790900E+00	0.120467E-03	0.165212E+03	0.105078E+03
0.145480E+01	0.140111E+03	0.792829E+00	0.120821E-03	0.165203E+03	0.104328E+03
0.160028E+01	0.141092E+03	0.794756E+00	0.121172E-03	0.165213E+03	0.103575E+03
0.176031E+01	0.142277E+03	0.796690E+00	0.121523E-03	0.165229E+03	0.102814E+03
0.193634E+01	0.142644E+03	0.798626E+00	0.121873E-03	0.165221E+03	0.102048E+03
0.212997E+01	0.142807E+03	0.800547E+00	0.122219E-03	0.165212E+03	0.101283E+03
0.234297E+01	0.143804E+03	0.802464E+00	0.122563E-03	0.165222E+03	0.100515E+03
0.257727E+01	0.145026E+03	0.804388E+00	0.122906E-03	0.165238E+03	0.997398E+02
0.283500E+01	0.146736E+03	0.806314E+00	0.123249E-03	0.165296E+03	0.989589E+02
0.311850E+01	0.147466E+03	0.808259E+00	0.123592E-03	0.165296E+03	0.981651E+02
0.343035E+01	0.147287E+03	0.810180E+00	0.123930E-03	0.165301E+03	0.973764E+02
0.377338E+01	0.147534E+03	0.812095E+00	0.124266E-03	0.165314E+03	0.965845E+02
0.415072E+01	0.147523E+03	0.814473E+00	0.124736E-03	0.165310E+03	0.958053E+02
0.456579E+01	0.149520E+03	0.817056E+00	0.125264E-03	0.165302E+03	0.950315E+02

Table F-4

Simulated and Computed kk_{ro} Values
Buildup Test
Case 1

Δt days	p_{ws} psi	DD Sim. So	Sim. kk_{ro} md	Comp. kk_{ro} md
0.150000E-05	0.207823E+04	0.598796E+00	0.374849E+01	0.303296E+02
0.205000E-05	0.208392E+04	0.598930E+00	0.375181E+01	0.277733E+02
0.265500E-05	0.208958E+04	0.599064E+00	0.375514E+01	0.235545E+02
0.332050E-05	0.209522E+04	0.599200E+00	0.375854E+01	0.207009E+02
0.405255E-05	0.210084E+04	0.599337E+00	0.376194E+01	0.186260E+02
0.485780E-05	0.210647E+04	0.599470E+00	0.376525E+01	0.170304E+02
0.574359E-05	0.211211E+04	0.599602E+00	0.376853E+01	0.157482E+02
0.671794E-05	0.211778E+04	0.599738E+00	0.377191E+01	0.146841E+02
0.778974E-05	0.212351E+04	0.599886E+00	0.377560E+01	0.137754E+02
0.896871E-05	0.212929E+04	0.600036E+00	0.377936E+01	0.129848E+02
0.102656E-04	0.213516E+04	0.600189E+00	0.378326E+01	0.122862E+02
0.116921E-04	0.214111E+04	0.600345E+00	0.378723E+01	0.116581E+02
0.132614E-04	0.214717E+04	0.600502E+00	0.379123E+01	0.110907E+02
0.149875E-04	0.215334E+04	0.600660E+00	0.379528E+01	0.105777E+02
0.168862E-04	0.215964E+04	0.600822E+00	0.379940E+01	0.101104E+02
0.189749E-04	0.216606E+04	0.600988E+00	0.380362E+01	0.968209E+01
0.212724E-04	0.217262E+04	0.601157E+00	0.380793E+01	0.928673E+01
0.237996E-04	0.217933E+04	0.601329E+00	0.381233E+01	0.892028E+01
0.265795E-04	0.218619E+04	0.601507E+00	0.381688E+01	0.858068E+01
0.296375E-04	0.219320E+04	0.601699E+00	0.382177E+01	0.826503E+01
0.330012E-04	0.220038E+04	0.601894E+00	0.382673E+01	0.797089E+01
0.367014E-04	0.220772E+04	0.602086E+00	0.383163E+01	0.769467E+01
0.407715E-04	0.221523E+04	0.602283E+00	0.383665E+01	0.743438E+01
0.452487E-04	0.222292E+04	0.602484E+00	0.384180E+01	0.719115E+01
0.501735E-04	0.223078E+04	0.602691E+00	0.384706E+01	0.696354E+01
0.555909E-04	0.223883E+04	0.602902E+00	0.385245E+01	0.674534E+01
0.615500E-04	0.224706E+04	0.603132E+00	0.385831E+01	0.653308E+01
0.681050E-04	0.225550E+04	0.603363E+00	0.386420E+01	0.632954E+01
0.753155E-04	0.226415E+04	0.603593E+00	0.387008E+01	0.613763E+01
0.832470E-04	0.227300E+04	0.603829E+00	0.387609E+01	0.594929E+01
0.919717E-04	0.228208E+04	0.604072E+00	0.388229E+01	0.575965E+01
0.101569E-03	0.229141E+04	0.604324E+00	0.388872E+01	0.554510E+01
0.112126E-03	0.230109E+04	0.604609E+00	0.389598E+01	0.527531E+01
0.123738E-03	0.231129E+04	0.604924E+00	0.390402E+01	0.510608E+01
0.136512E-03	0.232153E+04	0.605245E+00	0.391245E+01	0.505274E+01
0.150563E-03	0.233185E+04	0.605560E+00	0.392078E+01	0.499104E+01
0.166020E-03	0.234227E+04	0.605884E+00	0.392936E+01	0.492375E+01
0.183022E-03	0.235279E+04	0.606214E+00	0.393808E+01	0.485602E+01
0.201724E-03	0.236341E+04	0.606549E+00	0.394696E+01	0.478832E+01
0.222296E-03	0.237416E+04	0.606889E+00	0.395597E+01	0.472216E+01
0.244926E-03	0.238501E+04	0.607231E+00	0.396502E+01	0.465850E+01
0.269818E-03	0.239598E+04	0.607574E+00	0.397409E+01	0.459757E+01
0.297200E-03	0.240705E+04	0.607935E+00	0.398367E+01	0.453860E+01

Table F-4 (Cont'd)

Δt days	p_{ws} psi	DD Sim. So	Sim. kk_{ro} md	Comp. kk_{ro} md
0.327320E-03	0.241824E+04	0.608296E+00	0.399321E+01	0.448183E+01
0.360452E-03	0.242953E+04	0.608661E+00	0.400287E+01	0.442812E+01
0.396898E-03	0.244092E+04	0.609029E+00	0.401261E+01	0.437613E+01
0.436987E-03	0.245241E+04	0.609409E+00	0.402267E+01	0.432630E+01
0.481086E-03	0.246401E+04	0.609791E+00	0.403278E+01	0.427926E+01
0.529595E-03	0.247570E+04	0.610175E+00	0.404295E+01	0.423213E+01
0.582954E-03	0.248749E+04	0.610563E+00	0.405322E+01	0.418298E+01
0.641650E-03	0.249939E+04	0.610961E+00	0.406376E+01	0.413072E+01
0.706215E-03	0.251142E+04	0.611371E+00	0.407461E+01	0.407152E+01
0.777236E-03	0.252361E+04	0.611783E+00	0.408551E+01	0.398612E+01
0.855360E-03	0.253610E+04	0.612200E+00	0.409656E+01	0.390331E+01
0.941296E-03	0.254875E+04	0.612639E+00	0.410817E+01	0.388325E+01
0.103583E-02	0.256132E+04	0.613078E+00	0.411979E+01	0.389829E+01
0.113981E-02	0.257383E+04	0.613504E+00	0.413108E+01	0.390767E+01
0.125419E-02	0.258629E+04	0.613941E+00	0.414265E+01	0.391346E+01
0.138001E-02	0.259871E+04	0.614397E+00	0.415472E+01	0.391685E+01
0.151841E-02	0.261110E+04	0.614904E+00	0.416813E+01	0.391891E+01
0.167065E-02	0.262347E+04	0.615408E+00	0.418188E+01	0.392040E+01
0.183811E-02	0.263580E+04	0.615921E+00	0.419597E+01	0.392115E+01
0.202233E-02	0.264812E+04	0.616437E+00	0.421013E+01	0.385242E+01
0.222496E-02	0.266085E+04	0.616971E+00	0.422480E+01	0.383813E+01
0.244785E-02	0.267321E+04	0.617487E+00	0.423897E+01	0.390155E+01
0.269304E-02	0.268549E+04	0.618011E+00	0.425336E+01	0.391446E+01
0.296274E-02	0.269772E+04	0.618542E+00	0.426794E+01	0.391916E+01
0.325942E-02	0.270993E+04	0.619086E+00	0.428287E+01	0.387146E+01
0.358576E-02	0.272242E+04	0.619677E+00	0.429910E+01	0.384476E+01
0.394473E-02	0.273474E+04	0.620286E+00	0.431601E+01	0.387462E+01
0.433961E-02	0.274700E+04	0.620899E+00	0.433326E+01	0.386916E+01
0.477397E-02	0.275932E+04	0.621520E+00	0.435072E+01	0.381761E+01
0.525177E-02	0.277185E+04	0.622157E+00	0.436864E+01	0.374288E+01
0.577734E-02	0.278463E+04	0.622824E+00	0.438740E+01	0.375885E+01
0.635548E-02	0.279702E+04	0.623478E+00	0.440581E+01	0.384252E+01
0.699142E-02	0.280921E+04	0.624154E+00	0.442483E+01	0.389105E+01
0.769097E-02	0.282126E+04	0.624877E+00	0.444516E+01	0.391523E+01
0.846046E-02	0.283326E+04	0.625607E+00	0.446612E+01	0.390425E+01
0.930691E-02	0.284534E+04	0.626345E+00	0.448739E+01	0.393101E+01
0.102380E-01	0.285715E+04	0.627085E+00	0.450871E+01	0.399161E+01
0.112622E-01	0.286883E+04	0.627848E+00	0.453069E+01	0.402118E+01
0.123888E-01	0.288043E+04	0.628624E+00	0.455306E+01	0.402228E+01
0.136281E-01	0.289207E+04	0.629453E+00	0.457695E+01	0.401719E+01
0.149913E-01	0.290366E+04	0.630331E+00	0.460247E+01	0.405319E+01
0.164908E-01	0.291506E+04	0.631205E+00	0.462825E+01	0.409640E+01
0.181403E-01	0.292637E+04	0.632085E+00	0.465423E+01	0.411910E+01
0.199548E-01	0.293761E+04	0.633006E+00	0.468142E+01	0.410023E+01

Table F-4 (Cont'd)

Δt days	p_{ws} psi	DD Sim. So	Sim. kk_{ro} md	Comp. kk_{ro} md
0.219506E-01	0.294898E+04	0.634018E+00	0.471126E+01	0.410187E+01
0.241461E-01	0.296017E+04	0.635059E+00	0.474202E+01	0.414446E+01
0.265611E-01	0.297127E+04	0.636113E+00	0.477389E+01	0.415792E+01
0.292176E-01	0.298235E+04	0.637224E+00	0.480745E+01	0.413367E+01
0.321398E-01	0.299355E+04	0.638413E+00	0.484336E+01	0.406621E+01
0.353542E-01	0.300495E+04	0.639694E+00	0.488207E+01	0.406796E+01
0.388900E-01	0.301609E+04	0.640995E+00	0.492209E+01	0.414474E+01
0.427794E-01	0.302704E+04	0.642332E+00	0.496345E+01	0.420373E+01
0.470577E-01	0.303784E+04	0.643707E+00	0.500598E+01	0.421802E+01
0.517639E-01	0.304867E+04	0.645143E+00	0.505048E+01	0.425601E+01
0.569407E-01	0.305924E+04	0.646593E+00	0.509640E+01	0.433178E+01
0.626351E-01	0.306966E+04	0.648063E+00	0.514295E+01	0.437807E+01
0.688991E-01	0.307995E+04	0.649550E+00	0.519002E+01	0.440058E+01
0.757894E-01	0.309022E+04	0.651067E+00	0.523883E+01	0.441964E+01
0.833687E-01	0.310038E+04	0.652595E+00	0.528834E+01	0.447190E+01
0.917060E-01	0.311036E+04	0.654115E+00	0.533758E+01	0.452805E+01
0.100877E+00	0.312022E+04	0.655626E+00	0.538699E+01	0.456911E+01
0.110965E+00	0.312997E+04	0.657131E+00	0.543689E+01	0.457732E+01
0.122062E+00	0.313974E+04	0.658637E+00	0.548679E+01	0.460630E+01
0.134269E+00	0.314931E+04	0.660106E+00	0.553560E+01	0.467205E+01
0.147696E+00	0.315874E+04	0.661553E+00	0.558465E+01	0.471690E+01
0.162466E+00	0.316806E+04	0.662973E+00	0.563279E+01	0.474669E+01
0.178713E+00	0.317730E+04	0.664374E+00	0.568031E+01	0.475850E+01
0.196584E+00	0.318650E+04	0.665756E+00	0.572777E+01	0.479631E+01
0.216243E+00	0.319552E+04	0.667093E+00	0.577415E+01	0.484980E+01
0.237868E+00	0.320443E+04	0.668402E+00	0.581954E+01	0.487904E+01
0.261655E+00	0.321326E+04	0.669689E+00	0.586418E+01	0.487794E+01
0.287821E+00	0.322208E+04	0.670951E+00	0.590869E+01	0.483683E+01
0.316604E+00	0.323095E+04	0.672210E+00	0.595334E+01	0.482191E+01
0.348264E+00	0.323971E+04	0.673434E+00	0.599676E+01	0.488700E+01
0.383091E+00	0.324823E+04	0.674622E+00	0.603890E+01	0.498232E+01
0.421401E+00	0.325655E+04	0.675764E+00	0.608002E+01	0.503681E+01
0.463541E+00	0.326476E+04	0.676888E+00	0.612078E+01	0.510139E+01
0.509896E+00	0.327273E+04	0.677961E+00	0.615969E+01	0.519148E+01
0.560886E+00	0.328051E+04	0.679010E+00	0.619772E+01	0.525866E+01
0.616975E+00	0.328813E+04	0.680024E+00	0.623453E+01	0.531881E+01
0.678673E+00	0.329558E+04	0.681007E+00	0.627097E+01	0.535177E+01
0.746540E+00	0.330293E+04	0.681975E+00	0.630687E+01	0.540346E+01
0.821195E+00	0.331006E+04	0.682900E+00	0.634116E+01	0.548228E+01
0.903315E+00	0.331701E+04	0.683802E+00	0.637460E+01	0.553918E+01
0.993647E+00	0.332379E+04	0.684675E+00	0.640697E+01	0.559245E+01
0.109301E+01	0.333040E+04	0.685525E+00	0.643890E+01	0.562481E+01
0.120231E+01	0.333689E+04	0.686353E+00	0.647029E+01	0.562935E+01
0.132254E+01	0.334316E+04	0.687155E+00	0.650067E+01	0.576780E+01

Table F-4 (Cont'd)

Δt days	p_{ws} psi	DD Sim. So	Sim. kk_{ro} md	Comp. kk_{ro} md
0.145480E+01	0.334924E+04	0.687921E+00	0.652970E+01	0.579133E+01
0.160028E+01	0.335514E+04	0.688668E+00	0.655801E+01	0.584037E+01
0.176031E+01	0.336086E+04	0.689384E+00	0.658516E+01	0.588181E+01
0.193634E+01	0.336640E+04	0.690082E+00	0.661168E+01	0.591227E+01
0.212997E+01	0.337177E+04	0.690753E+00	0.663767E+01	0.596128E+01
0.234297E+01	0.337692E+04	0.691388E+00	0.666224E+01	0.602181E+01
0.257727E+01	0.338188E+04	0.692003E+00	0.668608E+01	0.606740E+01
0.283500E+01	0.338664E+04	0.692595E+00	0.670900E+01	0.611084E+01
0.311850E+01	0.339121E+04	0.693159E+00	0.673084E+01	0.615187E+01
0.343035E+01	0.339558E+04	0.693697E+00	0.675166E+01	0.617511E+01
0.377338E+01	0.339978E+04	0.694213E+00	0.677166E+01	0.621140E+01
0.415072E+01	0.340377E+04	0.694703E+00	0.679065E+01	0.626649E+01
0.456579E+01	0.340756E+04	0.695169E+00	0.680880E+01	0.629580E+01

Table F-5

Simulated and Computed kk_{rg} Values
Buildup Test
Case 1

p_{ws} psi	Sim. kk_{rg} md	Comp. kk_{rg} md
0.207823E+04	0.392982E-01	0.317801E+00
0.208392E+04	0.391431E-01	0.289613E+00
0.208958E+04	0.389880E-01	0.244437E+00
0.209522E+04	0.388291E-01	0.213789E+00
0.210084E+04	0.386707E-01	0.191431E+00
0.210647E+04	0.385160E-01	0.174182E+00
0.211211E+04	0.383627E-01	0.160279E+00
0.211778E+04	0.382053E-01	0.148709E+00
0.212351E+04	0.380329E-01	0.138806E+00
0.212929E+04	0.378624E-01	0.130172E+00
0.213516E+04	0.377008E-01	0.122528E+00
0.214111E+04	0.375364E-01	0.115647E+00
0.214717E+04	0.373706E-01	0.109421E+00
0.215334E+04	0.372033E-01	0.103779E+00
0.215964E+04	0.370325E-01	0.986278E-01
0.216606E+04	0.368577E-01	0.938956E-01
0.217262E+04	0.366791E-01	0.895190E-01
0.217933E+04	0.364969E-01	0.854538E-01
0.218619E+04	0.363089E-01	0.816764E-01
0.219320E+04	0.361061E-01	0.781552E-01
0.220038E+04	0.359008E-01	0.748641E-01
0.220772E+04	0.356980E-01	0.717663E-01
0.221523E+04	0.354902E-01	0.688408E-01
0.222292E+04	0.352769E-01	0.660954E-01
0.223078E+04	0.350590E-01	0.635149E-01
0.223883E+04	0.348361E-01	0.610406E-01
0.224706E+04	0.345933E-01	0.586395E-01
0.225550E+04	0.343492E-01	0.563359E-01
0.226415E+04	0.341061E-01	0.541542E-01
0.227300E+04	0.338571E-01	0.520222E-01
0.228208E+04	0.336001E-01	0.498968E-01
0.229141E+04	0.333339E-01	0.475762E-01
0.230109E+04	0.330335E-01	0.448051E-01
0.231129E+04	0.327004E-01	0.429058E-01
0.232153E+04	0.323978E-01	0.419981E-01
0.233185E+04	0.321121E-01	0.410283E-01
0.234227E+04	0.318178E-01	0.400201E-01
0.235279E+04	0.315188E-01	0.390162E-01
0.236341E+04	0.312145E-01	0.380206E-01
0.237416E+04	0.309055E-01	0.370450E-01
0.238501E+04	0.305954E-01	0.360967E-01
0.239598E+04	0.302845E-01	0.351771E-01
0.240705E+04	0.299560E-01	0.342797E-01

Table F-5 (Cont'd)

p_{wo} psi	Sim. kk_{rg} md	Comp. kk_{rg} md
0.241824E+04	0.296290E-01	0.334059E-01
0.242953E+04	0.292977E-01	0.325618E-01
0.244092E+04	0.289638E-01	0.317369E-01
0.245241E+04	0.286189E-01	0.309341E-01
0.246401E+04	0.282722E-01	0.301574E-01
0.247570E+04	0.279234E-01	0.293863E-01
0.248749E+04	0.275714E-01	0.286074E-01
0.249939E+04	0.272099E-01	0.278137E-01
0.251142E+04	0.268381E-01	0.269806E-01
0.252361E+04	0.264645E-01	0.259837E-01
0.253610E+04	0.260855E-01	0.250107E-01
0.254875E+04	0.256874E-01	0.244424E-01
0.256132E+04	0.252891E-01	0.240987E-01
0.257383E+04	0.249020E-01	0.237195E-01
0.258629E+04	0.245053E-01	0.233185E-01
0.259871E+04	0.240917E-01	0.229037E-01
0.261110E+04	0.236320E-01	0.224816E-01
0.262347E+04	0.232311E-01	0.220570E-01
0.263580E+04	0.228368E-01	0.216291E-01
0.264812E+04	0.224408E-01	0.208263E-01
0.266085E+04	0.220304E-01	0.203129E-01
0.267321E+04	0.216342E-01	0.202181E-01
0.268549E+04	0.212314E-01	0.198562E-01
0.269772E+04	0.208237E-01	0.194524E-01
0.270993E+04	0.204060E-01	0.187944E-01
0.272242E+04	0.199518E-01	0.182368E-01
0.273474E+04	0.195090E-01	0.179528E-01
0.274700E+04	0.190913E-01	0.175053E-01
0.275932E+04	0.186684E-01	0.168534E-01
0.277185E+04	0.182343E-01	0.161020E-01
0.278463E+04	0.177799E-01	0.157363E-01
0.279702E+04	0.173340E-01	0.156560E-01
0.280921E+04	0.168734E-01	0.154251E-01
0.282126E+04	0.163809E-01	0.150948E-01
0.283326E+04	0.159331E-01	0.146294E-01
0.284534E+04	0.154906E-01	0.143010E-01
0.285715E+04	0.150471E-01	0.140966E-01
0.286883E+04	0.145899E-01	0.137775E-01
0.288043E+04	0.141246E-01	0.133611E-01
0.289207E+04	0.136277E-01	0.129230E-01
0.290366E+04	0.131272E-01	0.126161E-01
0.291506E+04	0.126709E-01	0.123306E-01
0.292637E+04	0.122111E-01	0.119801E-01
0.293761E+04	0.117299E-01	0.115112E-01

Table F-5 (Cont'd)

p_{wf} psi	Sim. kk_{rg} md	Comp. kk_{rg} md
0.294898E+04	0.112018E-01	0.110967E-01
0.296017E+04	0.106624E-01	0.107956E-01
0.297127E+04	0.101878E-01	0.104164E-01
0.298235E+04	0.968777E-02	0.994497E-02
0.299355E+04	0.915287E-02	0.937473E-02
0.300495E+04	0.857632E-02	0.895795E-02
0.301609E+04	0.805762E-02	0.870635E-02
0.302704E+04	0.754554E-02	0.841134E-02
0.303784E+04	0.701913E-02	0.802575E-02
0.304867E+04	0.647831E-02	0.767883E-02
0.305924E+04	0.601292E-02	0.739993E-02
0.306966E+04	0.554122E-02	0.706488E-02
0.307995E+04	0.506412E-02	0.669010E-02
0.309022E+04	0.463815E-02	0.630757E-02
0.310038E+04	0.423469E-02	0.597040E-02
0.311036E+04	0.383349E-02	0.563607E-02
0.312022E+04	0.346691E-02	0.527941E-02
0.312997E+04	0.314711E-02	0.488524E-02
0.313974E+04	0.282726E-02	0.450940E-02
0.314931E+04	0.251990E-02	0.416994E-02
0.315874E+04	0.227940E-02	0.380815E-02
0.316806E+04	0.204333E-02	0.343296E-02
0.317730E+04	0.181035E-02	0.304464E-02
0.318650E+04	0.161129E-02	0.267107E-02
0.319552E+04	0.144338E-02	0.230664E-02
0.320443E+04	0.127904E-02	0.192886E-02
0.321326E+04	0.111745E-02	0.154098E-02
0.322208E+04	0.992452E-03	0.114409E-02
0.323095E+04	0.878636E-03	0.755802E-03
0.323971E+04	0.767959E-03	0.380488E-03
0.324823E+04	0.660550E-03	0.604924E-05
0.325655E+04	0.579837E-03	0.000000E+00
0.326476E+04	0.511382E-03	0.000000E+00
0.327273E+04	0.446054E-03	0.000000E+00
0.328051E+04	0.382181E-03	0.000000E+00
0.328813E+04	0.320971E-03	0.000000E+00
0.329558E+04	0.284493E-03	0.000000E+00
0.330293E+04	0.248549E-03	0.000000E+00
0.331006E+04	0.214215E-03	0.000000E+00
0.331701E+04	0.180738E-03	0.000000E+00
0.332379E+04	0.148336E-03	0.000000E+00
0.333040E+04	0.126229E-03	0.000000E+00
0.333689E+04	0.110365E-03	0.000000E+00
0.334316E+04	0.950135E-04	0.000000E+00

Table F-5 (Cont'd)

p_{wf} psi	Sim. kk_{rg} md	Comp. kk_{rg} md
0.334924E+04	0.803398E-04	0.000000E+00
0.335514E+04	0.660327E-04	0.000000E+00
0.336086E+04	0.523161E-04	0.000000E+00
0.336640E+04	0.399400E-04	0.000000E+00
0.337177E+04	0.351845E-04	0.000000E+00
0.337692E+04	0.306872E-04	0.000000E+00
0.338188E+04	0.263238E-04	0.000000E+00
0.338664E+04	0.221281E-04	0.000000E+00
0.339121E+04	0.181321E-04	0.000000E+00
0.339558E+04	0.143212E-04	0.000000E+00
0.339978E+04	0.106604E-04	0.000000E+00
0.340377E+04	0.718570E-05	0.000000E+00
0.340756E+04	0.491232E-05	0.000000E+00

Table F-6

Parameter Values for the Computation of kk_{ro} and kk_{rg}
Buildup Test
Case 1

Δt days	p_{ws} psi	$dp_{ws}/dlog(R_{H1})$ psi	$\mu_o B_o$ cp-RB/STB	$\mu_g B_g$ cp-RB/STB	R_s STB/STB
0.150000E-05	0.207823E+04	0.419718E+02	0.811594E+00	0.124178E-03	0.967920E+02
0.205000E-05	0.208392E+04	0.457912E+02	0.810819E+00	0.124042E-03	0.971126E+02
0.265500E-05	0.208958E+04	0.539414E+02	0.810046E+00	0.123907E-03	0.974312E+02
0.332050E-05	0.209522E+04	0.613186E+02	0.809275E+00	0.123771E-03	0.977486E+02
0.405255E-05	0.210084E+04	0.680842E+02	0.808503E+00	0.123635E-03	0.980653E+02
0.485780E-05	0.210647E+04	0.743919E+02	0.807729E+00	0.123499E-03	0.983819E+02
0.574359E-05	0.211211E+04	0.803715E+02	0.806951E+00	0.123361E-03	0.986996E+02
0.671794E-05	0.211778E+04	0.861118E+02	0.806166E+00	0.123222E-03	0.990190E+02
0.778974E-05	0.212351E+04	0.917019E+02	0.805373E+00	0.123082E-03	0.993411E+02
0.896871E-05	0.212929E+04	0.971879E+02	0.804569E+00	0.122939E-03	0.996669E+02
0.102656E-04	0.213516E+04	0.102610E+03	0.803752E+00	0.122793E-03	0.999969E+02
0.116921E-04	0.214111E+04	0.108027E+03	0.802920E+00	0.122644E-03	0.100332E+03
0.132614E-04	0.214717E+04	0.113433E+03	0.802071E+00	0.122493E-03	0.100673E+03
0.149875E-04	0.215334E+04	0.118805E+03	0.801203E+00	0.122337E-03	0.101021E+03
0.168862E-04	0.215964E+04	0.124159E+03	0.800316E+00	0.122178E-03	0.101375E+03
0.189749E-04	0.216606E+04	0.129505E+03	0.799409E+00	0.122014E-03	0.101737E+03
0.212724E-04	0.217262E+04	0.134861E+03	0.798479E+00	0.121847E-03	0.102106E+03
0.237996E-04	0.217933E+04	0.140233E+03	0.797525E+00	0.121675E-03	0.102484E+03
0.265795E-04	0.218619E+04	0.145605E+03	0.796548E+00	0.121497E-03	0.102870E+03
0.296375E-04	0.219320E+04	0.150975E+03	0.795545E+00	0.121315E-03	0.103265E+03
0.330012E-04	0.220038E+04	0.156344E+03	0.794516E+00	0.121128E-03	0.103669E+03
0.367014E-04	0.220772E+04	0.161741E+03	0.793460E+00	0.120936E-03	0.104082E+03
0.407715E-04	0.221523E+04	0.167175E+03	0.792375E+00	0.120738E-03	0.104505E+03
0.452487E-04	0.222292E+04	0.172587E+03	0.791262E+00	0.120534E-03	0.104938E+03
0.501735E-04	0.223078E+04	0.177970E+03	0.790119E+00	0.120324E-03	0.105380E+03
0.555909E-04	0.223883E+04	0.183455E+03	0.788945E+00	0.120108E-03	0.105833E+03
0.615500E-04	0.224706E+04	0.189126E+03	0.787740E+00	0.119886E-03	0.106297E+03
0.681050E-04	0.225550E+04	0.194900E+03	0.786501E+00	0.119656E-03	0.106772E+03
0.753155E-04	0.226415E+04	0.200669E+03	0.785226E+00	0.119420E-03	0.107259E+03
0.832470E-04	0.227300E+04	0.206676E+03	0.783917E+00	0.119177E-03	0.107757E+03
0.919717E-04	0.228208E+04	0.213114E+03	0.782568E+00	0.118926E-03	0.108268E+03
0.101569E-03	0.229141E+04	0.220966E+03	0.781177E+00	0.118666E-03	0.108794E+03
0.112126E-03	0.230109E+04	0.231836E+03	0.779727E+00	0.118394E-03	0.109339E+03
0.123738E-03	0.231129E+04	0.239165E+03	0.778575E+00	0.118196E-03	0.109924E+03
0.136512E-03	0.232154E+04	0.241337E+03	0.777437E+00	0.118002E-03	0.110513E+03
0.150563E-03	0.233185E+04	0.243959E+03	0.776285E+00	0.117804E-03	0.111106E+03
0.166020E-03	0.234227E+04	0.246920E+03	0.775117E+00	0.117604E-03	0.111704E+03
0.183022E-03	0.235279E+04	0.249981E+03	0.773931E+00	0.117400E-03	0.112309E+03
0.201724E-03	0.236342E+04	0.253121E+03	0.772726E+00	0.117192E-03	0.112919E+03
0.222296E-03	0.237416E+04	0.256260E+03	0.771501E+00	0.116980E-03	0.113537E+03
0.244926E-03	0.238501E+04	0.259344E+03	0.770258E+00	0.116765E-03	0.114160E+03
0.269818E-03	0.239598E+04	0.262350E+03	0.768995E+00	0.116546E-03	0.114790E+03
0.297200E-03	0.240705E+04	0.265316E+03	0.767713E+00	0.116323E-03	0.115427E+03

Table F-6 (Cont'd)

Δt days	p_{ws} psi	$dp_{ws}/dlog(R_{H1})$ psi	$\mu_o B_o$ cp-RB/STB	$\mu_g B_g$ cp-RB/STB	R_s STB/STB
0.327320E-03	0.241824E+04	0.268220E+03	0.766411E+00	0.116096E-03	0.116070E+03
0.360452E-03	0.242953E+04	0.271005E+03	0.765089E+00	0.115835E-03	0.116718E+03
0.396898E-03	0.244092E+04	0.273745E+03	0.763749E+00	0.115631E-03	0.117373E+03
0.436987E-03	0.245242E+04	0.276404E+03	0.762388E+00	0.115392E-03	0.118034E+03
0.481086E-03	0.246401E+04	0.278938E+03	0.761009E+00	0.115150E-03	0.118700E+03
0.529595E-03	0.247570E+04	0.281525E+03	0.759611E+00	0.114904E-03	0.119372E+03
0.582954E-03	0.248749E+04	0.284302E+03	0.758193E+00	0.114653E-03	0.120049E+03
0.641650E-03	0.249939E+04	0.287352E+03	0.756754E+00	0.114399E-03	0.120733E+03
0.706215E-03	0.251142E+04	0.290967E+03	0.755291E+00	0.114139E-03	0.121425E+03
0.777236E-03	0.252361E+04	0.296614E+03	0.753800E+00	0.113875E-03	0.122125E+03
0.855360E-03	0.253610E+04	0.302325E+03	0.752353E+00	0.113619E-03	0.122846E+03
0.941296E-03	0.254875E+04	0.303421E+03	0.751201E+00	0.113420E-03	0.123586E+03
0.103583E-02	0.256132E+04	0.301787E+03	0.750049E+00	0.113221E-03	0.124322E+03
0.113961E-02	0.257383E+04	0.300599E+03	0.748894E+00	0.113022E-03	0.125054E+03
0.125419E-02	0.258629E+04	0.299691E+03	0.747737E+00	0.112821E-03	0.125784E+03
0.138001E-02	0.259871E+04	0.298966E+03	0.746575E+00	0.112621E-03	0.126511E+03
0.151841E-02	0.261110E+04	0.298342E+03	0.745408E+00	0.112419E-03	0.127237E+03
0.167065E-02	0.262347E+04	0.297760E+03	0.744236E+00	0.112216E-03	0.127961E+03
0.183811E-02	0.263581E+04	0.297232E+03	0.743059E+00	0.112012E-03	0.128683E+03
0.202233E-02	0.264812E+04	0.302053E+03	0.741877E+00	0.111807E-03	0.129404E+03
0.222496E-02	0.266085E+04	0.302675E+03	0.740647E+00	0.111593E-03	0.130149E+03
0.244785E-02	0.267321E+04	0.297272E+03	0.739445E+00	0.111385E-03	0.130873E+03
0.269304E-02	0.268549E+04	0.295811E+03	0.738244E+00	0.111176E-03	0.131592E+03
0.296274E-02	0.269772E+04	0.294973E+03	0.737039E+00	0.110967E-03	0.132308E+03
0.325942E-02	0.270993E+04	0.298118E+03	0.735830E+00	0.110757E-03	0.133023E+03
0.358576E-02	0.272242E+04	0.299680E+03	0.734585E+00	0.110540E-03	0.133754E+03
0.394473E-02	0.273475E+04	0.296870E+03	0.733348E+00	0.110325E-03	0.134476E+03
0.433961E-02	0.274700E+04	0.296788E+03	0.732111E+00	0.110109E-03	0.135193E+03
0.477397E-02	0.275932E+04	0.300281E+03	0.730860E+00	0.109891E-03	0.135914E+03
0.525177E-02	0.277185E+04	0.305819E+03	0.729768E+00	0.109696E-03	0.136655E+03
0.577734E-02	0.278463E+04	0.304120E+03	0.728809E+00	0.109520E-03	0.137416E+03
0.635548E-02	0.279702E+04	0.297115E+03	0.727872E+00	0.109349E-03	0.138154E+03
0.699142E-02	0.280921E+04	0.293035E+03	0.726944E+00	0.109179E-03	0.138880E+03
0.769097E-02	0.282126E+04	0.290855E+03	0.726020E+00	0.109010E-03	0.139597E+03
0.846046E-02	0.283326E+04	0.291300E+03	0.725092E+00	0.108841E-03	0.140312E+03
0.930691E-02	0.284534E+04	0.288943E+03	0.724152E+00	0.108670E-03	0.141032E+03
0.102380E-01	0.285715E+04	0.284192E+03	0.723228E+00	0.108502E-03	0.141735E+03
0.112622E-01	0.286883E+04	0.281743E+03	0.722306E+00	0.108334E-03	0.142431E+03
0.123888E-01	0.288043E+04	0.281307E+03	0.721386E+00	0.108167E-03	0.143121E+03
0.136281E-01	0.289207E+04	0.281301E+03	0.720456E+00	0.107999E-03	0.143815E+03
0.149913E-01	0.290366E+04	0.278441E+03	0.719524E+00	0.107830E-03	0.144505E+03
0.164908E-01	0.291506E+04	0.275151E+03	0.718601E+00	0.107663E-03	0.145184E+03
0.181403E-01	0.292637E+04	0.273284E+03	0.717680E+00	0.107497E-03	0.145857E+03

Table F-6 (Cont'd)

Δt days	p_{ws} psi	$dp_{ws}/dlog(R_{H1})$ psi	$\mu_o B_o$ cp-RB/STB	$\mu_g B_g$ cp-RB/STB	R_s STB/STB
0.199548E-01	0.293761E+04	0.274189E+03	0.716759E+00	0.107331E-03	0.146527E+03
0.219506E-01	0.294898E+04	0.273721E+03	0.715821E+00	0.107162E-03	0.147204E+03
0.241461E-01	0.296017E+04	0.270556E+03	0.714892E+00	0.106995E-03	0.147871E+03
0.265611E-01	0.297127E+04	0.269331E+03	0.713965E+00	0.106829E-03	0.148532E+03
0.292176E-01	0.298235E+04	0.270558E+03	0.713035E+00	0.106662E-03	0.149192E+03
0.321398E-01	0.299355E+04	0.274682E+03	0.712090E+00	0.106492E-03	0.149858E+03
0.353542E-01	0.300495E+04	0.274265E+03	0.711313E+00	0.106342E-03	0.150545E+03
0.388900E-01	0.301609E+04	0.268922E+03	0.710621E+00	0.106204E-03	0.151220E+03
0.427794E-01	0.302704E+04	0.264893E+03	0.709937E+00	0.106067E-03	0.151882E+03
0.470577E-01	0.303784E+04	0.263743E+03	0.709257E+00	0.105932E-03	0.152535E+03
0.517639E-01	0.304867E+04	0.261135E+03	0.708569E+00	0.105796E-03	0.153191E+03
0.569407E-01	0.305924E+04	0.256323E+03	0.707895E+00	0.105662E-03	0.153830E+03
0.626351E-01	0.306966E+04	0.253373E+03	0.707225E+00	0.105530E-03	0.154461E+03
0.688991E-01	0.307995E+04	0.251839E+03	0.706559E+00	0.105399E-03	0.155084E+03
0.757894E-01	0.309022E+04	0.250516E+03	0.705890E+00	0.105268E-03	0.155705E+03
0.833687E-01	0.310038E+04	0.247355E+03	0.705224E+00	0.105138E-03	0.156320E+03
0.917060E-01	0.311036E+04	0.244059E+03	0.704565E+00	0.105010E-03	0.156924E+03
0.100877E+00	0.312022E+04	0.241642E+03	0.703911E+00	0.104882E-03	0.157520E+03
0.110965E+00	0.312997E+04	0.240985E+03	0.703260E+00	0.104756E-03	0.158110E+03
0.122062E+00	0.313974E+04	0.239245E+03	0.702604E+00	0.104629E-03	0.158701E+03
0.134269E+00	0.314931E+04	0.235662E+03	0.701958E+00	0.104504E-03	0.159280E+03
0.147696E+00	0.315874E+04	0.233208E+03	0.701317E+00	0.104381E-03	0.159851E+03
0.162466E+00	0.316806E+04	0.231533E+03	0.700680E+00	0.104259E-03	0.160414E+03
0.178713E+00	0.317730E+04	0.230750E+03	0.700045E+00	0.104137E-03	0.160974E+03
0.196584E+00	0.318650E+04	0.228723E+03	0.699409E+00	0.104015E-03	0.161530E+03
0.216243E+00	0.319552E+04	0.225998E+03	0.698783E+00	0.103896E-03	0.162076E+03
0.237868E+00	0.320444E+04	0.224443E+03	0.698160E+00	0.103777E-03	0.162615E+03
0.261655E+00	0.321326E+04	0.224295E+03	0.697541E+00	0.103660E-03	0.163149E+03
0.287821E+00	0.322208E+04	0.225999E+03	0.696919E+00	0.103542E-03	0.163683E+03
0.316604E+00	0.323095E+04	0.226512E+03	0.696344E+00	0.103430E-03	0.164220E+03
0.348264E+00	0.323971E+04	0.223353E+03	0.695901E+00	0.103339E-03	0.164751E+03
0.383091E+00	0.324823E+04	0.218943E+03	0.695469E+00	0.103249E-03	0.165267E+03
0.421401E+00	0.325655E+04	0.216442E+03	0.695044E+00	0.103162E-03	0.165770E+03
0.463541E+00	0.326476E+04	0.213572E+03	0.694621E+00	0.103075E-03	0.166268E+03
0.509896E+00	0.327273E+04	0.209742E+03	0.694209E+00	0.102990E-03	0.166750E+03
0.560886E+00	0.328051E+04	0.206941E+03	0.693805E+00	0.102908E-03	0.167222E+03
0.616975E+00	0.328813E+04	0.204484E+03	0.693406E+00	0.102826E-03	0.167683E+03
0.678673E+00	0.329558E+04	0.203109E+03	0.693015E+00	0.102747E-03	0.168135E+03
0.746540E+00	0.330293E+04	0.201054E+03	0.692627E+00	0.102668E-03	0.168580E+03
0.821195E+00	0.331006E+04	0.198055E+03	0.692248E+00	0.102592E-03	0.169012E+03
0.903315E+00	0.331701E+04	0.195916E+03	0.691877E+00	0.102517E-03	0.169433E+03
0.993647E+00	0.332379E+04	0.193947E+03	0.691514E+00	0.102444E-03	0.169844E+03
0.109301E+01	0.333040E+04	0.192733E+03	0.691158E+00	0.102372E-03	0.170244E+03

Table F-6 (Cont'd)

Δt days	p_{ws} psi	$dp_{ws}/dlog(R_{H1})$ psi	$\mu_o B_o$ cp-RB/STB	$\mu_g B_g$ cp-RB/STB	R_s STB/STB
0.132254E+01	0.334316E+04	0.187766E+03	0.690467E+00	0.102234E-03	0.171017E+03
0.145480E+01	0.334925E+04	0.186914E+03	0.690135E+00	0.102168E-03	0.171386E+03
0.160028E+01	0.335515E+04	0.185258E+03	0.689813E+00	0.102104E-03	0.171743E+03
0.176031E+01	0.336086E+04	0.183869E+03	0.689498E+00	0.102041E-03	0.172090E+03
0.193634E+01	0.336640E+04	0.182840E+03	0.689193E+00	0.101981E-03	0.172425E+03
0.212997E+01	0.337177E+04	0.181259E+03	0.688896E+00	0.101922E-03	0.172750E+03
0.234297E+01	0.337692E+04	0.179362E+03	0.688610E+00	0.101865E-03	0.173062E+03
0.257727E+01	0.338188E+04	0.177943E+03	0.688333E+00	0.101811E-03	0.173363E+03
0.283500E+01	0.338664E+04	0.176610E+03	0.688067E+00	0.101758E-03	0.173651E+03
0.311850E+01	0.339121E+04	0.175367E+03	0.687811E+00	0.101708E-03	0.173928E+03
0.343035E+01	0.339558E+04	0.174644E+03	0.687565E+00	0.101660E-03	0.174193E+03
0.377338E+01	0.339978E+04	0.173564E+03	0.687328E+00	0.101613E-03	0.174447E+03
0.415072E+01	0.340377E+04	0.171982E+03	0.687103E+00	0.101569E-03	0.174689E+03
0.456579E+01	0.340756E+04	0.171128E+03	0.686888E+00	0.101527E-03	0.174919E+03

Table F-7

Nonlinear Parameter Estimation
Two Unknowns
Case 1

Iteration Number	kk_r^o md	λ
0	0.62958E+01	0.10000E+01
1	0.70241E+01	0.10384E+01
2	0.70087E+01	0.15576E+01
3	0.69988E+01	0.20054E+01
4	0.69987E+01	0.20071E+01

Table F-8

Nonlinear Parameter Estimation
Three Unknowns
Case 1

Iteration Number	kk_r^o md	λ	S_{gc}
0	0.62958E+01	0.10000E+01	0.10000E-09
1	0.70241E+01	0.10384E+01	0.12632E-09
2	0.70087E+01	0.15576E+01	0.15125E-09
3	0.69988E+01	0.20054E+01	0.18906E-09
4	0.69987E+01	0.20071E+01	0.19021E-09

Table F-9

Nonlinear Parameter Estimation
Four Unknowns
Case 1

Iteration Number	kk_r^o md	λ	S_{gc}	S_{wc}
0	0.62958E+01	0.10000E+01	0.10000E-09	0.10000E+00
1	0.72833E+01	0.84544E+00	0.13635E-09	0.13089E+00
2	0.69194E+01	0.16395E+01	0.20452E-09	0.20332E+00
3	0.69982E+01	0.14652E+01	0.30678E-09	0.23475E+00
4	0.69898E+01	0.16599E+01	0.46017E-09	0.26770E+00
5	0.69904E+01	0.21708E+01	0.69026E-09	0.27503E+00
6	0.69904E+01	0.21808E+01	0.69175E-09	0.27485E+00

Table F-10

Effects of the Initial Guess on the Values of Estimated Parameters
Case 1

	kk_r^o md	λ	S_{gc}	S_{wc}	Iteration No.
I.G.* # 1	6.296	0.500	-	-	-
Results	6.995	2.042	-	-	7
I.G. # 2	4.592	0.500	-	-	-
Results	6.990	2.066	-	-	8
I.G. # 3	6.296	3.000	-	-	-
Results	6.989	2.065	-	-	10
I.G. # 4	4.592	3.000	-	-	-
Results	6.989	2.065	-	-	8
I.G. # 5	6.296	7.000	-	-	-
Results	6.989	2.065	-	-	7
I.G. # 6	4.592	7.000	-	-	-
Results	6.896	3.187	-	-	5
I.G. # 7	6.296	1.000	1.0×10^{-10}	-	-
Results	6.999	2.008	1.9×10^{-10}	-	6
I.G. # 8	4.592	1.000	1.0×10^{-10}	-	-
Results	6.999	2.065	3.8×10^{-10}	-	7
I.G. # 9	6.296	1.000	1.0×10^{-10}	0.100	-
Results	6.990	2.181	6.9×10^{-10}	0.275	6
I.G. # 10	4.592	1.000	1.0×10^{-10}	0.100	-
Results	6.990	2.149	6.6×10^{-10}	0.260	12
I.G. # 11	6.296	3.000	1.0×10^{-10}	0.200	-
Results	6.993	2.142	4.8×10^{-10}	0.277	9
I.G. # 12	4.592	3.000	1.0×10^{-10}	0.200	-
Results	6.891	2.234	1.1×10^{-10}	2.8×10^{-4}	4
I.G. # 13	6.296	7.000	1.0×10^{-10}	0.100	-
Results	7.007	1.728	2.1×10^{-10}	6.3×10^{-2}	5
Actual	7.0	2.0	0.0	0.3	-

* I.G. = Initial Guess

Table F-11

Approximate Confidence Intervals of Estimated Parameters with 95% Confidence
Case 1

	kk_r^o md	λ	S_{gc}	S_{wc}
I.G. # 1	[6.937,7.053]	[1.984,2.099]	-	-
I.G. # 2	[6.932,7.048]	[2.007,2.124]	-	-
I.G. # 3	[6.932,7.048]	[2.007,2.124]	-	-
I.G. # 4	[6.932,7.048]	[2.007,2.124]	-	-
I.G. # 5	[6.932,7.048]	[2.007,2.124]	-	-
I.G. # 6	[6.838,6.955]	[3.128,3.246]	-	-
I.G. # 7	[6.940,7.057]	[1.949,2.066]	$[0,5.8 \times 10^{-2}]$	-
I.G. # 8	[6.931,7.048]	[2.007,2.124]	$[0,5.8 \times 10^{-2}]$	-
I.G. # 9	[6.929,7.051]	[2.120,2.242]	$[0,6.1 \times 10^{-2}]$	[0.2138,0.3359]
I.G. # 10	[6.930,7.050]	[2.089,2.209]	$[0,6.0 \times 10^{-2}]$	[0.1999,0.3198]
I.G. # 11	[6.932,7.053]	[2.082,2.203]	$[0,6.0 \times 10^{-2}]$	[0.2172,0.3378]
I.G. # 12	[6.802,6.981]	[2.143,2.323]	$[0,9.0 \times 10^{-2}]$	[0.0913,0.2718]
I.G. # 13	[6.936,7.079]	[1.656,1.799]	$[0,7.1 \times 10^{-2}]$	[0.0000,0.1339]

Rock and Fluid Properties for Tables F-12 and F-13

$r_w = 0.328$ ft ; $r_e = 6600$ ft

$h = 15.547$ ft ; $\phi = 0.3$

$k = 10$ md

$q_{o1} = 50$ STB/DAY for $t_1 = 0.5$ days

$q_{o2} = 100$ STB/DAY for $t_2 = 1.0$ days

$s = 5.0$; $S_{gc} = 0.0$

$S_{wc} = S_{iw} = 0.3$; $S_{or} = 0.0$

$C_D = 0.0$ $(\beta^* \rightarrow \infty)$

PVT Data are given by Set 2 (Table A-3)

Relative Permeability Data are given by Set 1 (Table A-2)

$p_i = p_{bi} = 4201.6$ psi

$c_{ti} = 0.25616 \times 10^{-4}$ psi^{-1}

$\mu_{oi} = 0.391$ cp

$B_{oi} = 1.516$ RB/STB

Table F-12

Simulated and Computed kk_{ro} Values
Drawdown Test
Case 3

t days	p_{wf} psi	Sim. So	Sim. kk_{ro} md	Comp. kk_{ro} md
0.20000E+00	0.37174E+04	0.63168E+00	0.46423E+01	0.48633E+01
0.22500E+00	0.37139E+04	0.63153E+00	0.46379E+01	0.48451E+01
0.25000E+00	0.37107E+04	0.63139E+00	0.46337E+01	0.47949E+01
0.27500E+00	0.37078E+04	0.63126E+00	0.46299E+01	0.47534E+01
0.30000E+00	0.37051E+04	0.63113E+00	0.46260E+01	0.46078E+01
0.32500E+00	0.37026E+04	0.63099E+00	0.46219E+01	0.46057E+01
0.35000E+00	0.37003E+04	0.63087E+00	0.46184E+01	0.46108E+01
0.37500E+00	0.36981E+04	0.63076E+00	0.46151E+01	0.46128E+01
0.40000E+00	0.36961E+04	0.63065E+00	0.46119E+01	0.47195E+01
0.42500E+00	0.36942E+04	0.63055E+00	0.46089E+01	0.46871E+01
0.45000E+00	0.36924E+04	0.63046E+00	0.46063E+01	0.46181E+01
0.47500E+00	0.36907E+04	0.63037E+00	0.46036E+01	0.45725E+01
0.49500E+00	0.36894E+04	0.63030E+00	0.46016E+01	0.45947E+01
0.75000E+00	0.30230E+04	0.61008E+00	0.40404E+01	0.41980E+01
0.80000E+00	0.30132E+04	0.60986E+00	0.40346E+01	0.41820E+01
0.85000E+00	0.30046E+04	0.60967E+00	0.40296E+01	0.40677E+01
0.90000E+00	0.29968E+04	0.60949E+00	0.40248E+01	0.40539E+01
0.95000E+00	0.29898E+04	0.60933E+00	0.40206E+01	0.40510E+01
0.10000E+01	0.29833E+04	0.60917E+00	0.40163E+01	0.40798E+01
0.10500E+01	0.29774E+04	0.60904E+00	0.40129E+01	0.40358E+01
0.11000E+01	0.29718E+04	0.60890E+00	0.40092E+01	0.39823E+01
0.11500E+01	0.29666E+04	0.60878E+00	0.40060E+01	0.39851E+01
0.12000E+01	0.29617E+04	0.60867E+00	0.40031E+01	0.40260E+01
0.12500E+01	0.29571E+04	0.60856E+00	0.40002E+01	0.39476E+01
0.13000E+01	0.29527E+04	0.60845E+00	0.39973E+01	0.39817E+01
0.13500E+01	0.29486E+04	0.60836E+00	0.39949E+01	0.39951E+01
0.14000E+01	0.29447E+04	0.60827E+00	0.39925E+01	0.39541E+01
0.14500E+01	0.29408E+04	0.60817E+00	0.39899E+01	0.39290E+01
0.14900E+01	0.29379E+04	0.60810E+00	0.39880E+01	0.39805E+01

Table F-13

Simulated and Computed kk_{rg} Values
Drawdown Test
Case 3

p_{wf} psi	Sim. kk_{rg} md	Comp. kk_{rg} md
0.37174E+04	0.12423E-01	0.13780E-01
0.37139E+04	0.12501E-01	0.13864E-01
0.37107E+04	0.12574E-01	0.12515E-01
0.37078E+04	0.12642E-01	0.12517E-01
0.37051E+04	0.12710E-01	0.12233E-01
0.37026E+04	0.12783E-01	0.12320E-01
0.37003E+04	0.12846E-01	0.12418E-01
0.36981E+04	0.12903E-01	0.12497E-01
0.36961E+04	0.12961E-01	0.12856E-01
0.36942E+04	0.13013E-01	0.12832E-01
0.36924E+04	0.13060E-01	0.12704E-01
0.36907E+04	0.13107E-01	0.12635E-01
0.36894E+04	0.13143E-01	0.12741E-01
0.30230E+04	0.28010E-01	0.28296E-01
0.30132E+04	0.28209E-01	0.28438E-01
0.30046E+04	0.28382E-01	0.27874E-01
0.29968E+04	0.28545E-01	0.27972E-01
0.29898E+04	0.28690E-01	0.28125E-01
0.29833E+04	0.28836E-01	0.28486E-01
0.29774E+04	0.28954E-01	0.28323E-01
0.29718E+04	0.29081E-01	0.28083E-01
0.29666E+04	0.29190E-01	0.28229E-01
0.29617E+04	0.29289E-01	0.28637E-01
0.29571E+04	0.29389E-01	0.28189E-01
0.29527E+04	0.29489E-01	0.28538E-01
0.29486E+04	0.29571E-01	0.28734E-01
0.29447E+04	0.29652E-01	0.28533E-01
0.29408E+04	0.29743E-01	0.28443E-01
0.29379E+04	0.29807E-01	0.28885E-01

Rock and Fluid Properties for Tables F-14 through F-20

$r_w = 0.328$ ft ; $r_e = 6600$ ft

$h = 15.547$ ft ; $\phi = 0.3$

$k = 10$ md

$q_o = 150$ STB/DAY

$s = 0.0$; $S_{gc} = 0.0$

$S_{wc} = S_{iw} = 0.3$; $S_{or} = 0.0$

$C_D = 0.0$ $(\beta^* \rightarrow \infty)$

PVT Data are given by Set 1 (Table A-3)

Relative Permeability Data are given by Set 1 (Table A-2)

$p_i = 4700$ psi ; $p_{bi} = 4201.6$ psi

$c_{ti} = 0.27299 \times 10^{-4}$ psi^{-1}

$\mu_{oi} = 0.40147$ cp

$B_{oi} = 1.50803$ RB/STB

Table F-14

Simulated and Computed kk_{ro} Values
Drawdown Test
Case 1

t days	p_{wf} psi	Sim. So	Sim. kk_{ro} md	Comp. kk_{ro} md
0.10000E-05	0.46449E+04	0.69996E+00	0.69984E+01	0.13517E+02
0.20000E-05	0.46238E+04	0.69994E+00	0.69976E+01	0.12794E+02
0.30000E-05	0.46096E+04	0.69993E+00	0.69972E+01	0.11346E+02
0.40000E-05	0.45987E+04	0.69992E+00	0.69968E+01	0.10649E+02
0.50000E-05	0.45899E+04	0.69991E+00	0.69964E+01	0.10212E+02
0.60000E-05	0.45824E+04	0.69990E+00	0.69960E+01	0.98630E+01
0.70000E-05	0.45759E+04	0.69990E+00	0.69960E+01	0.95957E+01
0.80000E-05	0.45701E+04	0.69989E+00	0.69956E+01	0.93711E+01
0.90000E-05	0.45649E+04	0.69989E+00	0.69956E+01	0.92431E+01
0.10000E-04	0.45602E+04	0.69988E+00	0.69953E+01	0.89504E+01
0.15000E-04	0.45415E+04	0.69987E+00	0.69949E+01	0.87106E+01
0.20000E-04	0.45276E+04	0.69986E+00	0.69945E+01	0.83327E+01
0.25000E-04	0.45164E+04	0.69985E+00	0.69941E+01	0.81340E+01
0.30000E-04	0.45072E+04	0.69984E+00	0.69937E+01	0.80027E+01
0.35000E-04	0.44992E+04	0.69983E+00	0.69933E+01	0.78957E+01
0.40000E-04	0.44923E+04	0.69982E+00	0.69929E+01	0.78431E+01
0.45000E-04	0.44861E+04	0.69982E+00	0.69929E+01	0.77291E+01
0.50000E-04	0.44805E+04	0.69981E+00	0.69925E+01	0.76634E+01
0.55000E-04	0.44754E+04	0.69981E+00	0.69925E+01	0.76005E+01
0.60000E-04	0.44707E+04	0.69980E+00	0.69921E+01	0.75815E+01
0.65000E-04	0.44664E+04	0.69980E+00	0.69921E+01	0.75846E+01
0.70000E-04	0.44624E+04	0.69980E+00	0.69921E+01	0.75882E+01
0.75000E-04	0.44587E+04	0.69979E+00	0.69917E+01	0.75713E+01
0.80000E-04	0.44552E+04	0.69979E+00	0.69917E+01	0.75132E+01
0.85000E-04	0.44519E+04	0.69979E+00	0.69917E+01	0.73955E+01
0.90000E-04	0.44487E+04	0.69978E+00	0.69913E+01	0.74407E+01
0.95000E-04	0.44458E+04	0.69978E+00	0.69913E+01	0.75420E+01
0.10000E-03	0.44430E+04	0.69978E+00	0.69913E+01	0.73947E+01
0.15000E-03	0.44206E+04	0.69976E+00	0.69905E+01	0.73572E+01
0.20000E-03	0.44046E+04	0.69974E+00	0.69897E+01	0.73005E+01
0.25000E-03	0.43921E+04	0.69973E+00	0.69893E+01	0.72395E+01
0.30000E-03	0.43818E+04	0.69972E+00	0.69889E+01	0.72061E+01
0.35000E-03	0.43731E+04	0.69972E+00	0.69889E+01	0.71790E+01
0.40000E-03	0.43655E+04	0.69971E+00	0.69885E+01	0.70967E+01
0.45000E-03	0.43587E+04	0.69970E+00	0.69881E+01	0.70868E+01
0.50000E-03	0.43527E+04	0.69970E+00	0.69881E+01	0.70917E+01
0.55000E-03	0.43472E+04	0.69969E+00	0.69877E+01	0.71230E+01
0.60000E-03	0.43423E+04	0.69969E+00	0.69877E+01	0.71434E+01
0.65000E-03	0.43377E+04	0.69968E+00	0.69873E+01	0.70346E+01
0.70000E-03	0.43334E+04	0.69968E+00	0.69873E+01	0.70865E+01
0.75000E-03	0.43295E+04	0.69968E+00	0.69873E+01	0.70408E+01
0.80000E-03	0.43257E+04	0.69967E+00	0.69869E+01	0.70568E+01

Table F-14 (Cont'd)

t days	p_{wf} psi	Sim. So	Sim. kk_{ro} md	Comp. kk_{ro} md
0.85000E-03	0.43223E+04	0.69967E+00	0.69869E+01	0.71352E+01
0.90000E-03	0.43190E+04	0.69967E+00	0.69869E+01	0.70528E+01
0.95000E-03	0.43159E+04	0.69966E+00	0.69865E+01	0.70085E+01
0.10000E-02	0.43129E+04	0.69966E+00	0.69865E+01	0.70731E+01
0.15000E-02	0.42897E+04	0.69964E+00	0.69858E+01	0.70766E+01
0.20000E-02	0.42732E+04	0.69963E+00	0.69854E+01	0.70614E+01
0.25000E-02	0.42604E+04	0.69961E+00	0.69846E+01	0.70444E+01
0.30000E-02	0.42499E+04	0.69961E+00	0.69846E+01	0.70177E+01
0.35000E-02	0.42410E+04	0.69960E+00	0.69842E+01	0.70095E+01
0.40000E-02	0.42333E+04	0.69959E+00	0.69838E+01	0.70079E+01
0.45000E-02	0.42265E+04	0.69958E+00	0.69834E+01	0.69921E+01
0.50000E-02	0.42204E+04	0.69958E+00	0.69834E+01	0.69908E+01
0.55000E-02	0.42149E+04	0.69957E+00	0.69830E+01	0.70153E+01
0.60000E-02	0.42099E+04	0.69957E+00	0.69830E+01	0.69564E+01
0.65000E-02	0.42052E+04	0.69956E+00	0.69826E+01	0.69170E+01
0.70000E-02	0.42009E+04	0.69956E+00	0.69826E+01	0.70474E+01
0.75000E-02	0.41970E+04	0.69956E+00	0.69826E+01	0.70078E+01
0.80000E-02	0.41932E+04	0.69955E+00	0.69822E+01	0.69331E+01
0.85000E-02	0.41897E+04	0.69955E+00	0.69822E+01	0.71129E+01
0.90000E-02	0.41865E+04	0.69897E+00	0.69592E+01	0.72625E+01
0.95000E-02	0.41835E+04	0.69803E+00	0.69220E+01	0.72331E+01
0.10000E-01	0.41806E+04	0.69676E+00	0.68718E+01	0.67554E+01
0.15000E-01	0.41561E+04	0.67536E+00	0.60654E+01	0.64545E+01
0.20000E-01	0.41369E+04	0.66728E+00	0.57806E+01	0.59583E+01
0.25000E-01	0.41211E+04	0.66219E+00	0.56063E+01	0.57427E+01
0.30000E-01	0.41080E+04	0.65925E+00	0.55071E+01	0.56107E+01
0.35000E-01	0.40965E+04	0.65691E+00	0.54296E+01	0.54991E+01
0.40000E-01	0.40865E+04	0.65492E+00	0.53637E+01	0.54449E+01
0.45000E-01	0.40775E+04	0.65352E+00	0.53183E+01	0.53483E+01
0.50000E-01	0.40693E+04	0.65223E+00	0.52765E+01	0.52762E+01
0.55000E-01	0.40618E+04	0.65095E+00	0.52350E+01	0.53065E+01
0.60000E-01	0.40551E+04	0.65001E+00	0.52046E+01	0.53167E+01
0.65000E-01	0.40488E+04	0.64919E+00	0.51786E+01	0.52330E+01
0.70000E-01	0.40429E+04	0.64851E+00	0.51571E+01	0.51584E+01
0.75000E-01	0.40373E+04	0.64780E+00	0.51346E+01	0.51300E+01
0.80000E-01	0.40321E+04	0.64707E+00	0.51115E+01	0.51460E+01
0.85000E-01	0.40272E+04	0.64649E+00	0.50931E+01	0.51524E+01
0.90000E-01	0.40226E+04	0.64600E+00	0.50776E+01	0.51396E+01
0.95000E-01	0.40182E+04	0.64552E+00	0.50624E+01	0.51585E+01
0.10000E+00	0.40141E+04	0.64506E+00	0.50479E+01	0.50722E+01
0.15000E+00	0.39807E+04	0.64173E+00	0.49448E+01	0.50285E+01
0.20000E+00	0.39564E+04	0.63946E+00	0.48750E+01	0.49452E+01
0.25000E+00	0.39373E+04	0.63787E+00	0.48270E+01	0.49236E+01

Table F-14 (Cont'd)

t days	p_{wf} psi	Sim. So	Sim. kk_{ro} md	Comp. kk_{ro} md
0.30000E+00	0.39217E+04	0.63675E+00	0.47931E+01	0.48501E+01
0.35000E+00	0.39080E+04	0.63566E+00	0.47602E+01	0.47933E+01
0.40000E+00	0.38963E+04	0.63478E+00	0.47338E+01	0.47992E+01
0.45000E+00	0.38858E+04	0.63409E+00	0.47134E+01	0.47372E+01
0.50000E+00	0.38763E+04	0.63348E+00	0.46954E+01	0.46880E+01
0.55000E+00	0.38676E+04	0.63288E+00	0.46777E+01	0.47041E+01
0.60000E+00	0.38598E+04	0.63242E+00	0.46641E+01	0.47465E+01
0.65000E+00	0.38526E+04	0.63200E+00	0.46517E+01	0.46976E+01
0.70000E+00	0.38458E+04	0.63160E+00	0.46399E+01	0.46297E+01
0.75000E+00	0.38394E+04	0.63119E+00	0.46278E+01	0.45662E+01
0.80000E+00	0.38333E+04	0.63078E+00	0.46157E+01	0.46161E+01
0.85000E+00	0.38278E+04	0.63046E+00	0.46063E+01	0.47130E+01
0.90000E+00	0.38226E+04	0.63017E+00	0.45977E+01	0.47184E+01
0.95000E+00	0.38177E+04	0.62990E+00	0.45898E+01	0.46571E+01
0.10000E+01	0.38129E+04	0.62963E+00	0.45820E+01	0.45816E+01
0.12500E+01	0.37920E+04	0.62846E+00	0.45483E+01	0.46035E+01
0.15000E+01	0.37750E+04	0.62765E+00	0.45250E+01	0.45637E+01
0.17500E+01	0.37602E+04	0.62686E+00	0.45022E+01	0.45543E+01
0.20000E+01	0.37477E+04	0.62629E+00	0.44858E+01	0.45714E+01
0.22500E+01	0.37364E+04	0.62576E+00	0.44705E+01	0.44586E+01
0.25000E+01	0.37260E+04	0.62521E+00	0.44547E+01	0.44682E+01
0.27500E+01	0.37169E+04	0.62478E+00	0.44424E+01	0.45291E+01

Table F-15

Simulated and Computed kk_{ro} Values
Buildup Test
Case 1

Δt days	p_{ws} psi	DD Sim. So	Sim. kk_{ro} md	Comp. kk_{ro} md
0.200000E-05	0.376944E+04	0.627353E+00	0.451644E+01	0.139901E+02
0.300000E-05	0.378195E+04	0.627981E+00	0.453453E+01	0.131808E+02
0.400000E-05	0.379210E+04	0.628466E+00	0.454849E+01	0.117105E+02
0.500000E-05	0.380072E+04	0.628948E+00	0.456239E+01	0.107835E+02
0.600000E-05	0.380826E+04	0.629370E+00	0.457455E+01	0.101231E+02
0.700000E-05	0.381499E+04	0.629748E+00	0.458543E+01	0.961754E+01
0.800000E-05	0.382109E+04	0.630087E+00	0.459526E+01	0.922103E+01
0.900000E-05	0.382667E+04	0.630397E+00	0.460441E+01	0.888870E+01
0.100000E-04	0.383184E+04	0.630695E+00	0.461321E+01	0.827652E+01
0.150000E-04	0.385308E+04	0.632028E+00	0.465255E+01	0.782898E+01
0.200000E-04	0.386961E+04	0.633019E+00	0.468178E+01	0.718922E+01
0.250000E-04	0.388332E+04	0.633931E+00	0.470870E+01	0.677756E+01
0.300000E-04	0.389502E+04	0.634696E+00	0.473128E+01	0.650862E+01
0.350000E-04	0.390524E+04	0.635452E+00	0.475392E+01	0.630749E+01
0.400000E-04	0.391433E+04	0.636164E+00	0.477541E+01	0.614559E+01
0.450000E-04	0.392253E+04	0.636810E+00	0.479492E+01	0.601732E+01
0.500000E-04	0.392999E+04	0.637345E+00	0.481111E+01	0.590696E+01
0.550000E-04	0.393686E+04	0.637838E+00	0.482601E+01	0.581585E+01
0.600000E-04	0.394320E+04	0.638361E+00	0.484180E+01	0.574096E+01
0.650000E-04	0.394911E+04	0.638853E+00	0.485667E+01	0.566754E+01
0.700000E-04	0.395464E+04	0.639313E+00	0.487058E+01	0.560994E+01
0.750000E-04	0.395983E+04	0.639780E+00	0.488469E+01	0.555725E+01
0.800000E-04	0.396473E+04	0.640238E+00	0.489869E+01	0.551096E+01
0.850000E-04	0.396936E+04	0.640671E+00	0.491206E+01	0.547535E+01
0.900000E-04	0.397375E+04	0.641081E+00	0.492475E+01	0.543835E+01
0.950000E-04	0.397793E+04	0.641471E+00	0.493683E+01	0.540033E+01
0.100000E-03	0.398192E+04	0.641852E+00	0.494859E+01	0.532015E+01
0.150000E-03	0.401386E+04	0.645036E+00	0.504711E+01	0.524142E+01
0.200000E-03	0.403699E+04	0.647756E+00	0.513323E+01	0.512686E+01
0.250000E-03	0.405520E+04	0.650024E+00	0.520504E+01	0.506003E+01
0.300000E-03	0.407014E+04	0.652362E+00	0.528079E+01	0.502758E+01
0.350000E-03	0.408282E+04	0.654348E+00	0.534511E+01	0.499498E+01
0.400000E-03	0.409386E+04	0.656385E+00	0.541215E+01	0.497426E+01
0.450000E-03	0.410359E+04	0.658353E+00	0.547738E+01	0.498025E+01
0.500000E-03	0.411225E+04	0.660204E+00	0.553890E+01	0.499057E+01
0.550000E-03	0.412007E+04	0.661959E+00	0.559841E+01	0.500177E+01
0.600000E-03	0.412717E+04	0.664145E+00	0.567256E+01	0.501805E+01
0.650000E-03	0.413368E+04	0.666243E+00	0.574464E+01	0.502404E+01
0.700000E-03	0.413970E+04	0.668458E+00	0.582149E+01	0.503267E+01
0.750000E-03	0.414528E+04	0.670807E+00	0.590357E+01	0.503453E+01
0.800000E-03	0.415051E+04	0.673008E+00	0.598164E+01	0.503627E+01
0.850000E-03	0.415540E+04	0.675065E+00	0.605468E+01	0.504968E+01
0.900000E-03	0.416000E+04	0.678767E+00	0.618891E+01	0.505225E+01

Table F-15 (Cont'd)

Δt days	p_{ws} psi	DD Sim. So	Sim. kk_{ro} md	Comp. kk_{ro} md
0.950000E-03	0.416435E+04	0.682566E+00	0.632878E+01	0.504729E+01
0.100000E-02	0.416848E+04	0.686174E+00	0.646348E+01	0.499744E+01
0.150000E-02	0.420145E+04	0.699560E+00	0.698259E+01	0.501708E+01
0.200000E-02	0.422424E+04	0.699580E+00	0.698338E+01	0.497177E+01
0.250000E-02	0.424295E+04	0.699602E+00	0.698426E+01	0.478751E+01
0.300000E-02	0.425847E+04	0.699610E+00	0.698457E+01	0.474405E+01
0.350000E-02	0.427163E+04	0.699628E+00	0.698526E+01	0.475977E+01
0.400000E-02	0.428292E+04	0.699636E+00	0.698559E+01	0.482204E+01
0.450000E-02	0.429272E+04	0.699643E+00	0.698586E+01	0.489540E+01
0.500000E-02	0.430137E+04	0.699650E+00	0.698615E+01	0.497797E+01
0.550000E-02	0.430904E+04	0.699657E+00	0.698641E+01	0.506336E+01
0.600000E-02	0.431595E+04	0.699660E+00	0.698655E+01	0.512893E+01
0.650000E-02	0.432223E+04	0.699670E+00	0.698694E+01	0.519830E+01
0.700000E-02	0.432796E+04	0.699676E+00	0.698718E+01	0.527397E+01
0.750000E-02	0.433322E+04	0.699680E+00	0.698734E+01	0.534996E+01
0.800000E-02	0.433807E+04	0.699681E+00	0.698737E+01	0.541673E+01
0.850000E-02	0.434258E+04	0.699690E+00	0.698773E+01	0.547160E+01
0.900000E-02	0.434679E+04	0.699690E+00	0.698773E+01	0.552842E+01
0.950000E-02	0.435073E+04	0.699696E+00	0.698799E+01	0.558649E+01
0.100000E-01	0.435443E+04	0.699700E+00	0.698813E+01	0.584209E+01
0.150000E-01	0.438238E+04	0.699721E+00	0.698894E+01	0.597760E+01
0.200000E-01	0.440139E+04	0.699737E+00	0.698961E+01	0.621054E+01
0.250000E-01	0.441566E+04	0.699754E+00	0.699026E+01	0.639657E+01
0.300000E-01	0.442701E+04	0.699766E+00	0.699073E+01	0.653358E+01
0.350000E-01	0.443645E+04	0.699774E+00	0.699106E+01	0.660913E+01
0.400000E-01	0.444456E+04	0.699780E+00	0.699129E+01	0.664441E+01
0.450000E-01	0.445168E+04	0.699789E+00	0.699166E+01	0.667137E+01
0.500000E-01	0.445801E+04	0.699790E+00	0.699169E+01	0.670958E+01
0.550000E-01	0.446369E+04	0.699800E+00	0.699209E+01	0.674457E+01
0.600000E-01	0.446885E+04	0.699800E+00	0.699209E+01	0.677062E+01
0.650000E-01	0.447357E+04	0.699806E+00	0.699233E+01	0.678835E+01
0.700000E-01	0.447793E+04	0.699810E+00	0.699248E+01	0.680203E+01
0.750000E-01	0.448197E+04	0.699813E+00	0.699258E+01	0.682544E+01
0.800000E-01	0.448573E+04	0.699819E+00	0.699285E+01	0.684462E+01
0.850000E-01	0.448925E+04	0.699820E+00	0.699288E+01	0.685529E+01
0.900000E-01	0.449256E+04	0.699820E+00	0.699289E+01	0.686617E+01
0.950000E-01	0.449568E+04	0.699825E+00	0.699307E+01	0.686830E+01
0.100000E+00	0.449864E+04	0.699829E+00	0.699324E+01	0.687715E+01
0.110000E+00	0.450411E+04	0.699836E+00	0.699352E+01	0.690449E+01
0.120000E+00	0.450906E+04	0.699842E+00	0.699375E+01	0.692540E+01
0.130000E+00	0.451360E+04	0.699847E+00	0.699394E+01	0.692589E+01
0.140000E+00	0.451779E+04	0.699851E+00	0.699411E+01	0.692571E+01
0.150000E+00	0.452168E+04	0.699855E+00	0.699425E+01	0.692288E+01

Table F-15 (Cont'd)

Δt days	p_{ws} psi	DD Sim. So	Sim. kk_{ro} md	Comp. kk_{ro} md
0.160000E+00	0.452531E+04	0.699858E+00	0.699438E+01	0.693025E+01
0.170000E+00	0.452870E+04	0.699861E+00	0.699449E+01	0.694728E+01
0.180000E+00	0.453188E+04	0.699863E+00	0.699458E+01	0.695349E+01
0.190000E+00	0.453488E+04	0.699865E+00	0.699467E+01	0.696123E+01
0.200000E+00	0.453771E+04	0.699867E+00	0.699475E+01	0.696291E+01
0.210000E+00	0.454040E+04	0.699869E+00	0.699482E+01	0.696416E+01
0.220000E+00	0.454295E+04	0.699871E+00	0.699489E+01	0.697321E+01
0.230000E+00	0.454538E+04	0.699872E+00	0.699494E+01	0.697164E+01
0.240000E+00	0.454770E+04	0.699873E+00	0.699499E+01	0.698431E+01
0.250000E+00	0.454991E+04	0.699874E+00	0.699503E+01	0.697726E+01
0.260000E+00	0.455204E+04	0.699876E+00	0.699508E+01	0.697805E+01
0.270000E+00	0.455407E+04	0.699877E+00	0.699512E+01	0.698482E+01
0.280000E+00	0.455603E+04	0.699878E+00	0.699516E+01	0.697746E+01
0.290000E+00	0.455791E+04	0.699879E+00	0.699520E+01	0.698975E+01
0.300000E+00	0.455972E+04	0.699880E+00	0.699524E+01	0.698261E+01
0.310000E+00	0.456147E+04	0.699883E+00	0.699536E+01	0.699263E+01
0.320000E+00	0.456315E+04	0.699886E+00	0.699550E+01	0.699889E+01
0.330000E+00	0.456478E+04	0.699890E+00	0.699564E+01	0.697755E+01
0.340000E+00	0.456636E+04	0.699890E+00	0.699565E+01	0.699198E+01
0.350000E+00	0.456788E+04	0.699890E+00	0.699565E+01	0.699799E+01
0.360000E+00	0.456936E+04	0.699890E+00	0.699565E+01	0.699347E+01
0.370000E+00	0.457079E+04	0.699891E+00	0.699569E+01	0.700110E+01
0.380000E+00	0.457218E+04	0.699894E+00	0.699579E+01	0.699546E+01
0.390000E+00	0.457353E+04	0.699896E+00	0.699588E+01	0.700068E+01
0.400000E+00	0.457484E+04	0.699898E+00	0.699597E+01	0.701692E+01
0.410000E+00	0.457611E+04	0.699900E+00	0.699604E+01	0.701636E+01
0.420000E+00	0.457735E+04	0.699900E+00	0.699604E+01	0.699681E+01
0.430000E+00	0.457856E+04	0.699900E+00	0.699604E+01	0.701488E+01
0.440000E+00	0.457973E+04	0.699900E+00	0.699604E+01	0.701259E+01
0.450000E+00	0.458088E+04	0.699900E+00	0.699604E+01	0.698775E+01
0.460000E+00	0.458200E+04	0.699900E+00	0.699604E+01	0.700142E+01
0.470000E+00	0.458309E+04	0.699901E+00	0.699608E+01	0.702365E+01
0.480000E+00	0.458415E+04	0.699902E+00	0.699613E+01	0.702111E+01
0.490000E+00	0.458519E+04	0.699904E+00	0.699619E+01	0.699154E+01
0.500000E+00	0.458621E+04	0.699905E+00	0.699624E+01	0.700234E+01
0.510000E+00	0.458720E+04	0.699906E+00	0.699630E+01	0.702037E+01
0.520000E+00	0.458817E+04	0.699908E+00	0.699635E+01	0.700909E+01
0.530000E+00	0.458912E+04	0.699909E+00	0.699640E+01	0.704096E+01
0.540000E+00	0.459004E+04	0.699910E+00	0.699644E+01	0.704191E+01
0.550000E+00	0.459095E+04	0.699911E+00	0.699649E+01	0.700954E+01
0.560000E+00	0.459184E+04	0.699912E+00	0.699653E+01	0.702129E+01
0.570000E+00	0.459271E+04	0.699913E+00	0.699656E+01	0.699830E+01
0.580000E+00	0.459357E+04	0.699914E+00	0.699660E+01	0.702098E+01

Table F-15 (Cont'd)

Δt days	p_{ws} psi	DD Sim. So	Sim. kk_{ro} md	Comp. kk_{ro} md
0.590000E+00	0.459440E+04	0.699915E+00	0.699664E+01	0.704983E+01
0.600000E+00	0.459522E+04	0.699916E+00	0.699668E+01	0.699812E+01
0.610000E+00	0.459603E+04	0.699917E+00	0.699671E+01	0.699325E+01
0.620000E+00	0.459682E+04	0.699918E+00	0.699675E+01	0.703759E+01
0.630000E+00	0.459759E+04	0.699919E+00	0.699678E+01	0.704244E+01
0.640000E+00	0.459835E+04	0.699920E+00	0.699682E+01	0.700513E+01
0.650000E+00	0.459910E+04	0.699920E+00	0.699685E+01	0.701809E+01
0.660000E+00	0.459983E+04	0.699921E+00	0.699688E+01	0.703568E+01
0.670000E+00	0.460055E+04	0.699922E+00	0.699690E+01	0.705800E+01
0.680000E+00	0.460125E+04	0.699922E+00	0.699693E+01	0.703458E+01
0.690000E+00	0.460195E+04	0.699923E+00	0.699695E+01	0.701423E+01
0.700000E+00	0.460263E+04	0.699924E+00	0.699698E+01	0.704875E+01
0.710000E+00	0.460330E+04	0.699924E+00	0.699700E+01	0.703515E+01
0.720000E+00	0.460396E+04	0.699925E+00	0.699703E+01	0.702460E+01
0.730000E+00	0.460461E+04	0.699925E+00	0.699705E+01	0.701710E+01
0.740000E+00	0.460525E+04	0.699926E+00	0.699707E+01	0.701267E+01
0.750000E+00	0.460588E+04	0.699927E+00	0.699709E+01	0.701130E+01
0.760000E+00	0.460650E+04	0.699927E+00	0.699712E+01	0.701302E+01
0.770000E+00	0.460711E+04	0.699928E+00	0.699714E+01	0.701785E+01
0.780000E+00	0.460771E+04	0.699928E+00	0.699716E+01	0.702585E+01
0.790000E+00	0.460830E+04	0.699929E+00	0.699718E+01	0.703704E+01
0.800000E+00	0.460888E+04	0.699929E+00	0.699720E+01	0.705149E+01
0.810000E+00	0.460945E+04	0.699930E+00	0.699722E+01	0.706925E+01
0.820000E+00	0.461001E+04	0.699930E+00	0.699724E+01	0.702710E+01
0.830000E+00	0.461057E+04	0.699931E+00	0.699726E+01	0.698685E+01
0.840000E+00	0.461112E+04	0.699931E+00	0.699727E+01	0.701219E+01
0.850000E+00	0.461166E+04	0.699931E+00	0.699729E+01	0.704103E+01
0.860000E+00	0.461219E+04	0.699932E+00	0.699730E+01	0.707349E+01
0.870000E+00	0.461271E+04	0.699932E+00	0.699732E+01	0.704132E+01
0.880000E+00	0.461323E+04	0.699933E+00	0.699733E+01	0.701092E+01
0.890000E+00	0.461374E+04	0.699933E+00	0.699735E+01	0.705139E+01
0.900000E+00	0.461424E+04	0.699933E+00	0.699736E+01	0.702485E+01
0.910000E+00	0.461474E+04	0.699934E+00	0.699737E+01	0.700002E+01
0.920000E+00	0.461523E+04	0.699934E+00	0.699739E+01	0.704881E+01
0.930000E+00	0.461571E+04	0.699934E+00	0.699740E+01	0.702786E+01
0.940000E+00	0.461619E+04	0.699935E+00	0.699741E+01	0.700859E+01
0.950000E+00	0.461666E+04	0.699935E+00	0.699743E+01	0.706615E+01
0.960000E+00	0.461712E+04	0.699935E+00	0.699744E+01	0.705083E+01
0.970000E+00	0.461758E+04	0.699936E+00	0.699745E+01	0.703718E+01
0.980000E+00	0.461803E+04	0.699936E+00	0.699746E+01	0.702519E+01
0.990000E+00	0.461848E+04	0.699936E+00	0.699748E+01	0.701487E+01
0.100000E+01	0.461892E+04	0.699937E+00	0.699749E+01	0.703299E+01
0.102500E+01	0.462000E+04	0.699937E+00	0.699752E+01	0.701795E+01

Table F-15 (Cont'd)

Δt days	p_{ws} psi	DD Sim. So	Sim. kk_{ro} md	Comp. kk_{ro} md
0.105000E+01	0.462105E+04	0.699938E+00	0.699755E+01	0.704016E+01
0.107500E+01	0.462206E+04	0.699939E+00	0.699758E+01	0.707488E+01
0.110000E+01	0.462304E+04	0.699939E+00	0.699760E+01	0.704926E+01
0.112500E+01	0.462400E+04	0.699940E+00	0.699763E+01	0.703229E+01
0.115000E+01	0.462493E+04	0.699941E+00	0.699767E+01	0.702401E+01
0.117500E+01	0.462584E+04	0.699942E+00	0.699770E+01	0.702448E+01
0.120000E+01	0.462672E+04	0.699943E+00	0.699774E+01	0.707453E+01
0.122500E+01	0.462757E+04	0.699944E+00	0.699777E+01	0.705241E+01
0.125000E+01	0.462841E+04	0.699944E+00	0.699780E+01	0.703747E+01
0.127500E+01	0.462922E+04	0.699945E+00	0.699783E+01	0.707367E+01
0.130000E+01	0.463001E+04	0.699946E+00	0.699786E+01	0.702929E+01
0.132500E+01	0.463079E+04	0.699947E+00	0.699789E+01	0.703625E+01
0.135000E+01	0.463154E+04	0.699947E+00	0.699792E+01	0.705077E+01
0.137500E+01	0.463228E+04	0.699948E+00	0.699794E+01	0.702463E+01
0.140000E+01	0.463300E+04	0.699949E+00	0.699797E+01	0.705341E+01
0.142500E+01	0.463370E+04	0.699949E+00	0.699800E+01	0.703941E+01
0.145000E+01	0.463439E+04	0.699950E+00	0.699802E+01	0.703109E+01
0.147500E+01	0.463506E+04	0.699951E+00	0.699805E+01	0.708176E+01
0.150000E+01	0.463571E+04	0.699951E+00	0.699807E+01	0.710988E+01
0.152500E+01	0.463635E+04	0.699952E+00	0.699810E+01	0.704090E+01
0.155000E+01	0.463698E+04	0.699952E+00	0.699812E+01	0.699966E+01
0.157500E+01	0.463760E+04	0.699953E+00	0.699814E+01	0.701954E+01
0.160000E+01	0.463820E+04	0.699954E+00	0.699817E+01	0.704571E+01
0.162500E+01	0.463879E+04	0.699954E+00	0.699819E+01	0.707841E+01
0.165000E+01	0.463936E+04	0.699955E+00	0.699821E+01	0.705547E+01
0.167500E+01	0.463993E+04	0.699955E+00	0.699823E+01	0.703659E+01
0.170000E+01	0.464048E+04	0.699956E+00	0.699825E+01	0.708618E+01
0.172500E+01	0.464102E+04	0.699956E+00	0.699827E+01	0.701099E+01
0.175000E+01	0.464156E+04	0.699957E+00	0.699829E+01	0.700431E+01
0.177500E+01	0.464208E+04	0.699957E+00	0.699831E+01	0.706972E+01
0.180000E+01	0.464259E+04	0.699958E+00	0.699833E+01	0.707269E+01
0.182500E+01	0.464309E+04	0.699958E+00	0.699835E+01	0.707998E+01
0.185000E+01	0.464358E+04	0.699959E+00	0.699837E+01	0.701934E+01
0.187500E+01	0.464407E+04	0.699959E+00	0.699839E+01	0.703390E+01
0.190000E+01	0.464454E+04	0.699960E+00	0.699840E+01	0.705300E+01
0.192500E+01	0.464501E+04	0.699960E+00	0.699842E+01	0.700066E+01
0.195000E+01	0.464547E+04	0.699960E+00	0.699843E+01	0.702725E+01
0.197500E+01	0.464592E+04	0.699961E+00	0.699845E+01	0.705868E+01
0.200000E+01	0.464636E+04	0.699961E+00	0.699846E+01	0.709515E+01
0.202500E+01	0.464679E+04	0.699961E+00	0.699847E+01	0.705389E+01
0.205000E+01	0.464722E+04	0.699962E+00	0.699848E+01	0.701505E+01
0.207500E+01	0.464764E+04	0.699962E+00	0.699850E+01	0.706269E+01
0.210000E+01	0.464805E+04	0.699962E+00	0.699851E+01	0.702919E+01

Table F-15 (Cont'd)

Δt days	p_{ws} psi	DD Sim. So	Sim. kk_{ro} md	Comp. kk_{ro} md
0.212500E+01	0.464846E+04	0.699963E+00	0.699852E+01	0.699806E+01
0.215000E+01	0.464886E+04	0.699963E+00	0.699853E+01	0.705748E+01
0.217500E+01	0.464925E+04	0.699963E+00	0.699854E+01	0.703177E+01
0.220000E+01	0.464964E+04	0.699963E+00	0.699855E+01	0.700839E+01
0.222500E+01	0.465002E+04	0.699964E+00	0.699856E+01	0.708050E+01
0.225000E+01	0.465039E+04	0.699964E+00	0.699857E+01	0.706276E+01
0.227500E+01	0.465076E+04	0.699964E+00	0.699859E+01	0.704737E+01
0.230000E+01	0.465112E+04	0.699965E+00	0.699860E+01	0.703435E+01
0.232500E+01	0.465148E+04	0.699965E+00	0.699861E+01	0.702369E+01
0.235000E+01	0.465183E+04	0.699965E+00	0.699862E+01	0.701540E+01
0.237500E+01	0.465218E+04	0.699965E+00	0.699863E+01	0.700949E+01
0.240000E+01	0.465252E+04	0.699966E+00	0.699864E+01	0.711056E+01
0.242500E+01	0.465285E+04	0.699966E+00	0.699865E+01	0.711105E+01
0.245000E+01	0.465318E+04	0.699966E+00	0.699865E+01	0.700629E+01
0.247500E+01	0.465351E+04	0.699966E+00	0.699866E+01	0.701015E+01
0.250000E+01	0.465383E+04	0.699966E+00	0.699867E+01	0.701654E+01
0.252500E+01	0.465415E+04	0.699967E+00	0.699868E+01	0.702549E+01
0.255000E+01	0.465446E+04	0.699967E+00	0.699869E+01	0.703706E+01
0.257500E+01	0.465477E+04	0.699967E+00	0.699870E+01	0.705130E+01
0.260000E+01	0.465507E+04	0.699967E+00	0.699871E+01	0.706828E+01
0.262500E+01	0.465537E+04	0.699968E+00	0.699872E+01	0.708807E+01
0.265000E+01	0.465566E+04	0.699968E+00	0.699873E+01	0.699021E+01
0.267500E+01	0.465596E+04	0.699968E+00	0.699873E+01	0.701332E+01
0.270000E+01	0.465624E+04	0.699968E+00	0.699874E+01	0.703936E+01
0.272500E+01	0.465653E+04	0.699968E+00	0.699875E+01	0.706840E+01
0.275000E+01	0.465680E+04	0.699969E+00	0.699876E+01	0.710056E+01
0.277500E+01	0.465708E+04	0.699969E+00	0.699877E+01	0.700621E+01
0.280000E+01	0.465735E+04	0.699969E+00	0.699877E+01	0.704183E+01
0.282500E+01	0.465762E+04	0.699969E+00	0.699878E+01	0.708076E+01
0.285000E+01	0.465788E+04	0.699969E+00	0.699879E+01	0.698872E+01
0.287500E+01	0.465815E+04	0.699970E+00	0.699880E+01	0.703121E+01
0.290000E+01	0.465840E+04	0.699970E+00	0.699880E+01	0.707722E+01
0.292500E+01	0.465866E+04	0.699970E+00	0.699881E+01	0.698720E+01
0.295000E+01	0.465891E+04	0.699970E+00	0.699882E+01	0.703692E+01
0.297500E+01	0.465916E+04	0.699970E+00	0.699883E+01	0.709047E+01

Table F-16

Simulated and Computed kk_{rg} Values
Drawdown Test
Case 1

p_{wf} psi	Sim. kk_{rg} md	Comp. kk_{rg} md
0.46449E+04	0.40670E-07	0.00000E+00
0.46238E+04	0.61006E-07	0.00000E+00
0.46096E+04	0.71173E-07	0.00000E+00
0.45987E+04	0.81341E-07	0.00000E+00
0.45899E+04	0.91508E-07	0.00000E+00
0.45824E+04	0.10168E-06	0.00000E+00
0.45759E+04	0.10168E-06	0.00000E+00
0.45701E+04	0.11184E-06	0.00000E+00
0.45649E+04	0.11184E-06	0.00000E+00
0.45602E+04	0.12201E-06	0.00000E+00
0.45415E+04	0.13218E-06	0.00000E+00
0.45276E+04	0.14235E-06	0.00000E+00
0.45164E+04	0.15251E-06	0.00000E+00
0.45072E+04	0.16268E-06	0.00000E+00
0.44992E+04	0.17285E-06	0.00000E+00
0.44923E+04	0.18302E-06	0.00000E+00
0.44861E+04	0.18302E-06	0.00000E+00
0.44805E+04	0.19318E-06	0.00000E+00
0.44754E+04	0.19318E-06	0.00000E+00
0.44707E+04	0.20335E-06	0.00000E+00
0.44664E+04	0.20335E-06	0.00000E+00
0.44624E+04	0.20335E-06	0.00000E+00
0.44587E+04	0.21352E-06	0.00000E+00
0.44552E+04	0.21352E-06	0.00000E+00
0.44519E+04	0.21352E-06	0.00000E+00
0.44487E+04	0.22369E-06	0.00000E+00
0.44458E+04	0.22369E-06	0.00000E+00
0.44430E+04	0.22369E-06	0.00000E+00
0.44206E+04	0.24402E-06	0.00000E+00
0.44046E+04	0.26436E-06	0.00000E+00
0.43921E+04	0.27453E-06	0.00000E+00
0.43818E+04	0.28469E-06	0.00000E+00
0.43731E+04	0.28469E-06	0.00000E+00
0.43655E+04	0.29486E-06	0.00000E+00
0.43587E+04	0.30503E-06	0.00000E+00
0.43527E+04	0.30503E-06	0.00000E+00
0.43472E+04	0.31520E-06	0.00000E+00
0.43423E+04	0.31520E-06	0.00000E+00
0.43377E+04	0.32536E-06	0.00000E+00
0.43334E+04	0.32536E-06	0.00000E+00
0.43295E+04	0.32536E-06	0.00000E+00
0.43257E+04	0.33553E-06	0.00000E+00

Table F-16 (Cont'd)

p_{wf} psi	Sim. kk_{rg} md	Comp. kk_{rg} md
0.43223E+04	0.33553E-06	0.00000E+00
0.43190E+04	0.33553E-06	0.00000E+00
0.43159E+04	0.34570E-06	0.00000E+00
0.43129E+04	0.34570E-06	0.00000E+00
0.42897E+04	0.36603E-06	0.00000E+00
0.42732E+04	0.37620E-06	0.00000E+00
0.42604E+04	0.39654E-06	0.00000E+00
0.42499E+04	0.39654E-06	0.00000E+00
0.42410E+04	0.40670E-06	0.00000E+00
0.42333E+04	0.41687E-06	0.00000E+00
0.42265E+04	0.42704E-06	0.00000E+00
0.42204E+04	0.42704E-06	0.00000E+00
0.42149E+04	0.43721E-06	0.00000E+00
0.42099E+04	0.43721E-06	0.00000E+00
0.42052E+04	0.44737E-06	0.00000E+00
0.42009E+04	0.44737E-06	0.00000E+00
0.41970E+04	0.44737E-06	0.00000E+00
0.41932E+04	0.45754E-06	0.00000E+00
0.41897E+04	0.45754E-06	0.22342E-04
0.41865E+04	0.10473E-05	0.22930E-03
0.41835E+04	0.20030E-05	0.42100E-03
0.41806E+04	0.32943E-05	0.56695E-03
0.41561E+04	0.60444E-03	0.19388E-02
0.41369E+04	0.14200E-02	0.27942E-02
0.41211E+04	0.21735E-02	0.34858E-02
0.41080E+04	0.26969E-02	0.40452E-02
0.40965E+04	0.31941E-02	0.45132E-02
0.40865E+04	0.36210E-02	0.49394E-02
0.40775E+04	0.39906E-02	0.52669E-02
0.40693E+04	0.43311E-02	0.55680E-02
0.40618E+04	0.46690E-02	0.59416E-02
0.40551E+04	0.49172E-02	0.62581E-02
0.40488E+04	0.51797E-02	0.64415E-02
0.40429E+04	0.53979E-02	0.66096E-02
0.40373E+04	0.56257E-02	0.68180E-02
0.40321E+04	0.58599E-02	0.70670E-02
0.40272E+04	0.60460E-02	0.72904E-02
0.40226E+04	0.62032E-02	0.74729E-02
0.40182E+04	0.63572E-02	0.76929E-02
0.40141E+04	0.65048E-02	0.77403E-02
0.39807E+04	0.77761E-02	0.90886E-02
0.39564E+04	0.86815E-02	0.99425E-02
0.39373E+04	0.93971E-02	0.10681E-01

Table F-16 (Cont'd)

p_{wf} psi	Sim. kk_{rg} md	Comp. kk_{rg} md
0.39217E+04	0.99012E-02	0.11147E-01
0.39080E+04	0.10392E-01	0.11557E-01
0.38963E+04	0.10804E-01	0.12033E-01
0.38858E+04	0.11164E-01	0.12285E-01
0.38763E+04	0.11483E-01	0.12521E-01
0.38676E+04	0.11796E-01	0.12897E-01
0.38598E+04	0.12036E-01	0.13314E-01
0.38526E+04	0.12256E-01	0.13452E-01
0.38458E+04	0.12464E-01	0.13512E-01
0.38394E+04	0.12679E-01	0.13563E-01
0.38333E+04	0.12893E-01	0.13939E-01
0.38278E+04	0.13060E-01	0.14440E-01
0.38226E+04	0.13211E-01	0.14654E-01
0.38177E+04	0.13360E-01	0.14647E-01
0.38129E+04	0.13522E-01	0.14586E-01
0.37920E+04	0.14223E-01	0.15426E-01
0.37750E+04	0.14709E-01	0.15910E-01
0.37602E+04	0.15182E-01	0.16412E-01
0.37477E+04	0.15524E-01	0.16925E-01
0.37364E+04	0.15841E-01	0.16904E-01
0.37260E+04	0.16171E-01	0.17305E-01
0.37169E+04	0.16447E-01	0.17864E-01

Table F-17

Simulated and Computed kk_{rg} Values
Buildup Test
Case 1

p_{wf} psi	Sim. kk_{rg} md	Comp. kk_{rg} md
0.376944E+04	0.148864E-01	0.493895E-01
0.378195E+04	0.145101E-01	0.452225E-01
0.379210E+04	0.142197E-01	0.392307E-01
0.380072E+04	0.139305E-01	0.353826E-01
0.380826E+04	0.136775E-01	0.326049E-01
0.381499E+04	0.134513E-01	0.304575E-01
0.382109E+04	0.132547E-01	0.287500E-01
0.382667E+04	0.130927E-01	0.273148E-01
0.383184E+04	0.129370E-01	0.250889E-01
0.385308E+04	0.122409E-01	0.223880E-01
0.386961E+04	0.117236E-01	0.195930E-01
0.388332E+04	0.112472E-01	0.177132E-01
0.389502E+04	0.108476E-01	0.163871E-01
0.390524E+04	0.104852E-01	0.153516E-01
0.391433E+04	0.101651E-01	0.144979E-01
0.392253E+04	0.987437E-02	0.137884E-01
0.392999E+04	0.963332E-02	0.131713E-01
0.393686E+04	0.941133E-02	0.126373E-01
0.394320E+04	0.917607E-02	0.121726E-01
0.394911E+04	0.895464E-02	0.117386E-01
0.395464E+04	0.874745E-02	0.113612E-01
0.395983E+04	0.853731E-02	0.110141E-01
0.396473E+04	0.834729E-02	0.106970E-01
0.396936E+04	0.818169E-02	0.104161E-01
0.397375E+04	0.802467E-02	0.101460E-01
0.397793E+04	0.787516E-02	0.988595E-02
0.398192E+04	0.772951E-02	0.956118E-02
0.401386E+04	0.651247E-02	0.800913E-02
0.403699E+04	0.563965E-02	0.682740E-02
0.405520E+04	0.491349E-02	0.595174E-02
0.407014E+04	0.429623E-02	0.526937E-02
0.408282E+04	0.377208E-02	0.468991E-02
0.409386E+04	0.330568E-02	0.419610E-02
0.410359E+04	0.288757E-02	0.378137E-02
0.411225E+04	0.250371E-02	0.341384E-02
0.412007E+04	0.221190E-02	0.308100E-02
0.412717E+04	0.184833E-02	0.278022E-02
0.413368E+04	0.155021E-02	0.249767E-02
0.413970E+04	0.127200E-02	0.223670E-02
0.414528E+04	0.100550E-02	0.199114E-02
0.415051E+04	0.806505E-03	0.176047E-02
0.415540E+04	0.622381E-03	0.154795E-02
0.416000E+04	0.396983E-03	0.134404E-02

Table F-17 (Cont'd)

p_{ws} psi	Sim. kk_{rg} md	Comp. kk_{rg} md
0.416435E+04	0.226618E-03	0.114908E-02
0.416848E+04	0.113804E-03	0.955486E-03
0.420145E+04	0.447374E-06	0.000000E+00
0.422424E+04	0.427039E-06	0.000000E+00
0.424295E+04	0.404476E-06	0.000000E+00
0.425847E+04	0.396536E-06	0.000000E+00
0.427163E+04	0.378695E-06	0.000000E+00
0.428292E+04	0.370212E-06	0.000000E+00
0.429272E+04	0.363387E-06	0.000000E+00
0.430137E+04	0.355805E-06	0.000000E+00
0.430904E+04	0.349082E-06	0.000000E+00
0.431595E+04	0.345534E-06	0.000000E+00
0.432223E+04	0.335531E-06	0.000000E+00
0.432796E+04	0.329484E-06	0.000000E+00
0.433322E+04	0.325363E-06	0.000000E+00
0.433807E+04	0.324545E-06	0.000000E+00
0.434258E+04	0.315196E-06	0.000000E+00
0.434679E+04	0.315196E-06	0.000000E+00
0.435073E+04	0.308670E-06	0.000000E+00
0.435443E+04	0.305028E-06	0.000000E+00
0.438238E+04	0.284120E-06	0.000000E+00
0.440139E+04	0.266969E-06	0.000000E+00
0.441566E+04	0.250301E-06	0.000000E+00
0.442701E+04	0.238203E-06	0.000000E+00
0.443645E+04	0.229633E-06	0.000000E+00
0.444456E+04	0.223687E-06	0.000000E+00
0.445168E+04	0.214219E-06	0.000000E+00
0.445801E+04	0.213520E-06	0.000000E+00
0.446369E+04	0.203352E-06	0.000000E+00
0.446885E+04	0.203352E-06	0.000000E+00
0.447357E+04	0.197143E-06	0.000000E+00
0.447793E+04	0.193184E-06	0.000000E+00
0.448197E+04	0.190515E-06	0.000000E+00
0.448573E+04	0.183689E-06	0.000000E+00
0.448925E+04	0.183017E-06	0.000000E+00
0.449256E+04	0.182634E-06	0.000000E+00
0.449568E+04	0.178036E-06	0.000000E+00
0.449864E+04	0.173674E-06	0.000000E+00
0.450411E+04	0.166609E-06	0.000000E+00
0.450906E+04	0.160626E-06	0.000000E+00
0.451360E+04	0.155608E-06	0.000000E+00
0.451779E+04	0.151252E-06	0.000000E+00
0.452168E+04	0.147721E-06	0.000000E+00

Table F-17 (Cont'd)

p_{ws} psi	Sim. kk_{rg} md	Comp. kk_{rg} md
0.452531E+04	0.144425E-06	0.000000E+00
0.452870E+04	0.141542E-06	0.000000E+00
0.453188E+04	0.139216E-06	0.000000E+00
0.453488E+04	0.137021E-06	0.000000E+00
0.453771E+04	0.134951E-06	0.000000E+00
0.454040E+04	0.132983E-06	0.000000E+00
0.454295E+04	0.131390E-06	0.000000E+00
0.454538E+04	0.130069E-06	0.000000E+00
0.454770E+04	0.128808E-06	0.000000E+00
0.454991E+04	0.127606E-06	0.000000E+00
0.455204E+04	0.126448E-06	0.000000E+00
0.455407E+04	0.125344E-06	0.000000E+00
0.455603E+04	0.124279E-06	0.000000E+00
0.455791E+04	0.123256E-06	0.000000E+00
0.455972E+04	0.122272E-06	0.000000E+00
0.456147E+04	0.119264E-06	0.000000E+00
0.456315E+04	0.115629E-06	0.000000E+00
0.456478E+04	0.112103E-06	0.000000E+00
0.456636E+04	0.111844E-06	0.000000E+00
0.456788E+04	0.111844E-06	0.000000E+00
0.456936E+04	0.111844E-06	0.000000E+00
0.457079E+04	0.110634E-06	0.000000E+00
0.457218E+04	0.108197E-06	0.000000E+00
0.457353E+04	0.105831E-06	0.000000E+00
0.457484E+04	0.103534E-06	0.000000E+00
0.457611E+04	0.101676E-06	0.000000E+00
0.457735E+04	0.101676E-06	0.000000E+00
0.457856E+04	0.101676E-06	0.000000E+00
0.457973E+04	0.101676E-06	0.000000E+00
0.458088E+04	0.101676E-06	0.000000E+00
0.458200E+04	0.101676E-06	0.000000E+00
0.458309E+04	0.100741E-06	0.000000E+00
0.458415E+04	0.993036E-07	0.000000E+00
0.458519E+04	0.978937E-07	0.000000E+00
0.458621E+04	0.965109E-07	0.000000E+00
0.458720E+04	0.951687E-07	0.000000E+00
0.458817E+04	0.938537E-07	0.000000E+00
0.458912E+04	0.925658E-07	0.000000E+00
0.459004E+04	0.913466E-07	0.000000E+00
0.459095E+04	0.902952E-07	0.000000E+00
0.459184E+04	0.892669E-07	0.000000E+00
0.459271E+04	0.882617E-07	0.000000E+00
0.459357E+04	0.872680E-07	0.000000E+00

Table F-17 (Cont'd)

p_{we} psi	Sim. kk_{rg} md	Comp. kk_{rg} md
0.459440E+04	0.863091E-07	0.000000E+00
0.459522E+04	0.853616E-07	0.000000E+00
0.459603E+04	0.844257E-07	0.000000E+00
0.459682E+04	0.835130E-07	0.000000E+00
0.459759E+04	0.826233E-07	0.000000E+00
0.459835E+04	0.817452E-07	0.000000E+00
0.459910E+04	0.809677E-07	0.000000E+00
0.459983E+04	0.802867E-07	0.000000E+00
0.460055E+04	0.796151E-07	0.000000E+00
0.460125E+04	0.789621E-07	0.000000E+00
0.460195E+04	0.783092E-07	0.000000E+00
0.460263E+04	0.776749E-07	0.000000E+00
0.460330E+04	0.770499E-07	0.000000E+00
0.460396E+04	0.764342E-07	0.000000E+00
0.460461E+04	0.758279E-07	0.000000E+00
0.460525E+04	0.752309E-07	0.000000E+00
0.460588E+04	0.746432E-07	0.000000E+00
0.460650E+04	0.740649E-07	0.000000E+00
0.460711E+04	0.734959E-07	0.000000E+00
0.460771E+04	0.729362E-07	0.000000E+00
0.460830E+04	0.723858E-07	0.000000E+00
0.460888E+04	0.718448E-07	0.000000E+00
0.460945E+04	0.713131E-07	0.000000E+00
0.461001E+04	0.708796E-07	0.000000E+00
0.461057E+04	0.704787E-07	0.000000E+00
0.461112E+04	0.700848E-07	0.000000E+00
0.461166E+04	0.696982E-07	0.000000E+00
0.461219E+04	0.693187E-07	0.000000E+00
0.461271E+04	0.689464E-07	0.000000E+00
0.461323E+04	0.685740E-07	0.000000E+00
0.461374E+04	0.682088E-07	0.000000E+00
0.461424E+04	0.678508E-07	0.000000E+00
0.461474E+04	0.674928E-07	0.000000E+00
0.461523E+04	0.671420E-07	0.000000E+00
0.461571E+04	0.667983E-07	0.000000E+00
0.461619E+04	0.664546E-07	0.000000E+00
0.461666E+04	0.661180E-07	0.000000E+00
0.461712E+04	0.657887E-07	0.000000E+00
0.461758E+04	0.654593E-07	0.000000E+00
0.461803E+04	0.651371E-07	0.000000E+00
0.461848E+04	0.648149E-07	0.000000E+00
0.461892E+04	0.644998E-07	0.000000E+00
0.462000E+04	0.637265E-07	0.000000E+00

Table F-17 (Cont'd)

p_{we} . psi	Sim. kk_{rg} md	Comp. kk_{rg} md
0.462105E+04	0.629747E-07	0.000000E+00
0.462206E+04	0.622515E-07	0.000000E+00
0.462304E+04	0.615498E-07	0.000000E+00
0.462400E+04	0.608128E-07	0.000000E+00
0.462493E+04	0.599166E-07	0.000000E+00
0.462584E+04	0.590395E-07	0.000000E+00
0.462672E+04	0.581914E-07	0.000000E+00
0.462757E+04	0.573722E-07	0.000000E+00
0.462841E+04	0.565627E-07	0.000000E+00
0.462922E+04	0.557821E-07	0.000000E+00
0.463001E+04	0.550207E-07	0.000000E+00
0.463079E+04	0.542690E-07	0.000000E+00
0.463154E+04	0.535461E-07	0.000000E+00
0.463228E+04	0.528330E-07	0.000000E+00
0.463300E+04	0.521391E-07	0.000000E+00
0.463370E+04	0.514644E-07	0.000000E+00
0.463439E+04	0.507994E-07	0.000000E+00
0.463506E+04	0.501537E-07	0.000000E+00
0.463571E+04	0.495273E-07	0.000000E+00
0.463635E+04	0.489105E-07	0.000000E+00
0.463698E+04	0.483033E-07	0.000000E+00
0.463760E+04	0.477058E-07	0.000000E+00
0.463820E+04	0.471275E-07	0.000000E+00
0.463879E+04	0.465589E-07	0.000000E+00
0.463936E+04	0.460096E-07	0.000000E+00
0.463993E+04	0.454603E-07	0.000000E+00
0.464048E+04	0.449302E-07	0.000000E+00
0.464102E+04	0.444098E-07	0.000000E+00
0.464156E+04	0.438893E-07	0.000000E+00
0.464208E+04	0.433882E-07	0.000000E+00
0.464259E+04	0.428967E-07	0.000000E+00
0.464309E+04	0.424148E-07	0.000000E+00
0.464358E+04	0.419426E-07	0.000000E+00
0.464407E+04	0.414703E-07	0.000000E+00
0.464454E+04	0.410174E-07	0.000000E+00
0.464501E+04	0.405892E-07	0.000000E+00
0.464547E+04	0.402497E-07	0.000000E+00
0.464592E+04	0.399175E-07	0.000000E+00
0.464636E+04	0.395927E-07	0.000000E+00
0.464679E+04	0.392754E-07	0.000000E+00
0.464722E+04	0.389580E-07	0.000000E+00
0.464764E+04	0.386480E-07	0.000000E+00
0.464805E+04	0.383453E-07	0.000000E+00

Table F-17 (Cont'd)

p_{wf} psi	Sim. kk_{rg} md	Comp. kk_{rg} md
0.464846E+04	0.380427E-07	0.000000E+00
0.464886E+04	0.377474E-07	0.000000E+00
0.464925E+04	0.374596E-07	0.000000E+00
0.464964E+04	0.371717E-07	0.000000E+00
0.465002E+04	0.368912E-07	0.000000E+00
0.465039E+04	0.366181E-07	0.000000E+00
0.465076E+04	0.363450E-07	0.000000E+00
0.465112E+04	0.360793E-07	0.000000E+00
0.465148E+04	0.358136E-07	0.000000E+00
0.465183E+04	0.355552E-07	0.000000E+00
0.465218E+04	0.352969E-07	0.000000E+00
0.465252E+04	0.350459E-07	0.000000E+00
0.465285E+04	0.348023E-07	0.000000E+00
0.465318E+04	0.345588E-07	0.000000E+00
0.465351E+04	0.343152E-07	0.000000E+00
0.465383E+04	0.340790E-07	0.000000E+00
0.465415E+04	0.338428E-07	0.000000E+00
0.465446E+04	0.336140E-07	0.000000E+00
0.465477E+04	0.333852E-07	0.000000E+00
0.465507E+04	0.331637E-07	0.000000E+00
0.465537E+04	0.329423E-07	0.000000E+00
0.465566E+04	0.327282E-07	0.000000E+00
0.465596E+04	0.325068E-07	0.000000E+00
0.465624E+04	0.323001E-07	0.000000E+00
0.465653E+04	0.320861E-07	0.000000E+00
0.465680E+04	0.318868E-07	0.000000E+00
0.465708E+04	0.316801E-07	0.000000E+00
0.465735E+04	0.314808E-07	0.000000E+00
0.465762E+04	0.312815E-07	0.000000E+00
0.465788E+04	0.310896E-07	0.000000E+00
0.465815E+04	0.308903E-07	0.000000E+00
0.465840E+04	0.307058E-07	0.000000E+00
0.465866E+04	0.305139E-07	0.000000E+00
0.465891E+04	0.303293E-07	0.000000E+00
0.465916E+04	0.301448E-07	0.000000E+00

Table F-18

Nonlinear Parameter Estimation
Two Unknowns
Case 1

Iteration Number	kk_r^o md	λ
0	0.69826E+01	0.10000E+01
1	0.70175E+01	0.22597E+01
2	0.70076E+01	0.14547E+01
3	0.70074E+01	0.18958E+01
4	0.70073E+01	0.19652E+01
5	0.70072E+01	0.19569E+01
6	0.70072E+01	0.19575E+01
7	0.70072E+01	0.19578E+01

Table F-19

Nonlinear Parameter Estimation
Three Unknowns
Case 1

Iteration Number	kk_r^o md	λ	S_{gc}
0	0.69826E+01	0.10000E+01	0.10000E-19
1	0.70175E+01	0.22597E+01	0.15000E-19
2	0.70125E+01	0.18572E+01	0.18750E-19
3	0.70112E+01	0.19124E+01	0.21100E-19
4	0.70102E+01	0.19379E+01	0.23728E-19

Table F-20

Nonlinear Parameter Estimation
Four Unknowns
Case 1

Iteration Number	kk_r^o md	λ	S_{gc}	S_{wc}
0	0.69826E+01	0.10000E+01	0.10000E-19	0.10000E+01
1	0.70163E+01	0.17665E+01	0.15000E-19	0.15195E+01
2	0.70072E+01	0.97414E+00	0.22500E-19	0.18791E+01
3	0.70074E+01	0.11898E+01	0.28125E-19	0.23004E+01
4	0.70073E+01	0.12925E+01	0.35156E-19	0.25987E+01
5	0.70073E+01	0.13946E+01	0.43945E-19	0.28183E+01
6	0.70073E+01	0.15119E+01	0.54932E-19	0.29711E+01
7	0.70073E+01	0.16457E+01	0.68665E-19	0.30659E+01
8	0.70073E+01	0.17948E+01	0.85831E-19	0.31109E+01
9	0.70072E+01	0.19741E+01	0.10729E-18	0.31093E+01

Rock and Fluid Properties for Tables F-21 through F-24

$r_w = 0.328$ ft ; $r_e = 6600$ ft

$h = 15.547$ ft ; $\phi = 0.3$

$k = k_g = 10$ md

$r_{iz} = 3.91$ ft

$q_o = 200$ STB/DAY

$s = 0.0$; $S_{gc} = 0.0$

$S_{wc} = S_{iw} = 0.3$; $S_{or} = 0.0$

$C_D = 0.0$ $(\beta^* \rightarrow \infty)$

PVT Data are given by Set 1 (Table A-1)

Inner Zone Relative Permeability Data are given by Set 4 (Table A-6)

Outer Zone Relative Permeability Data are given by Set 1 (Table A-2)

$p_i = p_{bi} = 3460$ psi

$c_{ti} = 0.23564 \times 10^{-4}$ psi^{-1}

$\mu_{oi} = 0.43059$ cp

$B_{oi} = 1.5882$ RB/STB

Table F-21

Simulated and Computed kk_{ro} Values
Drawdown Test
Case 1

t days	p_{wf} psi	Sim. So	Sim. kk_{ro} md	Comp. kk_{ro} md
0.10157E-03	0.32152E+04	0.67003E+00	0.76659E+01	0.94629E+01
0.11213E-03	0.32085E+04	0.66907E+00	0.76260E+01	0.93508E+01
0.12374E-03	0.32018E+04	0.66808E+00	0.75849E+01	0.92058E+01
0.13651E-03	0.31949E+04	0.66707E+00	0.75429E+01	0.90667E+01
0.15056E-03	0.31880E+04	0.66604E+00	0.75002E+01	0.89413E+01
0.16602E-03	0.31810E+04	0.66499E+00	0.74566E+01	0.88451E+01
0.18302E-03	0.31740E+04	0.66392E+00	0.74130E+01	0.87304E+01
0.20172E-03	0.31669E+04	0.66283E+00	0.73686E+01	0.85837E+01
0.22230E-03	0.31596E+04	0.66171E+00	0.73230E+01	0.84506E+01
0.24493E-03	0.31522E+04	0.66056E+00	0.72762E+01	0.83351E+01
0.26982E-03	0.31448E+04	0.65940E+00	0.72295E+01	0.82211E+01
0.29720E-03	0.31372E+04	0.65821E+00	0.71820E+01	0.80818E+01
0.32732E-03	0.31295E+04	0.65700E+00	0.71338E+01	0.79333E+01
0.36045E-03	0.31217E+04	0.65576E+00	0.70843E+01	0.77969E+01
0.39690E-03	0.31137E+04	0.65450E+00	0.70344E+01	0.76687E+01
0.43699E-03	0.31056E+04	0.65322E+00	0.69844E+01	0.75265E+01
0.48109E-03	0.30974E+04	0.65192E+00	0.69336E+01	0.73715E+01
0.52959E-03	0.30889E+04	0.65060E+00	0.68820E+01	0.72247E+01
0.58295E-03	0.30803E+04	0.64926E+00	0.68302E+01	0.70849E+01
0.64165E-03	0.30715E+04	0.64791E+00	0.67785E+01	0.69421E+01
0.70621E-03	0.30626E+04	0.64656E+00	0.67268E+01	0.67941E+01
0.77724E-03	0.30534E+04	0.64520E+00	0.66748E+01	0.66521E+01
0.85536E-03	0.30440E+04	0.64382E+00	0.66228E+01	0.65115E+01
0.94130E-03	0.30345E+04	0.64247E+00	0.65722E+01	0.63759E+01
0.10358E-02	0.30247E+04	0.64112E+00	0.65215E+01	0.62466E+01
0.11398E-02	0.30147E+04	0.63977E+00	0.64710E+01	0.61192E+01
0.12542E-02	0.30045E+04	0.63844E+00	0.64222E+01	0.59943E+01
0.13800E-02	0.29941E+04	0.63714E+00	0.63744E+01	0.58743E+01
0.15184E-02	0.29835E+04	0.63586E+00	0.63274E+01	0.57653E+01
0.16706E-02	0.29726E+04	0.63460E+00	0.62814E+01	0.56660E+01
0.18381E-02	0.29616E+04	0.63338E+00	0.62375E+01	0.55677E+01
0.20223E-02	0.29504E+04	0.63218E+00	0.61944E+01	0.54688E+01
0.22250E-02	0.29389E+04	0.63102E+00	0.61527E+01	0.53837E+01
0.24479E-02	0.29273E+04	0.62990E+00	0.61125E+01	0.53159E+01
0.26930E-02	0.29155E+04	0.62879E+00	0.60734E+01	0.52343E+01
0.29627E-02	0.29035E+04	0.62771E+00	0.60353E+01	0.51445E+01
0.32594E-02	0.28912E+04	0.62667E+00	0.59987E+01	0.50784E+01
0.35858E-02	0.28789E+04	0.62568E+00	0.59638E+01	0.50367E+01
0.39447E-02	0.28664E+04	0.62469E+00	0.59292E+01	0.49841E+01
0.43396E-02	0.28537E+04	0.62370E+00	0.58951E+01	0.49015E+01
0.47740E-02	0.28408E+04	0.62277E+00	0.58630E+01	0.48402E+01
0.52518E-02	0.28278E+04	0.62187E+00	0.58320E+01	0.48062E+01
0.57773E-02	0.28147E+04	0.62099E+00	0.58016E+01	0.47695E+01

Table F-21 (Cont'd)

t days	p_{wf} psi	Sim. So	Sim. kk_{ro} md	Comp. kk_{ro} md
0.63555E-02	0.28014E+04	0.62011E+00	0.57713E+01	0.47255E+01
0.69914E-02	0.27880E+04	0.61923E+00	0.57418E+01	0.46604E+01
0.76910E-02	0.27743E+04	0.61840E+00	0.57141E+01	0.45911E+01
0.84605E-02	0.27605E+04	0.61762E+00	0.56881E+01	0.45503E+01
0.93069E-02	0.27465E+04	0.61687E+00	0.56630E+01	0.45374E+01
0.10238E-01	0.27325E+04	0.61613E+00	0.56383E+01	0.45199E+01
0.11262E-01	0.27184E+04	0.61539E+00	0.56136E+01	0.44798E+01
0.12389E-01	0.27041E+04	0.61480E+00	0.55939E+01	0.46997E+01
0.13628E-01	0.26913E+04	0.61363E+00	0.55549E+01	0.45486E+01
0.14991E-01	0.26760E+04	0.61273E+00	0.55248E+01	0.41859E+01
0.16491E-01	0.26607E+04	0.61199E+00	0.55001E+01	0.41728E+01
0.18140E-01	0.26453E+04	0.61138E+00	0.54798E+01	0.42334E+01
0.19955E-01	0.26303E+04	0.61072E+00	0.54577E+01	0.42790E+01
0.21951E-01	0.26152E+04	0.61005E+00	0.54354E+01	0.42089E+01
0.24146E-01	0.25997E+04	0.60945E+00	0.54159E+01	0.42027E+01
0.26561E-01	0.25844E+04	0.60879E+00	0.53946E+01	0.42143E+01
0.29218E-01	0.25690E+04	0.60811E+00	0.53726E+01	0.41321E+01
0.32140E-01	0.25530E+04	0.60750E+00	0.53529E+01	0.41183E+01
0.35354E-01	0.25374E+04	0.60682E+00	0.53309E+01	0.41157E+01
0.38890E-01	0.25214E+04	0.60612E+00	0.53083E+01	0.40259E+01
0.42779E-01	0.25050E+04	0.60548E+00	0.52876E+01	0.40108E+01
0.47058E-01	0.24888E+04	0.60477E+00	0.52648E+01	0.39964E+01
0.51764E-01	0.24721E+04	0.60403E+00	0.52414E+01	0.38782E+01
0.56941E-01	0.24548E+04	0.60338E+00	0.52209E+01	0.38512E+01
0.62635E-01	0.24378E+04	0.60266E+00	0.51982E+01	0.38527E+01
0.68899E-01	0.24205E+04	0.60194E+00	0.51754E+01	0.37820E+01
0.75789E-01	0.24028E+04	0.60127E+00	0.51542E+01	0.37698E+01
0.83369E-01	0.23852E+04	0.60051E+00	0.51302E+01	0.37261E+01
0.91706E-01	0.23670E+04	0.59981E+00	0.51082E+01	0.36392E+01
0.10003E+00	0.23501E+04	0.59912E+00	0.50869E+01	0.35739E+01
0.10918E+00	0.23327E+04	0.59855E+00	0.50693E+01	0.36144E+01
0.11925E+00	0.23158E+04	0.59794E+00	0.50504E+01	0.36735E+01
0.13033E+00	0.22986E+04	0.59731E+00	0.50310E+01	0.36301E+01
0.14251E+00	0.22810E+04	0.59679E+00	0.50149E+01	0.36767E+01
0.15591E+00	0.22639E+04	0.59622E+00	0.49973E+01	0.37193E+01
0.17065E+00	0.22465E+04	0.59562E+00	0.49788E+01	0.36588E+01
0.18687E+00	0.22285E+04	0.59514E+00	0.49639E+01	0.37063E+01
0.20471E+00	0.22112E+04	0.59460E+00	0.49475E+01	0.37376E+01
0.22433E+00	0.21933E+04	0.59406E+00	0.49312E+01	0.36455E+01
0.24591E+00	0.21749E+04	0.59363E+00	0.49182E+01	0.36378E+01
0.26718E+00	0.21585E+04	0.59321E+00	0.49055E+01	0.36989E+01
0.29057E+00	0.21421E+04	0.59275E+00	0.48916E+01	0.36912E+01
0.31630E+00	0.21251E+04	0.59240E+00	0.48810E+01	0.37439E+01

Table F-21 (Cont'd)

t days	p_{wf} psi	Sim. So	Sim. kk_{ro} md	Comp. kk_{ro} md
0.34461E+00	0.21088E+04	0.59198E+00	0.48683E+01	0.37925E+01
0.37575E+00	0.20918E+04	0.59153E+00	0.48547E+01	0.37340E+01
0.41000E+00	0.20745E+04	0.59108E+00	0.48411E+01	0.37179E+01
0.44767E+00	0.20571E+04	0.59062E+00	0.48272E+01	0.37161E+01
0.48911E+00	0.20394E+04	0.59016E+00	0.48133E+01	0.36936E+01
0.53470E+00	0.20213E+04	0.58968E+00	0.47991E+01	0.36447E+01
0.58485E+00	0.20028E+04	0.58925E+00	0.47866E+01	0.35656E+01
0.63395E+00	0.19856E+04	0.58887E+00	0.47755E+01	0.35818E+01
0.68797E+00	0.19687E+04	0.58850E+00	0.47647E+01	0.36572E+01
0.74739E+00	0.19516E+04	0.58813E+00	0.47539E+01	0.36717E+01
0.81275E+00	0.19343E+04	0.58776E+00	0.47430E+01	0.36823E+01
0.88465E+00	0.19168E+04	0.58737E+00	0.47317E+01	0.36744E+01
0.96373E+00	0.18989E+04	0.58696E+00	0.47197E+01	0.36489E+01
0.10507E+01	0.18807E+04	0.58655E+00	0.47077E+01	0.35652E+01
0.11375E+01	0.18632E+04	0.58619E+00	0.46972E+01	0.35437E+01
0.12328E+01	0.18459E+04	0.58583E+00	0.46867E+01	0.36434E+01
0.13378E+01	0.18287E+04	0.58544E+00	0.46753E+01	0.36870E+01
0.14532E+01	0.18112E+04	0.58501E+00	0.46627E+01	0.36432E+01
0.15802E+01	0.17930E+04	0.58458E+00	0.46501E+01	0.35346E+01
0.17071E+01	0.17754E+04	0.58419E+00	0.46387E+01	0.35147E+01
0.18466E+01	0.17580E+04	0.58380E+00	0.46273E+01	0.35903E+01
0.20002E+01	0.17405E+04	0.58340E+00	0.46156E+01	0.35987E+01
0.21691E+01	0.17225E+04	0.58299E+00	0.46037E+01	0.35625E+01
0.23548E+01	0.17039E+04	0.58257E+00	0.45914E+01	0.34726E+01
0.25365E+01	0.16863E+04	0.58219E+00	0.45803E+01	0.34625E+01
0.27363E+01	0.16669E+04	0.58182E+00	0.45695E+01	0.35398E+01
0.29562E+01	0.16513E+04	0.58144E+00	0.45584E+01	0.35467E+01
0.31980E+01	0.16332E+04	0.58104E+00	0.45467E+01	0.35256E+01
0.34639E+01	0.16146E+04	0.58064E+00	0.45350E+01	0.34946E+01
0.37237E+01	0.15975E+04	0.58024E+00	0.45233E+01	0.35262E+01
0.40094E+01	0.15804E+04	0.57980E+00	0.45108E+01	0.34771E+01
0.43236E+01	0.15619E+04	0.57937E+00	0.44991E+01	0.32933E+01
0.46320E+01	0.15438E+04	0.57902E+00	0.44896E+01	0.33184E+01
0.49712E+01	0.15266E+04	0.57867E+00	0.44800E+01	0.28833E+01

Table F-22

Simulated and Computed kk_{ro} Values
Buildup Test
Case 1

Δt days	p_{ws} psi	DD Sim. So	Sim. kk_{ro} md	Comp. kk_{ro} md
0.101569E-03	0.181486E+04	0.585100E+00	0.466532E+01	0.709053E+01
0.112126E-03	0.182591E+04	0.585372E+00	0.467326E+01	0.680526E+01
0.123738E-03	0.183742E+04	0.585638E+00	0.468105E+01	0.644415E+01
0.136512E-03	0.184959E+04	0.585908E+00	0.468892E+01	0.621890E+01
0.150563E-03	0.186183E+04	0.586162E+00	0.469636E+01	0.614493E+01
0.166020E-03	0.187417E+04	0.586416E+00	0.470379E+01	0.606506E+01
0.183022E-03	0.188661E+04	0.586684E+00	0.471160E+01	0.598055E+01
0.201724E-03	0.189918E+04	0.586966E+00	0.471986E+01	0.589118E+01
0.222296E-03	0.191188E+04	0.587258E+00	0.472837E+01	0.580162E+01
0.244926E-03	0.192473E+04	0.587547E+00	0.473682E+01	0.570856E+01
0.269818E-03	0.193774E+04	0.587834E+00	0.474520E+01	0.561767E+01
0.297200E-03	0.195089E+04	0.588115E+00	0.475342E+01	0.553385E+01
0.327320E-03	0.196419E+04	0.588403E+00	0.476183E+01	0.545210E+01
0.360452E-03	0.197763E+04	0.588696E+00	0.477040E+01	0.536971E+01
0.396898E-03	0.199123E+04	0.588995E+00	0.477913E+01	0.528868E+01
0.436987E-03	0.200497E+04	0.589301E+00	0.478807E+01	0.520933E+01
0.481086E-03	0.201888E+04	0.589623E+00	0.479748E+01	0.512771E+01
0.529595E-03	0.203296E+04	0.589989E+00	0.480818E+01	0.503497E+01
0.582954E-03	0.204727E+04	0.590365E+00	0.481953E+01	0.492450E+01
0.641650E-03	0.206187E+04	0.590746E+00	0.483105E+01	0.478054E+01
0.706215E-03	0.207694E+04	0.591143E+00	0.484303E+01	0.467454E+01
0.777236E-03	0.209211E+04	0.591537E+00	0.485495E+01	0.465692E+01
0.855360E-03	0.210719E+04	0.591939E+00	0.486708E+01	0.466481E+01
0.941296E-03	0.212222E+04	0.592325E+00	0.487876E+01	0.454612E+01
0.103583E-02	0.213799E+04	0.592666E+00	0.488906E+01	0.445423E+01
0.113981E-02	0.215355E+04	0.593072E+00	0.490133E+01	0.453630E+01
0.125419E-02	0.216867E+04	0.593471E+00	0.491340E+01	0.460553E+01
0.138001E-02	0.218368E+04	0.593835E+00	0.492441E+01	0.461338E+01
0.151841E-02	0.219866E+04	0.594221E+00	0.493606E+01	0.460102E+01
0.167065E-02	0.221366E+04	0.594676E+00	0.494982E+01	0.448874E+01
0.183811E-02	0.222929E+04	0.595161E+00	0.496456E+01	0.438376E+01
0.202233E-02	0.224493E+04	0.595579E+00	0.497749E+01	0.440331E+01
0.222496E-02	0.226033E+04	0.596096E+00	0.499346E+01	0.440873E+01
0.244785E-02	0.227583E+04	0.596617E+00	0.500956E+01	0.434656E+01
0.269304E-02	0.229157E+04	0.597102E+00	0.502455E+01	0.419378E+01
0.296274E-02	0.230811E+04	0.597658E+00	0.504174E+01	0.401881E+01
0.325942E-02	0.232515E+04	0.598278E+00	0.506090E+01	0.400807E+01
0.358576E-02	0.234169E+04	0.598845E+00	0.507842E+01	0.406967E+01
0.394473E-02	0.235814E+04	0.599449E+00	0.509708E+01	0.406908E+01
0.433961E-02	0.237460E+04	0.600103E+00	0.511735E+01	0.398016E+01
0.477397E-02	0.239170E+04	0.600791E+00	0.513911E+01	0.391062E+01
0.525177E-02	0.240866E+04	0.601493E+00	0.516128E+01	0.393463E+01
0.577734E-02	0.242547E+04	0.602147E+00	0.518194E+01	0.393684E+01

Table F-22 (Cont'd)

Δt days	p_{ws} psi	DD Sim. So	Sim. kk_{ro} md	Comp. kk_{ro} md
0.635548E-02	0.244232E+04	0.602850E+00	0.520415E+01	0.387551E+01
0.699142E-02	0.245955E+04	0.603558E+00	0.522653E+01	0.378264E+01
0.769097E-02	0.247714E+04	0.604254E+00	0.524852E+01	0.376003E+01
0.846046E-02	0.249449E+04	0.605021E+00	0.527279E+01	0.376499E+01
0.930691E-02	0.251193E+04	0.605752E+00	0.529639E+01	0.368907E+01
0.102380E-01	0.252988E+04	0.606492E+00	0.532031E+01	0.356304E+01
0.112622E-01	0.254846E+04	0.607301E+00	0.534647E+01	0.352810E+01
0.122647E-01	0.256473E+04	0.607948E+00	0.536739E+01	0.358169E+01
0.133674E-01	0.258096E+04	0.608637E+00	0.538965E+01	0.358204E+01
0.145805E-01	0.259746E+04	0.609354E+00	0.541281E+01	0.354927E+01
0.159148E-01	0.261419E+04	0.610011E+00	0.543407E+01	0.357873E+01
0.173825E-01	0.263059E+04	0.610732E+00	0.545812E+01	0.363645E+01
0.189971E-01	0.264695E+04	0.611446E+00	0.548197E+01	0.362768E+01
0.207730E-01	0.266357E+04	0.612129E+00	0.550477E+01	0.358769E+01
0.227266E-01	0.268041E+04	0.612989E+00	0.553347E+01	0.360905E+01
0.248756E-01	0.269693E+04	0.614145E+00	0.557207E+01	0.365853E+01
0.272394E-01	0.271339E+04	0.615183E+00	0.560671E+01	0.363007E+01
0.298396E-01	0.273023E+04	0.616009E+00	0.563430E+01	0.358539E+01
0.326998E-01	0.274716E+04	0.616904E+00	0.566416E+01	0.358846E+01
0.358461E-01	0.276399E+04	0.617818E+00	0.569466E+01	0.358541E+01
0.393070E-01	0.278096E+04	0.618802E+00	0.572752E+01	0.353268E+01
0.431140E-01	0.279832E+04	0.619907E+00	0.576440E+01	0.356085E+01
0.473016E-01	0.281504E+04	0.621014E+00	0.580247E+01	0.366308E+01
0.519081E-01	0.283145E+04	0.622122E+00	0.584065E+01	0.368646E+01
0.569752E-01	0.284794E+04	0.623282E+00	0.588066E+01	0.367831E+01
0.625489E-01	0.286441E+04	0.624533E+00	0.592381E+01	0.373065E+01
0.686801E-01	0.288041E+04	0.625803E+00	0.596819E+01	0.380601E+01
0.754244E-01	0.289619E+04	0.627092E+00	0.601356E+01	0.378327E+01
0.828431E-01	0.291234E+04	0.628507E+00	0.606342E+01	0.378603E+01
0.910037E-01	0.292804E+04	0.629975E+00	0.611512E+01	0.386612E+01
0.999803E-01	0.294347E+04	0.631483E+00	0.616932E+01	0.389848E+01
0.109855E+00	0.295884E+04	0.633086E+00	0.622697E+01	0.385597E+01
0.120716E+00	0.297452E+04	0.634820E+00	0.628934E+01	0.386133E+01
0.132664E+00	0.298977E+04	0.636619E+00	0.635528E+01	0.381899E+01
0.145807E+00	0.300569E+04	0.638594E+00	0.642784E+01	0.381393E+01
0.160264E+00	0.302087E+04	0.640604E+00	0.650215E+01	0.394863E+01
0.176167E+00	0.303563E+04	0.642635E+00	0.657837E+01	0.403325E+01
0.193660E+00	0.305008E+04	0.644711E+00	0.665624E+01	0.404765E+01
0.212902E+00	0.306462E+04	0.646869E+00	0.673865E+01	0.406522E+01
0.234068E+00	0.307881E+04	0.649029E+00	0.682134E+01	0.416078E+01
0.257351E+00	0.309256E+04	0.651169E+00	0.690422E+01	0.425059E+01
0.282963E+00	0.310602E+04	0.653282E+00	0.698683E+01	0.430452E+01
0.311135E+00	0.311927E+04	0.655378E+00	0.706907E+01	0.428653E+01

Table F-22 (Cont'd)

Δt days	p_{ws} psi	DD Sim. So	Sim. kk_{ro} md	Comp. kk_{ro} md
0.342125E+00	0.313268E+04	0.657496E+00	0.715352E+01	0.432591E+01
0.376214E+00	0.314551E+04	0.659513E+00	0.723399E+01	0.444256E+01
0.413712E+00	0.315804E+04	0.661467E+00	0.731314E+01	0.450634E+01
0.454959E+00	0.317032E+04	0.663357E+00	0.739012E+01	0.453092E+01
0.500331E+00	0.318251E+04	0.665209E+00	0.746568E+01	0.452587E+01
0.550241E+00	0.319459E+04	0.667016E+00	0.754071E+01	0.458101E+01
0.605141E+00	0.320624E+04	0.668737E+00	0.761216E+01	0.466095E+01
0.665531E+00	0.321767E+04	0.670390E+00	0.768113E+01	0.467690E+01
0.731961E+00	0.322898E+04	0.672003E+00	0.774944E+01	0.462779E+01
0.805033E+00	0.324035E+04	0.673602E+00	0.781717E+01	0.463198E+01
0.885413E+00	0.325134E+04	0.675123E+00	0.788170E+01	0.475708E+01
0.973830E+00	0.326182E+04	0.676556E+00	0.794366E+01	0.488621E+01
0.107109E+01	0.327192E+04	0.677924E+00	0.800277E+01	0.497784E+01
0.117807E+01	0.328168E+04	0.679232E+00	0.805933E+01	0.501861E+01
0.129576E+01	0.329118E+04	0.680490E+00	0.811408E+01	0.507663E+01
0.142521E+01	0.330047E+04	0.681717E+00	0.816817E+01	0.514489E+01
0.156761E+01	0.330931E+04	0.682864E+00	0.821870E+01	0.525870E+01
0.172425E+01	0.331781E+04	0.683971E+00	0.826748E+01	0.533510E+01
0.189655E+01	0.332599E+04	0.685021E+00	0.831375E+01	0.540294E+01
0.208608E+01	0.333386E+04	0.686035E+00	0.835930E+01	0.543221E+01
0.229456E+01	0.334151E+04	0.687002E+00	0.840279E+01	0.546523E+01
0.252389E+01	0.334884E+04	0.687932E+00	0.844455E+01	0.555465E+01
0.277616E+01	0.335580E+04	0.688816E+00	0.848429E+01	0.564151E+01
0.305365E+01	0.336244E+04	0.689647E+00	0.852163E+01	0.570543E+01
0.335889E+01	0.336878E+04	0.690438E+00	0.855758E+01	0.576321E+01
0.369466E+01	0.337482E+04	0.691191E+00	0.859204E+01	0.581058E+01
0.406400E+01	0.338058E+04	0.691904E+00	0.862472E+01	0.582124E+01
0.447028E+01	0.338611E+04	0.692590E+00	0.865614E+01	0.587039E+01
0.491718E+01	0.339129E+04	0.693228E+00	0.868533E+01	0.588036E+01

Table F-23

Simulated and Computed kk_{rg} Values
Drawdown Test
Case 1

p_{wf} psi	Sim. kk_{rg} md	Comp. kk_{rg} md
0.32152E+04	0.11609E-02	0.14326E-02
0.32085E+04	0.12902E-02	0.15825E-02
0.32018E+04	0.14248E-02	0.17293E-02
0.31949E+04	0.15622E-02	0.18775E-02
0.31880E+04	0.17022E-02	0.20291E-02
0.31810E+04	0.18454E-02	0.21886E-02
0.31740E+04	0.20383E-02	0.24001E-02
0.31669E+04	0.22349E-02	0.26042E-02
0.31596E+04	0.24369E-02	0.28127E-02
0.31522E+04	0.26442E-02	0.30280E-02
0.31448E+04	0.28837E-02	0.32790E-02
0.31372E+04	0.31583E-02	0.35534E-02
0.31295E+04	0.34375E-02	0.38233E-02
0.31217E+04	0.37236E-02	0.40983E-02
0.31137E+04	0.40426E-02	0.44077E-02
0.31056E+04	0.44103E-02	0.47527E-02
0.30974E+04	0.47838E-02	0.50861E-02
0.30889E+04	0.51629E-02	0.54202E-02
0.30803E+04	0.55940E-02	0.58033E-02
0.30715E+04	0.60661E-02	0.62106E-02
0.30626E+04	0.65381E-02	0.66035E-02
0.30534E+04	0.70137E-02	0.69911E-02
0.30440E+04	0.75768E-02	0.74481E-02
0.30345E+04	0.81411E-02	0.78992E-02
0.30247E+04	0.87054E-02	0.83397E-02
0.30147E+04	0.92867E-02	0.87813E-02
0.30045E+04	0.99412E-02	0.92783E-02
0.29941E+04	0.10581E-01	0.97516E-02
0.29835E+04	0.11211E-01	0.10215E-01
0.29726E+04	0.11863E-01	0.10699E-01
0.29616E+04	0.12561E-01	0.11214E-01
0.29504E+04	0.13247E-01	0.11694E-01
0.29389E+04	0.13911E-01	0.12172E-01
0.29273E+04	0.14560E-01	0.12660E-01
0.29155E+04	0.15290E-01	0.13180E-01
0.29035E+04	0.16000E-01	0.13641E-01
0.28912E+04	0.16684E-01	0.14126E-01
0.28789E+04	0.17335E-01	0.14640E-01
0.28664E+04	0.18014E-01	0.15144E-01
0.28537E+04	0.18755E-01	0.15598E-01
0.28408E+04	0.19452E-01	0.16060E-01
0.28278E+04	0.20126E-01	0.16583E-01
0.28147E+04	0.20785E-01	0.17088E-01

Table F-23 (Cont'd)

p_{wf} psi	Sim. kk_{rg} md	Comp. kk_{rg} md
0.28014E+04	0.21444E-01	0.17557E-01
0.27880E+04	0.22217E-01	0.18030E-01
0.27743E+04	0.22961E-01	0.18449E-01
0.27605E+04	0.23660E-01	0.18930E-01
0.27465E+04	0.24333E-01	0.19493E-01
0.27325E+04	0.24997E-01	0.20034E-01
0.27184E+04	0.25660E-01	0.20477E-01
0.27041E+04	0.26189E-01	0.21381E-01
0.26913E+04	0.27239E-01	0.21851E-01
0.26760E+04	0.28046E-01	0.20931E-01
0.26607E+04	0.28709E-01	0.21549E-01
0.26453E+04	0.29256E-01	0.22440E-01
0.26303E+04	0.29848E-01	0.23317E-01
0.26152E+04	0.30449E-01	0.23573E-01
0.25997E+04	0.31075E-01	0.24110E-01
0.25844E+04	0.31771E-01	0.24820E-01
0.25690E+04	0.32489E-01	0.24988E-01
0.25530E+04	0.33133E-01	0.25490E-01
0.25374E+04	0.33851E-01	0.26134E-01
0.25214E+04	0.34590E-01	0.26236E-01
0.25050E+04	0.35265E-01	0.26749E-01
0.24888E+04	0.36041E-01	0.27360E-01
0.24721E+04	0.36906E-01	0.27310E-01
0.24548E+04	0.37665E-01	0.27782E-01
0.24378E+04	0.38507E-01	0.28541E-01
0.24205E+04	0.39348E-01	0.28750E-01
0.24028E+04	0.40131E-01	0.29352E-01
0.23852E+04	0.41019E-01	0.29792E-01
0.23670E+04	0.41859E-01	0.29818E-01
0.23501E+04	0.42747E-01	0.30037E-01
0.23327E+04	0.43481E-01	0.30999E-01
0.23158E+04	0.44266E-01	0.32202E-01
0.22986E+04	0.45076E-01	0.32527E-01
0.22810E+04	0.45746E-01	0.33538E-01
0.22639E+04	0.46479E-01	0.34597E-01
0.22465E+04	0.47251E-01	0.34722E-01
0.22285E+04	0.47869E-01	0.35740E-01
0.22112E+04	0.48613E-01	0.36722E-01
0.21933E+04	0.49375E-01	0.36508E-01
0.21749E+04	0.49982E-01	0.36968E-01
0.21585E+04	0.50574E-01	0.38141E-01
0.21421E+04	0.51223E-01	0.38646E-01
0.21251E+04	0.51717E-01	0.39674E-01

Table F-23 (Cont'd)

p_{wf} psi	Sim. kk_{rg} md	Comp. kk_{rg} md
0.21088E+04	0.52309E-01	0.40750E-01
0.20918E+04	0.52944E-01	0.40720E-01
0.20745E+04	0.53579E-01	0.41146E-01
0.20571E+04	0.54227E-01	0.41743E-01
0.20394E+04	0.54876E-01	0.42117E-01
0.20213E+04	0.55616E-01	0.42236E-01
0.20028E+04	0.56307E-01	0.41946E-01
0.19856E+04	0.56917E-01	0.42684E-01
0.19687E+04	0.57511E-01	0.44137E-01
0.19516E+04	0.58105E-01	0.44874E-01
0.19343E+04	0.58700E-01	0.45575E-01
0.19168E+04	0.59326E-01	0.46076E-01
0.18989E+04	0.59985E-01	0.46370E-01
0.18807E+04	0.60643E-01	0.45921E-01
0.18632E+04	0.61221E-01	0.46192E-01
0.18459E+04	0.61799E-01	0.48050E-01
0.18287E+04	0.62426E-01	0.49236E-01
0.18112E+04	0.63116E-01	0.49309E-01
0.17930E+04	0.63807E-01	0.48495E-01
0.17754E+04	0.64433E-01	0.48822E-01
0.17580E+04	0.65060E-01	0.50478E-01
0.17405E+04	0.65702E-01	0.51220E-01
0.17225E+04	0.66361E-01	0.51357E-01
0.17039E+04	0.67035E-01	0.50704E-01
0.16863E+04	0.67646E-01	0.51133E-01
0.16689E+04	0.68240E-01	0.52860E-01
0.16513E+04	0.68850E-01	0.53573E-01
0.16332E+04	0.69493E-01	0.53887E-01
0.16146E+04	0.70135E-01	0.54048E-01
0.15975E+04	0.70778E-01	0.55175E-01
0.15804E+04	0.71569E-01	0.55175E-01
0.15619E+04	0.72443E-01	0.53030E-01
0.15438E+04	0.73155E-01	0.54076E-01
0.15266E+04	0.73866E-01	0.47541E-01

Table F-24

Simulated and Computed kk_{rg} Values
Buildup Test
Case 1

p_{ws} psi	Sim. kk_{rg} md	Comp. kk_{rg} md
0.181486E+04	0.629719E-01	0.957305E-01
0.182591E+04	0.625357E-01	0.911244E-01
0.183742E+04	0.621073E-01	0.855434E-01
0.184959E+04	0.616748E-01	0.818595E-01
0.186183E+04	0.612658E-01	0.802015E-01
0.187417E+04	0.608577E-01	0.784771E-01
0.188661E+04	0.604284E-01	0.767044E-01
0.189918E+04	0.599744E-01	0.748814E-01
0.191188E+04	0.595064E-01	0.730681E-01
0.192473E+04	0.590417E-01	0.712237E-01
0.193774E+04	0.585813E-01	0.694186E-01
0.195089E+04	0.581295E-01	0.677135E-01
0.196419E+04	0.576674E-01	0.660457E-01
0.197763E+04	0.571963E-01	0.643822E-01
0.199123E+04	0.567162E-01	0.627467E-01
0.200497E+04	0.562250E-01	0.611434E-01
0.201888E+04	0.557077E-01	0.595254E-01
0.203296E+04	0.551195E-01	0.577920E-01
0.204727E+04	0.545873E-01	0.558704E-01
0.206187E+04	0.540496E-01	0.535889E-01
0.207694E+04	0.534903E-01	0.517595E-01
0.209211E+04	0.529339E-01	0.509372E-01
0.210719E+04	0.523675E-01	0.503978E-01
0.212222E+04	0.518223E-01	0.485078E-01
0.213799E+04	0.513416E-01	0.469014E-01
0.215355E+04	0.507687E-01	0.471365E-01
0.216867E+04	0.502055E-01	0.472350E-01
0.218368E+04	0.496917E-01	0.466975E-01
0.219866E+04	0.491477E-01	0.459570E-01
0.221366E+04	0.485057E-01	0.442339E-01
0.222929E+04	0.478424E-01	0.425867E-01
0.224493E+04	0.473039E-01	0.421608E-01
0.226033E+04	0.466389E-01	0.416051E-01
0.227583E+04	0.459686E-01	0.404153E-01
0.229157E+04	0.453441E-01	0.384034E-01
0.230811E+04	0.446285E-01	0.362078E-01
0.232515E+04	0.438303E-01	0.355041E-01
0.234169E+04	0.431007E-01	0.354517E-01
0.235814E+04	0.423238E-01	0.348516E-01
0.237460E+04	0.414948E-01	0.335078E-01
0.239170E+04	0.406902E-01	0.323279E-01
0.240866E+04	0.398703E-01	0.319331E-01
0.242547E+04	0.391063E-01	0.313630E-01

Table F-24 (Cont'd)

p_{wf} psi	Sim. kk_{rg} md	Comp. kk_{rg} md
0.244232E+04	0.382849E-01	0.302938E-01
0.245955E+04	0.374571E-01	0.289882E-01
0.247714E+04	0.366439E-01	0.282271E-01
0.249449E+04	0.357494E-01	0.276838E-01
0.251193E+04	0.349787E-01	0.265539E-01
0.252988E+04	0.341975E-01	0.250783E-01
0.254846E+04	0.333431E-01	0.242461E-01
0.256473E+04	0.326598E-01	0.240922E-01
0.258096E+04	0.319326E-01	0.235740E-01
0.259746E+04	0.311762E-01	0.228341E-01
0.261419E+04	0.304841E-01	0.224878E-01
0.263059E+04	0.298379E-01	0.223169E-01
0.264695E+04	0.291973E-01	0.217323E-01
0.266357E+04	0.285847E-01	0.209598E-01
0.268041E+04	0.278135E-01	0.205415E-01
0.269693E+04	0.267765E-01	0.202835E-01
0.271339E+04	0.258459E-01	0.195921E-01
0.273023E+04	0.251047E-01	0.188124E-01
0.274716E+04	0.243023E-01	0.182867E-01
0.276399E+04	0.234831E-01	0.177331E-01
0.278096E+04	0.226000E-01	0.169294E-01
0.279832E+04	0.216093E-01	0.165045E-01
0.281504E+04	0.207666E-01	0.164245E-01
0.283145E+04	0.199373E-01	0.159821E-01
0.284794E+04	0.190684E-01	0.153986E-01
0.286441E+04	0.181314E-01	0.150631E-01
0.288041E+04	0.172538E-01	0.148179E-01
0.289619E+04	0.164066E-01	0.141908E-01
0.291234E+04	0.154757E-01	0.136504E-01
0.292804E+04	0.145104E-01	0.133924E-01
0.294347E+04	0.136459E-01	0.129635E-01
0.295884E+04	0.127289E-01	0.122890E-01
0.297452E+04	0.117367E-01	0.117621E-01
0.298977E+04	0.108373E-01	0.111104E-01
0.300569E+04	0.986547E-02	0.105453E-01
0.302087E+04	0.892116E-02	0.103709E-01
0.303563E+04	0.807203E-02	0.100504E-01
0.305008E+04	0.720454E-02	0.955387E-02
0.306462E+04	0.643006E-02	0.905750E-02
0.307881E+04	0.567471E-02	0.873360E-02
0.309256E+04	0.499941E-02	0.839141E-02
0.310602E+04	0.439248E-02	0.797206E-02
0.311927E+04	0.381182E-02	0.742356E-02

Table F-24 (Cont'd)

p_{wf} psi	Sim. kk_{rg} md	Comp. kk_{rg} md
0.313268E+04	0.332313E-02	0.696625E-02
0.314551E+04	0.285750E-02	0.663789E-02
0.315804E+04	0.248064E-02	0.622221E-02
0.317032E+04	0.213978E-02	0.575317E-02
0.318251E+04	0.181517E-02	0.524836E-02
0.319459E+04	0.156950E-02	0.481267E-02
0.320624E+04	0.133550E-02	0.440643E-02
0.321767E+04	0.112566E-02	0.393983E-02
0.322898E+04	0.968051E-03	0.342675E-02
0.324035E+04	0.811802E-03	0.295477E-02
0.325134E+04	0.667080E-03	0.256348E-02
0.326182E+04	0.572858E-03	0.217214E-02
0.327192E+04	0.482959E-03	0.176039E-02
0.328168E+04	0.396960E-03	0.133422E-02
0.329118E+04	0.326922E-03	0.915717E-03
0.330047E+04	0.277823E-03	0.498758E-03
0.330931E+04	0.231960E-03	0.924979E-04
0.331781E+04	0.187677E-03	0.000000E+00
0.332599E+04	0.146106E-03	0.000000E+00
0.333386E+04	0.125224E-03	0.000000E+00
0.334151E+04	0.105283E-03	0.000000E+00
0.334884E+04	0.861380E-04	0.000000E+00
0.335580E+04	0.679177E-04	0.000000E+00
0.336244E+04	0.507999E-04	0.000000E+00
0.336878E+04	0.401854E-04	0.000000E+00
0.337482E+04	0.344554E-04	0.000000E+00
0.338058E+04	0.290233E-04	0.000000E+00
0.338611E+04	0.238000E-04	0.000000E+00
0.339129E+04	0.189471E-04	0.000000E+00

Rock and Fluid Properties for Tables F-25 through F-28

$r_w = 0.328$ ft ; $r_e = 6600$ ft

$h = 15.547$ ft ; $\phi = 0.3$

$k = k_g = 10$ md

$r_{iz} = 3.91$ ft

$q_o = 200$ STB/DAY

$s = 0.0$; $S_{gc} = 0.0$

$S_{wc} = S_{iw} = 0.3$; $S_{or} = 0.0$

$C_D = 0.0$ $(\beta^* \rightarrow \infty)$

PVT Data are given by Set 1 (Table A-1)

Inner Zone Oil Relative Permeability Data are given by Set 4 (Table A-6)

$(k_{rg})_{iz} = (k_{ro})_{iz}(k_{rg}/k_{ro})_{oz}$

Outer Zone Relative Permeability Data are given by Set 1 (Table A-2)

$p_i = p_{bi} = 3460$ psi

$c_{ti} = 0.23564 \times 10^{-4}$ psi^{-1}

$\mu_{oi} = 0.43059$ cp

$B_{oi} = 1.5882$ RB/STB

Table F-25

Simulated and Computed kk_{ro} Values
Drawdown Test
Case 1a

t days	p_{wf} psi	Sim. So	Sim. kk_{ro} md	Comp. kk_{ro} md
0.10157E-03	0.32151E+04	0.67005E+00	0.76667E+01	0.94480E+01
0.11213E-03	0.32084E+04	0.66909E+00	0.76268E+01	0.93342E+01
0.12374E-03	0.32017E+04	0.66811E+00	0.75861E+01	0.91862E+01
0.13651E-03	0.31948E+04	0.66711E+00	0.75446E+01	0.90450E+01
0.15056E-03	0.31879E+04	0.66608E+00	0.75018E+01	0.89203E+01
0.16602E-03	0.31809E+04	0.66504E+00	0.74587E+01	0.88226E+01
0.18302E-03	0.31738E+04	0.66398E+00	0.74155E+01	0.87042E+01
0.20172E-03	0.31667E+04	0.66290E+00	0.73715E+01	0.85554E+01
0.22230E-03	0.31594E+04	0.66180E+00	0.73267E+01	0.84203E+01
0.24493E-03	0.31520E+04	0.66067E+00	0.72807E+01	0.83034E+01
0.26982E-03	0.31445E+04	0.65953E+00	0.72347E+01	0.81880E+01
0.29720E-03	0.31369E+04	0.65837E+00	0.71884E+01	0.80457E+01
0.32732E-03	0.31292E+04	0.65718E+00	0.71409E+01	0.78945E+01
0.36045E-03	0.31213E+04	0.65598E+00	0.70931E+01	0.77575E+01
0.39690E-03	0.31133E+04	0.65476E+00	0.70446E+01	0.76306E+01
0.43699E-03	0.31052E+04	0.65352E+00	0.69961E+01	0.74866E+01
0.48109E-03	0.30968E+04	0.65227E+00	0.69473E+01	0.73280E+01
0.52959E-03	0.30883E+04	0.65101E+00	0.68980E+01	0.71812E+01
0.58295E-03	0.30797E+04	0.64974E+00	0.68485E+01	0.70468E+01
0.64165E-03	0.30709E+04	0.64847E+00	0.67999E+01	0.69047E+01
0.70621E-03	0.30618E+04	0.64719E+00	0.67509E+01	0.67532E+01
0.77724E-03	0.30526E+04	0.64591E+00	0.67019E+01	0.66133E+01
0.85536E-03	0.30432E+04	0.64464E+00	0.66536E+01	0.64846E+01
0.94130E-03	0.30336E+04	0.64339E+00	0.66067E+01	0.63534E+01
0.10358E-02	0.30238E+04	0.64214E+00	0.65598E+01	0.62191E+01
0.11398E-02	0.30138E+04	0.64091E+00	0.65136E+01	0.60979E+01
0.12542E-02	0.30035E+04	0.63971E+00	0.64688E+01	0.59908E+01
0.13800E-02	0.29931E+04	0.63852E+00	0.64251E+01	0.58744E+01
0.15184E-02	0.29825E+04	0.63736E+00	0.63825E+01	0.57588E+01
0.16706E-02	0.29716E+04	0.63624E+00	0.63414E+01	0.56646E+01
0.18381E-02	0.29606E+04	0.63516E+00	0.63017E+01	0.55924E+01
0.20223E-02	0.29495E+04	0.63408E+00	0.62627E+01	0.55023E+01
0.22250E-02	0.29381E+04	0.63302E+00	0.62246E+01	0.54006E+01
0.24479E-02	0.29264E+04	0.63201E+00	0.61883E+01	0.53211E+01
0.26930E-02	0.29147E+04	0.63106E+00	0.61541E+01	0.52682E+01
0.29627E-02	0.29028E+04	0.63011E+00	0.61200E+01	0.52213E+01
0.32594E-02	0.28908E+04	0.62914E+00	0.60857E+01	0.51330E+01
0.35858E-02	0.28785E+04	0.62823E+00	0.60537E+01	0.50510E+01
0.39447E-02	0.28660E+04	0.62736E+00	0.60230E+01	0.50092E+01
0.43396E-02	0.28535E+04	0.62651E+00	0.59931E+01	0.49701E+01
0.47740E-02	0.28408E+04	0.62567E+00	0.59635E+01	0.49218E+01
0.52518E-02	0.28280E+04	0.62484E+00	0.59344E+01	0.48760E+01
0.57773E-02	0.28150E+04	0.62401E+00	0.59058E+01	0.48155E+01

Table F-25 (Cont'd)

t days	p_{wf} psi	Sim. So	Sim. kk_{ro} md	Comp. kk_{ro} md
0.63555E-02	0.28018E+04	0.62323E+00	0.58789E+01	0.47514E+01
0.69914E-02	0.27885E+04	0.62247E+00	0.58527E+01	0.47216E+01
0.76910E-02	0.27751E+04	0.62173E+00	0.58272E+01	0.46990E+01
0.84605E-02	0.27616E+04	0.62100E+00	0.58020E+01	0.46625E+01
0.93069E-02	0.27479E+04	0.62026E+00	0.57765E+01	0.46210E+01
0.10238E-01	0.27341E+04	0.61953E+00	0.57516E+01	0.45716E+01
0.11262E-01	0.27202E+04	0.61881E+00	0.57273E+01	0.45174E+01
0.12389E-01	0.27060E+04	0.61813E+00	0.57044E+01	0.44765E+01
0.13628E-01	0.26917E+04	0.61747E+00	0.56821E+01	0.44652E+01
0.14991E-01	0.26774E+04	0.61682E+00	0.56602E+01	0.44501E+01
0.16491E-01	0.26629E+04	0.61616E+00	0.56379E+01	0.44064E+01
0.18140E-01	0.26483E+04	0.61550E+00	0.56157E+01	0.43794E+01
0.19955E-01	0.26336E+04	0.61484E+00	0.55936E+01	0.43539E+01
0.21951E-01	0.26187E+04	0.61418E+00	0.55720E+01	0.42710E+01
0.24146E-01	0.26034E+04	0.61358E+00	0.55524E+01	0.42232E+01
0.26561E-01	0.25881E+04	0.61300E+00	0.55335E+01	0.42350E+01
0.29218E-01	0.25728E+04	0.61242E+00	0.55145E+01	0.42190E+01
0.32140E-01	0.25574E+04	0.61183E+00	0.54952E+01	0.41887E+01
0.35354E-01	0.25418E+04	0.61124E+00	0.54760E+01	0.41641E+01
0.38890E-01	0.25261E+04	0.61065E+00	0.54567E+01	0.41308E+01
0.42779E-01	0.25102E+04	0.61006E+00	0.54374E+01	0.40998E+01
0.47058E-01	0.24942E+04	0.60946E+00	0.54178E+01	0.40781E+01
0.51764E-01	0.24781E+04	0.60886E+00	0.53982E+01	0.40462E+01
0.56941E-01	0.24617E+04	0.60825E+00	0.53783E+01	0.40151E+01
0.62635E-01	0.24452E+04	0.60765E+00	0.53587E+01	0.39967E+01
0.68899E-01	0.24286E+04	0.60704E+00	0.53387E+01	0.39726E+01
0.75789E-01	0.24119E+04	0.60644E+00	0.53191E+01	0.39452E+01
0.83369E-01	0.23950E+04	0.60584E+00	0.52995E+01	0.39256E+01
0.91706E-01	0.23780E+04	0.60526E+00	0.52806E+01	0.39166E+01
0.10088E+00	0.23609E+04	0.60467E+00	0.52617E+01	0.38810E+01
0.11097E+00	0.23435E+04	0.60411E+00	0.52440E+01	0.38277E+01
0.12206E+00	0.23258E+04	0.60361E+00	0.52282E+01	0.38349E+01
0.13427E+00	0.23084E+04	0.60313E+00	0.52130E+01	0.38767E+01
0.14770E+00	0.22911E+04	0.60264E+00	0.51975E+01	0.38734E+01
0.16247E+00	0.22735E+04	0.60216E+00	0.51824E+01	0.38547E+01
0.17871E+00	0.22558E+04	0.60169E+00	0.51675E+01	0.38672E+01
0.19658E+00	0.22383E+04	0.60121E+00	0.51523E+01	0.38635E+01
0.21624E+00	0.22205E+04	0.60073E+00	0.51372E+01	0.38375E+01
0.23787E+00	0.22026E+04	0.60027E+00	0.51226E+01	0.38304E+01
0.26166E+00	0.21846E+04	0.59979E+00	0.51076E+01	0.38091E+01
0.28782E+00	0.21663E+04	0.59933E+00	0.50934E+01	0.37225E+01
0.31389E+00	0.21491E+04	0.59893E+00	0.50810E+01	0.37097E+01
0.34256E+00	0.21322E+04	0.59854E+00	0.50690E+01	0.37720E+01

Table F-25 (Cont'd)

t days	p_{wf} psi	Sim. So	Sim. kk_{ro} md	Comp. kk_{ro} md
0.37410E+00	0.21151E+04	0.59816E+00	0.50572E+01	0.37893E+01
0.40879E+00	0.20980E+04	0.59777E+00	0.50452E+01	0.38034E+01
0.44695E+00	0.20807E+04	0.59737E+00	0.50328E+01	0.37982E+01
0.48893E+00	0.20633E+04	0.59695E+00	0.50199E+01	0.37693E+01
0.53511E+00	0.20454E+04	0.59652E+00	0.50066E+01	0.37451E+01
0.58591E+00	0.20274E+04	0.59609E+00	0.49933E+01	0.37428E+01
0.64178E+00	0.20092E+04	0.59565E+00	0.49797E+01	0.37351E+01
0.70324E+00	0.19908E+04	0.59521E+00	0.49661E+01	0.36472E+01
0.76394E+00	0.19733E+04	0.59481E+00	0.49539E+01	0.35948E+01
0.83072E+00	0.19559E+04	0.59444E+00	0.49427E+01	0.36529E+01
0.90417E+00	0.19384E+04	0.59408E+00	0.49318E+01	0.36957E+01
0.98496E+00	0.19209E+04	0.59371E+00	0.49206E+01	0.36914E+01
0.10738E+01	0.19029E+04	0.59333E+00	0.49091E+01	0.36633E+01
0.11716E+01	0.18846E+04	0.59295E+00	0.48976E+01	0.36071E+01
0.12688E+01	0.18674E+04	0.59260E+00	0.48871E+01	0.35951E+01
0.13758E+01	0.18502E+04	0.59225E+00	0.48765E+01	0.36605E+01
0.14934E+01	0.18329E+04	0.59188E+00	0.48653E+01	0.36917E+01
0.16228E+01	0.18154E+04	0.59149E+00	0.48535E+01	0.36631E+01
0.17652E+01	0.17973E+04	0.59109E+00	0.48414E+01	0.36370E+01
0.19218E+01	0.17790E+04	0.59067E+00	0.48287E+01	0.35673E+01
0.20771E+01	0.17614E+04	0.59028E+00	0.48170E+01	0.35239E+01
0.22480E+01	0.17438E+04	0.58990E+00	0.48056E+01	0.35439E+01
0.24360E+01	0.17257E+04	0.58952E+00	0.47945E+01	0.35106E+01
0.26427E+01	0.17070E+04	0.58918E+00	0.47845E+01	0.34802E+01
0.28443E+01	0.16899E+04	0.58886E+00	0.47752E+01	0.34986E+01
0.30659E+01	0.16728E+04	0.58854E+00	0.47658E+01	0.35532E+01
0.33098E+01	0.16554E+04	0.58821E+00	0.47562E+01	0.35543E+01
0.35780E+01	0.16375E+04	0.58788E+00	0.47466E+01	0.35589E+01
0.38730E+01	0.16194E+04	0.58754E+00	0.47366E+01	0.35918E+01
0.41976E+01	0.16011E+04	0.58716E+00	0.47255E+01	0.35770E+01
0.45194E+01	0.15839E+04	0.58676E+00	0.47138E+01	0.35029E+01
0.48734E+01	0.15658E+04	0.58637E+00	0.47024E+01	0.30224E+01

Table F-26

Simulated and Computed kk_{ro} Values
Buildup Test
Case 1a

Δt days	p_{ws} psi	DD Sim. So	Sim. kk_{ro} md	Comp. kk_{ro} md
0.101569E-03	0.184232E+04	0.592081E+00	0.487140E+01	0.696349E+01
0.112126E-03	0.185353E+04	0.592318E+00	0.487855E+01	0.678437E+01
0.123738E-03	0.186481E+04	0.592548E+00	0.488550E+01	0.669331E+01
0.136512E-03	0.187620E+04	0.592779E+00	0.489249E+01	0.659007E+01
0.150563E-03	0.188772E+04	0.593014E+00	0.489959E+01	0.648138E+01
0.166020E-03	0.189938E+04	0.593257E+00	0.490692E+01	0.637119E+01
0.183022E-03	0.191118E+04	0.593505E+00	0.491442E+01	0.626097E+01
0.201724E-03	0.192315E+04	0.593758E+00	0.492206E+01	0.615358E+01
0.222296E-03	0.193526E+04	0.594013E+00	0.492978E+01	0.605007E+01
0.244926E-03	0.194753E+04	0.594268E+00	0.493747E+01	0.594992E+01
0.269818E-03	0.195995E+04	0.594526E+00	0.494528E+01	0.585337E+01
0.297200E-03	0.197252E+04	0.594793E+00	0.495333E+01	0.575973E+01
0.327320E-03	0.198524E+04	0.595082E+00	0.496214E+01	0.566946E+01
0.360452E-03	0.199812E+04	0.595384E+00	0.497147E+01	0.557933E+01
0.396898E-03	0.201115E+04	0.595696E+00	0.498112E+01	0.548749E+01
0.436987E-03	0.202436E+04	0.596016E+00	0.499101E+01	0.539291E+01
0.481086E-03	0.203775E+04	0.596337E+00	0.500091E+01	0.529179E+01
0.529595E-03	0.205136E+04	0.596663E+00	0.501099E+01	0.517149E+01
0.582954E-03	0.206528E+04	0.596999E+00	0.502136E+01	0.501591E+01
0.641650E-03	0.207964E+04	0.597344E+00	0.503201E+01	0.492041E+01
0.706215E-03	0.209401E+04	0.597678E+00	0.504234E+01	0.491337E+01
0.777236E-03	0.210832E+04	0.598005E+00	0.505246E+01	0.491494E+01
0.855360E-03	0.212259E+04	0.598327E+00	0.506240E+01	0.480260E+01
0.941296E-03	0.213748E+04	0.598663E+00	0.507278E+01	0.467685E+01
0.103583E-02	0.215245E+04	0.599008E+00	0.508345E+01	0.473359E+01
0.113981E-02	0.216690E+04	0.599344E+00	0.509384E+01	0.482309E+01
0.125419E-02	0.218124E+04	0.599706E+00	0.510501E+01	0.483148E+01
0.138001E-02	0.219555E+04	0.600083E+00	0.511672E+01	0.481908E+01
0.151841E-02	0.220988E+04	0.600458E+00	0.512858E+01	0.467876E+01
0.167065E-02	0.222497E+04	0.600851E+00	0.514100E+01	0.457428E+01
0.183811E-02	0.223988E+04	0.601254E+00	0.515373E+01	0.461783E+01
0.202233E-02	0.225460E+04	0.601656E+00	0.516643E+01	0.462174E+01
0.222496E-02	0.226940E+04	0.602051E+00	0.517892E+01	0.456429E+01
0.244785E-02	0.228439E+04	0.602458E+00	0.519178E+01	0.440892E+01
0.269304E-02	0.230015E+04	0.602897E+00	0.520565E+01	0.420604E+01
0.296274E-02	0.231653E+04	0.603354E+00	0.522008E+01	0.416944E+01
0.325942E-02	0.233248E+04	0.603798E+00	0.523413E+01	0.422289E+01
0.358576E-02	0.234837E+04	0.604267E+00	0.524895E+01	0.421667E+01
0.394473E-02	0.236429E+04	0.604787E+00	0.526538E+01	0.409740E+01
0.433961E-02	0.238102E+04	0.605364E+00	0.528400E+01	0.403005E+01
0.477397E-02	0.239740E+04	0.605926E+00	0.530235E+01	0.407164E+01
0.525177E-02	0.241371E+04	0.606505E+00	0.532128E+01	0.406080E+01
0.577734E-02	0.243009E+04	0.607093E+00	0.534048E+01	0.396077E+01

Table F-26 (Cont'd)

Δt days	p_{ws} psi	DD Sim. So	Sim. kk_{ro} md	Comp. kk_{ro} md
0.635548E-02	0.244714E+04	0.607719E+00	0.536094E+01	0.387580E+01
0.699142E-02	0.246415E+04	0.608341E+00	0.538125E+01	0.388306E+01
0.769097E-02	0.248104E+04	0.608971E+00	0.540182E+01	0.387474E+01
0.846046E-02	0.249803E+04	0.609603E+00	0.542249E+01	0.376351E+01
0.930691E-02	0.251582E+04	0.610268E+00	0.544420E+01	0.366717E+01
0.102380E-01	0.253361E+04	0.610932E+00	0.546590E+01	0.364829E+01
0.112622E-01	0.255147E+04	0.611606E+00	0.548793E+01	0.363759E+01
0.123888E-01	0.256929E+04	0.612285E+00	0.551010E+01	0.358700E+01
0.136281E-01	0.258756E+04	0.612979E+00	0.553278E+01	0.358157E+01
0.148612E-01	0.260369E+04	0.613592E+00	0.555280E+01	0.364941E+01
0.162176E-01	0.261977E+04	0.614227E+00	0.557355E+01	0.363705E+01
0.177096E-01	0.263619E+04	0.614957E+00	0.559740E+01	0.359607E+01
0.193508E-01	0.265280E+04	0.615704E+00	0.562256E+01	0.362639E+01
0.211562E-01	0.266908E+04	0.616442E+00	0.564744E+01	0.368120E+01
0.231421E-01	0.268532E+04	0.617181E+00	0.567240E+01	0.363379E+01
0.253266E-01	0.270213E+04	0.617953E+00	0.569842E+01	0.360479E+01
0.277295E-01	0.271871E+04	0.618741E+00	0.572501E+01	0.365474E+01
0.303727E-01	0.273513E+04	0.619582E+00	0.575340E+01	0.365203E+01
0.332803E-01	0.275179E+04	0.620469E+00	0.578366E+01	0.356164E+01
0.364786E-01	0.276908E+04	0.621405E+00	0.581596E+01	0.353856E+01
0.399967E-01	0.278598E+04	0.622332E+00	0.584791E+01	0.361553E+01
0.438667E-01	0.280258E+04	0.623275E+00	0.588042E+01	0.359861E+01
0.481236E-01	0.281965E+04	0.624308E+00	0.591603E+01	0.361491E+01
0.528063E-01	0.283609E+04	0.625366E+00	0.595281E+01	0.372010E+01
0.579572E-01	0.285221E+04	0.626427E+00	0.599016E+01	0.373043E+01
0.636232E-01	0.286855E+04	0.627537E+00	0.602926E+01	0.371635E+01
0.698557E-01	0.288476E+04	0.628696E+00	0.607006E+01	0.378116E+01
0.767116E-01	0.290050E+04	0.629925E+00	0.611336E+01	0.385878E+01
0.842530E-01	0.291603E+04	0.631170E+00	0.615807E+01	0.381287E+01
0.925486E-01	0.293209E+04	0.632501E+00	0.620594E+01	0.381216E+01
0.101674E+00	0.294756E+04	0.633903E+00	0.625635E+01	0.390956E+01
0.111711E+00	0.296276E+04	0.635370E+00	0.630940E+01	0.394922E+01
0.122753E+00	0.297785E+04	0.636880E+00	0.636489E+01	0.393310E+01
0.134898E+00	0.299309E+04	0.638515E+00	0.642494E+01	0.384629E+01
0.148258E+00	0.300876E+04	0.640323E+00	0.649160E+01	0.386323E+01
0.162955E+00	0.302377E+04	0.642137E+00	0.655968E+01	0.398412E+01
0.179120E+00	0.303840E+04	0.644014E+00	0.663012E+01	0.406062E+01
0.196903E+00	0.305275E+04	0.645927E+00	0.670260E+01	0.405214E+01
0.216463E+00	0.306733E+04	0.647967E+00	0.678069E+01	0.407944E+01
0.237980E+00	0.308135E+04	0.649983E+00	0.685786E+01	0.419474E+01
0.261648E+00	0.309501E+04	0.651998E+00	0.693662E+01	0.427031E+01
0.287683E+00	0.310840E+04	0.654014E+00	0.701544E+01	0.430331E+01
0.316322E+00	0.312169E+04	0.656040E+00	0.709548E+01	0.429598E+01

Table F-26 (Cont'd)

Δt days	p_{ws} psi	DD Sim. So	Sim. kk_{ro} md	Comp. kk_{ro} md
0.347824E+00	0.313496E+04	0.658070E+00	0.717643E+01	0.435455E+01
0.382477E+00	0.314772E+04	0.660021E+00	0.725425E+01	0.445848E+01
0.420595E+00	0.316020E+04	0.661924E+00	0.733176E+01	0.451910E+01
0.462524E+00	0.317242E+04	0.663767E+00	0.740681E+01	0.452665E+01
0.508647E+00	0.318465E+04	0.665597E+00	0.748178E+01	0.453154E+01
0.559382E+00	0.319662E+04	0.667372E+00	0.755547E+01	0.460383E+01
0.615191E+00	0.320822E+04	0.669062E+00	0.762563E+01	0.467000E+01
0.676580E+00	0.321961E+04	0.670693E+00	0.769394E+01	0.467400E+01
0.744108E+00	0.323092E+04	0.672294E+00	0.776177E+01	0.461873E+01
0.818389E+00	0.324228E+04	0.673877E+00	0.782885E+01	0.464664E+01
0.900099E+00	0.325316E+04	0.675385E+00	0.789305E+01	0.478654E+01
0.989979E+00	0.326356E+04	0.676798E+00	0.795410E+01	0.490415E+01
0.108885E+01	0.327360E+04	0.678152E+00	0.801265E+01	0.499243E+01
0.119760E+01	0.328330E+04	0.679452E+00	0.806880E+01	0.503199E+01
0.131723E+01	0.329280E+04	0.680705E+00	0.812357E+01	0.510801E+01
0.144883E+01	0.330199E+04	0.681919E+00	0.817705E+01	0.516866E+01
0.159358E+01	0.331077E+04	0.683055E+00	0.822710E+01	0.527285E+01
0.175281E+01	0.331921E+04	0.684155E+00	0.827559E+01	0.534710E+01
0.192796E+01	0.332734E+04	0.685196E+00	0.832163E+01	0.541386E+01
0.212062E+01	0.333515E+04	0.686201E+00	0.836676E+01	0.543180E+01
0.233256E+01	0.334279E+04	0.687164E+00	0.841003E+01	0.547244E+01
0.256568E+01	0.335004E+04	0.688085E+00	0.845142E+01	0.557528E+01
0.282212E+01	0.335694E+04	0.688960E+00	0.849076E+01	0.565308E+01
0.310420E+01	0.336353E+04	0.689782E+00	0.852769E+01	0.571464E+01
0.341449E+01	0.336982E+04	0.690569E+00	0.856357E+01	0.577171E+01
0.375581E+01	0.337581E+04	0.691313E+00	0.859764E+01	0.580939E+01
0.413127E+01	0.338153E+04	0.692023E+00	0.863017E+01	0.582691E+01
0.454426E+01	0.338700E+04	0.692700E+00	0.866117E+01	0.588765E+01
0.499856E+01	0.339213E+04	0.693331E+00	0.869007E+01	0.594037E+01

Table F-27

Simulated and Computed kk_{rg} Values
Drawdown Test
Case 1a

p_{wf} psi	Sim. kk_{rg} md	Comp. kk_{rg} md
0.32151E+04	0.14010E-02	0.17262E-02
0.32084E+04	0.15570E-02	0.19055E-02
0.32017E+04	0.17186E-02	0.20816E-02
0.31948E+04	0.18836E-02	0.22592E-02
0.31879E+04	0.20535E-02	0.24412E-02
0.31809E+04	0.22250E-02	0.26313E-02
0.31738E+04	0.24551E-02	0.28807E-02
0.31667E+04	0.26918E-02	0.31238E-02
0.31594E+04	0.29328E-02	0.33714E-02
0.31520E+04	0.31804E-02	0.36265E-02
0.31445E+04	0.34593E-02	0.39148E-02
0.31369E+04	0.37852E-02	0.42377E-02
0.31292E+04	0.41195E-02	0.45537E-02
0.31213E+04	0.44567E-02	0.48750E-02
0.31133E+04	0.48161E-02	0.52181E-02
0.31052E+04	0.52505E-02	0.56176E-02
0.30968E+04	0.56884E-02	0.59990E-02
0.30883E+04	0.61299E-02	0.63813E-02
0.30797E+04	0.65948E-02	0.67864E-02
0.30709E+04	0.71374E-02	0.72493E-02
0.30618E+04	0.76843E-02	0.76867E-02
0.30526E+04	0.82312E-02	0.81201E-02
0.30432E+04	0.88042E-02	0.85784E-02
0.30336E+04	0.94437E-02	0.90829E-02
0.30238E+04	0.10083E-01	0.95575E-02
0.30138E+04	0.10712E-01	0.10026E-01
0.30035E+04	0.11353E-01	0.10513E-01
0.29931E+04	0.12071E-01	0.11034E-01
0.29825E+04	0.12772E-01	0.11520E-01
0.29716E+04	0.13448E-01	0.12014E-01
0.29606E+04	0.14099E-01	0.12514E-01
0.29495E+04	0.14843E-01	0.13042E-01
0.29381E+04	0.15588E-01	0.13522E-01
0.29264E+04	0.16298E-01	0.14011E-01
0.29147E+04	0.16966E-01	0.14526E-01
0.29028E+04	0.17634E-01	0.15046E-01
0.28908E+04	0.18407E-01	0.15526E-01
0.28785E+04	0.19144E-01	0.15976E-01
0.28660E+04	0.19849E-01	0.16504E-01
0.28535E+04	0.20537E-01	0.17029E-01
0.28408E+04	0.21217E-01	0.17510E-01
0.28280E+04	0.21908E-01	0.17997E-01
0.28150E+04	0.22675E-01	0.18484E-01

Table F-27 (Cont'd)

p_{wf} psi	Sim. kk_{rg} md	Comp. kk_{rg} md
0.28018E+04	0.23395E-01	0.18911E-01
0.27885E+04	0.24097E-01	0.19438E-01
0.27751E+04	0.24781E-01	0.19982E-01
0.27616E+04	0.25455E-01	0.20458E-01
0.27479E+04	0.26139E-01	0.20912E-01
0.27341E+04	0.26870E-01	0.21362E-01
0.27202E+04	0.27623E-01	0.21784E-01
0.27060E+04	0.28334E-01	0.22237E-01
0.26917E+04	0.29024E-01	0.22804E-01
0.26774E+04	0.29703E-01	0.23352E-01
0.26629E+04	0.30393E-01	0.23758E-01
0.26483E+04	0.31083E-01	0.24239E-01
0.26336E+04	0.31805E-01	0.24751E-01
0.26187E+04	0.32625E-01	0.25009E-01
0.26034E+04	0.33370E-01	0.25385E-01
0.25881E+04	0.34091E-01	0.26093E-01
0.25728E+04	0.34811E-01	0.26638E-01
0.25574E+04	0.35544E-01	0.27090E-01
0.25418E+04	0.36277E-01	0.27581E-01
0.25261E+04	0.37010E-01	0.28018E-01
0.25102E+04	0.37743E-01	0.28460E-01
0.24942E+04	0.38488E-01	0.28970E-01
0.24781E+04	0.39234E-01	0.29413E-01
0.24617E+04	0.39992E-01	0.29852E-01
0.24452E+04	0.40737E-01	0.30386E-01
0.24286E+04	0.41495E-01	0.30873E-01
0.24119E+04	0.42240E-01	0.31324E-01
0.23950E+04	0.42985E-01	0.31838E-01
0.23780E+04	0.43706E-01	0.32422E-01
0.23609E+04	0.44509E-01	0.32826E-01
0.23435E+04	0.45323E-01	0.33076E-01
0.23258E+04	0.46050E-01	0.33774E-01
0.23084E+04	0.46748E-01	0.34761E-01
0.22911E+04	0.47460E-01	0.35368E-01
0.22735E+04	0.48158E-01	0.35820E-01
0.22558E+04	0.48842E-01	0.36550E-01
0.22383E+04	0.49540E-01	0.37148E-01
0.22205E+04	0.50238E-01	0.37521E-01
0.22026E+04	0.50906E-01	0.38071E-01
0.21846E+04	0.51636E-01	0.38513E-01
0.21663E+04	0.52374E-01	0.38283E-01
0.21491E+04	0.53016E-01	0.38706E-01
0.21322E+04	0.53642E-01	0.39917E-01

Table F-27 (Cont'd)

p_{wf} psi	Sim. kk_{rg} md	Comp. kk_{rg} md
0.21151E+04	0.54251E-01	0.40654E-01
0.20980E+04	0.54877E-01	0.41371E-01
0.20807E+04	0.55519E-01	0.41901E-01
0.20633E+04	0.56193E-01	0.42202E-01
0.20454E+04	0.56883E-01	0.42554E-01
0.20274E+04	0.57573E-01	0.43156E-01
0.20092E+04	0.58279E-01	0.43710E-01
0.19908E+04	0.58985E-01	0.43316E-01
0.19733E+04	0.59657E-01	0.43286E-01
0.19559E+04	0.60309E-01	0.44564E-01
0.19384E+04	0.60944E-01	0.45661E-01
0.19209E+04	0.61596E-01	0.46209E-01
0.19029E+04	0.62266E-01	0.46469E-01
0.18846E+04	0.62935E-01	0.46352E-01
0.18674E+04	0.63552E-01	0.46751E-01
0.18502E+04	0.64169E-01	0.48162E-01
0.18329E+04	0.64821E-01	0.49178E-01
0.18154E+04	0.65509E-01	0.49446E-01
0.17973E+04	0.66214E-01	0.49747E-01
0.17790E+04	0.66954E-01	0.49466E-01
0.17614E+04	0.67641E-01	0.49480E-01
0.17438E+04	0.68336E-01	0.50394E-01
0.17257E+04	0.69102E-01	0.50593E-01
0.17070E+04	0.69786E-01	0.50769E-01
0.16899E+04	0.70431E-01	0.51607E-01
0.16728E+04	0.71075E-01	0.52991E-01
0.16554E+04	0.71740E-01	0.53617E-01
0.16375E+04	0.72404E-01	0.54292E-01
0.16194E+04	0.73089E-01	0.55430E-01
0.16011E+04	0.73854E-01	0.55903E-01
0.15839E+04	0.74659E-01	0.55473E-01
0.15658E+04	0.75445E-01	0.48484E-01

Table F-28

Simulated and Computed kk_{rg} Values
Buildup Test
Case 1a

p_{ws} psi	Sim. kk_{rg} md	Comp. kk_{rg} md
0.184232E+04	0.644665E-01	0.921512E-01
0.185353E+04	0.640490E-01	0.890895E-01
0.186481E+04	0.636442E-01	0.872061E-01
0.187620E+04	0.632365E-01	0.851767E-01
0.188772E+04	0.628219E-01	0.830902E-01
0.189938E+04	0.623947E-01	0.809985E-01
0.191118E+04	0.619569E-01	0.789204E-01
0.192315E+04	0.615113E-01	0.768918E-01
0.193526E+04	0.610612E-01	0.749256E-01
0.194753E+04	0.606127E-01	0.730143E-01
0.195995E+04	0.601572E-01	0.711604E-01
0.197252E+04	0.596877E-01	0.693546E-01
0.198524E+04	0.591900E-01	0.676020E-01
0.199812E+04	0.587054E-01	0.658638E-01
0.201115E+04	0.582045E-01	0.641180E-01
0.202436E+04	0.576911E-01	0.623536E-01
0.203775E+04	0.571767E-01	0.605274E-01
0.205136E+04	0.566534E-01	0.584983E-01
0.206528E+04	0.561150E-01	0.560900E-01
0.207964E+04	0.555616E-01	0.543852E-01
0.209401E+04	0.550254E-01	0.536802E-01
0.210832E+04	0.544997E-01	0.530721E-01
0.212259E+04	0.539838E-01	0.512490E-01
0.213748E+04	0.534448E-01	0.492867E-01
0.215245E+04	0.528907E-01	0.492533E-01
0.216690E+04	0.523512E-01	0.495631E-01
0.218124E+04	0.517713E-01	0.490310E-01
0.219555E+04	0.511783E-01	0.482893E-01
0.220988E+04	0.506329E-01	0.462842E-01
0.222497E+04	0.500615E-01	0.446337E-01
0.223988E+04	0.494754E-01	0.444428E-01
0.225460E+04	0.488912E-01	0.438719E-01
0.226940E+04	0.483164E-01	0.427219E-01
0.228439E+04	0.477248E-01	0.406756E-01
0.230015E+04	0.470867E-01	0.382103E-01
0.231653E+04	0.464226E-01	0.372707E-01
0.233248E+04	0.457762E-01	0.371500E-01
0.234837E+04	0.450942E-01	0.364999E-01
0.236429E+04	0.443380E-01	0.348878E-01
0.238102E+04	0.435763E-01	0.337148E-01
0.239740E+04	0.428786E-01	0.334700E-01
0.241371E+04	0.421588E-01	0.327921E-01
0.243009E+04	0.414287E-01	0.314075E-01

Table F-28 (Cont'd)

p_{w_s} psi	Sim. kk_{rg} md	Comp. kk_{rg} md
0.244714E+04	0.406508E-01	0.301464E-01
0.246415E+04	0.398783E-01	0.296155E-01
0.248104E+04	0.390963E-01	0.289704E-01
0.249803E+04	0.383102E-01	0.275704E-01
0.251582E+04	0.374848E-01	0.262850E-01
0.253361E+04	0.366595E-01	0.255727E-01
0.255147E+04	0.358219E-01	0.249157E-01
0.256929E+04	0.349789E-01	0.239967E-01
0.258756E+04	0.341166E-01	0.233744E-01
0.260369E+04	0.333554E-01	0.232902E-01
0.261977E+04	0.325662E-01	0.226882E-01
0.263619E+04	0.316591E-01	0.219042E-01
0.265280E+04	0.308699E-01	0.215504E-01
0.266908E+04	0.300988E-01	0.213403E-01
0.268532E+04	0.293257E-01	0.205383E-01
0.270213E+04	0.285194E-01	0.198332E-01
0.271871E+04	0.276954E-01	0.195671E-01
0.273513E+04	0.268158E-01	0.190176E-01
0.275179E+04	0.259461E-01	0.180178E-01
0.276908E+04	0.250807E-01	0.173534E-01
0.278598E+04	0.242245E-01	0.171772E-01
0.280258E+04	0.233537E-01	0.165562E-01
0.281965E+04	0.223995E-01	0.160727E-01
0.283609E+04	0.214633E-01	0.159875E-01
0.285221E+04	0.206043E-01	0.154886E-01
0.286855E+04	0.197054E-01	0.148821E-01
0.288476E+04	0.187672E-01	0.145885E-01
0.290050E+04	0.177718E-01	0.143404E-01
0.291603E+04	0.168886E-01	0.136364E-01
0.293209E+04	0.159527E-01	0.130826E-01
0.294756E+04	0.149672E-01	0.128729E-01
0.296276E+04	0.139726E-01	0.124635E-01
0.297785E+04	0.130610E-01	0.118797E-01
0.299309E+04	0.120743E-01	0.110911E-01
0.300876E+04	0.110130E-01	0.105896E-01
0.302377E+04	0.100847E-01	0.103755E-01
0.303840E+04	0.912423E-02	0.100331E-01
0.305275E+04	0.822378E-02	0.948294E-02
0.306733E+04	0.735220E-02	0.900577E-02
0.308135E+04	0.649088E-02	0.872568E-02
0.309501E+04	0.578376E-02	0.835318E-02
0.310840E+04	0.507747E-02	0.789487E-02
0.312169E+04	0.443975E-02	0.736345E-02

Table F-28 (Cont'd)

p_{ws} . psi	Sim. kk_{rg} md	Comp. kk_{rg} md
0.313496E+04	0.386944E-02	0.694037E-02
0.314772E+04	0.332261E-02	0.659088E-02
0.316020E+04	0.290552E-02	0.617046E-02
0.317242E+04	0.250169E-02	0.568044E-02
0.318465E+04	0.213315E-02	0.518623E-02
0.319662E+04	0.184043E-02	0.477138E-02
0.320822E+04	0.156169E-02	0.435114E-02
0.321961E+04	0.132492E-02	0.387511E-02
0.323092E+04	0.113542E-02	0.335839E-02
0.324228E+04	0.947991E-03	0.290253E-02
0.325316E+04	0.784523E-03	0.252099E-02
0.326356E+04	0.672285E-03	0.212355E-02
0.327360E+04	0.564649E-03	0.171078E-02
0.328330E+04	0.461411E-03	0.128520E-02
0.329280E+04	0.383802E-03	0.868537E-03
0.330199E+04	0.325208E-03	0.451853E-03
0.331077E+04	0.270381E-03	0.454637E-04
0.331921E+04	0.217257E-03	0.000000E+00
0.332734E+04	0.171614E-03	0.000000E+00
0.333515E+04	0.146680E-03	0.000000E+00
0.334279E+04	0.122774E-03	0.000000E+00
0.335004E+04	0.999081E-04	0.000000E+00
0.335694E+04	0.781759E-04	0.000000E+00
0.336353E+04	0.577711E-04	0.000000E+00
0.336982E+04	0.471405E-04	0.000000E+00
0.337581E+04	0.403264E-04	0.000000E+00
0.338153E+04	0.338189E-04	0.000000E+00
0.338700E+04	0.276182E-04	0.000000E+00
0.339213E+04	0.218390E-04	0.000000E+00

Rock and Fluid Properties for Tables F-29 through F-32

$r_w = 0.328$ ft ; $r_e = 6600$ ft

$h = 15.547$ ft ; $\phi = 0.3$

$k = 10$ md ; $k_s = 3.313$ md

$r_{iz} = 3.91$ ft

$q_o = 50$ STB/DAY

$s = 5.0$; $S_{gc} = 0.0$

$S_{wc} = S_{iw} = 0.3$; $S_{or} = 0.0$

$C_D = 0.0$ $(\beta^* \rightarrow \infty)$

PVT Data are given by Set 1 (Table A-1)

Inner Zone Relative Permeability Data are given by Set 4 (Table A-6)

Outer Zone Relative Permeability Data are given by Set 1 (Table A-2)

$p_i = p_{bi} = 3460$ psi

$c_{ti} = 0.23564 \times 10^{-4}$ psi^{-1}

$\mu_{oi} = 0.43059$ cp

$B_{oi} = 1.5882$ RB/STB

Table F-29

Simulated and Computed kk_{ro} Values
Drawdown Test
Case 6

t days	p_{wf} psi	Sim. So	Sim. kk_{ro} md	Comp. kk_{ro} md
0.10157E-03	0.33267E+04	0.68459E+00	0.82947E+01	0.37776E+01
0.11213E-03	0.33226E+04	0.68405E+00	0.82709E+01	0.37134E+01
0.12374E-03	0.33184E+04	0.68349E+00	0.82463E+01	0.36523E+01
0.13651E-03	0.33141E+04	0.68293E+00	0.82216E+01	0.35944E+01
0.15056E-03	0.33098E+04	0.68236E+00	0.81965E+01	0.35394E+01
0.16602E-03	0.33054E+04	0.68177E+00	0.81705E+01	0.34875E+01
0.18302E-03	0.33010E+04	0.68118E+00	0.81445E+01	0.34384E+01
0.20172E-03	0.32965E+04	0.68057E+00	0.81176E+01	0.33913E+01
0.22230E-03	0.32920E+04	0.67995E+00	0.80903E+01	0.33459E+01
0.24493E-03	0.32874E+04	0.67932E+00	0.80631E+01	0.33018E+01
0.26982E-03	0.32827E+04	0.67868E+00	0.80354E+01	0.32600E+01
0.29720E-03	0.32780E+04	0.67803E+00	0.80074E+01	0.32205E+01
0.32732E-03	0.32733E+04	0.67736E+00	0.79784E+01	0.31830E+01
0.36045E-03	0.32685E+04	0.67668E+00	0.79490E+01	0.31471E+01
0.39690E-03	0.32636E+04	0.67599E+00	0.79192E+01	0.31137E+01
0.43699E-03	0.32587E+04	0.67529E+00	0.78889E+01	0.30826E+01
0.48109E-03	0.32538E+04	0.67457E+00	0.78582E+01	0.30523E+01
0.52959E-03	0.32488E+04	0.67383E+00	0.78268E+01	0.30235E+01
0.58295E-03	0.32437E+04	0.67308E+00	0.77951E+01	0.29974E+01
0.64165E-03	0.32387E+04	0.67232E+00	0.77629E+01	0.29758E+01
0.70621E-03	0.32335E+04	0.67154E+00	0.77298E+01	0.29578E+01
0.77724E-03	0.32284E+04	0.67075E+00	0.76964E+01	0.29435E+01
0.85536E-03	0.32233E+04	0.66995E+00	0.76625E+01	0.29346E+01
0.94130E-03	0.32181E+04	0.66913E+00	0.76285E+01	0.29326E+01
0.10358E-02	0.32129E+04	0.66829E+00	0.75936E+01	0.29341E+01
0.11398E-02	0.32078E+04	0.66745E+00	0.75587E+01	0.29383E+01
0.12542E-02	0.32026E+04	0.66659E+00	0.75230E+01	0.29503E+01
0.13800E-02	0.31975E+04	0.66573E+00	0.74873E+01	0.29715E+01
0.15184E-02	0.31924E+04	0.66486E+00	0.74513E+01	0.30046E+01
0.16706E-02	0.31874E+04	0.66398E+00	0.74155E+01	0.30376E+01
0.18381E-02	0.31824E+04	0.66309E+00	0.73792E+01	0.30719E+01
0.20223E-02	0.31775E+04	0.66220E+00	0.73430E+01	0.31189E+01
0.22250E-02	0.31727E+04	0.66131E+00	0.73067E+01	0.31750E+01
0.24479E-02	0.31679E+04	0.66043E+00	0.72709E+01	0.32423E+01
0.26930E-02	0.31633E+04	0.65954E+00	0.72351E+01	0.33094E+01
0.29627E-02	0.31588E+04	0.65864E+00	0.71992E+01	0.33714E+01
0.32594E-02	0.31543E+04	0.65775E+00	0.71637E+01	0.34392E+01
0.35858E-02	0.31499E+04	0.65687E+00	0.71286E+01	0.35142E+01
0.39447E-02	0.31456E+04	0.65599E+00	0.70935E+01	0.35937E+01
0.43396E-02	0.31414E+04	0.65513E+00	0.70592E+01	0.36774E+01
0.47740E-02	0.31374E+04	0.65426E+00	0.70251E+01	0.37469E+01
0.52518E-02	0.31333E+04	0.65339E+00	0.69910E+01	0.38033E+01
0.57773E-02	0.31294E+04	0.65254E+00	0.69578E+01	0.38638E+01

Table F-29 (Cont'd)

t days	p_{wf} psi	Sim. So	Sim. kk_{ro} md	Comp. kk_{ro} md
0.63555E-02	0.31254E+04	0.65170E+00	0.69250E+01	0.39242E+01
0.69914E-02	0.31216E+04	0.65087E+00	0.68925E+01	0.39834E+01
0.76910E-02	0.31178E+04	0.65005E+00	0.68605E+01	0.40417E+01
0.84605E-02	0.31140E+04	0.64923E+00	0.68290E+01	0.40775E+01
0.93069E-02	0.31103E+04	0.64842E+00	0.67980E+01	0.40946E+01
0.10238E-01	0.31066E+04	0.64763E+00	0.67678E+01	0.41169E+01
0.11262E-01	0.31029E+04	0.64685E+00	0.67379E+01	0.41399E+01
0.12389E-01	0.30992E+04	0.64608E+00	0.67084E+01	0.41632E+01
0.13628E-01	0.30956E+04	0.64534E+00	0.66801E+01	0.41891E+01
0.14991E-01	0.30919E+04	0.64459E+00	0.66517E+01	0.41962E+01
0.16491E-01	0.30883E+04	0.64384E+00	0.66236E+01	0.41785E+01
0.18140E-01	0.30846E+04	0.64312E+00	0.65966E+01	0.41656E+01
0.19955E-01	0.30809E+04	0.64241E+00	0.65699E+01	0.41630E+01
0.21951E-01	0.30773E+04	0.64173E+00	0.65444E+01	0.41654E+01
0.24146E-01	0.30736E+04	0.64106E+00	0.65193E+01	0.41747E+01
0.26561E-01	0.30699E+04	0.64040E+00	0.64945E+01	0.41789E+01
0.29218E-01	0.30663E+04	0.63973E+00	0.64696E+01	0.41564E+01
0.32140E-01	0.30626E+04	0.63906E+00	0.64450E+01	0.41126E+01
0.35354E-01	0.30588E+04	0.63842E+00	0.64215E+01	0.40832E+01
0.38890E-01	0.30551E+04	0.63781E+00	0.63990E+01	0.40840E+01
0.42779E-01	0.30513E+04	0.63721E+00	0.63770E+01	0.40903E+01
0.47058E-01	0.30476E+04	0.63662E+00	0.63553E+01	0.40807E+01
0.51764E-01	0.30438E+04	0.63603E+00	0.63336E+01	0.40631E+01
0.56941E-01	0.30400E+04	0.63544E+00	0.63120E+01	0.40452E+01
0.62635E-01	0.30362E+04	0.63485E+00	0.62904E+01	0.40201E+01
0.68899E-01	0.30324E+04	0.63428E+00	0.62699E+01	0.39911E+01
0.75789E-01	0.30285E+04	0.63373E+00	0.62501E+01	0.39687E+01
0.83369E-01	0.30246E+04	0.63318E+00	0.62304E+01	0.39532E+01
0.91706E-01	0.30207E+04	0.63265E+00	0.62113E+01	0.39373E+01
0.10088E+00	0.30168E+04	0.63212E+00	0.61922E+01	0.39196E+01
0.11097E+00	0.30129E+04	0.63161E+00	0.61739E+01	0.39189E+01
0.12206E+00	0.30090E+04	0.63111E+00	0.61559E+01	0.39258E+01
0.13427E+00	0.30050E+04	0.63059E+00	0.61372E+01	0.39116E+01
0.14770E+00	0.30011E+04	0.63008E+00	0.61189E+01	0.38853E+01
0.16247E+00	0.29971E+04	0.62956E+00	0.61005E+01	0.38306E+01
0.17871E+00	0.29931E+04	0.62906E+00	0.60829E+01	0.37918E+01
0.19658E+00	0.29890E+04	0.62860E+00	0.60667E+01	0.38077E+01
0.21624E+00	0.29850E+04	0.62814E+00	0.60505E+01	0.38204E+01
0.23787E+00	0.29809E+04	0.62768E+00	0.60343E+01	0.38095E+01
0.26166E+00	0.29769E+04	0.62723E+00	0.60184E+01	0.37949E+01
0.28782E+00	0.29728E+04	0.62679E+00	0.60029E+01	0.37911E+01
0.31660E+00	0.29687E+04	0.62636E+00	0.59878E+01	0.38008E+01
0.34826E+00	0.29646E+04	0.62593E+00	0.59727E+01	0.38101E+01

Table F-29 (Cont'd)

t days	p_{wf} psi	Sim. So	Sim. kk_{ro} md	Comp. kk_{ro} md
0.38309E+00	0.29606E+04	0.62549E+00	0.59572E+01	0.38101E+01
0.42140E+00	0.29565E+04	0.62507E+00	0.59424E+01	0.38062E+01
0.46354E+00	0.29525E+04	0.62464E+00	0.59275E+01	0.37792E+01
0.50990E+00	0.29483E+04	0.62424E+00	0.59137E+01	0.37709E+01
0.56089E+00	0.29442E+04	0.62386E+00	0.59006E+01	0.38023E+01
0.61697E+00	0.29402E+04	0.62350E+00	0.58882E+01	0.38299E+01
0.67867E+00	0.29361E+04	0.62314E+00	0.58758E+01	0.38564E+01
0.74654E+00	0.29321E+04	0.62280E+00	0.58640E+01	0.38833E+01
0.82119E+00	0.29281E+04	0.62247E+00	0.58527E+01	0.39174E+01
0.90331E+00	0.29242E+04	0.62216E+00	0.58420E+01	0.39581E+01
0.99365E+00	0.29203E+04	0.62185E+00	0.58313E+01	0.39924E+01
0.10930E+01	0.29164E+04	0.62155E+00	0.58209E+01	0.40189E+01
0.12023E+01	0.29126E+04	0.62125E+00	0.58106E+01	0.40453E+01
0.13225E+01	0.29087E+04	0.62097E+00	0.58009E+01	0.40762E+01
0.14548E+01	0.29049E+04	0.62070E+00	0.57916E+01	0.41156E+01
0.16003E+01	0.29012E+04	0.62045E+00	0.57830E+01	0.41669E+01
0.17603E+01	0.28974E+04	0.62019E+00	0.57741E+01	0.42098E+01
0.19363E+01	0.28938E+04	0.61995E+00	0.57658E+01	0.42304E+01
0.21300E+01	0.28901E+04	0.61971E+00	0.57578E+01	0.42161E+01
0.23430E+01	0.28864E+04	0.61949E+00	0.57505E+01	0.42281E+01
0.25773E+01	0.28827E+04	0.61930E+00	0.57441E+01	0.42803E+01
0.28350E+01	0.28791E+04	0.61911E+00	0.57378E+01	0.43169E+01
0.31185E+01	0.28755E+04	0.61893E+00	0.57318E+01	0.43608E+01
0.34303E+01	0.28719E+04	0.61875E+00	0.57258E+01	0.43988E+01
0.37734E+01	0.28684E+04	0.61857E+00	0.57198E+01	0.44042E+01
0.41507E+01	0.28648E+04	0.61839E+00	0.57138E+01	0.43997E+01
0.45658E+01	0.28612E+04	0.61822E+00	0.57081E+01	0.43715E+01

Table F-30

Simulated and Computed kk_{ro} Values
Buildup Test
Case 6

Δt days	p_{ws} psi	DD Sim. So	Sim. kk_{ro} md	Comp. kk_{ro} md
0.104954E-03	0.300998E+04	0.631239E+00	0.616055E+01	0.285572E+01
0.116124E-03	0.301574E+04	0.631980E+00	0.618719E+01	0.280950E+01
0.128411E-03	0.302157E+04	0.632763E+00	0.621535E+01	0.276204E+01
0.141927E-03	0.302746E+04	0.633581E+00	0.624476E+01	0.271547E+01
0.156794E-03	0.303342E+04	0.634436E+00	0.627550E+01	0.267034E+01
0.173148E-03	0.303945E+04	0.635353E+00	0.630879E+01	0.262716E+01
0.191137E-03	0.304556E+04	0.636306E+00	0.634378E+01	0.258597E+01
0.210925E-03	0.305174E+04	0.637278E+00	0.637948E+01	0.254701E+01
0.232692E-03	0.305798E+04	0.638284E+00	0.641646E+01	0.251048E+01
0.256636E-03	0.306430E+04	0.639373E+00	0.645647E+01	0.247601E+01
0.282974E-03	0.307068E+04	0.640534E+00	0.649953E+01	0.244343E+01
0.311946E-03	0.307712E+04	0.641704E+00	0.654342E+01	0.241280E+01
0.343816E-03	0.308363E+04	0.642930E+00	0.658943E+01	0.238451E+01
0.378872E-03	0.309019E+04	0.644234E+00	0.663834E+01	0.235805E+01
0.417434E-03	0.309681E+04	0.645594E+00	0.668983E+01	0.233348E+01
0.459851E-03	0.310349E+04	0.646975E+00	0.674271E+01	0.231103E+01
0.506511E-03	0.311021E+04	0.648399E+00	0.679723E+01	0.229023E+01
0.557837E-03	0.311698E+04	0.649873E+00	0.685364E+01	0.227116E+01
0.614295E-03	0.312379E+04	0.651345E+00	0.691108E+01	0.225374E+01
0.676399E-03	0.313064E+04	0.652816E+00	0.696860E+01	0.223787E+01
0.744714E-03	0.313753E+04	0.654296E+00	0.702645E+01	0.222365E+01
0.819860E-03	0.314444E+04	0.655745E+00	0.708371E+01	0.221118E+01
0.902520E-03	0.315138E+04	0.657165E+00	0.714036E+01	0.220039E+01
0.993447E-03	0.315835E+04	0.658559E+00	0.719592E+01	0.219185E+01
0.109347E-02	0.316532E+04	0.659928E+00	0.725053E+01	0.218552E+01
0.120349E-02	0.317231E+04	0.661242E+00	0.730399E+01	0.218166E+01
0.132451E-02	0.317930E+04	0.662525E+00	0.735622E+01	0.218118E+01
0.145764E-02	0.318627E+04	0.663780E+00	0.740733E+01	0.218378E+01
0.160407E-02	0.319322E+04	0.665000E+00	0.745702E+01	0.218978E+01
0.176516E-02	0.320014E+04	0.666176E+00	0.750582E+01	0.220037E+01
0.194235E-02	0.320701E+04	0.667325E+00	0.755352E+01	0.221537E+01
0.213726E-02	0.321382E+04	0.668435E+00	0.759964E+01	0.223331E+01
0.235166E-02	0.322056E+04	0.669522E+00	0.764477E+01	0.224780E+01
0.258750E-02	0.322727E+04	0.670573E+00	0.768886E+01	0.224440E+01
0.284692E-02	0.323402E+04	0.671612E+00	0.773289E+01	0.228002E+01
0.313229E-02	0.324051E+04	0.672597E+00	0.777461E+01	0.237482E+01
0.344619E-02	0.324672E+04	0.673525E+00	0.781391E+01	0.247850E+01
0.379148E-02	0.325267E+04	0.674408E+00	0.785131E+01	0.258922E+01
0.417131E-02	0.325836E+04	0.675238E+00	0.788669E+01	0.270955E+01
0.458911E-02	0.326378E+04	0.676014E+00	0.792022E+01	0.284054E+01
0.504870E-02	0.326895E+04	0.676748E+00	0.795195E+01	0.298183E+01
0.555424E-02	0.327386E+04	0.677444E+00	0.798202E+01	0.313229E+01
0.611034E-02	0.327854E+04	0.678102E+00	0.801046E+01	0.329069E+01

Table F-30 (Cont'd)

Δt days	p_{ws} psi	DD Sim. So	Sim. kk_{ro} md	Comp. kk_{ro} md
0.672205E-02	0.328299E+04	0.678717E+00	0.803704E+01	0.345546E+01
0.739493E-02	0.328723E+04	0.679300E+00	0.806227E+01	0.362423E+01
0.813509E-02	0.329127E+04	0.679855E+00	0.808622E+01	0.379419E+01
0.894928E-02	0.329513E+04	0.680383E+00	0.810937E+01	0.396215E+01
0.984488E-02	0.329883E+04	0.680887E+00	0.813160E+01	0.412704E+01
0.108300E-01	0.330239E+04	0.681367E+00	0.815274E+01	0.428608E+01
0.119137E-01	0.330581E+04	0.681825E+00	0.817289E+01	0.443821E+01
0.131058E-01	0.330913E+04	0.682272E+00	0.819258E+01	0.458194E+01
0.144170E-01	0.331234E+04	0.682698E+00	0.821136E+01	0.471671E+01
0.158594E-01	0.331546E+04	0.683109E+00	0.822949E+01	0.484242E+01
0.174460E-01	0.331851E+04	0.683510E+00	0.824713E+01	0.495936E+01
0.191913E-01	0.332148E+04	0.683906E+00	0.826459E+01	0.506745E+01
0.211111E-01	0.332439E+04	0.684288E+00	0.828145E+01	0.516599E+01
0.232229E-01	0.332725E+04	0.684660E+00	0.829784E+01	0.525819E+01
0.255458E-01	0.333006E+04	0.685024E+00	0.831390E+01	0.534407E+01
0.281011E-01	0.333282E+04	0.685386E+00	0.833016E+01	0.542281E+01
0.309119E-01	0.333555E+04	0.685742E+00	0.834615E+01	0.549563E+01
0.340037E-01	0.333823E+04	0.686087E+00	0.836165E+01	0.556402E+01
0.374048E-01	0.334089E+04	0.686426E+00	0.837688E+01	0.562646E+01
0.411459E-01	0.334351E+04	0.686762E+00	0.839199E+01	0.568462E+01
0.452612E-01	0.334610E+04	0.687098E+00	0.840709E+01	0.574037E+01
0.497880E-01	0.334867E+04	0.687429E+00	0.842197E+01	0.579123E+01
0.547675E-01	0.335121E+04	0.687754E+00	0.843656E+01	0.583915E+01
0.602449E-01	0.335373E+04	0.688070E+00	0.845075E+01	0.588626E+01
0.662701E-01	0.335622E+04	0.688387E+00	0.846500E+01	0.592888E+01
0.728978E-01	0.335870E+04	0.688701E+00	0.847913E+01	0.596794E+01
0.801882E-01	0.336115E+04	0.689012E+00	0.849309E+01	0.600688E+01
0.882077E-01	0.336359E+04	0.689324E+00	0.850712E+01	0.604315E+01
0.970291E-01	0.336600E+04	0.689631E+00	0.852090E+01	0.607781E+01
0.106733E+00	0.336840E+04	0.689930E+00	0.853434E+01	0.611073E+01
0.117407E+00	0.337078E+04	0.690231E+00	0.854806E+01	0.614174E+01
0.129148E+00	0.337314E+04	0.690528E+00	0.856170E+01	0.617332E+01
0.142063E+00	0.337549E+04	0.690822E+00	0.857516E+01	0.620138E+01
0.156271E+00	0.337782E+04	0.691112E+00	0.858841E+01	0.622839E+01
0.171898E+00	0.338013E+04	0.691401E+00	0.860166E+01	0.625690E+01
0.189089E+00	0.338242E+04	0.691689E+00	0.861486E+01	0.628273E+01
0.207998E+00	0.338470E+04	0.691972E+00	0.862784E+01	0.630703E+01
0.228799E+00	0.338696E+04	0.692256E+00	0.864081E+01	0.633100E+01
0.251679E+00	0.338920E+04	0.692537E+00	0.865370E+01	0.635449E+01
0.276848E+00	0.339142E+04	0.692813E+00	0.866634E+01	0.637875E+01
0.304533E+00	0.339362E+04	0.693083E+00	0.867872E+01	0.640072E+01
0.334987E+00	0.339580E+04	0.693351E+00	0.869097E+01	0.642160E+01
0.368487E+00	0.339796E+04	0.693618E+00	0.870318E+01	0.644415E+01

Table F-30 (Cont'd)

Δt days	p_{ws} psi	DD Sim. So	Sim. kk_{ro} md	Comp. kk_{ro} md
0.405336E+00	0.340010E+04	0.693883E+00	0.871533E+01	0.646519E+01
0.445871E+00	0.340222E+04	0.694146E+00	0.872739E+01	0.648600E+01
0.490458E+00	0.340431E+04	0.694407E+00	0.873934E+01	0.650635E+01
0.539505E+00	0.340638E+04	0.694660E+00	0.875091E+01	0.652598E+01
0.593456E+00	0.340842E+04	0.694910E+00	0.876239E+01	0.654626E+01
0.652802E+00	0.341044E+04	0.695162E+00	0.877404E+01	0.656536E+01
0.718083E+00	0.341243E+04	0.695403E+00	0.878532E+01	0.658466E+01
0.789892E+00	0.341439E+04	0.695640E+00	0.879639E+01	0.660397E+01
0.868882E+00	0.341631E+04	0.695876E+00	0.880740E+01	0.662310E+01
0.955771E+00	0.341821E+04	0.696109E+00	0.881827E+01	0.664009E+01
0.105135E+01	0.342007E+04	0.696338E+00	0.882898E+01	0.665647E+01
0.115648E+01	0.342189E+04	0.696562E+00	0.883946E+01	0.666543E+01
0.127213E+01	0.342368E+04	0.696782E+00	0.884971E+01	0.669979E+01
0.139935E+01	0.342543E+04	0.696994E+00	0.885960E+01	0.670833E+01
0.153928E+01	0.342714E+04	0.697200E+00	0.886925E+01	0.672729E+01
0.169321E+01	0.342880E+04	0.697404E+00	0.887879E+01	0.674154E+01
0.186253E+01	0.343042E+04	0.697604E+00	0.888809E+01	0.675722E+01
0.204879E+01	0.343200E+04	0.697795E+00	0.889704E+01	0.677259E+01
0.225367E+01	0.343353E+04	0.697981E+00	0.890571E+01	0.678579E+01
0.247903E+01	0.343501E+04	0.698161E+00	0.891410E+01	0.679945E+01
0.272694E+01	0.343645E+04	0.698332E+00	0.892213E+01	0.681185E+01
0.299963E+01	0.343783E+04	0.698498E+00	0.892987E+01	0.682614E+01
0.329960E+01	0.343916E+04	0.698658E+00	0.893733E+01	0.683562E+01
0.362956E+01	0.344044E+04	0.698746E+00	0.894143E+01	0.684617E+01
0.399251E+01	0.344167E+04	0.698825E+00	0.894511E+01	0.685626E+01
0.439177E+01	0.344285E+04	0.698900E+00	0.894863E+01	0.686414E+01
0.483094E+01	0.344397E+04	0.698972E+00	0.895199E+01	0.679126E+01

Table F-31

Simulated and Computed kk_{rg} Values
Drawdown Test
Case 6

p_{wf} psi	Sim. kk_{rg} md	Comp. kk_{rg} md
0.33267E+04	0.16294E-03	0.74190E-04
0.33226E+04	0.18453E-03	0.82900E-04
0.33184E+04	0.20693E-03	0.91573E-04
0.33141E+04	0.22933E-03	0.10026E-03
0.33098E+04	0.25212E-03	0.10894E-03
0.33054E+04	0.27572E-03	0.11765E-03
0.33010E+04	0.29932E-03	0.12640E-03
0.32965E+04	0.32371E-03	0.13520E-03
0.32920E+04	0.34980E-03	0.14452E-03
0.32874E+04	0.39120E-03	0.16006E-03
0.32827E+04	0.43327E-03	0.17570E-03
0.32780E+04	0.47599E-03	0.19149E-03
0.32733E+04	0.52003E-03	0.20742E-03
0.32685E+04	0.56472E-03	0.22349E-03
0.32636E+04	0.61007E-03	0.23984E-03
0.32587E+04	0.65608E-03	0.25645E-03
0.32538E+04	0.71716E-03	0.27874E-03
0.32488E+04	0.78949E-03	0.30497E-03
0.32437E+04	0.86279E-03	0.33174E-03
0.32387E+04	0.93706E-03	0.35933E-03
0.32335E+04	0.10133E-02	0.38771E-03
0.32284E+04	0.10905E-02	0.41699E-03
0.32233E+04	0.11706E-02	0.44838E-03
0.32181E+04	0.12821E-02	0.49297E-03
0.32129E+04	0.13963E-02	0.53928E-03
0.32078E+04	0.15105E-02	0.58725E-03
0.32026E+04	0.16274E-02	0.63801E-03
0.31975E+04	0.17443E-02	0.69216E-03
0.31924E+04	0.18688E-02	0.75338E-03
0.31874E+04	0.20275E-02	0.83053E-03
0.31824E+04	0.21880E-02	0.91069E-03
0.31775E+04	0.23485E-02	0.99731E-03
0.31727E+04	0.25090E-02	0.10899E-02
0.31679E+04	0.26677E-02	0.11899E-02
0.31633E+04	0.28513E-02	0.13045E-02
0.31588E+04	0.30590E-02	0.14322E-02
0.31543E+04	0.32644E-02	0.15668E-02
0.31499E+04	0.34675E-02	0.17094E-02
0.31456E+04	0.36705E-02	0.18591E-02
0.31414E+04	0.38690E-02	0.20157E-02
0.31374E+04	0.41116E-02	0.21930E-02
0.31333E+04	0.43615E-02	0.23719E-02
0.31294E+04	0.46057E-02	0.25574E-02

Table F-31 (Cont'd)

p_{wf} psi	Sim. kk_{rg} md	Comp. kk_{rg} md
0.31254E+04	0.48470E-02	0.27468E-02
0.31216E+04	0.50854E-02	0.29392E-02
0.31178E+04	0.53209E-02	0.31339E-02
0.31140E+04	0.56045E-02	0.33459E-02
0.31103E+04	0.58878E-02	0.35461E-02
0.31066E+04	0.61640E-02	0.37507E-02
0.31029E+04	0.64367E-02	0.39559E-02
0.30992E+04	0.67060E-02	0.41613E-02
0.30956E+04	0.69647E-02	0.43680E-02
0.30919E+04	0.72550E-02	0.45766E-02
0.30883E+04	0.75685E-02	0.47733E-02
0.30846E+04	0.78694E-02	0.49699E-02
0.30809E+04	0.81662E-02	0.51738E-02
0.30773E+04	0.84504E-02	0.53793E-02
0.30736E+04	0.87304E-02	0.55896E-02
0.30699E+04	0.90063E-02	0.57946E-02
0.30663E+04	0.93064E-02	0.59787E-02
0.30626E+04	0.96361E-02	0.61484E-02
0.30588E+04	0.99510E-02	0.63279E-02
0.30551E+04	0.10251E-01	0.65432E-02
0.30513E+04	0.10546E-01	0.67631E-02
0.30476E+04	0.10837E-01	0.69578E-02
0.30438E+04	0.11127E-01	0.71383E-02
0.30400E+04	0.11417E-01	0.73170E-02
0.30362E+04	0.11720E-01	0.74879E-02
0.30324E+04	0.12046E-01	0.76668E-02
0.30285E+04	0.12360E-01	0.78503E-02
0.30246E+04	0.12675E-01	0.80415E-02
0.30207E+04	0.12978E-01	0.82282E-02
0.30168E+04	0.13281E-01	0.84067E-02
0.30129E+04	0.13573E-01	0.86148E-02
0.30090E+04	0.13859E-01	0.88396E-02
0.30050E+04	0.14157E-01	0.90208E-02
0.30011E+04	0.14448E-01	0.91745E-02
0.29971E+04	0.14783E-01	0.92847E-02
0.29931E+04	0.15112E-01	0.94192E-02
0.29890E+04	0.15415E-01	0.96762E-02
0.29850E+04	0.15717E-01	0.99243E-02
0.29809E+04	0.16020E-01	0.10111E-01
0.29769E+04	0.16316E-01	0.10287E-01
0.29728E+04	0.16605E-01	0.10487E-01
0.29687E+04	0.16888E-01	0.10721E-01
0.29646E+04	0.17170E-01	0.10956E-01

Table F-31 (Cont'd)

p_{wf} psi	Sim. kk_{rg} md	Comp. kk_{rg} md
0.29606E+04	0.17460E-01	0.11165E-01
0.29565E+04	0.17736E-01	0.11362E-01
0.29525E+04	0.18052E-01	0.11510E-01
0.29483E+04	0.18351E-01	0.11702E-01
0.29442E+04	0.18636E-01	0.12008E-01
0.29402E+04	0.18905E-01	0.12299E-01
0.29361E+04	0.19175E-01	0.12583E-01
0.29321E+04	0.19429E-01	0.12866E-01
0.29281E+04	0.19676E-01	0.13169E-01
0.29242E+04	0.19909E-01	0.13491E-01
0.29203E+04	0.20141E-01	0.13791E-01
0.29164E+04	0.20365E-01	0.14064E-01
0.29126E+04	0.20590E-01	0.14333E-01
0.29087E+04	0.20800E-01	0.14615E-01
0.29049E+04	0.21002E-01	0.14923E-01
0.29012E+04	0.21189E-01	0.15271E-01
0.28974E+04	0.21384E-01	0.15587E-01
0.28938E+04	0.21571E-01	0.15827E-01
0.28901E+04	0.21786E-01	0.15955E-01
0.28864E+04	0.21983E-01	0.16160E-01
0.28827E+04	0.22154E-01	0.16511E-01
0.28791E+04	0.22324E-01	0.16798E-01
0.28755E+04	0.22486E-01	0.17109E-01
0.28719E+04	0.22647E-01	0.17397E-01
0.28684E+04	0.22808E-01	0.17561E-01
0.28648E+04	0.22970E-01	0.17685E-01
0.28612E+04	0.23122E-01	0.17710E-01

Table F-32

Simulated and Computed kk_{rg} Values
Buildup Test
Case 6

p_{ws} psi	Sim. kk_{rg} md	Comp. kk_{rg} md
0.300998E+04	0.137854E-01	0.772796E-02
0.301574E+04	0.133615E-01	0.745520E-02
0.302157E+04	0.129137E-01	0.718258E-02
0.302746E+04	0.124459E-01	0.691561E-02
0.303342E+04	0.119569E-01	0.665560E-02
0.303945E+04	0.114601E-01	0.640357E-02
0.304556E+04	0.109913E-01	0.615941E-02
0.305174E+04	0.105131E-01	0.592339E-02
0.305798E+04	0.100179E-01	0.569577E-02
0.306430E+04	0.948200E-02	0.547536E-02
0.307068E+04	0.895038E-02	0.526158E-02
0.307712E+04	0.846138E-02	0.505427E-02
0.308363E+04	0.794891E-02	0.485404E-02
0.309019E+04	0.740398E-02	0.465958E-02
0.309681E+04	0.687601E-02	0.447075E-02
0.310349E+04	0.639298E-02	0.428777E-02
0.311021E+04	0.589497E-02	0.410951E-02
0.311698E+04	0.537968E-02	0.393589E-02
0.312379E+04	0.494900E-02	0.376656E-02
0.313064E+04	0.452642E-02	0.360115E-02
0.313753E+04	0.410137E-02	0.343962E-02
0.314444E+04	0.372711E-02	0.328188E-02
0.315138E+04	0.339929E-02	0.312763E-02
0.315835E+04	0.307780E-02	0.297742E-02
0.316532E+04	0.276183E-02	0.283094E-02
0.317231E+04	0.252117E-02	0.268818E-02
0.317930E+04	0.228988E-02	0.254996E-02
0.318627E+04	0.206353E-02	0.241549E-02
0.319322E+04	0.184354E-02	0.228472E-02
0.320014E+04	0.168373E-02	0.215841E-02
0.320701E+04	0.152754E-02	0.203585E-02
0.321382E+04	0.137652E-02	0.191520E-02
0.322056E+04	0.122872E-02	0.179097E-02
0.322727E+04	0.110783E-02	0.165259E-02
0.323402E+04	0.100625E-02	0.154001E-02
0.324051E+04	0.909982E-03	0.146515E-02
0.324672E+04	0.819312E-03	0.139032E-02
0.325267E+04	0.733025E-03	0.131369E-02
0.325836E+04	0.659485E-03	0.123601E-02
0.326378E+04	0.608502E-03	0.115705E-02
0.326895E+04	0.560244E-03	0.107595E-02
0.327386E+04	0.514522E-03	0.991700E-03
0.327854E+04	0.471273E-03	0.903419E-03

Table F-32 (Cont'd)

p_{w_s} psi	Sim. kk_{rg} md	Comp. kk_{rg} md
0.328299E+04	0.430842E-03	0.810412E-03
0.328723E+04	0.392489E-03	0.711944E-03
0.329127E+04	0.356054E-03	0.607558E-03
0.329513E+04	0.331195E-03	0.496951E-03
0.329883E+04	0.311023E-03	0.380408E-03
0.330239E+04	0.291830E-03	0.258167E-03
0.330581E+04	0.273536E-03	0.130699E-03
0.330913E+04	0.255663E-03	0.000000E+00
0.331234E+04	0.238622E-03	0.000000E+00
0.331546E+04	0.222163E-03	0.000000E+00
0.331851E+04	0.206148E-03	0.000000E+00
0.332148E+04	0.190300E-03	0.000000E+00
0.332439E+04	0.174997E-03	0.000000E+00
0.332725E+04	0.160122E-03	0.000000E+00
0.333006E+04	0.146036E-03	0.000000E+00
0.333282E+04	0.138579E-03	0.000000E+00
0.333555E+04	0.131249E-03	0.000000E+00
0.333823E+04	0.124145E-03	0.000000E+00
0.334089E+04	0.117160E-03	0.000000E+00
0.334351E+04	0.110232E-03	0.000000E+00
0.334610E+04	0.103310E-03	0.000000E+00
0.334867E+04	0.964911E-04	0.000000E+00
0.335121E+04	0.898011E-04	0.000000E+00
0.335373E+04	0.832937E-04	0.000000E+00
0.335622E+04	0.767621E-04	0.000000E+00
0.335870E+04	0.702826E-04	0.000000E+00
0.336115E+04	0.638834E-04	0.000000E+00
0.336359E+04	0.574526E-04	0.000000E+00
0.336600E+04	0.511320E-04	0.000000E+00
0.336840E+04	0.449719E-04	0.000000E+00
0.337078E+04	0.417672E-04	0.000000E+00
0.337314E+04	0.395004E-04	0.000000E+00
0.337549E+04	0.372616E-04	0.000000E+00
0.337782E+04	0.350594E-04	0.000000E+00
0.338013E+04	0.328576E-04	0.000000E+00
0.338242E+04	0.306621E-04	0.000000E+00
0.338470E+04	0.285052E-04	0.000000E+00
0.338696E+04	0.263485E-04	0.000000E+00
0.338920E+04	0.242062E-04	0.000000E+00
0.339142E+04	0.221049E-04	0.000000E+00
0.339362E+04	0.200469E-04	0.000000E+00
0.339580E+04	0.180092E-04	0.000000E+00
0.339796E+04	0.159792E-04	0.000000E+00

Table F-32 (Cont'd)

p_{wf} psi	Sim. kk_{rg} md	Comp. kk_{rg} md
0.340010E+04	0.139596E-04	0.000000E+00
0.340222E+04	0.119554E-04	0.000000E+00
0.340431E+04	0.996789E-05	0.000000E+00
0.340638E+04	0.804550E-05	0.000000E+00
0.340842E+04	0.613683E-05	0.000000E+00
0.341044E+04	0.527724E-05	0.000000E+00
0.341243E+04	0.501390E-05	0.000000E+00
0.341439E+04	0.475543E-05	0.000000E+00
0.341631E+04	0.449815E-05	0.000000E+00
0.341821E+04	0.424435E-05	0.000000E+00
0.342007E+04	0.399423E-05	0.000000E+00
0.342189E+04	0.374947E-05	0.000000E+00
0.342368E+04	0.350993E-05	0.000000E+00
0.342543E+04	0.327897E-05	0.000000E+00
0.342714E+04	0.305356E-05	0.000000E+00
0.342880E+04	0.283091E-05	0.000000E+00
0.343042E+04	0.261374E-05	0.000000E+00
0.343200E+04	0.240458E-05	0.000000E+00
0.343353E+04	0.220207E-05	0.000000E+00
0.343501E+04	0.200630E-05	0.000000E+00
0.343645E+04	0.181871E-05	0.000000E+00
0.343783E+04	0.163780E-05	0.000000E+00
0.343916E+04	0.146355E-05	0.000000E+00
0.344044E+04	0.136793E-05	0.000000E+00
0.344167E+04	0.128204E-05	0.000000E+00
0.344285E+04	0.119978E-05	0.000000E+00
0.344397E+04	0.112123E-05	0.000000E+00

Rock and Fluid Properties for Tables F-33 through F-35

$r_w = 0.328$ ft ; $r_e = 6600$ ft

$h = 15.547$ ft ; $\phi = 0.3$

$k = 10$ md

$q_o = 150$ STB/DAY

$s = 0.0$; $S_{gc} = 0.0$

$S_{wc} = S_{iw} = 0.3$; $S_{or} = 0.0$

$C_D \approx 117.4$ $(\beta^* = 6.8 \times 10^{-4})$

PVT Data are given by Set 1 (Table A-1)

Relative Permeability Data are given by Set 1 (Table A-2)

$p_i = p_{bi} = 3460$ psi

$c_{ti} = 0.23564 \times 10^{-4}$ psi^{-1}

$\mu_{oi} = 0.43059$ cp

$B_{oi} = 1.5882$ RB/STB

Table F-33

Simulated and Computed S_o Versus p_{wf} Relationship
Drawdown Test
Case 2

t days	p_{wf} psi	Sim. S_o	Comp. S_o
0.10000000E-05	0.34599960E+04	0.70000000E+00	0.69999950E+00
0.15000000E-05	0.34599940E+04	0.70000000E+00	0.69999925E+00
0.20500000E-05	0.34599910E+04	0.70000000E+00	0.69999887E+00
0.26550000E-05	0.34599870E+04	0.70000000E+00	0.69999837E+00
0.33205000E-05	0.34599820E+04	0.70000000E+00	0.69999776E+00
0.40525500E-05	0.34599770E+04	0.70000000E+00	0.69999715E+00
0.48578050E-05	0.34599710E+04	0.70000000E+00	0.69999643E+00
0.57435855E-05	0.34599640E+04	0.70000000E+00	0.69999557E+00
0.67179441E-05	0.34599560E+04	0.70000000E+00	0.69999460E+00
0.77897385E-05	0.34599470E+04	0.69999000E+00	0.69999351E+00
0.89687123E-05	0.34599360E+04	0.69999000E+00	0.69999217E+00
0.10265584E-04	0.34599240E+04	0.69999000E+00	0.69999071E+00
0.11692142E-04	0.34599100E+04	0.69999000E+00	0.69998901E+00
0.13261356E-04	0.34598930E+04	0.69999000E+00	0.69998694E+00
0.14987492E-04	0.34598740E+04	0.69999000E+00	0.69998463E+00
0.16886241E-04	0.34598530E+04	0.69998000E+00	0.69998208E+00
0.18974865E-04	0.34598280E+04	0.69998000E+00	0.69997904E+00
0.21272351E-04	0.34597990E+04	0.69998000E+00	0.69997552E+00
0.23799587E-04	0.34597670E+04	0.69997000E+00	0.69997162E+00
0.26579545E-04	0.34597300E+04	0.69997000E+00	0.69996713E+00
0.29637500E-04	0.34596880E+04	0.69997000E+00	0.69996202E+00
0.33001250E-04	0.34596400E+04	0.69996000E+00	0.69995618E+00
0.36701375E-04	0.34595860E+04	0.69995000E+00	0.69994962E+00
0.40771512E-04	0.34595240E+04	0.69995000E+00	0.69994208E+00
0.45248663E-04	0.34594540E+04	0.69994000E+00	0.69993357E+00
0.50173530E-04	0.34593750E+04	0.69993000E+00	0.69992396E+00
0.55590883E-04	0.34592840E+04	0.69992000E+00	0.69991290E+00
0.61549971E-04	0.34591820E+04	0.69991000E+00	0.69990049E+00
0.68104968E-04	0.34590670E+04	0.69990000E+00	0.69988651E+00
0.75315465E-04	0.34589360E+04	0.69988000E+00	0.69987057E+00
0.83247011E-04	0.34587890E+04	0.69986000E+00	0.69985269E+00
0.91971713E-04	0.34586220E+04	0.69985000E+00	0.69983238E+00
0.10156888E-03	0.34584340E+04	0.69982000E+00	0.69980950E+00
0.11212577E-03	0.34582210E+04	0.69980000E+00	0.69978359E+00
0.12373835E-03	0.34579820E+04	0.69977000E+00	0.69975450E+00
0.13651218E-03	0.34577120E+04	0.69974000E+00	0.69972164E+00
0.15056340E-03	0.34574080E+04	0.69971000E+00	0.69968463E+00
0.16601974E-03	0.34570660E+04	0.69967000E+00	0.69964299E+00
0.18302172E-03	0.34566820E+04	0.69962000E+00	0.69959622E+00
0.20172389E-03	0.34562490E+04	0.69957000E+00	0.69954346E+00
0.22229628E-03	0.34557630E+04	0.69952000E+00	0.69948423E+00
0.24492591E-03	0.34552170E+04	0.69945000E+00	0.69941766E+00
0.26981850E-03	0.34546040E+04	0.69938000E+00	0.69934289E+00

Table F-33 (Cont'd)

t days	p_{wf} psi	Sim. S_o	Comp. S_o
0.29720035E-03	0.34539170E+04	0.69930000E+00	0.69925905E+00
0.32732038E-03	0.34531460E+04	0.69921000E+00	0.69916490E+00
0.36045242E-03	0.34522820E+04	0.69911000E+00	0.69905931E+00
0.39689766E-03	0.34513140E+04	0.69900000E+00	0.69894092E+00
0.43698743E-03	0.34502310E+04	0.69887000E+00	0.69880834E+00
0.48108617E-03	0.34490190E+04	0.69873000E+00	0.69865979E+00
0.52959479E-03	0.34476640E+04	0.69857000E+00	0.69849351E+00
0.58295426E-03	0.34461500E+04	0.69839000E+00	0.69830742E+00
0.64164969E-03	0.34444590E+04	0.69819000E+00	0.69809922E+00
0.70621466E-03	0.34425730E+04	0.69797000E+00	0.69786653E+00
0.77723613E-03	0.34404690E+04	0.69772000E+00	0.69760632E+00
0.85535974E-03	0.34381250E+04	0.69744000E+00	0.69731561E+00
0.94129571E-03	0.34355160E+04	0.69713000E+00	0.69699097E+00
0.10358253E-02	0.34326120E+04	0.69678000E+00	0.69662825E+00
0.11398078E-02	0.34293850E+04	0.69639000E+00	0.69622337E+00
0.12541886E-02	0.34258010E+04	0.69596000E+00	0.69577134E+00
0.13800075E-02	0.34218240E+04	0.69548000E+00	0.69526671E+00
0.15184082E-02	0.34174160E+04	0.69494000E+00	0.69470353E+00
0.16706490E-02	0.34125360E+04	0.69435000E+00	0.69407494E+00
0.18381139E-02	0.34071390E+04	0.69368000E+00	0.69337302E+00
0.20223253E-02	0.34011770E+04	0.69294000E+00	0.69258882E+00
0.22249578E-02	0.33946010E+04	0.69212000E+00	0.69171239E+00
0.24478536E-02	0.33873580E+04	0.69121000E+00	0.69071239E+00
0.26930390E-02	0.33793920E+04	0.69020000E+00	0.68971239E+00
0.29627429E-02	0.33706450E+04	0.68907000E+00	0.68848588E+00
0.32594172E-02	0.33610560E+04	0.68782000E+00	0.68710943E+00
0.35857589E-02	0.33505660E+04	0.68644000E+00	0.68556222E+00
0.39447348E-02	0.33391140E+04	0.68492000E+00	0.68382584E+00
0.43396083E-02	0.33266390E+04	0.68322000E+00	0.68187794E+00
0.47739691E-02	0.33130750E+04	0.68136000E+00	0.67967648E+00
0.52517660E-02	0.32983730E+04	0.67931000E+00	0.67723099E+00
0.57773426E-02	0.32824770E+04	0.67706000E+00	0.67446573E+00
0.63554769E-02	0.32653320E+04	0.67461000E+00	0.67143740E+00
0.69914245E-02	0.32469090E+04	0.67192000E+00	0.66803003E+00
0.76190413E-02	0.32290060E+04	0.66928000E+00	0.66475238E+00
0.83094198E-02	0.32099490E+04	0.66644000E+00	0.66136696E+00
0.89681152E-02	0.31920060E+04	0.66373000E+00	0.65825709E+00
0.96926802E-02	0.31730030E+04	0.66088000E+00	0.65505868E+00
0.10385942E-01	0.31550600E+04	0.65818000E+00	0.65230466E+00
0.11148530E-01	0.31361050E+04	0.65539000E+00	0.64943494E+00
0.11880020E-01	0.31181770E+04	0.65278000E+00	0.64703263E+00
0.12684658E-01	0.30992760E+04	0.65015000E+00	0.64454626E+00
0.13458692E-01	0.30813830E+04	0.64771000E+00	0.64248727E+00

Table F-33 (Cont'd)

t days	p_{wf} psi	Sim. S_o	Comp. S_o
0.14310129E-01	0.30625930E+04	0.64531000E+00	0.64037520E+00
0.15134026E-01	0.30447560E+04	0.64312000E+00	0.63855297E+00
0.16040313E-01	0.30261360E+04	0.64099000E+00	0.63677302E+00
0.16925252E-01	0.30083790E+04	0.63907000E+00	0.63511509E+00
0.17898684E-01	0.29899950E+04	0.63720000E+00	0.63360613E+00
0.18861444E-01	0.29723010E+04	0.63555000E+00	0.63221478E+00
0.19920480E-01	0.29541610E+04	0.63392000E+00	0.63082320E+00
0.21085419E-01	0.29353260E+04	0.63233000E+00	0.62943957E+00
0.22209957E-01	0.29176900E+04	0.63098000E+00	0.62827728E+00
0.23446948E-01	0.28999180E+04	0.62967000E+00	0.62713258E+00
0.24807638E-01	0.28817600E+04	0.62835000E+00	0.62598741E+00
0.26304397E-01	0.28631090E+04	0.62711000E+00	0.62483628E+00
0.27763455E-01	0.28458920E+04	0.62605000E+00	0.62383628E+00
0.29368419E-01	0.28288520E+04	0.62502000E+00	0.62283628E+00
0.31133880E-01	0.28117600E+04	0.62399000E+00	0.62183628E+00
0.33075886E-01	0.27945300E+04	0.62303000E+00	0.62094398E+00
0.35212093E-01	0.27774280E+04	0.62212000E+00	0.62007763E+00
0.37561921E-01	0.27605590E+04	0.62127000E+00	0.61930711E+00
0.40146732E-01	0.27440810E+04	0.62047000E+00	0.61857919E+00
0.42990024E-01	0.27280230E+04	0.61969000E+00	0.61787940E+00
0.46117645E-01	0.27123750E+04	0.61895000E+00	0.61720605E+00
0.49558028E-01	0.26971670E+04	0.61830000E+00	0.61655940E+00
0.53342449E-01	0.26825330E+04	0.61770000E+00	0.61594418E+00
0.57505313E-01	0.26684610E+04	0.61714000E+00	0.61536350E+00
0.62084463E-01	0.26549510E+04	0.61661000E+00	0.61485386E+00
0.67121528E-01	0.26418970E+04	0.61610000E+00	0.61438783E+00
0.72662299E-01	0.26291790E+04	0.61560000E+00	0.61393716E+00
0.78757148E-01	0.26167440E+04	0.61513000E+00	0.61349960E+00
0.85461481E-01	0.26045830E+04	0.61465000E+00	0.61307453E+00
0.92836248E-01	0.25923610E+04	0.61419000E+00	0.61264995E+00
0.10094849E+00	0.25801870E+04	0.61377000E+00	0.61222963E+00
0.10987196E+00	0.25681660E+04	0.61336000E+00	0.61181712E+00
0.11968777E+00	0.25562570E+04	0.61296000E+00	0.61141086E+00
0.13048517E+00	0.25443390E+04	0.61254000E+00	0.61100660E+00
0.14236230E+00	0.25323480E+04	0.61213000E+00	0.61060249E+00
0.15542715E+00	0.25203300E+04	0.61172000E+00	0.61020320E+00
0.16979849E+00	0.25083190E+04	0.61132000E+00	0.60980637E+00
0.18560695E+00	0.24962400E+04	0.61091000E+00	0.60940949E+00
0.20299627E+00	0.24840660E+04	0.61050000E+00	0.60901168E+00
0.22212451E+00	0.24718810E+04	0.61010000E+00	0.60861570E+00
0.24316558E+00	0.24596870E+04	0.60969000E+00	0.60822161E+00
0.26631076E+00	0.24474030E+04	0.60928000E+00	0.60782678E+00
0.29177046E+00	0.24350170E+04	0.60887000E+00	0.60743084E+00

Table F-33 (Cont'd)

t days	p_{wf} psi	Sim. S_o	Comp. S_o
0.31977612E+00	0.24226210E+04	0.60847000E+00	0.60703675E+00
0.35058235E+00	0.24102120E+04	0.60807000E+00	0.60664442E+00
0.38446921E+00	0.23977090E+04	0.60766000E+00	0.60625127E+00
0.42174474E+00	0.23851010E+04	0.60726000E+00	0.60585700E+00
0.46274784E+00	0.23724840E+04	0.60686000E+00	0.60547153E+00
0.50785124E+00	0.23598540E+04	0.60646000E+00	0.60510506E+00
0.55746498E+00	0.23471270E+04	0.60605000E+00	0.60475272E+00
0.61204010E+00	0.23342910E+04	0.60565000E+00	0.60440318E+00
0.67207273E+00	0.23214480E+04	0.60525000E+00	0.60405513E+00
0.73810862E+00	0.23085920E+04	0.60485000E+00	0.60370840E+00
0.81074810E+00	0.22954960E+04	0.60445000E+00	0.60335575E+00
0.89065153E+00	0.22821120E+04	0.60406000E+00	0.60299584E+00
0.97854530E+00	0.22689170E+04	0.60373000E+00	0.60264279E+00
0.10752285E+01	0.22557820E+04	0.60338000E+00	0.60229311E+00
0.11815799E+01	0.22425660E+04	0.60301000E+00	0.60194303E+00
0.12985665E+01	0.22292390E+04	0.60266000E+00	0.60159179E+00
0.14272518E+01	0.22158960E+04	0.60231000E+00	0.60124193E+00
0.15688056E+01	0.22025330E+04	0.60195000E+00	0.60089335E+00
0.17245148E+01	0.21890640E+04	0.60159000E+00	0.60054662E+00
0.18957949E+01	0.21754790E+04	0.60124000E+00	0.60020752E+00
0.20842030E+01	0.21618790E+04	0.60089000E+00	0.59987790E+00
0.22914519E+01	0.21482610E+04	0.60053000E+00	0.59955423E+00
0.25194257E+01	0.21345340E+04	0.60017000E+00	0.59922957E+00
0.27701969E+01	0.21206860E+04	0.59981000E+00	0.59890369E+00
0.30460452E+01	0.21066610E+04	0.59947000E+00	0.59857530E+00
0.33494783E+01	0.20925990E+04	0.59914000E+00	0.59824774E+00
0.36832548E+01	0.20785690E+04	0.59881000E+00	0.59792260E+00
0.40504089E+01	0.20644950E+04	0.59847000E+00	0.59759238E+00
0.44542784E+01	0.20504410E+04	0.59813000E+00	0.59725578E+00
0.48985348E+01	0.20362960E+04	0.59779000E+00	0.59691885E+00
0.50000000E+01	0.20300050E+04	0.59773000E+00	0.59676941E+00

Table F-34

Simulated and Computed kk_{ro} Values
Drawdown Test
Case 2

t days	p_{wf} psi	Sim. So	Sim. kk_{ro} md	Comp. kk_{ro} md	Comp. Inst. kk_{ro} md
0.10157E-03	0.34584E+04	0.69982E+00	0.69929E+01	0.75061E+01	0.23021E+03
0.11213E-03	0.34582E+04	0.69980E+00	0.69921E+01	0.74759E+01	0.20351E+03
0.12374E-03	0.34580E+04	0.69977E+00	0.69909E+01	0.74479E+01	0.18014E+03
0.13651E-03	0.34577E+04	0.69974E+00	0.69897E+01	0.74096E+01	0.15927E+03
0.15056E-03	0.34574E+04	0.69971E+00	0.69885E+01	0.73833E+01	0.14115E+03
0.16602E-03	0.34571E+04	0.69967E+00	0.69869E+01	0.73655E+01	0.12530E+03
0.18302E-03	0.34567E+04	0.69962E+00	0.69850E+01	0.73340E+01	0.11110E+03
0.20172E-03	0.34562E+04	0.69957E+00	0.69830E+01	0.73049E+01	0.98576E+02
0.22230E-03	0.34558E+04	0.69952E+00	0.69810E+01	0.72849E+01	0.87628E+02
0.24493E-03	0.34552E+04	0.69945E+00	0.69782E+01	0.72623E+01	0.77902E+02
0.26982E-03	0.34546E+04	0.69938E+00	0.69755E+01	0.72462E+01	0.69353E+02
0.29720E-03	0.34539E+04	0.69930E+00	0.69723E+01	0.72274E+01	0.61758E+02
0.32732E-03	0.34531E+04	0.69921E+00	0.69687E+01	0.72069E+01	0.55008E+02
0.36045E-03	0.34523E+04	0.69911E+00	0.69648E+01	0.71892E+01	0.49042E+02
0.39690E-03	0.34513E+04	0.69900E+00	0.69604E+01	0.71748E+01	0.43765E+02
0.43699E-03	0.34502E+04	0.69887E+00	0.69553E+01	0.71603E+01	0.39080E+02
0.48109E-03	0.34490E+04	0.69873E+00	0.69497E+01	0.71455E+01	0.34913E+02
0.52959E-03	0.34477E+04	0.69857E+00	0.69434E+01	0.71322E+01	0.31218E+02
0.58295E-03	0.34462E+04	0.69839E+00	0.69363E+01	0.71185E+01	0.27930E+02
0.64165E-03	0.34445E+04	0.69819E+00	0.69284E+01	0.71075E+01	0.25013E+02
0.70621E-03	0.34426E+04	0.69797E+00	0.69197E+01	0.70954E+01	0.22415E+02
0.77724E-03	0.34405E+04	0.69772E+00	0.69098E+01	0.70830E+01	0.20100E+02
0.85536E-03	0.34381E+04	0.69744E+00	0.68987E+01	0.70748E+01	0.18046E+02
0.94130E-03	0.34355E+04	0.69713E+00	0.68864E+01	0.70629E+01	0.16209E+02
0.10358E-02	0.34326E+04	0.69678E+00	0.68726E+01	0.70508E+01	0.14573E+02
0.11398E-02	0.34294E+04	0.69639E+00	0.68571E+01	0.70409E+01	0.13117E+02
0.12542E-02	0.34258E+04	0.69596E+00	0.68401E+01	0.70294E+01	0.11816E+02
0.13800E-02	0.34218E+04	0.69548E+00	0.68211E+01	0.70173E+01	0.10655E+02
0.15184E-02	0.34174E+04	0.69494E+00	0.67998E+01	0.70061E+01	0.96204E+01
0.16706E-02	0.34125E+04	0.69435E+00	0.67770E+01	0.69955E+01	0.86960E+01
0.18381E-02	0.34071E+04	0.69368E+00	0.67510E+01	0.69821E+01	0.78695E+01
0.20223E-02	0.34012E+04	0.69294E+00	0.67224E+01	0.69671E+01	0.71316E+01
0.22250E-02	0.33946E+04	0.69212E+00	0.66906E+01	0.69508E+01	0.64728E+01
0.24479E-02	0.33874E+04	0.69121E+00	0.66554E+01	0.69324E+01	0.58837E+01
0.26930E-02	0.33794E+04	0.69020E+00	0.66162E+01	0.69119E+01	0.53569E+01
0.29627E-02	0.33706E+04	0.68907E+00	0.65732E+01	0.68876E+01	0.48856E+01
0.32594E-02	0.33611E+04	0.68782E+00	0.65259E+01	0.68607E+01	0.44643E+01
0.35858E-02	0.33506E+04	0.68644E+00	0.64736E+01	0.68312E+01	0.40882E+01
0.39447E-02	0.33391E+04	0.68492E+00	0.64160E+01	0.67977E+01	0.37521E+01
0.43396E-02	0.33266E+04	0.68322E+00	0.63530E+01	0.67588E+01	0.34508E+01
0.47740E-02	0.33131E+04	0.68136E+00	0.62841E+01	0.67152E+01	0.31820E+01
0.52518E-02	0.32984E+04	0.67931E+00	0.62086E+01	0.66670E+01	0.29426E+01
0.57773E-02	0.32825E+04	0.67706E+00	0.61270E+01	0.66107E+01	0.27281E+01

Table F-34 (Cont'd)

t days	p_{wf} psi	Sim. So	Sim. kk_{ro} md	Comp. kk_{ro} md	Comp. Inst. kk_{ro} md
0.63555E-02	0.32653E+04	0.67461E+00	0.60385E+01	0.65483E+01	0.25374E+01
0.69914E-02	0.32469E+04	0.67192E+00	0.59431E+01	0.64576E+01	0.23651E+01
0.76190E-02	0.32290E+04	0.66928E+00	0.58500E+01	0.63376E+01	0.22169E+01
0.83094E-02	0.32099E+04	0.66644E+00	0.57515E+01	0.62606E+01	0.20943E+01
0.89681E-02	0.31920E+04	0.66373E+00	0.56585E+01	0.61301E+01	0.19846E+01
0.96927E-02	0.31730E+04	0.66088E+00	0.55618E+01	0.60529E+01	0.18953E+01
0.10386E-01	0.31551E+04	0.65818E+00	0.54717E+01	0.59221E+01	0.18125E+01
0.11149E-01	0.31361E+04	0.65539E+00	0.53792E+01	0.58360E+01	0.17447E+01
0.11880E-01	0.31182E+04	0.65278E+00	0.52943E+01	0.57035E+01	0.16810E+01
0.12685E-01	0.30993E+04	0.65015E+00	0.52091E+01	0.56103E+01	0.16292E+01
0.13459E-01	0.30814E+04	0.64771E+00	0.51318E+01	0.54807E+01	0.15818E+01
0.14310E-01	0.30626E+04	0.64531E+00	0.50558E+01	0.53911E+01	0.15441E+01
0.15134E-01	0.30448E+04	0.64312E+00	0.49878E+01	0.52775E+01	0.15117E+01
0.16040E-01	0.30261E+04	0.64099E+00	0.49219E+01	0.51969E+01	0.14872E+01
0.16925E-01	0.30084E+04	0.63907E+00	0.48632E+01	0.51024E+01	0.14693E+01
0.17899E-01	0.29900E+04	0.63720E+00	0.48067E+01	0.50305E+01	0.14569E+01
0.18861E-01	0.29723E+04	0.63555E+00	0.47569E+01	0.49488E+01	0.14523E+01
0.19920E-01	0.29542E+04	0.63392E+00	0.47084E+01	0.49447E+01	0.14690E+01
0.21085E-01	0.29353E+04	0.63233E+00	0.46615E+01	0.48201E+01	0.14568E+01
0.22210E-01	0.29177E+04	0.63098E+00	0.46216E+01	0.47442E+01	0.14672E+01
0.23447E-01	0.28999E+04	0.62967E+00	0.45832E+01	0.47725E+01	0.15095E+01
0.24808E-01	0.28818E+04	0.62835E+00	0.45452E+01	0.47172E+01	0.15350E+01
0.26304E-01	0.28631E+04	0.62711E+00	0.45094E+01	0.45935E+01	0.15452E+01
0.27763E-01	0.28459E+04	0.62605E+00	0.44789E+01	0.45352E+01	0.15865E+01
0.29368E-01	0.28289E+04	0.62502E+00	0.44492E+01	0.45691E+01	0.16588E+01
0.31134E-01	0.28118E+04	0.62399E+00	0.44202E+01	0.45204E+01	0.17148E+01
0.33076E-01	0.27945E+04	0.62303E+00	0.43932E+01	0.44631E+01	0.17782E+01
0.35212E-01	0.27774E+04	0.62212E+00	0.43676E+01	0.44199E+01	0.18601E+01
0.37562E-01	0.27606E+04	0.62127E+00	0.43437E+01	0.43821E+01	0.19577E+01
0.40147E-01	0.27441E+04	0.62047E+00	0.43212E+01	0.43461E+01	0.20698E+01
0.42990E-01	0.27280E+04	0.61969E+00	0.42995E+01	0.43009E+01	0.21866E+01
0.46118E-01	0.27124E+04	0.61895E+00	0.42791E+01	0.42482E+01	0.23088E+01
0.49558E-01	0.26972E+04	0.61830E+00	0.42613E+01	0.42093E+01	0.24487E+01
0.53342E-01	0.26825E+04	0.61770E+00	0.42448E+01	0.41878E+01	0.26066E+01
0.57505E-01	0.26685E+04	0.61714E+00	0.42294E+01	0.41848E+01	0.27732E+01
0.62084E-01	0.26550E+04	0.61661E+00	0.42149E+01	0.41840E+01	0.29391E+01
0.67122E-01	0.26419E+04	0.61610E+00	0.42009E+01	0.41687E+01	0.30875E+01
0.72662E-01	0.26292E+04	0.61560E+00	0.41872E+01	0.41493E+01	0.32198E+01
0.78757E-01	0.26167E+04	0.61513E+00	0.41742E+01	0.41471E+01	0.33470E+01
0.85461E-01	0.26046E+04	0.61465E+00	0.41614E+01	0.41175E+01	0.34278E+01
0.92836E-01	0.25924E+04	0.61419E+00	0.41492E+01	0.40730E+01	0.34746E+01
0.10095E+00	0.25802E+04	0.61377E+00	0.41381E+01	0.40674E+01	0.35495E+01
0.10987E+00	0.25682E+04	0.61336E+00	0.41273E+01	0.40952E+01	0.36325E+01

Table F-34 (Cont'd)

t days	p_{wf} psi	Sim. So	Sim. kk_{ro} md	Comp. kk_{ro} md	Comp. Inst. kk_{ro} md
0.11969E+00	0.25563E+04	0.61296E+00	0.41167E+01	0.41100E+01	0.36893E+01
0.13049E+00	0.25443E+04	0.61254E+00	0.41056E+01	0.40847E+01	0.37151E+01
0.14236E+00	0.25323E+04	0.61213E+00	0.40947E+01	0.40687E+01	0.37357E+01
0.15543E+00	0.25203E+04	0.61172E+00	0.40839E+01	0.40699E+01	0.37681E+01
0.16980E+00	0.25083E+04	0.61132E+00	0.40733E+01	0.40653E+01	0.37918E+01
0.18561E+00	0.24962E+04	0.61091E+00	0.40624E+01	0.40444E+01	0.37975E+01
0.20300E+00	0.24841E+04	0.61050E+00	0.40516E+01	0.40338E+01	0.38102E+01
0.22212E+00	0.24719E+04	0.61010E+00	0.40410E+01	0.40378E+01	0.38346E+01
0.24317E+00	0.24597E+04	0.60969E+00	0.40301E+01	0.40291E+01	0.38448E+01
0.26631E+00	0.24474E+04	0.60928E+00	0.40193E+01	0.40055E+01	0.38390E+01
0.29177E+00	0.24350E+04	0.60887E+00	0.40084E+01	0.39953E+01	0.38444E+01
0.31978E+00	0.24226E+04	0.60847E+00	0.39978E+01	0.39995E+01	0.38623E+01
0.35058E+00	0.24102E+04	0.60807E+00	0.39872E+01	0.39903E+01	0.38658E+01
0.38447E+00	0.23977E+04	0.60766E+00	0.39764E+01	0.39666E+01	0.38542E+01
0.42174E+00	0.23851E+04	0.60726E+00	0.39658E+01	0.39567E+01	0.38547E+01
0.46275E+00	0.23725E+04	0.60686E+00	0.39552E+01	0.39611E+01	0.38683E+01
0.50785E+00	0.23599E+04	0.60646E+00	0.39446E+01	0.39518E+01	0.38676E+01
0.55746E+00	0.23471E+04	0.60605E+00	0.39338E+01	0.39278E+01	0.38517E+01
0.61204E+00	0.23343E+04	0.60565E+00	0.39232E+01	0.39178E+01	0.38488E+01
0.67207E+00	0.23214E+04	0.60525E+00	0.39126E+01	0.39224E+01	0.38596E+01
0.73811E+00	0.23086E+04	0.60485E+00	0.39021E+01	0.38917E+01	0.38351E+01
0.81075E+00	0.22955E+04	0.60445E+00	0.38919E+01	0.38228E+01	0.37723E+01
0.89065E+00	0.22821E+04	0.60408E+00	0.38825E+01	0.38187E+01	0.37728E+01
0.97855E+00	0.22689E+04	0.60373E+00	0.38736E+01	0.38648E+01	0.38226E+01
0.10752E+01	0.22558E+04	0.60338E+00	0.38646E+01	0.38716E+01	0.38331E+01
0.11816E+01	0.22426E+04	0.60301E+00	0.38552E+01	0.38534E+01	0.38186E+01
0.12986E+01	0.22292E+04	0.60266E+00	0.38463E+01	0.38448E+01	0.38132E+01
0.14273E+01	0.22159E+04	0.60231E+00	0.38373E+01	0.38493E+01	0.38205E+01
0.15688E+01	0.22025E+04	0.60195E+00	0.38282E+01	0.38408E+01	0.38147E+01
0.17245E+01	0.21891E+04	0.60159E+00	0.38190E+01	0.38187E+01	0.37952E+01
0.18958E+01	0.21755E+04	0.60124E+00	0.38101E+01	0.38098E+01	0.37884E+01
0.20842E+01	0.21619E+04	0.60089E+00	0.38011E+01	0.38146E+01	0.37951E+01
0.22915E+01	0.21483E+04	0.60053E+00	0.37919E+01	0.38061E+01	0.37885E+01
0.25194E+01	0.21345E+04	0.60017E+00	0.37828E+01	0.37836E+01	0.37676E+01
0.27702E+01	0.21207E+04	0.59981E+00	0.37737E+01	0.37522E+01	0.37378E+01
0.30460E+01	0.21067E+04	0.59947E+00	0.37652E+01	0.37327E+01	0.37197E+01
0.33495E+01	0.20926E+04	0.59914E+00	0.37570E+01	0.37411E+01	0.37292E+01
0.36833E+01	0.20786E+04	0.59881E+00	0.37488E+01	0.37485E+01	0.37377E+01
0.40504E+01	0.20645E+04	0.59847E+00	0.37404E+01	0.37554E+01	0.37456E+01
0.44543E+01	0.20504E+04	0.59813E+00	0.37319E+01	0.37580E+01	0.37490E+01
0.48985E+01	0.20363E+04	0.59779E+00	0.37235E+01	0.31618E+01	0.31547E+01

Table F-35

Simulated and Computed kk_{rg} Values
Drawdown Test
Case 2

p_{wf} psi	Sim. kk_{rg} md	Comp. kk_{rg} md	Comp. Inst. kk_{rg} md
0.34584E+04	0.18302E-06	0.17501E-06	0.53676E-05
0.34582E+04	0.20335E-06	0.24401E-06	0.66424E-05
0.34580E+04	0.23385E-06	0.24111E-06	0.58315E-05
0.34577E+04	0.26436E-06	0.29031E-06	0.62404E-05
0.34574E+04	0.29486E-06	0.33917E-06	0.64840E-05
0.34571E+04	0.33553E-06	0.37940E-06	0.64540E-05
0.34567E+04	0.38637E-06	0.37998E-06	0.57561E-05
0.34562E+04	0.43721E-06	0.45435E-06	0.61313E-05
0.34558E+04	0.48804E-06	0.50797E-06	0.61102E-05
0.34552E+04	0.55922E-06	0.57683E-06	0.61877E-05
0.34546E+04	0.63039E-06	0.66590E-06	0.63733E-05
0.34539E+04	0.71173E-06	0.71458E-06	0.61060E-05
0.34531E+04	0.80324E-06	0.80385E-06	0.61355E-05
0.34523E+04	0.90492E-06	0.90758E-06	0.61911E-05
0.34513E+04	0.10168E-05	0.10432E-05	0.63632E-05
0.34502E+04	0.11489E-05	0.11639E-05	0.63526E-05
0.34490E+04	0.12913E-05	0.13101E-05	0.64012E-05
0.34477E+04	0.14540E-05	0.14799E-05	0.64775E-05
0.34462E+04	0.16370E-05	0.16719E-05	0.65600E-05
0.34445E+04	0.18403E-05	0.19085E-05	0.67164E-05
0.34426E+04	0.20640E-05	0.21154E-05	0.66827E-05
0.34405E+04	0.23182E-05	0.24011E-05	0.68138E-05
0.34381E+04	0.26029E-05	0.26966E-05	0.68783E-05
0.34355E+04	0.29181E-05	0.29828E-05	0.68456E-05
0.34326E+04	0.32740E-05	0.33832E-05	0.69928E-05
0.34294E+04	0.36705E-05	0.37697E-05	0.70230E-05
0.34258E+04	0.41077E-05	0.42128E-05	0.70815E-05
0.34218E+04	0.45958E-05	0.47343E-05	0.71888E-05
0.34174E+04	0.55091E-05	0.56577E-05	0.77689E-05
0.34125E+04	0.96911E-05	0.10025E-04	0.12462E-04
0.34071E+04	0.14440E-04	0.14889E-04	0.16781E-04
0.34012E+04	0.19685E-04	0.20377E-04	0.20858E-04
0.33946E+04	0.25498E-04	0.26471E-04	0.24651E-04
0.33874E+04	0.31948E-04	0.33263E-04	0.28231E-04
0.33794E+04	0.39107E-04	0.40856E-04	0.31665E-04
0.33706E+04	0.58335E-04	0.61151E-04	0.43376E-04
0.33611E+04	0.82274E-04	0.86468E-04	0.56266E-04
0.33506E+04	0.10870E-03	0.11461E-03	0.68593E-04
0.33391E+04	0.13925E-03	0.14753E-03	0.81431E-04
0.33266E+04	0.20235E-03	0.21533E-03	0.10994E-03
0.33131E+04	0.27139E-03	0.29005E-03	0.13744E-03
0.32984E+04	0.36389E-03	0.39064E-03	0.17242E-03
0.32825E+04	0.50091E-03	0.54073E-03	0.22315E-03

Table F-35 (Cont'd)

p_{wf} psi	Sim. kk_{rg} md	Comp. kk_{rg} md	Comp. Inst. kk_{rg} md
0.32653E+04	0.66163E-03	0.71777E-03	0.27812E-03
0.32469E+04	0.90483E-03	0.98287E-03	0.35998E-03
0.32290E+04	0.11688E-02	0.12656E-02	0.44269E-03
0.32099E+04	0.15254E-02	0.16605E-02	0.55545E-03
0.31920E+04	0.19174E-02	0.20764E-02	0.67221E-03
0.31730E+04	0.23913E-02	0.26029E-02	0.81500E-03
0.31551E+04	0.29243E-02	0.31656E-02	0.96882E-03
0.31361E+04	0.35170E-02	0.38151E-02	0.11406E-02
0.31182E+04	0.41859E-02	0.45100E-02	0.13292E-02
0.30993E+04	0.48802E-02	0.52560E-02	0.15263E-02
0.30814E+04	0.56546E-02	0.60379E-02	0.17426E-02
0.30626E+04	0.64246E-02	0.68489E-02	0.19616E-02
0.30448E+04	0.72439E-02	0.76640E-02	0.21952E-02
0.30261E+04	0.80594E-02	0.85104E-02	0.24355E-02
0.30084E+04	0.88570E-02	0.92908E-02	0.26754E-02
0.29900E+04	0.96987E-02	0.10152E-01	0.29400E-02
0.29723E+04	0.10441E-01	0.10863E-01	0.31881E-02
0.29542E+04	0.11253E-01	0.11819E-01	0.35114E-02
0.29353E+04	0.12083E-01	0.12494E-01	0.37762E-02
0.29177E+04	0.12788E-01	0.13127E-01	0.40597E-02
0.28999E+04	0.13498E-01	0.14057E-01	0.44461E-02
0.28818E+04	0.14289E-01	0.14830E-01	0.48256E-02
0.28631E+04	0.15032E-01	0.15316E-01	0.51520E-02
0.28459E+04	0.15668E-01	0.15866E-01	0.55503E-02
0.28289E+04	0.16285E-01	0.16726E-01	0.60723E-02
0.28118E+04	0.16985E-01	0.17368E-01	0.65885E-02
0.27945E+04	0.17639E-01	0.17919E-01	0.71391E-02
0.27774E+04	0.18259E-01	0.18477E-01	0.77758E-02
0.27606E+04	0.18838E-01	0.19002E-01	0.84890E-02
0.27441E+04	0.19384E-01	0.19498E-01	0.92857E-02
0.27280E+04	0.19942E-01	0.19951E-01	0.10143E-01
0.27124E+04	0.20510E-01	0.20358E-01	0.11064E-01
0.26972E+04	0.21010E-01	0.20752E-01	0.12072E-01
0.26825E+04	0.21470E-01	0.21185E-01	0.13186E-01
0.26685E+04	0.21901E-01	0.21673E-01	0.14362E-01
0.26550E+04	0.22308E-01	0.22143E-01	0.15554E-01
0.26419E+04	0.22699E-01	0.22525E-01	0.16683E-01
0.26292E+04	0.23084E-01	0.22871E-01	0.17747E-01
0.26167E+04	0.23445E-01	0.23294E-01	0.18800E-01
0.26046E+04	0.23862E-01	0.23614E-01	0.19659E-01
0.25924E+04	0.24280E-01	0.23834E-01	0.20332E-01
0.25802E+04	0.24661E-01	0.24243E-01	0.21156E-01
0.25682E+04	0.25033E-01	0.24837E-01	0.22031E-01

Table F-35 (Cont'd)

p_{wf} psi	Sim. kk_{rg} md	Comp. kk_{rg} md	Comp. Inst. kk_{rg} md
0.25563E+04	0.25396E-01	0.25358E-01	0.22763E-01
0.25443E+04	0.25777E-01	0.25646E-01	0.23325E-01
0.25323E+04	0.26149E-01	0.25984E-01	0.23858E-01
0.25203E+04	0.26521E-01	0.26425E-01	0.24466E-01
0.25083E+04	0.26884E-01	0.26831E-01	0.25027E-01
0.24962E+04	0.27256E-01	0.27140E-01	0.25483E-01
0.24841E+04	0.27629E-01	0.27510E-01	0.25985E-01
0.24719E+04	0.27992E-01	0.27975E-01	0.26567E-01
0.24597E+04	0.28364E-01	0.28355E-01	0.27058E-01
0.24474E+04	0.28736E-01	0.28639E-01	0.27449E-01
0.24350E+04	0.29108E-01	0.29010E-01	0.27915E-01
0.24226E+04	0.29471E-01	0.29481E-01	0.28469E-01
0.24102E+04	0.29834E-01	0.29857E-01	0.28925E-01
0.23977E+04	0.30206E-01	0.30132E-01	0.29278E-01
0.23851E+04	0.30569E-01	0.30504E-01	0.29717E-01
0.23725E+04	0.30932E-01	0.30981E-01	0.30255E-01
0.23599E+04	0.31295E-01	0.31354E-01	0.30686E-01
0.23471E+04	0.31667E-01	0.31618E-01	0.31006E-01
0.23343E+04	0.32030E-01	0.31988E-01	0.31424E-01
0.23214E+04	0.32393E-01	0.32471E-01	0.31951E-01
0.23086E+04	0.32779E-01	0.32690E-01	0.32214E-01
0.22955E+04	0.33201E-01	0.32617E-01	0.32186E-01
0.22821E+04	0.33592E-01	0.33040E-01	0.32643E-01
0.22689E+04	0.33961E-01	0.33886E-01	0.33515E-01
0.22558E+04	0.34331E-01	0.34399E-01	0.34057E-01
0.22426E+04	0.34722E-01	0.34701E-01	0.34388E-01
0.22292E+04	0.35092E-01	0.35081E-01	0.34793E-01
0.22159E+04	0.35461E-01	0.35575E-01	0.35309E-01
0.22025E+04	0.35841E-01	0.35955E-01	0.35711E-01
0.21891E+04	0.36222E-01	0.36218E-01	0.35995E-01
0.21755E+04	0.36591E-01	0.36595E-01	0.36389E-01
0.21619E+04	0.36961E-01	0.37097E-01	0.36908E-01
0.21483E+04	0.37341E-01	0.37478E-01	0.37304E-01
0.21345E+04	0.37721E-01	0.37728E-01	0.37569E-01
0.21207E+04	0.38121E-01	0.37902E-01	0.37757E-01
0.21067E+04	0.38516E-01	0.38184E-01	0.38051E-01
0.20926E+04	0.38899E-01	0.38735E-01	0.38612E-01
0.20786E+04	0.39282E-01	0.39285E-01	0.39172E-01
0.20645E+04	0.39677E-01	0.39837E-01	0.39733E-01
0.20504E+04	0.40072E-01	0.40347E-01	0.40251E-01
0.20363E+04	0.40467E-01	0.34362E-01	0.34285E-01

Rock and Fluid Properties for Tables F-36 and F-37

$r_w = 0.328$ ft ; $r_e = 6600$ ft

$h = 15.547$ ft ; $\phi = 0.3$

$k = 10$ md

$q_o = 150$ STB/DAY

$s = 0.0$; $S_{gc} = 0.0$

$S_{wc} = S_{iw} = 0.3$; $S_{or} = 0.0$

Drawdown Test: $C_D = 0.0$ $(\beta^* \rightarrow \infty)$
Buildup Test: $C_D \approx 117.4$ $(\beta^* = 6.8 \times 10^{-4})$

PVT Data are given by Set 1 (Table A-1)

Relative Permeability Data are given by Set 1 (Table A-2)

$p_i = p_{bi} = 3460$ psi

$c_{ti} = 0.23564 \times 10^{-4}$ psi^{-1}

$\mu_{oi} = 0.43059$ cp

$B_{oi} = 1.5882$ RB/STB

Table F-36

Simulated and Computed kk_{ro} Values
Buildup Test
Case 2

Δt days	p_{ws} psi	DD Sim. So	Sim. kk_{ro} md	Comp. kk_{ro} md
0.105719E-02	0.208107E+04	0.598863E+00	0.375015E+01	0.353986E+01
0.116391E-02	0.208747E+04	0.599013E+00	0.375389E+01	0.353285E+01
0.128130E-02	0.209463E+04	0.599186E+00	0.375819E+01	0.353394E+01
0.141043E-02	0.210262E+04	0.599380E+00	0.376301E+01	0.354475E+01
0.155247E-02	0.211147E+04	0.599587E+00	0.376816E+01	0.359234E+01
0.170872E-02	0.212110E+04	0.599824E+00	0.377405E+01	0.366076E+01
0.188059E-02	0.213157E+04	0.600096E+00	0.378087E+01	0.369711E+01
0.206965E-02	0.214309E+04	0.600397E+00	0.378855E+01	0.370621E+01
0.227762E-02	0.215575E+04	0.600722E+00	0.379685E+01	0.370025E+01
0.250638E-02	0.216970E+04	0.601082E+00	0.380602E+01	0.370103E+01
0.275801E-02	0.218497E+04	0.601474E+00	0.381603E+01	0.371379E+01
0.303482E-02	0.220158E+04	0.601925E+00	0.382753E+01	0.372426E+01
0.333930E-02	0.221964E+04	0.602398E+00	0.383960E+01	0.371873E+01
0.367423E-02	0.223939E+04	0.602918E+00	0.385285E+01	0.369520E+01
0.398251E-02	0.225749E+04	0.603416E+00	0.386555E+01	0.368496E+01
0.432161E-02	0.227662E+04	0.603925E+00	0.387855E+01	0.373757E+01
0.464391E-02	0.229462E+04	0.604418E+00	0.389112E+01	0.374904E+01
0.499844E-02	0.231363E+04	0.604999E+00	0.390593E+01	0.380448E+01
0.533752E-02	0.233149E+04	0.605548E+00	0.392048E+01	0.382079E+01
0.571050E-02	0.235041E+04	0.606139E+00	0.393611E+01	0.386362E+01
0.606895E-02	0.236826E+04	0.606702E+00	0.395102E+01	0.388117E+01
0.646325E-02	0.238711E+04	0.607296E+00	0.396673E+01	0.392725E+01
0.684364E-02	0.240490E+04	0.607865E+00	0.398181E+01	0.394603E+01
0.726208E-02	0.242367E+04	0.608471E+00	0.399785E+01	0.399381E+01
0.766745E-02	0.244136E+04	0.609043E+00	0.401299E+01	0.401810E+01
0.811335E-02	0.246000E+04	0.609659E+00	0.402930E+01	0.406560E+01
0.854825E-02	0.247763E+04	0.610239E+00	0.404464E+01	0.409669E+01
0.902664E-02	0.249614E+04	0.610851E+00	0.406085E+01	0.414211E+01
0.949668E-02	0.251375E+04	0.611451E+00	0.407672E+01	0.416951E+01
0.100137E-01	0.253220E+04	0.612070E+00	0.409311E+01	0.421431E+01
0.105232E-01	0.254975E+04	0.612674E+00	0.410910E+01	0.424555E+01
0.110837E-01	0.256808E+04	0.613309E+00	0.412592E+01	0.428986E+01
0.116395E-01	0.258559E+04	0.613916E+00	0.414200E+01	0.431118E+01
0.122509E-01	0.260389E+04	0.614606E+00	0.416024E+01	0.434739E+01
0.128582E-01	0.262132E+04	0.615320E+00	0.417947E+01	0.436689E+01
0.135261E-01	0.263951E+04	0.616076E+00	0.420023E+01	0.439689E+01
0.141938E-01	0.265690E+04	0.616807E+00	0.422029E+01	0.441510E+01
0.149282E-01	0.267496E+04	0.617561E+00	0.424099E+01	0.446282E+01
0.157361E-01	0.269372E+04	0.618368E+00	0.426316E+01	0.446749E+01
0.165188E-01	0.271100E+04	0.619134E+00	0.428420E+01	0.447779E+01
0.173799E-01	0.272878E+04	0.619990E+00	0.430768E+01	0.453807E+01
0.183270E-01	0.274705E+04	0.620901E+00	0.433333E+01	0.456079E+01
0.192697E-01	0.276409E+04	0.621760E+00	0.435748E+01	0.458632E+01

Table F-36 (Cont'd)

Δt days	p_{ws} psi	DD Sim. So	Sim. kk_{ro} md	Comp. kk_{ro} md
0.203068E-01	0.278145E+04	0.622659E+00	0.438277E+01	0.464449E+01
0.214476E-01	0.279912E+04	0.623591E+00	0.440899E+01	0.467861E+01
0.227024E-01	0.281703E+04	0.624618E+00	0.443788E+01	0.470363E+01
0.240828E-01	0.283508E+04	0.625718E+00	0.446931E+01	0.472205E+01
0.256011E-01	0.285317E+04	0.626830E+00	0.450136E+01	0.473490E+01
0.272714E-01	0.287118E+04	0.628002E+00	0.453513E+01	0.474202E+01
0.291086E-01	0.288901E+04	0.629229E+00	0.457050E+01	0.474183E+01
0.311295E-01	0.290655E+04	0.630554E+00	0.460904E+01	0.473500E+01
0.333526E-01	0.292371E+04	0.631877E+00	0.464809E+01	0.472060E+01
0.357979E-01	0.294039E+04	0.633251E+00	0.468864E+01	0.469681E+01
0.384878E-01	0.295655E+04	0.634718E+00	0.473192E+01	0.466064E+01
0.414467E-01	0.297217E+04	0.636199E+00	0.477647E+01	0.459102E+01
0.447014E-01	0.298736E+04	0.637750E+00	0.482335E+01	0.449006E+01
0.482817E-01	0.300214E+04	0.639373E+00	0.487238E+01	0.444112E+01
0.522199E-01	0.301614E+04	0.641000E+00	0.492225E+01	0.444560E+01
0.565520E-01	0.302945E+04	0.642632E+00	0.497272E+01	0.445111E+01
0.613173E-01	0.304209E+04	0.644265E+00	0.502325E+01	0.445606E+01
0.665591E-01	0.305420E+04	0.645898E+00	0.507439E+01	0.445965E+01
0.723251E-01	0.306583E+04	0.647516E+00	0.512562E+01	0.446241E+01
0.786678E-01	0.307710E+04	0.649136E+00	0.517692E+01	0.448049E+01
0.856446E-01	0.308799E+04	0.650735E+00	0.522808E+01	0.449735E+01
0.933192E-01	0.309867E+04	0.652336E+00	0.527994E+01	0.451264E+01
0.101761E+00	0.310909E+04	0.653919E+00	0.533121E+01	0.455619E+01
0.111047E+00	0.311927E+04	0.655480E+00	0.538216E+01	0.458028E+01
0.121262E+00	0.312935E+04	0.657035E+00	0.543371E+01	0.460207E+01
0.132499E+00	0.313926E+04	0.658562E+00	0.548432E+01	0.465064E+01
0.144858E+00	0.314897E+04	0.660055E+00	0.553387E+01	0.469273E+01
0.158454E+00	0.315857E+04	0.661527E+00	0.558376E+01	0.470734E+01
0.173410E+00	0.316810E+04	0.662980E+00	0.563303E+01	0.474318E+01
0.189861E+00	0.317744E+04	0.664394E+00	0.568100E+01	0.479907E+01
0.207957E+00	0.318664E+04	0.665777E+00	0.572849E+01	0.482482E+01
0.227863E+00	0.319576E+04	0.667129E+00	0.577539E+01	0.483753E+01
0.249759E+00	0.320481E+04	0.668457E+00	0.582144E+01	0.486902E+01
0.273846E+00	0.321370E+04	0.669753E+00	0.586639E+01	0.489849E+01
0.300340E+00	0.322252E+04	0.671013E+00	0.591091E+01	0.486240E+01
0.329484E+00	0.323142E+04	0.672277E+00	0.595573E+01	0.481980E+01
0.361543E+00	0.324027E+04	0.673512E+00	0.599955E+01	0.488100E+01
0.396807E+00	0.324882E+04	0.674703E+00	0.604178E+01	0.499014E+01
0.435598E+00	0.325716E+04	0.675848E+00	0.608307E+01	0.506726E+01
0.478268E+00	0.326532E+04	0.676964E+00	0.612353E+01	0.511627E+01
0.525205E+00	0.327335E+04	0.678044E+00	0.616271E+01	0.518149E+01
0.576835E+00	0.328115E+04	0.679095E+00	0.620082E+01	0.526484E+01
0.633629E+00	0.328877E+04	0.680110E+00	0.623772E+01	0.532714E+01

Table F-36 (Cont'd)

Δt days	p_{ws} psi	DD Sim. So	Sim. kk_{ro} md	Comp. kk_{ro} md
0.696102E+00	0.329623E+04	0.681092E+00	0.627411E+01	0.537170E+01
0.764822E+00	0.330355E+04	0.682056E+00	0.630986E+01	0.541351E+01
0.840414E+00	0.331070E+04	0.682983E+00	0.634424E+01	0.547886E+01
0.923566E+00	0.331765E+04	0.683886E+00	0.637770E+01	0.554527E+01
0.101503E+01	0.332443E+04	0.684756E+00	0.640998E+01	0.559889E+01
0.111565E+01	0.333103E+04	0.685605E+00	0.644194E+01	0.563777E+01
0.122632E+01	0.333749E+04	0.686431E+00	0.647323E+01	0.564943E+01
0.134806E+01	0.334377E+04	0.687232E+00	0.650358E+01	0.577289E+01
0.148198E+01	0.334984E+04	0.687995E+00	0.653253E+01	0.579670E+01
0.162929E+01	0.335573E+04	0.688742E+00	0.656082E+01	0.584639E+01
0.179133E+01	0.336143E+04	0.689456E+00	0.658786E+01	0.589075E+01
0.196957E+01	0.336695E+04	0.690151E+00	0.661435E+01	0.591901E+01
0.216564E+01	0.337231E+04	0.690820E+00	0.664023E+01	0.596469E+01
0.238131E+01	0.337744E+04	0.691452E+00	0.666473E+01	0.602773E+01
0.261855E+01	0.338238E+04	0.692066E+00	0.668850E+01	0.607303E+01
0.287952E+01	0.338713E+04	0.692656E+00	0.671134E+01	0.611564E+01
0.316658E+01	0.339168E+04	0.693217E+00	0.673307E+01	0.615728E+01
0.348235E+01	0.339603E+04	0.693752E+00	0.675380E+01	0.618055E+01
0.382969E+01	0.340021E+04	0.694266E+00	0.677371E+01	0.621635E+01
0.421177E+01	0.340418E+04	0.694754E+00	0.679260E+01	0.627119E+01
0.463206E+01	0.340795E+04	0.695216E+00	0.681068E+01	0.627181E+01

Table F-37

Simulated and Computed kk_{rg} Values
Buildup Test
Case 2

p_{ws} psi	Sim. kk_{rg} md	Comp. kk_{rg} md
0.208107E+04	0.392206E-01	0.370021E-01
0.208747E+04	0.390464E-01	0.367284E-01
0.209463E+04	0.388456E-01	0.365152E-01
0.210262E+04	0.386206E-01	0.363757E-01
0.211147E+04	0.383800E-01	0.365817E-01
0.212110E+04	0.381054E-01	0.369653E-01
0.213157E+04	0.377997E-01	0.369883E-01
0.214309E+04	0.374818E-01	0.367000E-01
0.215575E+04	0.371379E-01	0.362240E-01
0.216970E+04	0.367585E-01	0.357720E-01
0.218497E+04	0.363437E-01	0.353904E-01
0.220158E+04	0.358676E-01	0.349391E-01
0.221964E+04	0.353678E-01	0.342884E-01
0.223939E+04	0.348194E-01	0.334203E-01
0.225749E+04	0.342933E-01	0.327325E-01
0.227662E+04	0.337552E-01	0.325614E-01
0.229462E+04	0.332348E-01	0.320589E-01
0.231363E+04	0.326216E-01	0.318896E-01
0.233149E+04	0.321225E-01	0.314209E-01
0.235041E+04	0.315865E-01	0.311243E-01
0.236826E+04	0.310754E-01	0.306506E-01
0.238711E+04	0.305366E-01	0.303575E-01
0.240490E+04	0.300197E-01	0.298795E-01
0.242367E+04	0.294697E-01	0.295759E-01
0.244136E+04	0.289509E-01	0.291247E-01
0.246000E+04	0.283914E-01	0.287963E-01
0.247763E+04	0.278655E-01	0.283755E-01
0.249614E+04	0.273100E-01	0.280100E-01
0.251375E+04	0.267658E-01	0.275437E-01
0.253220E+04	0.262038E-01	0.271501E-01
0.254975E+04	0.256555E-01	0.266852E-01
0.256808E+04	0.250789E-01	0.262599E-01
0.258559E+04	0.245278E-01	0.257155E-01
0.260389E+04	0.239022E-01	0.252199E-01
0.262132E+04	0.232985E-01	0.246527E-01
0.263951E+04	0.227177E-01	0.241076E-01
0.265690E+04	0.221566E-01	0.235222E-01
0.267496E+04	0.215774E-01	0.230570E-01
0.269372E+04	0.209572E-01	0.223332E-01
0.271100E+04	0.203687E-01	0.216952E-01
0.272878E+04	0.197118E-01	0.212680E-01
0.274705E+04	0.190896E-01	0.206325E-01
0.276409E+04	0.185046E-01	0.200520E-01

Table F-37 (Cont'd)

p_{wf} psi	Sim. kk_{rg} md	Comp. kk_{rg} md
0.278145E+04	0.178920E-01	0.195774E-01
0.279912E+04	0.172571E-01	0.189737E-01
0.281703E+04	0.165573E-01	0.183141E-01
0.283508E+04	0.158667E-01	0.176162E-01
0.285317E+04	0.152000E-01	0.168915E-01
0.287118E+04	0.144975E-01	0.161468E-01
0.288901E+04	0.137619E-01	0.153846E-01
0.290655E+04	0.130109E-01	0.146150E-01
0.292371E+04	0.123197E-01	0.138423E-01
0.294039E+04	0.116022E-01	0.130683E-01
0.295655E+04	0.108362E-01	0.122914E-01
0.297217E+04	0.101493E-01	0.114646E-01
0.298736E+04	0.945091E-02	0.106008E-01
0.300214E+04	0.872055E-02	0.989342E-02
0.301614E+04	0.805556E-02	0.933650E-02
0.302945E+04	0.743084E-02	0.880899E-02
0.304209E+04	0.680530E-02	0.830641E-02
0.305420E+04	0.623604E-02	0.782232E-02
0.306583E+04	0.571686E-02	0.735598E-02
0.307710E+04	0.519693E-02	0.692736E-02
0.308799E+04	0.472576E-02	0.650967E-02
0.309867E+04	0.430316E-02	0.609490E-02
0.310909E+04	0.388534E-02	0.572381E-02
0.311927E+04	0.349788E-02	0.533183E-02
0.312935E+04	0.316748E-02	0.493755E-02
0.313926E+04	0.284312E-02	0.457319E-02
0.314897E+04	0.252839E-02	0.420251E-02
0.315857E+04	0.228376E-02	0.380770E-02
0.316810E+04	0.204220E-02	0.342849E-02
0.317744E+04	0.180697E-02	0.306480E-02
0.318664E+04	0.160867E-02	0.268090E-02
0.319576E+04	0.143889E-02	0.229022E-02
0.320481E+04	0.127219E-02	0.190855E-02
0.321370E+04	0.110943E-02	0.152794E-02
0.322252E+04	0.986796E-03	0.113084E-02
0.323142E+04	0.872537E-03	0.734861E-03
0.324027E+04	0.760854E-03	0.355471E-03
0.324882E+04	0.653206E-03	0.000000E+00
0.325716E+04	0.574710E-03	0.000000E+00
0.326532E+04	0.506763E-03	0.000000E+00
0.327335E+04	0.440978E-03	0.000000E+00
0.328115E+04	0.376970E-03	0.000000E+00
0.328877E+04	0.317784E-03	0.000000E+00

Table F-37 (Cont'd)

p_{ws} psi	Sim. kk_{rg} md	Comp. kk_{rg} md
0.329623E+04	0.281348E-03	0.000000E+00
0.330355E+04	0.245554E-03	0.000000E+00
0.331070E+04	0.211141E-03	0.000000E+00
0.331765E+04	0.177640E-03	0.000000E+00
0.332443E+04	0.145324E-03	0.000000E+00
0.333103E+04	0.124691E-03	0.000000E+00
0.333749E+04	0.108878E-03	0.000000E+00
0.334377E+04	0.935432E-04	0.000000E+00
0.334984E+04	0.789127E-04	0.000000E+00
0.335573E+04	0.646129E-04	0.000000E+00
0.336143E+04	0.509520E-04	0.000000E+00
0.336695E+04	0.394527E-04	0.000000E+00
0.337231E+04	0.347152E-04	0.000000E+00
0.337744E+04	0.302304E-04	0.000000E+00
0.338238E+04	0.258808E-04	0.000000E+00
0.338713E+04	0.216999E-04	0.000000E+00
0.339168E+04	0.177243E-04	0.000000E+00
0.339603E+04	0.139299E-04	0.000000E+00
0.340021E+04	0.102857E-04	0.000000E+00
0.340418E+04	0.682749E-05	0.000000E+00
0.340795E+04	0.486406E-05	0.000000E+00